

Introduction to

Many-body quantum theory in condensed matter physics

Henrik Bruus and Karsten Flensberg

Ørsted Laboratory, Niels Bohr Institute, University of Copenhagen
Mikroelektronik Centret, Technical University of Denmark

Copenhagen, 15 August 2002

Preface

Preface for the 2001 edition

This introduction to quantum field theory in condensed matter physics has emerged from our courses for graduate and advanced undergraduate students at the Niels Bohr Institute, University of Copenhagen, held between the fall of 1999 and the spring of 2001. We have gone through the pain of writing these notes, because we felt the pedagogical need for a book which aimed at putting an emphasis on the physical contents and applications of the rather involved mathematical machinery of quantum field theory without losing mathematical rigor. We hope we have succeeded at least to some extent in reaching this goal.

We would like to thank the students who put up with the first versions of this book and for their enumerable and valuable comments and suggestions. We are particularly grateful to the students of *Many-particle Physics I & II*, the academic year 2000-2001, and to Niels Asger Mortensen and Brian Møller Andersen for careful proof reading. Naturally, we are solely responsible for the hopefully few remaining errors and typos.

During the work on this book H.B. was supported by the Danish Natural Science Research Council through Ole Rømer Grant No. 9600548.

Ørsted Laboratory, Niels Bohr Institute
1 September, 2001

Karsten Flensberg
Henrik Bruus

Preface for the 2002 edition

After running the course in the academic year 2001-2002 our students came up with more corrections and comments so that we felt a new edition was appropriate. We would like to thank our ever enthusiastic students for their valuable help in improving this book.

Karsten Flensberg
Ørsted Laboratory
Niels Bohr Institute

Henrik Bruus
Mikroelektronik Centret
Technical University of Denmark

Contents

List of symbols	xii
1 First and second quantization	1
1.1 First quantization, single-particle systems	2
1.2 First quantization, many-particle systems	4
1.2.1 Permutation symmetry and indistinguishability	5
1.2.2 The single-particle states as basis states	6
1.2.3 Operators in first quantization	7
1.3 Second quantization, basic concepts	9
1.3.1 The occupation number representation	10
1.3.2 The boson creation and annihilation operators	10
1.3.3 The fermion creation and annihilation operators	13
1.3.4 The general form for second quantization operators	14
1.3.5 Change of basis in second quantization	16
1.3.6 Quantum field operators and their Fourier transforms	17
1.4 Second quantization, specific operators	18
1.4.1 The harmonic oscillator in second quantization	18
1.4.2 The electromagnetic field in second quantization	19
1.4.3 Operators for kinetic energy, spin, density, and current	21
1.4.4 The Coulomb interaction in second quantization	23
1.4.5 Basis states for systems with different kinds of particles	24
1.5 Second quantization and statistical mechanics	25
1.5.1 The distribution function for non-interacting fermions	28
1.5.2 Distribution functions for non-interacting bosons	29
1.6 Summary and outlook	29
2 The electron gas	31
2.1 The non-interacting electron gas	32
2.1.1 Bloch theory of electrons in a static ion lattice	33
2.1.2 Non-interacting electrons in the jellium model	35
2.1.3 Non-interacting electrons at finite temperature	38
2.2 Electron interactions in perturbation theory	39
2.2.1 Electron interactions in 1 st order perturbation theory	41

2.2.2	Electron interactions in 2 nd order perturbation theory	43
2.3	Electron gases in 3, 2, 1, and 0 dimensions	44
2.3.1	3D electron gases: metals and semiconductors	45
2.3.2	2D electron gases: GaAs/Ga _{1-x} Al _x As heterostructures	46
2.3.3	1D electron gases: carbon nanotubes	48
2.3.4	0D electron gases: quantum dots	49
3	Phonons; coupling to electrons	51
3.1	Jellium oscillations and Einstein phonons	52
3.2	Electron-phonon interaction and the sound velocity	53
3.3	Lattice vibrations and phonons in 1D	53
3.4	Acoustical and optical phonons in 3D	56
3.5	The specific heat of solids in the Debye model	59
3.6	Electron-phonon interaction in the lattice model	61
3.7	Electron-phonon interaction in the jellium model	63
3.8	Summary and outlook	64
4	Mean field theory	65
4.1	The art of mean field theory	68
4.2	Hartree–Fock approximation	69
4.3	Broken symmetry	71
4.4	Ferromagnetism	73
4.4.1	The Heisenberg model of ionic ferromagnets	73
4.4.2	The Stoner model of metallic ferromagnets	75
4.5	Superconductivity	78
4.5.1	Breaking of global gauge symmetry and its consequences	78
4.5.2	Microscopic theory	81
4.6	Summary and outlook	85
5	Time evolution pictures	87
5.1	The Schrödinger picture	87
5.2	The Heisenberg picture	88
5.3	The interaction picture	88
5.4	Time-evolution in linear response	91
5.5	Time dependent creation and annihilation operators	91
5.6	Summary and outlook	93
6	Linear response theory	95
6.1	The general Kubo formula	95
6.2	Kubo formula for conductivity	98
6.3	Kubo formula for conductance	100
6.4	Kubo formula for the dielectric function	102
6.4.1	Dielectric function for translation-invariant system	104
6.4.2	Relation between dielectric function and conductivity	104

6.5	Summary and outlook	104
7	Transport in mesoscopic systems	107
7.1	The S -matrix and scattering states	108
7.1.1	Unitarity of the S -matrix	111
7.1.2	Time-reversal symmetry	112
7.2	Conductance and transmission coefficients	113
7.2.1	The Landauer-Büttiker formula, heuristic derivation	113
7.2.2	The Landauer-Büttiker formula, linear response derivation	115
7.3	Electron wave guides	116
7.3.1	Quantum point contact and conductance quantization	116
7.3.2	Aharonov-Bohm effect	120
7.4	Disordered mesoscopic systems	121
7.4.1	Statistics of quantum conductance, random matrix theory	121
7.4.2	Weak localization in mesoscopic systems	123
7.4.3	Universal conductance fluctuations	124
7.5	Summary and outlook	125
8	Green's functions	127
8.1	"Classical" Green's functions	127
8.2	Green's function for the one-particle Schrödinger equation	128
8.3	Single-particle Green's functions of many-body systems	131
8.3.1	Green's function of translation-invariant systems	132
8.3.2	Green's function of free electrons	132
8.3.3	The Lehmann representation	134
8.3.4	The spectral function	135
8.3.5	Broadening of the spectral function	136
8.4	Measuring the single-particle spectral function	137
8.4.1	Tunneling spectroscopy	137
8.4.2	Optical spectroscopy	141
8.5	Two-particle correlation functions of many-body systems	141
8.6	Summary and outlook	144
9	Equation of motion theory	145
9.1	The single-particle Green's function	145
9.1.1	Non-interacting particles	147
9.2	Anderson's model for magnetic impurities	147
9.2.1	The equation of motion for the Anderson model	149
9.2.2	Mean-field approximation for the Anderson model	150
9.2.3	Solving the Anderson model and comparison with experiments	151
9.2.4	Coulomb blockade and the Anderson model	153
9.2.5	Further correlations in the Anderson model: Kondo effect	153
9.3	The two-particle correlation function	153
9.3.1	The Random Phase Approximation (RPA)	153

9.4	Summary and outlook	156
10	Imaginary time Green's functions	157
10.1	Definitions of Matsubara Green's functions	160
10.1.1	Fourier transform of Matsubara Green's functions	161
10.2	Connection between Matsubara and retarded functions	161
10.2.1	Advanced functions	163
10.3	Single-particle Matsubara Green's function	164
10.3.1	Matsubara Green's function for non-interacting particles	164
10.4	Evaluation of Matsubara sums	165
10.4.1	Summations over functions with simple poles	167
10.4.2	Summations over functions with known branch cuts	168
10.5	Equation of motion	169
10.6	Wick's theorem	170
10.7	Example: polarizability of free electrons	173
10.8	Summary and outlook	174
11	Feynman diagrams and external potentials	177
11.1	Non-interacting particles in external potentials	177
11.2	Elastic scattering and Matsubara frequencies	179
11.3	Random impurities in disordered metals	181
11.3.1	Feynman diagrams for the impurity scattering	182
11.4	Impurity self-average	184
11.5	Self-energy for impurity scattered electrons	189
11.5.1	Lowest order approximation	190
11.5.2	1 st order Born approximation	190
11.5.3	The full Born approximation	193
11.5.4	The self-consistent Born approximation and beyond	194
11.6	Summary and outlook	197
12	Feynman diagrams and pair interactions	199
12.1	The perturbation series for \mathcal{G}	199
12.2	infinite perturbation series! Matsubara Green's function	199
12.3	The Feynman rules for pair interactions	201
12.3.1	Feynman rules for the denominator of $\mathcal{G}(b, a)$	201
12.3.2	Feynman rules for the numerator of $\mathcal{G}(b, a)$	202
12.3.3	The cancellation of disconnected Feynman diagrams	203
12.4	Self-energy and Dyson's equation	205
12.5	The Feynman rules in Fourier space	206
12.6	Examples of how to evaluate Feynman diagrams	208
12.6.1	The Hartree self-energy diagram	209
12.6.2	The Fock self-energy diagram	209
12.6.3	The pair-bubble self-energy diagram	210
12.7	Summary and outlook	211

13 The interacting electron gas	213
13.1 The self-energy in the random phase approximation	213
13.1.1 The density dependence of self-energy diagrams	214
13.1.2 The divergence number of self-energy diagrams	215
13.1.3 RPA resummation of the self-energy	215
13.2 The renormalized Coulomb interaction in RPA	217
13.2.1 Calculation of the pair-bubble	218
13.2.2 The electron-hole pair interpretation of RPA	220
13.3 The ground state energy of the electron gas	220
13.4 The dielectric function and screening	223
13.5 Plasma oscillations and Landau damping	227
13.5.1 Plasma oscillations and plasmons	228
13.5.2 Landau damping	230
13.6 Summary and outlook	231
14 Fermi liquid theory	233
14.1 Adiabatic continuity	233
14.1.1 The quasiparticle concept and conserved quantities	235
14.2 Semi-classical treatment of screening and plasmons	237
14.2.1 Static screening	238
14.2.2 Dynamical screening	238
14.3 Semi-classical transport equation	240
14.3.1 Finite life time of the quasiparticles	243
14.4 Microscopic basis of the Fermi liquid theory	245
14.4.1 Renormalization of the single particle Green's function	245
14.4.2 Imaginary part of the single particle Green's function	248
14.4.3 Mass renormalization?	251
14.5 Outlook and summary	251
15 Impurity scattering and conductivity	253
15.1 Vertex corrections and dressed Green's functions	254
15.2 The conductivity in terms of a general vertex function	259
15.3 The conductivity in the first Born approximation	261
15.4 The weak localization correction to the conductivity	264
15.5 Combined RPA and Born approximation	273
16 Green's functions and phonons	275
16.1 The Green's function for free phonons	275
16.2 Electron-phonon interaction and Feynman diagrams	276
16.3 Combining Coulomb and electron-phonon interactions	279
16.3.1 Migdal's theorem	279
16.3.2 Jellium phonons and the effective electron-electron interaction	280
16.4 Phonon renormalization by electron screening in RPA	281
16.5 The Cooper instability and Feynman diagrams	284

17 Superconductivity	287
17.1 The Cooper instability	287
17.2 The BCS groundstate	287
17.3 BCS theory with Green's functions	287
17.4 Experimental consequences of the BCS states	288
17.4.1 Tunneling density of states	288
17.4.2 specific heat	288
17.5 The Josephson effect	288
18 1D electron gases and Luttinger liquids	289
18.1 Introduction	289
18.2 First look at interacting electrons in one dimension	289
18.2.1 One-dimensional transmission line analog	289
18.3 The Luttinger-Tomonaga model - spinless case	289
18.3.1 Interacting one dimensional electron system	289
18.3.2 Bosonization of Tomonaga model-Hamiltonian	289
18.3.3 Diagonalization of bosonized Hamiltonian	289
18.3.4 Real space formulation	289
18.3.5 Electron operators in bosonized form	289
18.4 Luttinger liquid with spin	290
18.5 Green's functions	290
18.6 Tunneling into spinless Luttinger liquid	290
18.6.1 Tunneling into the end of Luttinger liquid	290
18.7 What is a Luttinger liquid?	290
18.8 Experimental realizations of Luttinger liquid physics	290
18.8.1 Edge states in the fractional quantum Hall effect	290
18.8.2 Carbon Nanotubes	290
A Fourier transformations	291
A.1 Continuous functions in a finite region	291
A.2 Continuous functions in an infinite region	292
A.3 Time and frequency Fourier transforms	292
A.4 Some useful rules	292
A.5 Translation invariant systems	293
B Exercises	295
C Index	326

List of symbols

Symbol	Meaning	Definition
$\hat{\heartsuit}$	operator \heartsuit in the interaction picture	Sec. 5.3
$\dot{\heartsuit}$	time derivative of \heartsuit	
$ \nu\rangle$	Dirac ket notation for a quantum state ν	Chap. 1
$\langle\nu $	Dirac bra notation for an adjoint quantum state ν	Chap. 1
$ 0\rangle$	vacuum state	
a	annihilation operator for particle (fermion or boson)	
a^\dagger	creation operator for particle (fermion or boson)	
a_ν, a_ν^\dagger	annihilation/creation operators (state ν)	
a_n^\pm	amplitudes of wavefunctions to the left	Sec. 7.1
a_0	Bohr radius	Eq. (2.36)
$\mathbf{A}(\mathbf{r}, t)$	electromagnetic vector potential	Sec. 1.4.2
$A(\nu, \omega)$	spectral function in frequency domain (state ν)	Sec. 8.3.4
$A(\mathbf{r}, \omega), A(\mathbf{k}, \omega)$	spectral function (real space, Fourier space)	Sec. 8.3.4
$A_0(\mathbf{r}, \omega), A_0(\mathbf{k}, \omega)$	spectral function for free particles	Sec. 8.3.4
A, A^\dagger	phonon annihilation and creation operator	Sec. 16.1
b	annihilation operator for particle (boson, phonon)	
b^\dagger	creation operator for particle (boson, phonon)	
b_n^\pm	amplitudes of wavefunctions to the right	Sec. 7.1
\mathbf{B}	magnetic field	
c	annihilation operator for particle (fermion, electron)	
c^\dagger	creation operator for particle (fermion, electron)	
c_ν, c_ν^\dagger	annihilation/creation operators (state ν)	
$C_{AB}^R(t, t')$	retarded correlation function between A and B (time)	Sec. 6.1
$C_{AB}^A(t, t')$	advanced correlation function between A and B (time)	Sec. 10.2.1
$C_{II}^R(\omega)$	retarded current-current correlation function (frequency)	Sec. 6.3
\mathcal{C}_{AB}	Matsubara correlation function	Sec. 10.1
$\mathcal{C}(\mathbf{Q}, ik_n, ik_n + iq_n)$	Cooperon in the Matsubara domain	Sec. 15.4
$C^R(\mathbf{Q}, \varepsilon, \varepsilon)$	Cooperon in the real time domain	Sec. 15.4
C_V^{ion}	specific heat for ions (constant volume)	

Symbol	Meaning	Definition
$d(\epsilon)$	density of states (including spin degeneracy for electrons)	Eq. (2.31)
$\delta(\mathbf{r})$	Dirac delta function	Eq. (1.11)
$D^R(\mathbf{r}t, \mathbf{r}t')$	retarded phonon propagator	Chap. 16
$D^R(\mathbf{q}, \omega)$	retarded phonon propagator (Fourier space)	Chap. 16
$\mathcal{D}(\mathbf{r}\tau, \mathbf{r}\tau')$	Matsubara phonon propagator	Chap. 16
$\mathcal{D}(\mathbf{q}, iq_n)$	Matsubara phonon propagator (Fourier space)	Chap. 16
$D^R(\nu t, \nu' t')$	retarded many particle Green's function	Eq. (9.9b)
$D_{\alpha\beta}(\mathbf{r})$	phonon dynamical matrix	Sec. 3.4
$\Delta_{\mathbf{k}}$	superconducting orderparameter	Eq. (4.58b)
e	elementary charge	
e_0^2	electron interaction strength	Eq. (1.101)
$\mathbf{E}(\mathbf{r}, t)$	electric field	
E	total energy of the electron gas	
$E^{(1)}$	interaction energy of the electron gas, 1st order perturbation	
$E^{(2)}$	interaction energy of the electron gas, 2nd order perturbation	
E_0	Rydberg energy	Eq. (2.36)
$E_{\mathbf{k}}$	dispersion relation for BCS quasiparticles	Eq. (4.64)
ε	energy variable	
ϵ_0	the dielectric constant of vacuum	
$\epsilon_{\mathbf{k}}$	dispersion relation	
ϵ_{ν}	energy of quantum state ν	
ϵ_F	Fermi energy	
$\epsilon_{\mathbf{k}\lambda}$	phonon polarization vector	Eq. (3.20)
$\varepsilon(\mathbf{r}t, \mathbf{r}t')$	dielectric function in real space	Sec. 6.4
$\varepsilon(\mathbf{k}, \omega)$	dielectric function in Fourier space	Sec. 6.4
F	free energy	Sec. 1.5
$ \text{FS}\rangle$	the filled Fermi sea N -particle quantum state	
$\phi(\mathbf{r}, t)$	electric potential	
ϕ_{ext}	external electric potential	
ϕ_{ind}	induced electric potential	
$\phi, \tilde{\phi}$	wavefunctions with different normalizations	Eq. (7.4)
$\phi_{LnE}^{\pm}, \phi_{RnE}^{\pm}$	wavefunctions in the left and right leads	Sec. 7.1
$g_{\mathbf{q}\lambda}$	electron-phonon coupling constant (lattice model)	
$g_{\mathbf{q}}$	electron-phonon coupling constant (jellium model)	
G	conductance	

Symbol	Meaning	Definition
$G(\mathbf{r}t, \mathbf{r}'t')$	Green's function for the Schrödinger equation	Sec. 8.2
$G_0(\mathbf{r}t, \mathbf{r}'t')$	unperturbed Green's function for Schrödingers eq.	Sec. 8.2
$G_0^<(\mathbf{r}t, \mathbf{r}'t')$	free lesser Green's function	Sec. 8.3.1
$G_0^>(\mathbf{r}t, \mathbf{r}'t')$	free greater Green's function	Sec. 8.3.1
$G_0^A(\mathbf{r}t, \mathbf{r}'t')$	free advanced Green's function	Sec. 8.3.1
$G_0^R(\mathbf{r}t, \mathbf{r}'t')$	free retarded Green's function	Sec. 8.3.1
$G_0^R(\mathbf{k}, \omega)$	free retarded Green's function (Fourier space)	Sec. 8.3.1
$G^<(\mathbf{r}t, \mathbf{r}'t')$	lesser Green's function	Sec. 8.3
$G^>(\mathbf{r}t, \mathbf{r}'t')$	greater Green's function	Sec. 8.3
$G^A(\mathbf{r}t, \mathbf{r}'t')$	advanced Green's function	Sec. 8.3
$G^R(\mathbf{r}t, \mathbf{r}'t')$	retarded Green's function (real space)	Sec. 8.3
$G^R(\mathbf{k}, \omega)$	retarded Green's function in Fourier space	Sec. 8.3
$G^R(\mathbf{k}, \omega)$	retarded Green's function (Fourier space)	Sec. 8.3.1
$G^R(\nu\tau, \nu'\tau')$	retarded single-particle Green's function ($\{\nu\}$ basis)	Eq. (8.32)
$\mathcal{G}(\mathbf{r}\sigma\tau, \mathbf{r}'\sigma'\tau')$	Matsubara Green's function (real space)	Sec. 10.3
$\mathcal{G}(\nu\tau, \nu'\tau')$	Matsubara Green's function ($\{\nu\}$ basis)	Sec. 10.3
$\mathcal{G}(1, 1')$	Matsubara Green's function (real space four-vectors)	Sec. 11.1
$\mathcal{G}(\tilde{k}, \tilde{k}')$	Matsubara Green's function (four-momentum notation)	Sec. 12.5
$\mathcal{G}_0(\mathbf{r}\sigma\tau, \mathbf{r}'\sigma'\tau')$	Matsubara Green's function (real space, free particles)	Sec. 10.3.1
$\mathcal{G}_0(\nu\tau, \nu'\tau')$	Matsubara Green's function ($\{\nu\}$ basis, free particles)	Sec. 10.3.1
$\mathcal{G}_0(\mathbf{k}, ik_n)$	Matsubara Green's function (Fourier space, free particles)	Sec. 10.3
$\mathcal{G}_0(\nu, ik_n)$	Matsubara Green's function (free particles)	Sec. 10.3
$\mathcal{G}_0^{(n)}$	n -particle Green's function (free particles)	Sec. 10.6
$\mathcal{G}(\mathbf{k}, ik_n)$	Matsubara Green's function (Fourier space)	Sec. 10.3
$\mathcal{G}(\nu, ik_n)$	Matsubara Green's function ($\{\nu\}$ basis, frequency domain)	Sec. 10.3
γ, γ^{RA}	scalar vertex function	Sec. 15.3
Γ	imaginary part of self-energy	
$\Gamma_x(\tilde{k}, \tilde{k} + \tilde{q})$	vertex function (x -component, four vector notation)	Eq. (15.20b)
$\Gamma_{0,x}$	free (undressed) vertex function	
H	a general Hamiltonian	
H_0	unperturbed part of an Hamiltonian	
H'	perturbative part of an Hamiltonian	
H_{ext}	external potential part of an Hamiltonian	
H_{int}	interaction part of an Hamiltonian	
H_{ph}	phonon part of an Hamiltonian	
η	positive infinitesimal	
I	current operator (particle current)	Sec. 6.3
I_e	electrical current (charge current)	Sec. 6.3

Symbol	Meaning	Definition
$J_\sigma(\mathbf{r})$	current density operator	Eq. (1.99a)
$J_\sigma^\Delta(\mathbf{r})$	current density operator, paramagnetic term	Eq. (1.99a)
$J_\sigma^A(\mathbf{r})$	current density operator, diamagnetic term	Eq. (1.99a)
$J_\sigma(\mathbf{q})$	current density operator (momentum space)	
$J_e(\mathbf{r}, t)$	electric current density operator	
J_{ij}	interaction strength in the Heisenberg model	Sec. 4.4.1
k_n	Matsubara frequency (fermions)	
k_F	Fermi wave number	
\mathbf{k}	general momentum or wave vector variable	
ℓ	mean free path or scattering length	
ℓ_0	mean free path (first Born approximation)	
ℓ_ϕ	phase breaking mean free path	
ℓ_{in}	inelastic scattering length	
\mathcal{L}	normalization length or system size in 1D	
λ_F	Fermi wave length	
Λ^{irr}	irreducible four-point function	Eq. (15.17)
m	mass (electrons and general particles)	
m^*	effective interaction renormalized mass	Sec. 14.4.1
μ	chemical potential	
μ	general quantum number label	
n	particle density	
$n_F(\varepsilon)$	Fermi-Dirac distribution function	Sec. 1.5.1
$n_B(\varepsilon)$	Bose-Einstein distribution function	Sec. 1.5.2
n_{imp}	impurity density	
N	number of particles	
N_{imp}	number of impurities	
ν	general quantum number label	
ω	frequency variable	
$\omega_{\mathbf{q}}$	phonon dispersion relation	
ω_n	Matsubara frequency	Chap. 10
Ω	thermodynamic potential	Sec. 1.5
\mathbf{p}	general momentum or wave number variable	
p_n	Matsubara frequency (fermion)	
$\Pi_{\alpha\beta}^R(\mathbf{r}t, \mathbf{r}'t')$	retarded current-current correlation function	Eq. (6.26)
$\Pi_{\alpha\beta}^R(\mathbf{q}, \omega)$	retarded current-current correlation function	
$\Pi_{\alpha\beta}(\mathbf{q}, i\omega_n)$	Matsubara current-current correlation function	Chap. 15
$\Pi^0(\mathbf{q}, iq_n)$	free pair-bubble diagram	Eq. (12.34)

Symbol	Meaning	Definition
\mathbf{q}	general momentum variable	
q_n	Matsubara frequency (bosons)	
\mathbf{r}	general space variable	
\mathbf{r}	reflection matrix coming from left	Sec. 7.1
\mathbf{r}'	reflection matrix coming from right	Sec. 7.1
r_s	electron gas density parameter	Eq. (2.37)
ρ	density matrix	Sec. 1.5
ρ_0	unperturbed density matrix	
$\rho_\sigma(\mathbf{r})$	particle density operator (real space)	Eq. (1.96)
$\rho_\sigma(\mathbf{q})$	particle density operator (momentum space)	Eq. (1.96)
S	entropy	
\mathbf{S}	scattering matrix	Sec. 7.1
σ	general spin index	
$\sigma_{\alpha\beta}(\mathbf{r}t, \mathbf{r}'t')$	conductivity tensor	Sec. 6.2
$\Sigma^R(\mathbf{q}, \omega)$	retarded self-energy (Fourier space)	
$\Sigma(\mathbf{q}, ik_n)$	Matsubara self-energy	
$\Sigma_{\mathbf{k}}$	impurity scattering self-energy	Sec. 11.5
$\Sigma_{\mathbf{k}}^{\text{IBA}}$	first Born approximation	Sec. 11.5.1
$\Sigma_{\mathbf{k}}^{\text{FBA}}$	full Born approximation	Sec. 11.5.3
$\Sigma_{\mathbf{k}}^{\text{SCBA}}$	self-consistent Born approximation	Sec. 11.5.4
$\Sigma(l, j)$	general electron self-energy	
$\Sigma_\sigma(\mathbf{k}, ik_n)$	general electron self-energy	
$\Sigma_\sigma^F(\mathbf{k}, ik_n)$	Fock self-energy	Sec. 12.6
$\Sigma_\sigma^H(\mathbf{k}, ik_n)$	Hartree self-energy	Sec. 12.6
$\Sigma_\sigma^P(\mathbf{k}, ik_n)$	pair-bubble self-energy	Sec. 12.6
$\Sigma_\sigma^{\text{RPA}}(\mathbf{k}, ik_n)$	RPA electron self-energy	Eq. (13.10)
t	general time variable	
\mathbf{t}	transmission matrix coming from left	Sec. 7.1
\mathbf{t}'	transmission matrix coming from right	Sec. 7.1
T	kinetic energy	
τ	general imaginary time variable	
τ^{tr}	transport scattering time	Eq. (14.39)
$\tau_0, \tau_{\mathbf{k}}$	life-time in the first Born approximation	
u_j	ion displacement (1D)	
$\mathbf{u}(\mathbf{R}_0)$	ion displacement (3D)	
$u_{\mathbf{k}}$	BCS coherence factor	Sec. 4.5.2
U	general unitary matrix	
$\hat{U}(t, t')$	real time-evolution operator, interaction picture	
$\hat{U}(\tau, \tau')$	imaginary time-evolution operator, interaction picture	

Symbol	Meaning	Definition
$v_{\mathbf{k}}$	BCS coherence factor	Sec. 4.5.2
$V(\mathbf{r}), V(\mathbf{q})$	general single impurity potential	
$V(\mathbf{r}), V(\mathbf{q})$	Coulomb interaction	
V_{eff}	combined Coulomb and phonon-mediated interaction	Sec. 13.2
\mathcal{V}	normalization volume	
W	pair interaction Hamiltonian	
$W(\mathbf{r}), W(\mathbf{q})$	general pair interaction	
$W(\mathbf{r}), W(\mathbf{q})$	Coulomb interaction	
W^{RPA}	RPA-screened Coulomb interaction	Sec. 13.2
$\xi_{\mathbf{k}}$	$\varepsilon_{\mathbf{k}} - \mu$	
ξ_{ν}	$\varepsilon_{\nu} - \mu$	
$\chi(\mathbf{q}, iq_n)$	Matsubara charge-charge correlation function	Sec. 13.4
$\chi^{\text{RPA}}(\mathbf{q}, iq_n)$	RPA Matsubara charge-charge correlation function	Sec. 13.4
$\chi^{\text{irr}}(\mathbf{q}, iq_n)$	irreducible Matsubara charge-charge correlation function	Sec. 13.4
$\chi_0(\mathbf{r}t, \mathbf{r}'t')$	free retarded charge-charge correlation function	
$\chi_0(\mathbf{q}, iq_n)$	free Matsubara charge-charge correlation function	Sec. 13.4
$\chi^R(\mathbf{r}t, \mathbf{r}'t')$	retarded charge-charge correlation function	Eq. (6.39)
$\chi^R(\mathbf{q}, \omega)$	retarded charge-charge correlation function (Fourier)	
$\chi_n(y)$	transverse wavefunction	Sec. 7.1
$\psi_{\nu}(\mathbf{r})$	single-particle wave function, quantum number ν	
ψ_{nE}^{\pm}	single-particle scattering states	Sec. 7.1
$\psi(\mathbf{r}_1, \mathbf{r}_2, \dots, \mathbf{r}_n)$	n -particle wave function (first quantization)	
$\Psi_{\sigma}(\mathbf{r})$	quantum field annihilation operator	Sec. 1.3.6
$\Psi_{\sigma}^{\dagger}(\mathbf{r})$	quantum field creation operator	Sec. 1.3.6
$\theta(x)$	Heaviside's step function	Eq. (1.12)

Chapter 1

First and second quantization

Quantum theory is the most complete microscopic theory we have today describing the physics of energy and matter. It has successfully been applied to explain phenomena ranging over many orders of magnitude, from the study of elementary particles on the sub-nucleonic scale to the study of neutron stars and other astrophysical objects on the cosmological scale. Only the inclusion of gravitation stands out as an unsolved problem in fundamental quantum theory.

Historically, quantum physics first dealt only with the quantization of the motion of particles leaving the electromagnetic field classical, hence the name quantum mechanics (Heisenberg, Schrödinger, and Dirac 1925-26). Later also the electromagnetic field was quantized (Dirac, 1927), and even the particles themselves got represented by quantized fields (Jordan and Wigner, 1928), resulting in the development of quantum electrodynamics (QED) and quantum field theory (QFT) in general. By convention, the original form of quantum mechanics is denoted first quantization, while quantum field theory is formulated in the language of second quantization.

Regardless of the representation, be it first or second quantization, certain basic concepts are always present in the formulation of quantum theory. The starting point is the notion of quantum states and the observables of the system under consideration. Quantum theory postulates that all quantum states are represented by state vectors in a Hilbert space, and that all observables are represented by Hermitian operators acting on that space. Parallel state vectors represent the same physical state, and one therefore mostly deals with normalized state vectors. Any given Hermitian operator A has a number of eigenstates $|\psi_\alpha\rangle$ that up to a real scale factor α is left invariant by the action of the operator, $A|\psi_\alpha\rangle = \alpha|\psi_\alpha\rangle$. The scale factors are denoted the eigenvalues of the operator. It is a fundamental theorem of Hilbert space theory that the set of all eigenvectors of any given Hermitian operator forms a complete basis set of the Hilbert space. In general the eigenstates $|\psi_\alpha\rangle$ and $|\phi_\beta\rangle$ of two different Hermitian operators A and B are not the same. By measurement of the type B the quantum state can be prepared to be in an eigenstate $|\phi_\beta\rangle$ of the operator B . This state can also be expressed as a superposition of eigenstates $|\psi_\alpha\rangle$ of the operator A as $|\phi_\beta\rangle = \sum_\alpha |\psi_\alpha\rangle C_{\alpha\beta}$. If one in this state measures the dynamical variable associated with the operator A , one cannot in general predict the outcome with

certainty. It is only described in probabilistic terms. The probability of having any given $|\psi_\alpha\rangle$ as the outcome is given as the absolute square $|C_{\alpha\beta}|^2$ of the associated expansion coefficient. This non-causal element of quantum theory is also known as the collapse of the wavefunction. However, between collapse events the time evolution of quantum states is perfectly deterministic. The time evolution of a state vector $|\psi(t)\rangle$ is governed by the central operator in quantum mechanics, the Hamiltonian H (the operator associated with the total energy of the system), through Schrödinger's equation

$$i\hbar\partial_t|\psi(t)\rangle = H|\psi(t)\rangle. \quad (1.1)$$

Each state vector $|\psi\rangle$ is associated with an adjoint state vector $(|\psi\rangle)^\dagger \equiv \langle\psi|$. One can form inner products, “bra(c)kets”, $\langle\psi|\phi\rangle$ between adjoint “bra” states $\langle\psi|$ and “ket” states $|\phi\rangle$, and use standard geometrical terminology, e.g. the norm squared of $|\psi\rangle$ is given by $\langle\psi|\psi\rangle$, and $|\psi\rangle$ and $|\phi\rangle$ are said to be orthogonal if $\langle\psi|\phi\rangle = 0$. If $\{|\psi_\alpha\rangle\}$ is an orthonormal basis of the Hilbert space, then the above mentioned expansion coefficient $C_{\alpha\beta}$ is found by forming inner products: $C_{\alpha\beta} = \langle\psi_\alpha|\phi_\beta\rangle$. A further connection between the direct and the adjoint Hilbert space is given by the relation $\langle\psi|\phi\rangle = \langle\phi|\psi\rangle^*$, which also leads to the definition of adjoint operators. For a given operator A the adjoint operator A^\dagger is defined by demanding $\langle\psi|A^\dagger|\phi\rangle = \langle\phi|A|\psi\rangle^*$ for any $|\psi\rangle$ and $|\phi\rangle$.

In this chapter we will briefly review standard first quantization for one and many-particle systems. For more complete reviews the reader is referred to the textbooks by Dirac, Landau and Lifshitz, Merzbacher, or Shankar. Based on this we will introduce second quantization. This introduction is not complete in all details, and we refer the interested reader to the textbooks by Mahan, Fetter and Walecka, and Abrikosov, Gorkov, and Dzyaloshinskii.

1.1 First quantization, single-particle systems

For simplicity consider a non-relativistic particle, say an electron with charge $-e$, moving in an external electromagnetic field described by the potentials $\varphi(\mathbf{r}, t)$ and $\mathbf{A}(\mathbf{r}, t)$. The corresponding Hamiltonian is

$$H = \frac{1}{2m} \left(\frac{\hbar}{i} \nabla_{\mathbf{r}} + e\mathbf{A}(\mathbf{r}, t) \right)^2 - e\varphi(\mathbf{r}, t). \quad (1.2)$$

An eigenstate describing a free spin-up electron travelling inside a box of volume \mathcal{V} can be written as a product of a propagating plane wave and a spin-up spinor. Using the Dirac notation the state ket can be written as $|\psi_{\mathbf{k}, \uparrow}\rangle = |\mathbf{k}, \uparrow\rangle$, where one simply lists the relevant quantum numbers in the ket. The state function (also denoted the wave function) and the ket are related by

$$\psi_{\mathbf{k}, \sigma}(\mathbf{r}) = \langle\mathbf{r}|\mathbf{k}, \sigma\rangle = \frac{1}{\sqrt{\mathcal{V}}} e^{i\mathbf{k}\cdot\mathbf{r}} \chi_\sigma \quad (\text{free particle orbital}), \quad (1.3)$$

i.e. by the inner product of the position bra $\langle\mathbf{r}|$ with the state ket.

The plane wave representation $|\mathbf{k}, \sigma\rangle$ is not always a useful starting point for calculations. For example in atomic physics, where electrons orbiting a point-like positively

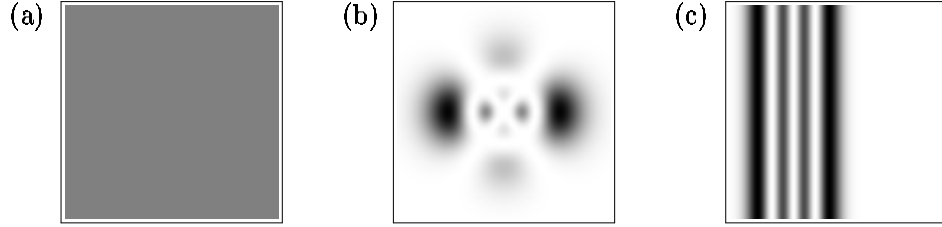


Figure 1.1: The probability density $|\langle \mathbf{r} | \psi_\nu \rangle|^2$ in the xy plane for (a) any plane wave $\nu = (k_x, k_y, k_z, \sigma)$, (b) the hydrogen orbital $\nu = (4, 2, 0, \sigma)$, and (c) the Landau orbital $\nu = (3, k_y, 0, \sigma)$.

charged nucleus are considered, the hydrogenic eigenstates $|n, l, m, \sigma\rangle$ are much more useful. Recall that

$$\langle \mathbf{r} | n, l, m, \sigma \rangle = R_{nl}(r) Y_{l,m}(\theta, \phi) \chi_\sigma \quad (\text{hydrogen orbital}), \quad (1.4)$$

where $R_{nl}(r)$ is a radial Coulomb function with $n-l$ nodes, while $Y_{l,m}(\theta, \phi)$ is a spherical harmonic representing angular momentum l with a z component m .

A third example is an electron moving in a constant magnetic field $\mathbf{B} = B \mathbf{e}_z$, which in the Landau gauge $\mathbf{A} = xB \mathbf{e}_y$ leads to the Landau eigenstates $|n, k_y, k_z, \sigma\rangle$, where n is an integer, k_y (k_z) is the y (z) component of \mathbf{k} , and σ the spin variable. Recall that

$$\langle \mathbf{r} | n, k_y, k_z, \sigma \rangle = H_n(x/\ell - k_y \ell) e^{-\frac{1}{2}(x/\ell - k_y \ell)^2} \frac{1}{\sqrt{L_y L_z}} e^{i(k_y y + k_z z)} \chi_\sigma \quad (\text{Landau orbital}), \quad (1.5)$$

where $\ell = \sqrt{\hbar/eB}$ is the magnetic length and H_n is the normalized Hermite polynomial of order n associated with the harmonic oscillator potential induced by the magnetic field. Examples of each of these three types of electron orbitals are shown in Fig. 1.1.

In general a complete set of quantum numbers is denoted ν . The three examples given above corresponds to $\nu = (k_x, k_y, k_z, \sigma)$, $\nu = (n, l, m, \sigma)$, and $\nu = (n, k_y, k_z, \sigma)$ each yielding a state function of the form $\psi_\nu(\mathbf{r}) = \langle \mathbf{r} | \nu \rangle$. The completeness of a basis state as well as the normalization of the state vectors play a central role in quantum theory. Loosely speaking the normalization condition means that with probability unity a particle in a given quantum state $\psi_\nu(\mathbf{r})$ must be somewhere in space: $\int d\mathbf{r} |\psi_\nu(\mathbf{r})|^2 = 1$, or in the Dirac notation: $1 = \int d\mathbf{r} \langle \nu | \mathbf{r} \rangle \langle \mathbf{r} | \nu \rangle = \langle \nu | (\int d\mathbf{r} |\mathbf{r}\rangle \langle \mathbf{r}|) | \nu \rangle$. From this we conclude

$$\int d\mathbf{r} |\mathbf{r}\rangle \langle \mathbf{r}| = 1. \quad (1.6)$$

Similarly, the completeness of a set of basis states $\psi_\nu(\mathbf{r})$ means that if a particle is in some state $\psi(\mathbf{r})$ it must be found with probability unity within the orbitals of the basis set: $\sum_\nu |\langle \nu | \psi \rangle|^2 = 1$. Again using the Dirac notation we find $1 = \sum_\nu \langle \psi | \nu \rangle \langle \nu | \psi \rangle = \langle \psi | (\sum_\nu |\nu\rangle \langle \nu|) | \psi \rangle$, and we conclude

$$\sum_\nu |\nu\rangle \langle \nu| = 1. \quad (1.7)$$

We shall often use the completeness relation Eq. (1.7). A simple example is the expansion of a state function in a given basis: $\psi(\mathbf{r}) = \langle \mathbf{r} | \psi \rangle = \langle \mathbf{r} | 1 | \psi \rangle = \langle \mathbf{r} | (\sum_{\nu} |\nu\rangle \langle \nu|) | \psi \rangle = \sum_{\nu} \langle \mathbf{r} | \nu \rangle \langle \nu | \psi \rangle$, which can be expressed as

$$\psi(\mathbf{r}) = \sum_{\nu} \psi_{\nu}(\mathbf{r}) \left(\int d\mathbf{r}' \psi_{\nu}^*(\mathbf{r}') \psi(\mathbf{r}') \right) \quad \text{or} \quad \langle \mathbf{r} | \psi \rangle = \sum_{\nu} \langle \mathbf{r} | \nu \rangle \langle \nu | \psi \rangle. \quad (1.8)$$

It should be noted that the quantum label ν can contain both discrete and continuous quantum numbers. In that case the symbol \sum_{ν} is to be interpreted as a combination of both summations and integrations. For example in the case in Eq. (1.5) with Landau orbitals in a box with side lengths L_x , L_y , and L_z , we have

$$\sum_{\nu} = \sum_{\sigma=\uparrow, \downarrow} \sum_{n=0}^{\infty} \int_{-\infty}^{\infty} \frac{L_y}{2\pi} dk_y \int_{-\infty}^{\infty} \frac{L_z}{2\pi} dk_z. \quad (1.9)$$

In the mathematical formulation of quantum theory we shall often encounter the following special functions.

Kronecker's delta-function $\delta_{k,n}$ for discrete variables,

$$\delta_{k,n} = \begin{cases} 1, & \text{for } k = n, \\ 0, & \text{for } k \neq n. \end{cases} \quad (1.10)$$

Dirac's delta-function $\delta(\mathbf{r})$ for continuous variables,

$$\delta(\mathbf{r}) = 0, \quad \text{for } \mathbf{r} \neq 0, \quad \text{while} \quad \int d\mathbf{r} \delta(\mathbf{r}) = 1, \quad (1.11)$$

and Heaviside's step-function $\theta(x)$ for continuous variables,

$$\theta(x) = \begin{cases} 0, & \text{for } x < 0, \\ 1, & \text{for } x > 0. \end{cases} \quad (1.12)$$

1.2 First quantization, many-particle systems

When turning to N -particle systems, i.e. a system containing N identical particles, say, electrons, three more assumptions are added to the basic assumptions defining quantum theory. The first assumption is the natural extension of the single-particle state function $\psi(\mathbf{r})$, which (neglecting the spin degree of freedom for the time being) is a complex wave function in 3-dimensional space, to the N -particle state function $\psi(\mathbf{r}_1, \mathbf{r}_2, \dots, \mathbf{r}_N)$, which is a complex function in the $3N$ -dimensional configuration space. As for one particle this N -particle state function is interpreted as a probability amplitude such that its absolute square is related to a probability:

$$|\psi(\mathbf{r}_1, \mathbf{r}_2, \dots, \mathbf{r}_N)|^2 \prod_{j=1}^N d\mathbf{r}_j = \left\{ \begin{array}{l} \text{The probability for finding the } N \text{ particles} \\ \text{in the } 3N\text{-dimensional volume } \prod_{j=1}^N d\mathbf{r}_j \\ \text{surrounding the point } (\mathbf{r}_1, \mathbf{r}_2, \dots, \mathbf{r}_N) \text{ in} \\ \text{the } 3N\text{-dimensional configuration space.} \end{array} \right\} \quad (1.13)$$

1.2.1 Permutation symmetry and indistinguishability

A fundamental difference between classical and quantum mechanics concerns the concept of indistinguishability of identical particles. In classical mechanics each particle can be equipped with an identifying marker (e.g. a colored spot on a billiard ball) without influencing its behavior, and moreover it follows its own continuous path in phase space. Thus in principle each particle in a group of identical particles can be identified. This is not so in quantum mechanics. Not even in principle is it possible to mark a particle without influencing its physical state, and worse, if a number of identical particles are brought to the same region in space, their wavefunctions will rapidly spread out and overlap with one another, thereby soon render it impossible to say which particle is where.

The second fundamental assumption for N -particle systems is therefore that identical particles, i.e. particles characterized by the same quantum numbers such as mass, charge and spin, are in principle indistinguishable.

From the indistinguishability of particles follows that if two coordinates in an N -particle state function are interchanged the same physical state results, and the corresponding state function can at most differ from the original one by a simple prefactor λ . If the same two coordinates then are interchanged a second time, we end with the exact same state function,

$$\psi(\mathbf{r}_1, \dots, \mathbf{r}_j, \dots, \mathbf{r}_k, \dots, \mathbf{r}_N) = \lambda \psi(\mathbf{r}_1, \dots, \mathbf{r}_k, \dots, \mathbf{r}_j, \dots, \mathbf{r}_N) = \lambda^2 \psi(\mathbf{r}_1, \dots, \mathbf{r}_j, \dots, \mathbf{r}_k, \dots, \mathbf{r}_N), \quad (1.14)$$

and we conclude that $\lambda^2 = 1$ or $\lambda = \pm 1$. Only two species of particles are thus possible in quantum physics, the so-called bosons and fermions¹:

$$\psi(\mathbf{r}_1, \dots, \mathbf{r}_j, \dots, \mathbf{r}_k, \dots, \mathbf{r}_N) = +\psi(\mathbf{r}_1, \dots, \mathbf{r}_k, \dots, \mathbf{r}_j, \dots, \mathbf{r}_N) \quad (\text{bosons}), \quad (1.15a)$$

$$\psi(\mathbf{r}_1, \dots, \mathbf{r}_j, \dots, \mathbf{r}_k, \dots, \mathbf{r}_N) = -\psi(\mathbf{r}_1, \dots, \mathbf{r}_k, \dots, \mathbf{r}_j, \dots, \mathbf{r}_N) \quad (\text{fermions}). \quad (1.15b)$$

The importance of the assumption of indistinguishability of particles in quantum physics cannot be exaggerated, and it has been introduced due to overwhelming experimental evidence. For fermions it immediately leads to the Pauli exclusion principle stating that two fermions cannot occupy the same state, because if in Eq. (1.15b) we let $\mathbf{r}_j = \mathbf{r}_k$ then $\psi = 0$ follows. It thus explains the periodic table of the elements, and consequently the starting point in our understanding of atomic physics, condensed matter physics and chemistry. It furthermore plays a fundamental role in the studies of the nature of stars and of the scattering processes in high energy physics. For bosons the assumption is necessary to understand Planck's radiation law for the electromagnetic field, and spectacular phenomena like Bose–Einstein condensation, superfluidity and laser light.

¹This discrete permutation symmetry is always obeyed. However, some quasiparticles in 2D exhibit **any** phase $e^{i\phi}$, a so-called Berry phase, upon adiabatic interchange. Such exotic beasts are called **anyons**

1.2.2 The single-particle states as basis states

We now show that the basis states for the N -particle system can be built from any complete orthonormal single-particle basis $\{\psi_\nu(\mathbf{r})\}$,

$$\sum_\nu \psi_\nu^*(\mathbf{r}') \psi_\nu(\mathbf{r}) = \delta(\mathbf{r} - \mathbf{r}'), \quad \int d\mathbf{r} \psi_\nu^*(\mathbf{r}) \psi_{\nu'}(\mathbf{r}) = \delta_{\nu, \nu'}. \quad (1.16)$$

Starting from an arbitrary N -particle state $\psi(\mathbf{r}_1, \dots, \mathbf{r}_N)$ we form the $(N-1)$ -particle function $A_{\nu_1}(\mathbf{r}_2, \dots, \mathbf{r}_N)$ by projecting onto the basis state $\psi_{\nu_1}(\mathbf{r}_1)$:

$$A_{\nu_1}(\mathbf{r}_2, \dots, \mathbf{r}_N) \equiv \int d\mathbf{r}_1 \psi_{\nu_1}^*(\mathbf{r}_1) \psi(\mathbf{r}_1, \dots, \mathbf{r}_N). \quad (1.17)$$

This can be inverted by multiplying with $\psi_{\nu_1}(\tilde{\mathbf{r}}_1)$ and summing over ν_1 ,

$$\psi(\tilde{\mathbf{r}}_1, \mathbf{r}_2, \dots, \mathbf{r}_N) = \sum_{\nu_1} \psi_{\nu_1}(\tilde{\mathbf{r}}_1) A_{\nu_1}(\mathbf{r}_2, \dots, \mathbf{r}_N). \quad (1.18)$$

Now define analogously $A_{\nu_1, \nu_2}(\mathbf{r}_3, \dots, \mathbf{r}_N)$ from $A_{\nu_1}(\mathbf{r}_2, \dots, \mathbf{r}_N)$:

$$A_{\nu_1, \nu_2}(\mathbf{r}_3, \dots, \mathbf{r}_N) \equiv \int d\mathbf{r}_2 \psi_{\nu_2}^*(\mathbf{r}_2) A_{\nu_1}(\mathbf{r}_2, \dots, \mathbf{r}_N). \quad (1.19)$$

Like before, we can invert this expression to give A_{ν_1} in terms of A_{ν_1, ν_2} , which upon insertion into Eq. (1.18) leads to

$$\psi(\tilde{\mathbf{r}}_1, \tilde{\mathbf{r}}_2, \mathbf{r}_3, \dots, \mathbf{r}_N) = \sum_{\nu_1, \nu_2} \psi_{\nu_1}(\tilde{\mathbf{r}}_1) \psi_{\nu_2}(\tilde{\mathbf{r}}_2) A_{\nu_1, \nu_2}(\mathbf{r}_3, \dots, \mathbf{r}_N). \quad (1.20)$$

Continuing all the way through $\tilde{\mathbf{r}}_N$ (and then writing \mathbf{r} instead of $\tilde{\mathbf{r}}$) we end up with

$$\psi(\mathbf{r}_1, \mathbf{r}_2, \dots, \mathbf{r}_N) = \sum_{\nu_1, \dots, \nu_N} A_{\nu_1, \nu_2, \dots, \nu_N} \psi_{\nu_1}(\mathbf{r}_1) \psi_{\nu_2}(\mathbf{r}_2) \dots \psi_{\nu_N}(\mathbf{r}_N), \quad (1.21)$$

where $A_{\nu_1, \nu_2, \dots, \nu_N}$ is just a complex number. Thus any N -particle state function can be written as a (rather complicated) linear superposition of product states containing N factors of single-particle basis states.

Even though the product states $\prod_{j=1}^N \psi_{\nu_j}(\mathbf{r}_j)$ in a mathematical sense form a perfectly valid basis for the N -particle Hilbert space, we know from the discussion on indistinguishability that physically it is not a useful basis since the coordinates have to appear in a symmetric way. No physical perturbation can ever break the fundamental fermion or boson symmetry, which therefore ought to be explicitly incorporated in the basis states. The symmetry requirements from Eqs. (1.15a) and (1.15b) are in Eq. (1.21) hidden in the coefficients A_{ν_1, \dots, ν_N} . A physical meaningful basis bringing the N coordinates on equal footing in the products $\psi_{\nu_1}(\mathbf{r}_1) \psi_{\nu_2}(\mathbf{r}_2) \dots \psi_{\nu_N}(\mathbf{r}_N)$ of single-particle state functions is obtained by

applying the bosonic symmetrization operator \hat{S}_+ or the fermionic anti-symmetrization operator \hat{S}_- defined by the following determinants and permanent:²

$$\hat{S}_{\pm} \prod_{j=1}^N \psi_{\nu_j}(\mathbf{r}_j) = \begin{vmatrix} \psi_{\nu_1}(\mathbf{r}_1) & \psi_{\nu_1}(\mathbf{r}_2) & \cdots & \psi_{\nu_1}(\mathbf{r}_N) \\ \psi_{\nu_2}(\mathbf{r}_1) & \psi_{\nu_2}(\mathbf{r}_2) & \cdots & \psi_{\nu_2}(\mathbf{r}_N) \\ \vdots & \vdots & \ddots & \vdots \\ \psi_{\nu_N}(\mathbf{r}_1) & \psi_{\nu_N}(\mathbf{r}_2) & \cdots & \psi_{\nu_N}(\mathbf{r}_N) \end{vmatrix}_{\pm}, \quad (1.22)$$

where $n_{\nu'}$ is the number of times the state $|\nu'\rangle$ appears in the set $\{|\nu_1\rangle, |\nu_2\rangle, \dots, |\nu_N\rangle\}$, i.e. 0 or 1 for fermions and between 0 and N for bosons. The fermion case involves ordinary determinants, which in physics are denoted Slater determinants,

$$\begin{vmatrix} \psi_{\nu_1}(\mathbf{r}_1) & \psi_{\nu_1}(\mathbf{r}_2) & \cdots & \psi_{\nu_1}(\mathbf{r}_N) \\ \psi_{\nu_2}(\mathbf{r}_1) & \psi_{\nu_2}(\mathbf{r}_2) & \cdots & \psi_{\nu_2}(\mathbf{r}_N) \\ \vdots & \vdots & \ddots & \vdots \\ \psi_{\nu_N}(\mathbf{r}_1) & \psi_{\nu_N}(\mathbf{r}_2) & \cdots & \psi_{\nu_N}(\mathbf{r}_N) \end{vmatrix}_{-} = \sum_{p \in S_N} \left(\prod_{j=1}^N \psi_{\nu_j}(\mathbf{r}_{p(j)}) \right) \text{sign}(p), \quad (1.23)$$

while the boson case involves a sign-less determinant, a so-called permanent,

$$\begin{vmatrix} \psi_{\nu_1}(\mathbf{r}_1) & \psi_{\nu_1}(\mathbf{r}_2) & \cdots & \psi_{\nu_1}(\mathbf{r}_N) \\ \psi_{\nu_2}(\mathbf{r}_1) & \psi_{\nu_2}(\mathbf{r}_2) & \cdots & \psi_{\nu_2}(\mathbf{r}_N) \\ \vdots & \vdots & \ddots & \vdots \\ \psi_{\nu_N}(\mathbf{r}_1) & \psi_{\nu_N}(\mathbf{r}_2) & \cdots & \psi_{\nu_N}(\mathbf{r}_N) \end{vmatrix}_{+} = \sum_{p \in S_N} \left(\prod_{j=1}^N \psi_{\nu_j}(\mathbf{r}_{p(j)}) \right). \quad (1.24)$$

Here S_N is the group of the $N!$ permutations p on the set of N coordinates³, and $\text{sign}(p)$, used in the Slater determinant, is the sign of the permutation p . Note how in the fermion case $\nu_j = \nu_k$ leads to $\psi = 0$, i.e. the Pauli principle. Using the symmetrized basis states the expansion in Eq. (1.21) gets replaced by the following, where the new expansion coefficients $B_{\nu_1, \nu_2, \dots, \nu_N}$ are completely symmetric in their ν -indices,

$$\psi(\mathbf{r}_1, \mathbf{r}_2, \dots, \mathbf{r}_N) = \sum_{\nu_1, \dots, \nu_N} B_{\nu_1, \nu_2, \dots, \nu_N} \hat{S}_{\pm} \psi_{\nu_1}(\mathbf{r}_1) \psi_{\nu_2}(\mathbf{r}_2) \cdots \psi_{\nu_N}(\mathbf{r}_N). \quad (1.25)$$

We need not worry about the precise relation between the two sets of coefficients A and B since we are not going to use it.

1.2.3 Operators in first quantization

We now turn to the third assumption needed to complete the quantum theory of N -particle systems. It states that single- and few-particle operators defined for single- and

²Note that to obtain a normalized state on the right hand side in Eq. (1.22) a prefactor $\frac{1}{\Pi_{\nu'} \sqrt{n_{\nu'}!}} \frac{1}{\sqrt{N!}}$ must be inserted. For fermions $n_{\nu'} = 0, 1$ (and thus $n_{\nu'}! = 1$) so here the prefactor reduces to $\frac{1}{\sqrt{N!}}$.

³For $N = 3$ we have, with the signs of the permutations as subscripts, $S_3 = \left\{ \begin{pmatrix} 1 \\ 2 \\ 3 \end{pmatrix}_{+}, \begin{pmatrix} 1 \\ 3 \\ 2 \end{pmatrix}_{-}, \begin{pmatrix} 2 \\ 1 \\ 3 \end{pmatrix}_{-}, \begin{pmatrix} 2 \\ 3 \\ 1 \end{pmatrix}_{+}, \begin{pmatrix} 3 \\ 1 \\ 2 \end{pmatrix}_{+}, \begin{pmatrix} 3 \\ 2 \\ 1 \end{pmatrix}_{-} \right\}$

few-particle states remain unchanged when acting on N -particle states. In this course we will only work with one- and two-particle operators.

Let us begin with one-particle operators defined on single-particle states described by the coordinate \mathbf{r}_j . A given local one-particle operator $T_j = T(\mathbf{r}_j, \nabla_{\mathbf{r}_j})$, say e.g. the kinetic energy operator $-\frac{\hbar^2}{2m} \nabla_{\mathbf{r}_j}^2$ or an external potential $V(\mathbf{r}_j)$, takes the following form in the $|\nu\rangle$ -representation for a single-particle system:

$$T_j = \sum_{\nu_a, \nu_b} T_{\nu_b \nu_a} |\psi_{\nu_b}(\mathbf{r}_j)\rangle \langle \psi_{\nu_a}(\mathbf{r}_j)|, \quad (1.26)$$

$$\text{where} \quad T_{\nu_b \nu_a} = \int d\mathbf{r}_j \psi_{\nu_b}^*(\mathbf{r}_j) T(\mathbf{r}_j, \nabla_{\mathbf{r}_j}) \psi_{\nu_a}(\mathbf{r}_j). \quad (1.27)$$

In an N -particle system all N particle coordinates must appear in a symmetrical way, hence the proper kinetic energy operator in this case must be the total (symmetric) kinetic energy operator T_{tot} associated with all the coordinates,

$$T_{\text{tot}} = \sum_{j=1}^N T_j, \quad (1.28)$$

and the action of T_{tot} on a simple product state is

$$\begin{aligned} T_{\text{tot}} |\psi_{\nu_{n_1}}(\mathbf{r}_1)\rangle |\psi_{\nu_{n_2}}(\mathbf{r}_2)\rangle \dots |\psi_{\nu_{n_N}}(\mathbf{r}_N)\rangle \\ = \sum_{j=1}^N \sum_{\nu_a \nu_b} T_{\nu_b \nu_a} \delta_{\nu_a, \nu_{n_j}} |\psi_{\nu_{n_1}}(\mathbf{r}_1)\rangle \dots |\psi_{\nu_b}(\mathbf{r}_j)\rangle \dots |\psi_{\nu_{n_N}}(\mathbf{r}_N)\rangle. \end{aligned} \quad (1.29)$$

Here the Kronecker delta comes from $\langle \nu_a | \nu_{n_j} \rangle = \delta_{\nu_a, \nu_{n_j}}$. It is straight forward to extend this result to the proper symmetrized basis states.

We move on to discuss symmetric two-particle operators V_{jk} , such as the Coulomb interaction $V(\mathbf{r}_j - \mathbf{r}_k) = \frac{e^2}{4\pi\epsilon_0 |\mathbf{r}_j - \mathbf{r}_k|}$ between a pair of electrons. For a two-particle system described by the coordinates \mathbf{r}_j and \mathbf{r}_k in the $|\nu\rangle$ -representation with basis states $|\psi_{\nu_a}(\mathbf{r}_j)\rangle |\psi_{\nu_b}(\mathbf{r}_k)\rangle$ we have the usual definition of V_{jk} :

$$V_{jk} = \sum_{\substack{\nu_a \nu_b \\ \nu_c \nu_d}} V_{\nu_c \nu_d, \nu_a \nu_b} |\psi_{\nu_c}(\mathbf{r}_j)\rangle |\psi_{\nu_d}(\mathbf{r}_k)\rangle \langle \psi_{\nu_a}(\mathbf{r}_j) | \langle \psi_{\nu_b}(\mathbf{r}_k) | \quad (1.30)$$

$$\text{where} \quad V_{\nu_c \nu_d, \nu_a \nu_b} = \int d\mathbf{r}_j d\mathbf{r}_k \psi_{\nu_c}^*(\mathbf{r}_j) \psi_{\nu_d}^*(\mathbf{r}_k) V(\mathbf{r}_j - \mathbf{r}_k) \psi_{\nu_a}(\mathbf{r}_j) \psi_{\nu_b}(\mathbf{r}_k). \quad (1.31)$$

In the N -particle system we must again take the symmetric combination of the coordinates, i.e. introduce the operator of the total interaction energy V_{tot} ,

$$V_{\text{tot}} = \sum_{j>k}^N V_{jk} = \frac{1}{2} \sum_{j,k \neq j}^N V_{jk}, \quad (1.32)$$

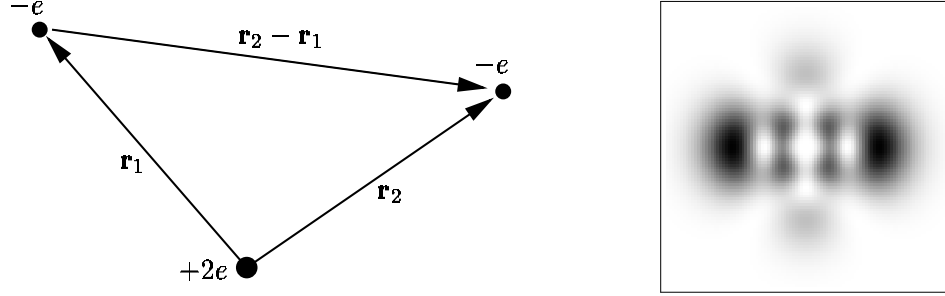


Figure 1.2: The position vectors of the two electrons orbiting the helium nucleus and the single-particle probability density $P(\mathbf{r}_1) = \int d\mathbf{r}_2 \frac{1}{2} |\psi_{\nu_1}(\mathbf{r}_1)\psi_{\nu_2}(\mathbf{r}_2) + \psi_{\nu_2}(\mathbf{r}_1)\psi_{\nu_1}(\mathbf{r}_2)|^2$ for the symmetric two-particle state based on the single-particle orbitals $|\nu_1\rangle = |(3, 2, 1, \uparrow)\rangle$ and $|\nu_2\rangle = |(4, 2, 0, \downarrow)\rangle$. Compare with the single orbital $|(4, 2, 0, \downarrow)\rangle$ depicted in Fig. 1.1(b).

V_{tot} acts as follows:

$$\begin{aligned} V_{\text{tot}}|\psi_{\nu_{n_1}}(\mathbf{r}_1)\rangle|\psi_{\nu_{n_2}}(\mathbf{r}_2)\rangle\cdots|\psi_{\nu_{n_N}}(\mathbf{r}_N)\rangle \\ = \frac{1}{2} \sum_{j \neq k}^N \sum_{\substack{\nu_a \nu_b \\ \nu_c \nu_d}} V_{\nu_c \nu_d, \nu_a \nu_b} \delta_{\nu_a, \nu_{n_j}} \delta_{\nu_b, \nu_{n_k}} |\psi_{\nu_{n_1}}(\mathbf{r}_1)\rangle \cdots |\psi_{\nu_c}(\mathbf{r}_j)\rangle \cdots |\psi_{\nu_d}(\mathbf{r}_k)\rangle \cdots |\psi_{\nu_{n_N}}(\mathbf{r}_N)\rangle. \end{aligned} \quad (1.33)$$

A typical Hamiltonian for an N -particle system thus takes the form

$$H = T_{\text{tot}} + V_{\text{tot}} = \sum_{j=1}^N T_j + \frac{1}{2} \sum_{j \neq k}^N V_{jk}. \quad (1.34)$$

A specific example is the Hamiltonian for the helium atom, which in a simple form neglecting spin interactions can be thought of as two electrons with coordinates $\mathbf{r} = \mathbf{r}_1$ and $\mathbf{r} = \mathbf{r}_2$ orbiting around a nucleus with charge $Z = +2$ at $\mathbf{r} = 0$,

$$H_{\text{He}} = \left(-\frac{\hbar^2}{2m} \nabla_1^2 - \frac{Ze^2}{4\pi\epsilon_0} \frac{1}{r_1} \right) + \left(-\frac{\hbar^2}{2m} \nabla_2^2 - \frac{Ze^2}{4\pi\epsilon_0} \frac{1}{r_2} \right) + \frac{e^2}{4\pi\epsilon_0} \frac{1}{|\mathbf{r}_1 - \mathbf{r}_2|}. \quad (1.35)$$

This Hamiltonian consists of four one-particle operators and one two-particle operator, see also Fig. 1.2.

1.3 Second quantization, basic concepts

Many-particle physics is formulated in terms of the so-called second quantization representation also known by the more descriptive name occupation number representation. The starting point of this formalism is the notion of indistinguishability of particles discussed in Sec. 1.2.1 combined with the observation in Sec. 1.2.2 that determinants or permanent of single-particle states form a basis for the Hilbert space of N -particle states. As we shall see, quantum theory can be formulated in terms of occupation numbers of these single-particle states.

1.3.1 The occupation number representation

The first step in defining the occupation number representation is to choose any ordered and complete single-particle basis $\{|\nu_1\rangle, |\nu_2\rangle, |\nu_3\rangle, \dots\}$, the ordering being of paramount importance for fermions. It is clear from the form $\hat{S}_{\pm} \psi_{\nu_{n_1}}(\mathbf{r}_1) \psi_{\nu_{n_2}}(\mathbf{r}_2) \dots \psi_{\nu_{n_N}}(\mathbf{r}_N)$ of the basis states in Eq. (1.25) that in each term only the occupied single-particle states $|\nu_{n_j}\rangle$ play a role. It must somehow be simpler to formulate a representation where one just counts how many particles there are in each orbital $|\nu\rangle$. This simplification is achieved with the occupation number representation.

The basis states for an N -particle system in the occupation number representation are obtained simply by listing the occupation numbers of each basis state,

$$N\text{-particle basis states : } |n_{\nu_1}, n_{\nu_2}, n_{\nu_3}, \dots\rangle, \quad \sum_j n_{\nu_j} = N. \quad (1.36)$$

It is therefore natural to define occupation number operators \hat{n}_{ν_j} which as eigenstates have the basis states $|n_{\nu_j}\rangle$, and as eigenvalues have the number n_{ν_j} of particles occupying the state ν_j ,

$$\hat{n}_{\nu_j} |n_{\nu_j}\rangle = n_{\nu_j} |n_{\nu_j}\rangle. \quad (1.37)$$

We shall show later that for fermions n_{ν_j} can be 0 or 1, while for bosons it can be any non-negative number,

$$n_{\nu_j} = \begin{cases} 0, 1 & (\text{fermions}) \\ 0, 1, 2, \dots & (\text{bosons}). \end{cases} \quad (1.38)$$

Naturally, the question arises how to connect the occupation number basis Eq. (1.36) with the first quantization basis Eq. (1.23). This will be answered in the next section.

The space spanned by the occupation number basis is denoted the Fock space \mathcal{F} . It can be defined as $\mathcal{F} = \mathcal{F}_0 \oplus \mathcal{F}_1 \oplus \mathcal{F}_2 \oplus \dots$, where $\mathcal{F}_N = \text{span}\{|n_{\nu_1}, n_{\nu_2}, \dots\rangle \mid \sum_j n_{\nu_j} = N\}$. In Table. 1.1 some of the fermionic and bosonic basis states in the occupation number representation are shown. Note how by virtue of the direct sum, states containing a different number of particles are defined to be orthogonal.

1.3.2 The boson creation and annihilation operators

To connect first and second quantization we first treat bosons. Given the occupation number operator it is natural to introduce the creation operator $b_{\nu_j}^{\dagger}$ that raises the occupation number in the state $|\nu_j\rangle$ by 1,

$$b_{\nu_j}^{\dagger} |\dots, n_{\nu_{j-1}}, n_{\nu_j}, n_{\nu_{j+1}}, \dots\rangle = B_+(n_{\nu_j}) |\dots, n_{\nu_{j-1}}, n_{\nu_j} + 1, n_{\nu_{j+1}}, \dots\rangle, \quad (1.39)$$

where $B_+(n_{\nu_j})$ is a normalization constant to be determined. The only non-zero matrix elements of $b_{\nu_j}^{\dagger}$ are $\langle n_{\nu_j} + 1 | b_{\nu_j}^{\dagger} | n_{\nu_j} \rangle$, where for brevity we only explicitly write the occupation number for ν_j . The adjoint of $b_{\nu_j}^{\dagger}$ is found by complex conjugation as $\langle n_{\nu_j} + 1 | b_{\nu_j}^{\dagger} | n_{\nu_j} \rangle^* = \langle n_{\nu_j} | (b_{\nu_j}^{\dagger})^{\dagger} | n_{\nu_j} + 1 \rangle$. Consequently, one defines the annihilation operator $b_{\nu_j} \equiv (b_{\nu_j}^{\dagger})^{\dagger}$, which lowers the occupation number of state $|\nu_j\rangle$ by 1,

$$b_{\nu_j} |\dots, n_{\nu_{j-1}}, n_{\nu_j}, n_{\nu_{j+1}}, \dots\rangle = B_-(n_{\nu_j}) |\dots, n_{\nu_{j-1}}, n_{\nu_j} - 1, n_{\nu_{j+1}}, \dots\rangle. \quad (1.40)$$

Table 1.1: Some occupation number basis states for N -particle systems.

N	fermion basis states $ n_{\nu_1}, n_{\nu_2}, n_{\nu_3}, \dots\rangle$
0	$ 0, 0, 0, 0, \dots\rangle$
1	$ 1, 0, 0, 0, \dots\rangle, 0, 1, 0, 0, \dots\rangle, 0, 0, 1, 0, \dots\rangle, \dots$
2	$ 1, 1, 0, 0, \dots\rangle, 0, 1, 1, 0, \dots\rangle, 1, 0, 1, 0, \dots\rangle, 0, 0, 1, 1, \dots\rangle, 0, 1, 0, 1, \dots\rangle, 1, 0, 0, 1, \dots\rangle, \dots$
\vdots	$\vdots \quad \quad \quad \vdots \quad \quad \quad \vdots \quad \quad \quad \vdots$

N	boson basis states $ n_{\nu_1}, n_{\nu_2}, n_{\nu_3}, \dots\rangle$
0	$ 0, 0, 0, 0, \dots\rangle$
1	$ 1, 0, 0, 0, \dots\rangle, 0, 1, 0, 0, \dots\rangle, 0, 0, 1, 0, \dots\rangle, \dots$
2	$ 2, 0, 0, 0, \dots\rangle, 0, 2, 0, 0, \dots\rangle, 1, 1, 0, 0, \dots\rangle, 0, 0, 2, 0, \dots\rangle, 0, 1, 1, 0, \dots\rangle, 1, 0, 1, 0, \dots\rangle, \dots$
\vdots	$\vdots \quad \quad \quad \vdots \quad \quad \quad \vdots \quad \quad \quad \vdots$

The creation and annihilation operators $b_{\nu_j}^\dagger$ and b_{ν_j} are the fundamental operators in the occupation number formalism. As we will demonstrate later any operator can be expressed in terms of them.

Let us proceed by investigating the properties of $b_{\nu_j}^\dagger$ and b_{ν_j} further. Since bosons are symmetric in the single-particle state index ν_j we of course demand that $b_{\nu_j}^\dagger$ and $b_{\nu_k}^\dagger$ must commute, and hence by Hermitian conjugation that also b_{ν_j} and b_{ν_k} commute. The commutator $[A, B]$ for two operators A and B is defined as

$$[A, B] \equiv AB - BA, \quad \text{so that } [A, B] = 0 \Rightarrow BA = AB. \quad (1.41)$$

We demand further that if $j \neq k$ then b_{ν_j} and $b_{\nu_k}^\dagger$ commute. However, if $j = k$ we must be careful. It is evident that since an unoccupied state can not be emptied further we must demand $b_{\nu_j}|\dots, 0, \dots\rangle = 0$, i.e. $B_-(0) = 0$. We also have the freedom to normalize the operators by demanding $b_{\nu_j}^\dagger|\dots, 0, \dots\rangle = |\dots, 1, \dots\rangle$, i.e. $B_+(0) = 1$. But since $\langle 1|b_{\nu_j}^\dagger|0\rangle^* = \langle 0|b_{\nu_j}|1\rangle$, it also follows that $b_{\nu_j}|\dots, 1, \dots\rangle = |\dots, 0, \dots\rangle$, i.e. $B_-(1) = 1$.

It is clear that b_{ν_j} and $b_{\nu_j}^\dagger$ do not commute: $b_{\nu_j}b_{\nu_j}^\dagger|0\rangle = |0\rangle$ while $b_{\nu_j}^\dagger b_{\nu_j}|0\rangle = 0$, i.e. we have $[b_{\nu_j}, b_{\nu_j}^\dagger]|0\rangle = |0\rangle$. We assume this commutation relation, valid for the state $|0\rangle$, also to be valid as an operator identity in general, and we calculate the consequences of this assumption. In summary, we define the operator algebra for the bosonic creation and annihilation operators by the following three commutation relations:

$$[b_{\nu_j}^\dagger, b_{\nu_k}^\dagger] = 0, \quad [b_{\nu_j}, b_{\nu_k}] = 0, \quad [b_{\nu_j}, b_{\nu_k}^\dagger] = \delta_{\nu_j, \nu_k}. \quad (1.42)$$

By definition b_ν^\dagger and b_ν are not Hermitian. However, the product $b_\nu^\dagger b_\nu$ is, and by using the operator algebra Eq. (1.42) we show below that this operator in fact is the

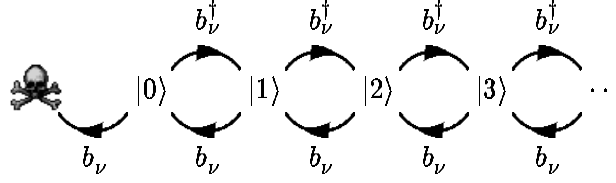


Figure 1.3: The action of the bosonic creation operator b_ν^\dagger and adjoint annihilation operator b_ν in the occupation number space. Note that b_ν^\dagger can act indefinitely, while b_ν eventually hits $|0\rangle$ and annihilates it yielding 0.

occupation number operator \hat{n}_ν . Firstly, Eq. (1.42) leads immediately to the following two very important commutation relations:

$$[b_\nu^\dagger b_\nu, b_\nu] = -b_\nu \quad [b_\nu^\dagger b_\nu, b_\nu^\dagger] = b_\nu^\dagger. \quad (1.43)$$

Secondly, for any state $|\phi\rangle$ we note that $\langle\phi|b_\nu^\dagger b_\nu|\phi\rangle$ is the norm of the state $b_\nu|\phi\rangle$ and hence a positive real number (unless $|\phi\rangle = |0\rangle$ for which $b_\nu|0\rangle = 0$). Let $|\phi_\lambda\rangle$ be any eigenstate of $b_\nu^\dagger b_\nu$, i.e. $b_\nu^\dagger b_\nu|\phi_\lambda\rangle = \lambda|\phi_\lambda\rangle$ with $\lambda > 0$. Now choose a particular λ_0 and study $b_\nu|\phi_{\lambda_0}\rangle$. We find that

$$(b_\nu^\dagger b_\nu)b_\nu|\phi_{\lambda_0}\rangle = (b_\nu b_\nu^\dagger - 1)b_\nu|\phi_{\lambda_0}\rangle = b_\nu(b_\nu^\dagger b_\nu - 1)|\phi_{\lambda_0}\rangle = b_\nu(\lambda_0 - 1)|\phi_{\lambda_0}\rangle, \quad (1.44)$$

i.e. $b_\nu|\phi_{\lambda_0}\rangle$ is also an eigenstate of $b_\nu^\dagger b_\nu$, but with the eigenvalue reduced by 1 to $(\lambda_0 - 1)$. If λ_0 is not a non-negative integer this lowering process can continue until a negative eigenvalue is encountered, but this violates the condition $\lambda_0 > 0$, and we conclude that $\lambda = n = 0, 1, 2, \dots$. Writing $|\phi_\lambda\rangle = |n_\nu\rangle$ we have shown that $b_\nu^\dagger b_\nu|n_\nu\rangle = n_\nu|n_\nu\rangle$ and $b_\nu|n_\nu\rangle \propto |n_\nu - 1\rangle$. Analogously, we find that

$$(b_\nu^\dagger b_\nu)b_\nu^\dagger|n_\nu\rangle = (n + 1)b_\nu^\dagger|n_\nu\rangle, \quad (1.45)$$

i.e. $b_\nu^\dagger|n_\nu\rangle \propto |n_\nu + 1\rangle$. The normalization factors for b_ν^\dagger and b_ν are found from

$$\|b_\nu|n_\nu\rangle\|^2 = (b_\nu|n_\nu\rangle)^\dagger(b_\nu|n_\nu\rangle) = \langle n_\nu|b_\nu^\dagger b_\nu|n_\nu\rangle = n_\nu, \quad (1.46a)$$

$$\|b_\nu^\dagger|n_\nu\rangle\|^2 = (b_\nu^\dagger|n_\nu\rangle)^\dagger(b_\nu^\dagger|n_\nu\rangle) = \langle n_\nu|b_\nu b_\nu^\dagger|n_\nu\rangle = n_\nu + 1. \quad (1.46b)$$

Hence we arrive at

$$b_\nu^\dagger b_\nu = \hat{n}_\nu, \quad b_\nu^\dagger b_\nu|n_\nu\rangle = n_\nu|n_\nu\rangle, \quad n_\nu = 0, 1, 2, \dots \quad (1.47)$$

$$b_\nu|n_\nu\rangle = \sqrt{n_\nu}|n_\nu - 1\rangle, \quad b_\nu^\dagger|n_\nu\rangle = \sqrt{n_\nu + 1}|n_\nu + 1\rangle, \quad (b_\nu^\dagger)^{n_\nu}|0\rangle = \sqrt{n_\nu!}|n_\nu\rangle, \quad (1.48)$$

and we can therefore identify the first and second quantized basis states,

$$\hat{S}_+|\psi_{\nu_{n_1}}(\tilde{\mathbf{r}}_1)\rangle|\psi_{\nu_{n_2}}(\tilde{\mathbf{r}}_2)\rangle\cdots|\psi_{\nu_{n_N}}(\tilde{\mathbf{r}}_N)\rangle = b_{\nu_{n_1}}^\dagger b_{\nu_{n_2}}^\dagger \cdots b_{\nu_{n_N}}^\dagger|0\rangle, \quad (1.49)$$

where both sides contain N -particle state-kets completely symmetric in the single-particle state index ν_{n_j} .

1.3.3 The fermion creation and annihilation operators

Also for fermions it is natural to introduce creation and annihilation operators, now denoted $c_{\nu_j}^\dagger$ and c_{ν_j} , being the Hermitian adjoint of each other:

$$c_{\nu_j}^\dagger |\dots, n_{\nu_{j-1}}, n_{\nu_j}, n_{\nu_{j+1}}, \dots\rangle = C_+(n_{\nu_j}) |\dots, n_{\nu_{j-1}}, n_{\nu_j}+1, n_{\nu_{j+1}}, \dots\rangle, \quad (1.50)$$

$$c_{\nu_j} |\dots, n_{\nu_{j-1}}, n_{\nu_j}, n_{\nu_{j+1}}, \dots\rangle = C_-(n_{\nu_j}) |\dots, n_{\nu_{j-1}}, n_{\nu_j}-1, n_{\nu_{j+1}}, \dots\rangle. \quad (1.51)$$

But to maintain the fundamental fermionic antisymmetry upon exchange of orbitals apparent in Eq. (1.23) it is in the fermionic case not sufficient just to list the occupation numbers of the states, also the order of the occupied states has a meaning. We must therefore demand

$$|\dots, n_{\nu_j} = 1, \dots, n_{\nu_k} = 1, \dots\rangle = -|\dots, n_{\nu_k} = 1, \dots, n_{\nu_j} = 1, \dots\rangle. \quad (1.52)$$

and consequently we must have that $c_{\nu_j}^\dagger$ and $c_{\nu_k}^\dagger$ anti-commute, and hence by Hermitian conjugation that also c_{ν_j} and c_{ν_k} anti-commute. The anti-commutator $\{A, B\}$ for two operators A and B is defined as

$$\{A, B\} \equiv AB + BA, \quad \text{so that } \{A, B\} = 0 \Rightarrow BA = -AB. \quad (1.53)$$

For $j \neq k$ we also demand that c_{ν_j} and $c_{\nu_k}^\dagger$ anti-commute. However, if $j = k$ we again must be careful. It is evident that since an unoccupied state can not be emptied further we must demand $c_{\nu_j} |\dots, 0, \dots\rangle = 0$, i.e. $C_-(0) = 0$. We also have the freedom to normalize the operators by demanding $c_{\nu_j}^\dagger |\dots, 0, \dots\rangle = |\dots, 1, \dots\rangle$, i.e. $C_+(0) = 1$. But since $\langle 1 | c_{\nu_j}^\dagger | 0 \rangle^* = \langle 0 | c_{\nu_j} | 1 \rangle$ it follows that $c_{\nu_j} |\dots, 1, \dots\rangle = |\dots, 0, \dots\rangle$, i.e. $C_-(1) = 1$.

It is clear that c_{ν_j} and $c_{\nu_j}^\dagger$ do not anti-commute: $c_{\nu_j} c_{\nu_j}^\dagger |0\rangle = |0\rangle$ while $c_{\nu_j}^\dagger c_{\nu_j} |0\rangle = 0$, i.e. we have $\{c_{\nu_j}, c_{\nu_j}^\dagger\} |0\rangle = |0\rangle$. We assume this anti-commutation relation to be valid as an operator identity and calculate the consequences. In summary, we define the operator algebra for the fermionic creation and annihilation operators by the following three anti-commutation relations:

$$\{c_{\nu_j}^\dagger, c_{\nu_k}^\dagger\} = 0, \quad \{c_{\nu_j}, c_{\nu_k}\} = 0, \quad \{c_{\nu_j}, c_{\nu_k}^\dagger\} = \delta_{\nu_j, \nu_k}. \quad (1.54)$$

An immediate consequence of the anti-commutation relations Eq. (1.54) is

$$(c_{\nu_j}^\dagger)^2 = 0, \quad (c_{\nu_j})^2 = 0. \quad (1.55)$$

Now, as for bosons we introduce the Hermitian operator $c_\nu^\dagger c_\nu$, and by using the operator algebra Eq. (1.54) we show below that this operator in fact is the occupation number operator \hat{n}_ν . In analogy with Eq. (1.43) we find

$$[c_\nu^\dagger c_\nu, c_\nu] = -c_\nu \quad [c_\nu^\dagger c_\nu, c_\nu^\dagger] = c_\nu^\dagger, \quad (1.56)$$

so that c_ν^\dagger and c_ν steps the eigenvalues of $c_\nu^\dagger c_\nu$ up and down by one, respectively. From Eqs. (1.54) and (1.55) we have $(c_\nu^\dagger c_\nu)^2 = c_\nu^\dagger (c_\nu c_\nu^\dagger) c_\nu = c_\nu^\dagger (1 - c_\nu^\dagger c_\nu) c_\nu = c_\nu^\dagger c_\nu$, so that

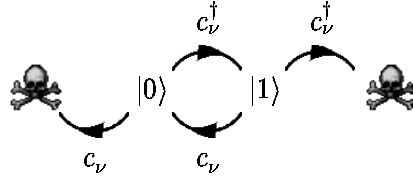


Figure 1.4: The action of the fermionic creation operator c_ν^\dagger and the adjoint annihilation operator c_ν in the occupation number space. Note that both c_ν^\dagger and c_ν can act at most twice before annihilating a state completely.

$c_\nu^\dagger c_\nu (c_\nu^\dagger c_\nu - 1) = 0$, and $c_\nu^\dagger c_\nu$ thus only has 0 and 1 as eigenvalues leading to a simple normalization for c_ν^\dagger and c_ν . In summary, we have

$$c_\nu^\dagger c_\nu = \hat{n}_\nu, \quad c_\nu^\dagger c_\nu |n_\nu\rangle = n_\nu |n_\nu\rangle, \quad n_\nu = 0, 1 \quad (1.57)$$

$$c_\nu |0\rangle = 0, \quad c_\nu^\dagger |0\rangle = |1\rangle, \quad c_\nu |1\rangle = |0\rangle, \quad c_\nu^\dagger |1\rangle = 0, \quad (1.58)$$

and we can readily identify the first and second quantized basis states,

$$\hat{S}_- |\psi_{\nu_{n_1}}(\tilde{\mathbf{r}}_1)\rangle |\psi_{\nu_{n_2}}(\tilde{\mathbf{r}}_2)\rangle \dots |\psi_{\nu_{n_N}}(\tilde{\mathbf{r}}_N)\rangle = c_{\nu_{n_1}}^\dagger c_{\nu_{n_2}}^\dagger \dots c_{\nu_{n_N}}^\dagger |0\rangle, \quad (1.59)$$

where both sides contain normalized N -particle state-kets completely anti-symmetric in the single-particle state index ν_{n_j} in accordance with the Pauli exclusion principle.

1.3.4 The general form for second quantization operators

In second quantization all operators can be expressed in terms of the fundamental creation and annihilation operators defined in the previous two sections. This rewriting of the first quantized operators in Eqs. (1.29) and (1.33) into their second quantized form is achieved by using the basis state identities Eqs. (1.49) and (1.59) linking the two representations.

For simplicity, let us first consider the single-particle operator T_{tot} from Eq. (1.29) acting on a bosonic N -particle system. In this equation we then act with the bosonic symmetrization operator S_+ on both sides. Utilizing that T_{tot} and S_+ commute and invoking the basis state identity Eq. (1.49) we obtain

$$T_{\text{tot}} b_{\nu_{n_1}}^\dagger \dots b_{\nu_{n_N}}^\dagger |0\rangle = \sum_{\nu_a \nu_b} T_{\nu_b \nu_a} \sum_{j=1}^N \delta_{\nu_a, \nu_{n_j}} b_{\nu_{n_1}}^\dagger \dots \overbrace{b_{\nu_b}^\dagger}^{\text{site } n_j} \dots b_{\nu_{n_N}}^\dagger |0\rangle, \quad (1.60)$$

where on the right hand side of the equation the operator $b_{\nu_b}^\dagger$ stands on the site n_j . To make the kets on the two sides of the equation look alike, we would like to reinsert the operator $b_{\nu_{n_j}}^\dagger$ at site n_j on the right. To do this we focus on the state $\nu \equiv \nu_{n_j}$. Originally, i.e. on the left hand side, the state ν may appear, say, p times leading to a contribution $(b_\nu^\dagger)^p |0\rangle$. We have $p > 0$ since otherwise both sides would yield zero. On the right hand



Figure 1.5: A graphical representation of the one- and two-particle operators in second quantization. The incoming and outgoing arrows represent initial and final states, respectively. The dashed and wiggled lines represent the transition amplitudes for the one- and two-particle processes contained in the operators.

side the corresponding contribution has changed into $b_{\nu_b}^\dagger (b_\nu^\dagger)^{p-1} |0\rangle$. This is then rewritten by use of Eqs. (1.42), (1.47) and (1.48) as

$$b_{\nu_b}^\dagger (b_\nu^\dagger)^{p-1} |0\rangle = b_{\nu_b}^\dagger \left(\frac{1}{p} b_\nu b_\nu^\dagger \right) (b_\nu^\dagger)^{p-1} |0\rangle = \left(\frac{1}{p} b_{\nu_b}^\dagger b_\nu \right) (b_\nu^\dagger)^p |0\rangle. \quad (1.61)$$

Now, the p operators b_ν^\dagger can be redistributed to their original places as they appear on the left hand side of Eq. (1.60). The sum over j together with $\delta_{\nu_a, \nu_{n_j}}$ yields p identical contributions cancelling the factor $1/p$ in Eq. (1.61), and we arrive at the simple result

$$T_{\text{tot}} \left[b_{\nu_{n_1}}^\dagger \dots b_{\nu_{n_N}}^\dagger |0\rangle \right] = \sum_{a,b} T_{\nu_b \nu_a} b_{\nu_b}^\dagger b_{\nu_a} \left[b_{\nu_{n_1}}^\dagger \dots b_{\nu_{n_N}}^\dagger |0\rangle \right]. \quad (1.62)$$

Since this result is valid for any basis state $b_{\nu_{n_1}}^\dagger \dots b_{\nu_{n_N}}^\dagger |0\rangle$, it is actually an operator identity stating $T_{\text{tot}} = \sum_{i,j} T_{\nu_i \nu_j} b_{\nu_i}^\dagger b_{\nu_j}$.

It is straightforward to generalize this result to two-particle (or any-number-of-particle) operators acting on boson states, and a similar reasoning can be made for the fermion case (see Exercise 1.1) when the necessary care is taken regarding the sign appearing from the anti-commutators in this case. If we let a^\dagger denote either a boson operator b^\dagger or a fermion operator c^\dagger we can state the general form for one- and two-particle operators in second quantization:

$$T_{\text{tot}} = \sum_{\nu_i, \nu_j} T_{\nu_i \nu_j} a_{\nu_i}^\dagger a_{\nu_j}, \quad (1.63)$$

$$V_{\text{tot}} = \frac{1}{2} \sum_{\substack{\nu_i \nu_j \\ \nu_k \nu_l}} V_{\nu_i \nu_j, \nu_k \nu_l} a_{\nu_i}^\dagger a_{\nu_j}^\dagger a_{\nu_l} a_{\nu_k}. \quad (1.64)$$

In Fig. 1.5 a graphical representation of these fundamental operator expressions is shown.

Operators in second quantization are thus composed of linear combinations of products of creation and annihilation operators weighted by the appropriate matrix elements of the operator calculated in first quantization. Note the order of the indices, which is extremely

important in the case of two-particle fermion operators. The first quantization matrix element can be read as a transition induced from the initial state $|\nu_k \nu_l\rangle$ to the final state $|\nu_i \nu_j\rangle$. In second quantization the initial state is annihilated by first annihilating state $|\nu_k\rangle$ and then state $|\nu_l\rangle$, while the final state is created by first creating state $|\nu_j\rangle$ and then state $|\nu_i\rangle$:

$$|0\rangle = a_{\nu_l} a_{\nu_k} |\nu_k \nu_l\rangle, \quad |\nu_i \nu_j\rangle = a_{\nu_i}^\dagger a_{\nu_j}^\dagger |0\rangle. \quad (1.65)$$

Note how all the permutation symmetry properties are taken care of by the operator algebra of a_ν^\dagger and a_ν . The matrix elements are all in the simple non-symmetrized form of Eq. (1.31).

1.3.5 Change of basis in second quantization

Different quantum operators are most naturally expressed in different representations making basis changes a central issue in quantum physics. In this section we give the general transformation rules which are to be exploited throughout this course.

Let $\{|\psi_{\nu_1}\rangle, |\psi_{\nu_2}\rangle, \dots\}$ and $\{|\tilde{\psi}_{\mu_1}\rangle, |\tilde{\psi}_{\mu_2}\rangle, \dots\}$ be two different complete and ordered single-particle basis sets. From the completeness condition Eq. (1.7) we have the basic transformation law for single-particle states:

$$|\tilde{\psi}_\mu\rangle = \sum_\nu |\psi_\nu\rangle \langle\psi_\nu|\tilde{\psi}_\mu\rangle = \sum_\nu \langle\tilde{\psi}_\mu|\psi_\nu\rangle^* |\psi_\nu\rangle. \quad (1.66)$$

In the case of single-particle systems we define quite naturally creation operators \tilde{a}_μ^\dagger and a_ν^\dagger corresponding to the two basis sets, and find directly from Eq. (1.66) that $\tilde{a}_\mu^\dagger|0\rangle = |\tilde{\psi}_\mu\rangle = \sum_\nu \langle\tilde{\psi}_\mu|\psi_\nu\rangle^* a_\nu^\dagger|0\rangle$, which guides us to the transformation rules for creation and annihilation operators (see also Fig. 1.6):

$$\tilde{a}_\mu^\dagger = \sum_\nu \langle\tilde{\psi}_\mu|\psi_\nu\rangle^* a_\nu^\dagger, \quad \tilde{a}_\mu = \sum_\nu \langle\tilde{\psi}_\mu|\psi_\nu\rangle a_\nu. \quad (1.67)$$

The general validity of Eq. (1.67) follows from applying the first quantization single-particle result Eq. (1.66) to the N -particle first quantized basis states $\hat{S}_\pm |\psi_{\nu_{n_1}} \dots \psi_{\nu_{n_N}}\rangle$ leading to

$$\tilde{a}_{\mu_{n_1}}^\dagger \tilde{a}_{\mu_{n_2}}^\dagger \dots \tilde{a}_{\mu_{n_N}}^\dagger |0\rangle = \left(\sum_{\nu_{n_1}} \langle\tilde{\psi}_{\mu_{n_1}}|\psi_{\nu_{n_1}}\rangle^* a_{\nu_{n_1}}^\dagger \right) \dots \left(\sum_{\nu_{n_N}} \langle\tilde{\psi}_{\mu_{n_N}}|\psi_{\nu_{n_N}}\rangle^* a_{\nu_{n_N}}^\dagger \right) |0\rangle. \quad (1.68)$$

The transformation rules Eq. (1.67) lead to two very desirable results. Firstly, that the basis transformation preserves the bosonic or fermionic particle statistics,

$$\begin{aligned} [\tilde{a}_{\mu_1}, \tilde{a}_{\mu_2}^\dagger]_\pm &= \sum_{\nu_j \nu_k} \langle\tilde{\psi}_{\mu_1}|\psi_{\nu_j}\rangle \langle\tilde{\psi}_{\mu_2}|\psi_{\nu_k}\rangle^* [a_{\nu_j}, a_{\nu_k}^\dagger]_\pm \\ &= \sum_{\nu_j \nu_k} \langle\tilde{\psi}_{\mu_1}|\psi_{\nu_j}\rangle \langle\psi_{\nu_k}|\tilde{\psi}_{\mu_2}\rangle \delta_{\nu_j, \nu_k} = \sum_{\nu_j} \langle\tilde{\psi}_{\mu_1}|\psi_{\nu_j}\rangle \langle\psi_{\nu_j}|\tilde{\psi}_{\mu_2}\rangle = \delta_{\mu_1, \mu_2}, \end{aligned} \quad (1.69)$$

and secondly, that it leaves the total number of particles unchanged,

$$\sum_\mu \tilde{a}_\mu^\dagger \tilde{a}_\mu = \sum_\mu \sum_{\nu_j \nu_k} \langle\psi_{\nu_j}|\tilde{\psi}_\mu\rangle \langle\tilde{\psi}_\mu|\psi_{\nu_k}\rangle a_{\nu_j}^\dagger a_{\nu_k} = \sum_{\nu_j \nu_k} \langle\psi_{\nu_j}|\psi_{\nu_k}\rangle a_{\nu_j}^\dagger a_{\nu_k} = \sum_{\nu_j} a_{\nu_j}^\dagger a_{\nu_j}. \quad (1.70)$$

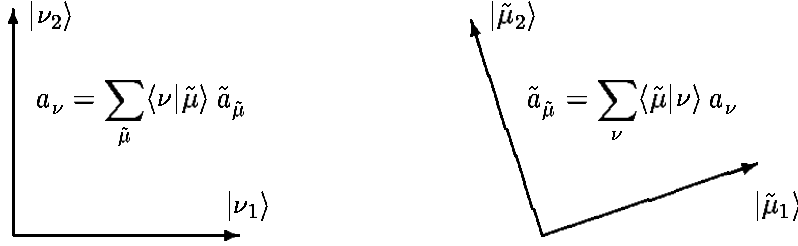


Figure 1.6: The transformation rules for annihilation operators a_ν and $\tilde{a}_{\tilde{\mu}}$ upon change of basis between $\{|\psi_\nu\rangle\} = \{|\nu\rangle\}$ and $\{|\tilde{\psi}_\mu\rangle\} = \{|\tilde{\mu}\rangle\}$.

1.3.6 Quantum field operators and their Fourier transforms

In particular one second quantization representation requires special attention, namely the real space representation leading to the definition of quantum field operators. If we in Sec. 1.3.5 let the transformed basis set $\{|\tilde{\psi}_\mu\rangle\}$ be the continuous set of position kets $\{|\mathbf{r}\rangle\}$ and, suppressing the spin index, denote \tilde{a}_μ^\dagger by $\Psi^\dagger(\mathbf{r})$ we obtain from Eq. (1.67)

$$\Psi^\dagger(\mathbf{r}) \equiv \sum_\nu \langle \mathbf{r} | \psi_\nu \rangle^* a_\nu^\dagger = \sum_\nu \psi_\nu^*(\mathbf{r}) a_\nu^\dagger, \quad \Psi(\mathbf{r}) \equiv \sum_\nu \langle \mathbf{r} | \psi_\nu \rangle a_\nu = \sum_\nu \psi_\nu(\mathbf{r}) a_\nu. \quad (1.71)$$

Note that $\Psi^\dagger(\mathbf{r})$ and $\Psi(\mathbf{r})$ are second quantization operators, while the coefficients $\psi_\nu^*(\mathbf{r})$ and $\psi_\nu(\mathbf{r})$ are ordinary first quantization wavefunctions. Loosely speaking, $\Psi^\dagger(\mathbf{r})$ is the sum of all possible ways to add a particle to the system at position \mathbf{r} through any of the basis states $\psi_\nu(\mathbf{r})$. Since $\Psi^\dagger(\mathbf{r})$ and $\Psi(\mathbf{r})$ are second quantization operators defined in every point in space they are called quantum field operators. From Eq. (1.69) it is straight forward to calculate the following fundamental commutator and anti-commutator,

$$[\Psi(\mathbf{r}_1), \Psi^\dagger(\mathbf{r}_2)] = \delta(\mathbf{r}_1 - \mathbf{r}_2), \quad \text{boson fields} \quad (1.72a)$$

$$\{\Psi(\mathbf{r}_1), \Psi^\dagger(\mathbf{r}_2)\} = \delta(\mathbf{r}_1 - \mathbf{r}_2), \quad \text{fermion fields.} \quad (1.72b)$$

In some sense the quantum field operators express the essence of the wave/particle duality in quantum physics. On the one hand they are defined as fields, i.e. as a kind of waves, but on the other hand they exhibit the commutator properties associated with particles.

The introduction of quantum field operators makes it easy to write down operators in the real space representation. By applying the definition Eq. (1.71) to the second quantized single-particle operator Eq. (1.63) one obtains

$$\begin{aligned} T &= \sum_{\nu_i \nu_j} \left(\int d\mathbf{r} \psi_{\nu_i}^*(\mathbf{r}) T_{\mathbf{r}} \psi_{\nu_j}(\mathbf{r}) \right) a_{\nu_i}^\dagger a_{\nu_j} \\ &= \int d\mathbf{r} \left(\sum_{\nu_i} \psi_{\nu_i}^*(\mathbf{r}) a_{\nu_i}^\dagger \right) T_{\mathbf{r}} \left(\sum_{\nu_j} \psi_{\nu_j}(\mathbf{r}) a_{\nu_j} \right) = \int d\mathbf{r} \Psi^\dagger(\mathbf{r}) T_{\mathbf{r}} \Psi(\mathbf{r}). \end{aligned} \quad (1.73)$$

So in the real space representation, i.e. using quantum field operators, second quantization operators have a form analogous to first quantization matrix elements.

Finally, when working with homogeneous systems it is often desirable to transform between the real space and the momentum representations, i.e. to perform a Fourier transformation. Substituting in Eq. (1.71) the $|\psi_\nu\rangle$ basis with the momentum basis $|\mathbf{k}\rangle$ yields

$$\Psi^\dagger(\mathbf{r}) = \frac{1}{\sqrt{\mathcal{V}}} \sum_{\mathbf{k}} e^{-i\mathbf{k}\cdot\mathbf{r}} a_{\mathbf{k}}^\dagger, \quad \Psi(\mathbf{r}) = \frac{1}{\sqrt{\mathcal{V}}} \sum_{\mathbf{k}} e^{i\mathbf{k}\cdot\mathbf{r}} a_{\mathbf{k}}. \quad (1.74)$$

The inverse expressions are obtained by multiplying by $e^{\pm i\mathbf{q}\cdot\mathbf{r}}$ and integrating over \mathbf{r} ,

$$a_{\mathbf{q}}^\dagger = \frac{1}{\sqrt{\mathcal{V}}} \int d\mathbf{r} e^{i\mathbf{q}\cdot\mathbf{r}} \Psi^\dagger(\mathbf{r}), \quad a_{\mathbf{q}} = \frac{1}{\sqrt{\mathcal{V}}} \int d\mathbf{r} e^{-i\mathbf{q}\cdot\mathbf{r}} \Psi(\mathbf{r}). \quad (1.75)$$

1.4 Second quantization, specific operators

In this section we will use the general second quantization formalism to derive some expressions for specific second quantization operators that we are going to use repeatedly in this course.

1.4.1 The harmonic oscillator in second quantization

The one-dimensional harmonic oscillator in first quantization is characterized by two conjugate variables appearing in the Hamiltonian: the position x and the momentum p ,

$$H = \frac{1}{2m} p^2 + \frac{1}{2} m \omega^2 x^2, \quad [p, x] = \frac{\hbar}{i}. \quad (1.76)$$

This can be rewritten in second quantization by identifying two operators a^\dagger and a satisfying the basic boson commutation relations Eq. (1.42). By inspection it can be verified that the following operators do the job,

$$\left. \begin{aligned} a &\equiv \frac{1}{\sqrt{2}} \left(\frac{x}{\ell} + i \frac{p}{\hbar/\ell} \right) \\ a^\dagger &\equiv \frac{1}{\sqrt{2}} \left(\frac{x}{\ell} - i \frac{p}{\hbar/\ell} \right) \end{aligned} \right\} \Rightarrow \left\{ \begin{aligned} x &\equiv \ell \frac{1}{\sqrt{2}} (a^\dagger + a), \\ p &\equiv \frac{\hbar}{\ell} \frac{i}{\sqrt{2}} (a^\dagger - a), \end{aligned} \right. \quad (1.77)$$

where x is given in units of the harmonic oscillator length $\ell = \sqrt{\hbar/m\omega}$ and p in units of the harmonic oscillator momentum \hbar/ℓ . Mnemotechnically, one can think of a as being the $(1/\sqrt{2}$ -normalized) complex number formed by the real part x/ℓ and the imaginary part $p/(\hbar/\ell)$, while a^\dagger is found as the adjoint operator to a . From Eq. (1.77) we obtain the Hamiltonian, H , and the eigenstates $|n\rangle$:

$$H = \hbar\omega \left(a^\dagger a + \frac{1}{2} \right) \quad \text{and} \quad |n\rangle = \frac{(a^\dagger)^n}{\sqrt{n!}} |0\rangle, \quad \text{with} \quad H|n\rangle = \hbar\omega \left(n + \frac{1}{2} \right) |n\rangle. \quad (1.78)$$

The excitation of the harmonic oscillator can thus be interpreted as filling the oscillator with bosonic quanta created by the operator a^\dagger . This picture is particularly useful in the studies of the photon and phonon fields, as we shall see during the course. If we as a

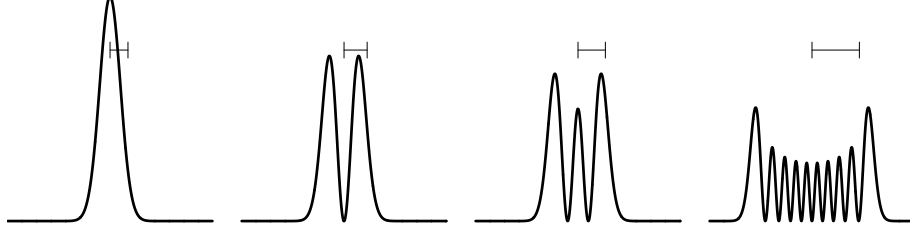


Figure 1.7: The probability density $|\langle \mathbf{r} | n \rangle|^2$ for $n = 0, 1, 2$, and 9 quanta in the oscillator state. Note that the width of the wave function is $\sqrt{\langle n | x^2 | n \rangle} = \sqrt{n + 1/2} \ell$.

measure of the amplitude of the oscillator in the state with n quanta, $|n\rangle$, use the square-root of the expectation value of $x^2 = \ell^2(a^\dagger a^\dagger + a^\dagger a + a a^\dagger + a a)/2$, we find $\sqrt{\langle n | x^2 | n \rangle} = \sqrt{n + 1/2} \ell$. Thus the width of the oscillator wavefunction scales roughly with the square-root of the number of quanta in the oscillator, as sketched in Fig. 1.7.

The creation operator can also be used to generate the specific form of the eigenfunctions $\psi_n(x)$ of the oscillator starting from the groundstate wavefunction $\psi_0(x)$:

$$\psi_n(x) = \langle x | n \rangle = \langle x | \frac{(a^\dagger)^n}{\sqrt{n!}} | 0 \rangle = \frac{1}{\sqrt{n!}} \langle x | \left(\frac{x}{\sqrt{2}\ell} - i \frac{p}{\hbar \sqrt{2}} \right)^n | 0 \rangle = \frac{1}{\sqrt{2^n n!}} \left(\frac{x}{\ell} - \ell \frac{d}{dx} \right)^n \psi_0(x). \quad (1.79)$$

1.4.2 The electromagnetic field in second quantization

Historically, the electromagnetic field was the first example of second quantization (Dirac, 1927). The quantum nature of the radiation field, and the associated concept of photons play a crucial role in the theory of interactions between matter and light. In most of the applications in this course we shall, however, treat the electromagnetic field classically.

The quantization of the electromagnetic field is based on the observation that the eigenmodes of the classical field can be thought of as a collection of harmonic oscillators. These are then quantized. In the free field case the electromagnetic field is completely determined by the vector potential $\mathbf{A}(\mathbf{r}, t)$ in a specific gauge. Normally, the transversality condition $\nabla \cdot \mathbf{A} = 0$ is chosen, in which case \mathbf{A} is denoted the radiation field, and we have

$$\begin{aligned} \mathbf{B} &= \nabla \times \mathbf{A} & \nabla \cdot \mathbf{A} &= 0 \\ \mathbf{E} &= -\partial_t \mathbf{A} & \nabla^2 \mathbf{A} - \frac{1}{c^2} \partial_t^2 \mathbf{A} &= 0. \end{aligned} \quad (1.80)$$

We assume periodic boundary conditions for \mathbf{A} enclosed in a huge box taken to be a cube of volume \mathcal{V} and hence side length $L = \sqrt[3]{\mathcal{V}}$. The dispersion law is $\omega_{\mathbf{k}} = kc$ and the two-fold polarization of the field is described by polarization vectors $\boldsymbol{\epsilon}_\lambda$, $\lambda = 1, 2$. The normalized eigenmodes $\mathbf{u}_{\mathbf{k}, \lambda}(\mathbf{r}, t)$ of the wave equation Eq. (1.80) are seen to be

$$\begin{aligned} \mathbf{u}_{\mathbf{k}, \lambda}(\mathbf{r}, t) &= \frac{1}{\sqrt{\mathcal{V}}} \boldsymbol{\epsilon}_\lambda e^{i(\mathbf{k} \cdot \mathbf{r} - \omega_{\mathbf{k}} t)}, & \lambda &= 1, 2, & \omega_{\mathbf{k}} &= ck \\ k_x &= \frac{2\pi}{L} n_x, & n_x &= 0, \pm 1, \pm 2, \dots & & \text{(same for } y \text{ and } z). \end{aligned} \quad (1.81)$$

The set $\{\epsilon_1, \epsilon_2, \mathbf{k}/k\}$ forms a right-handed orthonormal basis set. The field \mathbf{A} takes only real values and hence it has a Fourier expansion of the form

$$\mathbf{A}(\mathbf{r}, t) = \frac{1}{\sqrt{V}} \sum_{\mathbf{k}} \sum_{\lambda=1,2} \left(A_{\mathbf{k},\lambda} e^{i(\mathbf{k} \cdot \mathbf{r} - \omega_{\mathbf{k}} t)} + A_{\mathbf{k},\lambda}^* e^{-i(\mathbf{k} \cdot \mathbf{r} - \omega_{\mathbf{k}} t)} \right) \epsilon_{\lambda}, \quad (1.82)$$

where $A_{\mathbf{k},\lambda}$ are the complex expansion coefficients. We now turn to the Hamiltonian H of the system, which is simply the field energy known from electromagnetism. Using Eq. (1.80) we can express H in terms of the radiation field \mathbf{A} ,

$$H = \frac{1}{2} \int d\mathbf{r} \left(\epsilon_0 |\mathbf{E}|^2 + \frac{1}{\mu_0} |\mathbf{B}|^2 \right) = \frac{1}{2} \epsilon_0 \int d\mathbf{r} (\omega_{\mathbf{k}}^2 |\mathbf{A}|^2 + c^2 k^2 |\mathbf{A}|^2) = \epsilon_0 \omega_{\mathbf{k}}^2 \int d\mathbf{r} |\mathbf{A}|^2. \quad (1.83)$$

In Fourier space, using Parseval's theorem and the notation $A_{\mathbf{k},\lambda} = A_{\mathbf{k},\lambda}^R + iA_{\mathbf{k},\lambda}^I$ for the real and imaginary part of the coefficients, we have

$$H = \epsilon_0 \omega_{\mathbf{k}}^2 \sum_{\mathbf{k},\lambda} 2|A_{\mathbf{k},\lambda}|^2 = 4\epsilon_0 \omega_{\mathbf{k}}^2 \frac{1}{2} \sum_{\mathbf{k},\lambda} \left(|A_{\mathbf{k},\lambda}^R|^2 + |A_{\mathbf{k},\lambda}^I|^2 \right). \quad (1.84)$$

If in Eq. (1.82) we merge the time dependence with the coefficients, i.e. $\mathbf{A}_{\mathbf{k},\lambda}(t) = \mathbf{A}_{\mathbf{k},\lambda} e^{-i\omega_{\mathbf{k}} t}$, the time dependence for the real and imaginary parts are seen to be

$$\dot{A}_{\mathbf{k},\lambda}^R = +\omega_{\mathbf{k}} A_{\mathbf{k},\lambda}^I, \quad \dot{A}_{\mathbf{k},\lambda}^I = -\omega_{\mathbf{k}} A_{\mathbf{k},\lambda}^R. \quad (1.85)$$

From Eqs. (1.84) and (1.85) it thus follows that, up to some normalization constants, $\mathbf{A}_{\mathbf{k},\lambda}^R$ and $\mathbf{A}_{\mathbf{k},\lambda}^I$ are conjugate variables: $\frac{\partial H}{\partial A_{\mathbf{k},\lambda}^R} = -4\epsilon_0 \omega_{\mathbf{k}} \dot{A}_{\mathbf{k},\lambda}^I$ and $\frac{\partial H}{\partial A_{\mathbf{k},\lambda}^I} = +4\epsilon_0 \omega_{\mathbf{k}} \dot{A}_{\mathbf{k},\lambda}^R$. Proper normalized conjugate variables $Q_{\mathbf{k},\lambda}$ and $P_{\mathbf{k},\lambda}$ are therefore introduced:

$$\left. \begin{aligned} Q_{\mathbf{k},\lambda} &\equiv 2\sqrt{\epsilon_0} A_{\mathbf{k},\lambda}^R \\ P_{\mathbf{k},\lambda} &\equiv 2\omega_{\mathbf{k}} \sqrt{\epsilon_0} A_{\mathbf{k},\lambda}^I \end{aligned} \right\} \Rightarrow \left\{ \begin{aligned} H &= \sum_{\mathbf{k},\lambda} \frac{1}{2} \left(P_{\mathbf{k},\lambda}^2 + \omega_{\mathbf{k}}^2 Q_{\mathbf{k},\lambda}^2 \right) \\ \dot{Q}_{\mathbf{k},\lambda} &= P_{\mathbf{k},\lambda}, \quad \dot{P}_{\mathbf{k},\lambda} = -\omega_{\mathbf{k}}^2 Q_{\mathbf{k},\lambda} \\ \frac{\partial H}{\partial Q_{\mathbf{k},\lambda}} &= -\dot{P}_{\mathbf{k},\lambda}, \quad \frac{\partial H}{\partial P_{\mathbf{k},\lambda}} = \dot{Q}_{\mathbf{k},\lambda}. \end{aligned} \right. \quad (1.86)$$

This ends the proof that the radiation field \mathbf{A} can thought of as a collection of harmonic oscillator eigenmodes, where each mode are characterized by the conjugate variable $Q_{\mathbf{k},\lambda}$ and $P_{\mathbf{k},\lambda}$. Quantization is now obtained by imposing the usual condition on the commutator of the variables, and introducing the second quantized Bose operators $a_{\mathbf{k},\lambda}^\dagger$ for each quantized oscillator:

$$[P_{\mathbf{k},\lambda}, Q_{\mathbf{k},\lambda}] = \frac{\hbar}{i} \Rightarrow \left\{ \begin{aligned} H &= \sum_{\mathbf{k},\lambda} \hbar \omega_{\mathbf{k}} \left(a_{\mathbf{k},\lambda}^\dagger a_{\mathbf{k},\lambda} + \frac{1}{2} \right), \quad [a_{\mathbf{k},\lambda}, a_{\mathbf{k},\lambda}^\dagger] = 1, \\ Q_{\mathbf{k},\lambda} &= \sqrt{\frac{\hbar}{2\omega_{\mathbf{k}}}} (a_{\mathbf{k},\lambda}^\dagger + a_{\mathbf{k},\lambda}), \quad P_{\mathbf{k},\lambda} = \sqrt{\frac{\hbar \omega_{\mathbf{k}}}{2}} i(a_{\mathbf{k},\lambda}^\dagger - a_{\mathbf{k},\lambda}). \end{aligned} \right. \quad (1.87)$$

To obtain the final expression for \mathbf{A} in second quantization we simply express $\mathbf{A}_{\mathbf{k},\lambda}$ in terms of $P_{\mathbf{k},\lambda}$ and $Q_{\mathbf{k},\lambda}$, which in turn is expressed in terms of $a_{\mathbf{k},\lambda}^\dagger$ and $a_{\mathbf{k},\lambda}$:

$$A_{\mathbf{k},\lambda} = A_{\mathbf{k},\lambda}^R + iA_{\mathbf{k},\lambda}^I \rightarrow \frac{Q_{\mathbf{k},\lambda}}{2\sqrt{\epsilon_0}} + i \frac{P_{\mathbf{k},\lambda}}{2\omega_{\mathbf{k}}\sqrt{\epsilon_0}} = \sqrt{\frac{\hbar}{2\epsilon_0\omega_{\mathbf{k}}}} a_{\mathbf{k},\lambda}, \quad \text{and} \quad A_{\mathbf{k},\lambda}^* \rightarrow \sqrt{\frac{\hbar}{2\epsilon_0\omega_{\mathbf{k}}}} a_{\mathbf{k},\lambda}^\dagger. \quad (1.88)$$

Substituting this into the expansion Eq. (1.82) our final result is:

$$\mathbf{A}(\mathbf{r}, t) = \frac{1}{\sqrt{\mathcal{V}}} \sum_{\mathbf{k}} \sum_{\lambda=1,2} \sqrt{\frac{\hbar}{2\epsilon_0\omega_{\mathbf{k}}}} \left(a_{\mathbf{k},\lambda} e^{i(\mathbf{k}\cdot\mathbf{r}-\omega_{\mathbf{k}}t)} + a_{\mathbf{k},\lambda}^\dagger e^{-i(\mathbf{k}\cdot\mathbf{r}-\omega_{\mathbf{k}}t)} \right) \boldsymbol{\epsilon}_\lambda. \quad (1.89)$$

1.4.3 Operators for kinetic energy, spin, density, and current

In the following we establish the second quantization representation of the four important single-particle operators associated with kinetic energy, spin, particle density, and particle current density.

First, we study the kinetic energy operator T , which is independent of spin and hence diagonal in the spin indices. In first quantization it has the representations

$$T_{\mathbf{r},\sigma'\sigma} = -\frac{\hbar^2}{2m} \nabla_{\mathbf{r}}^2 \delta_{\sigma',\sigma}, \quad \text{real space representation,} \quad (1.90a)$$

$$\langle \mathbf{k}'\sigma' | T | \mathbf{k}\sigma \rangle = \frac{\hbar^2 k^2}{2m} \delta_{\mathbf{k}',\mathbf{k}} \delta_{\sigma',\sigma}, \quad \text{momentum representation.} \quad (1.90b)$$

Its second quantized forms with spin indices follow directly from Eqs. (1.63) and (1.73)

$$T = \sum_{\mathbf{k},\sigma} \frac{\hbar^2 k^2}{2m} a_{\mathbf{k},\sigma}^\dagger a_{\mathbf{k},\sigma} = -\frac{\hbar^2}{2m} \sum_{\sigma} \int d\mathbf{r} \Psi_{\sigma}^\dagger(\mathbf{r}) \left(\nabla_{\mathbf{r}}^2 \Psi_{\sigma}(\mathbf{r}) \right). \quad (1.91)$$

The second equality can also be proven directly by inserting $\Psi^\dagger(\mathbf{r})$ and $\Psi(\mathbf{r})$ from Eq. (1.74). For particles with charge q a magnetic field can be included in the expression for the kinetic energy by substituting the canonical momentum \mathbf{p} with the kinetic momentum⁴ $\mathbf{p} - q\mathbf{A}$,

$$T_{\mathbf{A}} = \frac{1}{2m} \sum_{\sigma} \int d\mathbf{r} \Psi_{\sigma}^\dagger(\mathbf{r}) \left(\frac{\hbar}{i} \nabla_{\mathbf{r}} - q\mathbf{A} \right)^2 \Psi_{\sigma}(\mathbf{r}). \quad (1.92)$$

Next, we treat the spin operator \mathbf{s} for electrons. In first quantization it is given by the Pauli matrices

$$\mathbf{s} = \frac{\hbar}{2} \boldsymbol{\tau}, \quad \text{with} \quad \boldsymbol{\tau} = \left\{ \begin{pmatrix} 0 & 1 \\ 1 & 0 \end{pmatrix}, \begin{pmatrix} 0 & -i \\ i & 0 \end{pmatrix}, \begin{pmatrix} 1 & 0 \\ 0 & -1 \end{pmatrix} \right\}. \quad (1.93)$$

⁴In analytical mechanics \mathbf{A} enters through the Lagrangian: $L = \frac{1}{2}mv^2 - V + q\mathbf{v}\cdot\mathbf{A}$, since this by the Euler-Lagrange equations yields the Lorentz force. But then $\mathbf{p} = \partial L / \partial \mathbf{v} = m\mathbf{v} + q\mathbf{A}$, and via a Legendre transform we get $H(\mathbf{r}, \mathbf{p}) = \mathbf{p}\cdot\mathbf{v} - L(\mathbf{r}, \mathbf{v}) = \frac{1}{2}mv^2 + V = \frac{1}{2m}(\mathbf{p} - q\mathbf{A})^2 + V$. Considering infinitesimal variations $\delta\mathbf{A}$ we get $\delta H = H(\mathbf{A} + \delta\mathbf{A}) - H(\mathbf{A}) = -q\mathbf{v}\cdot\delta\mathbf{A} = -q\int d\mathbf{r} \mathbf{J}\cdot\delta\mathbf{A}$, an expression used to find \mathbf{J} .

To obtain the second quantized operator we pull out the spin index explicitly in the basis kets, $|\nu\rangle = |\mu\rangle|\sigma\rangle$, and obtain with fermion operators the following vector expression,

$$\mathbf{s} = \sum_{\mu\sigma\mu'\sigma'} \langle\mu'|\langle\sigma'|\mathbf{s}|\sigma\rangle|\mu\rangle c_{\mu'\sigma'}^\dagger c_{\mu\sigma} = \frac{\hbar}{2} \sum_{\mu} \sum_{\sigma'\sigma} \langle\sigma'|(\tau^x, \tau^y, \tau^z)|\sigma\rangle c_{\mu\sigma'}^\dagger c_{\mu\sigma}, \quad (1.94a)$$

with components

$$s^x = \frac{\hbar}{2} \sum_{\mu} (c_{\mu\downarrow}^\dagger c_{\mu\uparrow} + c_{\mu\uparrow}^\dagger c_{\mu\downarrow}) \quad s^y = i\frac{\hbar}{2} \sum_{\mu} (c_{\mu\downarrow}^\dagger c_{\mu\uparrow} - c_{\mu\uparrow}^\dagger c_{\mu\downarrow}) \quad s^z = \frac{\hbar}{2} \sum_{\mu} (c_{\mu\uparrow}^\dagger c_{\mu\uparrow} - c_{\mu\downarrow}^\dagger c_{\mu\downarrow}). \quad (1.94b)$$

We then turn to the particle density operator $\rho(\mathbf{r})$. In first quantization the fundamental interpretation of the wave function $\psi_{\mu,\sigma}(\mathbf{r})$ gives us $\rho_{\mu,\sigma}(\mathbf{r}) = |\psi_{\mu,\sigma}(\mathbf{r})|^2$ which can also be written as $\rho_{\mu,\sigma}(\mathbf{r}) = \int d\mathbf{r}' \psi_{\mu,\sigma}^*(\mathbf{r}') \delta(\mathbf{r}' - \mathbf{r}) \psi_{\mu,\sigma}(\mathbf{r}')$, and thus the density operator for spin σ is given by $\rho_\sigma(\mathbf{r}) = \delta(\mathbf{r}' - \mathbf{r})$. In second quantization this combined with Eq. (1.63) yields

$$\rho_\sigma(\mathbf{r}) = \int d\mathbf{r}' \Psi_\sigma^\dagger(\mathbf{r}') \delta(\mathbf{r}' - \mathbf{r}) \Psi_\sigma(\mathbf{r}') = \Psi_\sigma^\dagger(\mathbf{r}) \Psi_\sigma(\mathbf{r}). \quad (1.95)$$

From Eq. (1.75) the momentum representation of this is found to be

$$\rho_\sigma(\mathbf{r}) = \frac{1}{V} \sum_{\mathbf{k}\mathbf{k}'} e^{i(\mathbf{k}-\mathbf{k}')\cdot\mathbf{r}} a_{\mathbf{k}'\sigma}^\dagger a_{\mathbf{k}\sigma} = \frac{1}{V} \sum_{\mathbf{k}\mathbf{q}} e^{-i\mathbf{q}\cdot\mathbf{r}} a_{\mathbf{k}+\mathbf{q}\sigma}^\dagger a_{\mathbf{k}\sigma} = \frac{1}{V} \sum_{\mathbf{q}} \left(\sum_{\mathbf{k}} a_{\mathbf{k}\sigma}^\dagger a_{\mathbf{k}+\mathbf{q}\sigma} \right) e^{i\mathbf{q}\cdot\mathbf{r}}, \quad (1.96)$$

where the momentum transfer $\mathbf{q} = \mathbf{k}' - \mathbf{k}$ has been introduced.

The fourth and last operator to be treated is the particle current density operator $\mathbf{J}(\mathbf{r})$. It is related to the particle density operator $\rho(\mathbf{r})$ through the continuity equation $\partial_t \rho + \nabla \cdot \mathbf{J} = 0$. This relationship can be used to actually define \mathbf{J} . However, we shall take a more general approach based on analytical mechanics, see Eq. (1.92) and the associated footnote. This allows us in a simple way to take the magnetic field, given by the vector potential \mathbf{A} , into account. By analytical mechanics it is found that variations δH in the Hamiltonian function due to variations $\delta \mathbf{A}$ in the vector potential is given by

$$\delta H = -q \int d\mathbf{r} \mathbf{J} \cdot \delta \mathbf{A} \quad (1.97)$$

We use this expression with H given by the kinetic energy Eq. (1.92). Variations due to a varying parameter are calculated as derivatives if the parameter appears as a simple factor. But expanding the square in Eq. (1.92) and writing only the \mathbf{A} dependent terms of the integrand, $-\Psi_\sigma^\dagger(\mathbf{r}) \frac{q\hbar}{2mi} [\nabla \cdot \mathbf{A} + \mathbf{A} \cdot \nabla] \Psi_\sigma(\mathbf{r}) + \frac{q^2}{2m} \mathbf{A}^2 \Psi_\sigma^\dagger(\mathbf{r}) \Psi_\sigma(\mathbf{r})$, reveals one term where ∇ is acting on \mathbf{A} . By partial integration this ∇ is shifted to $\Psi^\dagger(\mathbf{r})$, and we obtain

$$H = T + \sum_{\sigma} \int d\mathbf{r} \left\{ \frac{q\hbar}{2mi} \mathbf{A} \cdot \left[\left(\nabla \Psi_\sigma^\dagger(\mathbf{r}) \right) \Psi_\sigma(\mathbf{r}) - \Psi_\sigma^\dagger(\mathbf{r}) \left(\nabla \Psi_\sigma(\mathbf{r}) \right) \right] + \frac{q^2}{2m} \mathbf{A}^2 \Psi_\sigma^\dagger(\mathbf{r}) \Psi_\sigma(\mathbf{r}) \right\}. \quad (1.98)$$

The variations of Eq. (1.97) can in Eq. (1.98) be performed as derivatives and \mathbf{J} is immediately read off as the prefactor to $\delta\mathbf{A}$. The two terms in the current density operator are denoted the paramagnetic and the diamagnetic term, \mathbf{J}^∇ and \mathbf{J}^A , respectively:

$$\mathbf{J}_\sigma(\mathbf{r}) = \mathbf{J}_\sigma^\nabla(\mathbf{r}) + \mathbf{J}_\sigma^A(\mathbf{r}), \quad (1.99a)$$

$$\text{paramagnetic : } \mathbf{J}_\sigma^\nabla(\mathbf{r}) = \frac{\hbar}{2mi} \left[\Psi_\sigma^\dagger(\mathbf{r}) \left(\nabla \Psi_\sigma(\mathbf{r}) \right) - \left(\nabla \Psi_\sigma^\dagger(\mathbf{r}) \right) \Psi_\sigma(\mathbf{r}) \right], \quad (1.99b)$$

$$\text{diamagnetic : } \mathbf{J}_\sigma^A(\mathbf{r}) = -\frac{q}{m} \mathbf{A}(\mathbf{r}) \Psi_\sigma^\dagger(\mathbf{r}) \Psi_\sigma(\mathbf{r}). \quad (1.99c)$$

The momentum representation of \mathbf{J} is found in complete analogy with that of ρ

$$\mathbf{J}_\sigma^\nabla(\mathbf{r}) = \frac{\hbar}{m\mathcal{V}} \sum_{\mathbf{k}\mathbf{q}} (\mathbf{k} + \frac{1}{2}\mathbf{q}) e^{i\mathbf{q}\cdot\mathbf{r}} a_{\mathbf{k}\sigma}^\dagger a_{\mathbf{k}+\mathbf{q},\sigma}, \quad \mathbf{J}_\sigma^A(\mathbf{r}) = \frac{-q}{m\mathcal{V}} \mathbf{A}(\mathbf{r}) \sum_{\mathbf{k}\mathbf{q}} e^{i\mathbf{q}\cdot\mathbf{r}} a_{\mathbf{k}\sigma}^\dagger a_{\mathbf{k}+\mathbf{q},\sigma}. \quad (1.100)$$

The expression for \mathbf{J} in an arbitrary basis is treated in Exercise 1.2.

1.4.4 The Coulomb interaction in second quantization

The Coulomb interaction operator V is a two-particle operator not involving spin and thus diagonal in the spin indices of the particles. Using the same reasoning that led from Eq. (1.63) to Eq. (1.73) we can go directly from Eq. (1.64) to the following quantum field operator form of V :

$$V(\mathbf{r}_2 - \mathbf{r}_1) = \frac{1}{2} \sum_{\sigma_1\sigma_2} \int d\mathbf{r}_1 d\mathbf{r}_2 \frac{e_0^2}{|\mathbf{r}_2 - \mathbf{r}_1|} \Psi_{\sigma_1}^\dagger(\mathbf{r}_1) \Psi_{\sigma_2}^\dagger(\mathbf{r}_2) \Psi_{\sigma_2}(\mathbf{r}_2) \Psi_{\sigma_1}(\mathbf{r}_1). \quad (1.101)$$

Here we have introduced the abbreviation $e_0^2 = e^2/4\pi\epsilon_0$. We can also write the Coulomb interaction directly in the momentum basis by using Eq. (1.31) and Eq. (1.64) with $|\nu\rangle = |\mathbf{k}, \sigma\rangle$ and $\psi_{\mathbf{k},\sigma}(\mathbf{r}) = \frac{1}{\sqrt{\mathcal{V}}} e^{i\mathbf{k}\cdot\mathbf{r}} \chi_\sigma$. We can interpret the Coulomb matrix element as describing a transition from an initial state $|\mathbf{k}_1\sigma_1, \mathbf{k}_2\sigma_2\rangle$ to a final state $|\mathbf{k}_3\sigma_1, \mathbf{k}_4\sigma_2\rangle$ without flipping any spin, and we obtain

$$\begin{aligned} V &= \frac{1}{2} \sum_{\sigma_1\sigma_2} \sum_{\substack{\mathbf{k}_1\mathbf{k}_2 \\ \mathbf{k}_3\mathbf{k}_4}} \langle \mathbf{k}_3\sigma_1, \mathbf{k}_4\sigma_2 | V | \mathbf{k}_1\sigma_1, \mathbf{k}_2\sigma_2 \rangle a_{\mathbf{k}_3\sigma_1}^\dagger a_{\mathbf{k}_4\sigma_2}^\dagger a_{\mathbf{k}_2\sigma_2} a_{\mathbf{k}_1\sigma_1} \\ &= \frac{1}{2} \sum_{\sigma_1\sigma_2} \sum_{\substack{\mathbf{k}_1\mathbf{k}_2 \\ \mathbf{k}_3\mathbf{k}_4}} \left(\frac{e_0^2}{\mathcal{V}^2} \int d\mathbf{r}_1 d\mathbf{r}_2 \frac{e^{i(\mathbf{k}_1\cdot\mathbf{r}_1 + \mathbf{k}_2\cdot\mathbf{r}_2 - \mathbf{k}_3\cdot\mathbf{r}_1 - \mathbf{k}_4\cdot\mathbf{r}_2)}}{|\mathbf{r}_2 - \mathbf{r}_1|} \right) a_{\mathbf{k}_3\sigma_1}^\dagger a_{\mathbf{k}_4\sigma_2}^\dagger a_{\mathbf{k}_2\sigma_2} a_{\mathbf{k}_1\sigma_1}. \end{aligned} \quad (1.102)$$

Since $\mathbf{r}_2 - \mathbf{r}_1$ is the relevant variable for the interaction, the exponential is rewritten as

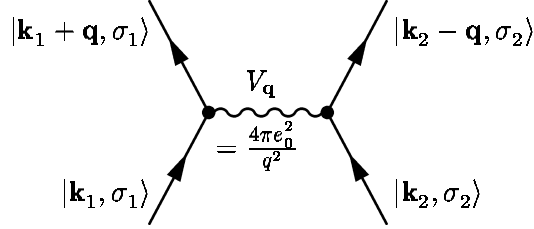


Figure 1.8: A graphical representation of the Coulomb interaction in second quantization. Under momentum and spin conservation the incoming states $|\mathbf{k}_1, \sigma_1\rangle$ and $|\mathbf{k}_2, \sigma_2\rangle$ are with probability amplitude $V_{\mathbf{q}}$ scattered into the outgoing states $|\mathbf{k}_1 + \mathbf{q}, \sigma_1\rangle$ and $|\mathbf{k}_2 - \mathbf{q}, \sigma_2\rangle$.

$e^{i[(\mathbf{k}_1 - \mathbf{k}_3) \cdot \mathbf{r}_1 + (\mathbf{k}_2 - \mathbf{k}_4) \cdot \mathbf{r}_2]} = e^{i(\mathbf{k}_1 - \mathbf{k}_3 + \mathbf{k}_2 - \mathbf{k}_4) \cdot \mathbf{r}_1} e^{i(\mathbf{k}_2 - \mathbf{k}_4) \cdot (\mathbf{r}_2 - \mathbf{r}_1)}$ leaving us with two integrals, which with the definitions $\mathbf{q} \equiv \mathbf{k}_2 - \mathbf{k}_4$ and $\mathbf{r} \equiv \mathbf{r}_2 - \mathbf{r}_1$ become

$$\int d\mathbf{r}_1 e^{i(\mathbf{k}_1 - \mathbf{k}_3 + \mathbf{q}) \cdot \mathbf{r}_1} = V \delta_{\mathbf{k}_3, \mathbf{k}_1 + \mathbf{q}}, \quad V_{\mathbf{q}} \equiv \int d\mathbf{r} \frac{e_0^2}{r} e^{i\mathbf{q} \cdot \mathbf{r}} = \frac{4\pi e_0^2}{q^2}. \quad (1.103)$$

These integrals express the Fourier transform of the Coulomb interaction⁵ and the explicit momentum conservation obeyed by the interaction. The momenta \mathbf{k}_3 and \mathbf{k}_4 of the final states can now be written as $\mathbf{k}_3 = \mathbf{k}_1 + \mathbf{q}$ and $\mathbf{k}_4 = \mathbf{k}_2 - \mathbf{q}$. The final second quantized form of the Coulomb interaction in momentum space is

$$V = \frac{1}{2\mathcal{V}} \sum_{\sigma_1 \sigma_2} \sum_{\mathbf{k}_1 \mathbf{k}_2 \mathbf{q}} V_{\mathbf{q}} a_{\mathbf{k}_1 + \mathbf{q} \sigma_1}^\dagger a_{\mathbf{k}_2 - \mathbf{q} \sigma_2}^\dagger a_{\mathbf{k}_2 \sigma_2} a_{\mathbf{k}_1 \sigma_1}. \quad (1.104)$$

We shall study this operator thoroughly in Sec. 2.2 in connection with the interacting electron gas. Here, in Fig. 1.8, we just show a graphical representation of the operator.

1.4.5 Basis states for systems with different kinds of particles

In the previous sections we have derived different fermion and boson operators. But so far we have not treated systems where different kinds of particles are coupled. In this course one important example of such a system is the fermionic electrons in a metal interacting with the bosonic lattice vibrations (phonons). We study this system in Chap. 3. Another example is electrons interacting with the photon field. Here we will briefly clarify how to construct the basis set for such composed systems in general.

Let us for simplicity just study two different kinds of particles. The arguments are easily generalized to include more complicated systems. The starting point is the case where the two kinds of particles do not interact with each other. Let the first kind of particles be described by the Hamiltonian H_1 and a complete set of basis states $\{|\nu\rangle\}$. Likewise we have H_2 and $\{|\mu\rangle\}$ for the second kind of particles. For the two decoupled

⁵We show in Exercise 1.5 how to calculate the Fourier transform $V_{\mathbf{q}}^{k_s}$ of the Yukawa potential $V^{k_s}(\mathbf{r}) = \frac{e_0^2}{r} e^{-k_s r}$. The result is $V_{\mathbf{q}}^{k_s} = \frac{4\pi e_0^2}{q^2 + k_s^2}$ from which Eq. (1.103) follows by setting $k_s = 0$.

systems an example of separate occupation number basis sets is

$$|\psi^{(1)}\rangle = |n_{\nu_1}, n_{\nu_2}, \dots, n_{\nu_j}, \dots\rangle \quad (1.105a)$$

$$|\psi^{(2)}\rangle = |n_{\mu_1}, n_{\mu_2}, \dots, n_{\mu_j}, \dots\rangle \quad (1.105b)$$

When a coupling H_{12} between the two system is introduced, we need to enlarge the Hilbert space. The natural definition of basis states is the outer product states written as

$$\begin{aligned} |\psi\rangle &= |\psi^{(1)}\rangle |\psi^{(2)}\rangle \\ &= |n_{\nu_1}, n_{\nu_2}, \dots, n_{\nu_j}, \dots\rangle |n_{\mu_1}, n_{\mu_2}, \dots, n_{\mu_l}, \dots\rangle \\ &= |n_{\nu_1}, n_{\nu_2}, \dots, n_{\nu_j}, \dots; n_{\mu_1}, n_{\mu_2}, \dots, n_{\mu_l}, \dots\rangle \end{aligned} \quad (1.106)$$

In the last line all the occupation numbers are simply listed within the same ket but the two groups are separated by a semicolon. A general state $|\Phi\rangle$ can of course be any superposition of the basis states:

$$|\Phi\rangle = \sum_{\{\nu_j\}\{\mu_l\}} C_{\{\nu_j\},\{\mu_l\}} |n_{\nu_1}, n_{\nu_2}, \dots, n_{\nu_j}, \dots; n_{\mu_1}, n_{\mu_2}, \dots, n_{\mu_l}, \dots\rangle. \quad (1.107)$$

As a concrete example we can write down the basis states for interacting electrons and photons in the momentum representation. The electronic basis states are the plane wave orbitals $|\mathbf{k}\sigma\rangle$ of Eq. (1.3), and the photon states are $|\mathbf{q}\lambda\rangle$ given in Eq. (1.81). We let $n_{\mathbf{k}\sigma}$ and $N_{\mathbf{q}\lambda}$ denote the occupation numbers for electrons and photons, respectively. A basis state $|\psi\rangle$ in this representation has the form:

$$|\psi\rangle = |n_{\mathbf{k}_1\sigma_1}, n_{\mathbf{k}_2\sigma_2}, \dots, n_{\mathbf{k}_j\sigma_j}, \dots; N_{\mathbf{q}_1\lambda_1}, N_{\mathbf{q}_2\lambda_2}, \dots, N_{\mathbf{q}_l\lambda_l}, \dots\rangle. \quad (1.108)$$

1.5 Second quantization and statistical mechanics

The basic assumption of statistical mechanics is the ergodicity assumption. It states that as time evolves a system assume all possible states complying with the given external constraints, e.g. with a given total energy E . In other words, because of the randomness of the system all of the available phase space is covered. The time it takes for the system to visit all of the phase is the ergodicity time, which is assumed to be smaller than typical time scales of the observation.

Suppose we are interested in some small system connected to the outside world, the so-called reservoir, and assume that, taken as a whole, they constitute a closed system with total energy E_T . Let us call the energy of the small system E_s and that of the reservoir E_r , i.e. $E_T = E_s + E_r$. Based on the ergodicity assumption it is natural to conjecture that the probability for a subsystem to have a definite energy E_s is proportional to the number of ways that the subsystem can have that energy. The density of states is defined as $d(E) = dN(E)/dE$, where $N(E)$ is the number of states with an energy less than E . We denote the density of states of the total system at a given total energy $d(E_T)$, while the small system and the reservoir have the densities of states $d_s(E_s)$ and $d_r(E_r)$,

respectively. Since for a given small energy interval ΔE the number of states in the reservoir is much larger than the number states in smaller subsystem, the total density of states is dominated by that of the reservoir and hence $d(E_T) \approx d_r(E_T)$. From the assumption about the probability being proportional to the number of states, we have for the probability for the subsystem to have energy E_s that

$$P(E_s) \propto d_r(E_T - E_s) \Delta E. \quad (1.109)$$

Now, we do not expect this probability to be dependent on the size of the reservoir, i.e. if we make it smaller by cutting it in half by some wall, nothing should happen to the state of the small system, provided of course that it is still much smaller than the new reservoir. This means that if we consider the ratio of two probabilities

$$\frac{P(E_s)}{P(E'_s)} = \frac{d_r(E_T - E_s)}{d_r(E_T - E'_s)}, \quad (1.110)$$

it must only depend on the energies E_s and E'_s and neither on the total energy E_T nor on d_r . But because the energy is only defined up to an additive constant, it can thus only depend on the difference $E_s - E'_s$. The only function $P(E)$ that satisfies the condition

$$\frac{P(E_s)}{P(E'_s)} = \frac{d_r(E_T - E_s)}{d_r(E_T - E'_s)} = f(E_s - E'_s), \quad (1.111)$$

is

$$P(E) \propto e^{-\beta E}. \quad (1.112)$$

We have thus arrived at the famous Boltzmann or Gibbs distribution which of course should be normalized. In conclusion: from statistical mechanics we know that both for classical and a quantum mechanical systems which are connected to a heat bath the probability for a given state s with energy E_s to be occupied is given by the Boltzmann distribution

$$P(E_s) = \frac{1}{Z} \exp(-\beta E_s), \quad (1.113)$$

where β is the inverse temperature, $\beta = 1/k_B T$, and where the normalization factor, Z , is the partition function

$$Z = \sum_s \exp(-\beta E_s). \quad (1.114)$$

When we sum over states, we must sum over a set of states which cover the entire space of possible states, i.e. the basis set that we use to compute the energy must be a complete set. For a quantum system with many particles, the states s are, as we have seen, in general quite complicated to write down, and it is therefore an advantage to have a form which is independent of the choice of basis states. Also for a quantum system it is not clear what is meant by the energy of a given state, unless of course it is an eigenstate of the Hamiltonian. Therefore the only meaningful interpretation of Eq. (1.114) is that the sum of states runs over eigenstates of the Hamiltonian. Using the basis states $|\nu\rangle$ defined by

$$H|\nu\rangle = E_\nu|\nu\rangle, \quad (1.115)$$

it is now quite natural to introduce the so-called density matrix operator ρ corresponding to the classical Boltzmann factor $e^{-\beta E}$,

$$\rho \equiv e^{-\beta H} = \sum_{\nu} |\nu\rangle e^{-\beta E_{\nu}} \langle \nu|. \quad (1.116)$$

We can thus write the expression Eq. (1.114) for the partition function as

$$Z = \sum_{\nu} \langle \nu | \rho | \nu \rangle = \text{Tr}[\rho]. \quad (1.117)$$

Likewise, the thermal average of any quantum operator A is easily expressed using the density matrix ρ . Following the elementary definition we have

$$\langle A \rangle = \frac{1}{Z} \sum_{\nu} \langle \nu | A | \nu \rangle e^{-\beta E_{\nu}} = \frac{1}{Z} \text{Tr}[\rho A] = \frac{\text{Tr}[\rho A]}{\text{Tr}[\rho]}. \quad (1.118)$$

Eqs. (1.117) and (1.118) are basis-independent expressions, since the sum over states is identified with the trace operation.⁶ This is of course true whatever formalism we use to evaluate the trace. In first quantization the trace runs over for example the determinant basis, which in second quantization translates to the Fock space of the corresponding quantum numbers. For the canonical ensemble the trace is however restricted to run over states with a given number of particles.

For the grand canonical ensemble the number of particles is not conserved. The small system is allowed to exchange particles with the reservoir while keeping its average particle number constant, and we introduce a chemical potential μ of the reservoir to accommodate this constraint. Basically, the result obtained from the canonical ensemble is carried over to the grand canonical ensemble by the substitution $H \rightarrow H - \mu N$, where N is the particle number operator. The corresponding density matrix ρ_G and partition function Z_G are defined as:

$$\rho_G \equiv e^{-\beta(H - \mu N)}, \quad Z_G = \text{Tr}[\rho_G]. \quad (1.119)$$

where the trace now includes states with any number of particles. Likewise, it is useful to introduce the Hamiltonian H_G corresponding to the grand canonical ensemble,

$$H_G \equiv H - \mu N. \quad (1.120)$$

Unfortunately, the symbol H is often used instead of H_G for the grand canonical Hamiltonian, so the reader must always carefully check whether H refers to the canonical or to the grand canonical ensemble. In this book we shall for brevity write H in both cases. This ought not cause any problems, since most of the times we are working in the grand canonical ensemble, i.e. we include the term μN in the Hamiltonian.

The partition functions are fundamental quantities in statistical mechanics. They are more than merely normalization factors. For example the free energy $F \equiv U -$

⁶Remember that if $t_{\nu} = \text{Tr}[A]$ is the trace of A in the basis $|\nu\rangle$, then in the transformed basis $U|\nu\rangle$ we have $t_{U\nu} = \text{Tr}[UAU^{-1}] = \text{Tr}[AU^{-1}U] = \text{Tr}[A] = t_{\nu}$. Here we have used that the trace is invariant under cyclic permutation, i.e. $\text{Tr}[ABC] = \text{Tr}[BCA]$.

TS , important in the grand canonical ensemble, and the thermodynamic potential $\Omega \equiv U - TS - \mu N$, important in the canonical ensemble, are directly related to Z and Z_G , respectively:

$$Z = e^{-\beta F} \quad (1.121a)$$

$$Z_G = e^{-\beta \Omega}. \quad (1.121b)$$

Let us now study the free energy, which is minimal when the entropy is maximal. Recall that

$$F = U - TS = \langle H \rangle - TS. \quad (1.122)$$

In various approximation schemes, for example the mean field approximation in Chap. 4, we shall use the principle of minimizing the free energy. This is based on the following inequality

$$F \leq \langle H \rangle_0 - TS_0, \quad (1.123)$$

where both $\langle H \rangle_0$ and S_0 are calculated in the approximation $\rho \approx \rho_0 = \exp(-\beta H_0)$, for example

$$\langle H \rangle_0 = \frac{\text{Tr}[\rho_0 H]}{\text{Tr}[\rho_0]}. \quad (1.124)$$

This inequality ensures that by minimizing the free energy calculated from the approximate Hamiltonian, we are guaranteed to make the best possible approximation based on the trial Hamiltonian, H_0 .

1.5.1 The distribution function for non-interacting fermions

As the temperature is raised from zero in a system of non-interacting fermions the occupation number for the individual energy eigenstates begins to fluctuate rather than being constantly 0 or constantly 1. Using the grand canonical ensemble we can derive the famous Fermi–Dirac distribution $n_F(\varepsilon)$.

Consider the electron state $|\mathbf{k}\sigma\rangle$ with energy $\varepsilon_{\mathbf{k}}$. The state can contain either 0 or 1 electron. The average occupation $n_F(\varepsilon_{\mathbf{k}})$ is therefore

$$n_F(\varepsilon_{\mathbf{k}}) = \frac{\text{Tr}[\rho_G n_{\mathbf{k}}]}{\text{Tr}[\rho_G]} = \frac{\sum_{n_{\mathbf{k}}=0,1} n_{\mathbf{k}} e^{-\beta(n_{\mathbf{k}}\varepsilon_{\mathbf{k}} - \mu n_{\mathbf{k}})}}{\sum_{n_{\mathbf{k}}=0,1} e^{-\beta(n_{\mathbf{k}}\varepsilon_{\mathbf{k}} - \mu n_{\mathbf{k}})}} = \frac{0 + e^{-\beta(\varepsilon_{\mathbf{k}} - \mu)}}{1 + e^{-\beta(\varepsilon_{\mathbf{k}} - \mu)}} = \frac{1}{e^{\beta(\varepsilon_{\mathbf{k}} - \mu)} + 1}. \quad (1.125)$$

We shall study the properties of the Fermi–Dirac distribution in Sec. 2.1.3. Note that the Fermi–Dirac distribution is defined in the grand canonical ensemble. The proper Hamiltonian is therefore $H_G = H - \mu N$. This is reflected in the single-particle energy variable. From Eq. (1.125) we see that the natural single-particle energy variable is not $\varepsilon_{\mathbf{k}}$ but rather $\xi_{\mathbf{k}}$ given by

$$\xi_{\mathbf{k}} \equiv \varepsilon_{\mathbf{k}} - \mu \quad (1.126)$$

For small excitation energies $\varepsilon_{\mathbf{k}}$ varies around μ whereas $\xi_{\mathbf{k}}$ varies around 0.

1.5.2 Distribution functions for non-interacting bosons

Next we find the distribution function for non-interacting bosons. Again using the grand canonical ensemble we derive the equally famous Bose–Einstein distribution $n_B(\varepsilon)$. It is derived like its fermionic counterpart, the Fermi–Dirac distribution $n_F(\varepsilon)$.

Consider a bosonic state characterized by its fundamental energy $\varepsilon_{\mathbf{k}}$. The occupation number of the state can be any non-negative integer $n_{\mathbf{k}} = 0, 1, 2, \dots$. In the grand canonical ensemble the average occupation number $n_B(\varepsilon_{\mathbf{k}})$ is found by writing $\lambda_{\mathbf{k}} = e^{-\beta(\varepsilon_{\mathbf{k}} - \mu)}$ and using the formulas $\sum_{n=0}^{\infty} n\lambda^n = \lambda \frac{d}{d\lambda} \sum_{n=0}^{\infty} \lambda^n$ and $\sum_{n=0}^{\infty} \lambda^n = \frac{1}{1-\lambda}$:

$$n_B(\varepsilon_{\mathbf{k}}) = \frac{\sum_{n_{\mathbf{k}}=0}^{\infty} n_{\mathbf{k}} e^{-\beta(n_{\mathbf{k}}\varepsilon_{\mathbf{k}} - \mu n_{\mathbf{k}})}}{\sum_{n_{\mathbf{k}}=0}^{\infty} e^{-\beta(n_{\mathbf{k}}\varepsilon_{\mathbf{k}} - \mu n_{\mathbf{k}})}} = \frac{\lambda_{\mathbf{k}} \frac{d}{d\lambda_{\mathbf{k}}} \sum_{n_{\mathbf{k}}=0}^{\infty} \lambda_{\mathbf{k}}^{n_{\mathbf{k}}}}{\sum_{n_{\mathbf{k}}=0}^{\infty} \lambda_{\mathbf{k}}^{n_{\mathbf{k}}}} = \frac{\frac{\lambda_{\mathbf{k}}}{(1-\lambda_{\mathbf{k}})^2}}{\frac{1}{1-\lambda_{\mathbf{k}}}} = \frac{1}{e^{\beta(\varepsilon_{\mathbf{k}} - \mu)} - 1}. \quad (1.127)$$

The Bose–Einstein distribution differs from the Fermi–Dirac distribution by having -1 in the denominator instead of $+1$. Both distributions converge towards the classical Maxwell–Boltzmann distribution, $n_{\mathbf{k}} = e^{-\beta(\varepsilon_{\mathbf{k}} - \mu)}$, for very small occupation numbers, where the particular particle statistics is not felt very strongly.

1.6 Summary and outlook

In this chapter we have introduced second quantization, the representation of quantum mechanics we are going to use throughout this course. The basic concepts are the occupation number basis states and the fundamental creation and annihilation operators, b_{ν}^{\dagger} and b_{ν} in the bosonic case (see Eq. (1.42)), and c_{ν}^{\dagger} and c_{ν} in the fermionic case (see Eq. (1.54)). The intricate permutation symmetries are manifestly ensured by the basic (anti-)commutator relations of these fundamental operators. The main result of the chapter is the derivation of the general form of one- and two-particle operators, Eqs. (1.63) and (1.64) and Fig. 1.5. In fact, perhaps after some measure of acquaintance, this main result appears so simple and intuitively clear that one could choose to define quantum theory directly in second quantization rather than going the cumbersome way from first to second quantization. However, students usually learn basic quantum theory in first quantization, so for pedagogical reasons we have chosen to start from the usual first quantization representation.

In Sec. 1.4 we presented a number of specific examples of second quantization operators, and we got a first glimpse of how second quantization leads to a formulation of quantum physics in terms of creation and annihilation of particles and field quanta. In the following three chapters we shall get more acquainted with second quantization through studies of simplified stationary problems for non-interacting systems or systems where a given particle only interacts with the mean field of the other particles. First in Chap. 5 will the question be raised of how to treat time evolution in second quantization. With an answer to that question we can proceed with the very interesting but also rather difficult studies of the full time dependent dynamics of many-particle quantum systems.

Chapter 2

The electron gas

The study of the interacting electron gas moving in a charge compensating background of positively charged ions is central in this course. Not only is this system a model of the solids that surrounds us, such as metals, semiconductors, and insulators, but historically this system played a major role as testing ground for the development of quantum field theory. In this chapter we shall study the basic properties of this system using the formalism of time-independent second quantization as developed in Chap. 1. The main emphasis will be on the non-interacting electron gas, since it will be clear that we need to develop our theoretical tools further to deal with the electron-electron interactions in full.

Any atom in a metal consists of three parts: the positively charged heavy nucleus at the center, the light cloud of the many negatively charged core electrons tightly bound to the nucleus, and finally, the outermost few valence electrons. The nucleus with its core electrons is denoted an ion. The ion mass is denoted M , and if the atom has Z valence electrons the charge of the ion is $+Ze$. To a large extent the inner degrees of freedom of the ions do not play a significant role leaving the center of mass coordinates \mathbf{R}_j and total spin \mathbf{S}_j of the ions as the only dynamical variables. In contrast to the core electrons the Z valence electrons, with mass m and charge $-e$, are often free to move away from their respective host atoms forming a gas of electrons swirling around among the ions. This is

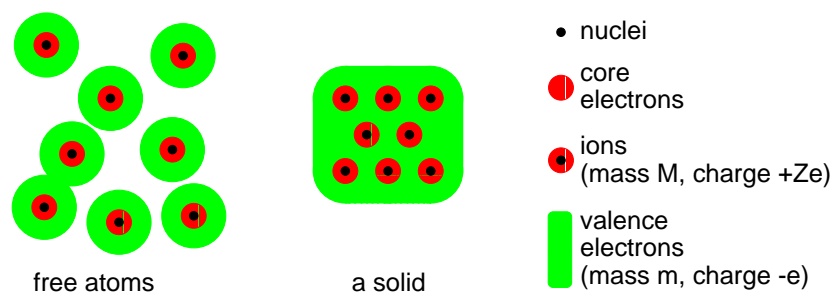


Figure 2.1: A sketch showing N free atoms merging into a metal. The ions are unchanged during the process where they end up by forming a periodic lattice. The valence electrons are freed from their host atoms and form an electron gas holding the ionic lattice together.

true for the alkali metals. The formation of a metal from N independent atoms is sketched in Fig. 2.1.

The Hamiltonian H of the system is written as the sum of kinetic and potential energy of the ionic system and the electronic system treated independently, and the Coulomb interaction between the two systems,

$$H = (T_{\text{ion}} + V_{\text{ion-ion}}) + (T_{\text{el}} + V_{\text{el-el}}) + V_{\text{el-ion}}. \quad (2.1)$$

The individual terms are easily written down in second quantization:

$$\begin{aligned} T_{\text{ion}} + V_{\text{ion-ion}} &= \int d\mathbf{R} \Psi_{\text{ion}}^\dagger(\mathbf{R}) \left(-\frac{\hbar^2}{2M} \nabla_{\mathbf{R}}^2 \right) \Psi_{\text{ion}}(\mathbf{R}) \\ &\quad + \frac{1}{2} \int d\mathbf{R}_1 d\mathbf{R}_2 \Psi_{\text{ion}}^\dagger(\mathbf{R}_1) \Psi_{\text{ion}}^\dagger(\mathbf{R}_2) \frac{Z^2 e_0^2}{|\mathbf{R}_1 - \mathbf{R}_2|} \Psi_{\text{ion}}(\mathbf{R}_2) \Psi_{\text{ion}}(\mathbf{R}_1), \end{aligned} \quad (2.2)$$

$$\begin{aligned} T_{\text{el}} + V_{\text{el-el}} &= \sum_{\sigma} \int d\mathbf{r} \Psi_{\sigma}^\dagger(\mathbf{r}) \left(-\frac{\hbar^2}{2m} \nabla_{\mathbf{r}}^2 \right) \Psi_{\sigma}(\mathbf{r}) \\ &\quad + \frac{1}{2} \sum_{\sigma_1 \sigma_2} \int d\mathbf{r}_1 d\mathbf{r}_2 \Psi_{\sigma_1}^\dagger(\mathbf{r}_1) \Psi_{\sigma_2}^\dagger(\mathbf{r}_2) \frac{e_0^2}{|\mathbf{r}_1 - \mathbf{r}_2|} \Psi_{\sigma_2}(\mathbf{r}_2) \Psi_{\sigma_1}(\mathbf{r}_1), \end{aligned} \quad (2.3)$$

$$V_{\text{el-ion}} = \sum_{\sigma} \int d\mathbf{r} d\mathbf{R} \Psi_{\sigma}^\dagger(\mathbf{r}) \Psi_{\text{ion}}^\dagger(\mathbf{R}) \frac{(-Ze_0^2)}{|\mathbf{R} - \mathbf{r}|} \Psi_{\text{ion}}(\mathbf{R}) \Psi_{\sigma}(\mathbf{r}). \quad (2.4)$$

Note that no double counting is involved in $V_{\text{el-ion}}$ since two different types of fields, $\Psi_{\sigma}^\dagger(\mathbf{r})$ and $\Psi_{\text{ion}}^\dagger(\mathbf{R})$ are involved, hence no factor $\frac{1}{2}$.

At zero temperature the ground state of the system is a periodic ion lattice held together by the cohesive forces of the surrounding electron gas. In principle it is possible in ab initio calculations to minimize the energy of the system and find the crystal structure and lattice parameters, i.e. the equilibrium positions \mathbf{R}_j of the ions in the lattice. From the obtained ground state one can then study the various excitations of the system: phonons (ion vibrations), electron-hole excitations (single-particle excitations), plasmons (collective electronic charge density waves), magnons (spin waves), etc. In this course we will not plunge into such full fledged ab initio calculations. Two approximation schemes will be used instead. One is the phenomenological lattice approach. We take the experimental determination of the crystal structure, lattice parameters and elasticity constants as input to the theory, and from there calculate the electronic and phononic properties. The other approximation scheme, the so-called jellium model, is in fact an ab initio calculation, where however the discrete nature of the ionic system is approximated by a positively charged, continuous and homogeneous fluid, the ion 'jellium'. Fortunately, most electronic and phononic properties of the system can be derived with good accuracy from the Hamiltonian describing the ion jellium combined with the electron gas.

2.1 The non-interacting electron gas

We first study the lattice model and the jellium model in the case of no electron-electron interaction. Later in Sec. 2.2 we attempt to include this interaction.

2.1.1 Bloch theory of electrons in a static ion lattice

Let us first consider the phenomenological lattice model. X-ray experiments show that the equilibrium positions of the ions form a periodic lattice. This lattice has an energy E_{latt} and an electrical potential $V_{\text{el-latt}}$ associated with it, both originating from a combination of T_{ion} , $V_{\text{ion-ion}}$, and $V_{\text{el-ion}}$ in the original Hamiltonian Eq. (2.1). At finite temperature the ions can vibrate around their equilibrium positions with the total electric field acting as the restoring force. As will be demonstrated in Chap. 3, these vibrations can be described in terms of quantized harmonic oscillators (much like the photon field of Sec. 1.4.2) giving rise to the concept of phonons. The non-interacting part of the phonon field is described by a Hamiltonian H_{ph} . Finally, the electrons are described by their kinetic energy T_{el} , their mutual interaction $V_{\text{el-el}}$, and their interaction with both the static part of the lattice, $V_{\text{el-latt}}$, and the vibrating part, i.e. the phonons, $V_{\text{el-ph}}$. The latter term must be there since a vibrating ion is giving rise to a vibrating electrical potential influencing the electrons. Thus the Hamiltonian for the phenomenological lattice model changes H of Eq. (2.1) into

$$H = (E_{\text{latt}} + H_{\text{ph}}) + (T_{\text{el}} + V_{\text{el-el}}) + (V_{\text{el-latt}} + V_{\text{el-ph}}). \quad (2.5)$$

At zero temperature the ions are not vibrating except for their quantum mechanical zero point motion. Thus we can drop all the phonon related terms of the Hamiltonian. If one furthermore neglects the electron-electron interaction (in Sec. 2.2 we study when this is reasonable) one arrives at the Hamiltonian H_{Bloch} used in Bloch's theory of non-interacting electrons moving in a static, periodic ion lattice:

$$H_{\text{Bloch}} = T_{\text{el}} + V_{\text{el-latt}}(\mathbf{r}), \quad \begin{cases} V_{\text{el-latt}}(\mathbf{r} + \mathbf{R}) = V_{\text{el-latt}}(\mathbf{r}) \\ \text{for any lattice vector } \mathbf{R}. \end{cases} \quad (2.6)$$

To solve the corresponding Schrödinger equation, and later the phonon problem, we have to understand the Fourier transform of periodic functions.

Let the static ion lattice be described by the ionic equilibrium positions \mathbf{R} in terms of the lattice basis vectors $\{\mathbf{a}_1, \mathbf{a}_2, \mathbf{a}_3\}$:

$$\mathbf{R} = n_1 \mathbf{a}_1 + n_2 \mathbf{a}_2 + n_3 \mathbf{a}_3, \quad n_1, n_2, n_3 \in \mathbb{Z}. \quad (2.7)$$

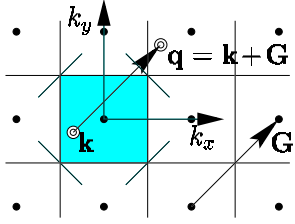
Working with periodic lattices it is often convenient to Fourier transform from the direct space to \mathbf{k} -space, also known as the reciprocal space, RS. It is useful to introduce the reciprocal lattice, RL, in RS defined by

$$\text{RL} = \left\{ \mathbf{G} \in \text{RS} \left| e^{i\mathbf{G} \cdot \mathbf{R}} = 1 \right. \right\} \Rightarrow \mathbf{G} = m_1 \mathbf{b}_1 + m_2 \mathbf{b}_2 + m_3 \mathbf{b}_3, \quad m_1, m_2, m_3 \in \mathbb{Z}, \quad (2.8)$$

where the basis vectors $\{\mathbf{b}_1, \mathbf{b}_2, \mathbf{b}_3\}$ in RL are defined as

$$\mathbf{b}_1 = 2\pi \frac{\mathbf{a}_2 \times \mathbf{a}_3}{\mathbf{a}_1 \cdot \mathbf{a}_2 \times \mathbf{a}_3}, \quad \mathbf{b}_2 = 2\pi \frac{\mathbf{a}_3 \times \mathbf{a}_1}{\mathbf{a}_2 \cdot \mathbf{a}_3 \times \mathbf{a}_1}, \quad \mathbf{b}_3 = 2\pi \frac{\mathbf{a}_1 \times \mathbf{a}_2}{\mathbf{a}_3 \cdot \mathbf{a}_1 \times \mathbf{a}_2}. \quad (2.9)$$

An important concept is the first Brillouin zone, FBZ, defined as all \mathbf{k} in RS lying closer to $\mathbf{G} = 0$ than to any other reciprocal lattice vector $\mathbf{G} \neq 0$. Using vectors $\mathbf{k} \in \text{FBZ}$, any wavevector $\mathbf{q} \in \text{RS}$ can be decomposed (the figure shows the FBZ for a 2D square lattice):



$$\text{FBZ} = \left\{ \mathbf{k} \in \text{RS} \mid |\mathbf{k}| < |\mathbf{k} - \mathbf{G}|, \text{ for all } \mathbf{G} \neq 0 \right\}$$

$$\Downarrow$$

$$\forall \mathbf{q}, \exists \mathbf{k} \in \text{FBZ}, \exists \mathbf{G} \in \text{RL} : \mathbf{q} = \mathbf{k} + \mathbf{G}. \quad (2.10)$$

The Fourier transform of any function periodic in the lattice is as follows:

$$V(\mathbf{r} + \mathbf{R}) = V(\mathbf{r}), \text{ for all } \mathbf{R} \quad \Leftrightarrow \quad V(\mathbf{r}) = \sum_{\mathbf{G} \in \text{RL}} V_{\mathbf{G}} e^{i\mathbf{G} \cdot \mathbf{r}}. \quad (2.11)$$

The solution of the Schrödinger equation $H_{\text{Bloch}}\psi = E\psi$ can be found in the plane wave basis $|\mathbf{k}\sigma\rangle$, which separates in spatial part $e^{i\mathbf{k} \cdot \mathbf{r}}$ and a spin part χ_{σ} , e.g. $\chi_{\uparrow} = \begin{pmatrix} 1 \\ 0 \end{pmatrix}$:

$$\psi_{\sigma}(\mathbf{r}) \equiv \frac{1}{\mathcal{V}} \sum_{\mathbf{k}'} c_{\mathbf{k}'} e^{i\mathbf{k}' \cdot \mathbf{r}} \chi_{\sigma} \Rightarrow \langle \mathbf{k}\sigma | H_{\text{Bloch}} | \psi_{\sigma} \rangle = \sum_{\mathbf{k}'} \left(\varepsilon_{\mathbf{k}} \delta_{\mathbf{k}, \mathbf{k}'} + \sum_{\mathbf{G}} V_{\mathbf{G}} \delta_{\mathbf{k}, \mathbf{k}'+\mathbf{G}} \right) c_{\mathbf{k}'}, \quad (2.12)$$

so the Schrödinger equation for a given \mathbf{k} is

$$c_{\mathbf{k}} \varepsilon_{\mathbf{k}} + \sum_{\mathbf{G}} V_{\mathbf{G}} c_{\mathbf{k}-\mathbf{G}} = E c_{\mathbf{k}}. \quad (2.13)$$

We see that any given coefficient $c_{\mathbf{k}}$ only couples to other coefficients of the form $c_{\mathbf{k}+\mathbf{G}}$, i.e. each Schrödinger equation of the form Eq. (2.13) for $c_{\mathbf{k}}$ couples to an infinite, but countable, number of similar equations for $c_{\mathbf{k}-\mathbf{G}}$. Each such infinite family of equations has exactly one representative $\mathbf{k} \in \text{FBZ}$, while any \mathbf{k} outside FBZ does not give rise to a new set of equations. The infinite family of equations generated by a given $\mathbf{k} \in \text{FBZ}$ gives rise to a discrete spectrum of eigenenergies $\varepsilon_{n\mathbf{k}}$, where $n \in \mathbb{N}$. The corresponding eigenfunctions $\psi_{n\mathbf{k}\sigma}$ are given by:

$$\psi_{n\mathbf{k}\sigma}(\mathbf{r}) = \frac{1}{\mathcal{V}} \sum_{\mathbf{G}} c_{\mathbf{k}+\mathbf{G}}^{(n)} e^{i(\mathbf{G}+\mathbf{k}) \cdot \mathbf{r}} \chi_{\sigma} = \left(\frac{1}{\mathcal{V}} \sum_{\mathbf{G}} c_{\mathbf{G}}^{(n\mathbf{k})} \right) e^{i\mathbf{k} \cdot \mathbf{r}} \chi_{\sigma} \equiv u_{n\mathbf{k}}(\mathbf{r}) e^{i\mathbf{k} \cdot \mathbf{r}} \chi_{\sigma}. \quad (2.14)$$

According to Eq. (2.11) the function $u_{n\mathbf{k}}(\mathbf{r})$ is periodic in the lattice, and thus we end with Bloch's theorem¹:

$$H_{\text{Bloch}} \psi_{n\mathbf{k}\sigma} = \varepsilon_{n\mathbf{k}} \psi_{n\mathbf{k}\sigma}, \quad \psi_{n\mathbf{k}\sigma}(\mathbf{r}) = u_{n\mathbf{k}}(\mathbf{r}) e^{i\mathbf{k} \cdot \mathbf{r}} \chi_{\sigma}, \quad \begin{cases} \mathbf{k} \in \text{FBZ}, \\ n \text{ is the band index}, \\ u_{n\mathbf{k}}(\mathbf{r} + \mathbf{R}) = u_{n\mathbf{k}}(\mathbf{r}). \end{cases} \quad (2.15)$$

¹An alternative derivation of Bloch's theorem with emphasis on the group theoretic aspects builds on the translation operator $T_{\mathbf{R}}$, with $T_{\mathbf{R}} f(\mathbf{r}) \equiv f(\mathbf{r} + \mathbf{R})$. We get $[H, T_{\mathbf{R}}] = 0 \Rightarrow T_{\mathbf{R}} \psi = \lambda_{\mathbf{R}} \psi$ for an eigenstate ψ . Applying $T_{\mathbf{P}}$ after $T_{\mathbf{R}}$ leads to $\lambda_{\mathbf{P}} \lambda_{\mathbf{R}} = \lambda_{\mathbf{P}+\mathbf{R}} \Rightarrow \lambda_{\mathbf{R}} = e^{i\mathbf{k} \cdot \mathbf{R}} \Rightarrow \psi_{n\mathbf{k}}(\mathbf{r}) = u_{n\mathbf{k}}(\mathbf{r}) e^{i\mathbf{k} \cdot \mathbf{r}}$.

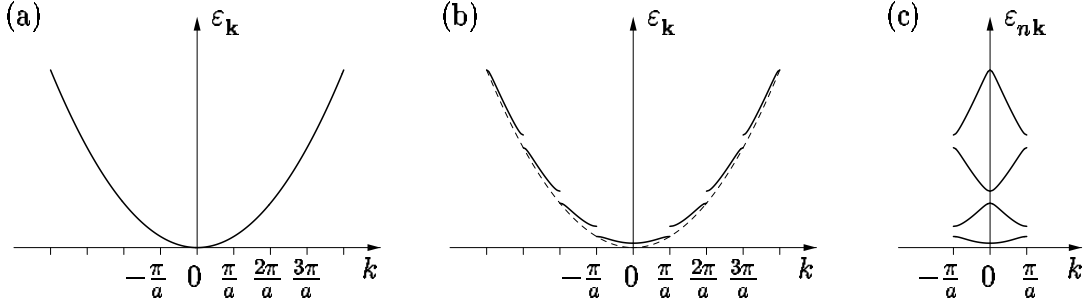


Figure 2.2: Bloch's theorem illustrated for a 1D lattice with lattice constant a . (a) The parabolic energy band for free electrons. (b) The Bloch bands viewed as a break-up of the parabolic free electron band in Brillouin zones (the extended zone scheme, $\mathbf{k} \in \text{RS}$). (c) All wavevectors are equivalent to those in the FBZ, so it is most natural to displace all the energy branches into the FBZ (the reduced zone scheme, $\mathbf{k} \in \text{FBZ}$).

The eigenfunctions are seen to be plane waves modulated by a periodic function $u_{n\mathbf{k}}(\mathbf{r})$ having the same periodicity as the lattice. For many applications it turns out that the Bloch electrons described by $\psi_{n\mathbf{k}\sigma}(\mathbf{r})$ can be approximated by plane waves if at the same time the electronic mass m is changed into a material dependent effective mass m^* . We shall use this so-called effective mass approximation throughout this course:²

$$\begin{array}{lcl} \text{The effective mass} & : & \left\{ \begin{array}{ll} \psi_{n\mathbf{k}\sigma} & \rightarrow \frac{1}{\sqrt{V}} e^{i\mathbf{k}\cdot\mathbf{r}} \chi_{\sigma} \\ m & \rightarrow m^* \\ \mathbf{k} & \text{unrestricted.} \end{array} \right. \end{array} \quad (2.16)$$

In the following, when no confusion is possible, m^* is often simply written as m .

2.1.2 Non-interacting electrons in the jellium model

In the effective mass approximation of the lattice model the electron eigenstates are plane waves. Also the jellium model results in plane wave solutions, which are therefore of major interest to study.

In the jellium model the ion charges are imagined to be smeared out to form a homogeneous and, to begin with, static positive charge density, $+Z\rho_{\text{jel}}$, the ion jellium. The periodic potential, $V_{\text{el-latt}}$, present in a real lattice becomes the constant potential $V_{\text{el-jel}}$ as sketched in Fig. 2.3. If we concentrate on the homogeneous part of the electron gas, i.e. discard the part of $V_{\text{el-el}}$ that leads to inhomogeneities, we notice that this part together with the ion jellium forms a completely charge neutral system. In other words, in H of Eq. (2.1) we have $V_{\text{ion-ion}} + V_{\text{el-el}} + V_{\text{el-ion}} = 0$, and we simply end up with

$$H_{\text{jel}} = T_{\text{el}}. \quad (2.17)$$

For a box with side lengths L_x , L_y , and L_z and volume $\mathcal{V} = L_x L_y L_z$ the single-particle basis states are the simple plane wave solutions to the free particle Schrödinger equation

²For a derivation of the effective mass approximation see e.g. Kittel or Ashcroft and Mermin.

with periodic boundary conditions $\psi(L, y, z) = \psi(0, y, z)$ and $\psi'(L, y, z) = \psi'(0, y, z)$ (likewise for the y and z directions). We prefer the periodic boundary conditions rather than the Dirichlet boundary conditions $\psi(0, y, z) = 0$ and $\psi(L, y, z) = 0$ (likewise for the y and z directions), since the former gives current carrying eigenstates well suited for the description of transport phenomena, while the latter yield standing waves carrying no current. The single-particle basis states are thus

$$H_{\text{jel}} \psi_{\mathbf{k}\sigma} = \frac{\hbar^2 k^2}{2m} \psi_{\mathbf{k}\sigma}, \quad \psi_{\mathbf{k}\sigma}(\mathbf{r}) = \frac{1}{\sqrt{\mathcal{V}}} e^{i\mathbf{k}\cdot\mathbf{r}} \chi_{\sigma}, \quad \begin{cases} k_x = \frac{2\pi}{L_x} n_x \text{ (same for } y \text{ and } z) \\ n_x = 0, \pm 1, \pm 2, \dots \\ \mathcal{V} = L_x L_y L_z, \end{cases} \quad (2.18)$$

and with this basis we obtain H_{jel} in second quantization:

$$H_{\text{jel}} = \sum_{\sigma} \int d\mathbf{r} \Psi_{\sigma}^{\dagger}(\mathbf{r}) \left(-\frac{\hbar^2}{2m} \nabla^2 \right) \Psi_{\sigma}(\mathbf{r}) = \sum_{\mathbf{k}\sigma} \frac{\hbar^2 k^2}{2m} c_{\mathbf{k}\sigma}^{\dagger} c_{\mathbf{k}\sigma}. \quad (2.19)$$

Note how the quantization of \mathbf{k} means that one state fills a volume $\frac{2\pi}{L_x} \frac{2\pi}{L_y} \frac{2\pi}{L_z} = \frac{(2\pi)^3}{\mathcal{V}}$ in \mathbf{k} -space, from which we obtain the following important rule of great practical value:

$$\sum_{\mathbf{k}} \rightarrow \frac{\mathcal{V}}{(2\pi)^3} \int d\mathbf{k}. \quad (2.20)$$

For the further analysis in second quantization it is natural to order the single-particle states $\psi_{\mathbf{k}\sigma}(\mathbf{r}) = |\mathbf{k}\sigma\rangle$ according to their energies $\varepsilon_{\mathbf{k}} = \frac{\hbar^2 k^2}{2m}$ in ascending order,

$$|\mathbf{k}_1, \uparrow\rangle, |\mathbf{k}_1, \downarrow\rangle, |\mathbf{k}_2, \uparrow\rangle, |\mathbf{k}_2, \downarrow\rangle, \dots, \quad \text{where } \varepsilon_{\mathbf{k}_1} \leq \varepsilon_{\mathbf{k}_2} \leq \varepsilon_{\mathbf{k}_3} \leq \dots \quad (2.21)$$

The ground state for N electrons at zero temperature is denoted the Fermi sea or the Fermi sphere $|\text{FS}\rangle$. It is obtained by filling up the N states with the lowest possible energy,

$$|\text{FS}\rangle \equiv c_{\mathbf{k}_{N/2}\uparrow}^{\dagger} c_{\mathbf{k}_{N/2}\downarrow}^{\dagger} \dots c_{\mathbf{k}_2\uparrow}^{\dagger} c_{\mathbf{k}_2\downarrow}^{\dagger} c_{\mathbf{k}_1\uparrow}^{\dagger} c_{\mathbf{k}_1\downarrow}^{\dagger} |0\rangle. \quad (2.22)$$

The energy of the topmost occupied state is denoted the Fermi energy, ε_{F} . Associated with ε_{F} is the Fermi wavenumber k_{F} , the Fermi wave length λ_{F} , and the Fermi velocity v_{F} :

$$k_{\text{F}} = \frac{1}{\hbar} \sqrt{2m\varepsilon_{\text{F}}}, \quad \lambda_{\text{F}} = \frac{2\pi}{k_{\text{F}}}, \quad v_{\text{F}} = \frac{\hbar k_{\text{F}}}{m}. \quad (2.23)$$

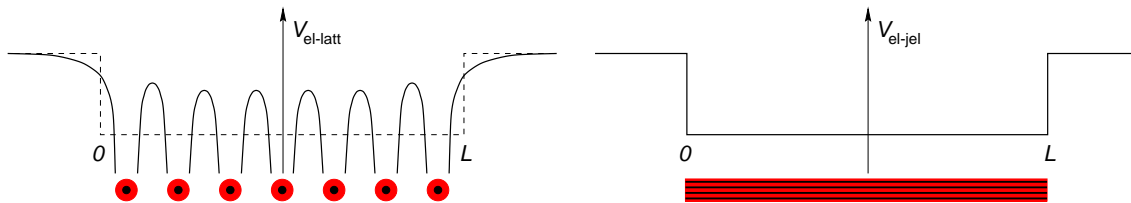


Figure 2.3: A sketch showing the periodic potential, $V_{\text{el-latt}}$, present in a real lattice, and the imagined smeared out potential $V_{\text{el-jel}}$ of the jellium model.

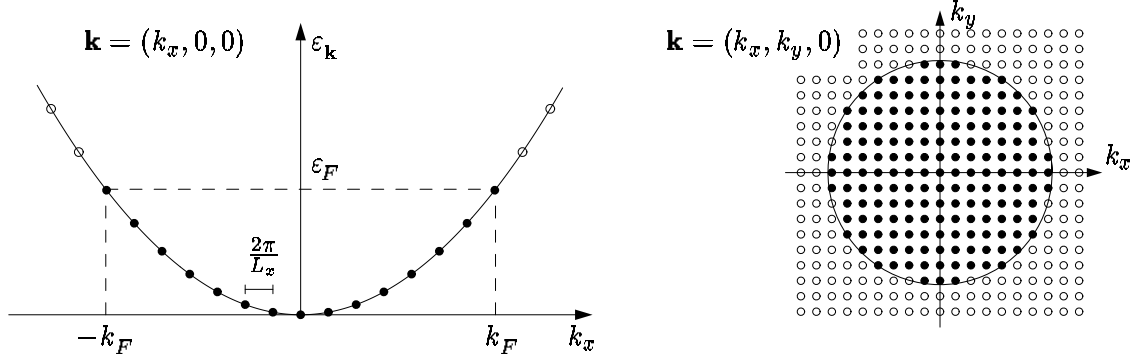


Figure 2.4: Two aspects of $|\text{FS}\rangle$ in \mathbf{k} -space. To the left the dispersion relation $\varepsilon_{\mathbf{k}}$ is plotted along the line $\mathbf{k} = (k_x, 0, 0)$, and ε_F and k_F are indicated. To the right the occupation of the states is shown in the plane $\mathbf{k} = (k_x, k_y, 0)$. The Fermi sphere is shown as a circle with radius k_F . Filled and empty circles represent occupied and unoccupied states, respectively.

Thus in $|\text{FS}\rangle$ all states with $\varepsilon_{\mathbf{k}} < \varepsilon_F$ or $|\mathbf{k}| < k_F$ are occupied and the rest are unoccupied. A sketch of $|\text{FS}\rangle$ in energy- and \mathbf{k} -space is shown in Fig. 2.4.

As a first exercise we calculate the relation between the macroscopic quantity $n = N/\mathcal{V}$, the density, and the microscopic quantity k_F , the Fermi wavenumber.

$$N = \langle \text{FS} | \hat{N} | \text{FS} \rangle = \langle \text{FS} | \sum_{\mathbf{k}\sigma} n_{\mathbf{k}\sigma} | \text{FS} \rangle = \sum_{\sigma} \frac{\mathcal{V}}{(2\pi)^3} \int d\mathbf{k} \langle \text{FS} | n_{\mathbf{k}\sigma} | \text{FS} \rangle. \quad (2.24)$$

The matrix element is easily evaluated, since $n_{\mathbf{k}\sigma} |\text{FS}\rangle = |\text{FS}\rangle$ for $|\mathbf{k}| < k_F$ and 0 otherwise. This is written in terms of the theta function³

$$N = \sum_{\sigma} \frac{\mathcal{V}}{(2\pi)^3} \int d\mathbf{k} \theta(k_F - |\mathbf{k}|) \langle \text{FS} | \text{FS} \rangle = \frac{2\mathcal{V}}{(2\pi)^3} \int_0^{k_F} dk k^2 \int_{-1}^1 d(\cos \theta) \int_0^{2\pi} d\phi 1 = \frac{\mathcal{V}}{3\pi^2} k_F^3, \quad (2.25)$$

and we arrive at the extremely important formula:

$$k_F^3 = 3\pi^2 n. \quad (2.26)$$

This formula allows us to obtain the values of the microscopic parameters k_F , ε_F , and v_F . Hall measurements yield the electron density of copper⁴, $n = 8.47 \times 10^{28} \text{ m}^{-3}$, and from Eqs. (2.23) and (2.26) it thus follows that for copper

$$\begin{aligned} k_F &= 13.6 \text{ nm}^{-1} & \varepsilon_F &= 7.03 \text{ eV} = 81600 \text{ K} \\ \lambda_F &= 0.46 \text{ nm} & v_F &= 1.57 \times 10^6 \text{ m/s} = 0.005 c. \end{aligned} \quad (2.27)$$

³ $\theta(x) = 1$ for $x > 0$ and $\theta(x) = 0$ for $x < 0$

⁴The density can also be estimated as follows. The inter-atomic distances are typically $\simeq 2 \text{ \AA}$. In monovalent Cu one electron thus occupies a volume $\simeq (2 \times 10^{-10} \text{ m})^3$, and $n \approx 10^{29} \text{ m}^{-3}$ follows.

Note that the Fermi energy corresponds to an extremely high temperature, which we shall return to shortly, and even though the Fermi velocity is large it is still less than a percent of the velocity of light, and we need not invoke relativistic considerations.

We move on to calculate the ground state energy $E^{(0)}$:

$$\begin{aligned} E^{(0)} &= \langle \text{FS} | H_{\text{jel}} | \text{FS} \rangle = \sum_{\mathbf{k}\sigma} \frac{\hbar^2 k^2}{2m} \langle \text{FS} | n_{\mathbf{k}\sigma} | \text{FS} \rangle = 2 \frac{\mathcal{V}}{(2\pi)^3} \frac{\hbar^2}{2m} \int d\mathbf{k} k^2 \theta(k_F - |\mathbf{k}|) \\ &= \frac{2\mathcal{V}}{(2\pi)^3} \frac{\hbar^2}{2m} \int_0^{k_F} dk k^4 \int_{-1}^1 d(\cos \theta) \int_0^{2\pi} d\phi = \frac{\mathcal{V}}{5\pi^2} \frac{\hbar^2}{2m} k_F^5 = \frac{3}{5} N \varepsilon_F. \end{aligned} \quad (2.28)$$

In the last equation we again used Eq. (2.26). The result is reasonable, since the system consists of N electrons each with an energy $0 < \varepsilon_{\mathbf{k}} < \varepsilon_F$. The kinetic energy per particle becomes an important quantity when we in the next section begin to study the Coulomb interaction. By Eqs. (2.26) and (2.28) it can be expressed in terms of n :

$$\frac{E^{(0)}}{N} = \frac{3}{5} \frac{\hbar^2}{2m} k_F^2 = \frac{3}{5} \frac{\hbar^2}{2m} (3\pi^2)^{\frac{2}{3}} n^{\frac{2}{3}}. \quad (2.29)$$

The next concept to be introduced for the non-interacting electron gas is the density of states $D(\varepsilon) = \frac{dN}{d\varepsilon}$, counting the number ΔN of states in the energy interval $\Delta\varepsilon$ around the energy ε , $\Delta N = D(\varepsilon)\Delta\varepsilon$, and the density of states per volume $d(\varepsilon) = D(\varepsilon)/\mathcal{V} = \frac{dn}{d\varepsilon}$. Again using Eq. (2.26) we find

$$\varepsilon_F = \frac{\hbar^2}{2m} k_F^2 = \frac{\hbar^2}{2m} (3\pi^2)^{\frac{2}{3}} n^{\frac{2}{3}} \Rightarrow n(\varepsilon) = \frac{1}{3\pi^2} \left(\frac{2m}{\hbar^2} \right)^{\frac{3}{2}} \varepsilon^{\frac{3}{2}}, \text{ for } \varepsilon > 0, \quad (2.30)$$

and from this

$$d(\varepsilon) = \frac{dn}{d\varepsilon} = \frac{1}{2\pi^2} \left(\frac{2m}{\hbar^2} \right)^{\frac{3}{2}} \varepsilon^{\frac{1}{2}} \theta(\varepsilon), \quad D(\varepsilon) = \frac{dN}{d\varepsilon} = \frac{\mathcal{V}}{2\pi^2} \left(\frac{2m}{\hbar^2} \right)^{\frac{3}{2}} \varepsilon^{\frac{1}{2}} \theta(\varepsilon). \quad (2.31)$$

The density of states is a very useful function. In the following we shall for example demonstrate how in terms of $D(\varepsilon)$ to calculate the particle number, $N = \int d\varepsilon D(\varepsilon)$, and the total energy, $E^{(0)} = \int d\varepsilon \varepsilon D(\varepsilon)$.

2.1.3 Non-interacting electrons at finite temperature

Finally, before turning to the problem of the Coulomb interaction, we study some basic temperature dependencies. As temperature is raised from zero the occupation number is given by the Fermi-Dirac distribution $n_F(\varepsilon_{\mathbf{k}})$, see Eq. (1.125). The main characteristics of this function is shown in Fig. 2.5. Note that to be able to see any effects of the temperature in Fig. 2.5, kT is set to $0.03 \varepsilon_F$ corresponding to $T \approx 2400$ K. Room temperature yields $kT/\varepsilon_F \approx 0.003$, thus the low temperature limit of $n_F(\varepsilon_{\mathbf{k}})$ is of importance:

$$n_F(\varepsilon_{\mathbf{k}}) = \frac{1}{e^{\beta(\varepsilon_{\mathbf{k}} - \mu)} + 1} \xrightarrow{T \rightarrow 0} \theta(\mu - \varepsilon_{\mathbf{k}}), \quad -\frac{\partial n_F}{\partial \varepsilon_{\mathbf{k}}} = \frac{\beta}{4 \cosh^2[\frac{\beta}{2}(\varepsilon_{\mathbf{k}} - \mu)]} \xrightarrow{T \rightarrow 0} \delta(\mu - \varepsilon_{\mathbf{k}}). \quad (2.32)$$

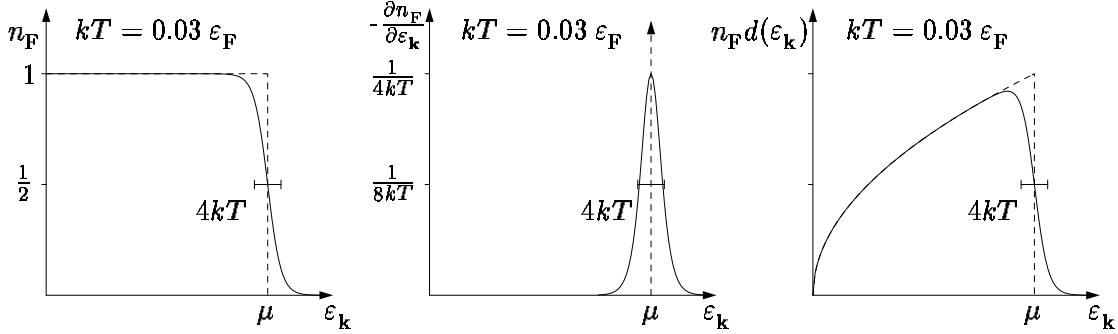


Figure 2.5: The Fermi-Dirac distribution $n_F(\epsilon_{\mathbf{k}})$, its derivative $-\frac{\partial n_F}{\partial \epsilon_{\mathbf{k}}}$, and its product with the density of states, $n_F(\epsilon_{\mathbf{k}})d(\epsilon_{\mathbf{k}})$, shown at the temperature $kT = 0.03 \epsilon_F$, corresponding to $T = 2400$ K in metals. This rather high value is chosen to have a clearly observable deviation from the $T = 0$ case, which is indicated by the dashed lines.

Note that, as mentioned in Sec. 1.5.1, the natural single-particle energy variable in these fundamental expressions actually is $\xi_{\mathbf{k}} = \epsilon_{\mathbf{k}} - \mu$ and not $\epsilon_{\mathbf{k}}$ itself.

At $T = 0$ the chemical potential μ is identical to ϵ_F . But in fact μ varies slightly with temperature. A careful analysis based on the so-called Sommerfeld expansion combined with the fact that the number of electrons does not change with temperature yields

$$n(T=0) = n(T) = \int_0^\infty d\epsilon d(\epsilon) f(\epsilon) \quad \Rightarrow \quad \mu(T) = \epsilon_F \left[1 - \frac{\pi^2}{12} \left(\frac{kT}{\epsilon_F} \right)^2 + \dots \right] \quad (2.33)$$

Because ϵ_F according to Eq. (2.27) is around 80000 K for metals, we find that even at the melting temperature of metals only a very limited number ΔN of electrons are affected by thermal fluctuations. Indeed, only the states within $2kT$ of ϵ_F are actually affected, and more precisely we have $\Delta N/N = 6kT/\epsilon_F$ ($\approx 10^{-3}$ at room temperature). The Fermi sphere is not destroyed by heating, it is only slightly smeared. Now we have at hand an explanation of the old paradox in thermodynamics, as to why only the ionic vibrational degrees of freedom contribute significantly to the specific heat of solids. The electronic degrees of freedom are simply 'frozen' in. Only at temperatures comparable to ϵ_F they begin to play a major role. As we shall see in Sec. 2.3.1 this picture is not true for semiconductors, where the electron density is much smaller than in metals.

2.2 Electron interactions in perturbation theory

We now apply standard perturbation theory to take the inhomogeneous part of the electron-electron interaction $V_{\text{el-el}}$ of Eq. (2.3) into account. The homogeneous part, which in \mathbf{k} -space (see Eqs. (1.103) and (1.104)) corresponds to a vanishing wavevector $\mathbf{q} = 0$, has already been taken into account in the jellium model to cancel the homogeneous positive background. We thus exclude the $\mathbf{q} = 0$ term in the following sums, which is indicated by

a prime:

$$V'_{\text{el-el}} = \frac{1}{2\mathcal{V}} \sum'_{\mathbf{k}_1 \mathbf{k}_2 \mathbf{q}} \sum_{\sigma_1 \sigma_2} \frac{4\pi e_0^2}{q^2} c_{\mathbf{k}_1 + \mathbf{q} \sigma_1}^\dagger c_{\mathbf{k}_2 - \mathbf{q} \sigma_2}^\dagger c_{\mathbf{k}_2 \sigma_2} c_{\mathbf{k}_1 \sigma_1}. \quad (2.34)$$

However, as we shall see, the direct use of this interaction with the tools developed so far becomes the story of the rise and fall of simple minded perturbation theory. The first order calculation works well and good physical conclusions can be drawn, but already in second order the calculation collapses due to divergent integrals. It turns out that to get rid of these divergences the more powerful tools of quantum field theory must be invoked. But let us see how we arrive at these conclusions.

A natural question arises: under which circumstances can the non-interacting electron gas actually serve as a starting point for a perturbation expansion in the interaction potential. The key to the answer lies in the density dependence of the kinetic energy $E_{\text{kin}} = E^{(0)}/N \propto n^{\frac{2}{3}}$ displayed in Eq. (2.29). This is to be compared to the typical potential energy of particles with a mean distance \bar{d} , $E_{\text{pot}} \simeq e_0^2/\bar{d} \propto n^{\frac{1}{3}}$. So we find that

$$\frac{E_{\text{pot}}}{E_{\text{kin}}} \propto \frac{n^{\frac{1}{3}}}{n^{\frac{2}{3}}} = n^{-\frac{1}{3}} \xrightarrow{n \rightarrow \infty} 0, \quad (2.35)$$

revealing the following perhaps somewhat counter intuitive fact: the importance of the electron-electron interacting diminishes as the density of the electron gas increases. Due to the Pauli exclusion principle the kinetic energy simply becomes the dominant energy scale in the interacting electron gas at high densities. Consequently, we approach the problem from this limit in the following analysis.

We begin the perturbation treatment by establishing the relevant length scale and energy scale for the problem of interacting charges. The prototypical example is of course the hydrogen atom, where a single electron orbits a proton. The ground state is a spherical symmetric s-wave with a radius denoted the Bohr radius a_0 and an energy E_0 . The following considerations may be helpful mnemotechnically. The typical length scale a_0 yields a typical momentum $p = \hbar/a_0$. Writing E_0 as the sum of kinetic energy $p^2/2m$ and potential energy $-e_0^2/a_0$, we arrive at $E_0 = \frac{\hbar^2}{2ma_0^2} - \frac{e_0^2}{a_0}$. The values of a_0 and E_0 are found either by minimization, $\frac{\partial E_0}{\partial a_0} = 0$, or by using the virial theorem $E_{\text{kin}} = -\frac{1}{2}E_{\text{pot}}$:

$$a_0 = \frac{\hbar^2}{me_0^2} = 0.053 \text{ nm}, \quad E_0 = -\frac{e_0^2}{2a_0} = -13.6 \text{ eV}, \quad 1 \text{ Ry} = \frac{e_0^2}{2a_0} = 13.6 \text{ eV}. \quad (2.36)$$

Here we have also introduced the energy unit 1 Ry often encountered in atomic physics as defining a natural energy scale. Lengths are naturally measured in units a_0 , and the dimensionless measure r_s of the average inter-electronic distance in the electron gas is introduced as the radius in a sphere containing exactly one electron:

$$\frac{4\pi}{3}(r_s a_0)^3 = \frac{1}{n} = \frac{3\pi^2}{k_F^3} \Rightarrow a_0 k_F = \left(\frac{9\pi}{4}\right)^{\frac{1}{3}} r_s^{-1} \Rightarrow r_s = \left(\frac{9\pi}{4}\right)^{\frac{1}{3}} \frac{1}{a_0 k_F}. \quad (2.37)$$

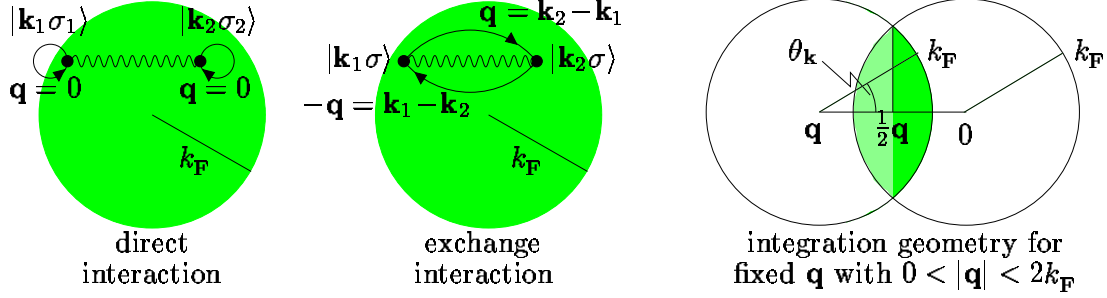


Figure 2.6: The two possible processes in first order perturbation theory for two states $|\mathbf{k}_1\sigma_1\rangle$ and $|\mathbf{k}_2\sigma_2\rangle$ in the Fermi sea. The direct process having $\mathbf{q} = 0$ is already taken into account in the homogeneous part, hence only the exchange process contributes to $V'_{\text{el-el}}$. Also the geometry for the \mathbf{k} -integration is shown for an arbitrary but fixed value of \mathbf{q} .

Rewriting the energy $E^{(0)}$ of the non-interacting electron gas to these units we obtain:

$$\frac{E^{(0)}}{N} = \frac{3}{5} \frac{1}{2} \frac{\hbar^2}{m} k_F^2 = \frac{3}{5} \frac{1}{2} (a_0 e_0^2) \frac{(a_0 k_F)^2}{a_0^2} = \frac{3}{5} \left(\frac{9\pi}{4} \right)^{\frac{2}{3}} \frac{e_0^2}{2a_0} r_s^{-2} \approx \frac{2.21}{r_s^2} \text{ Ry.} \quad (2.38)$$

This constitutes the zero'th order energy in our perturbation calculation.

2.2.1 Electron interactions in 1st order perturbation theory

The first order energy $E^{(1)}$ is found by the standard perturbation theory procedure:

$$\frac{E^{(1)}}{N} = \frac{\langle \text{FS} | V'_{\text{el-el}} | \text{FS} \rangle}{N} = \frac{1}{2\mathcal{V}N} \sum'_{\mathbf{q}} \sum_{\mathbf{k}_1, \mathbf{k}_2} \sum_{\sigma_1, \sigma_2} \frac{4\pi e_0^2}{q^2} \langle \text{FS} | c_{\mathbf{k}_1+\mathbf{q}\sigma_1}^\dagger c_{\mathbf{k}_2-\mathbf{q}\sigma_2}^\dagger c_{\mathbf{k}_2\sigma_2} c_{\mathbf{k}_1\sigma_1} | \text{FS} \rangle. \quad (2.39)$$

The matrix element is evaluated as follows. First, the two annihilation operators can only give a non-zero result if both $|\mathbf{k}_1| < k_F$ and $|\mathbf{k}_2| < k_F$. Second, the factor $\langle \text{FS} |$ demands that the two creation operators bring us back to $|\text{FS}\rangle$, thus either $\mathbf{q} = 0$ (but that is excluded from $V'_{\text{el-el}}$) or $\mathbf{k}_2 = \mathbf{k}_1 + \mathbf{q}$ and $\sigma_2 = \sigma_1$. These possibilities are sketched in Fig. 2.6. For $\mathbf{q} \neq 0$ we therefore end with

$$\begin{aligned} \langle \text{FS} | c_{\mathbf{k}_1+\mathbf{q}\sigma_1}^\dagger c_{\mathbf{k}_2-\mathbf{q}\sigma_2}^\dagger c_{\mathbf{k}_2\sigma_2} c_{\mathbf{k}_1\sigma_1} | \text{FS} \rangle &= \delta_{\mathbf{k}_2, \mathbf{k}_1+\mathbf{q}} \delta_{\sigma_1, \sigma_2} \langle \text{FS} | c_{\mathbf{k}_1+\mathbf{q}\sigma_1}^\dagger c_{\mathbf{k}_1\sigma_1}^\dagger c_{\mathbf{k}_1+\mathbf{q}\sigma_1} c_{\mathbf{k}_1\sigma_1} | \text{FS} \rangle \\ &= -\delta_{\mathbf{k}_2, \mathbf{k}_1+\mathbf{q}} \delta_{\sigma_1, \sigma_2} \langle \text{FS} | n_{\mathbf{k}_1+\mathbf{q}\sigma_1} n_{\mathbf{k}_1\sigma_1} | \text{FS} \rangle \\ &= -\delta_{\mathbf{k}_2, \mathbf{k}_1+\mathbf{q}} \delta_{\sigma_1, \sigma_2} \theta(k_F - |\mathbf{k}_1 + \mathbf{q}|) \theta(k_F - |\mathbf{k}_1|), \end{aligned} \quad (2.40)$$

where $\mathbf{q} \neq 0$ leads to $\mathbf{k}_1 + \mathbf{q} \neq \mathbf{k}_1$, which results in a simple anticommutator yielding the occupation number operators with a minus in front. Since only one \mathbf{k} -vector appears we now drop the index 1.

The \mathbf{k} - and \mathbf{q} -sum are converted into integrals, and polar coordinates (q, θ_q, ϕ_q) and (k, θ_k, ϕ_k) are employed. First note, that the integral is independent of the direction of \mathbf{q} so that $\int_{-1}^1 d(\cos \theta_q) \int_0^{2\pi} d\phi_q = 4\pi$. Second, only for $0 < q < 2k_F$ does the theta function

product give a non-zero result. For a given fixed value of q the rest of the integral is just the overlap volume between two spheres of radius k_F displaced by q . The geometry of this volume is sketched in Fig. 2.6, and is calculated by noting that $q/2k_F < \cos \theta_k < 1$, and that for a given $\cos \theta_k$ we have $q/(2 \cos \theta_k) < k < k_F$. The last variable is free: $0 < \phi_k < 2\pi$. We thus get

$$\frac{E^{(1)}}{N} = -\frac{4\pi e_0^2}{2\mathcal{V}N} 2(4\pi) \frac{\mathcal{V}}{(2\pi)^3} \int_0^{2k_F} dq \frac{q^2}{q^2} 2(2\pi) \int_{\frac{q}{2k_F}}^1 d(\cos \theta_k) \frac{\mathcal{V}}{(2\pi)^3} \int_{\frac{q}{2 \cos \theta_k}}^{k_F} dk k^2, \quad (2.41)$$

where the prefactors are a factor 2 for spin, 2 for symmetry, 4π for \mathbf{q} -angles, 2π for ϕ_k , and twice $\mathcal{V}/(2\pi)^3$ for the conversions of \mathbf{k} - and \mathbf{q} -sums to integrals. The integral is elementary and results in

$$\frac{E^{(1)}}{N} = -\frac{e_0^2}{2} \frac{\mathcal{V}}{N} \frac{k_F^4}{2\pi^3} = -\frac{e_0^2}{2a_0} (a_0 k_F) \frac{k_F^3}{2\pi^3 n} = -\frac{e_0^2}{2a_0} \left(\left(\frac{9\pi}{4} \right)^{\frac{1}{3}} \frac{1}{r_s} \right) \frac{3}{2\pi} \approx -\frac{0.916}{r_s} \text{ Ry}. \quad (2.42)$$

The final result for the first order perturbation theory is thus the simple expression

$$\frac{E}{N} \xrightarrow{r_s \rightarrow 0} \frac{E^{(0)} + E^{(1)}}{N} = \left(\frac{2.211}{r_s^2} - \frac{0.916}{r_s} \right) \text{ Ry}. \quad (2.43)$$

This result shows that the electron gas is stable when the repulsive Coulomb interaction is turned on. No external confinement potential is needed to hold the electron gas in the ion jellium together. There exists an optimal density n^* , or inter-particle distance r_s^* , which minimizes the energy and furthermore yields an energy $E^* < 0$. The negative exchange energy overcomes the positive kinetic energy. The equilibrium situation is obtained from $\frac{\partial}{\partial r_s}(E^{(0)} + E^{(1)}) = 0$, and we can compare the result with experiment:

$$\begin{aligned} r_s^* &= 4.83, & \frac{E^*}{N} &= -0.095 \text{ Ry} = -1.29 \text{ eV} & \text{(1st order perturbation theory)} \\ r_s &= 3.96, & \frac{E}{N} &= -0.083 \text{ Ry} = -1.13 \text{ eV} & \text{(experiment on Na)} \end{aligned} \quad (2.44)$$

We note that the negative binding energy is due to the exchange energy of the Coulomb interaction. Physically this can be interpreted as an effect of the Pauli exclusion principle: the electrons are forced to avoid each other, since only one electron at a time can be at a given point in space. The direct “classical” Coulomb interaction does not take this into account and is therefore over-estimating the energy, and the exchange part corrects for this by being negative.

One may wonder what happens to the Fermi sphere as the interaction is turned on. We found before that thermal smearing occurs but is rather insignificant compared to the huge Fermi energy, $\varepsilon_F \approx 7 \text{ eV}$. However, now we have learned that the interaction energy per particle is $\approx 1.3 \text{ eV}$, i.e. smaller than but certainly comparable to ε_F . One of the great results of quantum field theory, which we are going to study later in the course, is the explanation of why the Fermi surface is not destroyed by the strong Coulomb interaction between the electrons.

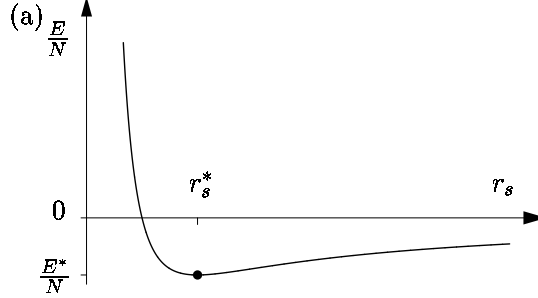


Figure 2.7: (a) The energy per particle E/N of the 3D electron gas in first order perturbation theory Eq. (2.43) as a function of the dimensionless inter-particle distance r_s . Due to the exchange interaction the electron gas is stable at $r_s = r_s^* = 4.83$ with an ionization energy $E/N = E^*/N = -1.29$ eV.

2.2.2 Electron interactions in 2nd order perturbation theory

One may try to improve on the first order result by going to second order perturbation theory. However, the result is disastrous. The matrix elements diverge without giving hope for a simple cure.

Here we can only reveal what goes wrong, and then later learn how to deal correctly with the infinities occurring in the calculations. According to second order perturbation theory $E^{(2)}$ is given by

$$\frac{E^{(2)}}{N} = \frac{1}{N} \sum_{|\nu\rangle \neq |\text{FS}\rangle} \frac{\langle \text{FS} | V'_{\text{el-el}} | \nu \rangle \langle \nu | V'_{\text{el-el}} | \text{FS} \rangle}{E^{(0)} - E_\nu}, \quad (2.45)$$

where all the intermediate states $|\nu\rangle$ must be different from $|\text{FS}\rangle$. As sketched in Fig. 2.8 this combined with the momentum conserving Coulomb interaction yields intermediate states where two particles are injected out of the Fermi sphere. From such an intermediate state, $|\text{FS}\rangle$ is restored by putting the excited electrons back into the holes they left behind. Only two types of processes are possible: the direct and the exchange process.

We now proceed to show that the direct interaction process gives a divergent contribution $E_{\text{dir}}^{(2)}$ to $E^{(2)}$ due to the singular behavior of the Coulomb interaction at small momentum transfers \mathbf{q} . For the direct process the constraint $|\nu\rangle \neq |\text{FS}\rangle$ leads to

$$|\nu\rangle = \theta(|\mathbf{k}_1 + \mathbf{q}| - k_F) \theta(|\mathbf{k}_2 - \mathbf{q}| - k_F) \theta(k_F - |\mathbf{k}_1|) \theta(k_F - |\mathbf{k}_2|) c_{\mathbf{k}_1 + \mathbf{q}\sigma_1}^\dagger c_{\mathbf{k}_2 - \mathbf{q}\sigma_2}^\dagger c_{\mathbf{k}_2\sigma_2} c_{\mathbf{k}_1\sigma_1} |\text{FS}\rangle. \quad (2.46)$$

To restore $|\text{FS}\rangle$ the same momentum transfer \mathbf{q} must be involved in both $\langle \nu | V'_{\text{el-el}} | \text{FS} \rangle$ and $\langle \text{FS} | V'_{\text{el-el}} | \nu \rangle$, and writing $V_{\mathbf{q}} = \frac{4\pi e_0^2}{q^2}$ we find

$$E_{\text{dir}}^{(2)} = \frac{1}{V^2} \sum_{\mathbf{q}} \sum_{\substack{\mathbf{k}_1\sigma_1 \\ \mathbf{k}_2\sigma_2}} \frac{(\frac{1}{2}V_{\mathbf{q}})^2}{E^{(0)} - E_\nu} \theta(|\mathbf{k}_1 + \mathbf{q}| - k_F) \theta(|\mathbf{k}_2 - \mathbf{q}| - k_F) \theta(k_F - |\mathbf{k}_1|) \theta(k_F - |\mathbf{k}_2|). \quad (2.47)$$

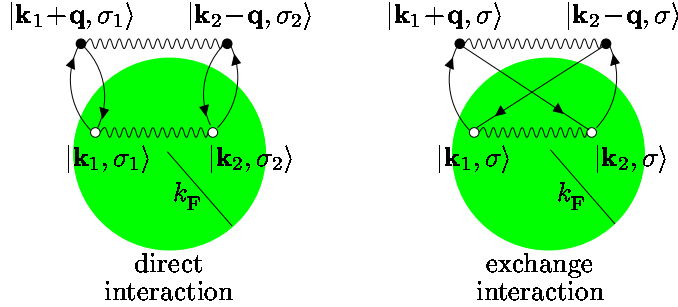


Figure 2.8: The two possible processes in second order perturbation theory for two states $|\mathbf{k}_1\sigma_1\rangle$ and $|\mathbf{k}_2\sigma_2\rangle$ in the Fermi sea. The direct process gives a divergent contribution to E/N while the exchange process gives a finite contribution.

The contribution from small values of \mathbf{q} to $E_{\text{dir}}^{(2)}$ is found by noting that

$$V_{\mathbf{q}}^2 \propto \frac{1}{q^4} \quad (2.48a)$$

$$E_0 - E_{\nu} \propto \mathbf{k}_1^2 + \mathbf{k}_2^2 - (\mathbf{k}_1 + \mathbf{q})^2 - (\mathbf{k}_2 - \mathbf{q})^2 \underset{q \rightarrow 0}{\propto} q \quad (2.48b)$$

$$\sum_{\mathbf{k}_1} \dots \theta(|\mathbf{k}_1 + \mathbf{q}| - k_F) \theta(k_F - |\mathbf{k}_1|) \underset{q \rightarrow 0}{\propto} q, \quad (2.48c)$$

from which we obtain

$$E_{\text{dir}}^{(2)} \propto \int_0 dq q^2 \frac{1}{q^4} \frac{1}{q} q = \int_0 dq \frac{1}{q} = \ln(q) \Big|_0 \propto \infty. \quad (2.49)$$

The exchange process does not lead to a divergence since in this case the momentum transfer in the excitation part is \mathbf{q} , but in the relaxation part it is $\mathbf{k}_2 - \mathbf{k}_1 - \mathbf{q}$. Thus $V_{\mathbf{q}}^2$ is replaced by $V_{\mathbf{q}} V_{\mathbf{k}_2 - \mathbf{k}_1 - \mathbf{q}} \propto q^{-2}$ for $q \rightarrow 0$, which is less singular than $V_{\mathbf{q}}^2 \propto q^{-4}$.

This divergent behavior of second order perturbation theory is a nasty surprise. We know that physically the energy of the electron gas must be finite. The only hope for rescue lies in regularization of the divergent behavior by taking higher order perturbation terms into account. In fact, as we shall see in Chap. 13, it turns out that one has to consider perturbation theory to infinite order, which is possible using the full machinery of quantum field theory to be developed in the coming chapters.

2.3 Electron gases in 3, 2, 1, and 0 dimensions

We end this chapter on the electron gas by mentioning a few experimental realizations of electron gases in 3D, 2D, and 1D. To work in various dimensions is a good opportunity to test ones understanding of the basic principles of the physics of electron gases. But as will become clear, this is not just an academic exercise. Electron gases at reduced dimensionality is of increasing experimental importance.

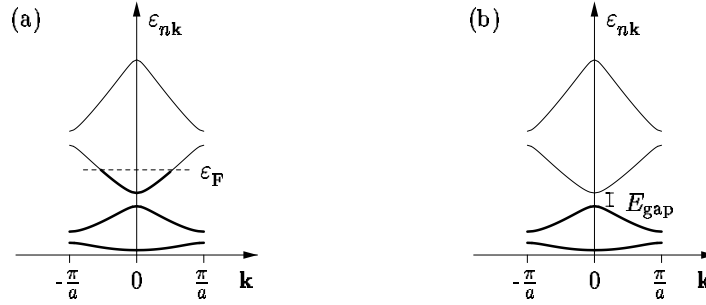


Figure 2.9: (a) A generic bandstructure for a metal. The Fermi level ε_F lies in the middle of a band resulting in arbitrarily small possible excitations energies. (b) A generic bandstructure for an insulator or a semiconductor. The Fermi level ε_F lies at the top of the valence band resulting in possible excitations energies of at least E_{gap} , the distance up to the unoccupied conduction band.

2.3.1 3D electron gases: metals and semiconductors

Bloch's theory of non-interacting electrons moving in a periodic lattice provides an explanation for the existence of metals, semiconductors, and band insulators. The important parameter is the position of the Fermi energy ε_F relative to the bands as sketched in Fig. 2.9. In the metallic case ε_F lies in the middle of a band. Consequently there is no energy gap between the last occupied level and the first unoccupied level, and any however small external field can excite the system and give rise to a significant response. In an insulator ε_F is at the top of a band, the so-called filled valence band, and filled bands does not carry any electrical or thermal current⁵. The system can only be excited by providing sufficient energy for the electrons to overcome the energy band gap E_{gap} between the top of the valence band and the bottom of the next empty band, the so-called conduction band. This is not possible for small external fields, and hence the inability of insulators to conduct electronic thermal and electrical currents. Semiconductors are insulators at $T = 0$, but their band gap E_{gap} is relatively small, typically less than 2 eV, such that at room temperature a sufficient number of electrons are excited thermally up into the conduction band to yield a significant conductivity.

We emphasize that at room temperature the electron gas in a metal is a degenerate Fermi gas since $k_B T \ll \varepsilon_F$. A semiconductor, on the other hand, is normally described as a classical gas since for energies $\varepsilon_{\mathbf{k}}$ in the conduction band we have $\varepsilon_{\mathbf{k}} - \mu > E_{\text{gap}}/2 \gg k_B T$, and consequently $n_F(\varepsilon_{\mathbf{k}}) \rightarrow e^{-(\varepsilon_{\mathbf{k}} - \mu)/k_B T}$, i.e. the Maxwell-Boltzmann distribution.

Finally, we note that in a typical metal most of the electron states at the Fermi surface are far away from the regions in \mathbf{k} -space where the free electron dispersion relation is strongly distorted by the periodic lattice. Therefore one finds effective masses m^* , see

⁵Transport properties are tightly connected to the electron velocity $v_{\mathbf{k}} = \frac{1}{\hbar} \frac{\partial \varepsilon_{\mathbf{k}}}{\partial \mathbf{k}}$. The current density is $\mathbf{J} = 2 \sum_{\mathbf{k} \in \text{FBZ}} \frac{1}{V} v_{\mathbf{k}} = 2 \int_{\text{FBZ}} \frac{d\mathbf{k}}{(2\pi)^3} \frac{1}{\hbar} \frac{\partial \varepsilon_{\mathbf{k}}}{\partial \mathbf{k}}$. Likewise, for the thermal current $\mathbf{J}_{\text{th}} = 2 \sum_{\mathbf{k} \in \text{FBZ}} \frac{1}{V} \varepsilon_{\mathbf{k}} v_{\mathbf{k}} = \int_{\text{FBZ}} \frac{d\mathbf{k}}{(2\pi)^3} \frac{1}{\hbar} \frac{\partial (\varepsilon_{\mathbf{k}}^2)}{\partial \mathbf{k}}$. Both currents are integrals over FBZ of gradients of periodic functions and therefore zero.

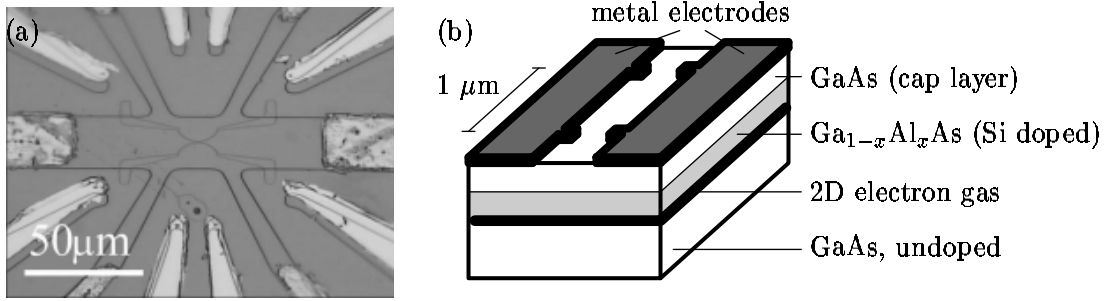


Figure 2.10: (a) A picture of a GaAs-device fabricated at the Ørsted Laboratory, Niels Bohr Institute. The metal contacts and wires are seen attached to the GaAs structure, which by wet etching has gotten a device geometry imprinted in its surface. (b) A sketch showing the different layers in the semiconductor structure as well as some surface gates defining the geometry of the device.

Eq. (2.16), close to the vacuum mass m . In contrast, all the electron states contributing to the transport properties in a semiconductor are close to these regions in \mathbf{k} -space, and one finds strongly modified effective masses, typically $m^* \approx 0.1 m$.

2.3.2 2D electron gases: GaAs/Ga_{1-x}Al_xAs heterostructures

For the past three decades it has been possible to fabricate 2D electron gases at semiconductor interfaces, the first realization being inversion layers in the celebrated silicon MOSFETs, the key component in integrated electronic circuits, and the more recent realization being in the gallium-arsenide/gallium-aluminum-arsenide (GaAs/Ga_{1-x}Al_xAs) heterostructures. In the latter system one can obtain extremely long mean free paths (more than 10 μm), which is technologically important for high-speed electronics, and which is essential for the basic research of many quantum effects in condensed matter physics.

The interface between the GaAs and the Ga_{1-x}Al_xAs semiconductor crystals in the GaAs/Ga_{1-x}Al_xAs heterostructure can be grown with mono-atomic-layer precision in molecular beam epitaxy (MBE) machines. This is because the two semiconductor crystals have nearly the same crystal structure leading to a stress-free interface. In Fig. 2.10 a picture of an actual device is shown as well as a sketch of the various layers in a GaAs heterostructure. The main difference between the two semiconductor crystals is the values of the bottom of the conduction band. For $x = 0.3$ the conduction band in Ga_{1-x}Al_xAs is 300 meV higher than the one in GaAs. Hence the electrons in the former conduction band can gain energy by moving to the latter. At $T = 0$ there are of course no free carriers in any of the conduction bands for pure semiconductor systems, but by doping the Ga_{1-x}Al_xAs with Si, conduction electrons are provided, which then accumulate on the GaAs side of the interface due to the energy gain. However, not all donor electrons will be transferred. The ionized Si donors left in the Ga_{1-x}Al_xAs provide an electrostatic energy that grows with an increasing number of transferred electrons. At some point the energy gained by

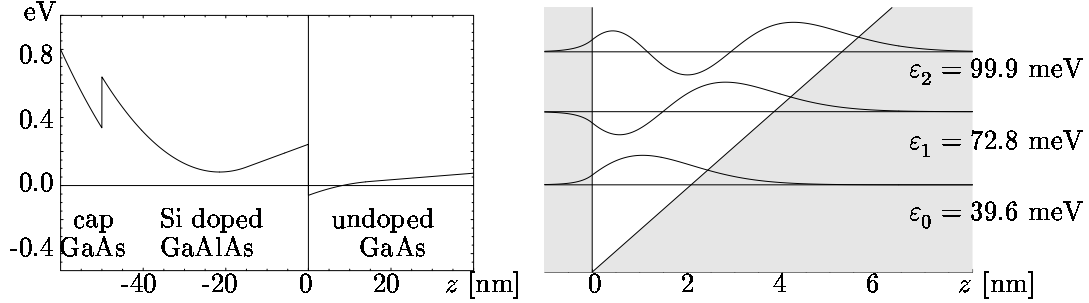


Figure 2.11: The conduction band in a GaAs/GaAlAs heterostructure. Note the triangular well forming at the interface. The wavefunctions $\zeta_n(z)$ and eigenvalues of the lowest three electron eigenstates in the triangular well.

transferring electrons to the GaAs layer is balanced by the growth in electrostatic energy. This is sketched in Fig. 2.11 where the resulting conduction band in equilibrium is shown as function of the position z perpendicular to the interface. The conduction band is not flat due to the curvature induced by the charge densities, as calculated from Poisson's equation: $\nabla^2 V = -e^2 n^{3D} / \epsilon^*$.

The key point to notice is the formation of the almost triangular quantum well at the GaAs side of the interface. The well is so narrow that a significant size-quantization is obtained. Without performing the full calculation we can get a grasp of the order of magnitude by the following estimate. We consider the positively charged layer of the ionized Si donors as one plate of a plate capacitor, while the conduction electrons at the GaAs/GaAlAs interface forms the other plate. The charge density outside this capacitor is zero. The electrical field \mathbf{E} at the interface is then found simply by forming a cylindrical Gauss box with its axis along the z direction and one circular 'bottom lid' at the interface and the other 'top lid' deep into the GaAs. All the contributions stems from the 'bottom lid', since for symmetry reasons \mathbf{E} must be perpendicular to the z axis, yielding zero from the side of the cylindrical box, and since for the reason of charge neutrality, $\mathbf{E} = 0$ at the 'top lid'. Thus at the interface $E = en / \epsilon^*$, n being the 2D electron density at the interface. The typical length scale l for the width of the triangular well is found by balancing the potential energy and the kinetic quantum energy: $eEl = \frac{\hbar^2}{m^* l^2} \Rightarrow l^3 = \frac{1}{4\pi} \frac{\epsilon^* / \epsilon_0}{m^* / m} \frac{a_0}{n}$, where we have used the Bohr radius a_0 of Eq. (2.36) to bring in atomic units. The experimental input for GaAs is $\epsilon^* = 13\epsilon_0$, $m^* = 0.067m$, and typically $n = 3 \times 10^{15} \text{ m}^{-2}$, which yields $l \approx 5 \text{ nm}$. From this we get the typical quantization energy ΔE due to the triangular well: $\Delta E = 13.6 \text{ eV} \frac{m}{m^*} \frac{a_0^2}{l^2} \approx 20 \text{ meV}$.

The significance of this quantization energy is the following. Due to the triangular well the 3D free electron wavefunction is modified,

$$\psi_{\mathbf{k}\sigma}(\mathbf{r}) = \frac{1}{\sqrt{V}} e^{ik_x x} e^{ik_y y} e^{ik_z z} \chi_\sigma \longrightarrow \psi_{k_x k_y n \sigma}(\mathbf{r}) = \frac{1}{\sqrt{A}} e^{ik_x x} e^{ik_y y} \zeta_n(z) \chi_\sigma, \quad (2.50)$$

where $\zeta_n(z)$ is the n th eigenfunction of the triangular well having the eigenenergy ε_n , see Fig. 2.11. Only the z direction is quantized leaving the x and y direction unaltered, and

the total energy for all three spatial directions is

$$\varepsilon_{k_x, k_y, n} = \frac{\hbar^2}{2m^*} (k_x^2 + k_y^2) + \varepsilon_n, \quad k_F^2 = 2\pi n \Rightarrow \varepsilon_F \approx 10 \text{ meV}, \quad (2.51)$$

where we have given the 2D version of the fundamental relation between k_F and n (see Exercise 2.4 and compare to Eq. (2.26) for the 3D case). The highest occupied state has the energy $E_0 + \varepsilon_F$ while the lowest unoccupied state has the energy E_1 . The difference is $E_1 - (E_0 + \varepsilon_F) = \Delta E - \varepsilon_F \approx 10 \text{ meV} \approx 100 \text{ K}$, and we arrive at our conclusion: At temperatures $T \ll 100 \text{ K}$ all occupied electron states have the same orbital in the z direction, $\zeta_0(z)$. Any changes of this orbital requires an excitation energy of at least 10 meV. If this is not provided the system has effectively lost one spatial degree of freedom and is dynamically a 2D system. This means that theoretical studies of 2D electron gases is far from an academic exercise; 2D systems do indeed exist in reality.

2.3.3 1D electron gases: carbon nanotubes

Since the mid-nineties a new research field has developed involving studies of the cylindrically shaped carbon based molecule, the so-called carbon nanotube. The carbon nanotube can be viewed as a normal graphite sheet rolled up into a cylinder with a radius $R_0 \approx 2 \text{ nm}$ and a length more than a thousand times R_0 , see Fig. 2.12. These long and thin carbon molecules have some extraordinary material characteristics. They are believed to be the strongest material in the world, and depending on the specific way the cylinder is rolled up the nanotubes are either metallic, semiconducting or insulating. In the same dynamical sense as the GaAs heterostructure is a 2D metal sheet, a metallic nanotube is a nearly ideal 1D wire, i.e. two of the three spatial degrees of freedom are frozen in. We briefly sketch how this comes about.

The cylindrical symmetry of the nanotube makes it natural to change the basis functions from the 3D (x, y, z) plane waves to cylindrical (x, r, ϕ) wavefunctions:

$$\psi_{\mathbf{k}\sigma}(\mathbf{r}) = \frac{1}{\sqrt{V}} e^{ik_x x} e^{ik_y y} e^{ik_z z} \chi_\sigma \longrightarrow \psi_{k_x, n, l, \sigma}(\mathbf{r}) = \frac{1}{\sqrt{L}} e^{ik_x x} R_{nl}(r) Y_l(\phi) \chi_\sigma. \quad (2.52)$$

This is of course more than just a mathematical transformation. The electrons are strongly bound to the surface of the cylinder in quantum states arising from the original π -bonds of the graphite system. This means that the extension ΔR of the radial wave function $R_{nl}(r)$ around the mean value R_0 is of atomic scale, i.e. $\Delta R \approx 0.1 \text{ nm}$, resulting in a radial confinement energy $E_0^R \sim \frac{\hbar^2}{2m\Delta R^2} \sim 10 \text{ eV}$. Likewise, in the azimuthal angle coordinate ϕ , there is a strong confinement, since the perimeter must contain an integer number of electron wavelengths λ_n , i.e. $\lambda_n = 2\pi R_0/n < 2 \text{ nm}$. The corresponding confinement energy is $E_n^\phi \sim \frac{\hbar^2}{2m\lambda_n^2} \sim 1 \text{ eV } n$. There are no severe constraints along the cylinder axis, i.e. in the x direction. We therefore end up with a total energy

$$\varepsilon_{k_x, n, l} = E_0^R + E_n^\phi + \frac{\hbar^2}{2m} k_x^2, \quad (2.53)$$

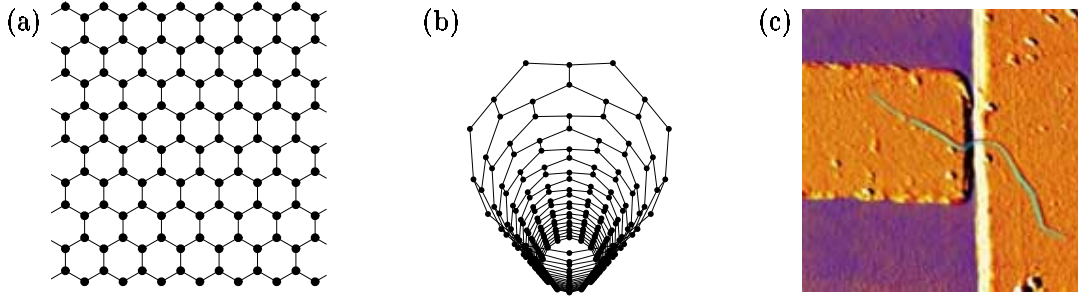


Figure 2.12: (a) Carbon atoms forming a sheet of graphite with a characteristic hexagonal lattice. (b) A carbon nanotube molecule is formed by rolling up a graphite sheet into a cylindrical geometry. (c) An atomic force micrograph taken at the Ørsted Laboratory, Niels Bohr Institute, showing a bundle of carbon nanotubes placed across a gap between two metal electrodes, thereby connecting them and allowing for electrical measurements on single molecules.

with a considerable gap ΔE from the center of the $(n, l) = (0, 0)$ band (the position of ε_F for the metallic case) to the bottom of the $(n, l) = (0, 1)$ band:

$$\Delta E = \frac{1}{2}(E_1^\phi - E_0^\phi) \approx 1 \text{ eV} \sim 12000 \text{ K}. \quad (2.54)$$

Thus at room temperature the only available degree of freedom is the axial one described by the continuous quantum number k_x and the associated plan waves $e^{ik_x x}$.

Not only are the nanotube very interesting from an experimental point of view, also from a pure theoretical point of view do they play an important role. The nanotubes is one of only a couple of systems exhibiting a nearly ideal 1D behavior. In particular that makes the nanotubes a key testing ground for the diagonalizable so-called Luttinger liquid model, a central quantum model for describing interacting electrons in 1D.

2.3.4 0D electron gases: quantum dots

Naturally one can think of confining the electrons in all three spatial dimensions. This has been realized experimentally in the so-called quantum dot systems, for example by using the device shown in Fig. 2.10(b). A simplified model of a quantum dot is studied in Exercise 8.4.

This section will be expanded in the next edition of these notes.

Chapter 3

Phonons; coupling to electrons

In this chapter we study the basic properties of ionic vibrations. These vibrations are well described by harmonic oscillators and therefore we can employ the results from Sec. 1.4.1 to achieve the second quantized form of the corresponding Hamiltonian. The quantized vibrations are denoted phonons, a name pointing to the connection between sound waves and lattice vibrations. Phonons play a fundamental role in our understanding of sound, specific heat, elasticity, and electrical resistivity of solids. And more surprising may be the fact that the electron-phonon coupling is the cause of conventional superconductivity. In the following sections we shall study the three types of matter oscillation sketched in Fig. 3.1. The ions will be treated using two models: the jellium model, where the ions are represented by a smeared-out continuous positive background, and the lattice model, where the ions oscillate around their equilibrium positions forming a regular crystal lattice.

Since phonons basically are harmonic oscillators, they are bosons according to the results of Sec. 1.4.1. Moreover, they naturally occur at finite temperature, so we will therefore often need the thermal distribution function for bosons, the Bose-Einstein distribution $n_B(\varepsilon)$ given in Eq. (1.127).

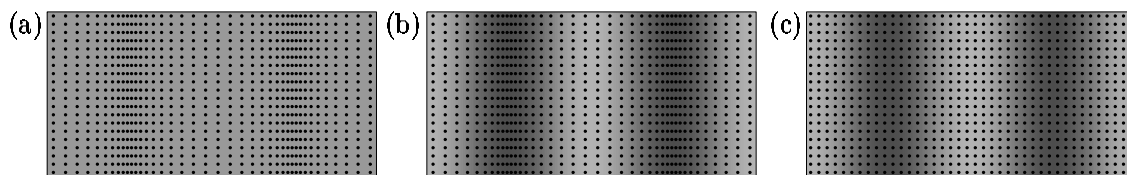


Figure 3.1: Three types of oscillations in metals. The grayscale represent the electron density and the dots the ions. (a) Slow ionic density oscillations in a static electron gas (ion plasma oscillations). The restoring force is the long range Coulomb interaction. (b) slow ion oscillations followed by the electron gas (sound waves, acoustic phonons). The restoring force is the compressibility of the disturbed electron gas. (c) Fast electronic plasma oscillations in a static ionic lattice (electronic plasma oscillations). The restoring force is the long range Coulomb interaction.

3.1 Jellium oscillations and Einstein phonons

Our first encounter with phonons will be those arising from a semiclassical treatment of the charge neutral jellium system. Let ρ_{ion}^0 be the particle density of the ion jellium, and $\rho_{\text{el}} = Z\rho_{\text{ion}}^0$ that of the homogeneous electron gas. We begin as depicted in Fig. 3.1(a) by studying oscillations in the smeared out ion density while neglecting the electron dynamics, i.e. we keep ρ_{el} fixed. If we study the limit of small harmonic deviations from equilibrium $\delta\rho_{\text{ion}}(\mathbf{r}, t) = \delta\rho_{\text{ion}}(\mathbf{r}) e^{-i\Omega t}$, we obtain linear equations of motion with solutions of the form

$$\rho_{\text{ion}}(\mathbf{r}, t) = \rho_{\text{ion}}^0 + \delta\rho_{\text{ion}}(\mathbf{r}) e^{-i\Omega t}. \quad (3.1)$$

A non-zero $\delta\rho_{\text{ion}}$ corresponds to a charge density $Ze\delta\rho_{\text{ion}}$ and hence is associated with an electric field \mathbf{E} obeying

$$\nabla \cdot \mathbf{E} = \frac{Ze}{\epsilon_0} \delta\rho_{\text{ion}} \quad \Rightarrow \quad \nabla \cdot \mathbf{f} = \frac{Z^2 e^2 \rho_{\text{ion}}^0}{\epsilon_0} \delta\rho_{\text{ion}}. \quad (3.2)$$

In the second equation we have introduced the force density \mathbf{f} , which to first order in $\delta\rho_{\text{ion}}$ becomes $\mathbf{f} = Ze\rho_{\text{ion}}\mathbf{E} \approx Ze\rho_{\text{ion}}^0\mathbf{E}$. This force equation is supplemented by the continuity equation, $\partial_t \rho_{\text{ion}} + \nabla \cdot (\rho_{\text{ion}} \mathbf{v}) = 0$, which to first order in $\delta\rho_{\text{ion}}$ becomes $\partial_t \delta\rho_{\text{ion}} + \rho_{\text{ion}}^0 \nabla \cdot \mathbf{v} = 0$, since the velocity \mathbf{v} is already a small quantity. Differentiating this with respect to time and using Newton's second law $\mathbf{f} = M\rho_{\text{ion}} \partial_t \mathbf{v}$ we obtain

$$\partial_t^2 \delta\rho_{\text{ion}} + \frac{1}{M} \nabla \cdot \mathbf{f} = 0 \quad \Rightarrow \quad \Omega^2 \delta\rho_{\text{ion}} = \frac{Z^2 e^2 \rho_{\text{ion}}^0}{\epsilon_0 M} \delta\rho_{\text{ion}} \quad \Rightarrow \quad \Omega = \sqrt{\frac{Z^2 e^2 \rho_{\text{ion}}^0}{\epsilon_0 M}} = \sqrt{\frac{Ze^2 \rho_{\text{el}}}{\epsilon_0 M}}. \quad (3.3)$$

Ω is the ionic plasma frequency. The ionic oscillations in the continuous jellium model are thus described by harmonic oscillators, which all have the same frequency Ω . Hence, the second quantization formalism leads to the following phonon Hamiltonian:

$$H_{\text{ph}} = \sum_{\mathbf{q}} \hbar \Omega \left(b_{\mathbf{q}}^\dagger b_{\mathbf{q}} + \frac{1}{2} \right). \quad (3.4)$$

These quantized ion oscillations are denoted phonons, and a model like this was proposed by Einstein in 1906 as the first attempt to explain the decrease of heat capacity C_V^{ion} of solids as a function of decreasing temperature (see Sec. 3.5). Note that the origin of the ionic plasma frequency is the long-range Coulomb interaction, which entered the analysis through the Maxwell equation $\nabla \cdot \mathbf{E} = Ze\delta\rho_{\text{ion}}/\epsilon_0$.

However, the Einstein phonons (also denoted optical phonons, see Sec. 3.3) are not a very good description of solids. Although it is correct that C_V^{ion} decreases at low temperature, the exact behavior is described by the Debye-model incorporating phonons with a photon-like dispersion $\omega_{\mathbf{q}} = v_s q$, where v_s is the sound velocity, instead of the Einstein dispersion $\omega_{\mathbf{q}} = \Omega$. These Debye phonons are also denoted acoustical phonons due to their relation to sound propagation. This is explained in details in Secs. 3.3 and 3.5. To fully understand how the optical Einstein phonons get renormalized to become the acoustic Debye phonons requires the full machinery of quantum field theory, but we hint at the solution of the problem in Fig. 3.1b and in Sec. 3.2.

3.2 Electron-phonon interaction and the sound velocity

Compared to the light and very mobile valence electrons, the ions are much heavier, more than a factor of 10^4 , and much slower. Consequently one would expect the electrons to follow the motion of the ions adiabatically and thereby always maintaining local charge neutrality and thus lowering the high ionic plasma frequency Ω , which is due to long-range charge Coulomb forces from the charge imbalance. This situation is depicted in Fig. 3.1b, and to illustrate its correctness we now use it to estimate the sound velocity in metals. The kinetic energy density associated with a sound wave is of the order $\frac{1}{2}Mv_s^2 \rho_{\text{ion}}$, while the potential energy density associated with the restoring force must be related to the density dependent energy content of the compressed electron gas, i.e. of the order $\frac{3}{5}\rho_{\text{el}}\varepsilon_{\text{F}}$. In a stationary state these two energy densities must be of the same order of magnitude. This gives an estimate for v_s , which in a more detailed treatment (see Exercise 3.4) is expressed by the Bohm-Staver formula,

$$v_s = \sqrt{\frac{Zm}{3M}} v_{\text{F}}, \quad (3.5)$$

which for typical numbers yields $v_s \simeq 3000$ m/s as found experimentally. Note how this estimate builds on classical considerations of the ionic motion while using the quantum result for the energy content of a degenerate electron gas. Surprisingly, an ordinary macroscopic phenomenon as sound propagation is deeply rooted in quantum physics.

3.3 Lattice vibrations and phonons in 1D

Even though we are not yet able to demonstrate how to turn the optical ion plasma oscillations into acoustical phonons, we can nevertheless learn a lot from simply postulating the existence of a periodic ion lattice (as observed in nature), in which the ions can execute small oscillatory motion around their equilibrium positions. The surroundings somehow provide the restoring force.

We begin by a simple one dimensional quantum mechanical model consisting of a 1D box of length L containing N ions of mass M each interacting with its two neighbors through a linear force field (a spring) with the force constant K . The equilibrium position of the j 'th ion is denoted R_j^0 , while its displacement away from this position is denoted u_j . The lattice spacing is denoted $a = R_j^0 - R_{j-1}^0$, so we have $L = Na$. This setup is shown in Fig. 3.2. The Hamiltonian is simply the sum of the kinetic energy of the ions and the potential energy of the springs, while the ion momentum p_j and the displacement u_j are canonical variables:

$$H_{\text{ph}} = \sum_{j=1}^N \left[\frac{1}{2M} p_j^2 + \frac{1}{2} K (u_j - u_{j-1})^2 \right], \quad [p_{j_1}, u_{j_2}] = \frac{\hbar}{i} \delta_{j_1, j_2}. \quad (3.6)$$

As for the photon model and the jellium model we impose periodic boundary conditions, $u_{N+1} = u_1$. Since the equilibrium system is periodic with the lattice spacing a it is natural

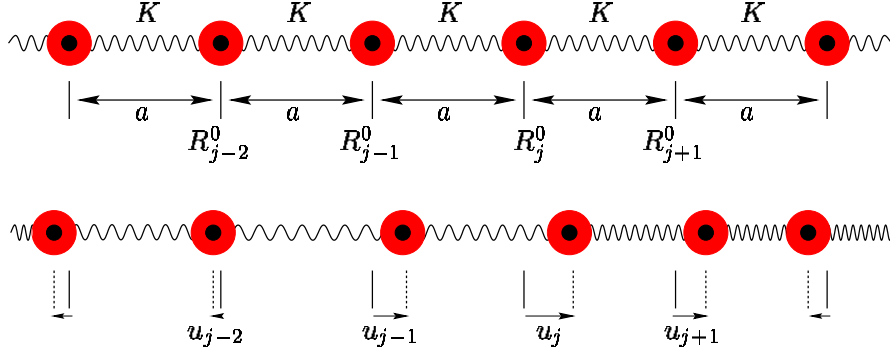


Figure 3.2: A 1D lattice of ions with mass M , lattice constant a , and a nearest neighbor linear force coupling of strength K . The equilibrium positions shown in the top row are denoted R_j^0 , while the displacements shown in the bottom row are denoted u_j .

to solve the problem in k -space by performing a discrete Fourier transform. In analogy with electrons moving in a periodic lattice, also the present system of N ions forming a periodic lattice leads to a first Brillouin zone, FBZ, in reciprocal space. By Fourier transformation the N ion coordinates becomes N wave vectors in FBZ:

$$\text{FBZ} = \left\{ -\frac{\pi}{a} + \Delta k, -\frac{\pi}{a} + 2\Delta k, \dots, -\frac{\pi}{a} + N\Delta k \right\}, \quad \Delta k = \frac{2\pi}{L} = \frac{2\pi}{a} \frac{1}{N}. \quad (3.7)$$

The Fourier transforms of the conjugate variables are:

$$\begin{aligned} p_j &\equiv \frac{1}{\sqrt{N}} \sum_{k \in \text{FBZ}} p_k e^{ikR_j^0}, & u_j &\equiv \frac{1}{\sqrt{N}} \sum_{k \in \text{FBZ}} u_k e^{ikR_j^0}, & \delta_{R_j^0, 0} &= \frac{1}{N} \sum_{k \in \text{FBZ}} e^{ikR_j^0}, \\ p_k &\equiv \frac{1}{\sqrt{N}} \sum_{j=1}^N p_j e^{-ikR_j^0}, & u_k &\equiv \frac{1}{\sqrt{N}} \sum_{j=1}^N u_j e^{-ikR_j^0}, & \delta_{k, 0} &= \frac{1}{N} \sum_{j=1}^N e^{-ikR_j^0}. \end{aligned} \quad (3.8)$$

By straight forward insertion of Eq. (3.8) into Eq. (3.6) we find

$$H = \sum_k \left[\frac{1}{2M} p_k p_{-k} + \frac{1}{2} M \omega_k^2 u_k u_{-k} \right], \quad \omega_k = \sqrt{\frac{K}{M}} 2 \left| \sin \frac{ka}{2} \right|, \quad [p_{k_1}, u_{k_2}] = \frac{\hbar}{i} \delta_{k_1, -k_2}. \quad (3.9)$$

This looks almost like the Hamiltonian for a set of harmonic oscillators except for some annoying details concerning k and $-k$. Note that while p_j in real space is a nice Hermitian operator, p_k in k -space is not self-adjoint. In fact, the hermiticity of p_j and the definition of the Fourier transform lead to $p_k^\dagger = p_{-k}$. Although the commutator in Eq. (3.9) tells us that u_k and p_{-k} form a pair of conjugate variables, we will not use this pair in analogy with x and p in Eq. (1.77) to form creation and annihilation operators. The reason is that the Hamiltonian in the present case contains products like $p_k p_{-k}$ and not p_k^2 as in the original case. Instead we combine u_k and p_k in the definition of the annihilation and

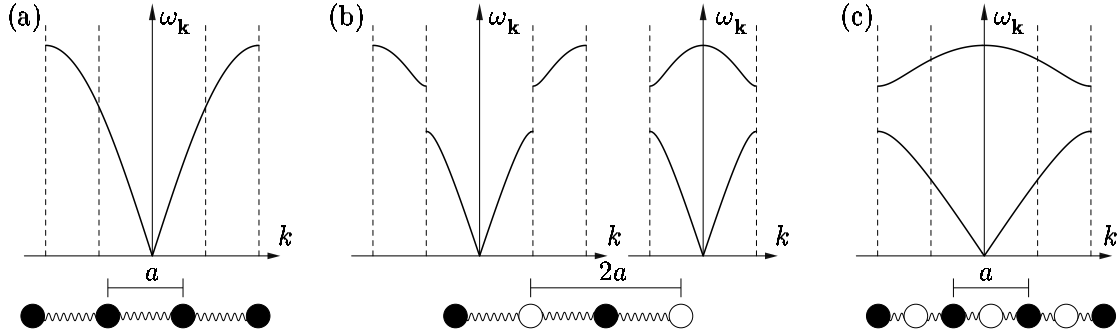


Figure 3.3: The phonon dispersion relation for three different 1D lattices. (a) A system with lattice constant a and one ion of mass M_1 (black disks) per unit cell. (b) As in (a) but now substituting every second ion of mass M_1 with one of mass M_2 (white disks) resulting in two ions per unit cell and a doubling of the lattice constant. To the left is shown the extended zone scheme, and to the right the reduced zone scheme. (c) As in (a) but now with the addition of mass M_2 ions in between the mass M_1 ions resulting in two ions per unit cell, but the same lattice constant as in (a).

creation operators b_k and b_{-k}^\dagger :

$$\begin{aligned} b_k &\equiv \frac{1}{\sqrt{2}} \left(\frac{u_k}{\ell_k} + i \frac{p_k}{\hbar/\ell_k} \right), & u_k &\equiv \ell_k \frac{1}{\sqrt{2}} (b_{-k}^\dagger + b_k), & \ell_k &= \sqrt{\frac{\hbar}{M\omega_k}}, \\ b_{-k}^\dagger &\equiv \frac{1}{\sqrt{2}} \left(\frac{u_k}{\ell_k} - i \frac{p_k}{\hbar/\ell_k} \right), & p_k &\equiv \frac{\hbar}{\ell_k} \frac{i}{\sqrt{2}} (b_{-k}^\dagger - b_k). \end{aligned} \quad (3.10)$$

Note how both the oscillator frequency $\omega_k = \omega_{-k}$ and the oscillator length $\ell_k = \ell_{-k}$ depends on the wavenumber k . Again by direct insertion it is readily verified that

$$H_{\text{ph}} = \sum_k \hbar \omega_k \left(b_k^\dagger b_k + \frac{1}{2} \right), \quad [b_{k_1}, b_{k_2}^\dagger] = \delta_{k_1, k_2}. \quad (3.11)$$

This is finally the canonical form of a Hamiltonian describing a set of independent harmonic oscillators in second quantization. The quantized oscillations are denoted phonons. Their dispersion relation is shown in Fig. 3.3(a). It is seen from Eq. (3.9) that $\omega_k \xrightarrow{k \rightarrow 0} \sqrt{\frac{K}{M}} a k$, so our solution Eq. (3.11) does in fact bring about the acoustical phonons. The sound velocity is found to be $v_s = \sqrt{\frac{K}{M}} a$, so upon measuring the value of it, one can determine the value of the free parameter K , the force constant in the model.

If, as shown in Fig. 3.3(b), the unit cell is doubled to hold two ions, the concept of phonon branches must be introduced. It is analogous to the Bloch bands for electrons. These came about as a consequence of breaking the translational invariance of the system by introducing a periodic lattice. Now we break the discrete translational invariance given by the lattice constant a . Instead the new lattice constant is $2a$. Hence the original BZ is halved in size and the original dispersion curve Fig. 3.3(a) is broken into sections. In

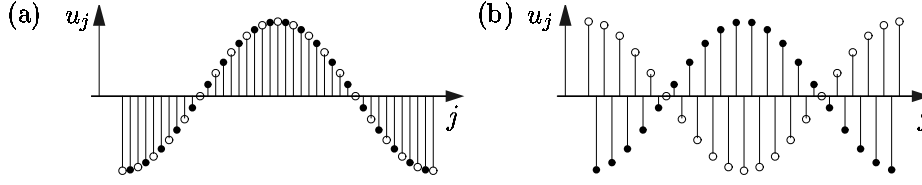


Figure 3.4: (a) An acoustical and (b) an optical phonon having the *same* wave length for a 1D system with two ions, ● and ○, per unit cell. In the acoustical case the two types of ions oscillate in phase, while in the optical case they oscillate π radians out of phase.

the reduced zone scheme in Fig. 3.3(b) we of course find two branches, since no states can be lost. The lower branch resembles the original dispersion so it corresponds to acoustic phonons. The upper band never approaches zero energy, so to excite these phonons high energies are required. In fact they can be excited by light, so they are known as optical phonons. The origin of the energy difference between an acoustical and an optical phonon at the *same* wave length is sketched in Fig. 3.4 for the case of a two-ion unit cell. For acoustical phonons the size of the displacement of neighboring ions differs only slightly and the sign of it is the same, whereas for optical phonons the sign of the displacement alternates between the two types of ions.

The generalization to p ions per unit cell is straight forward, and one finds the appearance of 1 acoustic branch and $(p-1)$ optical branches. The N appearing above, e.g. in Eq. (3.8), should be interpreted as the number of unit cells rather than the number of ions, so we have $N_{\text{ion}} = pN$. A branch index λ , analogous to the band index n for Bloch electrons is introduced to label the different branches, and in the general case the Hamiltonian Eq. (3.11) is changed into

$$H_{\text{ph}} = \sum_{k\lambda} \hbar\omega_{k\lambda} \left(b_{k\lambda}^\dagger b_{k\lambda} + \frac{1}{2} \right), \quad [b_{k_1\lambda_1}, b_{k_2\lambda_2}^\dagger] = \delta_{k_1, k_2} \delta_{\lambda_1, \lambda_2}. \quad (3.12)$$

3.4 Acoustical and optical phonons in 3D

The fundamental principles for constructing the second quantized phonon fields established for the 1D case carries over to the 3D case almost unchanged. The most notable difference is the appearance in 3D of polarization in analogy to what we have already seen for the photon field. We treat the general case of any monatomic Bravais lattice. The ionic equilibrium positions are denoted \mathbf{R}_j^0 and the displacements by $\mathbf{u}(\mathbf{R}_j^0)$ with components $u_\alpha(\mathbf{R}_j^0)$, $\alpha = x, y, z$. The starting point of the analysis is a second order Taylor expansion in $u_\alpha(\mathbf{R}_j^0)$ of the potential energy $U[\mathbf{u}(\mathbf{R}_1^0), \dots, \mathbf{u}(\mathbf{R}_N^0)]$,

$$U \approx U_0 + \frac{1}{2} \sum_{\mathbf{R}_1^0 \mathbf{R}_2^0} \sum_{\alpha\beta} u_\alpha(\mathbf{R}_1^0) \left. \frac{\partial^2 U}{\partial u_\alpha(\mathbf{R}_1^0) \partial u_\beta(\mathbf{R}_2^0)} \right|_{\mathbf{u}=0} u_\beta(\mathbf{R}_2^0). \quad (3.13)$$

Note that nothing has been assumed about the range of the potential. It may very well go much beyond the nearest neighbor case studied in the 1D case. The central object in

the theory is the force strength matrix $\frac{\partial^2 U}{\partial u_\alpha \partial u_\beta}$ (generalizing K from the 1D case) and its Fourier transform, the so-called dynamical matrix $\mathbf{D}(\mathbf{k})$ with components $D_{\alpha\beta}(\mathbf{k})$:

$$D_{\alpha\beta}(\mathbf{R}_1^0 - \mathbf{R}_2^0) = \left. \frac{\partial^2 U}{\partial u_\alpha(\mathbf{R}_1^0) \partial u_\beta(\mathbf{R}_2^0)} \right|_{\mathbf{u}=0}, \quad D_{\alpha\beta}(\mathbf{k}) = \sum_{\mathbf{R}} D_{\alpha\beta}(\mathbf{R}) e^{-i\mathbf{k} \cdot \mathbf{R}}. \quad (3.14)$$

The discrete Fourier transform in 3D is a straight forward generalization of the one in 1D, and for an arbitrary function $f(\mathbf{R}_j^0)$ we have

$$\begin{aligned} f(\mathbf{R}_j^0) &\equiv \frac{1}{\sqrt{N}} \sum_{\mathbf{k} \in \text{FBZ}} f(\mathbf{k}) e^{i\mathbf{k} \cdot \mathbf{R}_j^0}, & \delta_{\mathbf{R}_j^0, 0} &= \frac{1}{N} \sum_{\mathbf{k} \in \text{FBZ}} e^{i\mathbf{k} \cdot \mathbf{R}_j^0}, \\ f(\mathbf{k}) &= \frac{1}{\sqrt{N}} \sum_{j=1}^N f(\mathbf{R}_j^0) e^{-i\mathbf{k} \cdot \mathbf{R}_j^0}, & \delta_{\mathbf{k}, 0} &= \frac{1}{N} \sum_{j=1}^N e^{-i\mathbf{k} \cdot \mathbf{R}_j^0}. \end{aligned} \quad (3.15)$$

Due to the lattice periodicity $D_{\alpha\beta}(\mathbf{R}_1^0 - \mathbf{R}_2^0)$ depends only on the difference between any two ion positions. The D -matrix has the following three symmetry properties¹

$$\left[D(\mathbf{R}^0) \right]^t = D(\mathbf{R}^0), \quad \sum_{\mathbf{R}} D(\mathbf{R}^0) = \mathbf{0}, \quad D(-\mathbf{R}^0) = D(\mathbf{R}^0). \quad (3.16)$$

Using these symmetries in connection with $\mathbf{D}(\mathbf{k})$ we obtain

$$\begin{aligned} \mathbf{D}(\mathbf{k}) &= \sum_{\mathbf{R}^0} D(\mathbf{R}^0) e^{-i\mathbf{k} \cdot \mathbf{R}^0} = \frac{1}{2} \left(\sum_{\mathbf{R}^0} D(\mathbf{R}^0) e^{-i\mathbf{k} \cdot \mathbf{R}^0} + \sum_{\mathbf{R}^0} D(-\mathbf{R}^0) e^{i\mathbf{k} \cdot \mathbf{R}^0} \right) \\ &= \frac{1}{2} \sum_{\mathbf{R}^0} D(\mathbf{R}^0) \left(e^{i\mathbf{k} \cdot \mathbf{R}^0} + e^{-i\mathbf{k} \cdot \mathbf{R}^0} - 2 \right) = -2 \sum_{\mathbf{R}^0} D(\mathbf{R}^0) \sin^2 \left(\frac{1}{2} \mathbf{k} \cdot \mathbf{R}^0 \right) \end{aligned} \quad (3.17)$$

Thus $\mathbf{D}(\mathbf{k})$ is real and symmetric, hence diagonalizable in an orthonormal basis.

The classical equation of motions for the ions are simply

$$M \ddot{\mathbf{u}}_\alpha(\mathbf{R}_1^0) = - \frac{\partial U}{\partial u_\alpha(\mathbf{R}_1^0)} \Rightarrow -M \ddot{\mathbf{u}}(\mathbf{R}_1^0) = \sum_{\mathbf{R}_2^0} D(\mathbf{R}_2^0 - \mathbf{R}_1^0) \mathbf{u}(\mathbf{R}_2^0). \quad (3.18)$$

We seek simple harmonic solutions to the problem and find

$$\mathbf{u}(\mathbf{R}^0, t) \propto \boldsymbol{\epsilon} e^{i(\mathbf{k} \cdot \mathbf{R}^0 - \omega t)} \Rightarrow M \omega^2 \boldsymbol{\epsilon} = \mathbf{D}(\mathbf{k}) \boldsymbol{\epsilon}. \quad (3.19)$$

Since $\mathbf{D}(\mathbf{k})$ is a real symmetric matrix there exists for any value of \mathbf{k} an orthonormal basis set of vectors $\{\boldsymbol{\epsilon}_{\mathbf{k},1}, \boldsymbol{\epsilon}_{\mathbf{k},2}, \boldsymbol{\epsilon}_{\mathbf{k},3}\}$, the so-called polarization vectors, that diagonalizes $\mathbf{D}(\mathbf{k})$, i.e. they are eigenvectors:

$$\mathbf{D}(\mathbf{k}) \boldsymbol{\epsilon}_{\mathbf{k}\lambda} = K_{\mathbf{k}\lambda} \boldsymbol{\epsilon}_{\mathbf{k}\lambda}, \quad \boldsymbol{\epsilon}_{\mathbf{k}\lambda} \cdot \boldsymbol{\epsilon}_{\mathbf{k}\lambda'} = \delta_{\lambda,\lambda'}, \quad \lambda, \lambda' = 1, 2, 3. \quad (3.20)$$

¹The first follows from the interchangeability of the order of the differentiation in Eq. (3.14). The second follows from the fact that $U = 0$ if *all* the displacements are the same, but arbitrary, say \mathbf{d} , because then $0 = \sum_{R_1 R_2} \mathbf{d} \cdot \mathbf{D}(\mathbf{R}_1^0 - \mathbf{R}_2^0) \cdot \mathbf{d} = N \mathbf{d} \cdot [\sum_{\mathbf{R}} \mathbf{D}(\mathbf{R}^0)] \cdot \mathbf{d}$. The third follows from inversion symmetry always present in monatomic Bravais lattices.

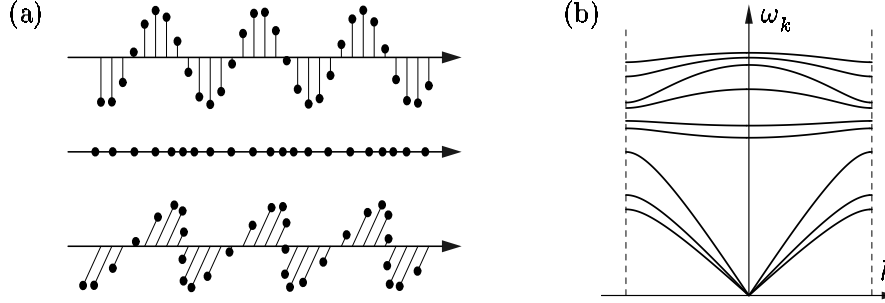


Figure 3.5: (a) Three examples of polarization in phonon modes: transverse, longitudinal and general. (b) A generic phonon spectrum for a system with 3 ions in the unit cell. The 9 modes divide into 3 acoustical and 6 optical modes.

We have now found the classical eigenmodes $\mathbf{u}_{\mathbf{k}\lambda}$ of the 3D lattice vibrations characterized by the wavevector \mathbf{k} and the polarization vector $\boldsymbol{\epsilon}_{\mathbf{k}\lambda}$:

$$M\omega_{\mathbf{k}\lambda}^2 \boldsymbol{\epsilon}_{\mathbf{k}\lambda} = K_{\mathbf{k}\lambda} \boldsymbol{\epsilon}_{\mathbf{k}\lambda} \quad \Rightarrow \quad \mathbf{u}_{\mathbf{k}\lambda}(\mathbf{R}^0, t) = \boldsymbol{\epsilon}_{\mathbf{k}\lambda} e^{i(\mathbf{k} \cdot \mathbf{R}^0 - \omega_{\mathbf{k}\lambda} t)}, \quad \omega_{\mathbf{k}\lambda} \equiv \sqrt{\frac{K_{\mathbf{k}\lambda}}{M}}. \quad (3.21)$$

Using as in Eq. (3.10) the now familiar second quantization procedure of harmonic oscillators we obtain

$$\mathbf{u}_{\mathbf{k}\lambda} \equiv \ell_{\mathbf{k}\lambda} \frac{1}{\sqrt{2}} (b_{-\mathbf{k},\lambda}^\dagger + b_{\mathbf{k},\lambda}) \boldsymbol{\epsilon}_{\mathbf{k}\lambda}, \quad \ell_{\mathbf{k}\lambda} \equiv \sqrt{\frac{\hbar}{M\omega_{\mathbf{k}\lambda}}}, \quad (3.22)$$

$$H_{\text{ph}} = \sum_{\mathbf{k}\lambda} \hbar\omega_{\mathbf{k}\lambda} \left(b_{\mathbf{k}\lambda}^\dagger b_{\mathbf{k}\lambda} + \frac{1}{2} \right), \quad [b_{\mathbf{k}\lambda}, b_{\mathbf{k}',\lambda'}^\dagger] = \delta_{\mathbf{k},\mathbf{k}'} \delta_{\lambda,\lambda'}. \quad (3.23)$$

Now, what about acoustical and optical phonons in 3D? It is clear from Eq. (3.17) that $\mathbf{D}(\mathbf{k}) \propto k^2$ for $k \rightarrow 0$, so the same holds true for its eigenvalues $K_{\mathbf{k}\lambda}$. The dispersion relation in Eq. (3.19) therefore becomes $\omega_{\mathbf{k}\lambda} = v_\lambda(\theta_k, \phi_k) k$, which describes an acoustical phonon with a sound velocity $v_\lambda(\theta_k, \phi_k)$ in general depending on both the direction of \mathbf{k} and the polarization λ . As in 1D the number of ions in the unit cell can be augmented from 1 to p . In that case it can be shown that of the resulting $3p$ modes 3 are acoustical and $3(p-1)$ optical modes. The acoustical modes are appearing because it is always possible to construct modes where all the ions have been given nearly the same displacement resulting in an arbitrarily low energy cost associated with such a deformation of the lattice. In Fig. 3.5 is shown the phonon modes for a unit cell with three ions.

A 3D lattice with N unit cells each containing p ions, each of which can oscillate in 3 directions, is described by $3pN$ modes. In terms of phonon modes we end up with $3p$ so-called phonon branches $\omega_{\mathbf{k}\lambda}$, which for each branch index λ are defined in N discrete points in \mathbf{k} -space. Thus in 3D the index λ contains information on both which polarization and which of the acoustical or optical modes we are dealing with.

3.5 The specific heat of solids in the Debye model

Debye's phonon model is a simple model, which describes the temperature dependence of the heat capacitance $C_V = \frac{\partial E}{\partial T}$ of solids exceedingly well, although it contains just one material dependent free parameter. The phonon spectrum Fig. 3.5(b) in the reduced zone scheme has $3p$ branches. In Fig. 3.6(a) is shown the acoustic and optical phonon branch in the extended zone scheme for a 1D chain with two ions per unit cell. Note how the optical branch appears as an extension of the acoustical branch. In d dimensions a reasonable average of the spectrum can be obtained by representing all the phonon branches in the reduced zone scheme with d acoustical branches in the extended zone scheme, each with a linear dispersion relation $\omega_{\mathbf{k}\lambda} = v_\lambda k$. Furthermore, since we will use the model to calculate the specific heat by averaging over all modes, we can even employ a suitable average v_D out the polarization dependent velocities v_λ and use the *same* linear dispersion relation for *all* acoustical branches,

$$\omega_{\mathbf{k}\lambda} \equiv v_D k \quad \Rightarrow \quad \varepsilon = \hbar v_D k. \quad (3.24)$$

Even though we have deformed the phonon spectrum we may not change the number of phonon modes. In the 3D Debye model we have $3N_{\text{ion}}$ modes, in the form of 3 acoustic branches each with N_{ion} allowed wavevectors, where N_{ion} is the number of ions in the lattice. Since we are using periodic boundary conditions the counting of the allowed phonon wavevectors is equivalent to that of Sec. 2.1.2 for plane wave electron states, i.e. $N_{\text{ion}} = [\mathcal{V}/(2\pi)^3] \times [\text{volume in } \mathbf{k}\text{-space}]$. Since the Debye spectrum Eq. (3.24) is isotropic in \mathbf{k} -space, the Debye phonon modes must occupy a sphere in this space, i.e. all modes with $|\mathbf{k}| < k_D$, where k_D is denoted the Debye wave number determined by

$$N_{\text{ion}} = \frac{\mathcal{V}}{(2\pi)^3} \frac{4}{3} \pi k_D^3. \quad (3.25)$$

Inserting k_D into Eq. (3.24) yields the characteristic Debye energy, $\hbar\omega_D$ and hence the characteristic Debye temperature T_D :

$$\hbar\omega_D \equiv k_B T_D \equiv \hbar v_D k_D \quad \Rightarrow \quad 6\pi^2 N_{\text{ion}} (\hbar v_D)^3 = \mathcal{V} (k_B T_D)^3. \quad (3.26)$$

Continuing the analogy with the electron case the density of phonon states $D_{\text{ph}}(\varepsilon)$ is found by combining Eq. (3.24) and Eq. (3.25) and multiplying by 3 for the number of acoustic branches,

$$N_{\text{ion}}(\varepsilon) = \frac{\mathcal{V}}{6\pi^2} \frac{1}{(\hbar v_D)^3} \varepsilon^3 \quad \Rightarrow \quad D_{\text{ph}}(\varepsilon) = 3 \frac{dN_{\text{ion}}(\varepsilon)}{d\varepsilon} = \frac{\mathcal{V}}{2\pi^2} \frac{1}{(\hbar v_D)^3} \varepsilon^2, \quad 0 < \varepsilon < k_B T_D. \quad (3.27)$$

The energy $E_{\text{ion}}(T)$ of the vibrating lattice is now easily computed using the Bose-Einstein distribution function $n_B(\varepsilon)$ Eq. (1.127) for the bosonic phonons:

$$E_{\text{ion}}(T) = \int_0^{k_B T_D} d\varepsilon \varepsilon D_{\text{ph}}(\varepsilon) n_B(\varepsilon) = \frac{\mathcal{V}}{2\pi^2} \frac{3}{(\hbar v_D)^3} \int_0^{k_B T_D} d\varepsilon \frac{\varepsilon^3}{e^{\beta\varepsilon} - 1}. \quad (3.28)$$

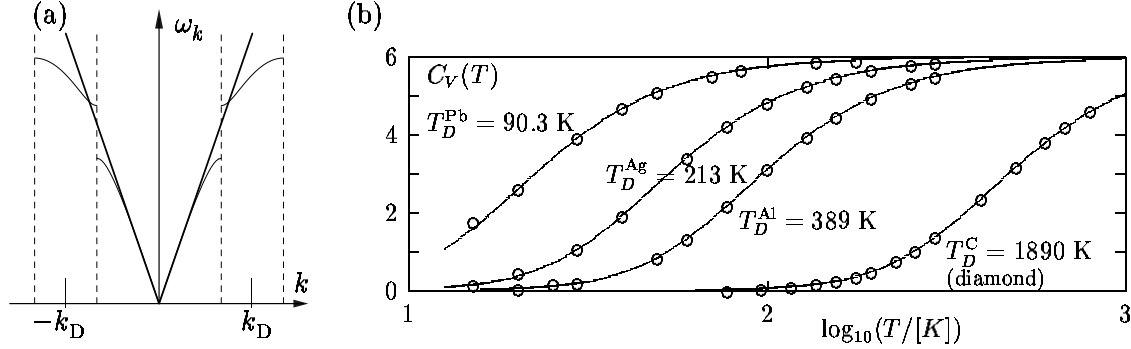


Figure 3.6: (a) The linear Debye approximation to the phonon spectrum with the Debye wave vector k_D shown. (b) Comparison between experiment and the Debye model of heat capacitance applied for lead, silver, aluminum, and diamond.

It is now straight forward to obtain C_V^{ion} from Eq. (3.28) by differentiation:

$$C_V^{\text{ion}}(T) = \frac{\partial E_{\text{ion}}}{\partial T} = 9N_{\text{ion}}k_B \left(\frac{T}{T_D}\right)^3 \int_0^{T_D/T} dx \frac{x^4 e^x}{(e^x - 1)^2}, \quad (3.29)$$

where the integrand is rendered dimensionless by introducing T_D from Eq. (3.26). Note that T_D is the only free parameter in the Debye model of heat capacitance; v_D dropped out of the calculation. Note also how the model reproduces the classical Dulong-Petit value in the high temperature limit, where all oscillators are thermally excited. In the low temperature limits the oscillators “freeze out” and the heat capacitance drops as T^3 ,

$$C_V^{\text{ion}}(T) \xrightarrow{T \ll T_D} \frac{12\pi^4}{5} N_{\text{ion}}k_B \left(\frac{T}{T_D}\right)^3, \quad C_V^{\text{ion}}(T) \xrightarrow{T \gg T_D} 3N_{\text{ion}}k_B. \quad (3.30)$$

In Fig. 3.6(b) the Debye model is compared to experiment. A remarkable agreement is obtained over the wide temperature range from 10 K to 1000 K after fitting T_D for each of the widely different materials lead, aluminum, silver and diamond.

We end this section by a historical remark. The very first published application of quantum theory to a condensed matter problem was in fact Einstein’s work from 1906, reproduced in Fig. 3.7(a), explaining the main features of Weber’s 1875 measurements on diamond. In analogy with Planck’s quantization of the oscillators related to the black body radiation, Einstein quantized the oscillators corresponding to the lattice vibrations, assuming that all oscillators had the same frequency ω_E . So instead of Eq. (3.27), Einstein employed the much simpler $D_{\text{ion}}^E(\varepsilon) = \delta(\varepsilon - \hbar\omega_E)$, which immediately leads to

$$C_V^{\text{ion,E}}(T) = 3N_{\text{ion}}k_B \left(\frac{T_E}{T}\right)^2 \frac{e^{T_E/T}}{(e^{T_E/T} - 1)^2}, \quad T_E \equiv \hbar\omega_E/k_B. \quad (3.31)$$

While this theory also gives the classical result $3N_{\text{ion}}k_B$ in the high temperature limit, it exaggerates the decrease of C_V^{ion} at low temperatures by predicting an exponential suppression. In Fig. 3.7(b) is shown a comparison of Debye’s and Einstein’s models. Nowadays, Einstein’s formula is still in use, since it provides a fairly accurate description of the optical phonons which in many cases have a reasonably flat dispersion relation.

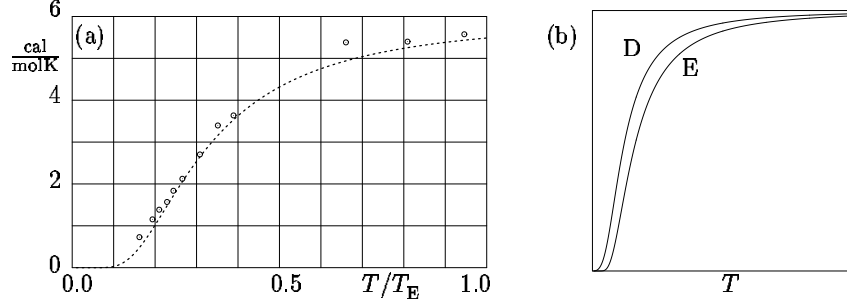


Figure 3.7: (a) The first application of quantum theory to condensed matter physics. Einstein's 1906 theory of heat capacitance of solids. The theory is compared to Weber's 1875 measurements on diamond. (b) A comparison between Debye's and Einstein's model.

3.6 Electron-phonon interaction in the lattice model

In Chap. 2 we mentioned that in the lattice model the electron-ion interaction splits in two terms, one arising from the static lattice and the other from the ionic vibrations, $V_{\text{el-ion}} = V_{\text{el-latt}} + V_{\text{el-ph}}$. The former has already been dealt with in the H_{Bloch} , so in this section the task is to derive the explicit second quantized form of the latter. Regarding the basis states for the combined electron and phonon system we are now in the situation discussed in Sec. 1.4.5. We will simply use the product states given in Eq. (1.108).

Our point of departure is the simple expression for the Coulomb energy of an electron density in the electric potential $V_{\text{ion}}(\mathbf{r} - \mathbf{R}_j)$ of an ion placed at the position \mathbf{R}_j ,

$$V_{\text{el-ion}} = \int d\mathbf{r} (-e)\rho_{\text{el}}(\mathbf{r}) \sum_{j=1}^N V_{\text{ion}}(\mathbf{r} - \mathbf{R}_j). \quad (3.32)$$

As before the actual ion coordinates are given by $\mathbf{R}_j = \mathbf{R}_j^0 + \mathbf{u}_j$, where \mathbf{R}_j^0 are the ionic equilibrium positions, i.e. the static periodic lattice, and where \mathbf{u}_j denotes the lattice vibrations. The respective contributions from these two sets of coordinates are separated by a Taylor expansion, $V_{\text{ion}}(\mathbf{r} - \mathbf{R}_j) \approx V_{\text{ion}}(\mathbf{r} - \mathbf{R}_j^0) - \nabla_{\mathbf{r}} V_{\text{ion}}(\mathbf{r} - \mathbf{R}_j^0) \cdot \mathbf{u}_j$, note the sign of the second term, and we obtain

$$V_{\text{el-ion}} = \int d\mathbf{r} (-e)\rho_{\text{el}}(\mathbf{r}) \sum_{j=1}^N V_{\text{ion}}(\mathbf{r} - \mathbf{R}_j^0) - \int d\mathbf{r} (-e)\rho_{\text{el}}(\mathbf{r}) \sum_{j=1}^N \nabla_{\mathbf{r}} V_{\text{ion}}(\mathbf{r} - \mathbf{R}_j^0) \cdot \mathbf{u}_j. \quad (3.33)$$

The first term is the one entering H_{Bloch} in Eq. (2.6), while the second is the electron-phonon interaction, also sketched in Fig. 3.8,

$$V_{\text{el-ph}} = \int d\mathbf{r} \rho_{\text{el}}(\mathbf{r}) \left\{ \sum_j e \mathbf{u}_j \cdot \nabla_{\mathbf{r}} V_{\text{ion}}(\mathbf{r} - \mathbf{R}_j^0) \right\}. \quad (3.34)$$

$V_{\text{el-ph}}$ is readily defined in real space, but a lot easier to use in \mathbf{k} -space, so we will proceed



Figure 3.8: (a) Being in an eigenstate a Bloch electron moves through a *perfect* lattice without being scattered. (b) A displaced ion results in an electric dipole relative to the perfect background, and this can scatter Bloch electrons from $|\mathbf{k}, \sigma\rangle$ to $|\mathbf{k}', \sigma\rangle$.

by Fourier transforming it. Let us begin with the ionic part, the $\mathbf{u} \cdot \nabla V$ -term. The Fourier transform of \mathbf{u}_j is given in Eq. (3.22), where we note that the phonon wavevector \mathbf{k} is restricted to the Brillouin zone $\mathbf{k} \in \text{FBZ}$. Defining $V_{\text{ion}}(\mathbf{r}) = \frac{1}{\mathcal{V}} \sum_{\mathbf{p}} V_{\mathbf{p}} e^{i\mathbf{p} \cdot \mathbf{r}}$, we see that $\nabla_{\mathbf{r}}$ simply brings down a factor $i\mathbf{p}$. To facilitate comparison to the phonon wavevector \mathbf{k} we decompose \mathbf{p} as in Eq. (2.10): $\mathbf{p} = \mathbf{q} + \mathbf{G}$, where $\mathbf{q} \in \text{FBZ}$ and $\mathbf{G} \in \text{RL}$. All in all we have

$$\nabla_{\mathbf{r}} V_{\text{ion}}(\mathbf{r} - \mathbf{R}_j^0) = \frac{1}{\mathcal{V}} \sum_{\mathbf{q} \in \text{FBZ}} \sum_{\mathbf{G} \in \text{RL}} i(\mathbf{q} + \mathbf{G}) V_{\mathbf{q}+\mathbf{G}} e^{i(\mathbf{q}+\mathbf{G}) \cdot (\mathbf{r} - \mathbf{R}_j^0)}, \quad (3.35)$$

$$\mathbf{u}_j = \frac{1}{\sqrt{N}} \sum_{\mathbf{k} \in \text{FBZ}} \sum_{\lambda} \frac{\ell_{\mathbf{k}\lambda}}{\sqrt{2}} (b_{\mathbf{k},\lambda} + b_{-\mathbf{k},\lambda}^{\dagger}) \boldsymbol{\epsilon}_{\mathbf{k}\lambda} e^{i\mathbf{k} \cdot \mathbf{R}_j^0}. \quad (3.36)$$

These expressions, together with $\sum_j e^{i\mathbf{k} \cdot \mathbf{R}_j} = N\delta_{\mathbf{k},0}$, and multiplying by e , lead to

$$\sum_j e \mathbf{u}_j \cdot \nabla_{\mathbf{r}} V_{\text{el}}(\mathbf{r} - \mathbf{R}_j^0) = \frac{1}{\mathcal{V}} \sum_{\substack{\mathbf{q} \in \text{FBZ} \\ \mathbf{G} \in \text{RL}, \lambda}} g_{\mathbf{q},\mathbf{G},\lambda} (b_{\mathbf{q},\lambda} + b_{-\mathbf{q},\lambda}^{\dagger}) e^{i(\mathbf{q}+\mathbf{G}) \cdot \mathbf{r}}, \quad (3.37)$$

where we have introduced the phonon coupling strength $g_{\mathbf{q},\mathbf{G},\lambda}$ given by

$$g_{\mathbf{q},\mathbf{G},\lambda} = ie \sqrt{\frac{N\hbar}{2M\omega_{\mathbf{q}\lambda}}} (\mathbf{q} + \mathbf{G}) \cdot \boldsymbol{\epsilon}_{\mathbf{q}\lambda} V_{\mathbf{q}+\mathbf{G}}. \quad (3.38)$$

The final result, $V_{\text{el-ph}}$, is now obtained by inserting the Fourier representation of the electron density, $\rho_{\text{el}}(\mathbf{r}) = \frac{1}{\mathcal{V}} \sum_{\mathbf{k}\mathbf{p}\sigma} e^{-i\mathbf{p} \cdot \mathbf{r}} c_{\mathbf{k}+\mathbf{p}\sigma}^{\dagger} c_{\mathbf{k}\sigma}$, derived in Eq. (1.96), together with Eq. (3.37) into Eq. (3.34), and utilizing $\int d\mathbf{r} e^{i\mathbf{k} \cdot \mathbf{r}} = \mathcal{V}\delta_{\mathbf{k},0}$:

$$V_{\text{el-ph}} = \frac{1}{\mathcal{V}} \sum_{\mathbf{k}\sigma} \sum_{\mathbf{q}\lambda} \sum_{\mathbf{G}} g_{\mathbf{q},\mathbf{G},\lambda} c_{\mathbf{k}+\mathbf{q}+\mathbf{G},\sigma}^{\dagger} c_{\mathbf{k}\sigma} (b_{\mathbf{q},\lambda} + b_{-\mathbf{q},\lambda}^{\dagger}). \quad (3.39)$$

The interpretation of this formula is quite simple. Under momentum conservation (but only up to an undetermined reciprocal lattice vector due to the periodicity of the lattice) and spin conservation the electrons can be scattered from any initial state $|\mathbf{k}, \sigma\rangle_{\text{el}}$ to the final state $|\mathbf{k} + \mathbf{q} + \mathbf{G}, \sigma\rangle_{\text{el}}$ either by absorbing a phonon from the state $|\mathbf{q}\lambda\rangle_{\text{ph}}$ or by emitting a phonon into the state $|- \mathbf{q}\lambda\rangle_{\text{ph}}$. A graphical representation of this fundamental process is shown in Fig. 3.9.

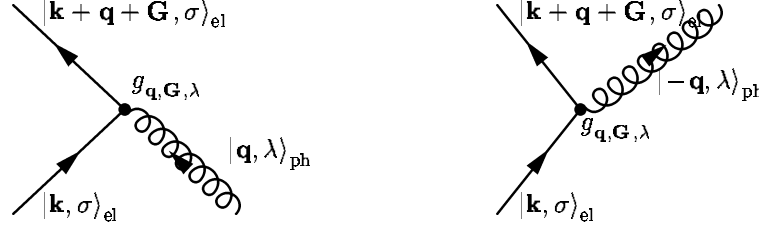


Figure 3.9: A graphical representation of the fundamental electron-phonon coupling. The electron states are represented by the straight lines, the phonon states by curly spring-like lines, and the coupling strength by a dot. To the left the electron is scattered by absorbing a phonon, to the right by emitting a phonon.

The normal processes, i.e. processes where per definition $\mathbf{G} = 0$, often tend to dominate over the so-called umklapp processes, where $\mathbf{G} \neq 0$, so in the following we shall completely neglect the latter.² Moreover, we shall treat only isotropic media, where $\epsilon_{\mathbf{q}\lambda}$ is either parallel to or perpendicular to \mathbf{q} , i.e. $\mathbf{q} \cdot \epsilon_{\mathbf{q}\lambda}$ in $g_{\mathbf{q},\mathbf{G}=0,\lambda}$ is only non-zero for longitudinally polarized phonons. So in the **I**sotropic case for **N**ormal phonon processes we have

$$V_{\text{el-ph}}^{\text{IN}} = \frac{1}{\mathcal{V}} \sum_{\mathbf{k}\sigma} \sum_{\mathbf{q}\lambda_l} g_{\mathbf{q},\lambda_l} c_{\mathbf{k}+\mathbf{q},\sigma}^\dagger c_{\mathbf{k}\sigma} (b_{\mathbf{q},\lambda_l} + b_{-\mathbf{q},\lambda_l}^\dagger). \quad (3.40)$$

Finally, the most significant physics of the electron-phonon coupling can often be extracted from considering just the acoustical modes. Due to their low energies they are excited significantly more than the high energy optical phonons at temperatures lower than the Debye temperature. Thus in the **I**sotropic case for **N**ormal **A**coustical phonon processes only the longitudinal acoustical branch enters and we have

$$V_{\text{el-ph}}^{\text{INA}} = \frac{1}{\mathcal{V}} \sum_{\mathbf{k}\sigma} \sum_{\mathbf{q}} g_{\mathbf{q}} c_{\mathbf{k}+\mathbf{q},\sigma}^\dagger c_{\mathbf{k}\sigma} (b_{\mathbf{q}} + b_{-\mathbf{q}}^\dagger). \quad (3.41)$$

If we for ions with charge $+Ze$ approximate $V_{\mathbf{q}}$ by a Yukawa potential, $V_{\mathbf{q}} = \frac{Ze}{\epsilon_0} \frac{1}{q^2 + k_s^2}$ (see Exercise 1.5), the explicit form of the coupling constant $g_{\mathbf{q}}$ is particularly simple:

$$g_{\mathbf{q}} = i \frac{Ze^2}{\epsilon_0} \frac{q}{q^2 + k_s^2} \sqrt{\frac{N\hbar}{2M\omega_{\mathbf{q}}}}. \quad (3.42)$$

3.7 Electron-phonon interaction in the jellium model

Finally, we return to the case of Einstein phonons in the jellium model treated in Sec. 3.1. The electron-phonon interaction in this case is derived in analogy with the that of normal

²There are mainly two reasons why the umklapp processes often can be neglected: (1) $V_{\mathbf{q}+\mathbf{G}}$ is small due to the $1/(\mathbf{q} + \mathbf{G})^2$ dependence, and (2) At low temperatures the phase space available for umklapp processes is small.

lattice phonons in the isotropic case, Eq. (3.41). If we as in Sec. 3.1 neglect the weak dispersion of the Einstein phonons and simply assume that they all vibrate with the ion plasma frequency Ω of Eq. (3.3), the result for N vibrating ions in the volume \mathcal{V} is

$$V_{\text{el-ph}}^{\text{jel}} = \frac{1}{\mathcal{V}} \sum_{\mathbf{k}\sigma} \sum_{\mathbf{q}} g_{\mathbf{q}}^{\text{jel}} c_{\mathbf{k}+\mathbf{q},\sigma}^{\dagger} c_{\mathbf{k}\sigma} (b_{\mathbf{q}} + b_{-\mathbf{q}}^{\dagger}), \quad (3.43)$$

with

$$g_{\mathbf{q}}^{\text{jel}} = i \frac{Ze^2}{\epsilon_0} \frac{1}{q} \sqrt{\frac{N\hbar}{2M\Omega}}. \quad (3.44)$$

3.8 Summary and outlook

In this chapter we have derived the second quantized form of the Hamiltonian of the isolated phonon system and the electron-phonon coupling. The solution of the phonon problem actually constitutes our first solution of a real interacting many-particle system, each ion is coupled to its neighbors. Also the treatment of the electron-phonon coupling marks an important step forward: here we dealt for the first time with the coupling between to different kinds of particles, electrons and phonons.

The electron-phonon coupling is a very important mechanism in condensed matter systems. It is the cause of a large part of electrical resistivity in metals and semiconductors, and it also plays a major role in studies of heat transport. In Exercise 3.1 and Exercise 3.2 give a first hint at how the electron-phonon coupling leads to a scattering or relaxation time for electrons.

We shall return to the electron-phonon coupling in Chap. 16, and there see the first hint of the remarkable interplay between electrons and phonons that lies at the heart of the understanding of conventional superconductivity. The very successful microscopic theory of superconductivity, the so-called BCS theory, is based on the electron-phonon scattering, even the simple form given in Eqs. (3.41) and (3.42) suffices to cause superconductivity.

Chapter 4

Mean field theory

The physics of interacting particles is often very complicated because the motions of the individual particles depend on the position of all the others, or in other words the particles motions become correlated. This is clearly the case for a system of charged particles interacting by Coulomb forces, such as e.g. the electron gas. There we expect the probability to find two electrons in close proximity to be small due to the strong repulsive interaction. Consequently, due to these correlation effects there is a suppressed density in the neighborhood of every electron, and one talks about a “correlation hole”.

Nevertheless, in spite of this complicated problem there are a number of cases where a more crude treatment, not fully including the correlations, gives a good physical model. In these cases it suffices to include correlations “on the average”, which means that the effect of the other particles is included as a mean density (or mean field), leaving an effective single particle problem, which is soluble. This idea is illustrated in Fig. 4.1. The mean fields are chosen as those which minimize the free energy, which in turn ensure that the method is consistent, as we shall see shortly. This approximation scheme is called “mean field theory”. Upon performing the mean field approximation we can neglect the detailed dynamics and the time-independent second quantization method described in Chap. 1 suffices.

There exist numerous examples of the success of the mean field method and its ability

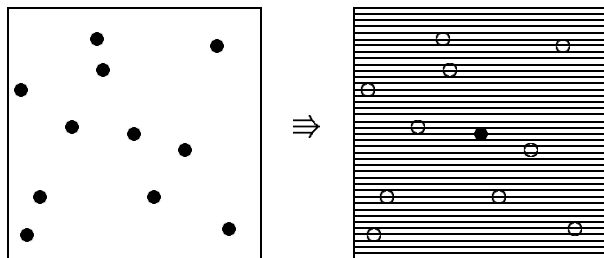


Figure 4.1: Illustration of the mean field idea. Left box shows the real physical system where the interaction leads to correlation between the particle motions. To the right are the interactions felt by the black particle replaced by an average interaction due to the average density of the white particles.

to explain various physical phenomena. In this chapter, we shall discuss a few examples from condensed matter physics, but before going to specific examples let us discuss the mathematical structure of the mean field theory.

First we consider a system with two kinds of particles, described by operators a_ν and b_μ , respectively. Let us assume that only interactions between different kind of particles are important. The Hamiltonian is

$$H = H_0 + V_{\text{int}}, \quad (4.1a)$$

$$H_0 = \sum_{\nu} \xi_{\nu}^a a_{\nu}^{\dagger} a_{\nu} + \sum_{\mu} \xi_{\mu}^b b_{\mu}^{\dagger} b_{\mu}, \quad (4.1b)$$

$$V_{\text{int}} = \sum_{\nu\nu',\mu\mu'} V_{\nu\mu,\nu'\mu'} a_{\nu}^{\dagger} b_{\mu}^{\dagger} b_{\mu'} a_{\nu'}. \quad (4.1c)$$

Now suppose that we expect, based on physical arguments, that the density operators $a_{\nu}^{\dagger} a_{\nu'}$ and $b_{\mu}^{\dagger} b_{\mu'}$ deviate only little from their average values, $\langle a_{\nu}^{\dagger} a_{\nu'} \rangle$ and $\langle b_{\mu}^{\dagger} b_{\mu'} \rangle$. It is then natural to use this deviation as a small parameter and perform an expansion. In order to do so we define the deviation operators

$$d_{\nu\nu'} = a_{\nu}^{\dagger} a_{\nu'} - \langle a_{\nu}^{\dagger} a_{\nu'} \rangle, \quad (4.2a)$$

$$e_{\mu\mu'} = b_{\mu}^{\dagger} b_{\mu'} - \langle b_{\mu}^{\dagger} b_{\mu'} \rangle, \quad (4.2b)$$

and insert them into (4.1a), which gives

$$H = H_0 + V_{\text{MF}} + \overbrace{\sum_{\nu\nu',\mu\mu'} V_{\nu\mu,\nu'\mu'} d_{\nu\nu'} e_{\mu\mu'}}^{\text{neglected in mean field}}, \quad (4.3)$$

where

$$V_{\text{MF}} = \sum_{\nu\nu',\mu\mu'} V_{\nu\mu,\nu'\mu'} \left(a_{\nu}^{\dagger} a_{\nu'} \langle b_{\mu}^{\dagger} b_{\mu'} \rangle + b_{\mu}^{\dagger} b_{\mu'} \langle a_{\nu}^{\dagger} a_{\nu'} \rangle \right) - \sum_{\nu\nu',\mu\mu'} V_{\nu\mu,\nu'\mu'} \langle a_{\nu}^{\dagger} a_{\nu'} \rangle \langle b_{\mu}^{\dagger} b_{\mu'} \rangle, \quad (4.4)$$

Because $d_{\nu\nu'}$ and $e_{\mu\mu'}$ are assumed to be small the second term in Eq. (4.3) is neglected, and the interaction V_{int} is approximated by the mean field interaction V_{MF} resulting in the so-called mean field Hamiltonian H_{MF} given by

$$H_{\text{MF}} = H_0 + V_{\text{MF}}. \quad (4.5)$$

The mean field Hamiltonian H_{MF} contains only single-particle operators, and thus the original many-body problem has been reduced to a single-particle problem, which in principle is always soluble.¹

¹To see that a single-particle problem or a quadratic Hamiltonian can always be diagonalized, write H as $H = \sum_{ij} a_i^{\dagger} h_{ij} a_j$. Now since \mathbf{h} is a hermitian matrix there exists a transformation, $\alpha_i = \sum_j U_{ij} a_j$, with \mathbf{U} being a unitary matrix, such that \mathbf{h} is diagonal, $\sum_{kk'} U_{ik}^{\dagger} h_{kk'} U_{k'j} = \delta_{ij} \epsilon_i$. In terms of the new basis the Hamiltonian then becomes $H = \sum_i \alpha_i^{\dagger} \epsilon_i \alpha_i$, and $\{\epsilon_i\}$ are thus the eigenvalues of \mathbf{h} .

Looking at Eq. (4.4) we can formulate the mean field procedure in a different way: If we have an interaction term involving two operators A and B given by a product of the two

$$H_{AB} = AB, \quad (4.6)$$

then the mean field approximation is given by A coupled to the mean field of B plus B coupled to the mean field of A and finally to avoid double counting subtracted by the product of the mean fields (such that $\langle H_{AB}^{\text{MF}} \rangle = \langle A \rangle \langle B \rangle$):

$$H_{AB}^{\text{MF}} = A\langle B \rangle + \langle A \rangle B - \langle A \rangle \langle B \rangle. \quad (4.7)$$

The question is however how to find the averages $\langle a_\nu^\dagger a_{\nu'} \rangle$ and $\langle b_\mu^\dagger b_{\mu'} \rangle$. There are two possible routes which in fact are equivalent. Method 1: The average is to be determined self-consistently, i.e. when calculating the averages

$$\bar{n}_{\nu\nu'}^a \equiv \langle a_\nu^\dagger a_{\nu'} \rangle, \quad (4.8a)$$

$$\bar{n}_{\mu\mu'}^b \equiv \langle b_\mu^\dagger b_{\mu'} \rangle, \quad (4.8b)$$

using the new mean field Hamiltonian, the same answer should come out. This means for \bar{n}^a (and similarly for \bar{n}^b) that

$$\bar{n}_{\nu\nu'}^a \equiv \langle a_\nu^\dagger a_{\nu'} \rangle_{\text{MF}} = \frac{1}{Z_{\text{MF}}} \text{Tr} \left(e^{-\beta H_{\text{MF}}} a_\nu^\dagger a_{\nu'} \right), \quad (4.9)$$

where Z_{MF} is the mean field partition function given by

$$Z_{\text{MF}} = \text{Tr} \left(e^{-\beta H_{\text{MF}}} \right). \quad (4.10)$$

Eq. (4.9) and the similar one for \bar{n}^b are called the self-consistency equations (because \bar{n}^a and \bar{n}^b are given in terms of H_{MF} and Z_{MF} , which themselves depend on \bar{n}^a and \bar{n}^b).

Next we turn to the alternative route. Method 2: Use the $n_{\nu\nu'}$ that minimizes the free energy F_{MF} of the mean field Hamiltonian. Using the expression for the free energy given in Sec. 1.5, we get

$$\begin{aligned} 0 &= \frac{d}{d\bar{n}_{\nu\nu'}^a} F_{\text{MF}} = \frac{d}{d\bar{n}_{\nu\nu'}^a} \left(-\frac{1}{\beta} \ln Z_{\text{MF}} \right) \\ &= \frac{1}{Z_{\text{MF}}} \text{Tr} \left(e^{-\beta H_{\text{MF}}} \frac{d}{d\bar{n}_{\nu\nu'}^a} H_{\text{MF}} \right) \\ &= \frac{1}{Z_{\text{MF}}} \text{Tr} \left(e^{-\beta H_{\text{MF}}} \left(\sum_{\mu\mu'} V_{\nu\mu,\nu'\mu'} (b_\mu^\dagger b_{\mu'} - \bar{n}_{\mu\mu'}^b) \right) \right) \\ &= \sum_{\mu\mu'} V_{\nu\mu,\nu'\mu'} \left(\langle b_\mu^\dagger b_{\mu'} \rangle_{\text{MF}} - \bar{n}_{\mu\mu'}^b \right). \end{aligned} \quad (4.11)$$

This should hold for any pair (ν, ν') and hence the last parenthesis has to vanish and we arrive at the self-consistency equation for \bar{n}^b . Similarly by minimizing with respect to \bar{n}^b we get Eq. (4.9). Thus the two methods are equivalent.

We can gain some more understanding of the physical content of the mean field approximation if we look at average interaction energy $\langle V_{\text{int}} \rangle$. A natural approximation would be to evaluate the expectation value of a and b operator separately,

$$\langle V_{\text{int}} \rangle \approx \sum_{\nu\nu', \mu\mu'} V_{\nu\mu, \nu'\mu'} \langle a_{\nu}^{\dagger} a_{\nu'} \rangle \langle b_{\mu}^{\dagger} b_{\mu'} \rangle, \quad (4.12)$$

which is equivalent to assuming that the a and b particles are uncorrelated². This is in essence the approximation done in the mean field approach. To see this let us evaluate $\langle V_{\text{int}} \rangle$ using the mean field Hamiltonian

$$\langle V_{\text{int}} \rangle_{\text{MF}} = \frac{1}{Z_{\text{MF}}} \text{Tr} \left(e^{-\beta H_{\text{MF}}} V_{\text{int}} \right). \quad (4.13)$$

Because the mean field Hamiltonian can be separated into a part containing only a -operators and a part containing only b -operators, $H_{\text{MF}} = H_{\text{MF}}^a + H_{\text{MF}}^b$, the average factorizes exactly as in Eq. (4.12), and we get

$$\langle V_{\text{int}} \rangle_{\text{MF}} = \sum_{\nu\nu', \mu\mu'} V_{\nu\mu, \nu'\mu'} \langle a_{\nu}^{\dagger} a_{\nu'} \rangle_{\text{MF}} \langle b_{\mu}^{\dagger} b_{\mu'} \rangle_{\text{MF}}. \quad (4.14)$$

The mean field approach hence provides a consistent and physically sensible method to study interacting systems where correlations are less important. Here “less important” should be quantified by checking the validity of the mean field approximation. That is, one should check that d indeed is small by calculating $\langle d \rangle$, using the neglected term in (4.3) as a perturbation, and then compare the result to $\langle a_{\nu}^{\dagger} a_{\nu'} \rangle$. If it is not small, one has either chosen the wrong mean field parameter, or the method simply fails and other tools more adequate to deal with the problem at hand must be applied.

4.1 The art of mean field theory

In practice one has to assume something about the averages $\langle a_{\nu}^{\dagger} a_{\nu'} \rangle$ and $\langle b_{\mu}^{\dagger} b_{\mu'} \rangle$ because even though (4.9) gives a recipe on how to find which averages are important, there are simply too many possible combinations. Suppose we have N different quantum numbers, then there are in principle N^2 different combinations, which gives N^2 coupled non-linear equations, which of course is only tractable for small systems. With modern computers one can treat hundreds of particles in this way, but for a condensed matter system, it is out of the question. Therefore, one must provide some physical insight to reduce the number of mean field parameters.

Often symmetry arguments can help reducing the number of parameters. Suppose for example that the Hamiltonian that we are interested in has translational symmetry, such that momentum space is a natural choice. For a system of particles described by operators c and c^{\dagger} , we then have

$$\langle c_{\mathbf{k}}^{\dagger} c_{\mathbf{k}'} \rangle = \frac{1}{\mathcal{V}} \int d\mathbf{r} \int d\mathbf{r}' e^{-i\mathbf{k}' \cdot \mathbf{r}'} e^{i\mathbf{k} \cdot \mathbf{r}} \langle \Psi^{\dagger}(\mathbf{r}) \Psi(\mathbf{r}') \rangle. \quad (4.15)$$

²Remember from usual statistics that the correlation function between two stochastic quantities X and Y is defined by $\langle XY \rangle - \langle X \rangle \langle Y \rangle$.

It is natural to assume that the system is homogeneous, which means

$$\langle \Psi^\dagger(\mathbf{r})\Psi(\mathbf{r}') \rangle = f(\mathbf{r} - \mathbf{r}') \Rightarrow \langle c_{\mathbf{k}}^\dagger c_{\mathbf{k}'} \rangle = \langle n_{\mathbf{k}} \rangle \delta_{\mathbf{k}, \mathbf{k}'}. \quad (4.16)$$

This assumption about homogeneity is however not always true, because in some cases the symmetry of the system is lower than that of the Hamiltonian. For example if the system spontaneously orders into a state with a spatial density variation, like a wave formation then the average $\langle \Psi^\dagger(\mathbf{r})\Psi(\mathbf{r}') \rangle$ is not function of the $\mathbf{r} - \mathbf{r}'$ only. Instead it has a lower and more restricted symmetry, namely that

$$\langle \Psi^\dagger(\mathbf{r})\Psi(\mathbf{r}') \rangle = h(\mathbf{r}, \mathbf{r}'), \quad h(\mathbf{r}, \mathbf{r}') = h(\mathbf{r} + \mathbf{R}, \mathbf{r}' + \mathbf{R}) \quad (4.17)$$

with \mathbf{R} being a lattice vector. The kind of crystal structure of course exists in Nature and when it happens we talk about phenomena with broken symmetry. It is important to realize that this solution cannot be found if we assumed Eq. (4.16) from line one. Instead we should have started by assuming Eq. (4.17) leading to the possibility of $\langle c_{\mathbf{k}}^\dagger c_{\mathbf{k}+\mathbf{Q}} \rangle$ being finite, where $\mathbf{R} \cdot \mathbf{Q} = 2\pi$. Thus the choice of the proper mean field parameters requires physical motivation about which possible states one expects.

4.2 Hartree–Fock approximation

Above we discussed the mean field theory for interactions between different particles. Here we go on to formulate the method for like particles. For the interaction term in Eq. (4.1a) we use the approximation to replace $a_\nu^\dagger a_{\nu'}$ and $b_\mu^\dagger b_{\mu'}$ by their average values plus small corrections. For interactions between identical particles this, however, does not exhaust the possibilities and only includes the so-called Hartree term and now we discuss the more general approximation scheme, called the Hartree–Fock approximation. Suppose we have a system of interacting particles described by the Hamiltonian

$$H = H_0 + V_{\text{int}}, \quad (4.18a)$$

$$H_0 = \sum_{\nu} \xi_{\nu} c_{\nu}^\dagger c_{\nu}, \quad (4.18b)$$

$$V_{\text{int}} = \frac{1}{2} \sum_{\nu\nu', \mu\mu'} V_{\nu\mu, \nu'\mu'} c_{\nu}^\dagger c_{\mu}^\dagger c_{\mu'} c_{\nu'}. \quad (4.18c)$$

The basic idea behind the mean field theory was that the operator

$$\rho_{\mu\mu'} = c_{\mu}^\dagger c_{\mu'}, \quad (4.19)$$

is large only when the average $\langle \rho_{\mu\mu'} \rangle$ is non-zero. For most of the combinations $\nu\nu'$ the average $\langle \rho_{\nu\nu'} \rangle$ is zero. We therefore use the same strategy as in the introduction and write the four operators in the interaction term in terms of a deviation from the average value

$$c_{\nu}^\dagger \left(c_{\mu}^\dagger c_{\mu'} - \langle c_{\mu}^\dagger c_{\mu'} \rangle \right) c_{\nu'} + c_{\nu}^\dagger c_{\nu'} \langle c_{\mu}^\dagger c_{\mu'} \rangle. \quad (4.20)$$

If the quantum number ν' is different from μ we can commute $c_{\nu'}$ with the parenthesis. This is true except in a set of measure zero. With this assumption we again write $c_{\nu}^\dagger c_{\nu'}$ as its average value plus a deviation, which gives

$$\left(c_{\nu}^\dagger c_{\nu'} - \langle c_{\nu}^\dagger c_{\nu'} \rangle\right) \left(c_{\mu}^\dagger c_{\mu'} - \langle c_{\mu}^\dagger c_{\mu'} \rangle\right) + c_{\nu}^\dagger c_{\nu'} \langle c_{\mu}^\dagger c_{\mu'} \rangle + c_{\mu}^\dagger c_{\mu'} \langle c_{\nu}^\dagger c_{\nu'} \rangle - \langle c_{\mu}^\dagger c_{\mu'} \rangle \langle c_{\nu}^\dagger c_{\nu'} \rangle. \quad (4.21)$$

If we neglect the first term, which is proportional to the deviation squared, we have arrived at the Hartree approximation for interactions

$$V_{\text{int}}^{\text{Hartree}} = \frac{1}{2} \sum V_{\nu\mu,\nu'\mu'} \bar{n}_{\mu\mu'} c_{\nu}^\dagger c_{\nu'} + \frac{1}{2} \sum V_{\nu\mu,\nu'\mu'} \bar{n}_{\nu\nu'} c_{\mu}^\dagger c_{\mu'} - \frac{1}{2} \sum V_{\nu\mu,\nu'\mu'} \bar{n}_{\nu\nu'} \bar{n}_{\mu\mu'}. \quad (4.22)$$

This is the same result we would get if we considered the operators with (ν, ν') and (μ, μ') to be different kinds of particles and used the formula from the previous section. However, this is not the full result because here the operators labelled by μ and ν represent identical, indistinguishable particles and there is therefore one combination we missed be the Hartree approximation, namely the so-called exchange or Fock term. This new term appears because the product of four operators in Eq. (4.18c) also gives a large contribution when $\langle c_{\nu}^\dagger c_{\mu'} \rangle$ is finite. To derive the mean field contribution from this possibility we thus have to first replace $c_{\nu}^\dagger c_{\mu'}$ by its average value and following the principle in Eq. (4.7) do the same with the combination $c_{\mu}^\dagger c_{\nu'}$. The mean field result for the Fock term thus becomes

$$V_{\text{int}}^{\text{Fock}} = -\frac{1}{2} \sum V_{\nu\mu,\nu'\mu'} \bar{n}_{\nu\mu'} c_{\mu}^\dagger c_{\nu'} - \frac{1}{2} \sum V_{\nu\mu,\nu'\mu'} \bar{n}_{\mu\nu'} c_{\nu}^\dagger c_{\mu'} + \frac{1}{2} \sum V_{\nu\mu,\nu'\mu'} \bar{n}_{\nu\mu'} \bar{n}_{\mu\nu'}. \quad (4.23)$$

The final mean field Hamiltonian within the Hartree–Fock approximation is

$$H^{\text{HF}} = H_0 + V_{\text{int}}^{\text{Fock}} + V_{\text{int}}^{\text{Hartree}} \quad (4.24)$$

Consider now the example of a homogeneous electron gas which is translation invariant, which means that the expectation value $\langle c_{\mathbf{k}}^\dagger c_{\mathbf{k}'} \rangle$ is diagonal. We can now read off the corresponding Hartree–Fock Hamiltonian, see Exercise 4.1 from Eq. (1.104). The result is

$$H^{\text{HF}} = \sum_{\mathbf{k}\sigma} \xi_{\mathbf{k}}^{\text{HF}} c_{\mathbf{k}\sigma}^\dagger c_{\mathbf{k}\sigma}, \quad (4.25a)$$

$$\begin{aligned} \xi_{\mathbf{k}}^{\text{HF}} &= \xi_{\mathbf{k}} + \sum_{\mathbf{k}'\sigma'} [V(0) - \delta_{\sigma\sigma'} V(\mathbf{k} - \mathbf{k}')] n_{\mathbf{k}'\sigma'}, \\ &= \xi_{\mathbf{k}} + V(0)N - \sum_{\mathbf{k}'\sigma'} V(\mathbf{k} - \mathbf{k}') n_{\mathbf{k}'\sigma'}. \end{aligned} \quad (4.25b)$$

The second term is the interaction with the average electron charge. As explained in Chap. 2 in condensed matter systems it is normally cancelled out by an equally large term due to the positively charged ionic background. The third term is the exchange correction.

Again we emphasize that the Hartree–Fock approximation depends crucially on what averages we assume to be finite, and these assumptions must be based on physical knowledge or clever guess-work. In deriving Eq. (4.25b) we assumed for example that the spin

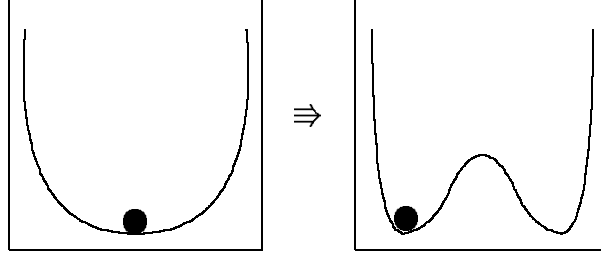


Figure 4.2: The energetics of a phase transition. Above the critical point the effective potential has a well-defined minimum at the symmetry point, and the system is in a state of large symmetry. Below the critical point a two well potential develops and the system has to choose one of the two possibilities. Even though the total potential is still symmetric the system will reside only in one well due to the macroscopically large energy barrier and thus the state of the system has “lower symmetry” than the potential.

symmetry is also maintained, which implies that $\langle c_{\mathbf{k}\downarrow}^\dagger c_{\mathbf{k}\downarrow} \rangle = \langle c_{\mathbf{k}\uparrow}^\dagger c_{\mathbf{k}\uparrow} \rangle$. If we allow them to be different we have the possibility of obtaining a ferromagnetic solution, which indeed happens in some cases. This is discussed in Sec. 4.4.2.

4.3 Broken symmetry

Mean field theory is often used to study phase transitions and thus changes of symmetry. For a given Hamiltonian with some symmetry (e.g. translational symmetry, rotational symmetry in real space or in spin space) there exists an operator which reflects this symmetry and therefore commutes with the Hamiltonian (e.g. translation operator, rotation operator in real space or spin space). Since the operator and the Hamiltonian commute according to the theory of Hermitian operators a common set of eigenstates exists. Consider for example the case of a liquid of particles where the Hamiltonian of course has translational symmetry, which means that the translational operator $T(\mathbf{R})$ commutes with Hamiltonian, $[H, T(\mathbf{R})] = 0$. Here $T(\mathbf{R})$ is an operator which displaces all particle coordinates by the amount \mathbf{R} . It can be written as $T = \exp(i\mathbf{R} \cdot \mathbf{P})$, where P is the total momentum operator. The total momentum operator is thus a conserved quantity and it is given by

$$\mathbf{P} = \hbar \sum_{\mathbf{k}\sigma} \mathbf{k} c_{\mathbf{k}\sigma}^\dagger c_{\mathbf{k}\sigma}, \quad (4.26)$$

We can now choose an orthogonal basis of states with definite total momentum, $|\mathbf{P}\rangle$. This fact we can use to “prove” the unphysical result that a density wave can never exist. A density wave, with wave vector \mathbf{Q} , means that the Fourier transform of the density operator

$$\rho(\mathbf{Q}) = \sum_{\mathbf{k}\sigma} c_{\mathbf{k}\sigma}^\dagger c_{\mathbf{k}+\mathbf{Q}\sigma}, \quad (4.27)$$

Phenomena	Order parameter physical	Order parameter mathematical
crystal	density wave	$\sum_{\mathbf{k}} \langle c_{\mathbf{k}}^{\dagger} c_{\mathbf{k}+\mathbf{Q}} \rangle$
ferromagnet	magnetization	$\sum_{\mathbf{k}} \langle c_{\mathbf{k}\uparrow}^{\dagger} c_{\mathbf{k}\uparrow} - c_{\mathbf{k}\downarrow}^{\dagger} c_{\mathbf{k}\downarrow} \rangle$
Bose-Einstein condensate	population of $\mathbf{k} = \mathbf{0}$ state	$\langle a_{\mathbf{k}=\mathbf{0}}^{\dagger} \rangle$
superconductor	pair condensate	$\langle c_{\mathbf{k}\uparrow} c_{-\mathbf{k}\downarrow} \rangle$

Table 4.1: Typical examples of spontaneous symmetry breakings and their corresponding order parameters.

has a finite expectation value, but

$$\langle c_{\mathbf{k}\sigma}^{\dagger} c_{\mathbf{k}+\mathbf{Q}\sigma} \rangle = \frac{1}{Z} \sum_{\mathbf{P}} e^{-\beta E_{\mathbf{P}}} \langle \mathbf{P} | c_{\mathbf{k}\sigma}^{\dagger} c_{\mathbf{k}+\mathbf{Q}\sigma} | \mathbf{P} \rangle = 0, \quad (4.28)$$

because $c_{\mathbf{k}}^{\dagger} c_{\mathbf{k}+\mathbf{Q}} | \mathbf{P} \rangle$ has momentum $\mathbf{P} - \mathbf{Q}$ and is thus orthogonal to $| \mathbf{P} \rangle$. We have therefore reached the senseless result that crystals do not exist. In the same way, we could “prove” that magnetism, superconductivity, and other well-known physical phenomena cannot happen. What is wrong?

The proof above breaks down if the sum of states in the thermodynamical average is restricted. Even though crystals with different spatial reference points (or ferromagnets with magnetization in different directions) have formally the same energy, they are effectively decoupled due to the large energy barrier it takes to melt and then recrystallize into a new state with a shifted reference (or direction of magnetization). In those cases where many states of the system are degenerate but separated by large energy barriers, it does not make sense to include them on equal footing in the statistical average as in Eq. (4.28) because they correspond to macroscopically totally different configurations. We are therefore forced to refrain from the fundamental ergodicity postulate of statistical mechanics, also discussed in Sec. 1.5, and built into the description that the phase space of the system falls into physically separated sections. This is often illustrated by the double barrier model of phase transitions shown in Fig. 4.2.

When at some critical temperature the thermodynamical state of the system develops a non-zero expectation value of some macroscopic quantity which has a symmetry lower than the original Hamiltonian it is called *spontaneous breaking of symmetry*. The quantity which signals that a phase transition has occurred is called the order parameter. Typical examples are listed in Table 4.1.

In order to arrive at the new phase in a calculation and to avoid the paradox in Eq. (4.28), one has to built in the possibility of the new phase into the theory. In the mean field approach the trick is to include the order parameter in the choice of finite mean fields and, of course, show that the resulting mean field Hamiltonian leads to a self-consistent finite result. Next we study in some detail examples of symmetry breaking phenomena and their corresponding order parameters.

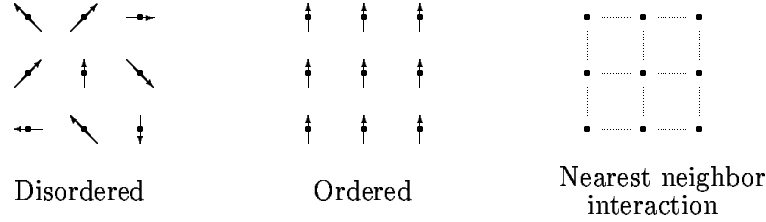


Figure 4.3: The left figure shows the Heisenberg model in the disordered state where there is no preferred direction for spins, while in the ferromagnetic state, shown in the middle, the spins form a collective state with a finite macroscopic moment along one direction. The model discussed here includes interactions between adjacent spins only, as shown in the right panel.

4.4 Ferromagnetism

4.4.1 The Heisenberg model of ionic ferromagnets

In ionic magnetic crystals the interaction between the magnetic ions is due to the exchange interactions originating from the Coulomb interactions. Here we will not go into the details of this interaction but simply give the effective Hamiltonian³, known as the Heisenberg model for interaction between spins in a crystal. It reads

$$H = -2 \sum_{ij} J_{ij} \mathbf{S}_i \cdot \mathbf{S}_j, \quad (4.29)$$

where \mathbf{S}_i is the spin operator for the ion on site i and J_{ij} is the strength of the interaction, between the magnetic moment of the ions on sites i and j . It depends only on the distance between the ions. The interaction is generally short ranged and we truncate it so that it, as in Fig. 4.3, is only non-zero for nearest neighbors

$$J_{ij} = \begin{cases} J_0 & \text{if } i \text{ and } j \text{ are neighbors,} \\ 0 & \text{otherwise.} \end{cases} \quad (4.30)$$

We immediately see that if $J < 0$, the spins tend to become antiparallel whereas for $J > 0$, it is energetically favorable for the spins to be parallel. The first case corresponds to the antiferromagnetic case, while the latter to the ferromagnetic case. Here we consider only the ferromagnetic case, $J > 0$.

As the model Hamiltonian stands, although simple looking, it is immensely complicated and cannot be solved in general, the spins of the individual ions being strongly correlated. However, it is a good example where a mean field solution gives an easy and also physical correct answer. The mean field decomposition then gives

$$H \approx H_{\text{MF}} = -2 \sum_{ij} J_{ij} \langle \mathbf{S}_i \rangle \cdot \mathbf{S}_j - 2 \sum_{ij} J_{ij} \mathbf{S}_i \cdot \langle \mathbf{S}_j \rangle + 2 \sum_{ij} J_{ij} \langle \mathbf{S}_i \rangle \cdot \langle \mathbf{S}_j \rangle. \quad (4.31)$$

³The term “effective Hamiltonian” has a well-defined meaning. It means the Hamiltonian describing the important degrees of freedom on the relevant low energy scale.

Here $\langle \mathbf{S}_i \rangle$ is the average spin at site i . From symmetry arguments we would then expect that the expectation value of this is zero, because all directions are equivalent. But since this is not the right answer we have to assume that the symmetry is broken, i.e. allow for $\langle \mathbf{S}_i \rangle$ to be non-zero. Furthermore, because of the translational symmetry we expect it to be independent of position coordinate i .⁴ So we assume a finite but spatial independent average spin polarization.

If we choose the z axis along the direction of the magnetization our mean field assumption is

$$\langle \mathbf{S}_i \rangle = \langle S_z \rangle \mathbf{e}_z, \quad (4.32)$$

and the magnetic moment \mathbf{m} (which by assumption is equal for all sites) felt by each spin thus becomes

$$\mathbf{m} = 2 \sum_j J_{ij} \langle S_z \rangle \mathbf{e}_z = 2nJ_0 \langle S_z \rangle \mathbf{e}_z, \quad (4.33)$$

where n is the number of neighbors. For a square lattice it is $n = 2d$, where d is the dimension. The mean field Hamiltonian

$$H_{\text{MF}} = -2 \sum_i \mathbf{m} \cdot \mathbf{S}_i + mN \langle S_z \rangle, \quad (4.34)$$

is now diagonal in the site index and hence easily solved. Here N is the number of sites and $m = |\mathbf{m}|$. Suppose for simplicity that the ions have spin $S = \frac{1}{2}$. With this simplification the mean field partition function is

$$Z_{\text{MF}} = \left(e^{\beta m} + e^{-\beta m} \right)^N e^{\beta N m \langle S_z \rangle} = \left[\left(e^{\beta m} + e^{-\beta m} \right) e^{\beta m^2 / 2nJ_0} \right]^N, \quad (4.35)$$

with one term for each possible spin projection, $S_z = \pm \frac{1}{2}$.

The self-consistency equation is found by minimizing the free energy

$$\frac{\partial F_{\text{MF}}}{\partial m} = -\frac{1}{\beta} \frac{\partial}{\partial m} \ln Z_{\text{MF}} = -N \left(\frac{e^{\beta m} - e^{-\beta m}}{e^{\beta m} + e^{-\beta m}} \right) + N \frac{m}{nJ_0} = 0,$$

which has a solution given by the transcendental equation

$$\alpha = \tanh(b\alpha), \quad \alpha = \frac{m}{nJ_0}, \quad b = nJ_0\beta. \quad (4.36)$$

It is evident from an expansion for small α ,

$$\alpha \approx b\alpha - \frac{1}{3}(b\alpha)^3, \quad (4.37)$$

that there is no solution for $b < 1$, and thus we can determine the critical temperature T_c where the magnetism disappears, by the condition $b_c = 1$ and hence $k_B T_c = nJ_0$.

⁴But had we reasons to believe that an antiferromagnetic solution (where the spins point in opposite direction on even and odd sites) was relevant (if $J_{ij} < 0$), we would have to assume that also this symmetry was broken.

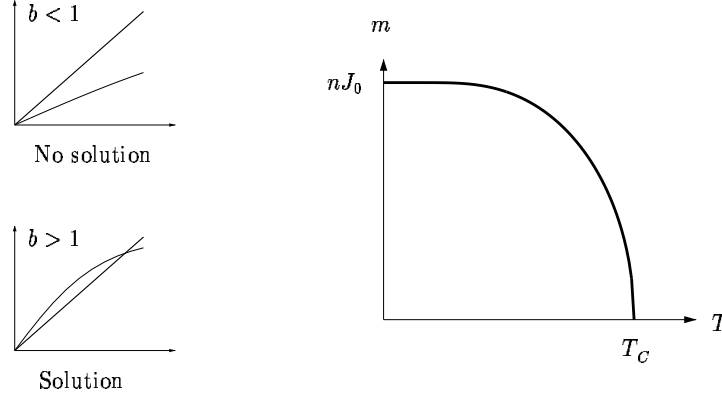


Figure 4.4: Left two panels show the graphical solution of the mean field equation for the Heisenberg model, Eq. (4.36). At temperatures larger than the critical temperature, $T_c = nJ_0$, corresponding to $b = nJ_0/T < 1$ there is no solution and hence no ferromagnetic moment. For $b > 1$ a solution exists. The resulting temperature dependence of the magnetization is shown to the right.

Furthermore, for small α we find the solution for the magnetization, $\alpha \approx \frac{1}{b} \sqrt{3(b-1)/b} \Rightarrow m \approx nJ_0 \sqrt{3 \frac{T_c - T}{T_c}}$, valid close to T_c . At $T = 0$ where $t = \infty$ the solution is $\alpha = 1$ and hence $m = nJ_0$. For the functional form of the magnetization in the entire range of temperature one must solve Eq. (4.36) numerically, which of course is a simple task. The solution is shown in Fig. 4.4.

4.4.2 The Stoner model of metallic ferromagnets

In magnets where the electrons both generate the magnetic moments and also form conduction bands the Heisenberg model cannot explain the magnetism. This is simply because the spins are not localized. Metallic magnetism happens e.g. in transition metals where the conduction bands are formed by the narrower d or f orbitals. The interaction between two particles in those orbitals is stronger than between electrons occupying the more spread out s or p orbitals and hence give a larger correlation between electrons. Typical metals where correlations between conduction band electrons are important are Fe and Ni.

Since the short range of the interaction is important it is relevant to study a model, the so-called Hubbard model, where this physical fact is reflected in a simple but extreme manner: the Coulomb interaction between electrons is taken to be point-like in real space and hence constant in momentum space.

$$H_{\text{hub}} = \sum_{\mathbf{k}\sigma} \xi_{\mathbf{k}} c_{\mathbf{k}\sigma}^\dagger c_{\mathbf{k}\sigma} + \frac{U}{2V} \sum_{\mathbf{k}'\mathbf{k}\mathbf{q}, \sigma\sigma'} c_{\mathbf{k}+\mathbf{q}\sigma}^\dagger c_{\mathbf{k}'-\mathbf{q}\sigma'}^\dagger c_{\mathbf{k}'\sigma'} c_{\mathbf{k}\sigma}. \quad (4.38)$$

We now use the Hartree–Fock approximation scheme on this model but search for a ferromagnetic solution by allowing for the expectation values to depend on the direction of

the spin. The mean field parameters are

$$\langle c_{\mathbf{k}\uparrow}^\dagger c_{\mathbf{k}'\uparrow} \rangle = \delta_{\mathbf{k}\mathbf{k}'} \bar{n}_{\mathbf{k}\uparrow}, \quad \langle c_{\mathbf{k}\downarrow}^\dagger c_{\mathbf{k}'\downarrow} \rangle = \delta_{\mathbf{k}\mathbf{k}'} \bar{n}_{\mathbf{k}\downarrow}, \quad (4.39)$$

and the mean field interaction Hamiltonian becomes

$$\begin{aligned} V_{\text{int}}^{\text{MF}} = & \frac{U}{\mathcal{V}} \sum_{\mathbf{k}'\mathbf{k}\mathbf{q}\sigma\sigma'} c_{\mathbf{k}+\mathbf{q}\sigma}^\dagger \langle c_{\mathbf{k}'-\mathbf{q}\sigma'}^\dagger c_{\mathbf{k}'\sigma'} \rangle c_{\mathbf{k}\sigma} - \frac{U}{\mathcal{V}} \sum_{\mathbf{k}'\mathbf{k}\mathbf{q}\sigma\sigma'} \langle c_{\mathbf{k}+\mathbf{q}\sigma}^\dagger c_{\mathbf{k}'\sigma'} \rangle c_{\mathbf{k}'-\mathbf{q}\sigma'}^\dagger c_{\mathbf{k}\sigma} \\ & - \frac{U}{2\mathcal{V}} \sum_{\mathbf{k}'\mathbf{k}\mathbf{q}\sigma\sigma'} \left[\langle c_{\mathbf{k}+\mathbf{q}\sigma}^\dagger c_{\mathbf{k}\sigma} \rangle \langle c_{\mathbf{k}'-\mathbf{q}\sigma'}^\dagger c_{\mathbf{k}'\sigma'} \rangle - \langle c_{\mathbf{k}+\mathbf{q}\sigma}^\dagger c_{\mathbf{k}'\sigma'} \rangle \langle c_{\mathbf{k}'-\mathbf{q}\sigma'}^\dagger c_{\mathbf{k}\sigma} \rangle \right]. \end{aligned} \quad (4.40)$$

The factor $\frac{1}{2}$ disappeared because there are two terms as in Eqs. (4.22) and (4.23). Using our mean field assumptions Eq. (4.39) we obtain

$$V_{\text{int}}^{\text{MF}} = U \sum_{\mathbf{k}\sigma\sigma'} c_{\mathbf{k}\sigma}^\dagger c_{\mathbf{k}\sigma} [\bar{n}_{\sigma'} - \bar{n}_\sigma \delta_{\sigma\sigma'}] - U\mathcal{V} \sum_{\sigma\sigma'} \bar{n}_\sigma \bar{n}_{\sigma'} + U\mathcal{V} \sum_{\sigma} \bar{n}_\sigma^2, \quad (4.41)$$

where the spin densities have been defined as

$$\bar{n}_\sigma = \frac{1}{\mathcal{V}} \sum_{\mathbf{k}} \langle c_{\mathbf{k}\sigma}^\dagger c_{\mathbf{k}\sigma} \rangle. \quad (4.42)$$

The full mean field Hamiltonian is now given by

$$H_{\text{MF}} = \sum_{\mathbf{k}\sigma} \xi_{\mathbf{k}\sigma}^{\text{MF}} c_{\mathbf{k}\sigma}^\dagger c_{\mathbf{k}\sigma} - \frac{U\mathcal{V}}{2} \sum_{\sigma\sigma'} \bar{n}_\sigma \bar{n}_{\sigma'} + \frac{U\mathcal{V}}{2} \sum_{\sigma} \bar{n}_\sigma^2, \quad (4.43a)$$

$$\xi_{\mathbf{k}\sigma}^{\text{MF}} = \xi_{\mathbf{k}} + U(n_\uparrow + \bar{n}_\downarrow - \bar{n}_\sigma) = \xi_{\mathbf{k}} + U\bar{n}_{\bar{\sigma}}. \quad (4.43b)$$

The mean field solution is found by minimization, which gives the self-consistency equations

$$\bar{n}_\sigma = \frac{1}{\mathcal{V}} \sum_{\mathbf{k}} \langle c_{\mathbf{k}\sigma}^\dagger c_{\mathbf{k}\sigma} \rangle_{\text{MF}} = \frac{1}{\mathcal{V}} \sum_{\mathbf{k}} n_F(\xi_{\mathbf{k}\sigma}^{\text{MF}}). \quad (4.44)$$

We obtain at zero temperature

$$\bar{n}_\uparrow = \int \frac{d\mathbf{k}}{(2\pi)^3} \theta \left(\mu - \frac{\hbar^2 k^2}{2m} - U\bar{n}_\downarrow \right) = \frac{1}{6\pi^2} k_{F\uparrow}^3, \quad (4.45)$$

where $\frac{\hbar^2}{2m} k_{F\uparrow}^2 + U\bar{n}_\downarrow = \mu$, and of course a similar equation for spin down. The two equations are

$$\frac{\hbar^2}{2m} (6\pi)^{2/3} \bar{n}_\uparrow^{2/3} + U\bar{n}_\downarrow = \mu, \quad \frac{\hbar^2}{2m} (6\pi)^{2/3} \bar{n}_\downarrow^{2/3} + U\bar{n}_\uparrow = \mu. \quad (4.46)$$

Define the variables,

$$\zeta = \frac{\bar{n}_\uparrow - \bar{n}_\downarrow}{\bar{n}}, \quad \gamma = \frac{2mU\bar{n}^{1/3}}{(3\pi^2)^{2/3} \hbar^2}, \quad \bar{n} = \bar{n}_\uparrow + \bar{n}_\downarrow. \quad (4.47)$$

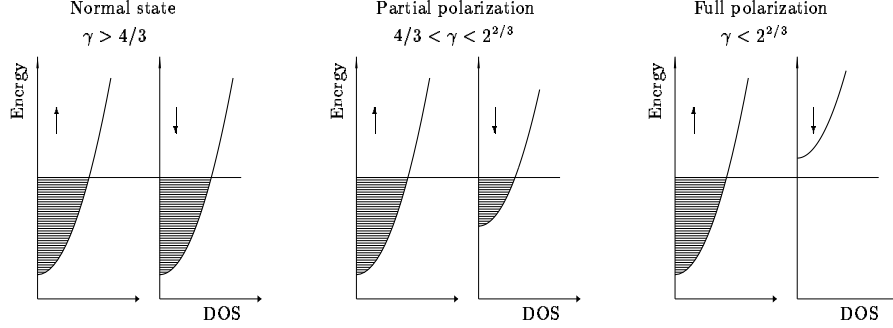


Figure 4.5: The three possible solutions of the Stoner model. The polarization is thus a function of the interaction strength; the stronger the interaction the larger the polarization. The Stoner model provides a clear physical picture for how the exchange interactions induce a ferromagnetic phase transition in a metal with strong on-site interactions.

Then by subtracting the self-consistency conditions (4.46), we get

$$\begin{aligned} \bar{n}_{\uparrow}^{2/3} - \bar{n}_{\downarrow}^{2/3} &= \frac{2mU}{\hbar^2} (6\pi)^{-2/3} (n_{\uparrow} - n_{\downarrow}), \\ &\Downarrow \\ \gamma\zeta &= (1 + \zeta)^{2/3} - (1 - \zeta)^{2/3}. \end{aligned} \quad (4.48)$$

This expression has three types of solutions:

$$\begin{array}{lll} \gamma < \frac{4}{3} : & \text{Isotropic solution: } \zeta = 0 & \text{Normal state} \\ \frac{4}{3} < \gamma < 2^{2/3} : & \text{Partial polarization: } 0 < \zeta < 1 & \text{Weak ferromagnet} \\ \gamma > 2^{2/3} : & \text{Full polarization } \zeta = 1 & \text{Strong ferromagnet} \end{array} \quad (4.49)$$

The different solutions are sketched in Fig. 4.5.

The possibility for a magnetic solution can be traced back to the spin-dependent energies Eq. (4.43a), where it is clear that the mean field energy of a given spin direction depends on the occupation of the opposite spin direction, whereas the energy does not depend on the occupation of the same spin direction. This resulted from two things: the short range interaction and the exchange term. One can understand this simply from the Pauli principle which ensures that electrons with the same spin never occupy the same spatial orbital and therefore, if the interaction is short-range, they cannot interact. This leaves interactions between opposite spin as the only possibility. Thus the interaction energy is lowered by having a polarized ground state, which on the other hand for a fixed density costs kinetic energy. The competition between the potential and the kinetic energy contributions is what gives rise to the phase transition.

The Stoner model gives a reasonable account of metallic magnets and it is also capable of qualitatively explaining the properties of excitations in the spin polarized states. This

is however outside the scope of this section and the interested reader should consult for example the book by Yosida.

4.5 Superconductivity

One of the most striking examples of symmetry breaking is the superconducting phase transition. Below the critical temperature the metal which turns superconducting has no resistance what so ever, and it exhibits perfect diamagnetism (called Meissner effect), which means that magnetic fields are totally expelled from the interior of the material. These astonishing phenomena result from the superconducting state having a new form of symmetry breaking, namely loss of global gauge invariance. Besides the superconductivity itself and the Meissner effect superconductors show a number of other characteristics, e.g. distinct single particle properties, which result from the appearance of a gap in the excitation spectrum.

Both the new type of phase and the appearance of an excitation gap are explained by the Bardeen-Cooper-Schrieffer (BCS) theory from 1957. It is probably the most successful theory in condensed matter physics and it has found application in other branches of physics as well, e.g. to explain the stability of nuclei with an even number of nucleons and also in the standard model of high-energy physics.

In this section, we give a short introduction to the BCS theory, which in its spirit is very much like the Hartree-Fock theory presented above. It is a mean field theory but with a quite unusual mean field and therefore we begin by discussing the nature of the superconducting phase.

4.5.1 Breaking of global gauge symmetry and its consequences

Let us start by understanding what kind of broken symmetry could give rise to a superconducting state. As was said above, the relevant symmetry is the global gauge symmetry, which means that we can give all electrons the same extra constant phase and still leave the Hamiltonian invariant. The analog to this in the case of a ferromagnet, is that all spins can be rotated by some angle without changing the Hamiltonian, which therefore has a global $SO(3)$ symmetry. In that case a broken $SO(3)$ symmetry means that the expectation value $\langle \mathbf{S} \rangle$ is *not* invariant under the rotation, because it will change the direction of the magnetization. In the same way the phase rotation also changes the superconducting order parameter, which is of the form $\langle c_\nu c_{\nu'} \rangle$. The order parameter for the superconductor thus involves an expectation value of two annihilation operators. Of course, the number of particles is conserved, but this is not a problem here where we discuss only superconductors connected to electron reservoirs. Schematically the analogies between superconductors and ferromagnets are as shown in Table 4.2.

While it is clear why the finite expectation $\langle \mathbf{S} \rangle$ gives a magnetization in the case of a ferromagnet, it is not so clear why broken symmetry in the superconducting case leads to a system without resistance. We have argued that the superconducting state is sensitive to a change of global phase, but it is also clear that a constant phase cannot have any measurable effect because all expectation values are given by the absolute square

Global $U(1)$ gauge symmetry, superconductor	Global $SO(3)$, ferromagnet
$c_\nu \rightarrow c_\nu e^{i\varphi} \Rightarrow H \rightarrow H$ Broken symmetry: $0 \neq \langle c_\nu c_{\nu'} \rangle \rightarrow \langle c_\nu c_{\nu'} \rangle e^{2i\varphi}$	$\mathbf{S} \rightarrow \mathbf{U}\mathbf{S} \Rightarrow H \rightarrow H$ Broken symmetry: $0 \neq \langle \mathbf{S} \rangle \rightarrow \mathbf{U}\langle \mathbf{S} \rangle$

Table 4.2: The analogy between the broken symmetries of a superconductor and a ferromagnet.

of the wave function. However, phase gradients can have an effect. Let us therefore assume that we ascribe a phase to the superconducting state which depends on position, $\varphi(\mathbf{r})$, but varies extremely slowly, such that it takes a macroscopic distance to see any significant changes in $\varphi(\mathbf{r})$. For any other non-superconducting system it would not make sense to talk about a quantum mechanical phase difference over macroscopic distances, simply because quantum coherence is destroyed by all sorts of scattering events on rather short length scales, maybe of the order of 10 nm or less in metals. To argue that the superconducting state depends on phase differences over macroscopic distances is therefore very unusual and tells us that superconductivity is a macroscopic quantum phenomenon.

In order to study the consequences of the phase change let us introduce a unitary transformation which changes the phase

$$U = \exp \left(i \int d\mathbf{r} \rho(\mathbf{r}) \varphi(\mathbf{r}) \right), \quad (4.50)$$

(recall that ρ , is the density operator $\rho(\mathbf{r}) = \Psi^\dagger(\mathbf{r}) \Psi(\mathbf{r})$) because it has the following properties when applied to quantum field operators

$$\begin{aligned} \tilde{\Psi}(\mathbf{r}) &= U \Psi(\mathbf{r}) U^{-1} = \exp \left(i \int d\mathbf{r} \rho(\mathbf{r}) \varphi(\mathbf{r}) \right) \Psi(\mathbf{r}) \exp \left(-i \int d\mathbf{r} \rho(\mathbf{r}) \varphi(\mathbf{r}) \right) \\ &= \Psi(\mathbf{r}) \exp(-i\varphi(\mathbf{r})), \end{aligned} \quad (4.51a)$$

$$\tilde{\Psi}^\dagger(\mathbf{r}) = U \Psi^\dagger(\mathbf{r}) U^{-1} = \Psi^\dagger(\mathbf{r}) \exp(i\varphi(\mathbf{r})). \quad (4.51b)$$

These equations follow from the differential equation (together with the boundary condition $\tilde{\Psi}_{\varphi=0} = \Psi$)

$$\frac{\delta}{\delta \varphi(\mathbf{r}')} \tilde{\Psi}(\mathbf{r}) = iU[\rho(\mathbf{r}'), \Psi(\mathbf{r})]U^{-1} = i\tilde{\Psi}(\mathbf{r})\delta(\mathbf{r} - \mathbf{r}'). \quad (4.52)$$

(See also Eq. (5.24) in Chap. 5 which is derived in the same way.) If we transform the density operator and calculate the transformed partition function, we get

$$\tilde{Z} = \text{Tr}' \left[U e^{-\beta H} U^{-1} \right] = \text{Tr}' \left[e^{-\beta \tilde{H}} \right]. \quad (4.53)$$

Note here that if we had used the cyclic properties of the trace, U would have disappeared all together. However, we learned above that when dealing with systems with broken

symmetry, the sum-over-states has to be restricted so that the cyclic properties does not necessarily hold. This we have anticipated by the symbol Tr' which means that the trace is restricted due to the spontaneous symmetry breaking. The transformation only changes in the kinetic energy term of the Hamiltonian, because both the Coulomb interaction term, the impurity scattering term, and the phonon coupling term, only involve the electron density operator $\rho(\mathbf{r})$ which according to (4.51) is unchanged under the phase shift transformation. The kinetic part reads

$$\begin{aligned}\tilde{H} &= \frac{1}{2m_e} \int d\mathbf{r} \Psi^\dagger(\mathbf{r}) e^{i\varphi(\mathbf{r})} \left(\frac{\hbar}{i} \nabla + e\mathbf{A} \right)^2 e^{-i\varphi(\mathbf{r})} \Psi(\mathbf{r}) \\ &= \frac{1}{2m_e} \int d\mathbf{r} \Psi^\dagger(\mathbf{r}) \left(\frac{\hbar}{i} \nabla + e\mathbf{A} - \hbar \nabla \varphi(\mathbf{r}) \right)^2 \Psi(\mathbf{r}), \\ &= H - \hbar \int d\mathbf{r} \nabla \varphi(\mathbf{r}) \cdot \mathbf{J}(\mathbf{r}) + \frac{\hbar^2}{2m_e} \int d\mathbf{r} \rho(\mathbf{r}) (\nabla \varphi(\mathbf{r}))^2,\end{aligned}\tag{4.54}$$

where the last step closely follows the derivation of the current operator in Sec. 1.4.3.

The claim above was that contrary to the non-superconducting state in the superconductor the phase is a macroscopic quantity. Let us therefore minimize the free energy with respect to the phase in order to find the condition for the lowest free energy. It is clear from (4.54) that the energy doesn't depend on φ itself, but only on the gradient of φ . We obtain

$$\frac{\delta F}{\delta \nabla \varphi} = -\langle \mathbf{J}(\mathbf{r}) \rangle + \frac{\hbar}{m_e} \langle \rho(\mathbf{r}) \rangle \nabla \varphi(\mathbf{r}) = 0,\tag{4.55}$$

and hence the energy is minimized if it carries a current, even in equilibrium, given by

$$\langle \mathbf{J} \rangle = \frac{\hbar \rho_0}{m_e} \nabla \varphi.\tag{4.56}$$

The meaning of this result is that by forcing a phase gradient onto the system it minimizes its energy by carrying a current even in thermodynamical equilibrium, meaning a dissipationless current⁵. In the normal state of metals a current is always associated with a non-equilibrium state, where energy is constantly dissipated from the driving source and absorbed in the conductor. Of course there is an energy cost for the system to carry the current, but as long as this cost is smaller than the alternative which is to go out of the superconducting state, the current carrying state is chosen. The critical current is reached when the energies are equal, and then the superconductor goes into the normal state.

What we have done so far is to show that if a phase gradient is imposed on a system, where the energy is assumed to depend on phase differences on a macroscopic scale, it unavoidably leads to the conclusion that the system will carry a dissipationless current in order to minimize the energy cost of the phase gradient.

Finally, it should be noted that the appearance of the excitation gap is not the reason for the superconductivity itself. The superconductivity is, as we have argued, due to the lack of gauge invariance, and in fact gapless superconductors do exist.

⁵In reality the electron density appearing in Eq. (4.56) should only be the electrons participating in the superconducting condensate, the so-called superfluid. However, the simple minded derivation presented here assumes that all electrons participates.

4.5.2 Microscopic theory

The understanding that superconductivity was closely related to the electron-phonon coupling was clear from the early 1950's when for example the isotope effect was discovered. Also the idea that the superconductivity was somehow similar to Bose-Einstein condensation, with the bosons being electron pairs, had been tried and in fact was the underlying idea of London's theory in 1935. However, only in 1956 Cooper showed that the Fermi surface of the normal metal state was unstable towards formation of bound pairs of electrons (see Chap. 16). Subsequently in 1957 when the superconducting state was derived using a variational wavefunction by BCS, were the principles fully understood. Here we give an outline of the main principles in the BCS theory.

In Chap. 16 we will see that the phonon mediated electron-electron interaction (derived from the electron-phonon interaction found in Sec. 3.6) in fact has a range in frequency and momentum space where it is negative, i.e. attractive. This happens for energy exchanges of order the Debye energy, ω_D , which as we saw in Chap. 3 for metals is much smaller than the Fermi energy, $\omega_D \ll E_F$. Furthermore, from the Cooper instability we know that the phonon-mediated interaction tends to pair electrons with opposite spin and momentum. We define a Cooper pair operator

$$b_k = c_{k\downarrow} c_{-k\uparrow}.$$

These two physical inputs led BCS to suggest the following remarkably successful model Hamiltonian to explain the superconducting state. The BCS effective Hamiltonian model is

$$H_{\text{BCS}} = \sum_{\mathbf{k}\sigma} \xi_{\mathbf{k}} c_{\mathbf{k}\sigma}^\dagger c_{\mathbf{k}\sigma} + \sum_{\mathbf{k}\mathbf{k}'} V_{\mathbf{k}\mathbf{k}'} c_{\mathbf{k}\uparrow}^\dagger c_{-\mathbf{k}\downarrow}^\dagger c_{-\mathbf{k}'\downarrow} c_{\mathbf{k}'\uparrow}, \quad (4.57)$$

where $V_{\mathbf{k}\mathbf{k}'}$ is the coupling strength which is only non-zero for states with energy $\xi_{\mathbf{k}}$ within $\xi_F \pm \omega_D$ and furthermore constant and negative, $V_{\mathbf{k}\mathbf{k}'} = -V_0$, in this range. The interaction includes only pair interactions and the remaining interaction is supposed to be included in $\xi_{\mathbf{k}}$ via a Hartree-Fock term. The origin of the attractive interaction can intuitively be thought of in the following way: when an electron propagates through the crystal it attracts the positive ions and thus effectively creates a positive trace behind it. This trace is felt by the other electrons as an attractive interaction. It turns out that this effective interaction is most important for electrons occupying time reversed states and in fact they can form a bound state which is the Cooper pair. The Cooper pair is thus a bound state of an electron in state $\psi_{\nu}(\mathbf{r})$ and an electron in state $\psi_{\nu}^*(\mathbf{r})$ or in the homogeneous case electrons in state \mathbf{k} and $-\mathbf{k}$.

Because the typical energy exchange due to the attractive interaction is the Debye energy, ω_D , one would naively expect that the energy scale for the superconducting transition temperature would be of the order ω_D/k . This is however far from the truth because while ω_D/k is typically of the order of several hundred kelvin, the critical temperatures found in "conventional" low superconductors are in most cases less than 10 K and never more than 30 K. It therefore seems that a new energy scale is generated and we shall indeed see that this is the case.

The mean field assumption made by BCS, is that the pair operator has a finite expectation value and that it varies only little from its average value. The BCS mean field Hamiltonian is derived in full analogy with Hartree–Fock mean field theory described above

$$H_{\text{BCS}}^{\text{MF}} = \sum_{\mathbf{k}\sigma} \xi_{\mathbf{k}} c_{\mathbf{k}\sigma}^\dagger c_{\mathbf{k}\sigma} - \sum_{\mathbf{k}} \Delta_{\mathbf{k}} c_{\mathbf{k}\uparrow}^\dagger c_{-\mathbf{k}\downarrow}^\dagger - \sum_{\mathbf{k}} \Delta_{\mathbf{k}}^* c_{\mathbf{k}\downarrow} c_{-\mathbf{k}\uparrow} + \sum_{\mathbf{k}\mathbf{k}'} V_{\mathbf{k}\mathbf{k}'} \langle c_{\mathbf{k}\uparrow}^\dagger c_{-\mathbf{k}\downarrow}^\dagger \rangle \langle c_{\mathbf{k}'\downarrow} c_{-\mathbf{k}'\uparrow} \rangle, \quad (4.58a)$$

$$\Delta_{\mathbf{k}} = - \sum_{\mathbf{k}\mathbf{k}'} V_{\mathbf{k}\mathbf{k}'} \langle c_{-\mathbf{k}'\downarrow} c_{\mathbf{k}'\uparrow} \rangle \quad (4.58b)$$

The mean field Hamiltonian is quadratic in electron operators and should be readily solvable. It is however somewhat unusual in that terms like $c^\dagger c^\dagger$ and cc appear. The way to solve it is by a so-called Bogoliubov transformation. For this purpose it is convenient to write the Hamiltonian in matrix notation

$$\begin{aligned} H_{\text{BCS}}^{\text{MF}} &= \sum_{\mathbf{k}} \begin{pmatrix} c_{\mathbf{k}\uparrow}^\dagger & c_{-\mathbf{k}\downarrow} \end{pmatrix} \begin{pmatrix} \xi_{\mathbf{k}} & \Delta_{\mathbf{k}} \\ \Delta_{\mathbf{k}}^* & -\xi_{\mathbf{k}} \end{pmatrix} \begin{pmatrix} c_{\mathbf{k}\uparrow} \\ c_{-\mathbf{k}\downarrow}^\dagger \end{pmatrix} \\ &+ \sum_{\mathbf{k}} \xi_{\mathbf{k}} + \sum_{\mathbf{k}\mathbf{k}'} V_{\mathbf{k}\mathbf{k}'} \langle c_{\mathbf{k}\uparrow}^\dagger c_{-\mathbf{k}\downarrow}^\dagger \rangle \langle c_{\mathbf{k}'\downarrow} c_{-\mathbf{k}'\uparrow} \rangle, \\ &= \sum_{\mathbf{k}} \mathbf{A}_{\mathbf{k}}^\dagger \mathbf{H}_{\mathbf{k}} \mathbf{A}_{\mathbf{k}} + \text{constant}, \end{aligned} \quad (4.59)$$

where

$$\mathbf{A}_{\mathbf{k}} = \begin{pmatrix} c_{\mathbf{k}\uparrow} \\ c_{-\mathbf{k}\downarrow}^\dagger \end{pmatrix}, \quad \mathbf{H}_{\mathbf{k}} = \begin{pmatrix} \xi_{\mathbf{k}} & \Delta_{\mathbf{k}} \\ \Delta_{\mathbf{k}}^* & -\xi_{\mathbf{k}} \end{pmatrix}. \quad (4.60)$$

To bring the Hamiltonian into a diagonal form, we introduce the unitary transformation

$$\mathbf{B}_{\mathbf{k}} = \begin{pmatrix} \gamma_{\mathbf{k}\uparrow} \\ \gamma_{-\mathbf{k}\downarrow}^\dagger \end{pmatrix} = \mathbf{U}_{\mathbf{k}}^{-1} \mathbf{A}_{\mathbf{k}}, \quad \mathbf{U}_{\mathbf{k}} = \begin{pmatrix} u_{\mathbf{k}} & -v_{\mathbf{k}} \\ v_{\mathbf{k}}^* & u_{\mathbf{k}}^* \end{pmatrix}, \quad (4.61)$$

which diagonalizes the problem if

$$\mathbf{U}_{\mathbf{k}}^\dagger \mathbf{H}_{\mathbf{k}} \mathbf{U}_{\mathbf{k}} = \begin{pmatrix} E_{\mathbf{k}} & 0 \\ 0 & \tilde{E}_{\mathbf{k}} \end{pmatrix}. \quad (4.62)$$

After some algebra, we find the following solution for u, v and the energies, E and \tilde{E}

$$|u_{\mathbf{k}}|^2 = \frac{1}{2} \left(1 + \frac{\xi_{\mathbf{k}}}{E_{\mathbf{k}}} \right), \quad |v_{\mathbf{k}}|^2 = \frac{1}{2} \left(1 - \frac{\xi_{\mathbf{k}}}{E_{\mathbf{k}}} \right), \quad (4.63)$$

$$E_{\mathbf{k}} = \sqrt{\xi_{\mathbf{k}}^2 + |\Delta_{\mathbf{k}}|^2} = -\tilde{E}_{\mathbf{k}}. \quad (4.64)$$

The new fermion operators that diagonalize the Hamiltonian are called bogoliubons and they are superpositions of electrons and holes. This rather unusual particle appears because of the lack of particle conservation in the mean field Hamiltonian. There are two different bogoliubons inherited from the two fold spin degeneracy. From (4.61) we have the transformations from old to new operators

$$\begin{pmatrix} \gamma_{\mathbf{k}\uparrow} \\ \gamma_{-\mathbf{k}\downarrow}^\dagger \end{pmatrix} = \begin{pmatrix} u_{\mathbf{k}}^* & v_{\mathbf{k}} \\ -v_{\mathbf{k}}^* & u_{\mathbf{k}} \end{pmatrix} \begin{pmatrix} c_{\mathbf{k}\uparrow} \\ c_{-\mathbf{k}\downarrow}^\dagger \end{pmatrix} \Leftrightarrow \begin{pmatrix} c_{\mathbf{k}\uparrow} \\ c_{-\mathbf{k}\downarrow}^\dagger \end{pmatrix} = \begin{pmatrix} u_{\mathbf{k}} & -v_{\mathbf{k}} \\ v_{\mathbf{k}}^* & u_{\mathbf{k}}^* \end{pmatrix} \begin{pmatrix} \gamma_{\mathbf{k}\uparrow} \\ \gamma_{-\mathbf{k}\downarrow}^\dagger \end{pmatrix}, \quad (4.65)$$

and the Hamiltonian is in terms of the new bogoliubons

$$H_{\text{BCS}}^{\text{MF}} = \sum_{\mathbf{k}} E_{\mathbf{k}} \left(\gamma_{\mathbf{k}\uparrow}^\dagger \gamma_{\mathbf{k}\uparrow} + \gamma_{\mathbf{k}\downarrow}^\dagger \gamma_{\mathbf{k}\downarrow} \right) + \text{constant}. \quad (4.66)$$

As is evident from the new Hamiltonian and the solution in Eq. (4.64) there are no fermion excitations possible with energy less than $|\Delta|$. The mean field parameter provides an energy gap, which is why it is called the superconducting gap. The excitation gap has a number of important consequences.

The self-consistent solution is found from Eq. (4.58b), the so-called gap equation, by calculating the expectation value of the right hand side using the diagonalized Hamiltonian. Above in the general section on mean field theory we saw that this procedure is equivalent to minimizing the free energy with respect to the mean field parameter, which is here $\langle b_{\mathbf{k}} \rangle$. Using Eqs. (4.61), (4.63), and (4.64) we find

$$\begin{aligned} \Delta_{\mathbf{k}} &= - \sum_{\mathbf{k}'} V_{\mathbf{k}\mathbf{k}'} \langle c_{-\mathbf{k}'\downarrow} c_{\mathbf{k}'\uparrow} \rangle, \\ &= - \sum_{\mathbf{k}'} V_{\mathbf{k}\mathbf{k}'} \left\langle \left(u_{\mathbf{k}'}^* \gamma_{-\mathbf{k}'\downarrow} - v_{\mathbf{k}'} \gamma_{\mathbf{k}'\uparrow}^\dagger \right) \left(u_{\mathbf{k}'}^* \gamma_{\mathbf{k}'\uparrow} + v_{\mathbf{k}'} \gamma_{-\mathbf{k}'\downarrow}^\dagger \right) \right\rangle, \\ &= - \sum_{\mathbf{k}'} V_{\mathbf{k}\mathbf{k}'} \left(u_{\mathbf{k}'}^* v_{\mathbf{k}'} \langle \gamma_{-\mathbf{k}'\downarrow} \gamma_{-\mathbf{k}'\downarrow}^\dagger \rangle - v_{\mathbf{k}'} u_{\mathbf{k}'}^* \langle \gamma_{\mathbf{k}'\uparrow}^\dagger \gamma_{\mathbf{k}'\uparrow} \rangle \right) \\ &= - \sum_{\mathbf{k}'} V_{\mathbf{k}\mathbf{k}'} u_{\mathbf{k}'}^* v_{\mathbf{k}'} [1 - 2n_F(E_{\mathbf{k}'})], \end{aligned} \quad (4.67)$$

where we used in the last step that according to the Hamiltonian Eq. (4.66) the bogoliubons are free fermions and therefore their distribution function is the usual Fermi-Dirac distribution. Now using the approximation that $V_{\mathbf{k}\mathbf{k}'}$ is finite only for $\xi_{\mathbf{k}}, \xi_{\mathbf{k}'} \in [-\omega_D, \omega_D]$, and that $\omega_D \ll E_F$, such that the density of states is constant in the energy interval in question, we get

$$|\Delta| = V_0 \frac{d(E_F)}{2} \int_{-\omega_D}^{\omega_D} d\xi \frac{|\Delta|}{2E} [1 - 2n_F(E)], \quad (4.68)$$

and the gap $|\Delta|$ is determined by the integral equation,

$$\frac{2}{V_0 d(E_F)} = \int_0^{\omega_D} d\xi \frac{\tanh\left(\beta \sqrt{\xi^2 + |\Delta|^2}/2\right)}{\sqrt{\xi^2 + |\Delta|^2}}, \quad (4.69)$$

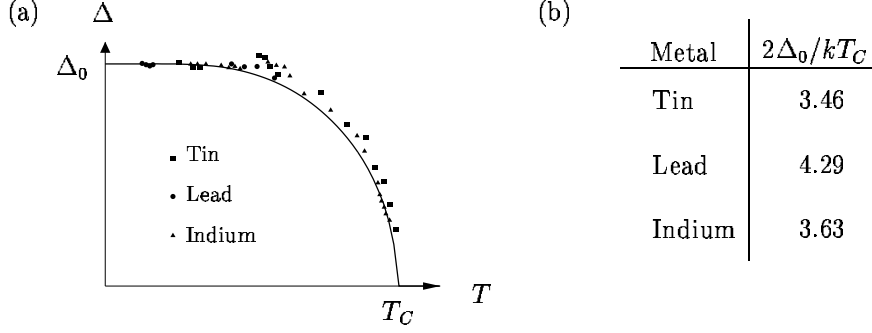


Figure 4.6: Measured values of the gap parameter for three different metals compared to the BCS predictions. To the left the temperature dependence is shown as it follows from the BCS gap equation in Eq. (4.69) together with experimental values. The right table shows the measured value of the ratio between twice the gap at zero temperature and critical temperature, determined from tunneling measurements. The theoretical BCS value is given in Eq. (4.72).

which can be solved numerically. In Fig. 4.6, we show the temperature dependence of the gap together with measured values. The critical temperature is found by setting $\Delta = 0$ in the integral and one finds approximately

$$kT_C = 1.13\omega_D e^{-2/V_0 d(E_F)}. \quad (4.70)$$

At zero temperature the gap, Δ_0 , is found from

$$\begin{aligned} \frac{2}{V_0 d(E_F)} &= \int_0^{\omega_D} d\xi \frac{1}{\sqrt{\xi^2 + \Delta_0^2}} = \sinh^{-1} \frac{2\omega_D}{\Delta_0^2}, \\ \Downarrow \\ \Delta_0 &= \frac{\omega_D}{\sinh(2/V_0 d(E_F))} \approx 2\omega_D e^{-2/V_0 d(E_F)}, \end{aligned} \quad (4.71)$$

because in metals $V_0 d(E_F)$ is typically a very small number. Combining (4.70) and (4.71), we get the BCS prediction that the ratio of gap to critical temperature is

$$\frac{2\Delta_0}{kT_C} = 3.53. \quad (4.72)$$

This is in very good agreement with experimental findings, see Fig. 4.6(b), where the ratio typically range between 3 and 4.5. This is just one of the successes of the BCS theory, but there are many others but the reader is referred to the many very good books on superconductivity.

Both the gap and the critical temperature are thus reduced by the exponential factor $\exp(-1/V_0 d(E_F))$ as compared to the bare energy scale of the interaction, ω_D . This strong renormalization is what generates the new scale, $\omega_D \exp(-2/V_0 d(E_F))$, as we foresaw in

the discussion above. Note that the interaction strength appears in a non-perturbative fashion in this expression, because the function $\exp(-1/x)$ has no Taylor expansion at $x = 0$. This tells us that the result could never have been derived using perturbation theory in the interaction, no matter how many orders were included. This is in fact a general feature of phase transitions. It is not possible by perturbation expansions to cross a phase transition line, because the two states have no analytic connection. Once again we see that there is no automatic way to predict the phase diagram of a given physical system, and one must rely on a combination of technical skill and most importantly physical intuition.

The BCS theory has provided an excellent model for the behavior of low temperature superconductors. It is however not clear to what extent the theory can be used to explain the superconductivity of high temperature superconductors and other exotic superconducting materials. This is still a very active and interesting area of research.

4.6 Summary and outlook

Mean field theories are widely used to study phase transitions in matter and also in e.g. atomic physics to compute the energetics of a finite size systems. The mean field approximation is in many cases sufficient to understand the important physical features, at least those that have to do with static properties. We have seen examples of this in the case of magnets and superconductors, where the important concept of symmetry breaking was introduced. It means that the state of the system chooses to have a lower symmetry than the original Hamiltonian, e.g. all spins point in the same direction. Of course we have not covered the vast fields of both magnetism and superconductivity in detail and the interested reader should consult the book by Yosida to learn more about magnetism, and the books by Schrieffer, Tinkham and de Gennes to learn about superconductivity.

In the remaining part of this course we shall deal with the dynamical properties of many-particle systems. Also for the time-dependent case Hartree–Fock type approximations will be invoked, e.g. for the so-called Random Phase Approximation treatment of the dielectric function in Sec. 8.5. The RPA result will later be derived later based on a more rigorous quantum field theoretical approach in Chap. 12.

Chapter 5

Time evolution pictures

Using the second quantization procedure, we have so far only treated energy eigenstates with a trivial time dependence $e^{i\omega t}$, instant processes at a single time $t = 0$, and systems where interactions are approximated by time-independent mean field theory. But how does one then treat the general case of time dependence in second quantization? That question will be addressed in this chapter, where time evolution is discussed using three representations, or “pictures”: the Schrödinger picture, the Heisenberg picture, and the interaction picture. These representations are used in the following chapters to develop general methods for treating many-particle systems.

5.1 The Schrödinger picture

The Schrödinger picture is useful when dealing with a time-independent Hamiltonian H , i.e. $\partial_t H = 0$. Any other operator A may or may not depend on time. The state vectors $|\psi(t)\rangle$ does depend on time, and their time evolution is governed by Schrödinger’s equation. The time-independence of H leads to a simple formal solution:

$$i\hbar\partial_t |\psi(t)\rangle = H |\psi(t)\rangle \quad \Rightarrow \quad |\psi(t)\rangle = e^{-\frac{i}{\hbar}Ht} |\psi_0\rangle. \quad (5.1)$$

In the following we will measure the energy in units of frequency, such that \hbar drops out of the time-evolution equations: $\varepsilon/\hbar \rightarrow \varepsilon$ and $H/\hbar \rightarrow H$. At the end of the calculations one can easily convert frequencies back to energies. With this notation we can summarize the Schrödinger picture with its states $|\psi(t)\rangle$ and operators A as:

$$\text{The Schrödinger picture} \quad \left\{ \begin{array}{ll} \text{states :} & |\psi(t)\rangle = e^{-iHt} |\psi_0\rangle, \\ \text{operators :} & A, \text{ may or may not depend on time.} \\ & H, \text{ does not depend on time.} \end{array} \right. \quad (5.2)$$

To interpret the operator e^{-iHt} we recall that a function $f(B)$ of any operator B is defined by the Taylor expansion of f ,

$$f(B) = \sum_{n=0}^{\infty} \frac{f^{(n)}(0)}{n!} B^n. \quad (5.3)$$

While the Schrödinger picture is quite useful for time-independent operators A , it may sometimes be preferable to collect all time dependencies in the operators and work with time-independent state vectors. We can do that using the Heisenberg picture.

5.2 The Heisenberg picture

The central idea behind the Heisenberg picture is to obtain a representation where all the time dependence is transferred to the operators, $A(t)$, leaving the state vectors $|\psi_0\rangle$ time independent. The Hamiltonian H remains time-independent in the Heisenberg picture. If the matrix elements of any operator between any two states are identical in the two representations, then the two representations are fully equivalent. By using Eq. (5.2) we obtain the identity

$$\langle\psi'(t)|A|\psi(t)\rangle = \langle\psi'_0|e^{iHt}Ae^{-iHt}|\psi_0\rangle \equiv \langle\psi'_0|A(t)|\psi_0\rangle. \quad (5.4)$$

Thus we see that the correspondence between the Heisenberg picture with time-independent state vectors $|\psi_0\rangle$, but time-dependent operators $A(t)$, and the Schrödinger picture is given by the unitary transformation operator $\exp(iHt)$,

$$\text{The Heisenberg picture} \quad \left\{ \begin{array}{ll} \text{states :} & |\psi_0\rangle \equiv e^{iHt} |\psi(t)\rangle, \\ \text{operators :} & A(t) \equiv e^{iHt} A e^{-iHt}. \\ & H \quad \text{does not depend on time.} \end{array} \right. \quad (5.5)$$

As before the original operator A may be time dependent. The important equation of motion governing the time evolution of $A(t)$ is easily established. Since H is time independent, the total time derivative of A in the Heisenberg picture is denoted with a dot, \dot{A} , while the explicit time derivative of the original Schrödinger operator is denoted $\partial_t A$:

$$\dot{A}(t) = e^{iHt} (iHA - iAH + \partial_t A) e^{-iHt} \Rightarrow \dot{A}(t) = i[H, A(t)] + (\partial_t A)(t), \quad (5.6)$$

where $X(t)$ always means $e^{iHt} X e^{-iHt}$ for any symbol X , in particular for $X = \partial_t A$. In this way an explicit time-dependence of A is taken into account. Note how carefully the order of the operators is kept during the calculation.

Both the Schrödinger and the Heisenberg picture require a time-independent Hamiltonian. In the general case of time-dependent Hamiltonians, we have to switch to the interaction picture.

5.3 The interaction picture

The third and last representation, the interaction picture, is introduced to deal with the situation where a system described by a time-independent Hamiltonian H_0 , with known energy eigenstates $|n_0\rangle$, is perturbed by some, possibly time-dependent, interaction $V(t)$,

$$H = H_0 + V(t), \quad \text{with} \quad H_0|n_0\rangle = \varepsilon_{n_0}|n_0\rangle. \quad (5.7)$$

The key idea behind the interaction picture is to separate the trivial time evolution due to H_0 from the intricate one due to $V(t)$. This is obtained by using only H_0 , not the full H , in the unitary transformation Eq. (5.5). As a result, in the interaction picture both the state vectors $|\hat{\psi}(t)\rangle$ and the operators $\hat{A}(t)$ depend on time. The defining equations for the interaction picture are

$$\text{The interaction picture} \quad \left\{ \begin{array}{ll} \text{states :} & |\hat{\psi}(t)\rangle \equiv e^{iH_0 t} |\psi(t)\rangle, \\ \text{operators :} & \hat{A}(t) \equiv e^{iH_0 t} A e^{-iH_0 t}. \\ & H_0 \quad \text{does not depend on time.} \end{array} \right. \quad (5.8)$$

The interaction picture and the Heisenberg picture coincide when $V = 0$; i.e., in the non-perturbed case. If $V(t)$ is a weak perturbation, then one can think of Eq. (5.8) as a way to pull out the fast, but trivial, time dependence due to H_0 , leaving states that vary only slowly in time due to $V(t)$.

The first hint of the usefulness of the interaction picture comes from calculating the time derivative of $|\hat{\psi}(t)\rangle$ using the definition Eq. (5.8):

$$i\partial_t |\hat{\psi}(t)\rangle = \left(i\partial_t e^{iH_0 t} \right) |\psi(t)\rangle + e^{iH_0 t} \left(i\partial_t |\psi(t)\rangle \right) = e^{iH_0 t} (-H_0 + H) |\psi(t)\rangle, \quad (5.9)$$

which by Eq. (5.8) is reduced to

$$i\partial_t |\hat{\psi}(t)\rangle = \hat{V}(t) |\hat{\psi}(t)\rangle. \quad (5.10)$$

The resulting Schrödinger equation for $|\hat{\psi}(t)\rangle$ thus contains explicit reference only to the interaction part $\hat{V}(t)$ of the full Hamiltonian H . This means that in the interaction picture the time evolution of a state $|\hat{\psi}(t_0)\rangle$ from time t_0 to t must be given in terms of a unitary operator $\hat{U}(t, t_0)$ which also only depends on $\hat{V}(t)$. $\hat{U}(t, t_0)$ is completely determined by

$$|\hat{\psi}(t)\rangle = \hat{U}(t, t_0) |\hat{\psi}(t_0)\rangle. \quad (5.11)$$

When V and thus H are time-independent, an explicit form for $\hat{U}(t, t_0)$ is obtained by inserting $|\hat{\psi}(t)\rangle = e^{iH_0 t} |\psi(t)\rangle = e^{iH_0 t} e^{-iHt} |\psi_0\rangle$ and $|\hat{\psi}(t_0)\rangle = e^{iH_0 t_0} e^{-iHt_0} |\psi_0\rangle$ into Eq. (5.11),

$$e^{iH_0 t} e^{-iHt} |\psi_0\rangle = \hat{U}(t, t_0) e^{iH_0 t_0} e^{-iHt_0} |\psi_0\rangle \Rightarrow \hat{U}(t, t_0) = e^{iH_0 t} e^{-iH(t-t_0)} e^{-iH_0 t_0}. \quad (5.12)$$

From this we observe that $\hat{U}^{-1} = \hat{U}^\dagger$, i.e. \hat{U} is indeed a unitary operator.

In the general case with a time-dependent $\hat{V}(t)$ we must rely on the differential equation appearing when Eq. (5.11) is inserted in Eq. (5.10). We remark that Eq. (5.11) naturally implies the boundary condition $\hat{U}(t_0, t_0) = 1$, and we obtain:

$$i\partial_t \hat{U}(t, t_0) = \hat{V}(t) \hat{U}(t, t_0), \quad \hat{U}(t_0, t_0) = 1. \quad (5.13)$$

By integration of this differential equation we get the integral equation

$$\hat{U}(t, t_0) = 1 + \frac{1}{i} \int_{t_0}^t dt' \hat{V}(t') \hat{U}(t', t_0), \quad (5.14)$$

which we can solve iteratively for $\hat{U}(t, t_0)$ starting from $\hat{U}(t', t_0) = 1$. The solution is

$$\hat{U}(t, t_0) = 1 + \frac{1}{i} \int_{t_0}^t dt_1 \hat{V}(t_1) + \frac{1}{i^2} \int_{t_0}^t dt_1 \hat{V}(t_1) \int_{t_0}^{t_1} dt_2 \hat{V}(t_2) + \dots \quad (5.15)$$

Note that in the iteration the ordering of all operators is carefully kept. A more compact form is obtained by the following rewriting. Consider for example the second order term, paying special attention to the dummy variables t_1 and t_2 :

$$\begin{aligned} & \int_{t_0}^t dt_1 \hat{V}(t_1) \int_{t_0}^{t_1} dt_2 \hat{V}(t_2) \\ &= \frac{1}{2} \int_{t_0}^t dt_1 \hat{V}(t_1) \int_{t_0}^{t_1} dt_2 \hat{V}(t_2) + \frac{1}{2} \int_{t_0}^t dt_2 \hat{V}(t_2) \int_{t_0}^{t_2} dt_1 \hat{V}(t_1) \\ &= \frac{1}{2} \int_{t_0}^t dt_1 \int_{t_0}^t dt_2 \hat{V}(t_1) \hat{V}(t_2) \theta(t_1 - t_2) + \frac{1}{2} \int_{t_0}^t dt_2 \int_{t_0}^t dt_1 \hat{V}(t_2) \hat{V}(t_1) \theta(t_2 - t_1) \\ &= \frac{1}{2} \int_{t_0}^t dt_1 \int_{t_0}^t dt_2 \left[\hat{V}(t_1) \hat{V}(t_2) \theta(t_1 - t_2) + \hat{V}(t_2) \hat{V}(t_1) \theta(t_2 - t_1) \right] \\ &\equiv \frac{1}{2} \int_{t_0}^t dt_1 \int_{t_0}^t dt_2 T_t[\hat{V}(t_1) \hat{V}(t_2)], \end{aligned} \quad (5.16)$$

where we have introduced the time ordering operator T_t . Time ordering is easily generalized to higher order terms. In n -th order, where n factors $\hat{V}(t_j)$ appear, all $n!$ permutations $p \in S_n$ of the n times t_j are involved, and we define¹

$$T_t[\hat{V}(t_1) \hat{V}(t_2) \dots \hat{V}(t_n)] \equiv \sum_{p \in S_n} \hat{V}(t_{p(1)}) \hat{V}(t_{p(2)}) \dots \hat{V}(t_{p(n)}) \times \theta(t_{p(1)} - t_{p(2)}) \theta(t_{p(2)} - t_{p(3)}) \dots \theta(t_{p(n-1)} - t_{p(n)}). \quad (5.17)$$

Using the time ordering operator, we obtain the final compact form (see also Exercise 5.2):

$$\hat{U}(t, t_0) = \sum_{n=0}^{\infty} \frac{1}{n!} \left(\frac{1}{i} \right)^n \int_{t_0}^t dt_1 \dots \int_{t_0}^t dt_n T_t \left(\hat{V}(t_1) \dots \hat{V}(t_n) \right) = T_t \left(e^{-i \int_{t_0}^t dt' \hat{V}(t')} \right). \quad (5.18)$$

Note the similarity with a usual time evolution factor $e^{-i\varepsilon t}$. This expression for $\hat{U}(t, t_0)$ is the starting point for infinite order perturbation theory and for introducing the concept of Feynman diagrams; it is therefore one of the central equations in quantum field theory. A graphical sketch of the contents of the formula is given in Fig. 5.1.

¹For $n = 3$ we have $T_t[\hat{V}(t_1) \hat{V}(t_2) \hat{V}(t_3)] = \hat{V}(t_1) \hat{V}(t_2) \hat{V}(t_3) \theta(t_1 - t_2) \theta(t_2 - t_3) + \hat{V}(t_1) \hat{V}(t_3) \hat{V}(t_2) \theta(t_1 - t_3) \theta(t_3 - t_2) + \hat{V}(t_2) \hat{V}(t_3) \hat{V}(t_1) \theta(t_2 - t_3) \theta(t_3 - t_1) + \hat{V}(t_2) \hat{V}(t_1) \hat{V}(t_3) \theta(t_2 - t_1) \theta(t_1 - t_3) + \hat{V}(t_3) \hat{V}(t_1) \hat{V}(t_2) \theta(t_3 - t_1) \theta(t_1 - t_2) + \hat{V}(t_3) \hat{V}(t_2) \hat{V}(t_1) \theta(t_3 - t_2) \theta(t_2 - t_1)$.

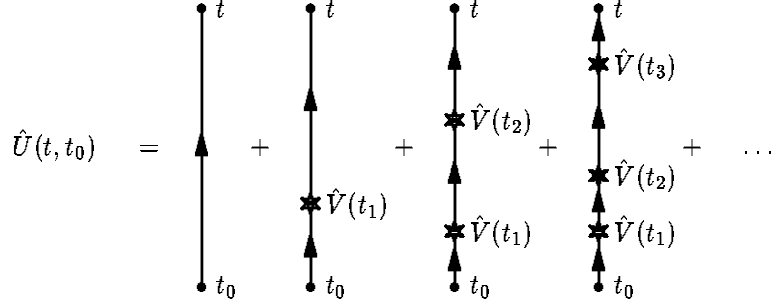


Figure 5.1: The time evolution operator $\hat{U}(t, t_0)$ can be viewed as the sum of additional phase factors due to \hat{V} on top of the trivial phase factors arising from H_0 . The sum contains contributions from processes with 0, 1, 2, 3, \dots scattering events \hat{V} , which happen during the evolution from time t_0 to time t .

5.4 Time-evolution in linear response

In many applications the perturbation $\hat{V}(t)$ is weak compared to H_0 . It can therefore be justified to approximate $\hat{U}(t, t_0)$ by the first order approximation

$$\hat{U}(t, t_0) \approx 1 + \frac{1}{i} \int_{t_0}^t dt' \hat{V}(t'). \quad (5.19)$$

This simple time evolution operator forms the basis for the Kubo formula in linear response theory, which, as we shall see in the following chapters, is applicable to a wide range of physical problems.

5.5 Time dependent creation and annihilation operators

It is of fundamental interest to study how the basic creation and annihilation operators a_ν^\dagger and a_ν evolve in time given some set of basis states $\{|\nu\rangle\}$ for a time-independent Hamiltonian H . As in Sec. 1.3.4 these operators can be taken to be either bosonic or fermionic. Let us first apply the definition of the Heisenberg picture, Eq. (5.5):

$$a_\nu^\dagger(t) \equiv e^{iHt} a_\nu^\dagger e^{-iHt}, \quad (5.20a)$$

$$a_\nu(t) \equiv e^{iHt} a_\nu e^{-iHt}. \quad (5.20b)$$

In the case of a general time-independent Hamiltonian with complicated interaction terms, the commutators $[H, a_\nu^\dagger]$ and $[H, a_\nu]$ are not simple, and consequently the fundamental (anti-)commutator $[a_\nu(t_1), a_\nu^\dagger(t_2)]_{F,B}$ involving two different times t_1 and t_2 cannot be given in a simple closed form:

$$[a_{\nu_1}(t_1), a_{\nu_2}^\dagger(t_2)]_{F,B} = e^{iHt_1} a_{\nu_1} e^{-iH(t_1-t_2)} a_{\nu_2}^\dagger e^{-iHt_2} \pm e^{iHt_2} a_{\nu_2}^\dagger e^{-iH(t_2-t_1)} a_{\nu_1} e^{-iHt_1} = ?? \quad (5.21)$$

No further reduction is possible in the general case. In fact, as we shall see in the following chapters, calculating (anti-)commutators like Eq. (5.21) is *the* problem in many-particle physics.

But let us investigate some simple cases to get a grasp of the time evolution pictures. Consider first a time-independent Hamiltonian H which is diagonal in the $|\nu\rangle$ -basis,

$$H = \sum_{\nu} \varepsilon_{\nu} a_{\nu}^{\dagger} a_{\nu}. \quad (5.22)$$

The equation of motion, Eq. (5.6), is straightforward:²

$$\begin{aligned} \dot{a}_{\nu}(t) &= i[H, a_{\nu}(t)] = i e^{iHt} [H, a_{\nu}] e^{-iHt} \\ &= i e^{iHt} \sum_{\nu'} \varepsilon_{\nu'} [a_{\nu'}^{\dagger} a_{\nu'}, a_{\nu}] e^{-iHt} = i e^{iHt} \sum_{\nu'} \varepsilon_{\nu'} (-\delta_{\nu, \nu'}) a_{\nu'} e^{-iHt} \\ &= -i \varepsilon_{\nu} e^{iHt} a_{\nu} e^{-iHt} = -i \varepsilon_{\nu} a_{\nu}(t). \end{aligned} \quad (5.23)$$

By integration we obtain

$$a_{\nu}(t) = e^{-i\varepsilon_{\nu}t} a_{\nu}, \quad (5.24)$$

which by Hermitian conjugation leads to

$$a_{\nu}^{\dagger}(t) = e^{+i\varepsilon_{\nu}t} a_{\nu}^{\dagger}. \quad (5.25)$$

In this very simple case the basic (anti-)commutator Eq. (5.21) can be evaluated directly:

$$[a_{\nu_1}(t_1), a_{\nu_2}^{\dagger}(t_2)]_{F,B} = e^{-i\varepsilon_{\nu_1}(t_1-t_2)} \delta_{\nu_1, \nu_2}. \quad (5.26)$$

For the diagonal Hamiltonian the time evolution is thus seen to be given by trivial phase factors $e^{\pm i\varepsilon t}$.

We can also gain some insight into the interaction picture by a trivial extension of the simple model. Assume that

$$H = H_0 + \gamma H_0, \quad \gamma \ll 1, \quad (5.27)$$

where H_0 is diagonalized in the basis $\{|\nu\rangle\}$ with the eigenenergies ε_{ν} . Obviously, the full Hamiltonian H is also diagonalized in the same basis, but with the eigenenergies $(1+\gamma)\varepsilon$. Let us however try to treat γH_0 as a perturbation V to H_0 , and then use the interaction picture of Sec. 5.3. From Eq. (5.8) we then obtain

$$|\hat{\nu}(t)\rangle = e^{i\varepsilon_{\nu}t} |\nu(t)\rangle. \quad (5.28)$$

But we actually know the time evolution of the Schrödinger state on the right-hand side of the equation, so

$$|\hat{\nu}(t)\rangle = e^{i\varepsilon_{\nu}t} e^{-i(1+\gamma)\varepsilon_{\nu}t} |\nu\rangle = e^{-i\gamma\varepsilon_{\nu}t} |\nu\rangle. \quad (5.29)$$

²We are using the identities $[AB, C] = A[B, C] + [A, C]B$ and $[AB, C] = A\{B, C\} - \{A, C\}B$, which are valid for any set of operators. Note that the first identity is particularly useful for bosonic operators and the second for fermionic operators (see Exercise 5.4).

Here we clearly see that the fast Schrödinger time dependence given by the phase factor $e^{i\varepsilon_\nu t}$, is replaced in the interaction picture by the slow phase factor $e^{i\gamma\varepsilon_\nu t}$. The reader can try to obtain Eq. (5.29) directly from Eq. (5.18).

Finally, we briefly point to the complications that arise when the interaction is given by a time-independent operator V not diagonal in the same basis as H_0 . Consider for example the Coulomb-like interaction written symbolically as

$$H = H_0 + V = \sum_{\nu'} \varepsilon_{\nu'} a_{\nu'}^\dagger a_{\nu'} + \sum_{\nu_1 \nu_2} \sum_q V_q a_{\nu_1+q}^\dagger a_{\nu_2-q}^\dagger a_{\nu_2} a_{\nu_1}. \quad (5.30)$$

The equation of motion for $a_\nu(t)$ is:

$$\begin{aligned} \dot{a}_\nu(t) &= i[H, a_\nu(t)] = -i\varepsilon_\nu a_\nu(t) + i \sum_{\nu_1 \nu_2 q} V_q \left[a_{\nu_1+q}^\dagger(t) a_{\nu_2-q}^\dagger(t), a_\nu(t) \right] a_{\nu_2}(t) a_{\nu_1}(t) \\ &= -i\varepsilon_\nu a_\nu(t) + i \sum_{\nu_1 \nu_2} (V_{\nu_2-\nu} - V_{\nu-\nu_1}) a_{\nu_1+\nu_2-\nu}^\dagger(t) a_{\nu_2}(t) a_{\nu_1}(t). \end{aligned} \quad (5.31)$$

The problem in this more general case is evident. The equation of motion for the single operator $a_\nu(t)$ contains terms with both one and three operators, and we do not know the time evolution of the three-operator product $a_{\nu_1+\nu_2-\nu}^\dagger(t) a_{\nu_2}(t) a_{\nu_1}(t)$. If we write down the equation of motion for this three-operator product we discover that terms are generated involving five operator products. This feature is then repeated over and over again generating a never-ending sequence of products containing seven, nine, eleven, etc. operators. In the following chapters we will learn various approximate methods to deal with this problem.

5.6 Summary and outlook

In this chapter we have introduced the fundamental representations used in the description of time evolution in many-particle systems: the Schrödinger picture, Eq. (5.2), the Heisenberg picture, Eq. (5.5), and the interaction picture, Eq. (5.8). The first two pictures rely on a time-independent Hamiltonian H , while the interaction picture involves a time-dependent Hamiltonian H of the form $H = H_0 + V(t)$, where H_0 is a time-independent Hamiltonian with known eigenstates. Which picture to use depends on the problem at hand.

We have derived an explicit expression, Eq. (5.18), for the time evolution operator $\hat{U}(t, t_0)$ describing the evolution of an interaction picture state $|\hat{\psi}(t_0)\rangle$ at time t_0 to $|\hat{\psi}(t)\rangle$ at time t . We shall see in the following chapters how the operator $\hat{U}(t, t_0)$ plays an important role in the formulation of infinite order perturbation theory and the introduction of Feynman diagrams, and how its linearized form Eq. (5.19) forms the basis of the widely used linear response theory and the associated Kubo formalism.

Finally, by studying the basic creation and annihilation operators we have gotten a first glimpse of the problems we are facing, when we are trying to study the full time dependence, or equivalently the full dynamics, of interacting many-particle systems.

Chapter 6

Linear response theory

Linear response theory is an extremely widely used concept in all branches of physics. It simply states that the response to a weak external perturbation is proportional to the perturbation, and therefore all one needs to understand is the proportionality constant. Below we derive the general formula for the linear response of a quantum system exerted by a perturbation. The physical question we ask is thus: supposing some perturbation H' , what is the measured consequence for an observable quantity, A . In other words, what is $\langle A \rangle$ to linear order in H' ?

Among the numerous applications of the linear response formula, one can mention charge and spin susceptibilities of e.g. electron systems due to external electric or magnetic fields. Responses to external mechanical forces or vibrations can also be calculated using the very same formula. Here we utilize the formalism to derive a general expression for the electrical conductivity and briefly mention other applications.

6.1 The general Kubo formula

Consider a quantum system described by the (time independent) Hamiltonian H_0 in thermodynamic equilibrium. According to Sec. 1.5 this means that an expectation value of a physical quantity, described by the operator A , can be evaluated as

$$\langle A \rangle = \frac{1}{Z_0} \text{Tr} [\rho_0 A] = \frac{1}{Z_0} \sum_n \langle n | A | n \rangle e^{-\beta E_n}, \quad (6.1a)$$

$$\rho_0 = e^{-\beta H_0} = \sum_n |n\rangle \langle n| e^{-\beta E_n}, \quad (6.1b)$$

where ρ_0 is the density operator and $Z_0 = \text{Tr}[\rho_0]$ is the partition function. Here as in Sec. 1.5, we write the density operator in terms of a complete set of eigenstates, $\{|n\rangle\}$, of the Hamiltonian, H_0 , with eigenenergies $\{E_n\}$.

Suppose now that at some time, $t = t_0$, an external perturbation is applied to the system, driving it out of equilibrium. The perturbation is described by an additional time dependent term in the Hamiltonian

$$H(t) = H_0 + H'(t)\theta(t - t_0). \quad (6.2)$$

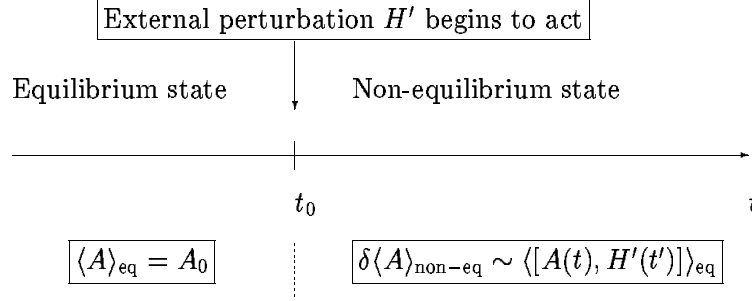


Figure 6.1: Illustration of the linear response theory. At times before t_0 the system is in equilibrium, after which the perturbation is turned on. The system is now evolving according to the new Hamiltonian and is in a non-equilibrium state. The Kubo formula relates the expectation value $\delta\langle A \rangle_{\text{non-eq}}$ in the non-equilibrium state to a equilibrium expectation value $\langle \cdots \rangle_{\text{eq}}$ of the more complicated time-dependent commutator $[\hat{A}(t), \hat{H}'(t')]$.

We emphasize that H_0 is the Hamiltonian describing the system before the perturbation was applied, see Fig. 6.1 for an illustration. Now we wish to find the expectation value of the operator A at times t greater than t_0 . In order to do so we must find the time evolution of the density matrix or equivalently the time evolution of the eigenstates of the unperturbed Hamiltonian. Once we know the $|n(t)\rangle$, we can obtain $\langle A(t) \rangle$ as

$$\langle A(t) \rangle = \frac{1}{Z_0} \sum_n \langle n(t) | A | n(t) \rangle e^{-\beta E_n} = \frac{1}{Z_0} \text{Tr} [\rho(t) A], \quad (6.3a)$$

$$\rho(t) = \sum_n |n(t)\rangle \langle n(t)| e^{-\beta E_n}. \quad (6.3b)$$

The philosophy behind this expression is as follows. The initial states of the system are distributed according to the usual Boltzmann distribution $e^{-\beta E_{0n}}/Z_0$. At later times the system is described by the same distribution of states but the states are now time-dependent and they have evolved according to the new Hamiltonian. The time dependence of the states $|n(t)\rangle$ is of course governed by the Schrödinger equation

$$i\partial_t |n(t)\rangle = H(t) |n(t)\rangle. \quad (6.4)$$

Since H' is to be regarded as a small perturbation, it is convenient to utilize the interaction picture representation $|\hat{n}(t)\rangle$ introduced in Sec. 5.3. The time dependence in this representation is given by

$$|n(t)\rangle = e^{-iH_0 t} |\hat{n}(t)\rangle = e^{-iH_0 t} \hat{U}(t, t_0) |\hat{n}(t_0)\rangle, \quad (6.5)$$

where by definition $|\hat{n}(t_0)\rangle = e^{iH_0 t_0} |n(t_0)\rangle = |n\rangle$.

To linear order in H' , Eq. (5.19) states that $\hat{U}(t, t_0) = 1 - i \int_{t_0}^t dt' \hat{H}'(t')$. Inserting this into (6.3a), one obtains the expectation value of A up to linear order in the perturbation

$$\begin{aligned} \langle A(t) \rangle &= \langle A \rangle_0 - i \int_{t_0}^t dt' \frac{1}{Z_0} \sum_n e^{-\beta E_n} \langle n(t_0) | \hat{A}(t) \hat{H}'(t') - \hat{H}'(t') \hat{A}(t) | n(t_0) \rangle \\ &= \langle A \rangle_0 - i \int_{t_0}^t dt' \langle [\hat{A}(t), \hat{H}'(t')] \rangle_0. \end{aligned} \quad (6.6)$$

The brackets $\langle \rangle_0$ mean an equilibrium average with respect to the Hamiltonian H_0 . This is in fact a remarkable and very useful result, because the inherently non-equilibrium quantity $\langle A(t) \rangle$ has been expressed as a correlation function of the system in equilibrium. The physical reason for this is that the interaction between excitations created in the non-equilibrium state is an effect to second order in the weak perturbation, and hence not included in linear response.

The correlation function that appears in Eq. (6.6), is called a retarded correlation function, and for later reference we rewrite the linear response result as

$$\delta \langle A(t) \rangle \equiv \langle A(t) \rangle - \langle A \rangle_0 = \int_{t_0}^{\infty} dt' C_{AH'}^R(t, t') e^{-\eta(t-t')}, \quad (6.7)$$

where

$$C_{AH'}^R(t, t') = -i\theta(t - t') \left\langle [\hat{A}(t), \hat{H}'(t')] \right\rangle_0. \quad (6.8)$$

This is the famous Kubo formula which expresses the linear response to a perturbation, H' . We have added a very important detail here: the factor $e^{-\eta(t-t')}$, with an infinitesimal positive parameter η , has been included to force the response at time t due to the influence of H' at time t' to decay when $t \gg t'$. In the end of a calculation we must therefore take the limit $\eta \rightarrow 0^+$. For physical reasons the (retarded) effect of a perturbation must of course decrease in time. You can think of the situation that one often has for differential equations with two solutions: one which increases exponentially with time (physically not acceptable) and one which decreases exponentially with time; the factor $e^{-\eta(t-t')}$ is there to pick out the physically relevant solution by introducing an artificial relaxation mechanism.

Kubo formula in the frequency domain

It is often convenient to express the response to an external disturbance in the frequency domain. Let us therefore write the perturbation in terms of its Fourier components

$$H'(t) = \int \frac{d\omega}{2\pi} e^{-i\omega t} H'_\omega, \quad (6.9)$$

such that $C_{AH'}^R$ becomes

$$C_{AH'}^R(t, t') = \int_{-\infty}^{\infty} \frac{d\omega}{2\pi} e^{-i\omega t'} C_{AH'_\omega}^R(t - t'), \quad (6.10)$$

because $\langle [\hat{A}(t), \hat{H}'_\omega(t')] \rangle_0$ only depends on the difference between t and t' , which can easily be proven using the definition of the expectation value. When inserted into the Kubo formula, one gets (after setting $t_0 = -\infty$, because we are not interested in the transient behavior)

$$\begin{aligned} \delta \langle A(t) \rangle &= \int_{-\infty}^{\infty} dt' \int_{-\infty}^{\infty} \frac{d\omega}{2\pi} e^{-i\omega t} e^{-i(\omega+i\eta)(t'-t)} C_{AH'_\omega}^R(t-t') \\ &= \int_{-\infty}^{\infty} \frac{d\omega}{2\pi} e^{-i\omega t} C_{AH'_\omega}^R(\omega), \end{aligned} \quad (6.11)$$

and therefore the final result reads in frequency domain

$$\delta \langle A_\omega \rangle = C_{AH'_\omega}^R(\omega), \quad (6.12a)$$

$$C_{AH'_\omega}^R(\omega) = \int_{-\infty}^{\infty} dt e^{i\omega t} e^{-\eta t} C_{AH'_\omega}^R(t). \quad (6.12b)$$

Note again that the infinitesimal η is incorporated in order to ensure the correct physical result, namely that the retarded response function decays at large times.

6.2 Kubo formula for conductivity

Consider a system of charged particles, electrons say, which is subjected to an external electromagnetic field. The electromagnetic field induces a current, and the conductivity is the linear response coefficient. In the general case the conductivity may be non-local in both time and space, such that the electric current \mathbf{J}_e at some point \mathbf{r} at time t depends on the electric field at points \mathbf{r}' at times t'

$$J_e^\alpha(\mathbf{r}, t) = \int dt' \int d\mathbf{r}' \sum_{\beta} \sigma^{\alpha\beta}(\mathbf{r}t, \mathbf{r}'t') E^\beta(\mathbf{r}', t') \quad (6.13)$$

where $\sigma^{\alpha\beta}(\mathbf{r}, \mathbf{r}'; t, t')$ is the conductivity tensor which describes the current response in direction \hat{e}_α to an applied electric field in direction \hat{e}_β .

The electric field \mathbf{E} is given by the electric potential ϕ_{ext} and the vector potential \mathbf{A}_{ext}

$$\mathbf{E}(\mathbf{r}, t) = -\nabla_{\mathbf{r}} \phi_{\text{ext}}(\mathbf{r}, t) - \partial_t \mathbf{A}_{\text{ext}}(\mathbf{r}, t). \quad (6.14)$$

The current density operator of charged particles in the presence of an electromagnetic field was given in Chap. 1. For simplicity we assume only one kind of particles, electrons say, but generalization to more kinds of charge carrying particles is straightforward by simple addition of more current components.¹ For electrons $\mathbf{J}_e = -e\langle \mathbf{J} \rangle$. The perturbing term in the Hamiltonian due to the external electromagnetic field is given by the coupling

¹With more carriers the operator for the electrical current becomes $\mathbf{J}_e(\mathbf{r}) = \sum_i q_i \mathbf{J}_i(\mathbf{r})$, where q_i are the charges of the different carriers. Note that in this case the currents of the individual species are not necessarily independent.

of the electrons to the scalar potential and the vector potential. To linear order in the external potential

$$H_{\text{ext}} = -e \int d\mathbf{r} \rho(\mathbf{r}) \phi_{\text{ext}}(\mathbf{r}, t) + e \int d\mathbf{r} \mathbf{J}(\mathbf{r}) \cdot \mathbf{A}_{\text{ext}}(\mathbf{r}, t), \quad (6.15)$$

where the latter term was explained in Sec. 1.4.3. Let \mathbf{A}_0 denote the vector potential in the equilibrium, i.e. prior to the onset of the perturbation \mathbf{A}_{ext} , and let \mathbf{A} denote the total vector potential. Then we have

$$\mathbf{A} = \mathbf{A}_0 + \mathbf{A}_{\text{ext}}, \quad (6.16)$$

Again according to Sec. 1.4.3, the current operator has two components, the diamagnetic term and the paramagnetic term

$$\mathbf{J}(\mathbf{r}) = \mathbf{J}^\nabla(\mathbf{r}) + \frac{e}{m} \mathbf{A}(\mathbf{r}) \rho(\mathbf{r}), \quad (6.17)$$

In order to simplify the expressions, we can choose a gauge where the external electrical potential is zero, $\phi_{\text{ext}} = 0$. This is always possible by a suitable choice of $\mathbf{A}(\mathbf{r}, t)$ as you can see in Eq. (6.14). The final result should of course not depend on the choice of gauge. The conductivity is most easily expressed in the frequency domain, and therefore we Fourier transform the perturbation. Since ∂_t becomes $-i\omega$ in the frequency domain we have $\mathbf{A}_{\text{ext}}(\mathbf{r}, \omega) = (1/i\omega) \mathbf{E}_{\text{ext}}(\mathbf{r}, \omega)$, and therefore the external perturbation in Eq. (6.15) becomes in the Fourier domain

$$H_{\text{ext}, \omega} = \frac{e}{i\omega} \int d\mathbf{r} \mathbf{J}(\mathbf{r}) \cdot \mathbf{E}_{\text{ext}}(\mathbf{r}, \omega). \quad (6.18)$$

In order to exploit the frequency domain formulation of linear response we want to write the definition of the conductivity tensor in Eq. (6.13) in frequency domain. Because we are only considering linear response the conductivity tensor is a property of the equilibrium system and can thus only depend on time differences $\sigma^{\alpha\beta}(\mathbf{r}t, \mathbf{r}'t') = \sigma^{\alpha\beta}(\mathbf{r}, \mathbf{r}', t - t')$. The frequency transform of Eq. (6.13) is therefore simply that of a convolution and hence

$$J_e^\alpha(\mathbf{r}, \omega) = \int d\mathbf{r}' \sum_\beta \sigma^{\alpha\beta}(\mathbf{r}, \mathbf{r}', \omega) E^\beta(\mathbf{r}', \omega). \quad (6.19)$$

Now since Eq. (6.18) is already linear in the external potential \mathbf{E}_{ext} and since we are only interested in the linear response, we can replace \mathbf{J} in Eq. (6.18) by $\mathbf{J}_0 = \mathbf{J}^\nabla + \frac{e}{m} \mathbf{A}_0 \rho$, thus neglecting the term proportional to $\mathbf{E}_{\text{ext}} \cdot \mathbf{A}_{\text{ext}}$. Eq. (6.18) is therefore replaced by

$$H_{\text{ext}, \omega} = \frac{e}{i\omega} \int d\mathbf{r} \mathbf{J}_0(\mathbf{r}) \cdot \mathbf{E}_{\text{ext}}(\mathbf{r}, \omega). \quad (6.20)$$

To find the expectation value of the current we write

$$\langle \mathbf{J}(\mathbf{r}, \omega) \rangle = \langle \mathbf{J}_0(\mathbf{r}, \omega) \rangle + \langle \frac{e}{m} \mathbf{A}_{\text{ext}}(\mathbf{r}, \omega) \rho(\mathbf{r}) \rangle. \quad (6.21)$$

For the last term in Eq. (6.21) we use that to linear order in \mathbf{A}_{ext} the expectation value can be evaluated in the equilibrium state

$$\left\langle \frac{e}{m} \mathbf{A}_{\text{ext}}(\mathbf{r}, \omega) \rho(\mathbf{r}) \right\rangle = \frac{e}{m} \mathbf{A}_{\text{ext}}(\mathbf{r}, \omega) \langle \rho(\mathbf{r}) \rangle_0 = \frac{e}{i\omega} \mathbf{E}_{\text{ext}}(\mathbf{r}, \omega) \langle \rho(\mathbf{r}) \rangle_0. \quad (6.22)$$

For the first term in Eq. (6.21) we use the general Kubo formula in Eq. (6.7). Since the equilibrium state does not carry any current, i.e. $\langle J_0 \rangle_0 = 0$, we conclude that $\langle J_0 \rangle = \delta \langle J_0 \rangle$. In frequency domain we should use the results Eq. (6.12a) and substitute $\mathbf{J}_0(\mathbf{r})$ for the operator “ A ”, and $H_{\text{ext},\omega}$ for “ H'_ω ”, which leads to $\langle J_0(\mathbf{r}, \omega) \rangle = \mathbf{C}_{J_0(\mathbf{r})H_{\text{ext},\omega}}^R(\omega)$. Collecting things we now have

$$\langle \mathbf{J}(\mathbf{r}, \omega) \rangle = \mathbf{C}_{J_0(\mathbf{r})H_{\text{ext},\omega}}^R(\omega) + \frac{e}{m} \langle \rho(\mathbf{r}) \rangle_0 \mathbf{A}_{\text{ext}}(\mathbf{r}, \omega). \quad (6.23)$$

Writing out the first term

$$\mathbf{C}_{J_0(\mathbf{r})H_{\text{ext},\omega}}^R(\omega) = \int d\mathbf{r}' \sum_{\beta} \mathbf{C}_{J_0(\mathbf{r})J_0^\beta(\mathbf{r}')}^R(\omega) \frac{e}{i\omega} E^\beta(\mathbf{r}', \omega). \quad (6.24)$$

Comparing with the definition of the non-local conductivity in Eq. (6.19), we can now collect the two contributions to the conductivity tensor. The first term comes from Eq. (6.24) and it is seen to be of the same form as (6.12a), in particular the response is non-local in space. In contrast, the second term in Eq. (6.22) stemming from the diamagnetic part of the current operator is local in space. Now collecting the two terms and using that $\mathbf{J}_e = -e\langle \mathbf{J} \rangle$, we finally arrive at the linear response formula for the conductivity tensor

$$\sigma^{\alpha\beta}(\mathbf{r}, \mathbf{r}', \omega) = \frac{ie^2}{\omega} \Pi_{\alpha\beta}^R(\mathbf{r}, \mathbf{r}', \omega) + \frac{ie^2 n(\mathbf{r})}{i\omega m} \delta(\mathbf{r} - \mathbf{r}') \delta_{\alpha\beta}, \quad (6.25)$$

where we have used the symbol $\Pi^R = C_{J_0 J_0}^R$ for the retarded current-current correlation function. In the time domain it is given by

$$\Pi_{\alpha\beta}^R(\mathbf{r}, \mathbf{r}', t - t') = C_{J_0^\alpha(\mathbf{r})J_0^\beta(\mathbf{r}')}^R(t - t') = -i\theta(t - t') \left\langle \left[\hat{J}_0^\alpha(\mathbf{r}, t), \hat{J}_0^\beta(\mathbf{r}', t') \right] \right\rangle_0. \quad (6.26)$$

Finding the conductivity of a given system has thus been reduced to finding the retarded current-current correlation function. This formula will be used extensively in Chap. 14.

6.3 Kubo formula for conductance

The conductivity σ is the proportionality coefficient between the electric field \mathbf{E} and the current density \mathbf{J} , and it is an intrinsic property of a material. The conductance on the other hand is the proportionality coefficient between the current I through a sample and the voltage V applied to it, i.e. a sample specific quantity. The conductance G is defined by the usual Ohm's law

$$I = GV. \quad (6.27)$$

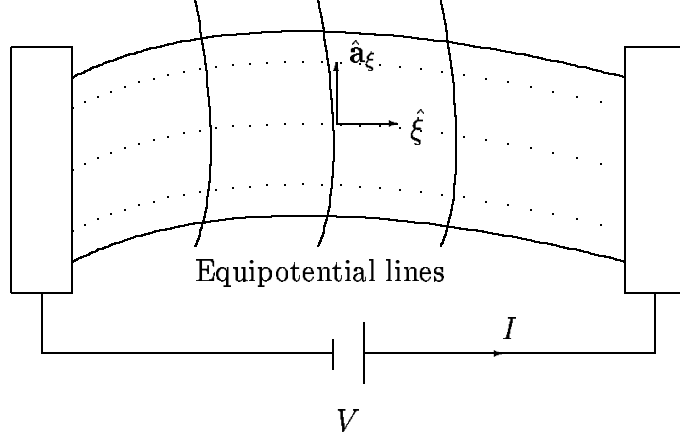


Figure 6.2: The principle of a conductance measurement, which, in contrast to the conductivity, is a sample-specific quantity. In the Kubo formula derivation we use a coordinate system given by the equipotential lines, which together with use of current conservation allows a simple derivation.

For a material where the conductivity can be assumed to be local in space one can find the conductance of a specific sample by the relation

$$G = \frac{W}{L} \sigma, \quad (6.28)$$

where L is the length of the sample, and W the area of the cross-section. For samples which are inhomogeneous such that this simple relation is not applicable, one must use the Kubo formula for conductance rather than that for conductivity. One example is the so-called mesoscopic conductors, which are systems smaller than a typical thermalization or equilibration length, whereby a local description is inadequate.

The current passing through the sample is equal to the integrated current density through a cross-section. Here we are interested in the DC-response only (or in frequencies where the corresponding wave length is much longer than the sample size). Because of current conservation we can of course choose any cross section, and it is convenient to choose an equipotential surface and to define a coordinate system (ξ, \mathbf{a}_ξ) , where ξ is a coordinate parallel to the field line and where \mathbf{a}_ξ are coordinates on the plane perpendicular to the ξ -direction; see Figure 6.2. In this coordinate system the electric field is directed along the $\hat{\xi}$ -direction, $\mathbf{E}(\mathbf{r}) = \hat{\xi} E(\xi)$. The current I is

$$\begin{aligned} I_e &= \int d\mathbf{a}_\xi \hat{\xi} \cdot \mathbf{J}_e(\xi, \mathbf{a}_\xi) = \int d\mathbf{a}_\xi \int d\mathbf{r}' \hat{\xi} \cdot \sigma(\mathbf{r}, \mathbf{r}'; \omega = 0) \mathbf{E}(\mathbf{r}'), \\ &= \int d\mathbf{a}_\xi \int d\mathbf{a}_{\xi'} \int d\xi' \hat{\xi} \cdot \sigma(\xi, \mathbf{a}_\xi, \xi', \mathbf{a}_{\xi'}; \omega = 0) \cdot \hat{\xi}' E(\xi'), \end{aligned} \quad (6.29)$$

where $\hat{\xi}$ is a unit vector normal to the surface element $d\mathbf{a}_\xi$ and σ is the conductivity tensor. In order to get the dc-response we should take the limit $\omega \rightarrow 0$ of this expression. If

we furthermore take the real part of (6.29) we see that what determines the dc-current is the real part of the first term in Eq. (6.25) and hence the retarded correlation function of the current densities. Since the total particle current at the coordinate ξ is given by $I(\xi) = \int d\mathbf{a}_\xi \hat{\xi} \cdot J$, the conductance can instead be written as

$$I_e(\xi) = \lim_{\omega \rightarrow 0} \int d\xi' \operatorname{Re} \left[\frac{ie^2}{\omega} C_{I(\xi)I(\xi')}^R(\omega) \right] E(\xi') \equiv \int d\xi' G(\xi, \xi') E(\xi'), \quad (6.30)$$

where $C_{I(\xi)I(\xi')}^R$ is the correlation function between total currents. Because of current conservation the dc-current may be calculated at any point ξ and thus the result cannot depend on ξ . Consequently the function inside the square brackets in Eq. (6.30) cannot depend on ξ . Furthermore, since the conductance function $G(\xi, \xi')$ can be shown to be a symmetric function it cannot depend on ξ' either. This simplification is the reason for choosing the skew coordinate system defined by the field lines. We can therefore perform the integration over ξ' which is just the voltage difference $V = \int d\xi' E(\xi') = \phi(-\infty) - \phi(\infty)$, and we finally arrive at the for linear response formula for the conductance

$$G = \lim_{\omega \rightarrow 0} \frac{ie^2}{\omega} C_{II}^R(\omega). \quad (6.31)$$

Here C_{II}^R is the retarded current-current function. In the time domain it is

$$C_{II}^R(t - t') = -i\theta(t - t') \langle [\hat{I}(t), \hat{I}(t')] \rangle, \quad (6.32)$$

where the current operator I denote the current through an arbitrary cross section along the sample.

6.4 Kubo formula for the dielectric function

When dealing with systems containing charged particles, as for example the electron gas, one is often interested in the dielectric properties of the system, and in particular the linear response properties. When such a system is subjected to an external electromagnetic perturbation the charge is redistributed and the system gets polarized. This in turn affects the measurements. The typical experiment is to exert an external potential, ϕ_{ext} , and measure the resulting total potential, ϕ_{tot} . The total potential is the sum of the external one and the potential created by the induced polarization, ϕ_{ind} ,

$$\phi_{\text{tot}} = \phi_{\text{ext}} + \phi_{\text{ind}}. \quad (6.33)$$

Alternatively to working with the potentials we can work with electric fields or charges. The charges are related to the potentials through a set of Poisson equations

$$\rho_{\text{tot}} = \rho_{\text{ext}} + \rho_{\text{ind}}, \quad \left\{ \begin{array}{l} \nabla^2 \phi_{\text{tot}} = -\frac{1}{\varepsilon_0} \rho_{e,\text{tot}} \\ \nabla^2 \phi_{\text{ext}} = -\frac{1}{\varepsilon_0} \rho_{e,\text{ext}} \\ \nabla^2 \phi_{\text{ind}} = -\frac{1}{\varepsilon_0} \rho_{e,\text{ind}} \end{array} \right\}, \quad (6.34)$$

and likewise for electric fields, E_{tot} , E_{ext} , and E_{ind} , which are related to the corresponding charges by a set of Gauss laws, $\nabla \cdot \mathbf{E} = \rho_e/\varepsilon_0$. Here we have used the symbols ρ_e for the charge density, where ρ as defined in Chap. 1 defines particle densities.

The ratio between the external and the total potential is the dielectric response function, also called the relative permittivity ε

$$\phi_{\text{tot}} = \varepsilon^{-1} \phi_{\text{ext}}, \quad (6.35)$$

which is well-known from classical electrodynamics.² However, in reality the permittivity is non-local both in time and space and the general relations between the total and the external potentials are

$$\phi_{\text{tot}}(\mathbf{r}, t) = \int d\mathbf{r}' \int dt' \varepsilon^{-1}(\mathbf{r}t, \mathbf{r}'t') \phi_{\text{ext}}(\mathbf{r}', t'), \quad (6.36a)$$

$$\phi_{\text{ext}}(\mathbf{r}, t) = \int d\mathbf{r}' \int dt' \varepsilon(\mathbf{r}t, \mathbf{r}'t') \phi_{\text{tot}}(\mathbf{r}', t'). \quad (6.36b)$$

Our present task is to find the dielectric function $\varepsilon(\mathbf{r}t, \mathbf{r}'t')$, or rather its inverse $\varepsilon^{-1}(\mathbf{r}t, \mathbf{r}'t')$ assuming linear response theory and for this purpose the induced potential is needed.

The external perturbation is represented as the following term to the Hamiltonian

$$H' = \int d\mathbf{r} \rho_e(\mathbf{r}) \phi_{\text{ext}}(\mathbf{r}, t). \quad (6.37)$$

The induced charge density follows from linear response theory (if we assume that the system is charge neutral in equilibrium, i.e. $\langle \rho_e(\mathbf{r}, t) \rangle_0 = 0$) as

$$\rho_{e,\text{ind}}(\mathbf{r}, t) = \langle \rho_e(\mathbf{r}, t) \rangle = \int d\mathbf{r}' \int_{t_0}^{\infty} dt' C_{\rho_e \rho_e}^R(\mathbf{r}t, \mathbf{r}'t') e^{-\eta(t-t')} \phi_{\text{ext}}(\mathbf{r}', t'), \quad (6.38)$$

$$C_{\rho_e \rho_e}^R(\mathbf{r}t, \mathbf{r}'t') \equiv \chi_e^R(\mathbf{r}t, \mathbf{r}'t') = -i\theta(t-t') \langle [\hat{\rho}_e(\mathbf{r}, t), \hat{\rho}_e(\mathbf{r}', t')] \rangle_0. \quad (6.39)$$

The charge-charge correlation function, χ_e^R , is called the polarizability function and it is an important function which we will encounter many times. Once the induced charge is known the potential follows from the Coulomb interaction $V_c(\mathbf{r} - \mathbf{r}') = 1/(\epsilon_0 |\mathbf{r} - \mathbf{r}'|)$ as

$$\phi_{\text{ind}}(\mathbf{r}) = \int d\mathbf{r}' V_c(\mathbf{r} - \mathbf{r}') \rho_{e,\text{ind}}(\mathbf{r}'), \quad (6.40)$$

and hence

$$\phi_{\text{tot}}(\mathbf{r}, t) = \phi_{\text{ext}}(\mathbf{r}, t) + \int d\mathbf{r}' \int d\mathbf{r}'' \int_{t_0}^{\infty} dt' V_c(\mathbf{r} - \mathbf{r}') \chi^R(\mathbf{r}'t, \mathbf{r}''t') \phi_{\text{ext}}(\mathbf{r}'', t'). \quad (6.41)$$

From this expression we read off the inverse of the dielectric function as

$$\varepsilon^{-1}(\mathbf{r}t, \mathbf{r}'t') = \delta(\mathbf{r} - \mathbf{r}') \delta(t - t') + \int d\mathbf{r}'' V_c(\mathbf{r} - \mathbf{r}'') \chi^R(\mathbf{r}''t, \mathbf{r}'t'), \quad (6.42)$$

²In electrodynamics the permittivity is defined as the proportionality constant between the electric displacement field, \mathbf{D} , and the electric field, $\mathbf{D} = \varepsilon \mathbf{E}$. In the present formulation, \mathbf{E}_{ext} plays the role of the \mathbf{D} -field, i.e. $\mathbf{D} = \varepsilon_0 \mathbf{E}_{\text{ext}}$, while \mathbf{E}_{tot} is the \mathbf{E} -field

which ends our derivation. In later chapters we will make extensive use of the dielectric function ε and the polarizability χ . The dielectric function expressed in Eq. (6.42) includes all correlation effects, but often we must use some approximation to compute the polarizability.

6.4.1 Dielectric function for translation-invariant system

In the translation-invariant case the polarizability can only depend on the differences of the arguments, i.e. $\chi^R(\mathbf{r}t, \mathbf{r}'t') = \chi^R(\mathbf{r} - \mathbf{r}'; t - t')$, and therefore the problem is considerably simplified by going to frequency and momentum space, where both Eqs. (6.36) have the form of convolutions. After Fourier transformation they become products

$$\phi_{\text{tot}}(\mathbf{q}, \omega) = \varepsilon^{-1}(\mathbf{q}, \omega) \phi_{\text{ext}}(\mathbf{q}, \omega), \quad \text{or} \quad \phi_{\text{ext}}(\mathbf{q}, \omega) = \varepsilon(\mathbf{q}, \omega) \phi_{\text{tot}}(\mathbf{q}, \omega), \quad (6.43)$$

with the dielectric function being

$$\varepsilon^{-1}(\mathbf{q}, \omega) = 1 + V_c(\mathbf{q}) \chi_e^R(\mathbf{q}, \omega). \quad (6.44)$$

6.4.2 Relation between dielectric function and conductivity

Both ε and σ give the response of a system to an applied electromagnetic field, and one should therefore expect that they were related, and of course they are. Here we consider again the translational-invariant case, and using the definition of conductivity

$$\mathbf{J}(\mathbf{q}, \omega) = \sigma(\mathbf{q}, \omega) \mathbf{E}_{\text{ext}}(\mathbf{q}, \omega) = -i\sigma(\mathbf{q}, \omega) \mathbf{q} \phi_{\text{ext}}(\mathbf{q}, \omega), \quad (6.45)$$

and the continuity equation,

$$-i\omega\rho(\mathbf{q}, \omega) + i\mathbf{q} \cdot \mathbf{J}(\mathbf{q}, \omega) = 0, \quad (\text{continuity equation}), \quad (6.46)$$

we obtain

$$-i\mathbf{q} \cdot \sigma(\mathbf{q}, \omega) \mathbf{q} \phi_{\text{ext}}(\mathbf{q}, \omega) = \omega\rho_e(\mathbf{q}, \omega) = \omega\chi_e^R(\mathbf{q}, \omega) \phi_{\text{ext}}(\mathbf{q}, \omega). \quad (6.47)$$

Finally, using Eq. (6.44) and knowing that for a homogeneous system, the conductivity tensor is diagonal, we arrive at the relation

$$\varepsilon^{-1}(\mathbf{q}, \omega) = 1 - i \frac{q^2}{\omega} V_c(\mathbf{q}) \sigma(\mathbf{q}, \omega). \quad (6.48)$$

So if we know the conductivity we can find the dielectric response and vice versa. This formula also tells us what information about the interactions within a given system can be extracted from measurements of the dielectric properties.

6.5 Summary and outlook

We have developed a general method for calculating the response to weak perturbations. This method, called linear response theory, is widely used because many experimental

investigations are done in the linear response regime. In this regime the lack of equilibrium is not important, and one can think of this as probing the individual excitations of the systems. Because the perturbation is weak it is not necessary to include interactions between these excitations.

The general formula is a correlation function of the quantity that we measure and the quantity to which the weak external perturbation couples. In the case of conductivity we saw that it was the current-current correlation function, and the dielectric response reduces to a charge-charge correlation. These two will be used later in Chaps. 12 and 14. Also in the next chapter we will make use of the linear response result, when discussing tunneling current between two conductors.

Chapter 7

Transport in mesoscopic systems

In this chapter we give an introduction to electronic transport in mesoscopic structures and it is our first in-depth use of the Kubo formalism. The physics of mesoscopic systems is a vast field, and we shall concentrate on the Landauer-Büttiker single-particle approach to conductance of small nanometer-sized coherent systems. By coherent we mean that the quantum mechanical coherence length is longer than the sample size, and the phenomena that we discuss in the following all rely on quantum effects. They are all clear manifestations of the wave propagation of electrons through the structures. The field of mesoscopic transport is interesting in that it combines physics on many length scales.

The important length scales are the coherence length ℓ_ϕ , the energy relaxation length, ℓ_{in} , the elastic mean free path, ℓ_0 , the Fermi wave length of the electron, λ_F , the atomic Bohr radius, a_0 , and of course the sample size, \mathcal{L} . Typical mesoscopic structures that we have mind are those which are fabricated on semiconductor chips, e.g. by electrostatic confinement of two dimensional electron gases (see e.g. Sec. 2.3.2). At low temperatures, typically the range from 50 mK to 4 K, the length scales for these system are related as

$$a_0 \ll \lambda_F \lesssim \ell_0 < \mathcal{L} < \ell_\phi \lesssim \ell_{\text{in}}. \quad (7.1)$$

Metallic systems are more difficult to bring into the mesoscopic regime because of their small Fermi wave length, $\lambda_F \approx a_0$. However, there is one relatively simple experiment involving a narrow metallic wire where the conductance as a clear signature of quantum transport decreases in pronounced steps of size $2e^2/h$ as the wire is stretched and pulled apart. This even happens at room temperature, whereas the more high-tech devices based on semiconductor nanostructures only show quantum effects at low temperatures (see e.g. Fig. 7.2).

This chapter deals with the physics of quantum transport which can be understood by invoking the Fermi liquid picture of non-interacting electrons to be discussed in Chap. 14. When interactions are important another rich field of physics appears, but this we will have to study at some other time.

7.1 The S-matrix and scattering states

We consider a mesoscopic sample connected to electron reservoirs in the form of macroscopic metal contacts. By mesoscopic we mean that the size \mathcal{L} of the sample region between the two reservoirs is much smaller than the energy relaxation length ℓ_{in} , and the phase breaking length, ℓ_ϕ . This implies that we can consider the electron motion to be quantum mechanically coherent in this region. Furthermore, since the reservoir is a macroscopic conductor, much larger than the entrance to the mesoscopic region, we can safely assume that electrons entering the reservoir will be thermalized at the temperature and chemical potential of the contact before returning to the mesoscopic sample. The contact is thus required to be reflectionless. Fig. 7.1 illustrates how a contact formed as a “horn” can give a reflectionless contact.

In the following we solve for the eigenstates in a geometry similar to Fig. 7.1. The system is divided into five regions: left reservoir, left lead, (L), mesoscopic region (M), right lead (R), and right reservoir. For simplicity, it is assumed that the left and right leads are perfect straight segments with hard walls, that they are identical as in the figure, and furthermore that the system is two-dimensional. In this case, the Hamiltonian and the eigenstates with energy E in the leads are given by

$$H_L = H_R = \begin{cases} \frac{1}{2m}p_x^2 + \frac{1}{2m}p_y^2, & y \in [0, W] \\ \infty, & \text{otherwise,} \end{cases} \quad (7.2a)$$

$$\phi_{LnE}^\pm(x, y) = \frac{1}{\sqrt{k_n(E)}} e^{\pm i k_n(E)x} \chi_n(y), \quad (x, y) \in L, \quad (7.2b)$$

$$\phi_{RnE}^\pm(x, y) = \frac{1}{\sqrt{k_n(E)}} e^{\pm i k_n(E)x} \chi_n(y), \quad (x, y) \in R, \quad (7.2c)$$

$$\chi_n(y) = \sqrt{\frac{2}{W}} \sin\left(\frac{\pi n y}{W}\right), \quad n = 1, 2, \dots, N \quad (7.2d)$$

$$E = \frac{\hbar^2}{2m} k_n^2 + \varepsilon_n, \quad \varepsilon_n = \frac{\hbar^2}{2m} \left(\frac{\pi n}{W}\right)^2. \quad (7.2e)$$

Here χ_n denote the transverse wavefunction and W is the width of the leads. In principle n can be any positive integer, but in practice we can introduce a cut-off at some large value N without affecting the lowest occupied states. The quantum number ± 1 represents right and left moving states with wavenumber $k_n(E) = \sqrt{2m(E - \varepsilon_n)}/\hbar$. The wavefunctions ϕ^\pm have been normalized in a particular manner so that they all carry the same absolute probability current in a given cross section:

$$\int_0^W dy \left(\phi_{\alpha n, E}^\eta(x, y) \right)^* \frac{p_x}{m} \phi_{\alpha n, E}^\eta(x, y) = \eta \frac{\hbar}{m}, \quad \eta = \pm 1, \quad (7.3)$$

Because of this normalization, it is more natural to label the states in terms of their energy E rather than as usual their k values. The transformation from a discrete to a continuous set of energy levels looks a bit different in the two cases. In the following $\tilde{\phi}_k$ means a state

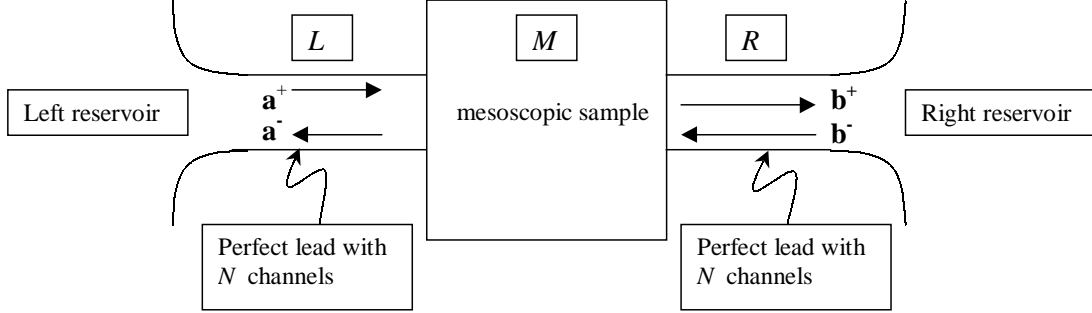


Figure 7.1: The geometry considered in the derivation of the Landauer formula. Two reflectionless contacts each with N channels connect to a mesoscopic region. The wave function is written as a superposition of incoming and outgoing wave at the two entrances. When solving the Schrödinger equation, the system is separated in three regions: L , R and M .

with the usual normalization, $\tilde{\phi}_k = e^{ikx}/\sqrt{L}$, while $\phi_k = e^{ikx}/\sqrt{k}$.

$$\begin{aligned}
 \sum_{k>0} \langle \tilde{\phi}_k | A | \tilde{\phi}_k \rangle &\rightarrow L \int_0^\infty \frac{dk}{2\pi} \langle \tilde{\phi}_k | A | \tilde{\phi}_k \rangle \\
 &= \int_0^\infty \frac{dk}{2\pi} k \langle \phi_k | A | \phi_k \rangle \\
 &= \int_0^\infty \frac{dE}{2\pi} \frac{k}{dE/dk} \langle \phi_k | A | \phi_k \rangle, \\
 &= \frac{m}{2\pi\hbar^2} \int_0^\infty dE \langle \phi_k | A | \phi_k \rangle.
 \end{aligned} \tag{7.4}$$

As we shall see in detail later, that the quantization of the conductance in units of the universal conductance quantum e^2/h is due to the cancellation of the velocity, $\propto k$, by the density of states, $\propto dk/dE$, a feature particular of one dimension.

The eigenfunctions in the middle region, M , are in general not easy to find, but fortunately we need not specify the wavefunction in the complicated region. All we will need is the transmission coefficients, relating incoming and outgoing electron waves. Let us therefore introduce the so-called scattering matrix or S -matrix formalism.

A given eigenstate with energy E is some linear combination of $\phi_{Ln,E}^\pm$ and $\phi_{Rn,E}^\pm$ in the leads L and R , and some unknown complicated function $\phi_{M,E}$, in the middle region M . We can therefore write an eigenstate as

$$\psi_E(x, y) = \begin{cases} \sum_n a_n^+ \phi_{Ln,E}^+(x, y) + \sum_n a_n^- \phi_{Ln,E}^-(x, y), & (x, y) \in L, \\ \sum_n b_n^+ \phi_{Rn,E}^+(x, y) + \sum_n b_n^- \phi_{Rn,E}^-(x, y), & (x, y) \in R, \\ \psi_{M,E}(x, y), & (x, y) \in M, \end{cases} \tag{7.5}$$

where a_n^\pm and b_n^\pm are some unknown sets of coefficients, which in vector form are written as $\mathbf{a}^+ = (a_1^+, a_2^+, \dots)$ and similarly for \mathbf{a}^- and \mathbf{b}^\pm . As usual the wavefunction and its

derivative must be continuous. For a given $\psi_{M,E}$ in the middle region this condition gives $4 \times N$ linearly independent equations to determine a_n^\pm and b_n^\pm . These equations are

$$\begin{aligned} (a_n^+ + a_n^-) &= \sqrt{k_n(E)} \int dy \chi_n(y) \psi_{M,E}(0, y), \\ (b_n^+ e^{ik_n(E)L} + b_n^- e^{-ik_n(E)L}) &= \sqrt{k_n(E)} \int dy \chi_n(y) \psi_{M,E}(L, y), \\ (a_n^+ - a_n^-) &= \frac{1}{i\sqrt{k_n(E)}} \int dy \chi_n(y) (\partial_x \psi_M(x, y))_{x=0}, \\ (b_n^+ e^{ik_n(E)L} - b_n^- e^{-ik_n(E)L}) &= \frac{1}{i\sqrt{k_n(E)}} \int dy \chi_n(y) (\partial_x \psi_{M,E}(x, y))_{x=L}. \end{aligned}$$

Fortunately, we will not have to solve such a system of equations unless we want an exact expression for the wavefunction. It is merely written down in order to illustrate the linear dependence of the coefficients, $\{a_n^\pm\}$ and $\{b_n^\pm\}$. A particular useful way of representing the linear dependence is through the so-called scattering matrix, or S -matrix, which relates the amplitudes of outgoing waves, ϕ_L^- and ϕ_R^+ , to incoming waves, ϕ_L^+ and ϕ_R^- ,

$$\mathbf{c}_{\text{out}} \equiv \begin{pmatrix} \mathbf{a}^- \\ \mathbf{b}^+ \end{pmatrix} = \begin{pmatrix} \mathbf{r} & \mathbf{t}' \\ \mathbf{t} & \mathbf{r}' \end{pmatrix} \begin{pmatrix} \mathbf{a}^+ \\ \mathbf{b}^- \end{pmatrix} \equiv \mathbf{S} \begin{pmatrix} \mathbf{a}^+ \\ \mathbf{b}^- \end{pmatrix} \equiv \mathbf{S} \mathbf{c}_{\text{in}}. \quad (7.7)$$

Here we have defined the important S -matrix to be a matrix of size $2N \times 2N$ with the $N \times N$ reflection and transmission matrices as block elements

$$\mathbf{S} = \begin{pmatrix} \mathbf{r} & \mathbf{t}' \\ \mathbf{t} & \mathbf{r}' \end{pmatrix}. \quad (7.8)$$

Here the matrix element $t_{nn'}$ represents the transmission amplitude for an incoming wave from the left in state n' to be transmitted into state n on the right hand side. The amplitude for transmission in the opposite direction is given by $t'_{nn'}$. Similarly the element $r_{nn'}$ gives the amplitude for being reflected back into the left lead in state n . The coefficients of the scattering matrix are of course energy dependent. Most of the time, we suppress this dependence in the notation.

We now define the so-called scattering states, which are states with an incoming wave in one particular lead state, i.e. $\mathbf{c}_{\text{in}} = (0, \dots, 0, 1, 0, \dots)$. The scattering states are denoted ψ^\pm , where the superscript \pm refers to the direction from which the incoming wave comes. In the plus direction (an incoming wave from the left) the scattering states are

$$\psi_{nE}^+(x, y) = \begin{cases} \phi_{Ln,E}^+(x, y) + \sum_{n'} r_{n'n} \phi_{Ln',E}^-(x, y), & (x, y) \in L, \\ \sum_{n'} t_{n'n} \phi_{Rn',E}^+(x, y), & (x, y) \in R, \\ ? & (x, y) \in M. \end{cases} \quad (7.9)$$

and in the minus direction (an electron incoming from the right hand side)

$$\psi_{nE}^-(x, y) = \begin{cases} \phi_{Rn,E}^-(x, y) + \sum_{n'} r'_{n'n} \phi_{Rn',E}^+(x, y), & (x, y) \in R, \\ \sum_{n'} t'_{n'n} \phi_{Ln',E}^-(x, y), & (x, y) \in L, \\ ? & (x, y) \in M. \end{cases} \quad (7.10)$$

The wavefunction in the scattering region is not specified, because to find the conductance all we need is the transmission probabilities of electrons, and that we can get from the S -matrix.

7.1.1 Unitarity of the S-matrix

Before we calculate the transport properties of a mesoscopic system, let us look at some properties of the S -matrix. First of all, it must be unitary, i.e. $\mathbf{S}^{-1} = \mathbf{S}^\dagger$. This is a consequence of probability current conservation. The incoming electron flux $\sum_n |c_{\text{in}}|^2 = |\mathbf{c}_{\text{in}}|^2$ must equal the outgoing flux $\sum_n |c_{\text{out}}|^2 = |\mathbf{c}_{\text{out}}|^2$ and therefore

$$\mathbf{c}_{\text{out}}^\dagger \mathbf{c}_{\text{out}} = \mathbf{c}_{\text{in}}^\dagger \mathbf{c}_{\text{in}} \quad \Rightarrow \quad \mathbf{c}_{\text{in}}^\dagger (1 - \mathbf{S}^\dagger \mathbf{S}) \mathbf{c}_{\text{in}} = 0, \quad (7.11)$$

and hence $\mathbf{S}^\dagger = \mathbf{S}^{-1}$. From the unitarity follows some properties of \mathbf{r} and \mathbf{t} , which we will make use of below:

$$\mathbf{S}^\dagger \mathbf{S} = \mathbf{1} \quad \Leftrightarrow \quad \begin{cases} 1 = \mathbf{r}^\dagger \mathbf{r} + \mathbf{t}^\dagger \mathbf{t} = \mathbf{r}'^\dagger \mathbf{r}' + \mathbf{t}'^\dagger \mathbf{t}', \\ 0 = \mathbf{r}^\dagger \mathbf{t}' + \mathbf{t}^\dagger \mathbf{r}' = \mathbf{t}'^\dagger \mathbf{r} + \mathbf{r}'^\dagger \mathbf{t}, \end{cases}, \quad (7.12)$$

and furthermore

$$\mathbf{S} \mathbf{S}^\dagger = \mathbf{1} \quad \Leftrightarrow \quad \begin{cases} 1 = \mathbf{r}' \mathbf{r}'^\dagger + \mathbf{t} \mathbf{t}^\dagger = \mathbf{r} \mathbf{r}^\dagger + \mathbf{t}' \mathbf{t}'^\dagger, \\ 0 = \mathbf{r} \mathbf{t}^\dagger + \mathbf{t}' \mathbf{r}'^\dagger = \mathbf{t} \mathbf{r}^\dagger + \mathbf{r}' \mathbf{t}'^\dagger. \end{cases} \quad (7.13)$$

We also show the unitarity in a bit more explicit way by calculating the currents on the left and right hand sides of the system. This we do because we will need the currents later on anyway. The current through a cross section for a given state is, cf. Eq. (1.99b),

$$I(x) = \int_0^W dy \Psi^*(x, y) \overleftrightarrow{J}_x \Psi(x, y), \quad \overleftrightarrow{J}_x = \frac{\hbar}{2mi} \left(\overrightarrow{\partial}_x - \overleftarrow{\partial}_x \right), \quad (7.14)$$

where the arrows indicate to which side the differential operators are acting. For a stationary state, i.e. an eigenstate with energy E , the continuity equation gives $\partial_x J = -\dot{\rho} = 0$, i.e. $I(x)$ cannot depend on x . Let us compute $I(x)$ for a state with incoming coefficients $\mathbf{c}_{\text{in}} = (\mathbf{a}^+, \mathbf{b}^-)$. First calculate the current in region L

$$\begin{aligned} I_L(x) &= \int_0^W dy \left(\mathbf{a}^+ \cdot \phi_{L,E}^+ + \mathbf{a}^- \cdot \phi_{L,E}^- \right)^* \overleftrightarrow{J}_x \left(\mathbf{a}^+ \cdot \phi_{L,E}^+ + \mathbf{a}^- \cdot \phi_{L,E}^- \right) \\ &= \frac{\hbar}{m} \left(|\mathbf{a}^+|^2 - |\mathbf{r} \mathbf{a}^+ + \mathbf{t}' \mathbf{b}^-|^2 \right), \end{aligned} \quad (7.15)$$

where $\phi_{L,E}^+ = (\phi_{L,1E}^+, \phi_{L,2E}^+, \dots)$ and $\phi_{L,E}^- = (\phi_{L,1E}^-, \phi_{L,2E}^-, \dots)$. In the same way for R we obtain

$$I_R(x) = \frac{\hbar}{m} \left(-|\mathbf{b}^-|^2 + |\mathbf{t} \mathbf{a}^+ + \mathbf{r}' \mathbf{b}^-|^2 \right), \quad (7.16)$$

or more detailed

$$I_L = \frac{\hbar}{m} \left[(\mathbf{a}^+)^\dagger (1 - \mathbf{r}^\dagger \mathbf{r}) \cdot \mathbf{a}^+ - (\mathbf{b}^-)^\dagger (\mathbf{t}^\dagger \mathbf{t}') \mathbf{b}^- - 2 \operatorname{Re}[(\mathbf{a}^+)^\dagger \mathbf{r}^\dagger \mathbf{t}' \mathbf{b}^-] \right] \quad (7.17a)$$

$$I_R = \frac{\hbar}{m} \left[(\mathbf{b}^+)^\dagger (-1 + \mathbf{r}'^\dagger \mathbf{r}') \mathbf{b}^+ + (\mathbf{a}^+)^\dagger (\mathbf{t}^\dagger \mathbf{t}) \mathbf{a}^+ - 2 \operatorname{Re}[(\mathbf{a}^+)^\dagger \mathbf{t}^\dagger \mathbf{r}' \mathbf{b}^-] \right]. \quad (7.17b)$$

From the continuity equation we know that the current on the two sides must be equal, $I_L = I_R$, and we obtain Eq. (7.12) and hence \mathbf{S} is unitary.

7.1.2 Time-reversal symmetry

Time-reversal symmetry means that $H = H^*$, because if $\Psi(\mathbf{r}, t)$ is a solution to the Schrödinger equation so is $\Psi^*(\mathbf{r}, -t)$. In that case the scattering matrix is not only unitary it is also symmetric, $\mathbf{S} = \mathbf{S}^T$. This has some important consequences for the statistics of S -matrices in disordered systems, which can be seen experimentally by studying transport with and without an applied magnetic field.

A non-zero magnetic field $\mathbf{B} = \nabla \times \mathbf{A}$ breaks time-reversal symmetry, and in this case the Schrödinger equation is

$$H_{\mathbf{B}} \Psi_{\mathbf{B}}(\mathbf{r}) = \left[-\frac{\hbar^2}{2m} \left(\nabla_{\mathbf{r}} + i \frac{e}{\hbar} \mathbf{A} \right)^2 + V(\mathbf{r}) \right] \Psi_{\mathbf{B}}(\mathbf{r}) = E \Psi_{\mathbf{B}}(\mathbf{r}). \quad (7.18)$$

Now, since $H_{\mathbf{B}} = H_{-\mathbf{B}}^*$ we see that

$$H_{\mathbf{B}} \Psi_{\mathbf{B}}(\mathbf{r}) = E \Psi_{\mathbf{B}}(\mathbf{r}) \quad \Leftrightarrow \quad H_{-\mathbf{B}}^* \Psi_{-\mathbf{B}}^*(\mathbf{r}) = E \Psi_{-\mathbf{B}}^*(\mathbf{r}), \quad (7.19)$$

or in short: if $\Psi_{\mathbf{B}}(\mathbf{r})$ is a solution so is $\Psi_{-\mathbf{B}}^*(\mathbf{r})$. We can therefore construct new eigenstates by complex conjugation followed by reversal of the magnetic field. Suppose we have an eigenstate which is a linear combination of incoming and outgoing waves $\Psi_{\mathbf{B}}(\mathbf{r}) = (\mathbf{c}_{\text{in}} \phi_{\text{in}}, \mathbf{c}_{\text{out}} \phi_{\text{out}})$, then we can make a new eigenstate by $\Psi_{-\mathbf{B}}^{\text{new}}(\mathbf{r}) = \Psi_{\mathbf{B}}^*(\mathbf{r})$, which is a solution for $-\mathbf{B}$. However, because complex conjugation reverses the direction of propagation, the new in- and outgoing wave functions are $\mathbf{c}_{\text{in}}^{\text{new}} = \mathbf{c}_{\text{out}}^*$, and $\mathbf{c}_{\text{out}}^{\text{new}} = \mathbf{c}_{\text{in}}^*$. Since Ψ^{new} is a solution for $-\mathbf{B}$, we have

$$\mathbf{c}_{\text{out}}^{\text{new}} = \mathbf{S}_{-\mathbf{B}} \mathbf{c}_{\text{in}}^{\text{new}} \quad \Rightarrow \quad \mathbf{c}_{\text{in}}^* = \mathbf{S}_{-\mathbf{B}} \mathbf{c}_{\text{out}}^* = \mathbf{S}_{-\mathbf{B}} \mathbf{S}_{\mathbf{B}}^* \mathbf{c}_{\text{in}}^*, \quad (7.20)$$

which shows that

$$\mathbf{S}_{-\mathbf{B}} \mathbf{S}_{\mathbf{B}}^* = 1 \quad \Rightarrow \quad \mathbf{S}_{-\mathbf{B}}^* = \mathbf{S}_{\mathbf{B}}^\dagger \quad \Rightarrow \quad \mathbf{S}_{\mathbf{B}} = \mathbf{S}_{-\mathbf{B}}^T. \quad (7.21)$$

In case of time-reversal symmetry, the scattering matrix therefore has an additional symmetry besides being unitary: it is also a symmetric matrix. This will be of importance when we look at disordered systems below.

7.2 Conductance and transmission coefficients

Next we calculate the conductance. This will be done in two different ways: first we will argue on physical grounds that the population of the scattering state is given by the equilibrium distribution function of the reservoir, which allows us to calculate the current directly. Secondly, we calculate the conductance using linear response theory, and, fortunately, we find the same result. While the first method is more physically appealing, one could get in doubt if the Pauli principle is treated correctly. The linear response result shows that indeed the first method gave the right answer, at least in the linear response limit.

The answer we find, the celebrated Landauer-Büttiker formula, is very simple and physically sensible: the conductance of a mesoscopic sample is given by the sum of all the transmission possibilities a given electron has, i.e. by the sum of transmission probabilities

$$G = \frac{2e^2}{h} \sum_n \mathcal{T}_n = \frac{2e^2}{h} \text{Tr}[\mathbf{t}^\dagger \mathbf{t}], \quad (7.22)$$

where \mathcal{T}_n are the eigenvalues of the matrix $\mathbf{t}^\dagger \mathbf{t}$. This should not be confused with the transmission probabilities, i.e. the probability that an electron in a given incoming state, n , ends up on the other side. This probability is $T_n = (\mathbf{t}^\dagger \mathbf{t})_{nn}$, but when summing over all incoming states n we in fact get, $\sum_n \mathcal{T}_n = \sum_n T_n$. So we can write Eq. (7.22) in terms of \mathcal{T}_n or T_n as we please.

The Landauer-Büttiker formula tells us that the conductance of a mesoscopic sample is quantized in units of $2e^2/h$. The number of quanta will be the number of channels connecting the two sides. However, since \mathcal{T}_n is a number between 0 and 1 one expects this quantization to show up only for some special geometries where T_n is either 0 or 1. This is in fact what happens for the quantum point contact, which is discussed below in Sec. 7.3.1. There a particular smooth interface between the two reservoirs ensures that T_n changes in a well-controlled manner between 0 and 1. However, there are other examples where the conductance quantum e^2/h shows up, namely in the fluctuations of conductance. These fluctuations are universal in the sense that they have an amplitude of the order e^2/h independent of the average conductance. This is discussed in Sec. 7.4.3.

7.2.1 The Landauer-Büttiker formula, heuristic derivation

We argued above that if the reservoirs are much wider than the mesoscopic region and its leads, then we can assume reflectionless transmission from the leads to the reservoirs, i.e. the electrons entering the reservoir from the sample are thermalized before returning. Thus all electrons entering from the contacts are distributed according to the Fermi-Dirac distribution n_F of the given reservoirs. Furthermore, since the mesoscopic region is defined to be phase coherent, no energy relaxation takes place there, and consequently electrons originating from, say, the left reservoir maintain their distribution function equal to that of that reservoir. Therefore it is natural to express the occupation of the scattering eigenstates $\psi_{n\epsilon}^\pm$ by two different distribution functions f^\pm and the chemical potentials $\mu_{L/R}$

of the relevant reservoirs,

$$f^+(\varepsilon) = n_F(\varepsilon - \mu_L), \quad f^-(\varepsilon) = n_F(\varepsilon - \mu_R). \quad (7.23)$$

Now it is a simple matter to calculate the current through the mesoscopic system. Because of current conservation, we can calculate it in either of the regions L , R , or M . Naturally, we choose to do so in the perfect leads L or R where the wavefunctions are known. Let us look at the current in the left lead:

$$I = I_L = e \sum_{nk} \left[\tilde{I}_{nk}^+ f^+(E_{nk}) + \tilde{I}_{nk}^- f^-(E_{nk}) \right]. \quad (7.24)$$

The currents carried by a scattering state $\psi_{n\varepsilon}^\pm$ can be read off from Eqs. (7.17a) and (7.17b) by substituting $(\mathbf{a}^+)_{n'} = \delta_{nn'}$ for a state moving in the positive direction and $(\mathbf{b}^-)_{n'} = \delta_{nn'}$ for a state moving in the negative direction. We get

$$I_{nk}^+ = \frac{\hbar}{m} \left[1 - (\mathbf{r}^\dagger \mathbf{r})_{nn} \right] = \frac{\hbar}{m} (\mathbf{t}^\dagger \mathbf{t})_{nn}, \quad (7.25)$$

$$I_{nk}^- = -\frac{\hbar}{m} (\mathbf{t}'^\dagger \mathbf{t}')_{nn} = \frac{\hbar}{m} \left[-1 + (\mathbf{r}'^\dagger \mathbf{r}')_{nn} \right]. \quad (7.26)$$

Transforming to an energy integral as in Eq. (7.4), the current is therefore simply

$$I = \frac{e}{2\pi\hbar} \sum_n \int_0^\infty dE \left[(\mathbf{t}^\dagger \mathbf{t})_{nn} n_F(E - \mu_L) - (\mathbf{t}'^\dagger \mathbf{t}')_{nn} n_F(E - \mu_R) \right]. \quad (7.27)$$

The sum over diagonal elements of $(\mathbf{t}^\dagger \mathbf{t})$ is nothing but the trace. The unitarity condition Eq. (7.13), then leads to $\text{Tr}[\mathbf{t}'^\dagger \mathbf{t}'] = \text{Tr}[\mathbf{t}^\dagger \mathbf{t}]$, and the current can be written as

$$I = \frac{e}{2\pi\hbar} \int_0^\infty dE \text{Tr} \left[\mathbf{t}_E^\dagger \mathbf{t}_E \right] \left[n_F(E - \mu_L) - n_F(E - \mu_R) \right]. \quad (7.28)$$

In Eq. (7.28), we have stressed the energy dependence of the transmission matrix, but at low voltages V and temperatures T we can assume \mathcal{T}_n to be energy independent and the integral can be done. For $|eV| = |\mu_R - \mu_L| \ll \mu$, where μ is the equilibrium electrochemical potential, we Taylor expand around μ and find after integration

$$I = \overbrace{2}^{\text{From spin}} \frac{e^2}{h} V \text{Tr} \left[\mathbf{t}_E^\dagger \mathbf{t}_E \right] \Rightarrow G = \frac{2e^2}{h} \text{Tr} \left[\mathbf{t}^\dagger \mathbf{t} \right] = \frac{2e^2}{h} \sum_n \mathcal{T}_n. \quad (7.29)$$

This is the famous Landauer-Büttiker formula. Here we have assumed that the spin degrees of freedom are degenerate which gives rise to a simple factor of two. If they are not degenerate the trace must also include a trace over the spin degrees of freedom.

The expression Eq. (7.27) for current relies on the fact that the scattering states are eigenstates of the system, which means that we should not include any kind of blocking factors $(1 - n_F)$ to ensure that the final state is empty, as one would normally do in a Boltzmann equation. Once a state is occupied in one lead, it is automatically also occupied in the other. Thus we are not talking about a scattering event from one reservoir to the other, but rather about the thermal population of eigenmodes. In order to dismiss any concern about this point, the next section is devoted to a derivation of Eq. (7.22) from first principles using the linear response formalism of Chap. 6.

7.2.2 The Landauer-Büttiker formula, linear response derivation

Our starting point is Eq. (6.31) expressing the conductance G in terms of the current-current correlation function,

$$G(\omega) = -\frac{2e^2}{\hbar\omega} \text{Im} \int_{-\infty}^{\infty} dt e^{i(\omega+i\eta)t} (-i)\Theta(t) \langle [I(x, t), I(x, 0)] \rangle_0, \quad (7.30)$$

where the current operator $I(x)$ due to current conservation can be evaluated at any cross section x in the perfect leads, rendering G independent of x . (Again we consider the spin degenerate case which is the reason for the factor of two.) In second quantization the current operator is given by

$$I(x) = \sum_{\lambda\lambda'} j_{\lambda\lambda'}(x) c_{\lambda}^{\dagger} c_{\lambda'}, \quad (7.31)$$

$$j_{\lambda\lambda'}(x) = \frac{\hbar}{2mi} \int dy \psi_{\lambda}^*(x, y) \left(\vec{\partial}_x - \overleftarrow{\partial}_x \right) \psi_{\lambda'}(x, y), \quad (7.32)$$

where we choose $\{\psi_{\lambda}\}$ as a set of eigenstates, and where $j_{\lambda\lambda'}$ is a matrix element of the current operator. We will of course use the scattering states that we found above as our basis, which means that the quantum number λ is specified by $\lambda = \{E, n, \eta = \pm\}$. We start by calculating the commutator in Eq. (7.30)

$$\begin{aligned} \langle [I(x', t), I(x', 0)] \rangle_0 &= \sum_{\nu\nu'} j_{\nu\nu'}(x') \sum_{\lambda\lambda'} j_{\lambda\lambda'}(x') e^{i(E_{\lambda}-E_{\lambda'})t/\hbar} \left\langle [c_{\lambda}^{\dagger} c_{\lambda'}, c_{\nu}^{\dagger} c_{\nu'}] \right\rangle_0 \\ &= \sum_{\lambda\lambda'} |j_{\lambda\lambda'}(x')|^2 e^{i(E_{\lambda}-E_{\lambda'})t/\hbar} [n_F(E_{\lambda}) - n_F(E_{\lambda'})], \end{aligned} \quad (7.33)$$

where we used that $\langle c_{\lambda}^{\dagger} c_{\lambda'} \rangle_0 = \delta_{\lambda\lambda'} n_F(E_{\lambda})$, and that $j_{\lambda\lambda'}(x') = (j_{\lambda'\lambda}(x'))^*$. Inserting this into Eq. (7.30) yields

$$G(\omega) = -\frac{2e^2}{\omega} \text{Im} \sum_{\lambda\lambda'} \frac{|j_{\lambda\lambda'}(x')|^2}{(\hbar\omega + i\eta + E_{\lambda} - E_{\lambda'})} [n_F(E_{\lambda}) - n_F(E_{\lambda'})], \quad (7.34)$$

and in the dc-limit, $\omega \rightarrow 0$, one has

$$G(0) = -2\hbar e^2 \pi \sum_{\lambda\lambda'} |j_{\lambda\lambda'}(x')|^2 \left(-\frac{\partial n_F(E_{\lambda})}{\partial E_{\lambda}} \right) \delta(E_{\lambda} - E_{\lambda'}). \quad (7.35)$$

Changing the sum over eigenstates to integrals over energy, i.e. $\sum_{\lambda} \rightarrow \sum_{n\eta} \frac{m}{2\pi\hbar^2} \int dE$, and setting $T = 0$ such that $(-\partial n_F(E)/\partial E) = \delta(E - E_F)$, the conductance becomes

$$G(0) = -2\hbar e^2 \pi \left(\frac{m}{2\pi\hbar^2} \right)^2 \sum_{nn', \eta\eta'} |j_{n\eta E_F, n'\eta' E_F}(x')|^2, \quad (7.36)$$

Due to current conservation the current matrix elements $j_{n\eta E_F, n'\eta' E_F}(x')$ are independent of x' , and we evaluate them in the L or R region at our convenience. We obtain

$$j_{n\eta E_F, n'\eta' E_F}(x') = \frac{\hbar}{m} \begin{pmatrix} (\mathbf{t}^\dagger \mathbf{t})_{nn'} & (\mathbf{t}^\dagger \mathbf{r}')_{nn'} \\ -(\mathbf{t}'^\dagger \mathbf{r})_{nn'} & (-\mathbf{t}'^\dagger \mathbf{t}')_{nn'} \end{pmatrix} \equiv \frac{\hbar}{m} \mathbf{j}, \quad (7.37)$$

where the rows and columns correspond to $\eta = +1$ and -1 , respectively. Hence we get

$$\begin{aligned} \sum_{nn', \eta\eta'} |j_{n\eta E_F, n'\eta' E_F}(x')|^2 &= \left(\frac{\hbar}{m}\right)^2 \text{Tr} [\mathbf{j}^\dagger \mathbf{j}] \\ &= \left(\frac{\hbar}{m}\right)^2 \text{Tr} \left[(\mathbf{t}^\dagger \mathbf{t})^2 + (\mathbf{t}'^\dagger \mathbf{t}')^2 + \mathbf{r}'^\dagger \mathbf{t} \mathbf{t}^\dagger \mathbf{r}' + \mathbf{r}^\dagger \mathbf{t}' \mathbf{t}'^\dagger \mathbf{r} \right] \\ &= 2 \left(\frac{\hbar}{m}\right)^2 \text{Tr} [\mathbf{t}^\dagger \mathbf{t}], \end{aligned} \quad (7.38)$$

after using the result Eq. (7.13). The final result is therefore

$$I = -\frac{2e^2}{h} \text{Tr} [\mathbf{t}^\dagger \mathbf{t}] \int dx' E(x') = \frac{2e^2}{h} \text{Tr} [\mathbf{t}^\dagger \mathbf{t}] V, \quad (7.39)$$

which again is the Landauer-Büttiker formula. We have thus seen that it can be derived microscopically, and any doubt about the validity of the treatment of the occupation factor in the heuristic derivation, has been removed.

7.3 Electron wave guides

7.3.1 Quantum point contact and conductance quantization

One of the most striking consequences of the Landauer-Büttiker formula for conductance is that the conductance of a perfect channel is $2e^2/h$, and if there are N “perfect” channels it is $N2e^2/h$. This has been experimentally tested in numerous experiments and it is now a well-established fact. The first experiments showing this was done by groups in Delft (Holland) and Cambridge (England) in 1988. The technique they used was a so-called splitgate geometry where a set of metallic gate electrodes was put on top of a two-dimensional electron gas such that a narrow contact between the two sides of the 2DEG was formed, see Fig. 2.10b. By applying voltage to the gates the width of the constriction could be controlled very accurately. As the width decreases quantum channels are squeezed out one by one, until only one remains, leading to a staircase of conductance, each step being of height $2e^2/h$, see Fig. 7.2. We will now see how this nice effect can happen.

Suppose there is a smooth constriction between two electron reservoirs. Smooth here means a horn-like shape where the curvature at all points is large compared to the wavelength of the wave which is going to be transmitted through the horn. The relevant wave equation for an electron horn is of course the Schrödinger equation, but there is in principle no difference between the electron wave guide and horn wave guides used in loud

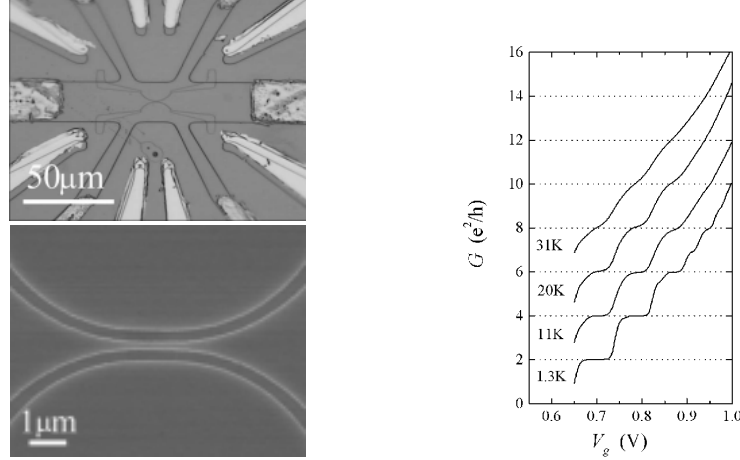


Figure 7.2: An experiment on quantized conductance. The upper left panel is a picture of the surface of an GaAs chip with an etched point contact structure. The lower left panel is an zoom-in of this structure recorded in an electron microscope. The right panel shows the conductance versus sidegate voltage. At the lowest temperature (1.3 K) the conductance shows clear steps at integer values of $2e^2/h$. By clever design this point contact yields a particularly large subband splitting, which is why the conductance quantization persists up to “high” temperatures of the order 20 K. The device was fabricated and measured at the Ørsted Laboratory, Niels Bohr Institute.

speakers, water waves or other wave phenomena. So the quantized conductance is nothing but a manifestation of the wave nature of a quantum particle, but you might say a very striking one.

The Schrödinger equation for the quantum point contact geometry is

$$\left[-\frac{\hbar^2}{2m} (\partial_x^2 + \partial_y^2) + V_{\text{conf}}(x, y) \right] \Psi(x, y) = E \Psi(x, y), \quad (7.40)$$

where $V_{\text{conf}}(x, y)$ is the confinement potential. Because the change along the x -direction is assumed to be smooth, we try to separate the motion in longitudinal and transverse motion. Had the confinement potential been rectangular we would have eigenstates as ϕ^\pm in Eq. (7.2b). Inspired by that we expand the wave function in terms of the transverse eigenstates $\chi_{nx}(y)$ which however are x -dependent now, as are the expansion coefficients $\phi_n(x)$,

$$\Psi(x, y) = \sum_n \phi_n(x) \chi_{nx}(y). \quad (7.41)$$

This is always possible at any given fixed x since, being solutions of the transverse Schrödinger equation, $\{\chi_n(x)\}$ forms a complete set,

$$\left[-\frac{\hbar^2}{2m} \partial_y^2 + V_{\text{conf}}(x, y) \right] \chi_{nx}(y) = \varepsilon_n(x) \chi_{nx}(y). \quad (7.42)$$

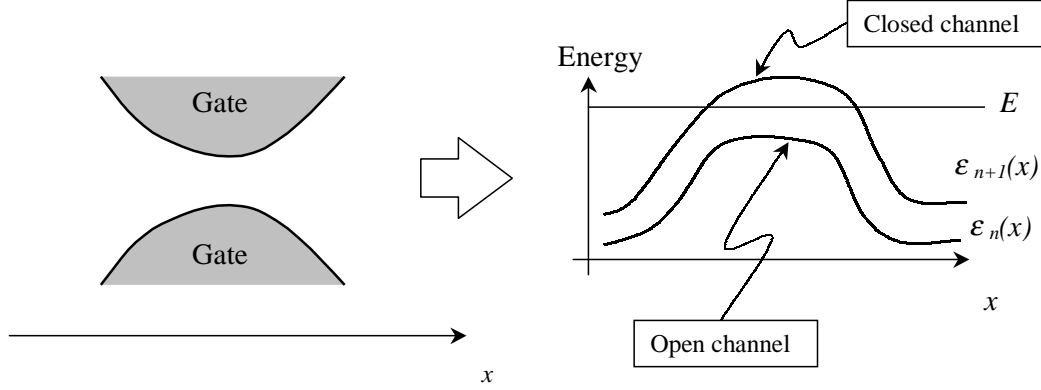


Figure 7.3: Illustration of the adiabatic contact giving rise to an effective one-dimensional barrier. When the energy of the incident electron is larger than the maximum transverse kinetic energy, i.e. the maximum of $\varepsilon_n(x)$, it is transmitted through without reflection, otherwise not. The width of constriction and thereby the height of $\varepsilon_n(x)$ is controlled by a voltage applied to the gate electrodes.

Inserting Eq. (7.41) into Eq. (7.40) and multiplying from the left with $\chi_{nx}^*(y)$ followed by integration over the transverse direction, y , yields

$$\left[-\frac{\hbar^2}{2m} \partial_x^2 + \varepsilon_n(x) \right] \phi_n(x) = E \phi_n(x) + \delta_n, \quad (7.43)$$

where

$$\delta_n = \frac{\hbar^2}{m} \sum_{n'} \int dy \chi_{nx}^*(y) \left[(\partial_x \phi_{n'}(x)) (\partial_x \chi_{n'x}(y)) + \frac{1}{2} \phi_{n'}(x) \partial_x^2 \chi_{n'x}(y) \right]. \quad (7.44)$$

As mentioned, the fundamental approximation we wanted to impose was the smooth geometry approximation, often referred to as the adiabatic approximation. It means that the derivative of the transverse mode with respect to longitudinal direction is neglected, i.e. $\partial_x \chi_{n'x}(y) \approx 0$. In the case of hard walls,

$$V_{\text{conf}}(x, y) = \begin{cases} 0 & \text{for } y \in [-d(x)/2, d(x)/2], \\ \infty & \text{otherwise,} \end{cases} \quad (7.45)$$

the transverse wavefunctions are the well-known wavefunction for a particle in a box

$$\chi_{nx}(y) = \sqrt{\frac{2}{d(x)}} \sin \left(\frac{\pi n (y - d(x)/2)}{d(x)} \right), \quad (7.46)$$

with the corresponding eigenenergies

$$\varepsilon_n(x) = \frac{\hbar^2 \pi^2}{2m [d(x)]^2} n^2. \quad (7.47)$$

Taking the derivative $\partial_x \chi_{n'x}(y)$, will give something proportional to $d'(x)$. The essence of the adiabatic approximation is that $d'(x) \ll 1$, such we end up with an effective one-dimensional problem of decoupled modes, ϕ_n , which obey the 1D Schrödinger equation with an energy barrier $\varepsilon_n(x)$

$$\left[-\frac{\hbar^2}{2m} \partial_x^2 + \varepsilon_n(x) \right] \phi_n(x) = E \phi_n(x). \quad (7.48)$$

The transverse direction has thus been translated into an effective 1D barrier. The barrier is there because some of the kinetic energy is bound into the transverse motion. Let $x = 0$ be the position in the constriction where this is most narrow, i.e. $d_{\min} = d(0)$. If the transverse kinetic energy, $\varepsilon_n^{\max} \equiv \varepsilon_n(0)$, at this place is larger than E , the mode cannot transmit (neglecting tunneling through the barrier, of course). If, however, it is smaller than E the mode has sufficient energy to pass over the barrier and get through the constriction, this is illustrated in Fig. 7.3.

For smooth barriers, we can use the WKB approximation result for the wavefunction

$$\phi_n(x) \approx \phi_n^{\text{WKB}}(x) = \frac{1}{\sqrt{p(x)}} \exp \left(i \int_{-\infty}^x dx' p(x') / \hbar \right), \quad p(x) = \sqrt{2m(E - \varepsilon_n(x))}, \quad (7.49)$$

which is a solution to Eq. (7.48) if $|p'(x)/\hbar p^2(x)| \ll 1$. In this case we can directly read off the transmission amplitude because in the notation used for the scattering states, we have $r = 0$ and hence $|t| = 1$. The conductance is therefore

$$G = \frac{2e^2}{h} \sum_n \Theta(E_F - \varepsilon_n^{\max}). \quad (7.50)$$

All subbands with energy smaller than E_F contribute with one conductance quantum, which results in a step structure of the conductance as a function of ε_n^{\max} . This is roughly what is seen experimentally, where ε_n^{\max} is changed by changing the width of the constriction through the voltage of the gate electrodes.

Obviously the WKB approximation breaks down if $p(x)$ is too small. Right at the point where a new channel opens, which happens when $E_F = \varepsilon_n(0)$, we would expect some smearing of the step. The shape of the smearing will in general depend on the geometry of the constriction and is, in contrast to the step heights, not universal. A useful model is the so-called saddle point model for the constriction, where the confinement potential is modelled by

$$V_{\text{conf}}(x, y) = \frac{1}{2} m \omega_y^2 y^2 - \frac{1}{2} m \omega_x^2 x^2 + V_0, \quad (7.51)$$

where V_0 is a constant. The saddle point model can be thought of as a quadratic expansion of the confinement potential near its maximum. Using this potential it can be shown that the transmission probability has a particular simple form, namely

$$T_n(E) = \frac{1}{\exp \left(\pi \left(E - V_0 - (n + \frac{1}{2}) \hbar \omega_x \right) / \hbar \omega_y \right) + 1}. \quad (7.52)$$

For this model the smearing of the conductance steps thus has the form of a Fermi function. Experiments using the splitgate geometry indeed show that the conductance traces (meaning conductance versus gate voltage) are well described by Eq. (7.52).

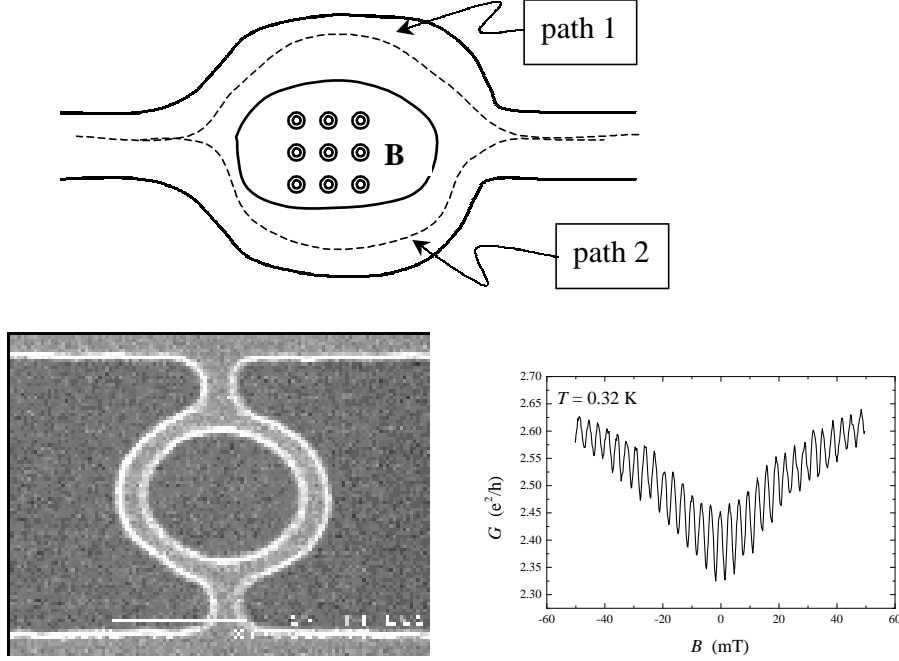


Figure 7.4: A device which shows Aharonov-Bohm effect, because of interference between path 1 and path 2. The interference is modulated by magnetic flux enclosed by the paths. This is shown in the bottom part, where the left panel shows the experimental realization, while the right panel depicts the conductance versus B -field trace. Both the device fabrication and the measurements have been performed at the Ørsted Laboratory.

7.3.2 Aharonov-Bohm effect

A particular nice example of interference effects in mesoscopic systems is the Aharonov-Bohm effect, where an applied magnetic field \mathbf{B} is used to control the phase of two interfering paths. The geometry is illustrated in Fig. 7.4. Each of the arms in the ring could be an adiabatic wave guide, where the wave function can be assumed to be of the form in Eq. (7.49). Because of the applied \mathbf{B} -field we must add a vector potential \mathbf{A} to the Schrödinger equation Eq. (7.40) as in Eq. (7.18). At small magnetic fields we can neglect the orbital changes induced by \mathbf{B} in the arms of the ring and absorb the vector potential due to the \mathbf{B} -field through the hole of the ring as a phase factor

$$\Psi_{\mathbf{B} \neq 0}(\mathbf{r}) = \Psi_{\mathbf{B} = 0}(\mathbf{r}) \exp \left(-i \frac{e}{\hbar} \int^{\mathbf{r}} d\mathbf{l} \cdot \mathbf{A} \right). \quad (7.53)$$

We now approximate the line integral by an integral following the center of the waveguides and furthermore assume ideal adiabatic arms, i.e. no backscattering. In that case the transmission coefficient is given by a sum corresponding to the two paths

$$t \propto \exp \left(-i \frac{e}{\hbar} \int_{\text{path 1}}^{\mathbf{r}} d\mathbf{l} \cdot \mathbf{A} \right) + e^{i\phi_0} \exp \left(-i \frac{e}{\hbar} \int_{\text{path 2}}^{\mathbf{r}} d\mathbf{l} \cdot \mathbf{A} \right), \quad (7.54)$$

where ϕ_0 is some phase shift due to different length of the two arms. The transmission probability now becomes

$$|t|^2 \propto 1 + \cos \left(\phi_0 - \frac{e}{\hbar} \int_{\text{path } 1+2}^{\mathbf{r}} d\mathbf{l} \cdot \mathbf{A} \right) = 1 + \cos \left(\phi_0 - \pi \frac{\Phi_{\text{path } 1+2}}{\Phi_0} \right), \quad (7.55)$$

where Φ is the flux enclosed and $\Phi_0 = h/2e$ is the flux quantum. The conductance will oscillate as with the applied magnetic, a signature of quantum interference. Note that the effect persists even if there is no magnetic field along the electron trajectories, which is a manifestation of the non-locality of quantum mechanics. Experiments have verified this picture. See Fig. 7.4.

7.4 Disordered mesoscopic systems

In this section we shall study disordered mesoscopic systems. The experiments we have in mind are e.g. experiments on disordered “quantum dots”, which is a mesoscopic region connected to reservoirs just as we have discussed above where the Landauer-Büttiker formula was derived, see Fig. 7.5. Again we use the Landauer-Büttiker to calculate the conductance, but because the system is disordered it makes little sense to talk about the conductance for specific sample geometries. One cannot precisely neither locate nor control the positions of the impurities. Instead one studies the statistical properties of the conductance for an ensemble of systems. The average and the variance of the conductance will turn out to exhibit interesting quantum phenomena, namely weak localization and universal conductance fluctuations, respectively. In order to understand these two phenomena, we must first learn about how to average over S -matrices.

Fig. 7.5 shows an example of a disorder mesoscopic system. It cannot be a surprise that the classical motion in such a geometry is expected to be chaotic and the system to be ergodic, which means that all parts of the phase-space are visited with equal probability. Quantum mechanically this means that there are no symmetries and hence no systematic degeneracies of energy levels. In fact, as a function of any external parameter (e.g. shape, magnetic field, or density) the energy levels avoid to cross one another. This important phenomenon is known as level repulsion.

7.4.1 Statistics of quantum conductance, random matrix theory

Let us consider the statistical properties of some ensemble of disordered or chaotic systems influenced by some external parameter. Such ensembles have been studied for a long time, initially atomic nuclei containing a large number of nucleons. The basic assumption being made is that the Hamiltonians describing each of the systems of the ensemble are drawn randomly according to some probability distribution only constrained by the symmetry of the system. This statistical method is known as random matrix theory (RMT). The matrix elements of the Hamiltonians are assumed to follow a Gaussian distribution, and from this one can argue that the S -matrix follows the so-called circular ensemble distribution. This means that all unitary matrixes are equally likely, or in other words the distribution $P(\mathbf{S})$

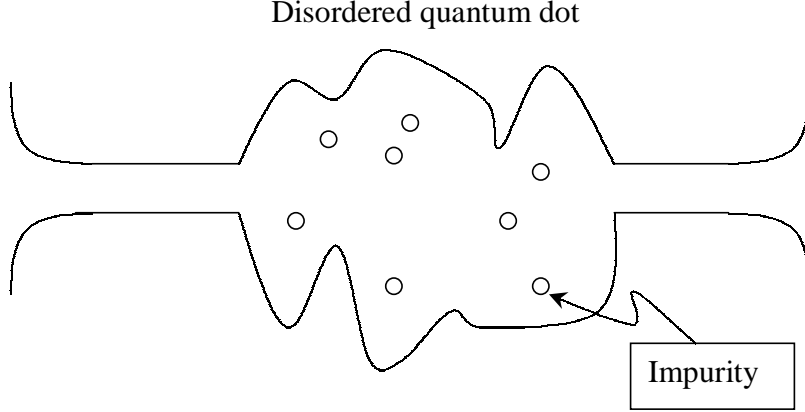


Figure 7.5: Disordered quantum dot geometry. The averaged over different geometries could be an average over positions of impurities, dot boundaries or Fermi energy.

of scattering matrices \mathbf{S} is uniform in the group of unitary matrices of size $2N \times 2N$, denoted $\mathcal{U}(2N)$. This claim can also be justified by “entropy” considerations, in sense that it is the distribution which maximizes the entropy and hence is the ensemble with “maximal randomness”.

Here we will not be concerned with the microscopic justification for the ensemble averaging, but simply say that since we have no information about the scattering matrix the most sensible thing to assume is that all scattering matrices in $\mathcal{U}(2N)$ will appear with equal probability only subject to normalization conditions and symmetry constraints. For the time-reversal symmetry case, we are therefore restricted to symmetric members of $\mathcal{U}(2N)$. The TR case can be realized by writing $\mathbf{S} = \mathbf{U}\mathbf{U}^T$, where $\mathbf{U} \in \mathcal{U}(2N)$. We skip the derivation and simply list the first few moments of a random unitary matrix of dimension $M = 2N$:

$$\langle U_{\alpha\beta} \rangle = 0, \quad (7.56)$$

$$\langle U_{\alpha a}^* U_{\beta b} \rangle = \frac{1}{M} \delta_{\alpha\beta} \delta_{ab}, \quad (7.57)$$

$$\begin{aligned} \langle U_{\alpha a}^* U_{\alpha' a'}^* U_{\beta b} U_{\beta' b'} \rangle &= \frac{1}{M^2 - 1} (\delta_{\alpha\beta} \delta_{ab} \delta_{\alpha'\beta'} \delta_{a'b'} + \delta_{\alpha\beta'} \delta_{ab'} \delta_{\alpha'\beta} \delta_{a'b}) \\ &\quad - \frac{1}{M(M^2 - 1)} (\delta_{\alpha\beta} \delta_{ab'} \delta_{\alpha'\beta'} \delta_{a'b} + \delta_{\alpha\beta'} \delta_{ab} \delta_{\alpha'\beta} \delta_{a'b'}). \end{aligned} \quad (7.58)$$

The method to derive these result is to utilize $\langle f(\mathbf{U}) \rangle = \langle f(\mathbf{U}_0 \mathbf{U}) \rangle = \langle f(\mathbf{U} \mathbf{U}_0) \rangle$, which for any fixed unitary matrix \mathbf{U}_0 is a consequence of the constant probability assumption. By suitable choice of \mathbf{U}_0 the various averages can be derived. The first term in Eq. (7.58) is equivalent to assuming the real and imaginary parts of $U_{\alpha a}$ to be independent, while the last term corrects for that because the unitarity condition gives some constraints on the elements of \mathbf{U} . These correlations however become less important in limit of large M .

7.4.2 Weak localization in mesoscopic systems

In Sec. 14.4 studied the weak localization in self-averaging macroscopic samples. The origin of this effect was found to be the constructive interference between time-reversed pairs of paths beginning and ending in the same point in space. Also mesoscopic systems exhibit weak localization. In this case the coherence length is larger than the sample, hence the conductance is given by the S -matrix through the Landauer-Büttiker formula, and we can find the weak localization correction not for an individual sample but for an ensemble of samples using random matrix theory of the S -matrix.

It is important to realize that the weak localization correction survives ensemble averaging. The average conductance is therefore

$$\langle G \rangle = \frac{2e^2}{h} \left\langle \text{Tr} [\mathbf{t}^\dagger \mathbf{t}] \right\rangle = \frac{2e^2}{h} \sum_{n=1}^N \sum_{m=N+1}^{2N} \langle S_{mn}^* S_{mn} \rangle. \quad (7.59)$$

The result now depends on whether time-reversal symmetry is present or not, i.e. if a \mathbf{B} -field is applied or not. First take the case of broken time-reversal symmetry, $\mathbf{B} \neq 0$. In this case there is no other constraints on \mathbf{S} than that it is unitary and there we can use Eq. (7.57) directly

$$\langle G \rangle_{\mathbf{B} \neq 0} = \frac{2e^2}{h} N^2 \frac{1}{2N} = \frac{2e^2}{h} \frac{N}{2}. \quad (7.60)$$

The case $\mathbf{B} = 0$ means that in addition to unitarity \mathbf{S} is also symmetric. Writing $\mathbf{S} = \mathbf{U}\mathbf{U}^T$ we get

$$\langle G \rangle_{\mathbf{B}=0} = \frac{2e^2}{h} \sum_{n=1}^N \sum_{m=N+1}^{2N} \sum_{i=1}^{2N} \sum_{j=1}^{2N} \langle U_{mi}^* U_{ni}^* U_{mj} U_{nj} \rangle, \quad (7.61)$$

and now applying Eq. (7.58), we have

$$\langle G \rangle_{\mathbf{B}=0} = \frac{2e^2}{h} \sum_{n=1}^N \sum_{m=N+1}^{2N} \sum_{i=1}^{2N} \sum_{j=1}^{2N} (\delta_{ij} + \delta_{mn} \delta_{ij}) \left(1 - \frac{1}{2N}\right) \frac{1}{4N^2 - 1} \quad (7.62)$$

$$= \frac{2e^2}{h} \frac{1}{4N^2 - 1} (2N^3) \left(1 - \frac{1}{2N}\right) = \frac{2e^2}{h} \frac{N^2}{2N + 1}, \quad (7.63)$$

which is smaller than the $\mathbf{B} \neq 0$ result. It is natural to compare the conductance with the classical conductance i.e. the series connection between two leads with N channels

$$\frac{\langle \delta G \rangle}{2e^2/h} = \frac{\langle G \rangle}{2e^2/h} - \frac{N}{2} = \begin{cases} -\frac{N}{2(2N+1)} & , \text{ for } B = 0, \\ 0 & , \text{ for } B \neq 0. \end{cases} \quad (7.64)$$

This result clearly shows that quantum corrections, which comes from the last term in Eq. (7.58), give a reduced conductance and that the quantum coherence is destroyed by a magnetic field. Of course in reality the transition from the $\mathbf{B} = 0$ to the finite \mathbf{B} -field case is a smooth transition. The transition happens when the flux enclosed by a typical trajectory is of order the flux quantum, which we saw from the arguments leading to Eq. (7.55).

7.4.3 Universal conductance fluctuations

The fluctuations of the conductance contains some interesting information about the nature of the eigenstates of a chaotic system. Historically the study of these fluctuations were the first in the field of mesoscopic transport. They were observed experimentally around 1980 and explained theoretically about five years later.

It is an experimental fact that the fluctuations turn out to be independent of the size of the conductance itself, which has given rise to the name universal conductance fluctuations (UCF). Naively, one would expect that if the average conductance is $\langle G \rangle = N_0(2e^2/h)$, corresponding to N_0 open channels, then the fluctuations in the number of open channels would be $\sqrt{N_0}$, so that $\langle \delta G \rangle = (2e^2/h)\sqrt{N_0}$. This is not seen experimentally, the reason being that the transmission probabilities are not independent. The number of conducting channels in a given energy window does therefore not follow a Poisson distribution.

For a completely random system without any symmetries, we do not expect degeneracies to occur. In fact one can show from RMT that the statistical measure vanishes when two eigenvalues coincide. Given an eigenvalue $x = 0$, the probability for the next eigenvalue to be at x can be shown to be

$$P(x) = \frac{\pi}{2} x \exp\left(-\frac{\pi}{4} x^2\right), \quad (7.65)$$

for the case with time-reversal symmetry. This is called the Wigner surmise, and a suggestive derivation is as follows. Suppose that the probability of finding an eigenvalue in dx is $f(x) dx$, then $P(x) dx$ is the probability of finding an eigenvalue at x , $f(x) dx$, times the probability that there was no eigenvalues in the interval $[0, x]$:

$$P(x)dx = \exp\left(-\int_0^x dx' f(x')\right) f(x)dx, \quad (7.66)$$

and hence

$$P(x) = f(x) \exp\left(-\int_0^x dx' f(x')\right). \quad (7.67)$$

For f constant, we recover the Poisson distribution result. Assuming “linear repulsion” $f(x) \propto x$, we get Eq. (7.65) after suitable normalization. The fluctuations of the number of eigenvalues in a given interval is therefore far from $1/\sqrt{N}$, which is the physical reason for the “universal” behavior.

In the following we calculate the fluctuations of G using the statistical RMT for the S -matrix as outlined above. The fluctuation of the conductance in the non-TRS case are

$$\begin{aligned} \langle G^2 \rangle_{\mathbf{B} \neq 0} &= \left(\frac{2e^2}{h}\right)^2 \sum_{n=1}^N \sum_{m=N+1}^{2N} \sum_{n'=1}^N \sum_{m'=N+1}^{2N} \langle S_{mn}^* S_{mn} S_{m'n'}^* S_{m'n'} \rangle, \\ &= \left(\frac{2e^2}{h}\right)^2 \sum_{n=1}^N \sum_{m=N+1}^{2N} \sum_{n'=1}^N \sum_{m'=N+1}^{2N} \frac{1}{4N^2 - 1} \left(1 + \delta_{mm'} \delta_{nn'} - \frac{1}{2N} (\delta_{nn'} + \delta_{mm'})\right), \\ &= \left(\frac{2e^2}{h}\right)^2 \frac{N^4}{4N^2 - 1} \approx \left(\frac{2e^2}{h}\right)^2 \left(\frac{N}{2}\right)^2 \left(1 + \frac{1}{4N^2}\right), \quad \text{for } N \gg 1 \end{aligned} \quad (7.68)$$

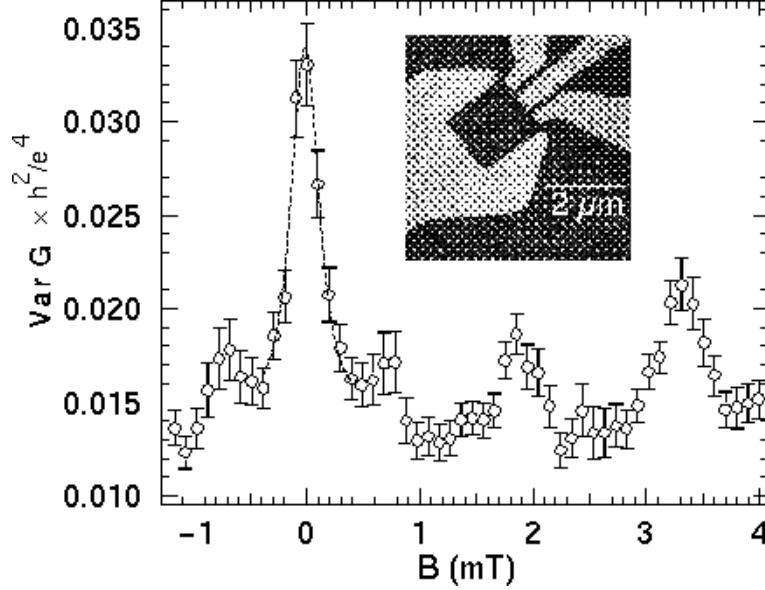


Figure 7.6: Variance of the conductance of a quantum dot as a function of magnetic field. The trace is taken at 30 mK. The decrease of the variance when the time-reversal symmetry is broken by the magnetic field is clearly seen and the decreases by approximately a factor of 2 is in agreement with the theory. The inset shows the geometry of the quantum dot, which has additional gates by which the shape can be changed. After Chan et al., Phys. Rev. Lett. **74**, 3876 (1995).

and the variance is

$$\frac{\langle \delta G^2 \rangle_{\mathbf{B} \neq 0}}{(2e^2/h)^2} \approx \frac{1}{16}, \quad \text{for } N \gg 1. \quad (7.69)$$

A similar calculation for the $\mathbf{B} = 0$ case gives

$$\frac{\langle \delta G^2 \rangle_{\mathbf{B}=0}}{(2e^2/h)^2} \approx \frac{1}{8}, \quad \text{for } N \gg 1. \quad (7.70)$$

The variance is thus independent of the average value of G and furthermore it is expected to decrease by a factor of 2 when a magnetic field is applying. Indeed this is what is seen experimentally for example as shown in Fig. 7.6.

7.5 Summary and outlook

Below we list a few text books and review papers about mesoscopic physics.

TEXT BOOKS:

1. *Electronic transport in mesoscopic systems*,
S. Datta, (Cambridge University Press), 1995.

2. *Transport in nanostructures*,
D.K. Ferry and S.M. Goodnick, (Cambridge University Press), 1995.

REVIEW PAPERS:

1. *Quantum transport in semiconductor nanostructures*,
C.W.J. Beenakker and H. van Houten,
Solid State Physics **44**, eds. H. Ehrenreich and D. Turnbull, (Academic Press), 1991.
2. *Random-matrix theory of quantum transport*,
C.W.J. Beenakker, Review of Modern Physics **69**, 731 (1997).
3. *Conductance quantisation in metallic point contacts*,
J.M. van Ruitenbeek, cond-mat/9910394.
4. *The statistical theory of quantum dots*,
Y. Alhassid, Review of Modern Physics **72**, 895 (2000)

Chapter 8

Green's functions

8.1 “Classical” Green's functions

The Green's function method is a very useful method in the theory of ordinary and partial differential equations. It has a long history with numerous applications.

To illustrate the idea of the method let us consider the familiar problem of finding the electrical potential ϕ given a fixed charge distribution, ρ_e , i.e. we want to solve Poisson's equation

$$\nabla^2 \phi(\mathbf{r}) = -\frac{1}{\varepsilon_0} \rho_e(\mathbf{r}). \quad (8.1)$$

It turns out to be a good idea instead to look for the solution G of a related but simpler differential equation

$$\nabla_{\mathbf{r}}^2 G(\mathbf{r}) = \delta(\mathbf{r}), \quad (8.2)$$

where $\delta(\mathbf{r})$ is the Dirac delta function. $G(\mathbf{r})$ is called the Green's function for the Laplace operator, $\nabla_{\mathbf{r}}^2$. This is a good idea because once we have found $G(\mathbf{r})$, the electrical potential follows as

$$\phi(\mathbf{r}) = -\frac{1}{\varepsilon_0} \int d\mathbf{r}' G(\mathbf{r} - \mathbf{r}') \rho_e(\mathbf{r}'). \quad (8.3)$$

That this is a solution to Eq. (8.1) is easily verified by letting $\nabla_{\mathbf{r}}^2$ act directly on the integrand and then use Eq. (8.2).

The easiest way to find $G(\mathbf{r})$ is by Fourier transformation, which immediately gives

$$-k^2 G(\mathbf{k}) = 1 \quad \Rightarrow \quad G(\mathbf{k}) = -\frac{1}{k^2}, \quad (8.4)$$

and hence

$$G(\mathbf{r}) = \int \frac{d\mathbf{k}}{(2\pi)^3} e^{i\mathbf{k}\cdot\mathbf{r}} G(\mathbf{k}) = - \int \frac{d\mathbf{k}}{(2\pi)^3} \frac{e^{i\mathbf{k}\cdot\mathbf{r}}}{k^2} = -\frac{1}{4\pi r}. \quad (8.5)$$

When inserting this into (8.3) we obtain the well-known potential created by a charge distribution

$$\phi(\mathbf{r}) = \frac{1}{4\pi\varepsilon_0} \int d\mathbf{r}' \frac{\rho_e(\mathbf{r}')}{|\mathbf{r} - \mathbf{r}'|}. \quad (8.6)$$

8.2 Green's function for the one-particle Schrödinger equation

Green's functions are particularly useful for problems where one looks for perturbation theory solutions. Consider for example the Schrödinger equation

$$[H_0(\mathbf{r}) + V(\mathbf{r})] \Psi_E = E \Psi_E, \quad (8.7)$$

where we know the eigenstates of H_0 , and where we want to treat V as a perturbation. Here we consider the case of an open system, i.e. there is a continuum of states and hence we are free to choose any E . This situation is relevant for scattering problems where a flux of incoming particles (described by H_0) interacts with a system (described by V). The interaction induces transitions from the incoming state to different outgoing states. The procedure outlined below is then a systematic way of calculating the effect of the interaction between the “beam” and the “target” on the outgoing states.

In order to solve the Schrödinger equation, we define the corresponding Green's function by the differential equation

$$[E - H_0(\mathbf{r})] G_0(\mathbf{r}, \mathbf{r}', E) = \delta(\mathbf{r} - \mathbf{r}'), \quad (8.8)$$

with the boundary condition, $G_0(\mathbf{r}, \mathbf{r}') = G_0(\mathbf{r}', \mathbf{r})$. It is natural to identify the operator $[E - H_0(\mathbf{r})]$ as the inverse of $G_0(\mathbf{r}, \mathbf{r}')$ and therefore we write¹

$$G_0^{-1}(\mathbf{r}, E) = E - H_0(\mathbf{r}) \quad \text{or} \quad G_0^{-1}(\mathbf{r}, E) G_0(\mathbf{r}, \mathbf{r}', E) = \delta(\mathbf{r} - \mathbf{r}'). \quad (8.9)$$

Now the Schrödinger equation can be rewritten as

$$[G_0^{-1}(\mathbf{r}, E) - V(\mathbf{r})] \Psi_E = 0, \quad (8.10)$$

and by inspection we see that the solution may be written as an integral equation

$$\Psi_E(\mathbf{r}) = \Psi_E^0(\mathbf{r}) + \int d\mathbf{r}' G_0(\mathbf{r}, \mathbf{r}', E) V(\mathbf{r}') \Psi_E(\mathbf{r}'). \quad (8.11)$$

This is verified by inserting ψ_E from Eq. (8.11) into the $G_0^{-1}\psi_E$ term of Eq. (8.10) and then using Eq. (8.9). One can now solve the integral equation Eq. (8.11) by iteration, and up to first order in V the solution is

$$\Psi_E(\mathbf{r}) = \Psi_E^0(\mathbf{r}) + \int d\mathbf{r}' G_0(\mathbf{r}, \mathbf{r}', E) V(\mathbf{r}') \Psi_E^0(\mathbf{r}') + \mathcal{O}(V^2), \quad (8.12)$$

where Ψ_E^0 is an eigenstate to H_0 with eigenenergy E . What we have generated by the iteration procedure is nothing but the ordinary (non-degenerate) perturbation theory. The next leading terms are also easily found by continuing the iteration procedure. The Green's

¹In order to emphasize the matrix structure we could have written this as $\int d\mathbf{r}'' G_0^{-1}(\mathbf{r}, \mathbf{r}'') G_0(\mathbf{r}'', \mathbf{r}') = \delta(\mathbf{r} - \mathbf{r}')$, where the inverse Green's function is a function of two arguments. But in the \mathbf{r} -representation it is in fact diagonal $G_0^{-1}(\mathbf{r}, \mathbf{r}') = (E - H_0(\mathbf{r}))\delta(\mathbf{r} - \mathbf{r}')$.

function method is thus useful for this kind of iterative calculations and one can regard the Green's function of the unperturbed system, G_0 , as simple building blocks from which the solutions of more complicated problems can be build.

Before we introduce the many-body Green's function in the next section, we continue to study the case of non-interaction particles some more and include time dependence. Again we consider the case where the Hamiltonian has a free particle part H_0 of some perturbation V , $H = H_0 + V$. The time dependent Schrödinger equation is

$$[i\partial_t - H_0(\mathbf{r}) - V(\mathbf{r})] \Psi(\mathbf{r}, t) = 0. \quad (8.13)$$

Similar to Eq. (8.8) we define the Green's functions by

$$[i\partial_t - H_0(\mathbf{r})] G_0(\mathbf{r}, \mathbf{r}'; t, t') = \delta(\mathbf{r} - \mathbf{r}')\delta(t - t'). \quad (8.14a)$$

$$[i\partial_t - H_0(\mathbf{r}) - V(\mathbf{r})] G(\mathbf{r}, \mathbf{r}'; t, t') = \delta(\mathbf{r} - \mathbf{r}')\delta(t - t'). \quad (8.14b)$$

The inverse of the Green's functions are thus

$$G_0^{-1}(\mathbf{r}, t) = i\partial_t - H_0(\mathbf{r}) \quad (8.15a)$$

$$G^{-1}(\mathbf{r}, t) = i\partial_t - H_0(\mathbf{r}) - V(\mathbf{r}). \quad (8.15b)$$

From these building blocks we easily build the solution of the time dependent Schrödinger equation. First we observe that the following self-consistent expression is a solution to Eq. (8.13)

$$\Psi(\mathbf{r}, t) = \Psi^0(\mathbf{r}, t) + \int d\mathbf{r}' \int dt' G_0(\mathbf{r}, \mathbf{r}'; t, t') V(\mathbf{r}') \Psi(\mathbf{r}', t'), \quad (8.16)$$

or in terms of the full Green's function

$$\Psi(\mathbf{r}, t) = \Psi^0(\mathbf{r}, t) + \int d\mathbf{r}' \int dt' G(\mathbf{r}, \mathbf{r}'; t, t') V(\mathbf{r}') \Psi^0(\mathbf{r}', t'), \quad (8.17)$$

which both can be shown by inspection, see Exercise 7.1. As for the static case in Eq. (8.11) we can iterate the solution and get

$$\begin{aligned} \Psi &= \Psi^0 + G_0 V \Psi^0 + G_0 V G_0 V \Psi^0 + G_0 V G_0 V G_0 V \Psi^0 + \dots \\ &= \Psi^0 + (G_0 + G_0 V G_0 + G_0 V G_0 V G_0 + \dots) V \Psi^0, \end{aligned} \quad (8.18)$$

where the integration variables have been suppressed. By comparison with Eq. (8.17), we see that the full Green's function G is given by

$$\begin{aligned} G &= G_0 + G_0 V G_0 + G_0 V G_0 V G_0 + \dots \\ &= G_0 + G_0 V (G_0 + G_0 V G_0 + \dots). \end{aligned} \quad (8.19)$$

Noting that the last parenthesis is nothing but G itself we have derived the so-called Dyson equation

$$G = G_0 + G_0 V G. \quad (8.20)$$

This equation will play an important role when we introduce the Feynman diagrams later in the course. The Dyson equation can also be derived directly from Eqs. (8.14) by multiplying Eq. (8.14b) with G_0 from the left.

The Green's function $G(\mathbf{r}, t)$ we have defined here is the non-interaction version of the retarded single particle Green's function that will be introduced in the following section. It is also often called a propagator because it propagates the wavefunction, i.e. if the wavefunction is known at some time then the wavefunction at later times is given by

$$\Psi(\mathbf{r}, t) = \int d\mathbf{r}' \int dt' G(\mathbf{r}t, \mathbf{r}'t') \Psi(\mathbf{r}', t'), \quad (8.21)$$

which can be checked by inserting Eq. (8.21) into the Schrödinger equation and using the definition Eq. (8.14b).

That the Green's function is nothing but a propagator is immediately clear when we write it as

$$G(\mathbf{r}t, \mathbf{r}'t') = -i\theta(t - t') \langle \mathbf{r} | e^{-iH(t-t')} | \mathbf{r}' \rangle, \quad (8.22)$$

which indeed is a solution of the partial differential equation defining the Green's function, Eq. (8.14b), the proof being left as an exercise; see Exercise 7.2. Looking at Eq. (8.22) the Green's function expresses the amplitude for the particle to be in state $|\mathbf{r}\rangle$ at time t , given that it was in the state $|\mathbf{r}'\rangle$ at time t' . We could of course calculate the propagator in a different basis, e.g. suppose it was in a state $|\phi_{n'}\rangle$ and time t' then the propagator for ending in state $|\phi_n\rangle$ is

$$G(nt, n't') = -i\theta(t - t') \langle \phi_n | e^{-iH(t-t')} | \phi_{n'} \rangle. \quad (8.23)$$

The Green's functions are related by a simple change of basis

$$G(\mathbf{r}t, \mathbf{r}'t') = \sum_{nn'} \langle \mathbf{r} | \phi_n \rangle G(nt, n't') \langle \phi_{n'} | \mathbf{r}' \rangle. \quad (8.24)$$

If we choose the basis state $|\phi_n\rangle$ as the eigenstates of the Hamiltonian, then the Green's function becomes

$$G(\mathbf{r}t, \mathbf{r}'t') = -i\theta(t - t') \sum_n \langle \mathbf{r} | \phi_n \rangle \langle \phi_n | \mathbf{r}' \rangle e^{-iE_n(t-t')}. \quad (8.25)$$

Propagation from one point to another in quantum mechanics is generally expressed in terms of transmission amplitudes. As a simple example we end this section by a typical scattering problem in one dimension. Consider an electron incident on a barrier, located between $x > 0$ and $x < L$, the incoming wave is for $x < 0$ given by $\exp(ikx)$ while the outgoing wave on the other side $x > L$ is given by $t \exp(ikx)$. Here t is the transmission amplitude. The eigenstates are for this example thus given by

$$\psi(\mathbf{k}) = \begin{cases} \exp(ikx), & \text{for } x < 0, \\ t \exp(ikx), & \text{for } x > L. \end{cases} \quad (8.26)$$

When this is inserted into Eq. (8.25) we see that the Green's function for the $x > L$ and $x' < 0$ precisely describes propagator across the scattering region becomes

$$G(xt, x't') = t G_0(x, x'; t, t'), \quad x > L \quad \text{and} \quad x' < 0. \quad (8.27)$$

where G_0 is the Green's function in the absence of the scattering potential. From this example it is evident that the Green's function contains information about the transmission amplitudes for the particle. See also Exercise 10.2.

8.3 Single-particle Green's functions of many-body systems

In many-particle physics we adopt the Green's function philosophy and define some simple building blocks, also called Green's functions, from which we obtain solutions to our problems. The Green's functions contain only part of the full information carried by the wave functions of the systems but they include the relevant information for the given problem. When we define the many-body Green's functions it is not immediately clear that they are solutions to differential equations as for the Schrödinger equation Green's functions defined above. But as you will see later they are in fact solutions of equations of motions with similar structure justifying calling them Green's functions. Let us simply carry on and define the different types of Green's functions that we will be working with.

There are various types of single-particle Green's functions. The retarded Green's function is defined as

$$G^R(\mathbf{r}\sigma t, \mathbf{r}'\sigma't') = -i\theta(t - t') \langle [\Psi_\sigma(\mathbf{r}t), \Psi_{\sigma'}^\dagger(\mathbf{r}'t')]_{B,F} \rangle, \quad \left\{ \begin{array}{l} B : \text{ bosons} \\ F : \text{ fermions} \end{array} \right\} \quad (8.28)$$

where the (anti-) commutator $[\cdots, \cdots]_{B,F}$ is defined as

$$\begin{aligned} [A, B]_B &= [A, B] = AB - BA, \\ [A, B]_F &= \{A, B\} = AB + BA. \end{aligned} \quad (8.29)$$

Notice the similarity between the many-body Green's function Eq. (8.28) and the one for the propagator for the one particle wavefunction, in Eq. (8.22). For non-interacting particles they are indeed identical.

The second type of single-particle Green's functions is the so-called greater and lesser Green's functions

$$G^>(\mathbf{r}\sigma t, \mathbf{r}'\sigma't') = -i\langle \Psi_\sigma(\mathbf{r}t) \Psi_{\sigma'}^\dagger(\mathbf{r}'t') \rangle, \quad (8.30a)$$

$$G^<(\mathbf{r}\sigma t, \mathbf{r}'\sigma't') = -i(\pm 1) \langle \Psi_{\sigma'}^\dagger(\mathbf{r}'t') \Psi_\sigma(\mathbf{r}t) \rangle. \quad (8.30b)$$

We see that the retarded Green's function can be written in terms of these two functions as

$$G^R(\mathbf{r}\sigma t, \mathbf{r}'\sigma't') = \theta(t - t') [G^>(\mathbf{r}\sigma t, \mathbf{r}'\sigma't') - G^<(\mathbf{r}\sigma t, \mathbf{r}'\sigma't')].$$

Even though we call these Green's functions for "single-particle Green's functions", they are truly many-body objects because they describe the propagation of single particles

governed by the full many-body Hamiltonian. Therefore the single-particle functions can include all sorts of correlation effects.

The Green's functions in Eqs. (8.28), (8.30a), and (8.30b) are often referred to as propagators. The reason is that they give the amplitude of a particle inserted in point \mathbf{r}' at time t' to propagate to position \mathbf{r} at time t . In this sense G^R has its name “retarded” because it is required that $t > t'$.

The relation between the real space retarded Green's function and the corresponding one in a general $|\nu\rangle$ -basis as defined in Eq. (1.71) is

$$G^R(\sigma\mathbf{r}t, \sigma'\mathbf{r}'t') = \sum_{\nu\nu'} \psi_\nu(\sigma\mathbf{r}) G^R(\nu\sigma t, \nu'\sigma't') \psi_{\nu'}^*(\sigma'\mathbf{r}'), \quad (8.31)$$

where

$$G^R(\nu\sigma t, \nu'\sigma't') = -i\theta(t - t') \langle [a_{\nu\sigma}(t), a_{\nu'\sigma'}^\dagger(t')]_{B,F} \rangle, \quad (8.32)$$

and similarly for $G^>$ and $G^<$.

8.3.1 Green's function of translation-invariant systems

For a system with translation-invariance the usual \mathbf{k} -representation is a natural basis set. Since the system is translation-invariant $G(\mathbf{r}, \mathbf{r}')$ can only depend on the difference $\mathbf{r} - \mathbf{r}'$ and in this case

$$\begin{aligned} G^R(\mathbf{r} - \mathbf{r}', \sigma t, \sigma' t') &= \frac{1}{\mathcal{V}} \sum_{\mathbf{k}\mathbf{k}'} e^{i\mathbf{k}\cdot\mathbf{r}} G^R(\mathbf{k}\sigma t, \mathbf{k}'\sigma' t') e^{-i\mathbf{k}'\cdot\mathbf{r}'}, \\ &= \frac{1}{\mathcal{V}} \sum_{\mathbf{k}\mathbf{k}'} e^{i\mathbf{k}\cdot(\mathbf{r}-\mathbf{r}')} G^R(\mathbf{k}\sigma t, \mathbf{k}'\sigma' t') e^{i(\mathbf{k}-\mathbf{k}')\cdot\mathbf{r}'}. \end{aligned} \quad (8.33)$$

However, because the right hand side cannot explicitly dependent on the origin and on \mathbf{r}' , it follows that $G(\mathbf{k}, \mathbf{k}') = \delta_{\mathbf{k}, \mathbf{k}'} G(\mathbf{k})$, allowing us to write

$$G^R(\mathbf{r} - \mathbf{r}', \sigma t, \sigma' t') = \frac{1}{\mathcal{V}} \sum_{\mathbf{k}} e^{i\mathbf{k}\cdot(\mathbf{r}-\mathbf{r}')} G^R(\mathbf{k}, \sigma t, \sigma' t'), \quad (8.34a)$$

$$G^R(\mathbf{k}, \sigma t, \sigma' t') = -i\theta(t - t') \langle [a_{\mathbf{k}\sigma}(t), a_{\mathbf{k}\sigma'}^\dagger(t')]_{B,F} \rangle. \quad (8.34b)$$

The other types of Green's functions have similar forms.

8.3.2 Green's function of free electrons

A particular case often encountered in the theory of quantum liquids is the simple case of free particles. Consider therefore the Hamiltonian for free electrons (or other fermions)

$$H = \sum_{\mathbf{k}\sigma} \xi_{\mathbf{k}\sigma} c_{\mathbf{k}\sigma}^\dagger c_{\mathbf{k}\sigma}, \quad (8.35)$$

and the corresponding greater function in \mathbf{k} -space, which we denote $G_0^>$ to indicate that it is the propagator of free electrons. Because the Hamiltonian is diagonal in the quantum numbers \mathbf{k} and σ so is the Green's function and therefore

$$G_0^>(\mathbf{k}\sigma, t - t') = -i \left\langle c_{\mathbf{k}\sigma}(t) c_{\mathbf{k}\sigma}^\dagger(t') \right\rangle. \quad (8.36)$$

Because of the simple form of the Hamiltonian we are able to find the time dependence of the c -operators (see Eq. (5.24))

$$c_{\mathbf{k}\sigma}(t) = e^{iHt} c_{\mathbf{k}\sigma} e^{-iHt} = c_{\mathbf{k}\sigma} e^{-i\xi_{\mathbf{k}}t}, \quad (8.37)$$

and similarly $c_{\mathbf{k}}^\dagger(t) = c_{\mathbf{k}}^\dagger e^{i\xi_{\mathbf{k}}t}$. An easy way to remember this is to realize that the factor e^{-iHt} to the right of $c_{\mathbf{k}}$ must have one more electron in state \mathbf{k} than e^{iHt} to the left of $c_{\mathbf{k}}$.

Now $G^>$ becomes

$$G_0^>(\mathbf{k}\sigma; t - t') = -i \langle c_{\mathbf{k}\sigma} c_{\mathbf{k}\sigma}^\dagger \rangle e^{-i\xi_{\mathbf{k}}(t-t')}, \quad (8.38)$$

and because the Hamiltonian is diagonal in \mathbf{k} and the occupation of free electrons is given by the Fermi-Dirac distribution, we of course have $\langle c_{\mathbf{k}\sigma} c_{\mathbf{k}\sigma}^\dagger \rangle = 1 - n_F(\xi_{\mathbf{k}})$. In exactly the same way, we can evaluate $G_0^<$ and finally G_0^R

$$G_0^>(\mathbf{k}\sigma, t - t') = -i(1 - n_F(\xi_{\mathbf{k}})) e^{-i\xi_{\mathbf{k}}(t-t')}, \quad (8.39a)$$

$$G_0^<(\mathbf{k}\sigma, t - t') = i n_F(\xi_{\mathbf{k}}) e^{-i\xi_{\mathbf{k}}(t-t')}, \quad (8.39b)$$

$$G_0^R(\mathbf{k}\sigma, t - t') = -i\theta(t - t') e^{-i\xi_{\mathbf{k}}(t-t')}. \quad (8.39c)$$

We see that $G^>$ gives the propagation of electrons, because it requires an empty state while $G^<$ gives the propagation of holes, because it is proportional to the number of electrons. This is perhaps more clearly seen if we write the $T = 0$ definition of for example $G_0^>$

$$G_0^>(\mathbf{k}, \mathbf{k}', t - t') = -i \langle G | c_{\mathbf{k}}(t) c_{\mathbf{k}'}^\dagger(t') | 0 \rangle = -i \langle G | c_{\mathbf{k}} e^{-iH(t-t')} c_{\mathbf{k}'}^\dagger | G \rangle e^{iE_0(t-t')}, \quad (8.40)$$

which precisely is the overlap between a state with an added electron in state \mathbf{k}' and with a state with an added electron in \mathbf{k} and allowing time to evolve from t' to t . Here $|G\rangle$ denotes the groundstate of the free electrons, i.e. the filled Fermi sea, $|G\rangle = |\text{FS}\rangle$.

By Fourier transforming from the time domain to the frequency domain, we get information about the possible energies of the propagating particle. This is intuitively clear from Eqs. (8.39) because the propagators evolve periodically in time with the period given by the energy of the electron. For example, the electron propagator is in the frequency domain

$$G_0^>(\mathbf{k}\sigma, \omega) = -2\pi i [1 - n_F(\xi_{\mathbf{k}})] \delta(\xi_{\mathbf{k}} - \omega). \quad (8.41)$$

The corresponding \mathbf{r} -dependent propagator, which expresses propagation of a particle in real space is given by

$$\begin{aligned} \frac{G_0^>(\mathbf{r} - \mathbf{r}', \omega)}{-2\pi i} &= \int \frac{d\mathbf{k}}{(2\pi)^3} (1 - n_F(\xi_{\mathbf{k}})) e^{i\mathbf{k} \cdot (\mathbf{r} - \mathbf{r}')} \delta(\xi_{\mathbf{k}} - \omega) \\ &= d(\omega) (1 - n_F(\omega)) \frac{\sin(k_\omega \rho)}{k_\omega \rho}, \quad \frac{k_\omega^2}{2m} = \omega, \quad \rho = |\mathbf{r} - \mathbf{r}'|, \end{aligned} \quad (8.42)$$

where $d(\varepsilon) = m^{3/2} \sqrt{\varepsilon/2}/\pi^2$ is the density of states per spin in three dimensions, see also Eq. (2.31). The propagation from point \mathbf{r}' to \mathbf{r} of a particle with energy ω is thus determined by the density of states, d , the availability of an empty state $(1 - n_F)$, the interference function $\sin(x)/x$ that gives the amplitude of a spherical wave spreading out from the point \mathbf{r}' . See also Exercise 7.3.

8.3.3 The Lehmann representation

A method we will often be using when proving formal results is the so-called Lehmann representation, which is just another name for using the set of eigenstates, $\{|n\rangle\}$, of the full Hamiltonian, H , as basis set. Let us for example study the diagonal Green's function, $G^>(\nu t \nu t')$. If we insert $1 = \sum_n |n\rangle\langle n|$ we get

$$\begin{aligned} G^>(\nu; t, t') &= -i \langle c_\nu(t) c_\nu^\dagger(t') \rangle = -i \frac{1}{Z} \sum_n \langle n | e^{-\beta H} a_\nu(t) a_\nu^\dagger(t') | n \rangle \\ &= -i \frac{1}{Z} \sum_{nn'} e^{-\beta E_n} \langle n | c_\nu | n' \rangle \langle n' | a_\nu^\dagger | n \rangle e^{i(E_n - E_{n'})(t - t')}. \end{aligned} \quad (8.43)$$

In the frequency domain, we obtain

$$G^>(\nu; \omega) = \frac{-2\pi i}{Z} \sum_{nn'} e^{-\beta E_n} \langle n | a_\nu | n' \rangle \langle n' | c_\nu^\dagger | n \rangle \delta(E_n - E_{n'} + \omega). \quad (8.44)$$

In the same way we have (for fermions, c)

$$\begin{aligned} G^<(\nu; \omega) &= \frac{2\pi i}{Z} \sum_{nn'} e^{-\beta E_n} \langle n | c_\nu^\dagger | n' \rangle \langle n' | c_\nu | n \rangle \delta(E_n - E_{n'} - \omega), \\ &= \frac{2\pi i}{Z} \sum_{nn'} e^{-\beta E_{n'}} \langle n' | c_\nu^\dagger | n \rangle \langle n | c_\nu | n' \rangle \delta(E_{n'} - E_n - \omega), \\ &= \frac{2\pi i}{Z} \sum_{nn'} e^{-\beta(E_n + \omega)} \langle n' | c_\nu^\dagger | n \rangle \langle n | c_\nu | n' \rangle \delta(E_{n'} - E_n - \omega), \\ &= -G^>(\nu; \omega) e^{-\beta \omega}. \end{aligned} \quad (8.45)$$

The retarded Green's function becomes (again for fermions)

$$\begin{aligned} G^R(\nu, \omega) &= -i \int_0^\infty dt e^{i(\omega + i\eta)t} \frac{1}{Z} \sum_{nn'} e^{-\beta E_n} \left(\langle n | c_\nu | n' \rangle \langle n' | c_\nu^\dagger | n \rangle e^{i(E_n - E_{n'})t} \right. \\ &\quad \left. + \langle n | c_\nu^\dagger | n' \rangle \langle n' | c_\nu | n \rangle e^{-i(E_n - E_{n'})t} \right) \\ &= \frac{1}{Z} \sum_{nn'} e^{-\beta E_n} \left(\frac{\langle n | c_\nu | n' \rangle \langle n' | c_\nu^\dagger | n \rangle}{\omega + E_n - E_{n'} + i\eta} + \frac{\langle n | c_\nu^\dagger | n' \rangle \langle n' | c_\nu | n \rangle}{\omega - E_n + E_{n'} + i\eta} \right) \\ &= \frac{1}{Z} \sum_{nn'} \frac{\langle n | c_\nu | n' \rangle \langle n' | c_\nu^\dagger | n \rangle}{\omega + E_n - E_{n'} + i\eta} \left(e^{-\beta E_n} + e^{-\beta E_{n'}} \right). \end{aligned} \quad (8.46)$$

Taking the imaginary part of this and using $(\omega + i\eta)^{-1} = \mathcal{P}\frac{1}{\omega} - i\pi\delta(\omega)$, we get

$$2\text{Im } G^R(\nu, \omega) = -\frac{2\pi}{Z} \sum_{nn'} \langle n|c_\nu|n'\rangle \langle n'|c_\nu^\dagger|n\rangle \left(e^{-\beta E_n} + e^{-\beta E_{n'}} \right) \delta(\omega + E_n - E_{n'}) \quad (8.47)$$

$$\begin{aligned} &= -\frac{2\pi}{Z} \sum_{nn'} \langle n|c_\nu|n'\rangle \langle n'|c_\nu^\dagger|n\rangle e^{-\beta E_n} (1 + e^{-\beta\omega}) \delta(\omega + E_n - E_{n'}), \\ &= -i(1 + e^{-\beta\omega}) G^>(\nu, \omega), \end{aligned} \quad (8.48)$$

Defining the spectral function A as

$$A(\nu, \omega) = -2\text{Im } G^R(\nu, \omega), \quad (8.49)$$

we have derived the important general relations

$$iG^>(\nu, \omega) = A(\nu, \omega) [1 - n_F(\omega)], \quad (8.50a)$$

$$-iG^<(\nu, \omega) = A(\nu, \omega) n_F(\omega). \quad (8.50b)$$

Similar relations hold for bosons, see Exercise 7.4

8.3.4 The spectral function

The spectral function $A(\nu, \omega)$ can be thought of as either the quantum state resolution of a particle with given energy ω or as the energy resolution for a particle in a given quantum number ν . It gives an indication of how well the excitation created by adding a particle in state ν can be described by a free non-interacting particle. For example if we look at the retarded propagator for free electrons in Eq. (8.39c)

$$\begin{aligned} G_0^R(\mathbf{k}\sigma, \omega) &= -i \int_{-\infty}^{\infty} dt \theta(t - t') e^{i\omega(t-t')} e^{-i\xi_{\mathbf{k}}(t-t')\eta(t-t')} \\ &= \frac{1}{\omega - \xi_{\mathbf{k}} + i\eta}, \end{aligned} \quad (8.51)$$

the corresponding spectral function is

$$A_0(\mathbf{k}\sigma, \omega) = -2\text{Im } G_0^R(\mathbf{k}\sigma, \omega) = 2\pi\delta(\omega - \xi_{\mathbf{k}}). \quad (8.52)$$

Thus for the idealized case of non-interaction free electrons, the spectral function is a delta function, which tells us that an excitation with energy ω can only happen by adding an electron to the state \mathbf{k} given by $\xi_{\mathbf{k}} = \omega$, as expected.

This result is true for any quadratic Hamiltonian, i.e. non-interacting system. If we for example have

$$H_0 = \sum_{\nu} \xi_{\nu} c_{\nu}^{\dagger} c_{\nu}, \quad (8.53)$$

where ν labels the eigenstates of the system. Again the spectral function is given by a simple delta function

$$A_0(\nu, \omega) = 2\pi\delta(\omega - \xi_{\nu}). \quad (8.54)$$

Generally, due to interactions the spectral function differs from a delta function, but it may still be a peaked function, which then indicates that the non-interacting approximation is not too far from the truth. In Chap. 13 this is discussed in much more detail.

We will now show that the spectral function is like a probability distribution. Firstly, it is always positive as one must require. This follows from Eq. (8.46), the definition of the spectral function, Eq. (8.49) and the fact that $\langle n' | c_\nu | n' \rangle \langle n' | c_\nu^\dagger | n \rangle = |\langle n' | c_\nu | n' \rangle|^2$. Secondly, it obeys the sum rule

$$\int_{-\infty}^{\infty} \frac{d\omega}{2\pi} A(\nu, \omega) = 1. \quad (8.55)$$

This formula is easily derived by considering the Lehmann representation of $-2 \text{Im } G^R$ in Eq. (8.47)

$$\begin{aligned} \int_{-\infty}^{\infty} \frac{d\omega}{2\pi} A(\nu, \omega) &= - \int_{-\infty}^{\infty} \frac{d\omega}{2\pi} 2 \text{Im } G^R(\nu, \omega) \\ &= \int_{-\infty}^{\infty} d\omega \frac{1}{Z} \sum_{nn'} \langle n | c_\nu | n' \rangle \langle n' | c_\nu^\dagger | n \rangle \left(e^{-\beta E_n} + e^{-\beta E_{n'}} \right) \\ &\quad \times \delta(\omega + E_n - E_{n'}) \\ &= \frac{1}{Z} \sum_{nn'} \langle n | c_\nu | n' \rangle \langle n' | c_\nu^\dagger | n \rangle \left(e^{-\beta E_n} + e^{-\beta E_{n'}} \right) \\ &= \langle c_\nu c_\nu^\dagger \rangle + \langle c_\nu^\dagger c_\nu \rangle = \langle c_\nu c_\nu^\dagger + c_\nu^\dagger c_\nu \rangle = 1, \end{aligned} \quad (8.56)$$

where the last equality follows from the Fermi operator commutation relations.

Furthermore, the spectral function is similar to the density of states at a given energy. This is evident since the occupation n_ν of a given state ν is for fermions given by (8.50b)

$$\begin{aligned} \bar{n}_\nu &= \langle c_\nu^\dagger c_\nu \rangle = -i G^<(\nu, t=0) \\ &= -i \int_{-\infty}^{\infty} \frac{d\omega}{2\pi} G^<(\nu, \omega) \\ &= \int_{-\infty}^{\infty} \frac{d\omega}{2\pi} A(\nu, \omega) n_F(\omega). \end{aligned} \quad (8.57)$$

The physical interpretation is that the occupation of a quantum state $|\nu\rangle$ is an energy integral of the spectral density of single particle states projected onto the state $|\nu\rangle$ and weighted by the occupation at the given energy. We of course expect that if the state $|\nu\rangle$ is far below the Fermi surface, e.g. $\varepsilon_\nu \ll E_F$, then $\langle c_\nu^\dagger c_\nu \rangle \approx 1$. This in fact follows from the sum rule, because if $\varepsilon_\nu \ll E_F$ and the width of $A(\nu, \omega)$ is also small compared to E_F then the Fermi function in (8.57) is approximately unity and since $A(\nu, \omega)$ integrates to 2π , see above, the expected result follows.

8.3.5 Broadening of the spectral function

When interactions are present the spectral function changes from the ideal delta function to a broadened profile. One possible mechanism of broadening in a metal is by e.g. electron-phonon interaction, which redistributes the spectral weight because of energy exchange

between the electron and the phonon system. Another mechanism for broadening is the electron-electron interaction. See Chap. 13.

As a simple example we consider a Green's function which decays in time due to processes that scatters the particle out of the state ν . In this situation the retarded Green's function becomes

$$G^R(\nu, t) \approx -i\theta(t)e^{-i\xi_\nu t}e^{-t/\tau}, \quad (8.58)$$

where τ is the characteristic decay time. Such a decaying Green's function corresponds to a finite width of the spectral function

$$A(\nu, \omega) = -2 \operatorname{Im} \int_{-\infty}^{\infty} dt e^{i\omega t} G^R(\nu, t) \approx 2 \operatorname{Im} i \int_0^{\infty} dt e^{i\omega t} e^{-i\xi_\nu t} e^{-t/\tau} = \frac{2/\tau}{(\omega - \xi_\nu)^2 + (1/\tau)^2}. \quad (8.59)$$

Thus the width in energy space is given by τ^{-1} .

The simple notion of single electron propagators becomes less well defined for interacting systems, which is reflected in a broadening of the spectral function. Amazingly, the free electron picture is still a good distribution in many cases and in particular for metals, which is quite surprising since the Coulomb interaction between the electrons is a rather strong interaction. The reason for this will be discussed later in the Chap. 13 on Fermi liquid theory.

8.4 Measuring the single-particle spectral function

In order to probe the single-particle properties of a many-body system, a solid state sample say, one must have a way of measuring how the electrons propagate as a function of energy. In practice this means taking out or inserting a particle with definite energy. There are not too many ways for doing this because most experiments measure density or other two-particle properties. For example the response to an electromagnetic field couples to the charge or current, which, as we saw in the previous chapter, measures charge-charge or current-current correlation functions, both being two particle propagators.

In principle there is only one way to measure the single particle properties, which is to insert/remove a single electron into/out of a many-body system. This can be achieved by a so-called tunnel junction device or by subjecting the sample to a beam of electrons. However, in some cases also optical experiments approximately measures the single particle density of states. For example when a photon is absorbed and an electron is kicked out from an occupied state to e.g. a freely propagating state outside the material.

In the following we study in detail the tunneling case where an electron tunnels from one material to the other and show how the tunneling current is expressed in terms of the spectral functions and thus provides a direct measurement of these.

8.4.1 Tunneling spectroscopy

The tunnel experiment set-up consists of two conducting materials brought into close contact such that electrons can tunnel from one to the other. This is illustrated in Fig. 8.1.

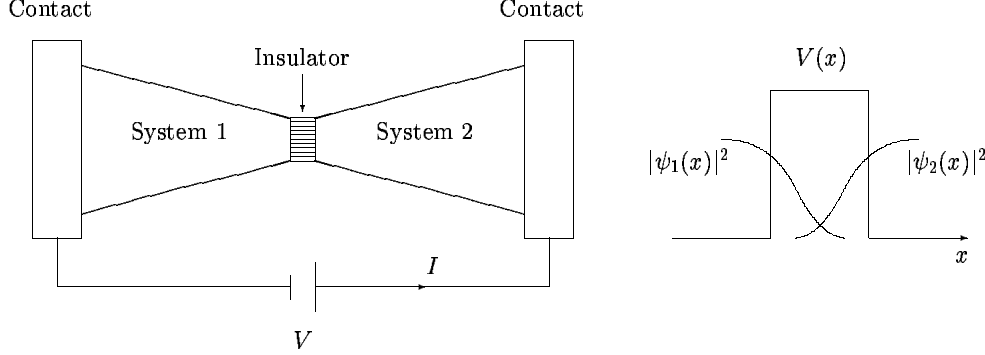


Figure 8.1: Measurement setup for the tunnel experiment. Two systems are brought into close contact, separated by an insulating material, e.g. an oxide or for the so-called scanning tunneling microscope (STM) simply vacuum. The right panel illustrates the electron wavefunctions in the two subsystems which have a small overlap in the insulator region. In the tunneling Hamiltonian this is modelled by the matrix element $T_{\nu\nu'}$.

Systems 1 and 2 are described by their respective Hamiltonians, H_1 and H_2 , involving electron operators, $c_{1,\nu}$ and $c_{2,\mu}$.

The coupling between the two sides of the junction is due to the finite overlap of the wavefunctions, which gives rise to a term in the Hamiltonian of the form

$$H_{12} = \sum_{\nu\mu} \left(T_{\nu\mu} c_{1,\nu}^\dagger c_{2,\mu} + T_{\nu\mu}^* c_{2,\mu}^\dagger c_{1,\nu} \right). \quad (8.60)$$

This is the most general one-particle operator which couples the two systems. The tunnel matrix element is defined as

$$T_{\nu\mu} = \int d\mathbf{r} \psi_\nu^*(\mathbf{r}) H(\mathbf{r}) \psi_\mu(\mathbf{r}), \quad (8.61)$$

with $H(\mathbf{r})$ being the (first quantization) one-particle Hamiltonian.

The current through the device is defined by the rate of change of particles, $I_e = -e\langle \dot{I} \rangle$, where $I = \dot{N}_1$, and hence

$$\begin{aligned} I &= i[H, N_1] = i[H_{12}, N_1] = i \sum_{\nu\mu} \sum_{\nu'} \left[\left(T_{\nu\mu} c_{1,\nu}^\dagger c_{2,\mu} + T_{\nu\mu}^* c_{2,\mu}^\dagger c_{1,\nu} \right), c_{1,\nu'}^\dagger c_{1,\nu'} \right] \\ &= -i \sum_{\nu\mu} \left(T_{\nu\mu} c_{1,\nu}^\dagger c_{2,\mu} - T_{\nu\mu}^* c_{2,\mu}^\dagger c_{1,\nu} \right) \equiv -i(L - L^\dagger). \end{aligned} \quad (8.62)$$

The current passing from 1 to 2 is driven by a shift of chemical potential difference, which means that $\mu_1 \neq \mu_2$. The coupling between the system is assumed to be very weak, since the tunnel matrix element is exponentially suppressed with distance between the two systems. Therefore we calculate the current to lowest order in the coupling. The current operator itself is already linear in $T_{\nu\mu}$ and therefore we need only one more order. This

means that linear response theory is applicable. According to the general Kubo formula derived in chap. 6 the particle current is to first order in H_{12} given by

$$\langle I \rangle(t) = \int_{-\infty}^{\infty} dt' C_{I_p H_{12}}^R(t, t'), \quad (8.63a)$$

$$C_{I_p H_{12}}^R(t - t') = -i\theta(t - t') \langle [\hat{I}_p(t), \hat{H}_{12}(t')] \rangle_{\text{eq}} \quad (8.63b)$$

where the time development is governed by $H = H_1 + H_2$. The correlation function $C_{I H_{12}}$ can be simplified a bit as

$$\begin{aligned} C_{I_p H_{12}}^R(t - t') &= -\theta(t - t') \left\langle \left[\hat{L}(t) - \hat{L}^\dagger(t), \hat{L}(t') + \hat{L}^\dagger(t') \right] \right\rangle_{\text{eq}} \\ &= -\theta(t - t') \left[\left\langle \left[\hat{L}(t), \hat{L}(t') \right] \right\rangle_{\text{eq}} - \left\langle \left[\hat{L}^\dagger(t), \hat{L}(t') \right] \right\rangle_{\text{eq}} + \text{c.c.} \right]. \end{aligned} \quad (8.64)$$

Now the combination $\left\langle \left[\hat{L}(t), \hat{L}(t') \right] \right\rangle$ involves terms of the form

$$\left\langle \left(c_{1,\nu}^\dagger c_{2,\mu} \right) (t) \left(c_{1,\nu}^\dagger c_{2,\mu} \right) (t') \right\rangle_{\text{eq}},$$

with two electrons created in system 1 and two electrons annihilated in system 2 and therefore it does not conserve the number of particles in each system. Naturally the number of particles is a conserved quantity and matrix elements of this type must vanish.² We are therefore left with

$$\begin{aligned} I_p(t) &= 2 \text{Re} \int_{-\infty}^{\infty} dt' \theta(t - t') \left\langle \left[\hat{L}^\dagger(t), \hat{L}(t') \right] \right\rangle_{\text{eq}} \\ &= 2 \text{Re} \int_{-\infty}^{\infty} dt' \theta(t - t') \sum_{\nu\mu} \sum_{\nu'\mu'} T_{\nu\mu}^* T_{\nu'\mu'} \left\langle \left[\hat{c}_{2,\mu}^\dagger(t) \hat{c}_{1,\nu}(t), \hat{c}_{1,\nu'}^\dagger(t') \hat{c}_{2,\mu'}(t') \right] \right\rangle_{\text{eq}} \\ &= 2 \text{Re} \int_{-\infty}^{\infty} dt' \theta(t - t') \sum_{\nu\mu} \sum_{\nu'\mu'} T_{\nu\mu}^* T_{\nu'\mu'} \left(\left\langle \hat{c}_{1,\nu}(t) \hat{c}_{1,\nu'}^\dagger(t') \right\rangle_{\text{eq}} \left\langle \hat{c}_{2,\mu}^\dagger(t) \hat{c}_{2,\mu'}(t') \right\rangle_{\text{eq}} \right. \\ &\quad \left. - \left\langle \hat{c}_{1,\nu'}^\dagger(t') \hat{c}_{1,\nu}(t) \right\rangle_{\text{eq}} \left\langle \hat{c}_{2,\mu'}(t') \hat{c}_{2,\mu}^\dagger(t) \right\rangle_{\text{eq}} \right). \end{aligned} \quad (8.65)$$

Now the time dependence due to the shift in energy by the applied voltages is explicitly pulled out such that

$$\hat{c}_1(t) = \tilde{c}_1(t) e^{-i(-e)V_1 t}, \quad (8.66a)$$

$$\hat{c}_2(t) = \tilde{c}_2(t) e^{-i(-e)V_2 t}, \quad (8.66b)$$

with the time dependence of \tilde{c} being given by the Hamiltonian with a common chemical potential μ . Furthermore, we are of course allowed to choose a basis set where the Green's

²This is in fact not true for superconductors which are characterized by having a spontaneous breaking of the symmetry corresponding to the conservation of particles and therefore such two-particle tunnel processes are allowed and give rise to the so-called Josephson current.

function of the decoupled system (i.e. without H_{12}) is diagonal, $G_{\nu\nu'}^> = \delta_{\nu\nu'} G_{\nu}^>$. The particle current then becomes (after change of variable $t' \rightarrow t' + t$)

$$I_p = 2 \operatorname{Re} \int_{-\infty}^0 dt' \sum_{\nu\mu} |T_{\nu\mu}|^2 e^{i(-e)(V_1 - V_2)t'} [G_1^>(\nu; -t') G_2^<(\mu; t') - G_1^<(\nu; -t') G_2^>(\mu; t')]. \quad (8.67)$$

After Fourier transformation (and reinsertion of the convergence factor $e^{\eta t'}$) this expression becomes

$$I_p = \int_{-\infty}^{\infty} \frac{d\omega}{2\pi} \sum_{\nu\mu} |T_{\nu\mu}|^2 [G_1^>(\nu; \omega) G_2^<(\mu; \omega + eV) - G_1^<(\nu; \omega) G_2^>(\mu; \omega + eV)], \quad (8.68)$$

with the voltage given by $V = V_2 - V_1$. The lesser and greater Green's functions are now written in terms of the spectral function, see Eq. (8.50), and we finally arrive at

$$I_p = \int_{-\infty}^{\infty} \frac{d\omega}{2\pi} \sum_{\nu\mu} |T_{\nu\mu}|^2 A_1(\nu, \omega) A_2(\mu, \omega + eV) [n_F(\omega + eV) - n_F(\omega)]. \quad (8.69)$$

In Eq. (8.69) we see that the current is determined by two factors: the availability of states, given by the difference of occupation functions, and by the density of states at a given energy. Therefore by sweeping the voltage across the junction one gets information about $A(\nu, \omega)$. This is a widely used spectroscopic principle in for example the study of superconductors where it was used to verify the famous prediction of the BCS theory of superconductivity that there is an excitation gap in the superconductor, and that the density of states peaks near the gap, see Exercise 4.3 and Exercise 7.5. Also it is used to study small structures such as quantum dots where the individual quantum levels become visible due to size quantization.

The tunnel spectroscopy technique amounts to a sweep of an external voltage which controls the chemical potential while measuring the differential conductance dI/dV . If the other material is a simple material where one can assume the density of states to be more or less constant, i.e.

$$\sum_{\mu} |T_{\nu\mu}|^2 A_2(\mu, \omega + eV) \approx \text{const.} \quad (8.70)$$

then

$$\frac{dI}{dV} \propto \int_{-\infty}^{\infty} d\omega \left(-\frac{\partial n_F(\omega + eV)}{\partial \omega} \right) \sum_{\nu} A_1(\nu, \omega). \quad (8.71)$$

At low temperatures where the derivative of the Fermi function tends to a delta function and (8.71) becomes

$$\frac{dI}{dV} \propto \sum_{\nu} A_1(\nu, -eV). \quad (8.72)$$

So the spectral function can in fact be measured in a rather direct way, which is illustrated in Fig. 8.2.

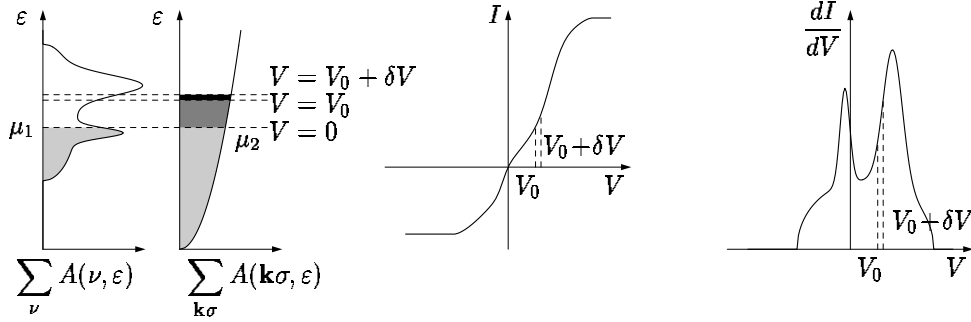


Figure 8.2: The principle used in tunneling spectroscopy. The left panel shows the two density of states in the two materials. The right one is metal, where there is little variations with energy and the experiment can therefore be used to get information about the density of states of the left material. The two right most panels show the resulting current and the differential conductance trace. It is seen how the differential conductance is a direct measure of $\sum_{\nu} A_1(\nu, \omega)$.

8.4.2 Optical spectroscopy

While the response to an electromagnetic field in principle is always given by the dielectric function, which was shown in Chap. 6, there are cases where it is well approximated by the one-particle spectral function. Such an example is photo emission spectroscopy.

8.5 Two-particle correlation functions of many-body systems

While the single-particle Green's functions defined above measure the properties of individual particles the higher order Green's functions give the response of the quantum system to processes involving several particles. One important type of higher order Green's functions are the correlation functions, which was encountered in the linear response chapter. For example, we saw that the response to electromagnetic radiation was determined by the auto correlation function of the charge and current densities. Typical correlation functions that we will meet are of the type

$$C_{AA}(t, t') = -i\theta(t - t') \langle [A(t), A(t')] \rangle, \quad (8.73)$$

where A is some two particle operator.

In order to treat a specific case, we evaluate the polarization function $\chi = C_{\rho\rho}$ for a non-interacting electron gas (see Eq. (6.39)). This function gives for example information about the dissipation due to an applied field, because the dissipation, which is the real part of the conductivity³, is according to Eq. (6.48) given by (take for simplicity the

³Because the power dissipated at any given point in space and time is $P(\mathbf{r}, t) = \mathbf{J}_e(\mathbf{r}, t) \cdot \mathbf{E}(\mathbf{r}, t)$, the

translation-invariant case)

$$\operatorname{Re} \sigma(\mathbf{q}, \omega) = -\frac{\omega e^2}{q^2} \operatorname{Im} \chi^R(\mathbf{q}, \omega). \quad (8.74)$$

In momentum space the polarization is given by

$$\begin{aligned} \chi^R(\mathbf{q}, t - t') &= \int d\mathbf{r} \chi(\mathbf{r} - \mathbf{r}', t - t') e^{-i\mathbf{q} \cdot (\mathbf{r} - \mathbf{r}')}, \\ &= -i\theta(t - t') \int d\mathbf{r} \langle [\rho(\mathbf{r}, t), \rho(\mathbf{r}', t')] \rangle e^{-i\mathbf{q} \cdot (\mathbf{r} - \mathbf{r}')}, \\ &= -i\theta(t - t') \int d\mathbf{r} \frac{1}{V^2} \sum_{\mathbf{q}_1 \mathbf{q}_2} \langle [\rho(\mathbf{q}_1, t), \rho(\mathbf{q}_2, t')] \rangle e^{i\mathbf{q}_1 \cdot \mathbf{r} + i\mathbf{q}_2 \cdot \mathbf{r}'} e^{-i\mathbf{q} \cdot (\mathbf{r} - \mathbf{r}')}, \\ &= -i\theta(t - t') \frac{1}{V} \sum_{\mathbf{q}_2} \langle [\rho(\mathbf{q}, t), \rho(\mathbf{q}_2, t')] \rangle e^{i(\mathbf{q}_2 + \mathbf{q}) \cdot \mathbf{r}'}. \end{aligned} \quad (8.75)$$

Due to the translation-invariance the result cannot depend on \mathbf{r}' and one sees that $\mathbf{q}_2 = -\mathbf{q}$ (or formally one can integrate over \mathbf{r}' and divide by volume to get a delta function, $\delta_{\mathbf{q}_2 + \mathbf{q}, 0}$) and thus

$$\chi^R(\mathbf{q}, t - t') = -i\theta(t - t') e^2 \frac{1}{V} \langle [\rho(\mathbf{q}, t), \rho(-\mathbf{q}, t')] \rangle. \quad (8.76)$$

The Fourier transform of the charge operator was derived in Eq. (1.96)

$$\rho(\mathbf{q}) = \sum_{\mathbf{k}\sigma} c_{\mathbf{k}\sigma}^\dagger c_{\mathbf{k}+\mathbf{q}\sigma}. \quad (8.77)$$

For free electrons, the time dependence is given by (see Eq. (8.37))

$$\rho(\mathbf{q}, t) = \sum_{\mathbf{k}\sigma} c_{\mathbf{k}\sigma}^\dagger c_{\mathbf{k}+\mathbf{q}\sigma} e^{i(\xi_{\mathbf{k}} - \xi_{\mathbf{k}+\mathbf{q}})t}, \quad (8.78)$$

which, when inserted into (8.76), yields

$$\chi_0^R(\mathbf{q}, t - t') = -i\theta(t - t') e^2 \frac{1}{V} \sum_{\mathbf{k}\mathbf{k}'\sigma\sigma'} \langle [c_{\mathbf{k}\sigma}^\dagger c_{\mathbf{k}+\mathbf{q}\sigma}, c_{\mathbf{k}'\sigma'}^\dagger c_{\mathbf{k}'-\mathbf{q}'\sigma'}] \rangle e^{i(\xi_{\mathbf{k}} - \xi_{\mathbf{k}+\mathbf{q}})t} e^{i(\xi_{\mathbf{k}'} - \xi_{\mathbf{k}'-\mathbf{q}})t'}, \quad (8.79)$$

where the subindex “0” indicates that we are using the free electron approximation. The commutator is easily evaluated using the formula, $[c_\nu^\dagger c_\mu, c_{\nu'}^\dagger c_{\mu'}] = c_\nu^\dagger c_{\mu'} \delta_{\mu, \nu'} - c_{\nu'}^\dagger c_\mu \delta_{\nu', \mu'}$, and we find

$$\chi_0^R(\mathbf{q}, t - t') = -i\theta(t - t') e^2 \frac{1}{V} \sum_{\mathbf{k}\sigma} [n_F(\xi_{\mathbf{k}}) - n_F(\xi_{\mathbf{k}+\mathbf{q}})] e^{i(\xi_{\mathbf{k}} - \xi_{\mathbf{k}+\mathbf{q}})(t - t')}, \quad (8.80)$$

total energy being dissipated is

$$W = \int d\mathbf{r} dt \mathbf{E}(\mathbf{r}, t) \cdot \mathbf{J}_e(\mathbf{r}, t) = \int \frac{d\omega}{2\pi} \frac{1}{V} \sum_{\mathbf{q}} \mathbf{E}^*(\mathbf{q}, \omega) \cdot \mathbf{J}_e(\mathbf{q}, \omega) = \int \frac{d\omega}{2\pi} \frac{1}{V} \sum_{\mathbf{q}} |\mathbf{E}(\mathbf{q}, \omega)|^2 \sigma(\mathbf{q}, \omega)$$

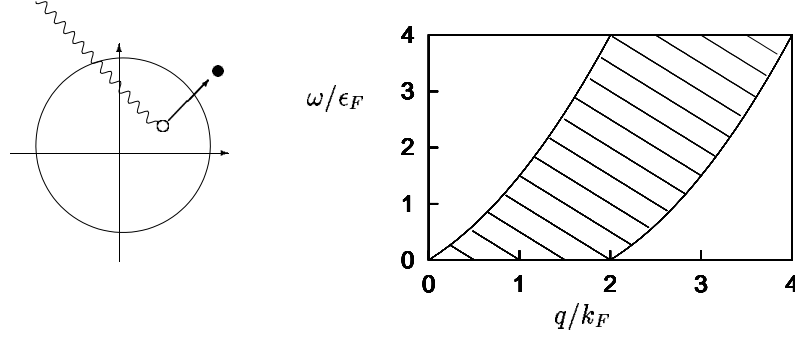


Figure 8.3: Absorption of a photon creates an electron-hole pair excitation in the free electron gas. The possible range of q and ω is given by the dashed area in the right plot. The strength of the interaction depends on the imaginary part of the polarization function, see Eq. (8.82)

because $\langle c_k^\dagger c_k \rangle = n_F(\xi_k)$. In the frequency space, we find

$$\begin{aligned}\chi_0^R(\mathbf{q}, \omega) &= -i \int_{t'}^{\infty} dt e^{i\omega t} \frac{1}{\mathcal{V}} \sum_{\mathbf{k}\sigma} [n_F(\xi_{\mathbf{k}}) - n_F(\xi_{\mathbf{k}+\mathbf{q}})] e^{i(\xi_{\mathbf{k}} - \xi_{\mathbf{k}+\mathbf{q}})(t-t')} e^{-\eta(t-t')}, \\ &= \frac{1}{\mathcal{V}} \sum_{\mathbf{k}\sigma} \frac{n_F(\xi_{\mathbf{k}}) - n_F(\xi_{\mathbf{k}+\mathbf{q}})}{\xi_{\mathbf{k}} - \xi_{\mathbf{k}+\mathbf{q}} + \omega + i\eta}.\end{aligned}\quad (8.81)$$

This function is known as the Lindhard function, and later on, when discussing the elementary excitations of the electron gas, we will study it in much more detail.

Within the non-interacting approximation and according to Eq. (8.74) we then have that the dissipation of the electron gas is proportional to

$$-\text{Im} \chi^R(\mathbf{q}, \omega) = \frac{\pi}{\mathcal{V}} \sum_{\mathbf{k}\sigma} [n_F(\xi_{\mathbf{k}}) - n_F(\xi_{\mathbf{k}+\mathbf{q}})] \delta(\xi_{\mathbf{k}} - \xi_{\mathbf{k}+\mathbf{q}} + \omega). \quad (8.82)$$

We can now analyze for what \mathbf{q} and ω excitations are possible, i.e. for which (\mathbf{q}, ω) Eq. (8.82) is non-zero. Let us take $T = 0$ where n_F is either zero or one, which means that $n_F(\xi_{\mathbf{k}}) - n_F(\xi_{\mathbf{k}+\mathbf{q}})$ is only non-zero if $(k > k_F \text{ and } |\mathbf{k} + \mathbf{q}| < k_F)$ or $(k < k_F \text{ and } |\mathbf{k} + \mathbf{q}| > k_F)$. The first case corresponds to $\omega < 0$, while the latter corresponds to $\omega > 0$. However, because of the symmetry $\chi_0^R(\mathbf{q}, \omega) = -\chi_0^R(-\mathbf{q}, -\omega)$, which is easily seen from Eq. (8.81), we need only study one case, for example $\omega > 0$. The delta function together with the second condition thus imply

$$0 < \omega = q^2 \frac{1}{2m} + \mathbf{k} \cdot \mathbf{q} \frac{1}{m} \Rightarrow \begin{cases} \omega_{\max} = \frac{1}{2m} q^2 + v_F q \\ \omega_{\min} = \frac{1}{2m} q^2 - v_F q \end{cases}, \quad q > 2k_F. \quad (8.83)$$

The possible range of excitations in (\mathbf{q}, ω) -space is shown in Fig.8.3. The excitations which give rise to the dissipation are electron-hole pair excitations, where an electron within the Fermi sea is excited to a state outside the Fermi sea. There is a continuum of such excitations given by conditions in (8.83).

While the electron-hole pair excitations are the only possible source of dissipation in the non-interacting electron gas, this is certainly not true for the interacting case which is more complicated. There is one particular type of excitation which is immensely important, namely the plasmon excitation. This we study in great detail later in this course.

The excitation of the electrons gas can be measured by for example inelastic light scattering (Raman scattering), where the change of momentum and energy of an incoming photon is measured. The process discussed here where an electron within the Fermi sea is scattering to an empty state outside the Fermi sea, is illustrated in the hand side of Fig. 8.3.

8.6 Summary and outlook

The concept of Green's functions in many-body physics has been introduced in this chapters, and we will use Green's functions in practically all discussions in the remaining part of the course. The Green's functions describe the dynamical properties of excitations. We have so far seen two examples of this: the density of states is related to the spectral function and it can be measured for example in a tunneling experiment, and secondly the absorption of electromagnetic radiation is given by the charge-charge correlation function.

The physical picture to remember is that the Green's function $G(\mathbf{r}\sigma t, \mathbf{r}'\sigma't')$ gives the amplitude for propagation from the space-time point $\mathbf{r}'t'$ to $\mathbf{r}t$, with initial spin σ' and final spin σ .

In this chapter we have defined the following many-body Green's functions

$$\begin{aligned} G^R(\mathbf{r}\sigma t, \mathbf{r}'\sigma't') &= -i\theta(t-t') \langle [\Psi_\sigma(\mathbf{r}t), \Psi_{\sigma'}^\dagger(\mathbf{r}'t')]_{B,F} \rangle && \text{retarded Green's function} \\ G^>(\mathbf{r}\sigma t, \sigma'\mathbf{r}'t') &= -i\langle \Psi_\sigma(\mathbf{r}t) \Psi_{\sigma'}^\dagger(\mathbf{r}'t') \rangle && \text{greater Green's function} \\ G^<(\mathbf{r}\sigma t, \sigma'\mathbf{r}'t') &= -i(\pm 1) \langle \Psi_{\sigma'}^\dagger(\mathbf{r}'t') \Psi_\sigma(\mathbf{r}t) \rangle && \text{lesser Green's function} \end{aligned}$$

and their corresponding Fourier transforms. The important spectral function is in the frequency domain and in a diagonal basis given by

$$A(\nu, \omega) = -2 \text{Im} G^R(\nu, \omega) \quad \text{spectral function}$$

The spectral function is related to the density of states. For non-interacting electrons the spectral function is given by a Dirac delta function

$$A_0(\nu, \omega) = 2\pi\delta(\xi_\nu - \omega) \quad \text{non-interacting case}$$

Chapter 9

Equation of motion theory

In the previous chapters we saw how various physical observables can be expressed in terms of retarded Green's functions and correlation functions. In many cases we need to calculate the time-dependence of these functions. There are several ways of attacking this problem, one of which is the equation of motion technique. The basic idea of this method is to generate a series of coupled differential equations by differentiating the correlation function at hand a number of times. If these equations close the problem is in principle solvable, and if not, one needs to invoke physical arguments to truncate the set of equations in a reasonable fashion. For example one can neglect certain correlations. We shall study examples of both situations in this chapter.

9.1 The single-particle Green's function

Let us consider the retarded Green's function G^R for either fermions or bosons, Eq. (8.28)

$$G^R(\mathbf{r}t, \mathbf{r}'t') = -i\theta(t - t') \langle [\Psi(\mathbf{r}t), \Psi^\dagger(\mathbf{r}'t')]_{B,F} \rangle. \quad (9.1)$$

We find the equation of motion for G^R as the derivative with respect to the first time argument

$$\begin{aligned} i\partial_t G^R(\mathbf{r}t, \mathbf{r}'t') &= (-i) (i\partial_t \theta(t - t')) \langle [\Psi(\mathbf{r}t), \Psi^\dagger(\mathbf{r}'t')]_{B,F} \rangle \\ &\quad + (-i) \theta(t - t') \langle [i\partial_t \Psi(\mathbf{r}t), \Psi^\dagger(\mathbf{r}'t')]_{B,F} \rangle, \\ &= \delta(t - t') \delta(\mathbf{r} - \mathbf{r}') + \\ &\quad + (-i) \theta(t - t') \langle [i\partial_t \Psi(\mathbf{r}t), \Psi^\dagger(\mathbf{r}'t')]_{B,F} \rangle. \end{aligned} \quad (9.2)$$

Here we used that the derivative of a step function is a delta function and the commutation relations for field operators at equal times $[\Psi(\mathbf{r}), \Psi^\dagger(\mathbf{r}')]_{B,F} = \delta(\mathbf{r} - \mathbf{r}')$. Next, let us study the time-derivative of the annihilation operator (throughout this chapter we assume that H is time independent)

$$i\partial_t \Psi(\mathbf{r}t) = -[H, \Psi(\mathbf{r})](t) = -[H_0, \Psi(\mathbf{r})](t) - [V_{\text{int}}, \Psi(\mathbf{r})](t), \quad (9.3)$$

where the interaction part of the Hamiltonian includes all the interactions in the given problem, while H_0 describes the quadratic part of the Hamiltonian, for example the kinetic energy. If H_0 is the usual kinetic energy Hamiltonian of free particles, we have

$$\begin{aligned} -[H_0, \Psi(\mathbf{r})] &= \frac{1}{2m} \int d\mathbf{r}' \left[\Psi^\dagger(\mathbf{r}') \nabla_{\mathbf{r}'}^2 \Psi(\mathbf{r}'), \Psi(\mathbf{r}) \right] \\ &= -\frac{1}{2m} \nabla_{\mathbf{r}}^2 \Psi(\mathbf{r}). \end{aligned} \quad (9.4)$$

In this case the equation of motion becomes

$$\left(i\partial_t + \frac{1}{2m} \nabla_{\mathbf{r}}^2 \right) G^R(\mathbf{r}t, \mathbf{r}'t') = \delta(t - t') \delta(\mathbf{r} - \mathbf{r}') + D^R(\mathbf{r}t, \mathbf{r}'t'), \quad (9.5a)$$

$$D^R(\mathbf{r}t, \mathbf{r}'t') = -i\theta(t - t') \left\langle \left[-[V_{\text{int}}, \Psi(\mathbf{r})](t), \Psi^\dagger(\mathbf{r}'t') \right]_{B,F} \right\rangle. \quad (9.5b)$$

The function D^R thus equals the corrections to the free particle Green's function. After evaluating $[V_{\text{int}}, \Psi(\mathbf{r})]$ we can, as in Sec. 5.5, continue the generation of differential equations. It is now evident why the many-body functions, G^R , are called Green's functions. The equation in (9.5a) has the structure of the classical Green's function we saw in Sec. 8.1, where the Green's function of a differential operator, L , was defined as $LG = \text{delta function}$.

Often it is convenient to work in some other basis, say $\{\nu\}$. The Hamiltonian is again written as $H = H_0 + V_{\text{int}}$, where the quadratic part of the Hamiltonian is

$$H_0 = \sum_{\nu\nu'} t_{\nu'\nu} a_{\nu'}^\dagger a_\nu. \quad (9.6)$$

The differential equation for the Green's function in this basis

$$G^R(\nu t, \nu' t') = -i\theta(t - t') \langle [a_\nu(t), a_{\nu'}^\dagger(t')]_{B,F} \rangle \quad (9.7)$$

is found in exactly the same way as above. By differentiation the commutator with H_0 is generated

$$-[H_0, a_\nu] = \sum_{\nu''} t_{\nu\nu''} a_{\nu''}, \quad (9.8)$$

and hence

$$\sum_{\nu''} (i\delta_{\nu\nu''} \partial_t - t_{\nu\nu''}) G^R(\nu'' t, \nu' t') = \delta(t - t') \delta_{\nu\nu'} + D^R(\nu t, \nu' t'), \quad (9.9a)$$

$$D^R(\nu t, \nu' t') = -i\theta(t - t') \left\langle \left[-[V_{\text{int}}, a_\nu](t), a_{\nu'}^\dagger(t') \right]_{B,F} \right\rangle. \quad (9.9b)$$

In this course we will mainly deal with problems where the Hamiltonian does not depend explicitly on time (linear response was an exception, but even there the time dependent problem was transformed into a correlation function of a time independent problem). Therefore the Green's function can only depend on the time difference $t - t'$ and in this case

it is always useful to work with the Fourier transforms. Recalling that when performing the Fourier transformation of the derivative it becomes $\partial_t \rightarrow -i\omega$, and that the Fourier transform of a delta function is unity, $\delta(t) \rightarrow 1$. We can write the equation of motion in frequency domain

$$\sum_{\nu''} [\delta_{\nu\nu''}(\omega + i\eta) - t_{\nu\nu''}] G^R(\nu''\nu'; \omega) = \delta_{\nu\nu'} + D^R(\nu, \nu'; \omega), \quad (9.10a)$$

$$D^R(\nu, \nu'; \omega) = -i \int_{-\infty}^{\infty} dt e^{i(\omega + i\eta)(t-t')} \theta(t-t') \left\langle \left[-[V_{\text{int}}, a_{\nu}](t), a_{\nu'}^{\dagger}(t') \right]_{B,F} \right\rangle. \quad (9.10b)$$

Here it is important to remember that the frequency of the retarded functions must carry a small positive imaginary part, η , to ensure proper convergence.

9.1.1 Non-interacting particles

For non-interacting particles, which means that the Hamiltonian is bilinear in annihilation or creation operators, we can in fact solve for the Green's function¹. In this case we have

$$\sum_{\nu''} (\delta_{\nu\nu''}(\omega + i\eta) - t_{\nu\nu''}) G_0^R(\nu''\nu'; \omega) = \delta_{\nu\nu'} \quad (9.11)$$

where the subindex 0 on G_0^R indicates that it is the Green's function corresponding to a non-interacting Hamiltonian. As in Sec. 8.1 we define the inverse Green's function as

$$(G_0^R)^{-1}(\nu\nu'; \omega) = \delta_{\nu\nu'}(\omega + i\eta) - t_{\nu\nu'} \equiv (\mathbf{G}_0^R)^{-1}_{\nu\nu'} \quad (9.12)$$

and in matrix notation Eq. (9.11) becomes

$$(\mathbf{G}_0^R)^{-1} \mathbf{G}_0^R = \mathbf{1}. \quad (9.13)$$

Therefore, in order to find the Green's function all we need to do is to invert the matrix $(\mathbf{G}_0^R)^{-1}_{\nu\nu'}$. For a diagonal basis, i.e. $t_{\nu\nu'} = \delta_{\nu\nu'} \varepsilon_{\nu}$, the solution is

$$(\mathbf{G}_0^R)_{\nu\nu'} = G_0^R(\nu, \omega) \delta_{\nu\nu'} = \frac{1}{\omega - \varepsilon_{\nu} + i\eta} \delta_{\nu\nu'}, \quad (9.14)$$

which of course agrees with the result found in Eq. (8.51).

9.2 Anderson's model for magnetic impurities

In order to exemplify the usefulness of the equation of motion technique, we proceed by solving a famous model for the appearance of a magnetic moment of impurities of certain

¹Here we only consider terms of the form $c^{\dagger}c$ but also anomalous terms like cc could be included. In Chap. 4 we saw that such a term is indeed relevant for superconductors. For the Green's function in a superconductor we should therefore solve the linear problem in a way similar to the Bogoliubov transformation introduced in Chap. 4. We return to this in Chap. 15.

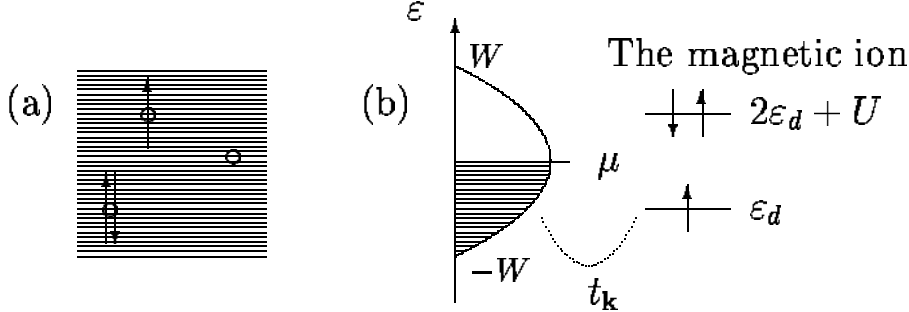


Figure 9.1: The Anderson model describing magnetic impurities embedded in a homogeneous host metal. The electrons in the conduction band of the non-magnetic host metal, indicated by the dashed areas, couple to the level of the magnetic impurity ion. The bare onsite energy of the state on the magnetic ion is ϵ_d . But the energy of electrons residing on the impurity ion also depends on whether it is doubly occupied or not, therefore the state with two electrons residing on the ion has energy $2\epsilon_d + U$, as seen in (b).

magnetic ions embedded in a non-magnetic host metal. The host metal, e.g. Nb or Mo, has a conduction band, which can be described by an effective non-interacting model

$$H_c = \sum_{\mathbf{k}\sigma} (\epsilon_{\mathbf{k}} - \mu) c_{\mathbf{k}\sigma}^\dagger c_{\mathbf{k}\sigma}. \quad (9.15)$$

For the impurity ion we assume that it has only one spin-degenerate state in the active shell, which is typically the d shell. In addition to the bare energy cost for an electron to reside in the d -state, there is an interaction energy that depends on the state being doubly occupied or not. The impurity ion Hamiltonian is thus modelled as

$$H_d + H_U = \sum_{\sigma} (\epsilon_d - \mu) c_{d\sigma}^\dagger c_{d\sigma} + U n_{d\uparrow} n_{d\downarrow}. \quad (9.16)$$

where $n_{d\sigma} = c_{d\sigma}^\dagger c_{d\sigma}$ is the number operator for d -electrons. The crucial input is here the correlation between electrons on the impurity ion, because the interaction in the narrower d -shell of a magnetic ion is particularly strong and this is in fact the reason for the magnetism. The states forming the conduction band are primarily s -states that are more extended in space, and hence interactions are less important for those.

The electrons occupying the conduction band couple to the outer-most electrons of the magnetic impurity ions, e.g. the d -shell of a Fe ion. The coupling occurs because the d -orbital and the conduction band states overlap spatially and also lie close in energy, giving rise to a “hybridization” between the two. The overlapping orbitals leads to a non-diagonal matrix element of the Hamiltonian

$$H_{\text{hyb}} = \sum_{\mathbf{k}\sigma} t_{\mathbf{k}} c_{d\sigma}^\dagger c_{\mathbf{k}\sigma} + \sum_{\mathbf{k}\sigma} t_{\mathbf{k}}^* c_{\mathbf{k}\sigma}^\dagger c_{d\sigma}. \quad (9.17)$$

The bare d -electron energy, ε_d , is below the chemical potential and from the kinetic energy point of view, it is favorable to fill the orbital by two electrons. However, this costs potential energy, U , and it is not possible if $2\varepsilon_d + U > 2\mu$. Furthermore, the system gains further kinetic energy by the hybridization, which on the other hand is complicated by the fact that the hopping in and out of the impurity orbital with, say, spin up electrons depends on the occupation of spin down electrons. The hybridization therefore seems to randomize the spin on the magnetic ion. The sum of these three energy contributions

$$H = H_c + H_d + H_U + H_{\text{hyb}} \quad (9.18)$$

is known as the Anderson model. See Fig. 9.1 for an illustration. Although the Anderson model looks simple, its full solution is very complicated and in fact the model has a very rich phase diagram. The Anderson model has been used to describe numerous effects in the physics of strongly correlated electron systems.²

It turns out that for certain values of the parameters it is energetically favorable for the system to have a magnetic moment (and thus minimizing the on-site interaction energy) while for other values there is no magnetic moment (thus gaining maximum hybridization energy). The physical question we try to answer here is: Under which circumstances is the material magnetic?

9.2.1 The equation of motion for the Anderson model

The magnetization in the z -direction is given by the expectation value of the difference $n_{\uparrow} - n_{\downarrow}$ between spin up and down occupancy. The occupation of a quantum state was found in Eq. (8.57) in terms of the spectral function. For the d -electron occupation we therefore have

$$n_{d\sigma} = \int \frac{d\omega}{2\pi} n_F(\omega) A(d\sigma, \omega), \quad (9.19)$$

where $A(d\sigma, \omega)$ is the spectral function, which follows from the retarded Green's function, G^R , see Eq. (8.49). All we need to find is then

$$G^R(d\sigma; t - t') = -i\theta(t - t') \langle \{c_{d\sigma}(t), c_{d\sigma}^\dagger(t')\} \rangle. \quad (9.20)$$

Let us write the equation of motion of this function using Eq. (9.10). Due to the hybridization term the Hamiltonian is not diagonal in the d -operators and the equations of motion will involve another Green's function, namely

$$G^R(\mathbf{k}\sigma, d\sigma, t - t') = -i\theta(t - t') \langle \{c_{\mathbf{k}\sigma}(t), c_{d\sigma}^\dagger(t')\} \rangle. \quad (9.21)$$

The equation of motion are thus found by letting ν'' in Eq. (9.10) run over both d and k and we obtain the coupled equations

$$(\omega + i\eta - \varepsilon_d + \mu) G^R(d\sigma, \omega) - \sum_{\mathbf{k}} t_{\mathbf{k}} G^R(\mathbf{k}\sigma, d\sigma, \omega) = 1 + U D^R(d\sigma, \omega), \quad (9.22)$$

$$(\omega + i\eta - \varepsilon_{\mathbf{k}} + \mu) G^R(\mathbf{k}\sigma, d\sigma, \omega) - t_{\mathbf{k}}^* G^R(d\sigma, \omega) = 0, \quad (9.23)$$

²The model in fact has a known exact solution, but the solution fills an entire book, and it is hard to extract useful physical information from this solution.

where

$$D^R(d\sigma, \omega) = -i \int_{-\infty}^{\infty} dt e^{i(\omega+i\eta)(t-t')} \theta(t-t') \left\langle \left\{ -[n_{d\uparrow} n_{d\downarrow}, c_{d\sigma}](t), c_{d\sigma}^\dagger(t') \right\} \right\rangle. \quad (9.24)$$

The commutator in this expression is for $\sigma = \uparrow$

$$[n_{d\uparrow} n_{d\downarrow}, c_{d\uparrow}] = n_{d\downarrow} [n_{d\uparrow}, c_{d\uparrow}] = -U n_{d\downarrow} c_{d\uparrow}, \quad (9.25)$$

and likewise we find the commutator for spin down by interchanging up and down. We thus face the following more complicated Green's function

$$D^R(d\uparrow, t-t') = -i\theta(t-t') \langle \{n_{d\downarrow}(t) c_{d\uparrow}(t), c_{d\uparrow}^\dagger(t')\} \rangle. \quad (9.26)$$

9.2.2 Mean-field approximation for the Anderson model

Differentiating the function in Eq. (9.26) with respect to time would generate yet another function $\langle \{[H, n_{d\downarrow}(t) d_\uparrow(t)], d_\uparrow^\dagger(t')\} \rangle$ to be determined, and the set of equations does not close. However a mean-field approximation still grasps the important physics that the spin-up electron population depends on the spin-down population, therefore we replace the interaction part H_U by its mean-field version

$$H_U^{MF} = U \langle n_{d\uparrow} \rangle n_{d\downarrow} + U \langle n_{d\downarrow} \rangle n_{d\uparrow} - U \langle n_{d\uparrow} \rangle \langle n_{d\downarrow} \rangle. \quad (9.27)$$

With this truncation, the function D^R becomes

$$D^R(d\uparrow, t-t') = -i\theta(t-t') \langle n_{d\downarrow} \rangle \langle \{c_{d\uparrow}(t), c_{d\uparrow}^\dagger(t')\} \rangle = \langle n_{d\downarrow} \rangle G^R(d\uparrow, t-t'). \quad (9.28)$$

In other words, since the mean-field approximation makes the Hamiltonian quadratic we can include $U \langle n_{d\downarrow} \rangle$ to the energy of the spin-up d -electrons in our equation of motion. Inserting (9.28) in Eq. (9.22), and solving Eq. (9.23) for $G^R(d\uparrow, \omega)$ gives

$$(\omega + i\eta - \varepsilon_d + \mu - U \langle n_{d\downarrow} \rangle) G^R(d\uparrow, \omega) - \sum_{\mathbf{k}} \frac{|t_{\mathbf{k}}|^2}{\omega - \varepsilon_{\mathbf{k}} + \mu + i\eta} G^R(d\uparrow, \omega) = 1, \quad (9.29)$$

and likewise for the spin-down Green's function. The final answer is

$$G^R(d\uparrow, \omega) = \frac{1}{\omega - \varepsilon_d + \mu - U \langle n_{d\downarrow} \rangle - \Sigma^R(\omega)}, \quad (9.30a)$$

$$\Sigma^R(\omega) = \sum_{\mathbf{k}} \frac{|t_{\mathbf{k}}|^2}{\omega - \varepsilon_{\mathbf{k}} + \mu + i\eta}. \quad (9.30b)$$

The function $\Sigma^R(\omega)$ is our first encounter with the concept known as “self-energy”. The self-energy changes the pole of G^R and furthermore gives some broadening to the spectral function. Due to this term the “bare” d -electron energy, ε_d , is seen to be renormalized by two effects: first the energy is shifted by $U \langle n_{d\downarrow} \rangle$ due to the interaction with the averaged density of electrons having opposite spin, and secondly, the coupling to the conduction band electrons gives through $\Sigma(\omega)$ an energy shift and most importantly an imaginary part. In the time domain the imaginary part translates into a life-time. It arises because the coupling to the c -electrons introduces off diagonal terms in the Hamiltonian, so that it is no longer diagonal in the d -operators. The diagonal modes are instead superpositions of c - and d -states.

9.2.3 Solving the Anderson model and comparison with experiments

Assuming that the coupling $t_{\mathbf{k}}$ only depends on the length of \mathbf{k} and thus on ε , the self-energy Σ is

$$\Sigma^R(\omega) = \int d\varepsilon d(\varepsilon) \frac{|t(\varepsilon)|^2}{\omega - \varepsilon + \mu + i\eta} = \mathcal{P} \int d\varepsilon d(\varepsilon) \frac{|t(\varepsilon)|^2}{\omega - \varepsilon + \mu} - i\pi d(\omega + \mu) |t(\omega + \mu)|^2. \quad (9.31)$$

The density of states $d(\varepsilon)$ and the coupling matrix element $t(\varepsilon)$ depend on the details of the material, but fortunately it is not important for the present considerations. Let us assume that the product $d(\varepsilon)|t(\varepsilon)|^2$ is constant within the band limits, $-W < \varepsilon < W$, and define the important parameter Γ by

$$\pi d(\varepsilon) |t(\varepsilon)|^2 = \Gamma \theta(W - |\varepsilon|). \quad (9.32)$$

This approximation is good if the width of the Green's function (which we shall see shortly is given by Γ) turns out to be small compared to the scale on which $d(\varepsilon)|t(\varepsilon)|^2$ typically changes. Since in practice $\Gamma \ll \varepsilon_F$, the approximation is indeed valid. For $\omega + \mu \in [-W, W]$ we get

$$\begin{aligned} \Sigma^R(\omega) &\approx \frac{\Gamma}{\pi} \int_{-W}^W \frac{d\varepsilon}{\omega - \varepsilon + \mu} - i\Gamma \\ &= -\frac{\Gamma}{\pi} \ln \left| \frac{W + \omega + \mu}{W - \omega - \mu} \right| - i\Gamma, \quad -W < \omega + \mu < W. \end{aligned} \quad (9.33)$$

The real part gives a shift of energy and since it is a slowly varying function, we simply include it as a shift of ε and define the new onsite energy $\tilde{\varepsilon} = \varepsilon + \text{Re } \Sigma^R$.

The spectral function hence becomes

$$\begin{aligned} A(d \uparrow, \omega) &= -2 \text{Im } G^R(d \uparrow, \omega) \\ &= \frac{2\Gamma}{(\omega - \tilde{\varepsilon} + \mu - U \langle n_{d\downarrow} \rangle)^2 + \Gamma^2} \theta(W - |\varepsilon|), \end{aligned} \quad (9.34)$$

where Γ is the width of the spectral function. Note that the spectral function derived here is an example of the Lorentzian form discussed in Sec. 8.3.5.

Now the self-consistent mean-field equation for $\langle n_{d\uparrow} \rangle$ follows as

$$\begin{aligned} \langle n_{d\uparrow} \rangle &= \int \frac{d\omega}{2\pi} n_F(\omega) A(d \uparrow, \omega) \\ &= \int_{-W}^W \frac{d\omega}{2\pi} n_F(\omega) \frac{2\Gamma}{(\omega - \tilde{\varepsilon} + \mu - U \langle n_{d\downarrow} \rangle)^2 + \Gamma^2}. \end{aligned} \quad (9.35)$$

If we neglect the finite bandwidth, which is justified because $\Gamma \ll W$, and if we furthermore consider low temperatures, $T = 0$, we get

$$\begin{aligned} \langle n_{d\uparrow} \rangle &\approx \int_{-\infty}^0 \frac{d\omega}{2\pi} \frac{2\Gamma}{(\omega - \tilde{\varepsilon} + \mu - U \langle n_{d\downarrow} \rangle)^2 + \Gamma^2}, \\ &= \frac{1}{2} - \frac{1}{\pi} \tan^{-1} \left(\frac{\tilde{\varepsilon} - \mu + U \langle n_{d\downarrow} \rangle}{\Gamma} \right). \end{aligned} \quad (9.36)$$

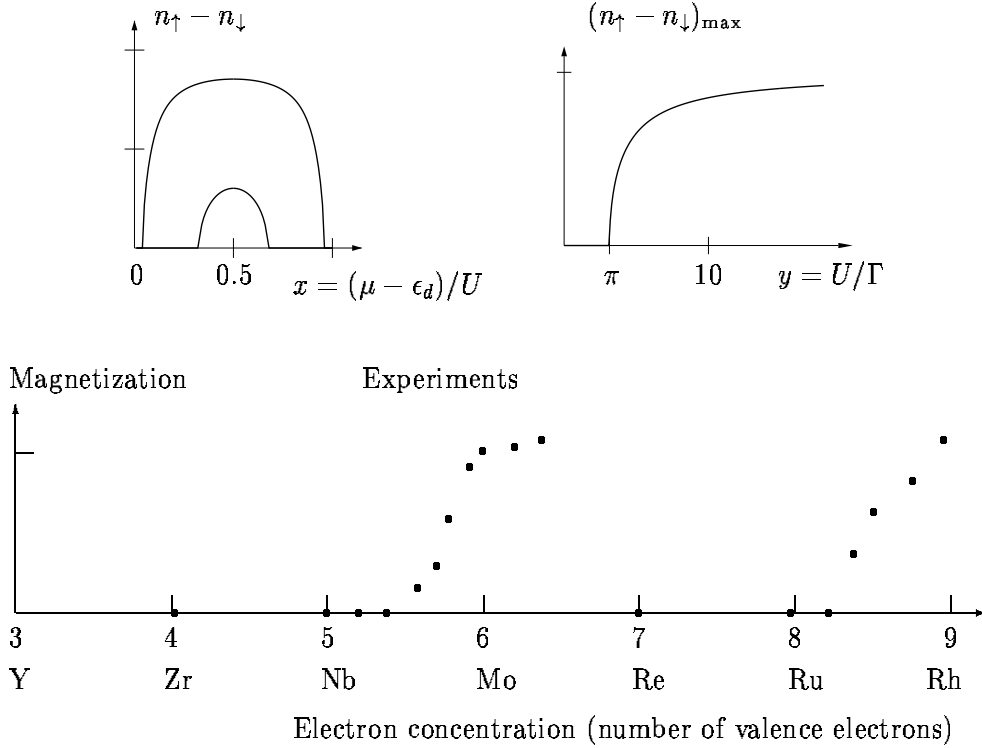


Figure 9.2: The upper part shows the mean field solution of the Anderson model with the left panel being magnetization as a function of electron density n_{el} , i.e. the chemical potential, for two different Γ -values, while the right panel is the maximum magnetization as function of the correlation energy. We see that there is a critical density and a critical U/Γ where the magnetization sets in. The latter means that too strong hybridization destroys the magnetization. The bottom panel shows experimental results (Clogston et al. (1962)) for the magnetic moment of Fe embedded in transition metals. The electron concentration and hence μ is varied by changing the alloy. For $4 < n_{\text{el}} < 8$ the magnetization curve is seen to be quite similar to the prediction of the model. For $n_{\text{el}} > 8$ the effect of having more than two d -orbitals in the Fe-atoms becomes important and the simple model is no longer adequate.

We obtain the two coupled equations

$$\cot(\pi n_{\uparrow}) = y(n_{\downarrow} - x), \quad x = -(\tilde{\varepsilon} - \mu)/U, \quad (9.37a)$$

$$\cot(\pi n_{\downarrow}) = y(n_{\uparrow} - x), \quad y = U/\Gamma. \quad (9.37b)$$

The solution of these equation gives the occupation of the d -orbital and in particular tells us whether there is a finite magnetization, i.e. whether there exists a solution $n_{\downarrow} \neq n_{\uparrow}$, different from the trivial solution $n_{\downarrow} = n_{\uparrow}$.³ In Fig. 9.2 solutions of these equations are shown together with experimental data. As is evident there, the model describes the observed behavior, at least qualitatively.

9.2.4 Coulomb blockade and the Anderson model

Above we applied the mean-field approximation to the interaction. This means that the energy of a given spin direction is only affected by the average occupation of the opposite spin direction. In an experiment where one probes the actual occupation of the atom this approach would not be sufficient. Such an experiment is for example a tunneling experiment where current is passed through a single atom or a small metallic island which can be thought of as an artificial atom. For the electron that wants to enter the island it does matter whether the island is already occupied, because, if it is, the tunneling barrier is increased by U . To capture this physics one must go one step beyond the mean-field approximation and truncate the equations of motion at a later stage. This is the topic for Exercise 8.4. See also Exercise 8.3.

9.2.5 Further correlations in the Anderson model: Kondo effect

9.3 The two-particle correlation function

The two particle correlation functions, such as the density-density correlation, was in Chap. 6 shown to give the linear response properties. Also for this quantity one can generate a set of equation of motions, and as for the single particle Green's function they are not solvable in general. But even so they may provide a good starting point for various approximation schemes.

Consider for example the retarded charge-charge correlation function

$$\chi^R(\mathbf{r}t, \mathbf{r}'t') = -i\theta(t - t') \langle [\rho(\mathbf{r}t), \rho(\mathbf{r}'t')] \rangle. \quad (9.38)$$

In Chap. 6 it was shown that this function is related to the dielectric response function and therefore tells about the screening properties of the material.

9.3.1 The Random Phase Approximation (RPA)

A commonly used approximation scheme for correlation functions is the so-called Random Phase Approximation (RPA). For the case of the electron gas, which is one of our

³We should also convince ourselves that the magnetic solution has lower energy, which it in fact does have.

main topics in this course, RPA is exact in some limits, but also in general gives a decent description of the interacting electron gas. In Chap.12 RPA is derived using Feynman diagrams, but here we derive it using the equation of motion technique. The two derivations give complementary insight into the physical content of the approximation.

We will for simplicity work with the translation-invariant electron gas with the Hamiltonian given by the usual kinetic energy plus interaction energy (here we disregard the spin degree of freedom because it is not important)

$$H = \sum_{\mathbf{k}} \xi_{\mathbf{k}} c_{\mathbf{k}}^{\dagger} c_{\mathbf{k}} + \frac{1}{2} \sum_{\mathbf{k}\mathbf{k}'\mathbf{q} \neq 0} V(\mathbf{q}) c_{\mathbf{k}+\mathbf{q}}^{\dagger} c_{\mathbf{k}-\mathbf{q}}^{\dagger} c_{\mathbf{k}'} c_{\mathbf{k}} = H_0 + V_{\text{int}}. \quad (9.39)$$

Furthermore, the $\mathbf{q} = \mathbf{0}$ component is cancelled by the positively charged background.

The charge-charge correlation function is

$$\chi^R(\mathbf{q}, t - t') = -i\theta(t - t') \frac{1}{\mathcal{V}} \langle [\rho(\mathbf{q}, t), \rho(-\mathbf{q}, t')] \rangle, \quad \rho(\mathbf{q}) = \sum_{\mathbf{k}} c_{\mathbf{k}}^{\dagger} c_{\mathbf{k}+\mathbf{q}}. \quad (9.40)$$

However, it turns out to be better to work with the function

$$\chi^R(\mathbf{k}\mathbf{q}, t - t') = -i\theta(t - t') \langle [(c_{\mathbf{k}}^{\dagger} c_{\mathbf{k}+\mathbf{q}})(t), \rho(-\mathbf{q}, t')] \rangle, \quad (9.41)$$

from which we can easily obtain $\chi(\mathbf{q})$ by summing over \mathbf{k} , $\chi^R(\mathbf{q}) = \sum_{\mathbf{k}} \chi^R(\mathbf{k}\mathbf{q})$. Let us find the equation of motion

$$\begin{aligned} i\partial_t \chi^R(\mathbf{k}\mathbf{q}, t - t') &= \delta(t - t') \langle [(c_{\mathbf{k}}^{\dagger} c_{\mathbf{k}+\mathbf{q}})(t), \rho(-\mathbf{q}, t')] \rangle \\ &\quad - i\theta(t - t') \langle [-[H, c_{\mathbf{k}}^{\dagger} c_{\mathbf{k}+\mathbf{q}}](t), \rho(-\mathbf{q}, t')] \rangle, \end{aligned} \quad (9.42)$$

and for this purpose we need the following commutators

$$[c_{\mathbf{k}}^{\dagger} c_{\mathbf{k}+\mathbf{q}}, \rho(-\mathbf{q})] = \sum_{\mathbf{k}'} [c_{\mathbf{k}}^{\dagger} c_{\mathbf{k}+\mathbf{q}}, c_{\mathbf{k}'}^{\dagger} c_{\mathbf{k}'-\mathbf{q}}] = c_{\mathbf{k}}^{\dagger} c_{\mathbf{k}} - c_{\mathbf{k}+\mathbf{q}}^{\dagger} c_{\mathbf{k}+\mathbf{q}}, \quad (9.43)$$

$$[H_0, c_{\mathbf{k}}^{\dagger} c_{\mathbf{k}+\mathbf{q}}] = (\xi_{\mathbf{k}} - \xi_{\mathbf{k}+\mathbf{q}}) c_{\mathbf{k}}^{\dagger} c_{\mathbf{k}+\mathbf{q}}, \quad (9.44)$$

$$\begin{aligned} [V_{\text{int}}, c_{\mathbf{k}}^{\dagger} c_{\mathbf{k}+\mathbf{q}}] &= -\frac{1}{2} \sum_{\mathbf{k}'\mathbf{q}'} V(\mathbf{q}') \left\{ c_{\mathbf{k}+\mathbf{q}'}^{\dagger} c_{\mathbf{k}'-\mathbf{q}'}^{\dagger} c_{\mathbf{k}'} c_{\mathbf{k}+\mathbf{q}} + c_{\mathbf{k}'+\mathbf{q}'}^{\dagger} c_{\mathbf{k}-\mathbf{q}'}^{\dagger} c_{\mathbf{k}+\mathbf{q}} c_{\mathbf{k}'} \right. \\ &\quad \left. - c_{\mathbf{k}'+\mathbf{q}'}^{\dagger} c_{\mathbf{k}}^{\dagger} c_{\mathbf{k}+\mathbf{q}+\mathbf{q}'} c_{\mathbf{k}'} - c_{\mathbf{k}}^{\dagger} c_{\mathbf{k}'-\mathbf{q}'}^{\dagger} c_{\mathbf{k}'} c_{\mathbf{k}+\mathbf{q}-\mathbf{q}'} \right\}. \end{aligned} \quad (9.45)$$

When this is inserted into Eq. (9.42) a new 6-particle Green's function is generated. Furthermore for each level of the equation of motion a Green's function with two more electron operators pops up. At this stage we truncate this series by the random phase approximation which says that the right hand side of (9.45) is replaced by a mean-field expression where pairs of operators are replaced by their average values. Using the recipe from Chap.

4, we get

$$\begin{aligned}
[V_{\text{int}}, c_{\mathbf{k}}^\dagger c_{\mathbf{k}+\mathbf{q}}] &\approx -\frac{1}{2} \sum_{\mathbf{k}' \mathbf{q}' \neq 0} V(q') \left\{ c_{\mathbf{k}+\mathbf{q}'}^\dagger c_{\mathbf{k}+\mathbf{q}} \langle c_{\mathbf{k}'-\mathbf{q}'}^\dagger c_{\mathbf{k}'} \rangle + \langle c_{\mathbf{k}+\mathbf{q}'}^\dagger c_{\mathbf{k}+\mathbf{q}} \rangle c_{\mathbf{k}'-\mathbf{q}'}^\dagger c_{\mathbf{k}'} \right. \\
&\quad + \langle c_{\mathbf{k}-\mathbf{q}'}^\dagger c_{\mathbf{k}+\mathbf{q}} \rangle c_{\mathbf{k}'+\mathbf{q}'}^\dagger c_{\mathbf{k}'} + c_{\mathbf{k}-\mathbf{q}'}^\dagger c_{\mathbf{k}+\mathbf{q}} \langle c_{\mathbf{k}'+\mathbf{q}'}^\dagger c_{\mathbf{k}'} \rangle \\
&\quad - c_{\mathbf{k}'+\mathbf{q}'}^\dagger c_{\mathbf{k}'} \langle c_{\mathbf{k}}^\dagger c_{\mathbf{k}+\mathbf{q}+\mathbf{q}'} \rangle - \langle c_{\mathbf{k}'+\mathbf{q}'}^\dagger c_{\mathbf{k}'} \rangle c_{\mathbf{k}}^\dagger c_{\mathbf{k}+\mathbf{q}+\mathbf{q}'} \\
&\quad \left. - c_{\mathbf{k}}^\dagger c_{\mathbf{k}+\mathbf{q}-\mathbf{q}'} \langle c_{\mathbf{k}'-\mathbf{q}'}^\dagger c_{\mathbf{k}'} \rangle - \langle c_{\mathbf{k}}^\dagger c_{\mathbf{k}+\mathbf{q}-\mathbf{q}'} \rangle c_{\mathbf{k}'-\mathbf{q}'}^\dagger c_{\mathbf{k}'} + \text{const.} \right\} \\
&= \sum_{\mathbf{k}'} V(q) (\langle n_{\mathbf{k}+\mathbf{q}} \rangle - \langle n_{\mathbf{k}} \rangle) c_{\mathbf{k}'-\mathbf{q}'}^\dagger c_{\mathbf{k}'}, \tag{9.46}
\end{aligned}$$

where we used that $\langle c_{\mathbf{k}}^\dagger c_{\mathbf{k}'} \rangle = \langle n_{\mathbf{k}} \rangle \delta_{\mathbf{k}, \mathbf{k}'}$. Note that the exchange pairings which we included in the Hartree-Fock approximation is not included here.

Collecting everything and going to the frequency domain the equation of motion becomes,

$$(\omega + i\eta + \xi_{\mathbf{k}} - \xi_{\mathbf{k}+\mathbf{q}}) \chi^R(\mathbf{k}\mathbf{q}, \omega) = (\langle n_{\mathbf{k}+\mathbf{q}} \rangle - \langle n_{\mathbf{k}} \rangle) \left(1 - V(q) \sum_{\mathbf{k}'} \chi^R(\mathbf{k}'\mathbf{q}, \omega) \right), \tag{9.47}$$

which, when summed over \mathbf{k} , allows us to find an equation for $\chi^R(\mathbf{q}, \omega)$

$$\chi^R(\mathbf{q}, \omega) = \frac{1}{V} \sum_{\mathbf{k}} \chi^R(\mathbf{k}\mathbf{q}, \omega) = \frac{1}{V} \sum_{\mathbf{k}} \frac{\langle n_{\mathbf{k}+\mathbf{q}} \rangle - \langle n_{\mathbf{k}} \rangle}{\omega + \xi_{\mathbf{k}} - \xi_{\mathbf{k}+\mathbf{q}} + i\delta} (1 + V(q) \chi^R(\mathbf{q}, \omega)), \tag{9.48}$$

and hence

$$\chi^{R,\text{RPA}}(\mathbf{q}, \omega) = \frac{\chi_0^R(\mathbf{q}, \omega)}{1 - V(q) \chi_0^R(\mathbf{q}, \omega)}. \tag{9.49}$$

This is the RPA result of the polarizability function. The free particle polarizability $\chi_0^R(\mathbf{q}, \omega)$ was derived in Sec. 8.5. The RPA dielectric function becomes

$$\epsilon^{\text{RPA}}(\mathbf{q}, \omega) = [1 + V(q) \chi^R(\mathbf{q}, \omega)]^{-1} = 1 - V(q) \chi_0^R(\mathbf{q}, \omega). \tag{9.50}$$

Replacing the expectation values, $n_{\mathbf{k}}$, by the Fermi-Dirac distribution function, we recognize the Lindhard function studied in Sec. 8.5. There we studied a non-interacting electron gas and found that $\chi^R(\mathbf{q}, \omega)$ indeed was equal to the numerator in (9.49) and the two results therefore agree nicely.

In Sec. 8.5 we also analyzed the excitation of the non-interacting electrons gas and the analysis there is basically still correct. The excitations which were shown in Sec. 8.5 to be related to the imaginary part of $\chi^R(\mathbf{q}, \omega)$ and therefore the structure of the electron-hole excitations of the non-interacting gas (depicted in Fig. 8.3) is preserved here, but of course the strength is modified by the real part of the denominator of (9.49).

However, the interactions add other fundamental excitations, namely collective modes, and in the case of a charge liquid these modes are the plasmon modes. The additional

modes are given by the part where the imaginary part of $\chi_0^R(\mathbf{q}, \omega)$ is zero because then there is a possibility of a pole in the polarizability. If we set $\text{Im } \chi_0^R(\mathbf{q}, \omega) = -i\delta$, we have

$$-\text{Im } \chi^R(\mathbf{q}, \omega) = \frac{\delta}{[1 - V(q) \text{Re } \chi_0^R(\mathbf{q}, \omega)]^2 + \delta^2} = \pi\delta (1 - V(q) \text{Re } \chi_0^R(\mathbf{q}, \omega)). \quad (9.51)$$

This means that there is a well-defined mode when $1 - V(q) \text{Re } \chi_0^R(\mathbf{q}, \omega) = 0$ and this is the plasma oscillation mode, also called a plasmon. The plasmon is studied in detail in Chap. 12, here we just mention that the condition for the mode turns out to be $\omega \propto \sqrt{\omega_{\text{pl}}^2 + \text{const. } q^2}$.

9.4 Summary and outlook

In this chapter we have seen a method to deal with the dynamical aspects of interacting many-body systems, namely the equation of motion method applied to the Green's functions. The set of differential equation is not soluble in general, and in fact only a very small set of Hamiltonians describing interacting systems can be solved exactly. Therefore approximations are necessary and we saw particular examples of this, namely the mean-field solution of a magnetic impurity embedded in a metallic host, and the RPA approximation for the charge auto correlation function.

In the following chapter we use the equation of motion to derive the Green's functions in the imaginary time formalism and to derive the famous Wick's theorem. Wick's theorem will then pave the way for introducing the Feynman diagrams.

Chapter 10

Imaginary time Green's functions

We have seen that physical observables often have the form of Green's functions, or that they can be derived in a simple way from the Green's functions. In all the situations we have studied so far the physical observables have been related to the retarded Green's functions, which in general are defined as

$$C_{AB}^R(t, t') = -i\theta(t - t') \left\langle [A(t), B(t')]_{B,F} \right\rangle, \quad \left\{ \begin{array}{l} B : \text{for bosons} \\ F : \text{for fermions} \end{array} \right\}, \quad (10.1)$$

When A and B are single particle annihilation and creation operators, it is the single particle Green's function defined in Eq. (8.28) from which one could derive the density of states. When A and B are two-particle operators, e.g. the density or current operators, C^R has the form of a retarded correlation function that was shown to give the linear response results of Chap. 6. In Eq. (10.1) boson operators mean either single particle operators like b or b^\dagger or an even number of fermion operators such as $c^\dagger c$ appearing in for example the density operator ρ . The important thing that distinguishes the boson case from the fermion case is the sign change that is obtained upon interchange.

In this chapter, we introduce a mathematical method to work out the retarded Green's functions. For technical reasons it is convenient to use a mapping to a more general Green's function, where the time and frequency arguments are imaginary quantities. This has no real physical meaning, and is only a clever mathematical trick, which we need to learn. This is much like treating electrical circuit theory with complex numbers even though all currents and voltages are real. The present chapter concentrates on the mathematical details of the technique and applications are left for later. The imaginary time formalism is particularly useful when we want to perform perturbation theory, and this will eventually lead us to the Feynman diagrams.

Let us for example look at the definition of the following correlation function

$$C_{AB}(t, t') = -\langle A(t)B(t') \rangle, \quad (10.2)$$

from which we can find the retarded function as $C^R = i\theta(t - t')(C_{AB} \mp C_{BA})$. By definition we have

$$C_{AB}(t, t') = -\frac{1}{Z} \text{Tr}(e^{-\beta H} A(t)B(t')). \quad (10.3)$$

Suppose the Hamiltonian is $H = H_0 + V$, where V is the perturbation. Then we saw in Chap. 5 that the interaction picture provides a systematic way of expanding in powers of V . We could try to utilize this and write C_{AB} as

$$C_{AB}(t, t') = -\frac{1}{Z} \text{Tr} \left[e^{-\beta H} \hat{U}(0, t) \hat{A}(t) \hat{U}(t, t') \hat{B}(t') \hat{U}(t', 0) \right], \quad (10.4)$$

In Eq. (5.18) we saw also how a single \hat{U} operator could be expanded as a time-ordered exponential. This would in Eq. (10.4) result in three time-ordered exponentials, which could be collected into a single time-ordered exponential. But the trouble arises for the density matrix $e^{-\beta H}$, which should also be expanded in powers of the interaction. To make a long story short: this is a mess and a new idea is therefore needed. The solution to this problem is to use imaginary times instead of real times, but bare in mind that this is purely a mathematical trick without physical contents.

To employ imaginary time is not as far fetched as it might look, because both the density operator $\rho = e^{-\beta H}/Z$ and the time evolution operator $U(t) = e^{-iHt}$ are both exponential functions of the Hamiltonian.¹ They therefore satisfy similar differential equations: U satisfies the Schrödinger equation, $i\partial_t U = HU$ while ρ is the solution to $\partial_\beta \rho = -H\rho$, which is known as the Bloch equation. In order to treat both U and ρ in one go, one replaces the time argument by a imaginary quantity $t \rightarrow -i\tau$, where τ is real and has the dimension time. In the end this means that both U and ρ can be treated in just one expansion in powers of V . Furthermore, we will see that there is a well-defined method to obtain the physically relevant quantity, i.e. to go back to physical real times from the imaginary time function.

As for real time we can define an imaginary time Heisenberg picture by substituting it by τ . We define

$$A(\tau) = e^{\tau H} A e^{-\tau H}, \quad \tau \text{ a Greek letter.} \quad (10.5)$$

In this notation, you should use the imaginary time definitions when the time argument is a Greek letter and the usual definition when the times are written with roman letters, so

$$A(t) = e^{itH} A e^{-itH}, \quad t \text{ a Roman letter.} \quad (10.6)$$

Similar to the interaction picture defined for real times, we can define the interaction picture for imaginary times as

$$\hat{A}(\tau) = e^{\tau H_0} A e^{-\tau H_0}. \quad (10.7)$$

Letting $H = H_0 + V$, the relation between the Heisenberg and the interaction picture in imaginary time follows the arguments in Chap. 5. If we consider a product of operators $A(\tau)B(\tau')$ and write it in terms of the corresponding operators in the interaction representation, we get

$$A(\tau)B(\tau') = \hat{U}(0, \tau) \hat{A}(\tau) \hat{U}(\tau, \tau') \hat{B}(\tau') \hat{U}(\tau', 0), \quad (10.8)$$

¹Note that we consider only time-independent Hamiltonians in this section. If they are not time-independent, one cannot use the ordinary equilibrium statistical mechanics but instead one must use a non-equilibrium formalism. This we did in the linear response limit in Chap. 6, but we will not cover the more general case of non-linear time dependent response in this course.

where, like in Eq. (5.12), the time-evolution operator \hat{U} in the interaction picture is

$$\hat{U}(\tau, \tau') = e^{\tau H_0} e^{-(\tau - \tau')H} e^{-\tau' H_0}. \quad (10.9)$$

From this it follows directly that

$$\hat{U}(\tau, \tau'') \hat{U}(\tau'', \tau') = \hat{U}(\tau, \tau'). \quad (10.10)$$

An explicit expression for $U(\tau, \tau')$ is found in analogy with the derivation of Eq. (5.18). First we differentiate Eq. (10.9) with respect to τ and find

$$\partial_\tau \hat{U}(\tau, \tau') = e^{\tau H_0} (H_0 - H) e^{-(\tau - \tau')H} e^{-\tau' H_0} = -\hat{V}(\tau) \hat{U}(\tau, \tau'). \quad (10.11)$$

This is analogous to Eq. (5.13) and the boundary condition, $\hat{U}(\tau, \tau) = 1$, is of course the same. Now the same iterative procedure is applied and we end with

$$\begin{aligned} \hat{U}(\tau, \tau') &= \sum_{n=0}^{\infty} \frac{1}{n!} (-1)^n \int_{\tau'}^{\tau} d\tau_1 \cdots \int_{\tau'}^{\tau} d\tau_n T_\tau \left(\hat{V}(\tau_1) \cdots \hat{V}(\tau_n) \right) \\ &= T_\tau \exp \left(- \int_{\tau'}^{\tau} d\tau_1 \hat{V}(\tau_1) \right). \end{aligned} \quad (10.12)$$

The time ordering is again the same as defined in Sec. 5.3, i.e. the operators are ordered such that $T_\tau(A(\tau)B(\tau'))$ is equal to $A(\tau)B(\tau')$ for $\tau > \tau'$ and $B(\tau')A(\tau)$ when $\tau' > \tau$.

Above it was argued that the density operator naturally can be treated within the imaginary time formalism, and indeed it can, because by combining Eqs. (10.9) and (10.12) we obtain

$$e^{-\beta H} = e^{-\beta H_0} \hat{U}(\beta, 0) = e^{-\beta H_0} T_\tau \exp \left(- \int_0^\beta d\tau_1 \hat{V}(\tau_1) \right). \quad (10.13)$$

Consider now the time ordered expectation value of the pair of operators in Eq. (10.8)

$$\langle T_\tau A(\tau) B(\tau') \rangle = \frac{1}{Z} \text{Tr} \left[e^{-\beta H} T_\tau A(\tau) B(\tau') \right]. \quad (10.14)$$

Utilizing Eqs. (10.8) and (10.13) we can immediately expand in powers of V

$$\langle T_\tau A(\tau) B(\tau') \rangle = \frac{1}{Z} \text{Tr} \left[e^{-\beta H_0} \hat{U}(\beta, 0) T_\tau (\hat{U}(0, \tau) \hat{A}(\tau) \hat{U}(\tau, \tau') \hat{B}(\tau') \hat{U}(\tau', 0)) \right]. \quad (10.15)$$

This can be written in a much more compact way relying on the properties of T_τ and Eq. (10.10)

$$\langle T_\tau A(\tau) B(\tau') \rangle = \frac{1}{Z} \text{Tr} \left[e^{-\beta H_0} T_\tau \hat{U}(\beta, 0) \hat{A}(\tau) \hat{B}(\tau') \right] = \frac{\langle T_\tau \hat{U}(\beta, 0) \hat{A}(\tau) \hat{B}(\tau') \rangle_0}{\langle \hat{U}(\beta, 0) \rangle_0}, \quad (10.16)$$

where we have used $Z = \text{Tr} [e^{-\beta H}] = \text{Tr} [e^{-\beta H_0} \hat{U}(\beta, 0)]$, and where the averages $\langle \cdots \rangle_0$ depending on $e^{-\beta H_0}$ appear after normalizing with $1/Z_0 = 1/\text{Tr} [e^{-\beta H_0}]$. This result demonstrates that the trick of using imaginary time indeed allows for a systematic expansion of the complicated looking expression in Eq. (10.4). However, before we can see the usefulness fully, we need to relate the correlation functions written in imaginary time and the correlation function with real time arguments.

10.1 Definitions of Matsubara Green's functions

The imaginary time Green's functions, also called Matsubara Green's function, is defined in the following way

$$\mathcal{C}_{AB}(\tau, \tau') \equiv -\langle T_\tau (A(\tau)B(\tau')) \rangle, \quad (10.17)$$

where the time-ordering symbol in imaginary time has been introduced. It means that operators are ordered according to history and just like the time-ordering operator seen in Chap. 5 with the later "times" to the left

$$T_\tau (A(\tau)B(\tau')) = \theta(\tau - \tau')A(\tau)B(\tau') \pm \theta(\tau' - \tau)B(\tau')A(\tau), \quad \begin{cases} + \text{ for bosons,} \\ - \text{ for fermions.} \end{cases} \quad (10.18)$$

The next question is: What values can τ have? From the definition in Eq. (10.17) three things are clear. Firstly, $\mathcal{C}_{AB}(\tau, \tau')$ is a function of the time difference only, i.e. $\mathcal{C}_{AB}(\tau, \tau') = \mathcal{C}_{AB}(\tau - \tau')$. This follows from the cyclic properties of the trace. We have for $\tau > \tau'$

$$\begin{aligned} \mathcal{C}_{AB}(\tau, \tau') &= \frac{-1}{Z} \text{Tr} \left[e^{-\beta H} e^{\tau H} A e^{-\tau H} e^{\tau' H} B e^{-\tau' H} \right] \\ &= \frac{-1}{Z} \text{Tr} \left[e^{-\beta H} e^{-\tau' H} e^{\tau H} A e^{-\tau H} e^{\tau' H} B \right] \\ &= \frac{-1}{Z} \text{Tr} \left[e^{-\beta H} e^{(\tau - \tau') H} A e^{-(\tau - \tau') H} B \right] \\ &= \mathcal{C}_{AB}(\tau - \tau'), \end{aligned} \quad (10.19)$$

and of course likewise for $\tau' > \tau$. Secondly, convergence of $\mathcal{C}_{AB}(\tau, \tau')$ is guaranteed only if $-\beta < \tau - \tau' < \beta$. For $\tau > \tau'$ the equality $\tau - \tau' < \beta$ is clearly seen if one uses the Lehmann representation in Eq. (10.19) to get a factor $\exp(-[\beta - \tau + \tau'] E_n)$, and, likewise, the second equality is obtained if $\tau < \tau'$. Thirdly, we have the property

$$\mathcal{C}_{AB}(\tau) = \pm \mathcal{C}_{AB}(\tau + \beta), \quad \text{for } \tau < 0, \quad (10.20)$$

which again follows from the cyclic properties of the trace. The proof of Eq. (10.20) for $\tau < 0$ is

$$\begin{aligned} \mathcal{C}_{AB}(\tau + \beta) &= \frac{-1}{Z} \text{Tr} \left[e^{-\beta H} e^{(\tau + \beta) H} A e^{-(\tau + \beta) H} B \right] \\ &= \frac{-1}{Z} \text{Tr} \left[e^{\tau H} A e^{-\tau H} e^{-\beta H} B \right] \\ &= \frac{-1}{Z} \text{Tr} \left[e^{-\beta H} B e^{\tau H} A e^{-\tau H} \right] \\ &= \frac{-1}{Z} \text{Tr} \left[e^{-\beta H} B A(\tau) \right] \\ &= \pm \frac{-1}{Z} \text{Tr} \left[e^{-\beta H} T_\tau (A(\tau)B) \right] \\ &= \pm \mathcal{C}_{AB}(\tau), \end{aligned} \quad (10.21)$$

and similarly for $\tau > 0$.

10.1.1 Fourier transform of Matsubara Green's functions

Next we wish to find the Fourier transforms with respect to the “time” argument τ . Because of the properties above, we take $\mathcal{C}_{AB}(\tau)$ to be defined in the interval $-\beta < \tau < \beta$, and thus according to the theory of Fourier transformations we have a discrete Fourier series on that interval given by

$$\mathcal{C}_{AB}(n) \equiv \frac{1}{2} \int_{-\beta}^{\beta} d\tau e^{i\pi n\tau/\beta} \mathcal{C}_{AB}(\tau), \quad (10.22a)$$

$$\mathcal{C}_{AB}(\tau) = \frac{1}{\beta} \sum_{n=-\infty}^{\infty} e^{-i\pi n\tau/\beta} \mathcal{C}_{AB}(n). \quad (10.22b)$$

However, due to the symmetry property (10.21) this can be simplified as

$$\begin{aligned} \mathcal{C}_{AB}(n) &= \frac{1}{2} \int_0^{\beta} d\tau e^{i\pi n\tau/\beta} \mathcal{C}_{AB}(\tau) + \frac{1}{2} \int_{-\beta}^0 d\tau e^{i\pi n\tau/\beta} \mathcal{C}_{AB}(\tau), \\ &= \frac{1}{2} \int_0^{\beta} d\tau e^{i\pi n\tau/\beta} \mathcal{C}_{AB}(\tau) + e^{-i\pi n} \frac{1}{2} \int_0^{\beta} d\tau e^{i\pi n\tau/\beta} \mathcal{C}_{AB}(\tau - \beta), \\ &= \frac{1}{2} (1 \pm e^{-i\pi n}) \int_0^{\beta} d\tau e^{i\pi n\tau/\beta} \mathcal{C}_{AB}(\tau), \end{aligned} \quad (10.23)$$

and since the factor $(1 \pm e^{-i\pi n})$ is zero for plus sign and n odd or for minus sign and n even and 2 otherwise, we obtain

$$\mathcal{C}_{AB}(n) = \int_0^{\beta} d\tau e^{i\pi n\tau/\beta} \mathcal{C}_{AB}(\tau), \quad \begin{cases} n \text{ is even for bosons,} \\ n \text{ is odd for fermions.} \end{cases} \quad (10.24)$$

From now on we use the following notation for the Fourier transforms of the Matsubara Green's functions

$$\mathcal{C}_{AB}(i\omega_n) = \int_0^{\beta} d\tau e^{i\omega_n\tau} \mathcal{C}_{AB}(\tau), \quad \begin{cases} \omega_n = \frac{2n\pi}{\beta}, & \text{for bosons,} \\ \omega_n = \frac{(2n+1)\pi}{\beta}, & \text{for fermions.} \end{cases} \quad (10.25)$$

The frequency variable ω_n is denoted a Matsubara frequency. Note how the information about the temperature is contained in the Matsubara frequencies through β .

Finally, we remark that the boundaries of the integral $\int_0^{\beta} d\tau$ in Eq. (10.25) leads to a minor ambiguity of how to treat the boundary $\tau = 0$, for example if $\mathcal{C}_{AB}(\tau)$ includes a delta function $\delta(\tau)$. A consistent choice is always to move the time argument into the interior of the interval $[0, \beta]$, e.g. replace $\delta(\tau)$ by $\delta(\tau - 0^+)$.

10.2 Connection between Matsubara and retarded functions

We shall now see why the Matsubara Green's functions have been introduced at all. In the frequency domain they are in fact the same analytic function as the usual real times

Green's functions. In other words, there exists an analytic function $\mathcal{C}_{AB}(z)$, where z is a complex frequency argument in the upper half plane, that equals $\mathcal{C}_{AB}(i\omega_n)$ on the imaginary axis and $C_{AB}^R(\omega)$ on the real axis. This means that once we have one of the two, the other one follows by analytic continuation. Since it is in many cases much easier to compute the Matsubara function, $\mathcal{C}_{AB}(i\omega_n)$, this is a powerful method for finding the corresponding retarded function. Indeed we shall now show that the appropriate analytic continuation is $C_{AB}^R(\omega) = \mathcal{C}_{AB}(i\omega_n \rightarrow \omega + i\eta)$, where η is a positive infinitesimal.

The relation between the two functions \mathcal{C}_{AB} and C_{AB}^R is proven by use of the Lehmann representation. In Sec. 8.3.3 we calculated the retarded single particle Green's function and the result Eq. (8.46) can be carried over for fermions. In the general case we get²

$$C_{AB}^R(\omega) = \frac{1}{Z} \sum_{nn'} \frac{\langle n|A|n'\rangle \langle n'|B|n\rangle}{\omega + E_n - E_{n'} + i\eta} \left(e^{-\beta E_n} - (\pm) e^{-\beta E_{n'}} \right), \quad (10.26)$$

The Matsubara function is calculated in a similar way. For $\tau > 0$, we have

$$\begin{aligned} \mathcal{C}_{AB}(\tau) &= \frac{-1}{Z} \text{Tr} \left[e^{-\beta H} e^{\tau H} A e^{-\tau H} B \right] \\ &= \frac{-1}{Z} \sum_{nn'} e^{-\beta E_n} \langle n|A|n'\rangle \langle n'|B|n\rangle e^{\tau(E_n - E_{n'})}, \end{aligned} \quad (10.27)$$

and hence

$$\begin{aligned} \mathcal{C}_{AB}(i\omega_n) &= \int_0^\beta d\tau e^{i\omega_n \tau} \frac{-1}{Z} \sum_{nn'} e^{-\beta E_n} \langle n|A|n'\rangle \langle n'|B|n\rangle e^{\tau(E_n - E_{n'})}, \\ &= \frac{-1}{Z} \sum_{nn'} e^{-\beta E_n} \frac{\langle n|A|n'\rangle \langle n'|B|n\rangle}{i\omega_n + E_n - E_{n'}} \left(e^{i\omega_n \beta} e^{\beta(E_n - E_{n'})} - 1 \right), \\ &= \frac{-1}{Z} \sum_{nn'} e^{-\beta E_n} \frac{\langle n|A|n'\rangle \langle n'|B|n\rangle}{i\omega_n + E_n - E_{n'}} \left(\pm e^{\beta(E_n - E_{n'})} - 1 \right) \\ &= \frac{1}{Z} \sum_{nn'} \frac{\langle n|A|n'\rangle \langle n'|B|n\rangle}{i\omega_n + E_n - E_{n'}} \left(e^{-\beta E_n} - (\pm) e^{-\beta E_{n'}} \right), \end{aligned} \quad (10.28)$$

Eqs. (10.26) and (10.28) show that $\mathcal{C}_{AB}(i\omega_n)$ and $C_{AB}^R(\omega)$ coincide and that they are just special cases of the same function, because we can generate both $\mathcal{C}_{AB}(i\omega_n)$ and $C_{AB}^R(\omega)$ from the following function defined in the entire complex plane except for the real axis

$$C_{AB}(z) = \frac{1}{Z} \sum_{nn'} \frac{\langle n|A|n'\rangle \langle n'|B|n\rangle}{z + E_n - E_{n'}} \left(e^{-\beta E_n} - (\pm) e^{-\beta E_{n'}} \right). \quad (10.29)$$

This function is analytic in the upper (or lower) half plane, but has a series of poles at $E_{n'} - E_n$ along the real axis. According to the theory of analytic functions: if two functions

²Note that it is assumed that the grand canonical ensemble is being used because the complete set of states includes states with any number of particles. Therefore the connection between imaginary time functions and retarded real time functions derived here is only valid in this ensemble.

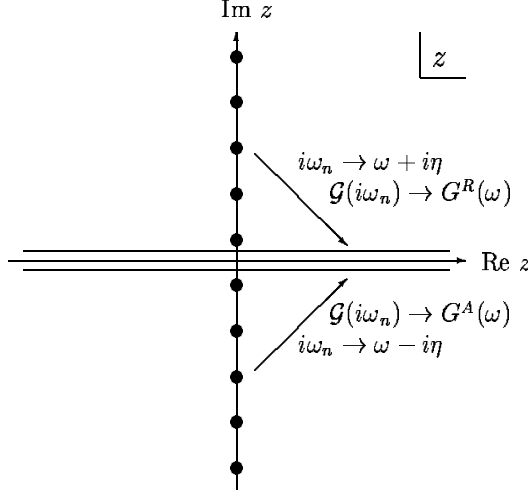


Figure 10.1: The analytic continuation procedure in the complex z -plane where the Matsubara function defined for $z = i\omega_n$ goes to the retarded or advanced Green's functions defined infinitesimally close to real axis.

coincide in an infinite set of points then they are fully identical functions within the entire domain where at least one of them is a analytic function and, furthermore, there is only one such common function. This means that if we know $\mathcal{C}_{AB}(i\omega_n)$ we can find $C_{AB}^R(\omega)$ by analytic continuation:

$$C_{AB}^R(\omega) = \mathcal{C}_{AB}(i\omega_n \rightarrow \omega + i\eta). \quad (10.30)$$

Warning: this way of performing the analytic continuation is only true when $\mathcal{C}_{AB}(i\omega_n)$ is written as a rational function which is analytic in the upper half plane. If not, it is not obvious how to perform the continuation. For example look at the definition in Eq. (10.25). If we naïvely insert $i\omega_n \rightarrow \omega + i\eta$ before doing the integral, the answer is completely different and of course wrong. Later we shall see examples of how to perform the analytic continuation correctly.

To summarize: Using the Lehmann representation we have shown that there exists a function $C_{AB}(z)$ which is analytic for z not purely real and which coincides with the Matsubara function, i.e. $C_{AB}(z = i\omega_n) = \mathcal{C}_{AB}(i\omega_n)$. On the real axis coming from above this function is identical to the retarded function, i.e. $C_{AB}(z = \omega + i0^+) = C_{AB}^R(\omega)$. However, it is not a simple task to determine $C_{AB}(z)$ unless it has been reduced to an rational function as in Eq. (10.28), where it is evident that the replacement in (10.30) $i\omega_n \rightarrow z \rightarrow \omega + i\eta$ gives the right analytic function. This is illustrated in Fig. 10.1.

10.2.1 Advanced functions

The function $C_{AB}(z)$ is analytic for all z away from the real axis. Therefore instead of the continuation in the upper half plane, we could do the same thing in the lower half

plane $i\omega_n \rightarrow z \rightarrow \omega - i\eta$, which gives the so-called advanced Green's function,

$$C_{AB}^A(\omega) = \mathcal{C}_{AB}(i\omega_n \rightarrow \omega - i\eta). \quad (10.31)$$

The advanced Green's function is in the time domain defined as

$$C_{AB}^A(t, t') = i\theta(t' - t) \left\langle [A(t), B(t')]_{B,F} \right\rangle. \quad (10.32)$$

The term “advanced” means that it gives the state of the system at previous times based on the state of system at present times. The retarded one, as was explained in Chap. 6, gives the present state of the system as it has evolved from the state at previous times, i.e. the effect of retardation.

10.3 Single-particle Matsubara Green's function

An important type of Matsubara functions are the single-particle Green's function \mathcal{G} . They are defined as

$$\mathcal{G}(\mathbf{r}\sigma\tau, \mathbf{r}'\sigma'\tau') = - \left\langle T_\tau \left(\Psi_\sigma(\mathbf{r}, \tau) \Psi_\sigma^\dagger(\mathbf{r}', \tau') \right) \right\rangle, \quad \text{real space}, \quad (10.33a)$$

$$\mathcal{G}(\nu\tau, \nu'\tau') = - \left\langle T_\tau \left(c_\nu(\tau) c_{\nu'}^\dagger(\tau') \right) \right\rangle, \quad \{\nu\} \text{ representation}. \quad (10.33b)$$

10.3.1 Matsubara Green's function for non-interacting particles

For non-interacting particles the Matsubara Green's functions can be evaluated in the same way we found the retarded Green's function in Sec. 8.3.2. Suppose the Hamiltonian is diagonal in the ν -quantum numbers

$$H_0 = \sum_\nu \xi_\nu c_\nu^\dagger c_\nu, \quad (10.34)$$

so that

$$c_\nu(\tau) = e^{\tau H_0} c_\nu e^{-\tau H_0} = e^{-\xi_\nu \tau} c_\nu, \quad c_\nu^\dagger(\tau) = e^{\tau H_0} c_\nu^\dagger e^{-\tau H_0} = e^{\xi_\nu \tau} c_\nu^\dagger, \quad (10.35)$$

which gives

$$\begin{aligned} \mathcal{G}_0(\nu, \tau - \tau') &= - \left\langle T_\tau \left(c_\nu(\tau) c_\nu^\dagger(\tau') \right) \right\rangle, \\ &= -\theta(\tau - \tau') \langle c_\nu(\tau) c_\nu^\dagger(\tau') \rangle - (\pm) \theta(\tau' - \tau) \langle c_\nu^\dagger(\tau') c_\nu(\tau) \rangle \\ &= - \left[\theta(\tau - \tau') \langle c_\nu c_\nu^\dagger \rangle (\pm) \theta(\tau' - \tau) \langle c_\nu^\dagger c_\nu \rangle \right] e^{-\xi_\nu(\tau - \tau')}, \end{aligned} \quad (10.36)$$

For fermions this is

$$\mathcal{G}_{0,F}(\nu, \tau - \tau') = - \left[\theta(\tau - \tau') (1 - n_F(\xi_\nu)) - \theta(\tau' - \tau) n_F(\xi_\nu) \right] e^{-\xi_\nu(\tau - \tau')} \quad (10.37)$$

while the bosonic free particle Green's function reads

$$\mathcal{G}_{0,B}(\nu, \tau - \tau') = - [\theta(\tau - \tau') (1 + n_B(\xi_\nu)) + \theta(\tau' - \tau) n_B(\xi_\nu)] e^{-\xi_\nu(\tau - \tau')}. \quad (10.38)$$

In the frequency representation, the fermionic Green's function is

$$\begin{aligned} \mathcal{G}_{0,F}(\nu, ik_n) &= \int_0^\beta d\tau e^{ik_n\tau} \mathcal{G}_{0,F}(\nu, \tau), \quad k_n = (2n+1)\pi/\beta \\ &= -(1 - n_F(\xi_\nu)) \int_0^\beta d\tau e^{ik_n\tau} e^{-\xi_\nu\tau}, \\ &= -(1 - n_F(\xi_\nu)) \frac{1}{ik_n - \xi_\nu} (e^{ik_n\beta} e^{-\xi_\nu\beta} - 1), \\ &= \frac{1}{ik_n - \xi_\nu}, \end{aligned} \quad (10.39)$$

because $e^{ik_n\beta} = -1$ and $1 - n_F(\varepsilon) = (e^{-\beta\varepsilon} + 1)^{-1}$, while the bosonic one becomes

$$\begin{aligned} \mathcal{G}_{0,B}(\nu, iq_n) &= \int_0^\beta d\tau e^{iq_n\tau} \mathcal{G}_{0,B}(\nu, \tau), \quad q_n = 2n\pi/\beta \\ &= -(1 + n_B(\xi_\nu)) \int_0^\beta d\tau e^{iq_n\tau} e^{-\xi_\nu\tau}, \\ &= -(1 + n_B(\xi_\nu)) \frac{1}{iq_n - \xi_\nu} (e^{iq_n\beta} e^{-\xi_\nu\beta} - 1), \\ &= \frac{1}{iq_n - \xi_\nu}, \end{aligned} \quad (10.40)$$

because $e^{iq_n\beta} = 1$ and $1 + n_B(\varepsilon) = -(e^{-\beta\varepsilon} - 1)^{-1}$. Here we have anticipated the notation that is used later: Matsubara frequencies ik_n and ip_n are used for fermion frequencies, while iq_n and $i\omega_n$ are used for boson frequencies.

According to our recipe Eq. (10.30), the retarded free particles Green's functions are for both fermions and bosons

$$G_0^R(\nu, \omega) = \frac{1}{\omega - \xi_\nu + i\eta}, \quad (10.41)$$

in agreement with Eq. (8.51).

10.4 Evaluation of Matsubara sums

When working with Matsubara Green's functions we will often encounter sums over Matsubara frequencies, similar to integrals over frequencies in the real time language. For example sums of the type

$$\mathcal{S}_1(\nu, \tau) = \frac{1}{\beta} \sum_{ik_n} \mathcal{G}(\nu, ik_n) e^{ik_n\tau}, \quad \tau > 0, \quad (10.42)$$

or sums with products of Green's functions. The imaginary time formalism has been introduced because it will be used to perform perturbation expansions, and therefore the types of sums we will meet are often products of the such free Green's functions, e.g.

$$\mathcal{S}_2(\nu_1, \nu_2, i\omega_n, \tau) = \frac{1}{\beta} \sum_{ik_n} \mathcal{G}_0(\nu_1, ik_n) \mathcal{G}_0(\nu_2, ik_n + i\omega_n) e^{ik_n \tau}, \quad \tau > 0. \quad (10.43)$$

This section is devoted to the mathematical techniques for evaluating such sums. In order to be more general, we define the two generic sums

$$\mathcal{S}^F(\tau) = \frac{1}{\beta} \sum_{ik_n} g(ik_n) e^{ik_n \tau}, \quad ik_n \text{ fermion frequency} \quad (10.44a)$$

$$\mathcal{S}^B(\tau) = \frac{1}{\beta} \sum_{i\omega_n} g(i\omega_n) e^{i\omega_n \tau}, \quad i\omega_n \text{ boson frequency} \quad (10.44b)$$

and study them for $\tau > 0$.

To evaluate these, the trick is to rewrite them as integrals over a complex variable and to use residue theory. For this we need two functions, $n(z)$, which have poles at $z = ik_n$ and $z = i\omega_n$, respectively. These functions turn out to be the well known Fermi and Bose distribution functions

$$n_F(z) = \frac{1}{e^{\beta z} + 1}, \quad \text{poles for } z = i(2n+1)\pi/\beta, \quad (10.45a)$$

$$n_B(z) = \frac{1}{e^{\beta z} - 1}, \quad \text{poles for } z = i(2n)\pi/\beta. \quad (10.45b)$$

The residues at these values are

$$\text{Res}_{z=ik_n} [n_F(z)] = \lim_{z \rightarrow ik_n} \frac{(z - ik_n)}{e^{\beta z} + 1} = \lim_{\delta \rightarrow 0} \frac{\delta}{e^{\beta ik_n} e^{\beta \delta} + 1} = -\frac{1}{\beta}, \quad (10.46a)$$

$$\text{Res}_{z=i\omega_n} [n_B(z)] = \lim_{z \rightarrow i\omega_n} \frac{(z - i\omega_n)}{e^{\beta z} - 1} = \lim_{\delta \rightarrow 0} \frac{\delta}{e^{\beta i\omega_n} e^{\beta \delta} - 1} = +\frac{1}{\beta}. \quad (10.46b)$$

According to the theory of analytic functions, the contour integral which encloses one of these points, but no singularity of $g(z)$, is given by

$$\oint dz n_F(z) g(z) = 2\pi i \text{Res}_{z=ik_n} [n_F(z) g(ik_n)] = -\frac{2\pi i}{\beta} g(ik_n), \quad (10.47)$$

for fermions and similarly for boson frequencies

$$\oint dz n_B(z) g(z) = 2\pi i \text{Res}_{z=i\omega_n} [n_B(z) g(i\omega_n)] = \frac{2\pi i}{\beta} g(i\omega_n). \quad (10.48)$$

If we therefore define contours, \mathcal{C} , which enclose all point $z = ik_n$ in the fermionic case and all points $z = i\omega_n$ in the bosonic case, but only regions where $g(z)$ is analytic, we can write

$$\mathcal{S}^F = - \int_{\mathcal{C}} \frac{dz}{2\pi i} n_F(z) g(z) e^{z\tau}, \quad (10.49a)$$

$$\mathcal{S}^B = + \int_{\mathcal{C}} \frac{dz}{2\pi i} n_B(z) g(z) e^{z\tau}. \quad (10.49b)$$

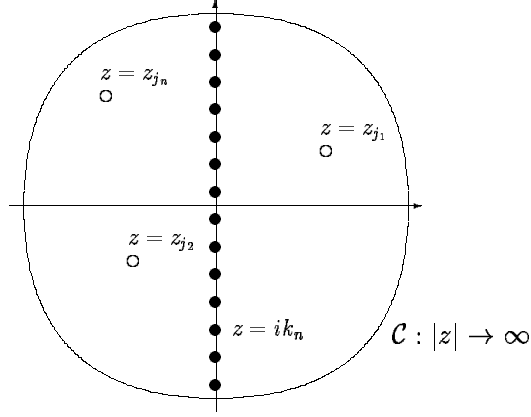


Figure 10.2: The contour used to perform the Matsubara sum for a function with known poles, z_j . The contribution from the contour goes to zero as $|z| \rightarrow \infty$ and hence the contributions from the $z = ik_n$ and $z = z_j$ poles add up to zero.

In the following two subsections, we use the contour integration technique in two special cases.

10.4.1 Summations over functions with simple poles

Consider a Matsubara frequency sum like Eq. (10.43) but let us take a slightly more general function which could include more free Green's function. Let us therefore consider the sum

$$\mathcal{S}_0^F(\tau) = \frac{1}{\beta} \sum_{ik_n} g_0(ik_n) e^{ik_n \tau}, \quad \tau > 0, \quad (10.50)$$

where $g_0(z)$, has a number of known simple poles, e.g. in the form of non-interacting Green's functions like (10.43)

$$g_0(z) = \prod_j \frac{1}{z - z_j}, \quad (10.51)$$

where $\{z_j\}$ is the set of known poles and hence $g_0(z)$ is analytic elsewhere in the z -plane. Because we know the poles of g_0 a good choice for a contour is to take one that covers the entire complex plane $\mathcal{C}_\infty : z = R e^{i\theta}$ where $R \rightarrow \infty$, see Fig. 10.2. Such a contour would give us the contribution for poles of $n_F(z)$ plus the contributions from poles of $g_0(z)$. Furthermore, the contour integral itself gives zero because the integrand goes to zero exponentially for $z \in \mathcal{C}_\infty$ (remember $0 < \tau < \beta$)

$$n_F(z) e^{\tau z} = \frac{e^{\tau z}}{e^{\beta z} + 1} \propto \begin{cases} e^{(\tau - \beta) \text{Re } z} \rightarrow 0, & \text{for } \text{Re } z > 0, \\ e^{\tau \text{Re } z} \rightarrow 0, & \text{for } \text{Re } z < 0. \end{cases} \quad (10.52)$$

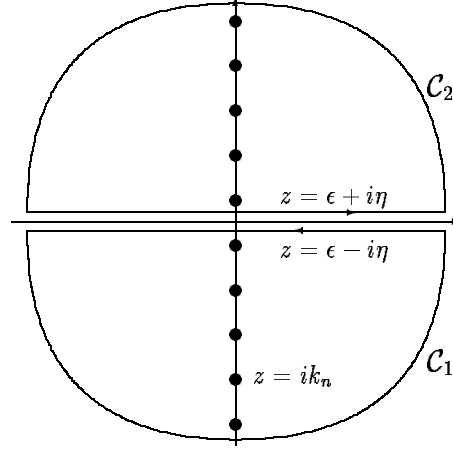


Figure 10.3: The contour used to perform the Matsubara sum for a function with known branch cuts, i.e. it is known to be an analytic function in the entire complex plane exempt on the branch cuts. The contribution from the outer parts of the contour goes to zero as $|z| \rightarrow \infty$ and hence only the paths parallel to the cut (here the real axis) contribute.

Hence

$$\begin{aligned}
 0 &= \int_{C_\infty} \frac{dz}{2\pi i} n_F(z) g_0(z) e^{z\tau} \\
 &= -\frac{1}{\beta} \sum_{ik_n} g_0(ik_n) e^{ik_n\tau} + \sum_j \text{Res}_{z=z_j} [g_0(z)] n_F(z_j) e^{z_j\tau},
 \end{aligned} \tag{10.53}$$

and thus

$$S_0^F(\tau) = \sum_j \text{Res}_{z=z_j} [g_0(z)] n_F(z_j) e^{z_j\tau}. \tag{10.54}$$

The Matsubara sum has thus been simplified considerably and we shall use this formula several times during the course. For bosons the derivation is almost identical and we get

$$\frac{1}{\beta} \sum_{i\omega_n} g_0(i\omega_n) e^{i\omega_n\tau} = S_0^B(\tau) = - \sum_j \text{Res}_{z=z_j} [g_0(z)] n_B(z_j) e^{z_j\tau}. \tag{10.55}$$

10.4.2 Summations over functions with known branch cuts

The second type of sums we will meet are of the form in Eq.(10.42). If it is the full Green's function, including for example the influence of interaction, we do not know the poles of the Green's function, but we do know that it is analytic for z not on the real axis. This general property of the Green's function was shown in Sec. 10.2.

In general, consider the sum

$$S(\tau) = \frac{1}{\beta} \sum_{ik_n} g(ik_n) e^{ik_n\tau}, \quad \tau > 0, \tag{10.56}$$

where it is known that $g(z)$ is analytic in the entire complex plane except on the real axis. A contour which includes all points $z = ik_n$ and no singularities of g is therefore $\mathcal{C} = \mathcal{C}_1 + \mathcal{C}_2$ depicted in Fig. 10.3. As for the example in the previous section, see Eq. (10.52), the part where $|z| \rightarrow \infty$ does not contribute to the integral and we are left with the parts of the contour running parallel to the real axis. They are shifted by an infinitesimal amount η away from the real axis on either side

$$\begin{aligned}\mathcal{S}(\tau) &= - \int_{\mathcal{C}_1 + \mathcal{C}_2} \frac{dz}{2\pi i} n_F(z) g(z) e^{z\tau}, \\ &= - \frac{1}{2\pi i} \int_{-\infty}^{\infty} d\varepsilon n_F(\varepsilon) [g(\varepsilon + i\eta) - g(\varepsilon - i\eta)] e^{\varepsilon\tau}.\end{aligned}\quad (10.57)$$

For example, the sum in Eq. (10.42), becomes in this way

$$\begin{aligned}\mathcal{S}_1(\nu, \tau) &= - \frac{1}{2\pi i} \int_{-\infty}^{\infty} d\varepsilon n_F(\varepsilon) [\mathcal{G}(\nu, \varepsilon + i\eta) - \mathcal{G}(\nu, \varepsilon - i\eta)] e^{\varepsilon\tau}, \\ &= - \frac{1}{2\pi i} \int_{-\infty}^{\infty} d\varepsilon n_F(\varepsilon) 2i \operatorname{Im} [G^R(\nu, \varepsilon)] e^{\varepsilon\tau} \\ &= \int_{-\infty}^{\infty} \frac{d\varepsilon}{2\pi} n_F(\varepsilon) A(\nu, \varepsilon) e^{\varepsilon\tau},\end{aligned}\quad (10.58)$$

according to the definition of the spectral function in Eq. (8.49). In the second equality we used that $\mathcal{G}(\varepsilon - i\eta) = [\mathcal{G}(\varepsilon + i\eta)]^*$ which follows from Eq. (10.29) with $A = c_\nu$ and $B = c_\nu^\dagger$. Now setting the time argument in the single particle imaginary time Green's function, Eq. (10.33b), to a negative infinitesimal 0^- , we have in fact found an expression for the expectation value of the occupation, because

$$\begin{aligned}\langle c_\nu^\dagger c_\nu \rangle &= \mathcal{G}(\nu, 0^-) \\ &= \frac{1}{\beta} \sum_{ik_n} \mathcal{G}(\nu, ik_n) e^{-ik_n 0^-} = \mathcal{S}_1(\nu, 0^+) \\ &= \int_{-\infty}^{\infty} \frac{d\varepsilon}{2\pi} n_F(\varepsilon) A(\nu, \varepsilon),\end{aligned}\quad (10.59)$$

which agrees with our previous finding, Eq. (8.57).

10.5 Equation of motion

The equation of motion technique, used in Chap. 8 to find various Green's functions, can also be used for the Matsubara functions. In the imaginary time formalism the time derivative of an operator is

$$\partial_\tau A(\tau) = \partial_\tau (e^{\tau H} A e^{-\tau H}) = e^{\tau H} [H, A] e^{-\tau H} = [H, A](\tau) \quad (10.60)$$

If we differentiate the Matsubara function Eq. (10.17) with respect to τ , we obtain

$$\begin{aligned}-\partial_\tau \mathcal{C}_{AB}(\tau - \tau') &= \frac{\partial}{\partial \tau} (\theta(\tau - \tau') \langle A(\tau) B(\tau') \rangle \pm \theta(\tau' - \tau) \langle B(\tau') A(\tau) \rangle), \\ &= \delta(\tau - \tau') \langle AB - (\pm) BA \rangle + \langle T_\tau ([H, A](\tau) B(\tau')) \rangle,\end{aligned}$$

where the minus sign in $\langle AB - (\pm)BA \rangle$ is for fermion operators, whereas the plus sign should be used for boson operators.

For the single-particle Green's functions defined in Eqs. (10.33), we then get for both fermion and boson Green's functions

$$-\partial_\tau \mathcal{G}(\mathbf{r}\tau, \mathbf{r}'\tau') = \delta(\tau - \tau')\delta(\mathbf{r} - \mathbf{r}') + \left\langle T_\tau([H, \Psi(\mathbf{r})](\tau)\Psi^\dagger(\mathbf{r}', \tau')) \right\rangle, \quad (10.61a)$$

$$-\partial_\tau \mathcal{G}(\nu\tau, \nu'\tau') = \delta(\tau - \tau')\delta_{\nu\nu'} + \left\langle T_\tau([H, c_\nu](\tau)c_{\nu'}^\dagger(\tau')) \right\rangle. \quad (10.61b)$$

For non-interacting electrons the Hamiltonian is quadratic, i.e. of the general form

$$H_0 = \int d\mathbf{r} \int d\mathbf{r}' \Psi^\dagger(\mathbf{r})h_0(\mathbf{r}, \mathbf{r}')\Psi(\mathbf{r}'), \quad (10.62a)$$

$$H_0 = \sum_{\nu\nu'} t_{\nu\nu'} c_\nu^\dagger c_{\nu'}. \quad (10.62b)$$

In this case, the equations of motion therefore in the two representations reduce to

$$-\partial_\tau \mathcal{G}_0(\mathbf{r}\tau, \mathbf{r}'\tau') - \int d\mathbf{r}'' h_0(\mathbf{r}, \mathbf{r}'')\mathcal{G}_0(\mathbf{r}''\tau, \mathbf{r}'\tau') = \delta(\tau - \tau')\delta(\mathbf{r} - \mathbf{r}'), \quad (10.63a)$$

$$-\partial_\tau \mathcal{G}_0(\nu\tau, \nu'\tau') - \sum_{\nu''} t_{\nu\nu''}\mathcal{G}_0(\nu''\tau, \nu'\tau') = \delta(\tau - \tau')\delta_{\nu\nu'}, \quad (10.63b)$$

or in matrix form

$$\mathcal{G}_0^{-1}\mathcal{G}_0 = 1, \quad \mathcal{G}_0^{-1} = -\partial_\tau - H_0. \quad (10.64)$$

This equation together with the boundary condition $\mathcal{G}(\tau) = \pm\mathcal{G}(\tau + \beta)$ gives the solution. For example for free particle those given in Eqs. (10.37) and (10.38).

10.6 Wick's theorem

We end this rather technical part by proving an extremely useful theorem, which we will need later when doing perturbation theory, and which is used in the example ending this chapter. The theorem - called Wick's theorem - states that for non-interacting particles, i.e. when the Hamiltonian is quadratic, higher order Green's function involving more than one particle can be factorized into products of single-particle Green's functions.

Consider an n -particle Green's function defined as

$$\begin{aligned} \mathcal{G}_0^{(n)}(\nu_1\tau_1, \dots, \nu_n\tau_n; \nu'_1\tau'_1, \dots, \nu'_n\tau'_n) \\ = (-1)^n \left\langle T_\tau \left[\hat{c}_{\nu_1}(\tau_1) \cdots \hat{c}_{\nu_n}(\tau_n) \hat{c}_{\nu'_n}^\dagger(\tau'_n) \cdots \hat{c}_{\nu'_1}^\dagger(\tau'_1) \right] \right\rangle_0. \end{aligned} \quad (10.65)$$

The average is taken with respect to a non-interacting Hamiltonian H_0 (like Eq. (10.62)), which we have indicated by the subscript 0. The time-evolution is also with respect to H_0 and it is given by

$$\hat{c}(\tau) = e^{\tau H_0} c e^{-\tau H_0}. \quad (10.66)$$

The expression in (10.65) is indeed quite complicated to look at if we write out all the possible orderings and the conditions for that particular ordering. For example if $n = 2$, there are 4 time arguments which can be ordered in 4! different ways. Let us simplify the writing by defining one operator symbol for both creation and annihilation operators

$$d_j(\sigma_j) = \begin{cases} \hat{c}_{\nu_j}(\tau_j), & j \in [1, n], \\ \hat{c}_{\nu'_{(2n+1-j)}}^{\dagger}(\tau'_{(2n+1-j)}), & j \in [n+1, 2n], \end{cases} \quad (10.67)$$

and furthermore define the permutations of the $2n$ operators as

$$P(d_1(\sigma_1) \cdots d_{2n}(\sigma_{2n})) = d_{P_1}(\sigma_{P_1}) \cdots d_{P_{2n}}(\sigma_{P_{2n}}), \quad (10.68)$$

where P_j denotes the j 'th variable in the permutation P (e.g. define the list (a, b, c) and the permutation (c, a, b) then $P = (3, 1, 2)$). Which permutation is the correct one of course depends on how the time arguments in (10.65) are really ordered. Therefore if we sum over all permutations and include the corresponding conditions, we can rewrite $\mathcal{G}_0^{(n)}$ as

$$\begin{aligned} \mathcal{G}_0^{(n)}(j_1, \dots, j_{2n}) &= (-1)^n \sum_{P \in S_{2n}} (\pm 1)^P \theta(\sigma_{P_1} - \sigma_{P_2}) \cdots \theta(\sigma_{P_{n-1}} - \sigma_{P_n}) \\ &\quad \times \left\langle d_{P_1}(\sigma_{P_1}) \cdots d_{P_{2n}}(\sigma_{P_{2n}}) \right\rangle_0, \end{aligned} \quad (10.69)$$

where the factor $(\pm 1)^P$ takes into account that for fermions (minus sign) it costs a sign change every time a pair of operators are commuted.

The easiest way to show Wick's theorem is through the equation of motion for the n -particle Green's function. Thus we differentiate $\mathcal{G}_0^{(n)}$ with respect to one of time arguments, τ_1, \dots, τ_n . This gives two kinds of contributions: the terms coming from the derivative of the theta functions and one term from the derivative of the expectation value itself. The last one gives for example for τ_1

$$\left[-\frac{\partial}{\partial \tau_1} \mathcal{G}_0^{(n)} \right]_{\text{last term}} = -(-1)^n \left\langle T_{\tau} \left[[\hat{H}_0, \hat{c}_{\nu_1}](\tau_1) \cdots \hat{c}_{\nu_n}(\tau_n) \hat{c}_{\nu'_n}^{\dagger}(\tau'_n) \cdots \hat{c}_{\nu'_1}^{\dagger}(\tau'_1) \right] \right\rangle, \quad (10.70)$$

which is similar to the derivation that lead to Eqs. (10.63) and (10.64), so that we have

$$\mathcal{G}_{0i}^{-1} \mathcal{G}_0^{(n)} = -\partial_{\tau_i}^{\theta} \mathcal{G}_0^{(n)}, \quad (10.71)$$

where \mathcal{G}_{0i}^{-1} means that it works on the coordinate ν_i, τ_i . On the right hand side the derivative only acts on the theta functions in Eq. (10.69).

Take now for example the case where τ_i is next to τ'_j . There are two such terms in (10.69), corresponding to τ_i being either smaller or larger than τ'_j , and they will have different order of the permutation. In this case $\mathcal{G}^{(n)}$ has the structure

$$\begin{aligned} \mathcal{G}_0^{(n)} &= [\cdots \theta(\tau_i - \tau'_j) \cdots] \left\langle \cdots \hat{c}_{\nu_i}(\tau_i) \hat{c}_{\nu'_j}^{\dagger}(\tau'_j) \cdots \right\rangle \\ &\quad \pm [\cdots \theta(\tau'_j - \tau_i) \cdots] \left\langle \cdots \hat{c}_{\nu'_j}^{\dagger}(\tau'_j) \hat{c}_{\nu_i}(\tau_i) \cdots \right\rangle, \end{aligned} \quad (10.72)$$

and when this is differentiated with respect to τ_i it gives two delta functions, and hence

$$-\partial_{\tau_i}^\theta \mathcal{G}_0^{(n)} = \left([\dots] \left\langle \dots \hat{c}_{\nu_i}(\tau_i) \hat{c}_{\nu'_j}^\dagger(\tau'_j) \dots \right\rangle \mp [\dots] \left\langle \dots \hat{c}_{\nu'_j}^\dagger(\tau'_j) \hat{c}_{\nu_i}(\tau_i) \dots \right\rangle \right) \delta(\tau_i - \tau'_j). \quad (10.73)$$

We can pull out the equal time commutator or anti-commutator for boson or fermions, respectively

$$\left[\hat{c}_{\nu_i}(\tau_i), \hat{c}_{\nu'_j}^\dagger(\tau_i) \right]_{B,F} = \delta_{\nu_i, \nu'_j}. \quad (10.74)$$

If τ_i is next to τ_j instead of τ'_j , we get in the same manner the (anti-)commutator

$$\left[\hat{c}_{\nu_i}(\tau_i), \hat{c}_{\nu_j}(\tau_i) \right]_{B,F} = 0, \quad (10.75)$$

which therefore does not contribute. The number of creation and annihilation operators has thus both been reduced by one, and it leaves a Green's function which is no longer an n -particle Green's function but an $(n-1)$ -Green's function. In fact, we saw a special case of this in Eq. (10.63) where a one-particle Green's function was reduced to a zero-particle Green's function, i.e. a constant. What we have not determined is the sign of the new $(n-1)$ -Green's function, and this sign denoted $(-1)^x$ will (for fermions) depend on the τ'_j in question. Besides this undetermined sign, our equation of motion (10.71) now looks like

$$\mathcal{G}_{0i}^{-1} \mathcal{G}_0^{(n)} = \sum_{j=1}^n \delta_{\nu_i, \nu'_j} \delta(\tau_i - \tau'_j) (-1)^x \mathcal{G}_0^{(n-1)} \underbrace{(\nu_1 \tau_1, \dots, \nu_n \tau_n)}_{\text{without } i} \underbrace{(\nu'_1 \tau'_1, \dots, \nu'_n \tau'_n)}_{\text{without } j}. \quad (10.76)$$

Let us collect the signs that go into $(-1)^x$: (-1) from $(-\partial_\tau)$, $(-1)^n$ from the definition in (10.65) $[(-1)^{n-1}]^{-1}$ from the definition of $\mathcal{G}^{(n-1)}$, and for fermions $(-1)^{n-i+n-j}$ from moving $\hat{c}_{\nu'_j}^\dagger$ next to \hat{c}_{ν_i} . Hence

$$\text{fermions: } (-1)^x = -(-1)^n (-1)^{1-n} (-1)^{2n-i-j} = (-1)^{j+i}, \quad (10.77a)$$

$$\text{bosons: } (-1)^x = -(-1)^n (-1)^{1-n} = 1, \quad (10.77b)$$

Now Eq. (10.76) can be integrated and because $\mathcal{G}_0^{(n)}$ has the same boundary conditions as \mathcal{G}_0 , i.e. periodic in the time arguments, it gives the same result and hence

$$\mathcal{G}_0^{(n)} = \sum_{j=1}^n (\pm)^{j+i} \mathcal{G}_0(\nu_i \tau_i, \nu'_j \tau'_j) \mathcal{G}_0^{(n-1)} \underbrace{(\nu_1 \tau_1, \dots, \nu_n \tau_n)}_{\text{without } i} \underbrace{(\nu'_1 \tau'_1, \dots, \nu'_n \tau'_n)}_{\text{without } j}. \quad (10.78)$$

By recalling the definition of a determinants this formula is immediately recognized as the determinant in the case where the minus sign should be used. With the plus sign it is called a permanent. We therefore end up with

$$\mathcal{G}_0^{(n)}(1, \dots, n; 1', \dots, n') = \left| \begin{array}{ccc} \mathcal{G}_0(1, 1') & \cdots & \mathcal{G}_0(1, n') \\ \vdots & \ddots & \vdots \\ \mathcal{G}_0(n, 1') & \cdots & \mathcal{G}_0(n, n') \end{array} \right|_{B,F}, \quad i \equiv (\nu_i, \tau_i) \quad (10.79)$$

where we used a shorthand notation with the orbital and the time arguments being collected into one variable, and where the determinant $|\cdot|_{B,F}$ means that for fermions it is the usual determinant, while for bosons it should be understood as a permanent where all have terms come with a plus sign; this is Wick's theorem.

10.7 Example: polarizability of free electrons

In Sec. 8.5 we calculated the polarizability of *non-interacting free electrons*. In order to illustrate the working principle of the imaginary time formalism, we do it again here.

The starting point is the physical quantity which is needed: the frequency dependent retarded charge-charge correlation function, $\chi^R(\mathbf{q}, \omega)$, which follows from the corresponding Matsubara function by

$$\chi^R(\mathbf{q}, \omega) = \chi(\mathbf{q}, iq_n \rightarrow \omega + i\eta). \quad (10.80)$$

In order to find $\chi(\mathbf{q}, iq_n)$ we start from the time-dependent χ

$$\chi_0(\mathbf{q}, \tau) = -\frac{1}{\mathcal{V}} \langle T_\tau (\rho(\mathbf{q}, \tau) \rho(-\mathbf{q})) \rangle_0, \quad (10.81)$$

and expresses it as a two-particle Green's function

$$\chi_0(\mathbf{q}, \tau) = -\frac{1}{\mathcal{V}} \sum_{\mathbf{k}, \mathbf{k}', \sigma, \sigma'} \left\langle T_\tau \left(c_{\mathbf{k}\sigma}^\dagger(\tau) c_{\mathbf{k}+\mathbf{q}\sigma}(\tau) c_{\mathbf{k}'\sigma'}^\dagger c_{\mathbf{k}'-\mathbf{q}\sigma'} \right) \right\rangle_0. \quad (10.82)$$

By Wick's theorem this is given by a product of single-particle Green's functions with all possible pairings and with the sign given by the number of times we interchange two fermion operators, i.e.

$$\begin{aligned} \chi_0(\mathbf{q}, \tau) &= \frac{1}{\mathcal{V}} \sum_{\mathbf{k}, \mathbf{k}', \sigma, \sigma'} \left\langle T_\tau \left(c_{\mathbf{k}+\mathbf{q}\sigma}(\tau) c_{\mathbf{k}'\sigma'}^\dagger \right) \right\rangle_0 \left\langle T_\tau \left(c_{\mathbf{k}'-\mathbf{q}\sigma'}(0) c_{\mathbf{k}\sigma}^\dagger(\tau) \right) \right\rangle_0 - \frac{1}{\mathcal{V}} \overbrace{\langle \rho(\mathbf{q}) \rangle_0 \langle \rho(-\mathbf{q}) \rangle_0}^{=0 \text{ for } q \neq 0}, \\ &= \frac{1}{\mathcal{V}} \sum_{\mathbf{k}\sigma} \mathcal{G}_0(\mathbf{k} + \mathbf{q}\sigma, \tau) \mathcal{G}_0(\mathbf{k}\sigma, -\tau). \end{aligned} \quad (10.83)$$

where we consider only $q \neq 0$ and use that $\mathcal{G}_0(\mathbf{k}, \mathbf{k}') \propto \delta_{\mathbf{k}, \mathbf{k}'}$.

The next step is to calculate the frequency dependent function, i.e. to Fourier transform the product (10.83). The Fourier transform of a product in the time domain is a convolution in the frequency domain. Because one function has argument τ while the other has argument $-\tau$, the internal frequencies in the two come with the same sign

$$\chi_0(\mathbf{q}, iq_n) = \frac{1}{\beta} \sum_{ik_n} \frac{1}{\mathcal{V}} \sum_{\mathbf{k}\sigma} \mathcal{G}_0(\mathbf{k} + \mathbf{q}\sigma, ik_n + iq_n) \mathcal{G}_0(\mathbf{k}\sigma, ik_n). \quad (10.84)$$

The sum over Matsubara frequencies has exactly the form studied in Sec. 10.4.1. Remembering that $\mathcal{G}_0(\mathbf{k}\sigma, ik_n) = 1/(ik_n - \xi_{\mathbf{k}})$, we can read off the answer from Eq.(10.54)

by inserting the poles of the two $\mathcal{G}_0(\mathbf{k}\sigma, z)$ ($z = \xi_{\mathbf{k}}$ and $z = \xi_{\mathbf{k}+\mathbf{q}} - iq_n$) and obtain

$$\begin{aligned}\chi_0(\mathbf{q}, iq_n) &= \frac{1}{\mathcal{V}} \sum_{\mathbf{k}} \{n_F(\xi_{\mathbf{k}}) \mathcal{G}_0(\mathbf{k} + \mathbf{q}\sigma, \xi_{\mathbf{k}} + iq_n) + n_F(\xi_{\mathbf{k}+\mathbf{q}} - iq_n) \mathcal{G}_0(\mathbf{k}\sigma, \xi_{\mathbf{k}+\mathbf{q}} - iq_n)\} \\ &= \frac{1}{\mathcal{V}} \sum_{\mathbf{k}\sigma} \frac{n_F(\xi_{\mathbf{k}}) - n_F(\xi_{\mathbf{k}+\mathbf{q}})}{iq_n + \xi_{\mathbf{k}} - \xi_{\mathbf{k}+\mathbf{q}}}.\end{aligned}\quad (10.85)$$

Here we used that

$$n_F(\xi_{\mathbf{k}+\mathbf{q}} - iq_n) = \frac{1}{e^{\beta\xi_{\mathbf{k}+\mathbf{q}}} e^{-\beta iq_n} + 1} = \frac{1}{e^{\beta\xi_{\mathbf{k}+\mathbf{q}}} + 1}, \quad (10.86)$$

because iq_n is a bosonic frequency. After the substitution (10.80) Eq. (10.85) gives the result we found in Eq. (8.81).

10.8 Summary and outlook

When performing calculations of physical quantities at finite temperatures it turns out that the easiest way to find the “real time” introduced in Chap. 7 is often to go via the imaginary time formalism. This formalism has been introduced in this chapter, and in the following chapters on Feynman diagrams it is a necessary tool. There you will see why it is more natural to use the imaginary time Green’s function, also called Matsubara Green’s function. The reason is that the time evolution operator and the Boltzmann weight factor can be treated on an equal footing and one single perturbation expansion suffices. In the real time formalism there is no simple way of doing this.

We have also derived some very useful relations concerning sums over Matsubara frequencies. The things to remember are the following.

Non-interacting particle Green’s function, valid for both bosons and fermions

$$\mathcal{G}_0(\nu, i\omega_n) = \frac{1}{i\omega_n - \xi_\nu}. \quad (10.87)$$

Matsubara frequency sum over products of non-interacting Green’s functions (for $\tau > 0$)

$$\mathcal{S}^F(\tau) = \frac{1}{\beta} \sum_{ik_n} g_0(ik_n) e^{ik_n\tau} = \sum_j \text{Res}(g_0(z_j)) n_F(z_j) e^{z_j\tau}, \quad ik_n \text{ fermion frequency}, \quad (10.88a)$$

$$\mathcal{S}^B(\tau) = \frac{1}{\beta} \sum_{i\omega_n} g_0(i\omega_n) e^{i\omega_n\tau} = - \sum_j \text{Res}(g_0(z_j)) n_B(z_j) e^{z_j\tau}, \quad i\omega_n \text{ boson frequency}, \quad (10.88b)$$

with $g_0(z) = \prod_i 1/(z - \xi_i)$. If we perform a sum over functions where the poles are unknown but where the branch cuts are known, we can use a contour depicted in Fig.

10.3. For example if $g(ik_n)$ is known to be analytic everywhere but on the real axis we get

$$\begin{aligned}\mathcal{S}^F(\tau) &= \frac{1}{\beta} \sum_{ik_n} g(ik_n) e^{ik_n \tau} = - \int_{-\infty}^{\infty} \frac{d\varepsilon}{2\pi i} n_F(\varepsilon) [g(\varepsilon + i\eta) - g(\varepsilon - i\eta)] \\ &= - \int_{-\infty}^{\infty} \frac{d\varepsilon}{2\pi i} n_F(\varepsilon) [g^R(\varepsilon) - g^A(\varepsilon)] .\end{aligned}\quad (10.89)$$

Finally, we proved an important theorem, Wick's theorem, which says that for non-interacting an n -particle Green's function is equal to a sum of products of single-particle Green's functions, where all possible pairings should be included in the sum. For fermions we must furthermore keep track of the number of factors -1 , because each time we interchange two fermion operators we must include a factor -1 . The end result was

$$\mathcal{G}_0^{(n)}(1, \dots, n; 1', \dots, n') = \left| \begin{array}{ccc} \mathcal{G}_0(1, 1') & \cdots & \mathcal{G}_0(1, n') \\ \vdots & \ddots & \vdots \\ \mathcal{G}_0(n, 1') & \cdots & \mathcal{G}_0(n, n') \end{array} \right|_{B,F}, \quad i \equiv (\nu_i, \tau_i), \quad (10.90)$$

where

$$\mathcal{G}_0^{(n)}(1, \dots, n; 1', \dots, n') = (-1)^n \left\langle T_\tau \left[\hat{c}(1) \cdots \hat{c}(n) \hat{c}^\dagger(n') \cdots \hat{c}^\dagger(1') \right] \right\rangle_0. \quad (10.91)$$

Chapter 11

Feynman diagrams and external potentials

From the previous chapters on linear response theory and Green's functions, it is clear that complete calculations of thermal averages of time-dependent phenomena in quantum field theory are a rather formidable task. Even the basic imaginary time evolution operator $\hat{U}(\tau)$ itself is an infinite series to all orders in the interaction $\hat{V}(\mathbf{r}, \tau)$. One simply faces the problem of getting lost in the myriads of integrals, and not being able to maintain a good physical intuition of which terms are important. In 1948 Feynman solved this problem as part of his seminal work on quantum electrodynamics by inventing the ingenious diagrams that today bear his name. The Feynman diagrams are both an exact mathematical representation of perturbation theory to infinite order and a powerful pictorial method that elucidate the physical content of the complicated expressions. In this chapter we introduce the Feynman diagrams for the case of non-interacting particles in an external potential. Our main example of their use will be the analysis of electron-impurity scattering in disordered metals.

11.1 Non-interacting particles in external potentials

Consider a time-independent Hamiltonian H in the space representation describing non-interacting fermions in an external spin-diagonal single-particle potential $V_\sigma(\mathbf{r})$:

$$H = H_0 + V = \sum_{\sigma} \int d\mathbf{r} \Psi_{\sigma}^{\dagger}(\mathbf{r}) H_0(\mathbf{r}) \Psi_{\sigma}(\mathbf{r}) + \sum_{\sigma} \int d\mathbf{r} \Psi_{\sigma}^{\dagger}(\mathbf{r}) V_{\sigma}(\mathbf{r}) \Psi_{\sigma}(\mathbf{r}). \quad (11.1)$$

As usual we assume that the unperturbed system described by the time-independent Hamiltonian H_0 is solvable, and that we know the corresponding eigenstates $|\nu\rangle$ and Green's functions \mathcal{G}_{ν}^0 . In the following it will prove helpful to introduce the short-hand notation

$$(\mathbf{r}_1, \sigma_1, \tau_1) = (1) \quad \text{and} \quad \int d1 = \sum_{\sigma_1} \int d\mathbf{r}_1 \int_0^{\beta} d\tau_1 \quad (11.2)$$

for points and integrals in space-time.

We want to study the full Green's function, $\mathcal{G}(b, a) = -\langle T_\tau \Psi(b) \Psi^\dagger(a) \rangle$, governed by H , and the bare one, $\mathcal{G}^0(b, a) = -\langle T_\tau \hat{\Psi}(b) \hat{\Psi}^\dagger(a) \rangle_0$, governed by H_0 . We note that since no particle-particle interaction is present in Eq. (11.1) both the full Hamiltonian H and the bare H_0 have the simple form of Eq. (10.62), and the equations of motion for the two Green's functions have the same form as Eq. (10.63):

$$[-\partial_{\tau_b} - H_0(b)] \mathcal{G}^0(b, a) = \delta(b-a) \quad \Leftrightarrow \quad [-\partial_{\tau_b} - H(b) + V(b)] \mathcal{G}^0(b, a) = \delta(b-a) \quad (11.3a)$$

$$[-\partial_{\tau_b} - H(b)] \mathcal{G}(b, a) = \delta(b-a) \quad \Leftrightarrow \quad \mathcal{G}(b, a) = [-\partial_{\tau_b} - H(b)]^{-1} \delta(b-a), \quad (11.3b)$$

where we have also given the formal solution of \mathcal{G} , which is helpful in acquiring the actual solution for \mathcal{G} . Substituting $\delta(b-a)$ in Eq. (11.3b) by the expression from Eq. (11.3a) yields:

$$\begin{aligned} [-\partial_{\tau_b} - H(b)] \mathcal{G}(b, a) &= [-\partial_{\tau_b} - H(b) + V(b)] \mathcal{G}^0(b, a) \\ &= [-\partial_{\tau_b} - H(b)] \mathcal{G}^0(b, a) + V(b) \mathcal{G}^0(b, a) \\ &= [-\partial_{\tau_b} - H(b)] \mathcal{G}^0(b, a) + \int d1 \delta(b-1) V(1) \mathcal{G}^0(1, a). \end{aligned} \quad (11.4)$$

Acting from the left with $[-\partial_{\tau_b} - H(b)]^{-1}$ gives an integral equation for \mathcal{G} , the so-called Dyson equation,

$$\mathcal{G}(b, a) = \mathcal{G}^0(b, a) + \int d1 \mathcal{G}(b, 1) V(1) \mathcal{G}^0(1, a), \quad (11.5)$$

where we have used the second expression in Eq. (11.3b) to introduce \mathcal{G} in the integrand. By iteratively inserting \mathcal{G} itself in the integrand on the left-hand side we obtain the infinite perturbation series

$$\begin{aligned} \mathcal{G}(b, a) &= \mathcal{G}^0(b, a) + \int d1 \mathcal{G}^0(b, 1) V(1) \mathcal{G}^0(1, a) \\ &\quad + \int d1 \int d2 \mathcal{G}^0(b, 1) V(1) \mathcal{G}^0(1, 2) V(2) \mathcal{G}^0(2, a) \\ &\quad + \int d1 \int d2 \int d3 \mathcal{G}^0(b, 1) V(1) \mathcal{G}^0(1, 2) V(2) \mathcal{G}^0(2, 3) V(3) \mathcal{G}^0(3, a) + \dots \end{aligned} \quad (11.6)$$

The solutions Eqs. (11.5) and (11.6) for \mathcal{G} are easy to interpret. The propagator, \mathcal{G} , of a fermion in an external potential is given as the sum of all possible processes involving unperturbed propagation, described by \mathcal{G}^0 , intersected by any number of scattering events V . So in this simple case there is really no need for further elucidation, but we will anyway proceed by introducing the corresponding Feynman diagrams.

The first step is to define the basic graphical vocabulary, i.e. to define the pictograms representing the basic quantities \mathcal{G} , \mathcal{G}^0 , and V of the problem. This vocabulary is known

as the Feynman rules:

$$\mathcal{G}(b, a) = \text{double arrow from } a \text{ to } b \quad \mathcal{G}^0(b, a) = \text{single arrow from } a \text{ to } b \quad \int d1 V(1) \dots = \star 1 \quad (11.7)$$

Note how the fermion lines point from the points of creation, e.g. $\Psi^\dagger(a)$, to the points of annihilation, e.g. $\Psi(b)$. Using the Feynman rules the infinite perturbation series Eq. (11.6) becomes

$$\text{double arrow } a \rightarrow b = \text{single arrow } a \rightarrow b + \text{single arrow } a \rightarrow \star 1 \rightarrow \text{single arrow } 1 \rightarrow b + \text{single arrow } a \rightarrow \star 1 \rightarrow \star 2 \rightarrow \text{single arrow } 2 \rightarrow b + \dots \quad (11.8)$$

In this form we clearly see how the full propagator from a to b is the sum over all possible ways to connect a and b with bare propagators via any number of scattering events. We can also perform calculations by manipulating the diagrams. Let us for example derive an integral form equivalent to Eq. (11.5) from Eq. (11.8):

$$\text{double arrow } a \rightarrow b = \text{single arrow } a \rightarrow b + \left(\text{single arrow } a \rightarrow \star 1 \times \left(\text{single arrow } 1 \rightarrow a + \text{single arrow } 1 \rightarrow \star 2 \rightarrow \text{single arrow } 2 \rightarrow a + \dots \right) \right) = \text{single arrow } a \rightarrow b + \text{double arrow } a \rightarrow \star 1 \rightarrow b \quad (11.9)$$

which by using the Feynman rules can be written as

$$\mathcal{G}(b, a) = \mathcal{G}^0(b, a) + \int d1 \mathcal{G}^0(b, 1) V(1) \mathcal{G}(1, a). \quad (11.10)$$

The former integral equation Eq. (11.5) for \mathcal{G} is obtained by pulling out the bottom part $V(n) \mathcal{G}^0(n, a)$ of every diagram on the right hand side of Eq. (11.8), thereby exchanging the arrow and the double-arrow in the last diagram of Eq. (11.9).

This is a first demonstration of the compactness of the Feynman diagram, and how visual clarity is obtained without loss of mathematical rigor.

11.2 Elastic scattering and Matsubara frequencies

When a fermion system interacts with a static external potential no energy is transferred between the two systems, a situation referred to as elastic scattering. The lack of energy

transfer in elastic scattering is naturally reflected in a particularly simple form of the single-particle Green's function $\mathcal{G}(ik_n)$ in Matsubara frequency space. In the following the spin index σ is left out since the same answer is obtained for the two spin directions.

First we note that since the Hamiltonian H in Eq. (11.1) is time-independent for static potentials we know from Eq. (10.19) that $\mathcal{G}(\mathbf{r}\tau, \mathbf{r}'\tau')$ depends only on the time difference $\tau - \tau'$, and according to Eqs. (10.22b) and (10.25) it can therefore be expressed in terms of a Fourier transform with just one fermionic Matsubara frequency ik_n :

$$\mathcal{G}(\mathbf{r}\tau, \mathbf{r}'\tau') = \frac{1}{\beta} \sum_n \mathcal{G}(\mathbf{r}, \mathbf{r}'; ik_n) e^{-ik_n(\tau - \tau')}, \quad \mathcal{G}(\mathbf{r}, \mathbf{r}'; ik_n) = \int_0^\beta d\tau \mathcal{G}(\mathbf{r}\tau, \mathbf{r}'\tau') e^{ik_n(\tau - \tau')}. \quad (11.11)$$

The Fourier transform of the time convolution $\int d\tau_1 \mathcal{G}^0(\tau_b - \tau_1) V \mathcal{G}(\tau_1 - \tau_a)$ appearing in the integral equation of \mathcal{G} is the product $\mathcal{G}^0(ik_n) V \mathcal{G}(ik_n)$. The elastic scattering, i.e. the time-independent V , cannot change the frequencies of the propagators. In Matsubara frequency space the Dyson equation Eq. (11.10) takes the form

$$\mathcal{G}(\mathbf{r}_b, \mathbf{r}_a; ik_n) = \mathcal{G}^0(\mathbf{r}_b, \mathbf{r}_a; ik_n) + \int d\mathbf{r}_1 \mathcal{G}^0(\mathbf{r}_b, \mathbf{r}_1; ik_n) V(1) \mathcal{G}(\mathbf{r}_1, \mathbf{r}_a; ik_n). \quad (11.12)$$

As seen previously, the expressions are simplified by transforming from the $|\mathbf{r}\rangle$ -basis to the basis $|\nu\rangle$ which diagonalizes H_0 . We define the transformed Green's function in this basis as follows:

$$\mathcal{G}_{\nu\nu'} \equiv \int d\mathbf{r} d\mathbf{r}' \langle \nu | \mathbf{r} \rangle \mathcal{G}(\mathbf{r}, \mathbf{r}') \langle \mathbf{r}' | \nu' \rangle \quad \Leftrightarrow \quad \mathcal{G}(\mathbf{r}, \mathbf{r}') = \sum_{\nu\nu'} \langle \mathbf{r} | \nu \rangle \mathcal{G}_{\nu\nu'} \langle \nu' | \mathbf{r}' \rangle. \quad (11.13)$$

In a similar way we define the $|\nu\rangle$ -transform of $V(\mathbf{r})$ as $V_{\nu\nu'} \equiv \int d\mathbf{r} \langle \nu | \mathbf{r} \rangle V(\mathbf{r}) \langle \mathbf{r} | \nu' \rangle$. In the $|\nu, ik_n\rangle$ representation the equation of motion Eq. (11.3b) for \mathcal{G} is a matrix equation,

$$\sum_{\nu''} [(ik_n - \xi_\nu) \delta_{\nu, \nu''} - V_{\nu, \nu''}] \mathcal{G}_{\nu'', \nu'}(ik_n) = \delta_{\nu, \nu'} \quad \text{or} \quad [ik_n \bar{1} - \bar{E}_0 - \bar{V}] \bar{\mathcal{G}}(ik_n) = \bar{1}, \quad (11.14)$$

where \bar{E}_0 is a diagonal matrix with the eigenenergies $\xi_\nu = \varepsilon_\nu - \mu$ along the diagonal. We have thus reduced the problem of finding the full Green's function to a matrix inversion problem. We note in particular that in accordance with Eq. (10.40) the bare propagator \mathcal{G}^0 has the simple diagonal form

$$\sum_{\nu''} (ik_n - \xi_\nu) \delta_{\nu, \nu''} \mathcal{G}_{\nu'', \nu'}^0(ik_n) = \delta_{\nu, \nu'} \quad \Rightarrow \quad \mathcal{G}_{\nu, \nu'}^0(ik_n) = \frac{1}{ik_n - \xi_\nu} \delta_{\nu, \nu'}. \quad (11.15)$$

We can utilize this to rewrite the integral equation Eq. (11.12) as a simple matrix equation,

$$\mathcal{G}(\nu_b \nu_a; ik_n) = \delta_{\nu_b, \nu_a} \mathcal{G}^0(\nu_a \nu_a; ik_n) + \sum_{\nu_c} \mathcal{G}^0(\nu_b \nu_c; ik_n) V_{\nu_c \nu_a} \mathcal{G}(\nu_c \nu_a; ik_n). \quad (11.16)$$

We can also formulate Feynman rules in (ν, ik_n) -space. We note that $\bar{\mathcal{G}}_0$ is diagonal in ν , while \bar{V} is a general matrix. To get the sum of all possible quantum processes one must

sum over all matrix indices different from the externally given ν_a and ν_b . The frequency argument is suppressed, since the Green's functions are diagonal in ik_n .

$$\mathcal{G}_{\nu_b\nu_a} = \text{diagram with two vertical lines, top dot } \nu_b, \text{ bottom dot } \nu_a, \text{ and a double arrow pointing up} \quad \mathcal{G}_{\nu_b\nu_a}^0 = \delta_{\nu_b\nu_a} \text{diagram with two vertical lines, top dot } \nu_b, \text{ bottom dot } \nu_a, \text{ and a single arrow pointing up} = \frac{\delta_{\nu_a\nu_b}}{ik_n - \xi_{\nu_a}} \quad V_{\nu\nu'} = \star_{\nu'}^{\nu} \quad (11.17)$$

Using these Feynman rules in (ν, ik_n) -space we can express Dyson's equation Eq. (11.16) diagrammatically:

$$\text{diagram with two vertical lines, top dot } \nu_b, \text{ bottom dot } \nu_a, \text{ and a double arrow pointing up} = \delta_{\nu_b\nu_a} \text{diagram with two vertical lines, top dot } \nu_a, \text{ bottom dot } \nu_a, \text{ and a single arrow pointing up} + \text{diagram with two vertical lines, top dot } \nu_b, \text{ bottom dot } \nu_a, \text{ and a double arrow pointing up with a star in the middle} \quad (11.18)$$

11.3 Random impurities in disordered metals

An important example of elastic scattering by external potentials is the case of random impurities in a disordered metal. One well-controlled experimental realization of this is provided by a perfect metal Cu lattice with Mg^{II} ions substituting a small number of randomly chosen Cu^{I} ions. The valence of the impurity ions is one higher than the host ions, and as a first approximation an impurity ion at site \mathbf{P}_j gives rise to a simple screened mono-charge Coulomb potential $u_j(\mathbf{r}) = -(e_0^2/|\mathbf{r} - \mathbf{P}_j|) e^{-|\mathbf{r} - \mathbf{P}_j|/a}$. The screening is due to the electrons in the system trying to neutralize the impurity charge, and as a result the range of the potential is finite, given by the so-called screening length a . This will be discussed in detail in Chap. 13.

In Fig. 11.1(a) is sketched a number of randomly positioned impurities in an otherwise perfect metal lattice. The presence of the impurities can be detected by measuring the (longitudinal) resistivity ρ_{xx} of the metal as a function of temperature. At high temperature the resistivity is mainly due to electron-phonon scattering, and since the vibrational

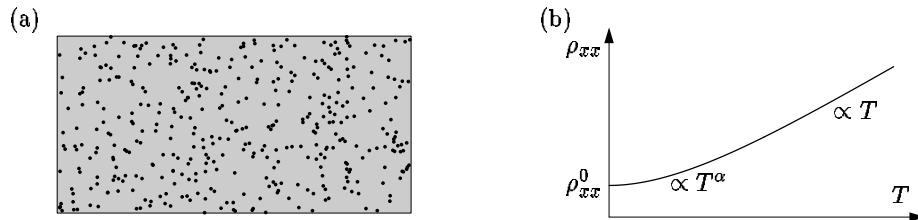


Figure 11.1: (a) A disordered metal consisting of an otherwise perfect metal lattice with a number of randomly positioned impurities giving rise to elastic electron-impurity scattering. (b) The electrical resistivity $\rho_{xx}(T)$ of the disordered metal as a function of temperature. At high T the electron-phonon scattering dominates giving rise to a linear behavior, while at low T only the electron-impurity scattering is effective and gives rise to the non-zero value ρ_{xx}^0 of ρ_{xx} at $T = 0$.

energy $\hbar\omega(n + \frac{1}{2})$ in thermal equilibrium is proportional to $k_B T$, the number n of phonons, and hence the electron-phonon scattering rate, is also proportional to T (see e.g. Exercise 3.2). At lower temperature the phonon degrees of freedom begin to freeze out and the phase space available for scattering also shrinks, and consequently the resistivity becomes proportional to some power α of T . Finally, at the lowest temperatures, typically a few kelvin, only the electron-impurity scattering is left preventing the Bloch electrons in moving unhindered through the crystal. As a result the resistivity levels off at some value, ρ_0 , the so-called residual resistivity. The temperature behavior of the resistivity is depicted in Fig. 11.1(b).

We postpone the calculation of the resistivity and in this section just concentrate on studying the electron Matsubara Green's function \mathcal{G} for electrons moving in such a disordered metal. We use the plane wave states $|\mathbf{k}\sigma\rangle$ from the effective mass approximation Eq. (2.16) as the unperturbed basis $|\nu\rangle$.

Now consider N_{imp} identical impurities situated at the randomly distributed but fixed positions \mathbf{P}_j . The elastic scattering potential $V(\mathbf{r})$ then acquires the form

$$V(\mathbf{r}) = \sum_{j=1}^{N_{\text{imp}}} u(\mathbf{r} - \mathbf{P}_j), \quad \mathbf{P}_j \text{ is randomly distributed.} \quad (11.19)$$

Two small dimensionless parameters of the system serve as guides to obtain good approximative solutions. One is stating that the ratio between the impurity density, $n_{\text{imp}} = N_{\text{imp}}/\mathcal{V}$, and the electron density n_{el} is much smaller than unity:

$$\frac{n_{\text{imp}}}{n_{\text{el}}} \ll 1. \quad (11.20)$$

The other small parameter is stating that the strength of the scattering potential is weak. We assume that the scattering potential $u(\mathbf{r} - \mathbf{P}_j)$ differs only significantly from 0 for $|\mathbf{r} - \mathbf{P}_j| < a$, and that the characteristic value in that region is \tilde{u} . Weak scattering means that \tilde{u} is much smaller than some characteristic level spacing \hbar^2/ma^2 as follows:¹

$$\tilde{u} \frac{ma^2}{\hbar^2} \ll \min \{1, k_F a\}. \quad (11.21)$$

11.3.1 Feynman diagrams for the impurity scattering

With the random potential Eq. (11.19) the Dyson equation Eq. (11.12) becomes

$$\mathcal{G}(\mathbf{r}_b, \mathbf{r}_a; ik_n) = \mathcal{G}^0(\mathbf{r}_b - \mathbf{r}_a; ik_n) + \sum_{j=1}^{N_{\text{imp}}} \int d\mathbf{r}_1 \mathcal{G}^0(\mathbf{r}_b - \mathbf{r}_1; ik_n) u(\mathbf{r}_1 - \mathbf{P}_j) \mathcal{G}(\mathbf{r}_1, \mathbf{r}_a; ik_n), \quad (11.22)$$

¹ Assume that u is only important in a sphere of radius a around the scattering center. The level spacing for non-perturbed states in that sphere is near the ground state given by the size quantization \hbar^2/ma^2 . For high energies around, say $\varepsilon = p^2/2m$, the level spacing is $(\partial\varepsilon/\partial p) \Delta p = (p/m) (\hbar/a) = ka \hbar^2/ma^2$, where $p = \hbar k$ has been used. Thus u is weak if it is smaller than the smallest of these level spacings.

where we have used the fact that the unperturbed system is translation-invariant and hence that $\mathcal{G}^0(\mathbf{r}_1, \mathbf{r}_a; ik_n) = \mathcal{G}^0(\mathbf{r}_1 - \mathbf{r}_a; ik_n)$. We now want to deduce the Feynman rules for constructing diagrams in this situation. First expand the Dyson equation Eq. (11.22) in orders n of the scattering potential $u(\mathbf{r} - \mathbf{P}_j)$, and obtain $\mathcal{G}(\mathbf{r}_b, \mathbf{r}_a) = \sum_{n=0}^{\infty} \mathcal{G}^{(n)}(\mathbf{r}_b, \mathbf{r}_a)$, where the frequency argument ik_n has been suppressed. The n -th order term $\mathcal{G}^{(n)}$ is

$$\begin{aligned} \mathcal{G}^{(n)}(\mathbf{r}_b, \mathbf{r}_a) = & \sum_{j_1}^{N_{\text{imp}}} \dots \sum_{j_n}^{N_{\text{imp}}} \int d\mathbf{r}_1 \dots \int d\mathbf{r}_n \\ & \times \mathcal{G}^0(\mathbf{r}_b - \mathbf{r}_n) u(\mathbf{r}_n - \mathbf{P}_{j_n}) \dots u(\mathbf{r}_2 - \mathbf{P}_{j_2}) \mathcal{G}^0(\mathbf{r}_2 - \mathbf{r}_1) u(\mathbf{r}_1 - \mathbf{P}_{j_1}) \mathcal{G}^0(\mathbf{r}_1 - \mathbf{r}_a). \end{aligned} \quad (11.23)$$

This n -th order contribution can be interpreted as the sum over all processes involving n scattering events in all possible combination of impurities. Naturally, we can never hope to solve this problem exactly. Not only is it for all practical purposes impossible to know where all the impurities in a given metallic sample de facto are situated, but even if we did, no simple solution for the Green's function could be found. However, if we are satisfied with the answer to the less ambitious and more practical question of what is the average behavior, then we shall soon find an answer. To this end we reformulate Dyson's equation in \mathbf{k} space since according to Eq. (11.15) $\mathcal{G}_{\mathbf{k}}^0$ of the impurity free, and therefore translation-invariant, problem has the simple form:

$$\mathcal{G}_{\mathbf{k}}^0(ik_n) = \frac{1}{ik_n - \xi_{\mathbf{k}}}, \quad \mathcal{G}_{\mathbf{k}}^0(\mathbf{r} - \mathbf{r}'; ik_n) = \frac{1}{\mathcal{V}} \sum_{\mathbf{k}} \mathcal{G}_{\mathbf{k}}^0(ik_n) e^{i\mathbf{k} \cdot (\mathbf{r} - \mathbf{r}')}. \quad (11.24)$$

The Fourier transform of the impurity potential $u(\mathbf{r} - \mathbf{P}_j)$ is:

$$u(\mathbf{r} - \mathbf{P}_j) = \frac{1}{\mathcal{V}} \sum_{\mathbf{q}} u_{\mathbf{q}} e^{i\mathbf{q} \cdot (\mathbf{r} - \mathbf{P}_j)} = \frac{1}{\mathcal{V}} \sum_{\mathbf{q}} e^{-i\mathbf{q} \cdot \mathbf{P}_j} u_{\mathbf{q}} e^{i\mathbf{q} \cdot \mathbf{r}}. \quad (11.25)$$

The Fourier expansion of $\mathcal{G}^{(n)}(\mathbf{r}_b, \mathbf{r}_a; ik_n)$ in Eq. (11.23) is:

$$\begin{aligned} \mathcal{G}^{(n)}(\mathbf{r}_b, \mathbf{r}_a) = & \sum_{j_1 \dots j_n}^{N_{\text{imp}}} \frac{1}{\mathcal{V}^n} \sum_{\mathbf{q}_1 \dots \mathbf{q}_n} \frac{1}{\mathcal{V}^2} \sum_{\mathbf{k}_a \mathbf{k}_b} \frac{1}{\mathcal{V}^{n-1}} \sum_{\mathbf{k}_1 \dots \mathbf{k}_{n-1}} \int d\mathbf{r}_1 \dots \int d\mathbf{r}_n \\ & \times \mathcal{G}_{\mathbf{k}_b}^0 u_{\mathbf{q}_n} \mathcal{G}_{\mathbf{k}_{n-1}}^0 u_{\mathbf{q}_{n-1}} \dots u_{\mathbf{q}_2} \mathcal{G}_{\mathbf{k}_1}^0 u_{\mathbf{q}_1} \mathcal{G}_{\mathbf{k}_a}^0 e^{-i(\mathbf{q}_n \cdot \mathbf{P}_{j_n} + \dots + \mathbf{q}_2 \cdot \mathbf{P}_{j_2} + \mathbf{q}_1 \cdot \mathbf{P}_{j_1})} \\ & \times e^{i\mathbf{k}_b \cdot (\mathbf{r}_b - \mathbf{r}_n)} e^{i\mathbf{q}_n \cdot \mathbf{r}_n} e^{i\mathbf{k}_{n-1} \cdot (\mathbf{r}_n - \mathbf{r}_{n-1})} \dots e^{i\mathbf{q}_2 \cdot \mathbf{r}_2} e^{i\mathbf{k}_1 \cdot (\mathbf{r}_2 - \mathbf{r}_1)} e^{i\mathbf{q}_1 \cdot \mathbf{r}_1} e^{i\mathbf{k}_a \cdot (\mathbf{r}_1 - \mathbf{r}_a)}. \end{aligned} \quad (11.26)$$

This complicated expression can be simplified a lot by performing the n spatial integrals, $\int d\mathbf{r}_j e^{i(\mathbf{k}_j - \mathbf{k}_{j-1} - \mathbf{q}_j) \cdot \mathbf{r}_j} = \mathcal{V} \delta_{\mathbf{k}_j, \mathbf{k}_{j-1} + \mathbf{q}_j}$, which may be interpreted as momentum conservation in each electron-impurity scattering: the change of the electron momentum is absorbed by the impurity. Utilizing these delta functions in the n \mathbf{q} -sums leads to

$$\begin{aligned} \mathcal{G}^{(n)}(\mathbf{r}_b, \mathbf{r}_a) = & \frac{1}{\mathcal{V}^2} \sum_{\mathbf{k}_a \mathbf{k}_b} e^{i\mathbf{k}_b \cdot \mathbf{r}_b} e^{-i\mathbf{k}_a \cdot \mathbf{r}_a} \sum_{j_1 \dots j_n}^{N_{\text{imp}}} \frac{1}{\mathcal{V}^{n-1}} \sum_{\mathbf{k}_1 \dots \mathbf{k}_{n-1}} \\ & \times \mathcal{G}_{\mathbf{k}_b}^0 u_{\mathbf{k}_b - \mathbf{k}_{n-1}} \mathcal{G}_{\mathbf{k}_{n-1}}^0 \dots u_{\mathbf{k}_2 - \mathbf{k}_1} \mathcal{G}_{\mathbf{k}_1}^0 u_{\mathbf{k}_1 - \mathbf{k}_a} \mathcal{G}_{\mathbf{k}_a}^0 e^{-i[(\mathbf{k}_b - \mathbf{k}_{n-1}) \cdot \mathbf{P}_{j_n} + \dots + (\mathbf{k}_1 - \mathbf{k}_a) \cdot \mathbf{P}_{j_1}]}. \end{aligned} \quad (11.27)$$

Introducing the Fourier transform $\mathcal{G}_{\mathbf{k}_b \mathbf{k}_a}^{(n)}$ of $\mathcal{G}^{(n)}(\mathbf{r}_b, \mathbf{r}_a)$ as

$$\mathcal{G}^{(n)}(\mathbf{r}_b, \mathbf{r}_a) = \frac{1}{\mathcal{V}^2} \sum_{\mathbf{k}_a \mathbf{k}_b} e^{i\mathbf{k}_b \cdot \mathbf{r}_b} e^{-i\mathbf{k}_a \cdot \mathbf{r}_a} \mathcal{G}_{\mathbf{k}_b \mathbf{k}_a}^{(n)}, \quad (11.28)$$

with

$$\begin{aligned} \mathcal{G}_{\mathbf{k}_b \mathbf{k}_a}^{(n)} &= \sum_{j_1 \dots j_n}^{N_{\text{imp}}} \frac{1}{\mathcal{V}^{n-1}} \sum_{\mathbf{k}_1 \dots \mathbf{k}_{n-1}} e^{-i[(\mathbf{k}_b - \mathbf{k}_{n-1}) \cdot \mathbf{P}_{j_n} + \dots + (\mathbf{k}_1 - \mathbf{k}_a) \cdot \mathbf{P}_{j_1}]} \\ &\times \mathcal{G}_{\mathbf{k}_b}^0 u_{\mathbf{k}_b - \mathbf{k}_{n-1}} \mathcal{G}_{\mathbf{k}_{n-1}}^0 \dots u_{\mathbf{k}_2 - \mathbf{k}_1} \mathcal{G}_{\mathbf{k}_1}^0 \dots u_{\mathbf{k}_1 - \mathbf{k}_a} \mathcal{G}_{\mathbf{k}_a}^0. \end{aligned} \quad (11.29)$$

we can now easily deduce the Feynman rules for the diagrams corresponding to $\mathcal{G}_{\mathbf{k}_b \mathbf{k}_a}^{(n)}$:

- (1) Let dashed arrows $j \bullet \text{---} \leftarrow \text{---} \star \mathbf{q}, \mathbf{P}_j$ denote a scattering event $u_{\mathbf{q}} e^{-i\mathbf{q} \cdot \mathbf{P}_j}$.
- (2) Draw n scattering events.
- (3) Let straight arrows $\text{---} \leftarrow \text{---} \mathbf{k}$ denote $\mathcal{G}_{\mathbf{k}}^0$.
- (4) Let $\mathcal{G}_{\mathbf{k}_a}^0$ go into vertex $\bullet 1$ and $\mathcal{G}_{\mathbf{k}_b}^0$ away from vertex $\bullet n$.
- (5) Let $\mathcal{G}_{\mathbf{k}_j}^0$ go from vertex j to vertex $j+1$.
- (6) Maintain momentum conservation at each vertex.
- (7) Perform the sums $\frac{1}{\mathcal{V}} \sum_{\mathbf{k}_j}$ over all internal momenta \mathbf{k}_j , and $\sum_{j_1 \dots j_n}^{N_{\text{imp}}}$ over \mathbf{P}_{j_i} .

(11.30)

The diagram corresponding to Eq. (11.29) is:

$$\mathcal{G}_{\mathbf{k}_b \mathbf{k}_a}^{(n)} = \begin{array}{c} \star \mathbf{P}_n \\ \downarrow \mathbf{k}_b - \mathbf{k}_{n-1} \\ \leftarrow \mathbf{k}_b \quad \bullet n \quad \leftarrow \mathbf{k}_{n-1} \quad \dots \quad \leftarrow \mathbf{k}_3 \quad \bullet 3 \quad \leftarrow \mathbf{k}_2 \quad \bullet 2 \quad \leftarrow \mathbf{k}_1 \quad \bullet 1 \quad \leftarrow \mathbf{k}_a \\ \star \mathbf{P}_3 \quad \star \mathbf{P}_2 \quad \star \mathbf{P}_1 \\ \downarrow \mathbf{k}_3 - \mathbf{k}_2 \quad \downarrow \mathbf{k}_2 - \mathbf{k}_1 \quad \downarrow \mathbf{k}_1 - \mathbf{k}_a \end{array} \quad (11.31)$$

This diagram is very suggestive. One can see how an incoming electron with momentum \mathbf{k}_a is scattered n times under momentum conservation with the impurities and leaves the system with momentum \mathbf{k}_b . However, as mentioned above, it is not possible to continue the study of impurity scattering on general grounds without further assumptions. We therefore begin to consider the possibility of performing an average over the random positions \mathbf{P}_j of the impurities.

11.4 Impurity self-average

If the electron wavefunctions are completely coherent throughout the entire disordered metal each true electronic eigenfunction exhibit an extremely complex diffraction pattern spawned by the randomly positioned scatterers. If one imagine changing some external parameter, e.g. the average electron density or an external magnetic field, each individual

diffraction pattern will of course change drastically due to the sensitivity of the scattering phases of the wavefunctions. Significant quantum fluctuations must therefore occur in any observable at sufficiently low temperatures.

Using modern nano-technology to fabricate small (but still macroscopic) samples, and standard cryogenic equipment to cool down these samples to ultra-low temperatures, one can in fact obtain an experimental situation where the electrons can traverse the sample without losing their quantum-mechanical phase coherence. In Fig. 11.2(a) is shown the conductance trace of a GaAs nano-device, such as the one shown in Fig. 2.10, at 0.31 K as a function of the electron density. This density can be controlled by applying a gate voltage V_g on an external electrode. The conductance G is seen to fluctuate strongly for minute changes of V_g . These fluctuations turn out to be perfectly reproducible as V_g is swept up and down several times.

As the temperature of a given sample is raised, the amount of electron-electron and electron-phonon scattering increases because of an increased phase space for scattering and an increased number of phonons. The quantum mechanical phase of each individual electron is changed by a small random amount at each inelastic scattering event, and as a result the coherence length l_φ for the electrons diminishes. At sufficiently high temperature (e.g. 4.1 K) l_φ is much smaller than the size of the device, and we can think of the device as being composed as a number of phase-independent small phase coherent sub-systems. Therefore, when one measures an observable the result is in fact an incoherent average of all these sub-systems. Note that this average is imposed by the physical properties of the system itself, and this effective averaging is consequently denoted *self-averaging*. This effect is illustrated in Fig. 11.2(b) where the conductance trace at 4.1 K is seen to be much smoother than the one at 0.31 K, and where the many small phase coherent sub-systems of the sample are indicated below the experimental graph.

For very large (mm sized) macroscopic samples l_φ is much smaller than the sample size at all experimental realizable temperatures ($T > 10$ mK for electron gases in metals and semiconductors), and we are in the impurity self-averaging case. Mathematically, the impurity average is performed by summing over all the phase-independent coherent sub-systems and dividing by their number N_{sys} . But due to the random distribution of the impurities, this average is the same as an average over the impurity position within a single subsystem - as can be seen from Fig. 11.2. However, even on the rather small length scale l_φ the system is already homogeneous, and one can as well perform the position average over the entire volume of the sample. Thus in the following we average over all possible uncorrelated positions \mathbf{P}_j of the N_{imp} impurities for the entire system:

$$\frac{1}{V} \langle \mathcal{G}_{\mathbf{k}_b \mathbf{k}_a} \rangle_{\text{imp}} \equiv \delta_{\mathbf{k}_b, \mathbf{k}_a} \bar{\mathcal{G}}_{\mathbf{k}_a} \equiv \frac{\delta_{\mathbf{k}_b, \mathbf{k}_a}}{N_{\text{sys}}} \sum_{i=1}^{N_{\text{sys}}} \mathcal{G}_{\mathbf{k}_a}^{\text{sys}_i} \sim \delta_{\mathbf{k}_b, \mathbf{k}_a} \frac{1}{V} \int d\mathbf{P}_1 \frac{1}{V} \int d\mathbf{P}_2 \dots \frac{1}{V} \int d\mathbf{P}_{N_{\text{imp}}} \mathcal{G}_{\mathbf{k}_a} \quad (11.32)$$

Here we have anticipated that the impurity averaged Green's function is diagonal in \mathbf{k} due to the restoring of translation-invariance upon average. Some care must be taken regarding the average over the impurity positions \mathbf{P}_j . Any n -th order contribution to $\mathcal{G}_{\mathbf{k}}$ contains n scattering events, but they need not be on n different scatterers. In fact, any

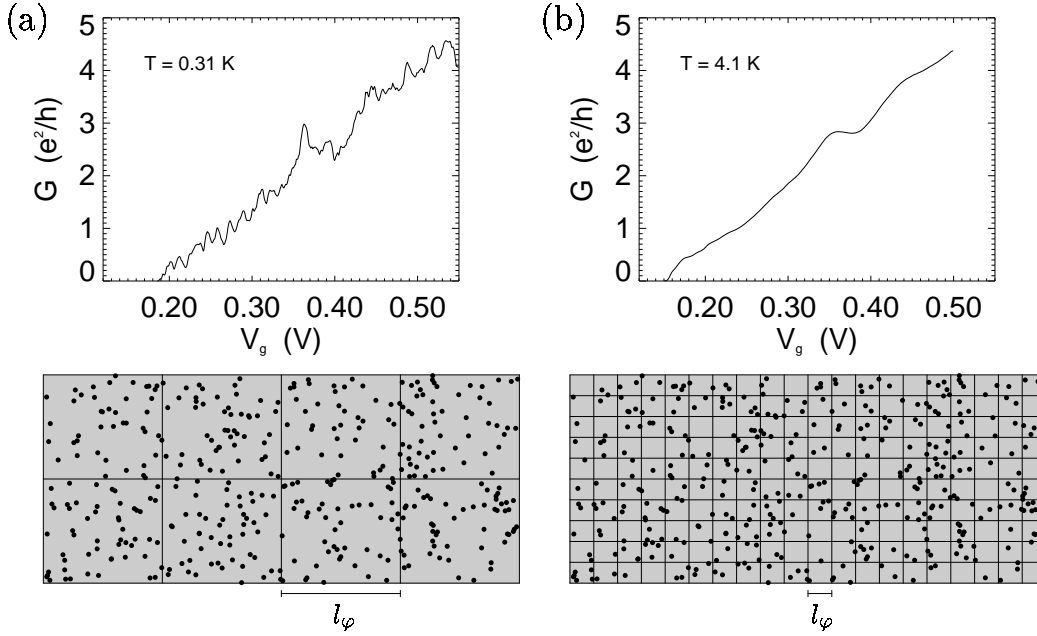


Figure 11.2: (a) The measured conductance of a disordered GaAs sample at $T = 0.31$ K displaying random but reproducible quantum fluctuations as a function of a gate voltage V_g controlling the electron density. The fluctuations are due to phase coherent scattering against randomly positioned impurities. Below is indicated that the phase coherence length l_φ is large compared to the size of the sample. (b) The same system at $T = 4.1$ K. The fluctuations are almost gone due to the smallness of l_φ at this temperature. The sample now contains a large number of independent but phase-coherent sub-systems of size l_φ . As a result a substantial self-averaging occurs, which suppresses the quantum fluctuations.

number p , $1 \leq p \leq n$ of scatterers could be involved. We must therefore carefully sort out all possible ways to scatter on p different impurities.

As mentioned in Eq. (11.20) we work in the limit of small impurity densities n_{imp} . For a given fixed number n of scattering events the most important contribution therefore comes from processes involving just one impurity. Then, down by the small factor $n_{\text{imp}}/n_{\text{el}}$, follow processes involving two impurities, etc. We note that in Eq. (11.29) the only reference to the impurity positions is the exponential $e^{i(\mathbf{q}_1 \cdot \mathbf{P}_{j_1} + \mathbf{q}_2 \cdot \mathbf{P}_{j_2} + \dots + \mathbf{q}_n \cdot \mathbf{P}_{j_n})}$, with the scattering vectors $\mathbf{q}_i = \mathbf{k}_i - \mathbf{k}_{i-1}$. The sum in Eq. (11.29) over impurity positions in this exponential is now ordered according to how many impurities are involved:

$$\begin{aligned}
& \sum_{j_1, \dots, j_n}^{N_{\text{imp}}} e^{i \sum_{l=1}^n \mathbf{q}_l \cdot \mathbf{P}_{j_l}} = \sum_{h_1}^{N_{\text{imp}}} e^{i(\sum_{\mathbf{q}_{j_1} \in Q} \mathbf{q}_{j_1}) \cdot \mathbf{P}_{h_1}} \\
& + \sum_{Q_1 \cup Q_2 = Q} \sum_{h_1}^{N_{\text{imp}}} \sum_{h_2}^{N_{\text{imp}}} e^{i(\sum_{\mathbf{q}_{l_1} \in Q_1} \mathbf{q}_{l_1}) \cdot \mathbf{P}_{h_1}} e^{i(\sum_{\mathbf{q}_{l_2} \in Q_2} \mathbf{q}_{l_2}) \cdot \mathbf{P}_{h_2}} \\
& + \sum_{Q_1 \cup Q_2 \cup Q_3 = Q} \sum_{h_1}^{N_{\text{imp}}} \sum_{h_2}^{N_{\text{imp}}} \sum_{h_3}^{N_{\text{imp}}} e^{i(\sum_{\mathbf{q}_{l_1} \in Q_1} \mathbf{q}_{l_1}) \cdot \mathbf{P}_{h_1}} e^{i(\sum_{\mathbf{q}_{l_2} \in Q_2} \mathbf{q}_{l_2}) \cdot \mathbf{P}_{h_2}} e^{i(\sum_{\mathbf{q}_{l_3} \in Q_3} \mathbf{q}_{l_3}) \cdot \mathbf{P}_{h_3}} \\
& + \dots
\end{aligned} \tag{11.33}$$

Here $Q = \{\mathbf{q}_1, \mathbf{q}_2, \dots, \mathbf{q}_n\}$ is the set of the n scattering vectors, while $Q_1 \cup Q_2 \cup \dots \cup Q_p = Q$ denotes all possible unions of non-empty disjunct subsets spanning Q . All the scattering vectors in one particular subset Q_i are connected to the same impurity \mathbf{P}_{h_i} . Note, that strictly speaking two different impurities cannot occupy the same position. However, in Eq. (11.33) we let the j -sums run unrestricted. This introduces a small error of the order $1/N_{\text{imp}}$ for the important terms in the low impurity density limit involving only a few impurities.²

Since all the p positions \mathbf{P}_h now are manifestly different we can perform the impurity average indicated in Eq. (11.32) over each exponential factor independently. The detailed calculation is straightforward but somewhat cumbersome; the result may perhaps be easier to understand than the derivation. As depicted in Eq. (11.38) the impurity averaged Green's function is a sum scattering processes against the position-averaged impurities. Since translation-invariance is restored by the averaging, the sum of all scattering momenta on the same impurity must be zero, cf. Fig. 11.3. But let us see how these conclusions are reached.

The impurity average indicated in Eq. (11.32) over each independent exponential factor results in some Kronecker delta's meaning that all scattering vectors \mathbf{q}_{h_i} connected to the same impurity must add up to zero:

$$\left\langle e^{i(\sum_{\mathbf{q}_{h_i} \in Q_i} \mathbf{q}_{h_i}) \cdot \mathbf{P}_{h_i}} \right\rangle_{\text{imp}} = \frac{1}{V} \int d\mathbf{P}_{h_i} e^{i(\sum_{\mathbf{q}_{h_i} \in Q_h} \mathbf{q}_{h_i}) \cdot \mathbf{P}_{h_i}} = \delta_{0, \sum_{\mathbf{q}_{h_i} \in Q_h} \mathbf{q}_{h_i}}. \tag{11.34}$$

This of course no longer depends on the p impurity positions \mathbf{P}_{h_i} ; the averaging has restored translation-invariance. The result of the impurity averaging can now be written as

$$\left\langle \sum_{j_1, \dots, j_n}^{N_{\text{imp}}} e^{i \sum_{l=1}^n \mathbf{q}_l \cdot \mathbf{P}_{j_l}} \right\rangle_{\text{imp}} = \sum_{p=1}^n \sum_{\bigcup_{h=1}^p Q_h = Q} \prod_{h=1}^p \left(N_{\text{imp}} \delta_{0, \sum_{\mathbf{q}_{h_i} \in Q_h} \mathbf{q}_{h_i}} \right), \tag{11.35}$$

²This error occurs since our approximation amounts to saying that the $(p+1)$ -st impurity can occupy any of the N_{imp} impurity sites, and not just the $N_{\text{imp}} - p$ available sites. For the important terms $p \ll N_{\text{imp}}$ and the error is $p/N_{\text{imp}} \ll 1$.

which, when inserted in Eq. (11.29), leads to

$$\begin{aligned} \langle \mathcal{G}_{\mathbf{k}}^{(n)} \rangle_{\text{imp}} = & \frac{1}{\mathcal{V}^{n-1}} \sum_{\mathbf{k}_1 \dots \mathbf{k}_{n-1}} \sum_{p=1}^n \sum_{\bigcup_{h=1}^p Q_h = Q} \prod_{h=1}^p \left(N_{\text{imp}} \delta_{0, \sum_{Q_h} (\mathbf{k}_{h_i} - \mathbf{k}_{(h_i-1)})} \right) \\ & \times \mathcal{G}_{\mathbf{k}}^0 u_{\mathbf{k}-\mathbf{k}_1} \mathcal{G}_{\mathbf{k}_1}^0 u_{\mathbf{k}_1-\mathbf{k}_2} \mathcal{G}_{\mathbf{k}_2}^0 \dots u_{\mathbf{k}_{n-1}-\mathbf{k}} \mathcal{G}_{\mathbf{k}}^0. \end{aligned} \quad (11.36)$$

We note that due to the p factors containing δ -functions there are in fact only $n-1-p$ free momenta sums $\frac{1}{\mathcal{V}} \sum_{\mathbf{k}'}$ to perform. The remaining p volume prefactors are combined with N_{imp} to yield p impurity density factors $n_{\text{imp}} = N_{\text{imp}}/\mathcal{V}$.

The Feynman rules for constructing the n -th order contribution $\langle \mathcal{G}_{\mathbf{k}}^{(n)} \rangle_{\text{imp}}$ to the impurity averaged Green's function $\langle \mathcal{G}_{\mathbf{k}} \rangle_{\text{imp}}$ are now easy to establish:

- (1) Let scattering lines $--\blacktriangleleft---$ \mathbf{q} denote the scattering amplitude $u_{\mathbf{q}}$.
- (2) Let \star denote a momentum conserving impurity averaged factor $n_{\text{imp}} \delta_{0, \sum \mathbf{q}}$.
- (3) Let fermion lines \longrightarrow \mathbf{k} denote the unperturbed Green's function $\mathcal{G}_{\mathbf{k}}^0$.
- (4) Draw p impurity stars. Let n_1 scattering lines go out from star 1, n_2 from star 2, etc, so that the total number $n_1 + n_2 + \dots + n_p$ of scattering lines is n .
- (5) Draw all topological different diagrams containing an unbroken chain of $n+1$ fermion lines connecting once to each of the n scattering line end-points.
- (7) Let the first and last fermion line be $\mathcal{G}_{\mathbf{k}}^0$.
- (8) Maintain momentum conservation at each vertex.
- (9) Make sure that the sum of all momenta leaving an impurity star is zero.
- (10) Perform the sum $\frac{1}{\mathcal{V}} \sum_{\mathbf{k}_j}$ over all free internal momenta \mathbf{k}_j .
- (11) Sum over all orders n of scattering and over p , with $1 \leq p \leq n$.

(11.37)

The diagrammatic expansion of $\langle \mathcal{G}_{\mathbf{k}} \rangle_{\text{imp}}$ has a direct intuitive appeal:

$$\begin{aligned} \langle \mathcal{G}_{\mathbf{k}} \rangle_{\text{imp}} = & \text{---} + \text{---} \star \text{---} + \left(\text{---} \star \text{---} + \text{---} \star \star \text{---} \right) \\ & + \left(\text{---} \star \text{---} + \text{---} \star \star \text{---} + \text{---} \star \star \text{---} + \text{---} \star \star \star \text{---} + \text{---} \star \star \star \star \text{---} \right) \\ & + \left(\text{---} \star \text{---} + \dots + \text{---} \star \star \text{---} + \dots + \text{---} \star \star \star \star \text{---} \right) + \dots \end{aligned} \quad (11.38)$$

In this expression, showing all diagrams up to third order and three diagrams of fourth order, we have for visual clarity suppressed all momentum labels and even the arrows of the scattering lines. For each order the diagrams are arranged after powers of n_{imp} , i.e. the number of impurity stars. In Fig. 11.3 two diagrams with complete labels are shown. In the following section we gain further insight in the solution of $\langle \mathcal{G}_{\mathbf{k}} \rangle_{\text{imp}}$ by rearranging the terms in the diagrammatic expansion, a procedure known as resummation.

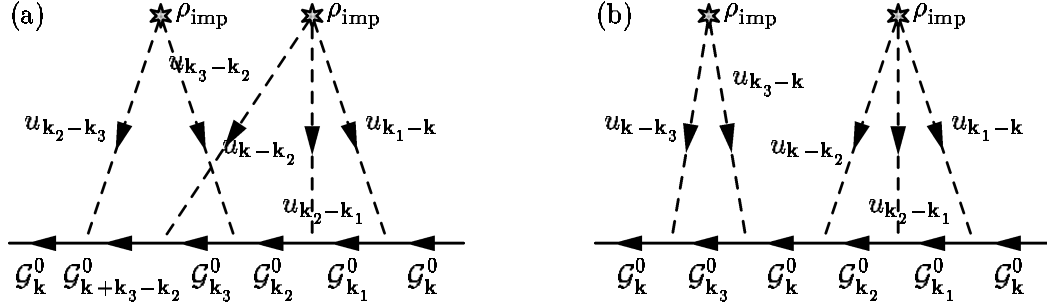


Figure 11.3: Two fully labelled fifth order diagrams both with two impurity scatterers. Diagram (a) is a so-called irreducible diagram, i.e. it cannot be cut into two pieces by cutting one internal fermion line. In contrast, diagram (b) is reducible. It consists of two irreducible parts.

11.5 Self-energy for impurity scattered electrons

In Fig. 11.3 we introduce the concept of irreducible diagrams, i.e. diagrams in the expansion of $\langle \mathcal{G}_{\mathbf{k}} \rangle_{\text{imp}}$ that cannot be cut into two pieces by cutting a single internal fermion line. We now use this concept to resum the diagrammatic expansion Eq. (11.38) for $\langle \mathcal{G}_{\mathbf{k}} \rangle_{\text{imp}}$. We remind the reader that this resummation is correct only in the limit of low impurity density. First we define the so-called self-energy $\Sigma_{\mathbf{k}}$:

$$\begin{aligned}
 \Sigma_{\mathbf{k}} &\equiv \left\{ \begin{array}{l} \text{The sum of all irreducible diagrams in } \langle \mathcal{G}_{\mathbf{k}} \rangle_{\text{imp}} \\ \text{without the two external fermion lines } \mathcal{G}_{\mathbf{k}}^0 \end{array} \right\} \\
 &= \begin{array}{c} \text{Diagram 1} + \text{Diagram 2} + \left(\text{Diagram 3} + \text{Diagram 4} \right) + \left(\text{Diagram 5} + \dots \right) + \dots \\ \text{Diagram 1: } \text{Star} \text{---} \text{Dashed line} \text{---} \text{Star} \\ \text{Diagram 2: } \text{Star} \text{---} \text{Dashed line} \text{---} \text{Dashed line} \text{---} \text{Star} \\ \text{Diagram 3: } \text{Star} \text{---} \text{Dashed line} \text{---} \text{Dashed line} \text{---} \text{Dashed line} \text{---} \text{Star} \\ \text{Diagram 4: } \text{Star} \text{---} \text{Dashed line} \text{---} \text{Dashed line} \text{---} \text{Star} \end{array} \\
 &= \text{Diagram 1} \quad (11.39)
 \end{aligned}$$

Using $\Sigma_{\mathbf{k}}$ and the product form of $\langle \mathcal{G}_{\mathbf{k}} \rangle_{\text{imp}}$ in Fourier space, Eq. (11.38) becomes

$$\begin{aligned}
 \langle \mathcal{G}_{\mathbf{k}} \rangle_{\text{imp}} &= \text{Diagram 1} + \text{Diagram 2} + \text{Diagram 3} + \dots \\
 &= \text{Diagram 1} + \text{Diagram 2} \times \left(\text{Diagram 1} + \text{Diagram 2} + \dots \right) \\
 &= \mathcal{G}_{\mathbf{k}}^0 + \mathcal{G}_{\mathbf{k}}^0 \Sigma_{\mathbf{k}} \langle \mathcal{G}_{\mathbf{k}} \rangle_{\text{imp}}. \quad (11.40)
 \end{aligned}$$

This algebraic Dyson equation, equivalent to Eqs. (11.9) and (11.18), is readily solved:

$$\langle \mathcal{G}_{\mathbf{k}}(ik_n) \rangle_{\text{imp}} = \frac{\mathcal{G}_{\mathbf{k}}^0}{1 - \mathcal{G}_{\mathbf{k}}^0 \Sigma_{\mathbf{k}}} = \frac{1}{(\mathcal{G}_{\mathbf{k}}^0)^{-1} - \Sigma_{\mathbf{k}}} = \frac{1}{ik_n - \xi_{\mathbf{k}} - \Sigma_{\mathbf{k}}(ik_n)}. \quad (11.41)$$

From this solution we immediately learn that $\Sigma_{\mathbf{k}}$ enters $\langle \mathcal{G}_{\mathbf{k}} \rangle_{\text{imp}}$ as an additive correction to the original unperturbed energy, $\xi_{\mathbf{k}} \rightarrow \xi_{\mathbf{k}} + \Sigma_{\mathbf{k}}$, hence the name self-energy. The problem

of finding $\langle \mathcal{G}_{\mathbf{k}} \rangle_{\text{imp}}$ is thus reduced to a calculation of $\Sigma_{\mathbf{k}}$. In the following we go through various approximations for $\Sigma_{\mathbf{k}}$.

11.5.1 Lowest order approximation

One marvellous feature of the self-energy $\Sigma_{\mathbf{k}}$ is that even if it is approximated by a finite number of diagrams, the Dyson equation Eq. (11.40) actually ensures that some diagrams of all orders are included in the perturbation series for $\langle \mathcal{G}_{\mathbf{k}} \rangle_{\text{imp}}$. This allows for essential changes in $\langle \mathcal{G}_{\mathbf{k}} \rangle_{\text{imp}}$, notably one can move the poles of $\langle \mathcal{G}_{\mathbf{k}} \rangle_{\text{imp}}$ and hence change the excitation energies. This would not be possible if only a finite number of diagrams were used in the expansion of $\langle \mathcal{G}_{\mathbf{k}} \rangle_{\text{imp}}$ itself.

Bearing in mind the inequalities Eqs. (11.20) and (11.21), the lowest order approximation $\Sigma_{\mathbf{k}}^{\text{LOA}}$ to $\Sigma_{\mathbf{k}}$ is obtained by including only the diagram with the fewest number of impurity stars and scattering lines,

$$\Sigma_{\mathbf{k}}^{\text{LOA}}(ik_n) \equiv \text{---} \overset{\star}{\underset{\bullet}{\uparrow}} \text{---} = n_{\text{imp}} u_0 = n_{\text{imp}} \int d\mathbf{r} u(\mathbf{r}), \quad (11.42)$$

i.e. a constant, which upon insertion into Dyson's equation Eq. (11.41) yields

$$\mathcal{G}_{\mathbf{k}}^{\text{LOA}}(ik_n) = \frac{1}{ik_n - (\xi_{\mathbf{k}} + n_{\text{imp}} u_0)}. \quad (11.43)$$

But this just reveals a simple constant shift of all the energy levels with the amount $n_{\text{imp}} u_0$. This shift constitutes a redefinition of the origin of the energy axis with no dynamical consequences. In the following it is absorbed into the definition of the chemical potential and will therefore not appear in the equations.

11.5.2 1st order Born approximation

The simplest non-trivial low-order approximation to the self-energy is the so-called first order Born approximation given by the 'wigwam'-diagram

$$\Sigma_{\mathbf{k}}^{\text{1BA}}(ik_n) \equiv \text{---} \overset{\mathbf{k}-\mathbf{k}'}{\underset{\mathbf{k}'}{\uparrow}} \overset{\star}{\text{---}} \overset{\mathbf{k}'-\mathbf{k}}{\text{---}} \text{---} = n_{\text{imp}} \sum_{\mathbf{k}'} |u_{\mathbf{k}-\mathbf{k}'}|^2 \frac{1}{ik_n - \xi_{\mathbf{k}'}} , \quad (11.44)$$

where we have used that $u_{-\mathbf{k}} = u_{\mathbf{k}}^*$ since $u(\mathbf{r})$ is real. We shall see shortly that $\Sigma_{\mathbf{k}}^{\text{1BA}} = \text{Re } \Sigma_{\mathbf{k}}^{\text{1BA}} + i \text{Im } \Sigma_{\mathbf{k}}^{\text{1BA}}$ moves the poles of $\langle \mathcal{G}_{\mathbf{k}} \rangle_{\text{imp}} = \text{---} \text{---}$ away from the real axis, i.e. the propagator acquires a finite life-time. By Eq. (11.40) we see that $\mathcal{G}_{\mathbf{k}}^{\text{1BA}}$ is the sum of propagations with any number of sequential wigwam-diagrams:

$$\text{---} \text{---}^{\text{1BA}} \text{---} = \text{---} \text{---} + \text{---} \overset{\star}{\uparrow} \text{---} + \text{---} \overset{\star}{\uparrow} \text{---} \overset{\star}{\uparrow} \text{---} + \text{---} \overset{\star}{\uparrow} \text{---} \overset{\star}{\uparrow} \text{---} \overset{\star}{\uparrow} \text{---} + \dots \quad (11.45)$$

In the evaluation of $\Sigma_{\mathbf{k}}^{\text{1BA}}$ we shall rely on our physical insight to facilitate the math. We know that for the electron gas in a typical metal $\varepsilon_{\text{F}} \sim 7 \text{ eV} \sim 80\,000 \text{ K}$, so as usual only electrons with an energy $\varepsilon_{\mathbf{k}}$ in a narrow shell around $\varepsilon_{\text{F}} \approx \mu$ play a role. For

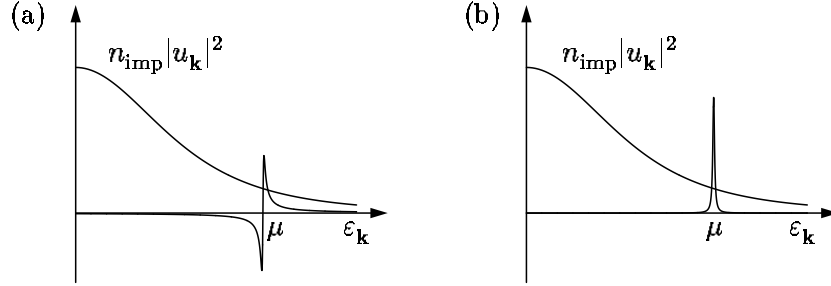


Figure 11.4: (a) The functions $n_{\text{imp}} |u_{\mathbf{k}}|^2$ and $(\omega - \epsilon_{\mathbf{k}} + \mu) / [(\omega - \epsilon_{\mathbf{k}} + \mu)^2 + \eta^2]$ appearing in the expression for $\text{Re } \Sigma_{\mathbf{k}}^{1\text{BA}}(ik_n)$. (b) The functions $n_{\text{imp}} |u_{\mathbf{k}}|^2$ and $|k_n| / [(\omega - \epsilon_{\mathbf{k}} + \mu)^2 + \eta^2]$ appearing in the expression for $\text{Im } \Sigma_{\mathbf{k}}^{1\text{BA}}(ik_n)$.

$T < 800$ K we have $k_B T / \varepsilon_F < 10^{-2}$, and for applied voltage drops V_{ext} less than 70 mV over the coherence length $l_\varphi < 10^{-5}$ m (the typical size we are looking at), i.e. applied electrical fields less than 7000 V/m, we have $eV_{\text{ext}} / \varepsilon_F < 10^{-2}$. Thus we are only interested in $\Sigma_{\mathbf{k}}^{1\text{BA}}(ik_n)$ for

$$|\mathbf{k}| \sim k_F \quad \text{and} \quad |ik_n \rightarrow \omega + i \text{sgn}(k_n)\eta| \ll \varepsilon_F. \quad (11.46)$$

Here we have also anticipated that at the end of the calculation, as sketched in Fig. 10.1, we need to perform an analytical continuation down to the real axis, either from the upper half-plane, where $k_n > 0$, as $ik_n \rightarrow \omega + i\eta$, or from the lower half-plane, where $k_n < 0$, as $ik_n \rightarrow \omega - i\eta$.

Furthermore, as we shall study in great detail later, the electron gas redistributes itself to screen out the external charges from the impurities, and as a result $u_{\mathbf{k}-\mathbf{k}'}$ varies in a smooth and gentle way for $0 < |\mathbf{k} - \mathbf{k}'| < 2k_F$.

With this physical input in mind we continue:

$$\begin{aligned} \Sigma_{\mathbf{k}}^{1\text{BA}}(\omega + i \text{sgn}(k_n)\eta) &= n_{\text{imp}} \sum_{\mathbf{k}'} |u_{\mathbf{k}-\mathbf{k}'}|^2 \frac{1}{(\omega - \xi_{\mathbf{k}'} + i \text{sgn}(k_n)\eta)} \\ &= \sum_{\mathbf{k}'} n_{\text{imp}} |u_{\mathbf{k}-\mathbf{k}'}|^2 \left[\frac{\omega - \xi_{\mathbf{k}'}}{(\omega - \xi_{\mathbf{k}'})^2 + \eta^2} - i \text{sgn}(k_n) \pi \delta(\omega - \xi_{\mathbf{k}'}) \right]. \end{aligned} \quad (11.47)$$

Since $|u_{\mathbf{k}-\mathbf{k}'}|^2$ vary smoothly and $|\omega - \xi_{\mathbf{k}'}| \ll \varepsilon_F \approx \mu$ we get the functional behavior shown in Fig. 11.4. Since $(\omega - \xi_{\mathbf{k}'}) / ((\omega - \xi_{\mathbf{k}'})^2 + \eta^2)$ is an odd function of $\omega - \xi_{\mathbf{k}'}$ and the width η is small, we have³ $\text{Re } \Sigma_{\mathbf{k}}^{1\text{BA}}(ik_n) \approx 0$; For the imaginary part of $\Sigma_{\mathbf{k}}^{1\text{BA}}$ we obtain the usual delta function for $\eta \rightarrow 0$. Finally, since the spectral function for the unperturbed system forces ω to equal $\xi_{\mathbf{k}}$, we obtain:

$$\Sigma_{\mathbf{k}}^{1\text{BA}}(ik_n) = -i\pi \text{sgn}(k_n) \sum_{\mathbf{k}'} n_{\text{imp}} |u_{\mathbf{k}-\mathbf{k}'}|^2 \delta(\xi_{\mathbf{k}} - \xi_{\mathbf{k}'}) = -i \text{sgn}(k_n) \frac{1}{2\tau_{\mathbf{k}}}, \quad (11.48)$$

³Strictly speaking, we only get vanishing real part if the slope of $|u_{\mathbf{k}-\mathbf{k}'}|^2$ is zero near μ . If this is not the case we do get a non-zero real part. However, since $|u_{\mathbf{k}-\mathbf{k}'}|^2$ is slowly varying near μ we get the same real part for all \mathbf{k} and \mathbf{k}' near k_F . This contribution can be absorbed into the definition of μ .

where we have introduced the impurity scattering time $\tau_{\mathbf{k}}$ defined as

$$\frac{1}{\tau_{\mathbf{k}}} \equiv 2\pi \sum_{\mathbf{k}'} n_{\text{imp}} |u_{\mathbf{k}-\mathbf{k}'}|^2 \delta(\xi_{\mathbf{k}} - \xi_{\mathbf{k}'}). \quad (11.49)$$

This result can also be found using Fermi's golden rule. Now we have obtained the 1st order Born approximation for $\mathcal{G}_{\mathbf{k}}(ik_n)$ in Eq. (11.41) and the analytic continuation $ik_n \rightarrow z$ thereof into the entire complex plane:

$$\mathcal{G}_{\mathbf{k}}^{1\text{BA}}(ik_n) = \frac{1}{ik_n - \xi_{\mathbf{k}} + i \frac{\text{sgn}(k_n)}{2\tau_{\mathbf{k}}}} \xrightarrow{ik_n \rightarrow z} \mathcal{G}_{\mathbf{k}}^{1\text{BA}}(z) = \begin{cases} \frac{1}{z - \xi_{\mathbf{k}} + \frac{i}{2\tau_{\mathbf{k}}}}, & \text{Im } z > 0 \\ \frac{1}{z - \xi_{\mathbf{k}} - \frac{i}{2\tau_{\mathbf{k}}}}, & \text{Im } z < 0. \end{cases} \quad (11.50)$$

We see that $\mathcal{G}_{\mathbf{k}}^{1\text{BA}}(z)$ has a branch cut along the real axis, but that it is analytic separately in the upper and the lower half-plane. This is a property that will play an important role later, when we calculate the electrical resistivity of disordered metals. Note that this behavior is in accordance with the general results obtained in Sec. 9.2 concerning the analytic properties of Matsubara Green's functions.

We close this section by remarking three properties summarized in Fig. 11.5 related to the retarded Green's function $G_{\mathbf{k}}^{\text{R,1BA}}(\omega) = \mathcal{G}_{\mathbf{k}}^{1\text{BA}}(\omega + i\eta)$. First, it is seen by Fourier transforming to the time domain that $G_{\mathbf{k}}^{\text{R,1BA}}(t)$ decays exponentially in time with $\tau_{\mathbf{k}}$ as the typical time scale:

$$G_{\mathbf{k}}^{\text{R,1BA}}(t) \equiv \int \frac{d\omega}{2\pi} \frac{e^{-i(\omega+i\eta)t}}{\omega - \xi_{\mathbf{k}} + i/2\tau_{\mathbf{k}}} = -i \theta(t) e^{-i\xi_{\mathbf{k}}t} e^{-t/2\tau_{\mathbf{k}}}. \quad (11.51)$$

Second, exploiting that $\omega, \tau_{\mathbf{k}}^{-1} \ll \varepsilon_{\text{F}}$, it is seen by Fourier transforming back to real space that $G^{\text{R,1BA}}(r, \omega)$ decays exponentially in space with $l_{\mathbf{k}} \equiv v_{\text{F}}\tau_{\mathbf{k}}$ as the typical length scale:

$$G^{\text{R,1BA}}(r, \omega) \equiv \int \frac{d\mathbf{k}}{(2\pi)^3} \frac{e^{i\mathbf{k}\cdot\mathbf{r}}}{\omega - \xi_{\mathbf{k}} + i/2\tau_{\mathbf{k}}} = \frac{\pi d(\varepsilon_{\text{F}})}{k_{\text{F}}|\mathbf{r}|} e^{ik_{\text{F}}|\mathbf{r}|} e^{-|\mathbf{r}|/2l_{\mathbf{k}}}. \quad (11.52)$$

Thirdly, the spectral function $A_{\mathbf{k}}^{1\text{BA}}(\omega)$ is a Lorentzian of width $2\tau_{\mathbf{k}}$:

$$A_{\mathbf{k}}^{1\text{BA}}(\omega) \equiv -2 \text{Im } \mathcal{G}_{\mathbf{k}}^{1\text{BA}}(\omega + i\eta) = \frac{1/\tau_{\mathbf{k}}}{(\omega - \xi_{\mathbf{k}})^2 + 1/4\tau_{\mathbf{k}}^2} \quad (11.53)$$

In conclusion the impurity averaged 1st Born approximation has resulted in a self-energy with a non-zero imaginary part. The poles of the Matsubara Green's function $\mathcal{G}_{\mathbf{k}}^{1\text{BA}}(ik_n)$ are therefore shifted away from the real axis, resulting in a both temporal and spatial exponential decay of the retarded Green's function. This is interpreted as follows: the impurity scattering transforms the free electrons into quasiparticles with a finite life time given by the scattering time $\tau_{\mathbf{k}}$ and a finite mean free path given by $l_{\mathbf{k}} = v_{\text{F}}\tau_{\mathbf{k}}$. The finite life time of the quasiparticles is also reflected in the broadening of the spectral function. The characteristic sharp δ -function for free electrons, $A_{\mathbf{k}}(\omega) = 2\pi\delta(\omega - \xi_{\mathbf{k}})$, is

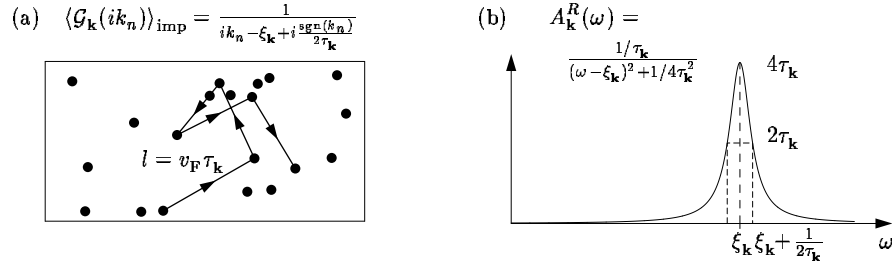


Figure 11.5: (a) The impurity averaged Green's function $\langle \mathcal{G}_k(ik_n) \rangle_{\text{imp}}$. The imaginary part of the self-energy is related to the scattering time τ_k and hence also to the elastic scattering length $l = v_F \tau_k$. (b) In the Born approximation the spectral function $A_k(\omega)$ is a Lorentzian centered around $\xi_k = 0$ with a width $1/2\tau_k$.

broadened into a Lorentzian of width $1/2\tau_k$. This means that a particle with momentum \mathbf{k} can have an energy ω that differs from ξ_k with an amount $\hbar/2\tau_k$.

This calculation of self-averaged impurity scattering constitutes a first and very important example of what can happen in a many-particle system. Note in particular the important role played by the self-energy, and the fact that it can have a non-zero imaginary part. The results is obtained in the 1st order Born approximation, where the self-energy is approximated by a single diagram. But what happens if we take more diagrams into account? The surprising answer is that in the low impurity density limit, $n_{\text{imp}} \ll n_{\text{el}}$ no qualitative difference arises by taking more diagrams into account. Only at higher impurity densities where scattering events from different impurities begin to interfere new physical effects, such as weak localization, appear. Let us see how this conclusion is reached.

11.5.3 The full Born approximation

A natural extension of the 1st Born approximation is the full Born approximation, which is exact to lowest order in n_{imp} . It is defined by the following self-energy $\Sigma_k^{\text{FBA}}(ik_n)$, where any number of scattering on the same impurity is taken into account, i.e. more dashed lines on the wigwam-diagram:

$$\begin{aligned}
 \Sigma_k^{\text{FBA}} &\equiv \text{[Diagram 1]} + \text{[Diagram 2]} + \text{[Diagram 3]} + \text{[Diagram 4]} + \dots \\
 &= \text{[Diagram 5]} + \text{[Diagram 6]} \times \left(\text{[Diagram 7]} + \text{[Diagram 8]} + \text{[Diagram 9]} + \dots \right) \quad (11.54)
 \end{aligned}$$

The diagrams are Feynman diagrams representing the self-energy. Diagram 1 is a single dashed line with a star at the top and a dot at the bottom labeled k . Diagram 2 is a dashed line with a star at the top, a dot at the bottom labeled k , and a dashed line loop with a dot at the top labeled k . Diagram 3 is a dashed line with a star at the top, a dot at the bottom labeled k , and a dashed line loop with a dot at the top labeled k . Diagram 4 is a dashed line with a star at the top, a dot at the bottom labeled k , and a dashed line loop with a dot at the top labeled k . Diagram 5 is a dashed line with a star at the top, a dot at the bottom labeled k , and a dashed line loop with a dot at the top labeled k . Diagram 6 is a dashed line with a star at the top, a dot at the bottom labeled k , and a dashed line loop with a dot at the top labeled k . Diagram 7 is a dashed line with a star at the top, a dot at the bottom labeled k , and a dashed line loop with a dot at the top labeled k . Diagram 8 is a dashed line with a star at the top, a dot at the bottom labeled k , and a dashed line loop with a dot at the top labeled k . Diagram 9 is a dashed line with a star at the top, a dot at the bottom labeled k , and a dashed line loop with a dot at the top labeled k .

In the parenthesis at the end of the second line we find a factor, which we denote $t_{k',k}$, that is not diagonal in \mathbf{k} but with a diagonal that equals the self-energy $t_{k,k} = \Sigma_k^{\text{FBA}}$. In scattering theory $t_{k',k}$ is known as the transition matrix. When this matrix is known all

consequences of the complete scattering sequence can be calculated. An integral equation for the transition matrix is derived diagrammatically:

$$\begin{aligned}
 t_{\mathbf{k}_1, \mathbf{k}_2}(ik_n) &\equiv \text{diagram 1} + \text{diagram 2} + \text{diagram 3} + \dots \\
 &= \text{diagram 1} + \text{diagram 4} \times \left(\text{diagram 1} + \text{diagram 2} + \text{diagram 3} + \dots \right) \\
 &= n_{\text{imp}} u_0 \delta_{\mathbf{k}_1, \mathbf{k}_2} + \sum_{\mathbf{k}'} u_{\mathbf{k}_1 - \mathbf{k}'} \mathcal{G}_{\mathbf{k}'}^0 t_{\mathbf{k}', \mathbf{k}_2}.
 \end{aligned} \tag{11.55}$$

This equation can in many cases be solved numerically. As before the task is simplified by the fact that we are only interested at electrons moving at the Fermi surface. The real part of the diagonal element $t_{\mathbf{k}, \mathbf{k}}(ik_n)$, the one yielding the self-energy, is almost constant for $|\mathbf{k}| \sim k_F$ and is absorbed into the definition of the chemical potential μ . We are then left with $\text{Im} t_{\mathbf{k}, \mathbf{k}}(ik_n)$, and by applying the optical theorem,⁴ $\text{Im} t_{\mathbf{k}, \mathbf{k}} = \text{Im} \sum_{\mathbf{k}'} t_{\mathbf{k}, \mathbf{k}'}^\dagger \mathcal{G}_{\mathbf{k}'}^0 t_{\mathbf{k}', \mathbf{k}}$, we obtain

$$\begin{aligned}
 \text{Im} \Sigma_{\mathbf{k}}^{\text{FBA}}(ik_n) &= \text{Im} t_{\mathbf{k}, \mathbf{k}}(ik_n) = \text{Im} \sum_{\mathbf{k}'} \frac{|t_{\mathbf{k}, \mathbf{k}'}|^2}{ik_n - \xi_{\mathbf{k}'}} \\
 &\xrightarrow{ik_n \rightarrow \omega + i \text{sgn}(k_n)\eta} -\text{sgn}(k_n) \pi \sum_{\mathbf{k}'} |t_{\mathbf{k}, \mathbf{k}'}|^2 \delta(\omega - \xi_{\mathbf{k}'}).
 \end{aligned} \tag{11.56}$$

This has the same form as Eq. (11.48) with $|t_{\mathbf{k}, \mathbf{k}'}|^2$ instead of $n_{\text{imp}} |u_{\mathbf{k} - \mathbf{k}'}|^2$, and we write

$$\Sigma_{\mathbf{k}}^{\text{FBA}}(ik_n) = -i \text{sgn}(k_n) \frac{1}{2\tau_{\mathbf{k}}}, \quad \text{with} \quad \frac{1}{\tau_{\mathbf{k}}} \equiv 2\pi \sum_{\mathbf{k}'} |t_{\mathbf{k}, \mathbf{k}'}|^2 \delta(\xi_{\mathbf{k}} - \xi_{\mathbf{k}'}). \tag{11.57}$$

By iteration of Dyson's equation we find that \mathcal{G}^{FBA} is the sum of propagations with any number and any type of sequential wigwam-diagrams:

$$\text{FBA} = \text{diagram 1} + \text{diagram 2} + \text{diagram 3} + \text{diagram 4} + \dots \tag{11.58}$$

11.5.4 The self-consistent Born approximation and beyond

Many more diagrams can be taken into account using the self-consistent Born approximation defined by substituting the bare \mathcal{G}^0 with the full \mathcal{G} in the full Born approximation

⁴Eq. (11.55) states (i): $t = u + u\mathcal{G}^0 t$. Since $u^\dagger = u$ the Hermitian conjugate of (i) is (ii): $u = -t^\dagger (\mathcal{G}^0)^\dagger u + t^\dagger$. Insert (ii) into (i): $t = u + (t^\dagger \mathcal{G}^0 t - t^\dagger (\mathcal{G}^0)^\dagger u \mathcal{G}^0 t)$. Both u and $t^\dagger (\mathcal{G}^0)^\dagger u \mathcal{G}^0 t$ are Hermitian so $\text{Im} t_{\mathbf{k}, \mathbf{k}} = \text{Im} \langle \mathbf{k} | t^\dagger \mathcal{G}^0 t | \mathbf{k} \rangle = \text{Im} \sum_{\mathbf{k}'} t_{\mathbf{k}, \mathbf{k}'}^\dagger \mathcal{G}_{\mathbf{k}'}^0 t_{\mathbf{k}', \mathbf{k}}$.

Eqs. (11.54) and (11.55) yields:

$$\begin{aligned}
 \Sigma_{\mathbf{k}}^{\text{SCBA}} &\equiv \text{diagram 1} + \text{diagram 2} + \text{diagram 3} + \text{diagram 4} + \dots \\
 &= n_{\text{imp}} u_0 \delta_{\mathbf{k},\mathbf{k}} + \sum_{\mathbf{k}'} u_{\mathbf{k}-\mathbf{k}'} \mathcal{G}_{\mathbf{k}'} t_{\mathbf{k}',\mathbf{k}},
 \end{aligned} \tag{11.59}$$

a self-consistent equation in $\Sigma_{\mathbf{k}}^{\text{SCBA}}$ since $\mathcal{G}_{\mathbf{k}'} = (ik_n - \xi_{\mathbf{k}'} - \Sigma_{\mathbf{k}'}^{\text{SCBA}})^{-1}$. We again utilize that $t_{\mathbf{k},\mathbf{k}}$ is only weakly dependent on energy for $|\mathbf{k}| \approx k_F$ and $\omega \ll \varepsilon_F$, and if furthermore the scattering strength is moderate, i.e. $|\Sigma_{\mathbf{k}}^{\text{SCBA}}| \ll \varepsilon_F$ we obtain almost the same result as in Eq. (11.56). Only the imaginary part $\Sigma_{\mathbf{k}}^i$ of $\Sigma_{\mathbf{k}}^{\text{SCBA}} = \Sigma_{\mathbf{k}}^R + i\Sigma_{\mathbf{k}}^i$ plays a role, since the small real part $\Sigma_{\mathbf{k}}^R$ can be absorbed into μ .

$$\Sigma_{\mathbf{k}}^i = \text{Im } t_{\mathbf{k},\mathbf{k}} = \text{Im } \sum_{\mathbf{k}'} \frac{|t_{\mathbf{k},\mathbf{k}'}|^2}{ik_n - \xi_{\mathbf{k}'} - i\Sigma_{\mathbf{k}'}^i} \approx -\text{sgn}(k_n - \Sigma_{\mathbf{k}}^i) \pi \sum_{\mathbf{k}'} |t_{\mathbf{k},\mathbf{k}'}|^2 \delta(\omega - \xi_{\mathbf{k}'}). \tag{11.60}$$

The only self-consistency requirement is thus connected with the sign of the imaginary part. But this requirement is fulfilled by taking $\text{Im } \Sigma_{\mathbf{k}}^{\text{SCBA}}(ik_n) \propto -\text{sgn}(k_n)$ as seen by direct substitution. The only difference between the full Born and the self-consistent Born approximation is in the case of strong scattering, where the limiting δ -function in Eq. (11.60) may acquire a small renormalization. The final result is

$$\Sigma_{\mathbf{k}}^{\text{SCBA}}(ik_n) = -i \text{sgn}(k_n) \frac{1}{2\tau_{\mathbf{k}}}, \quad \text{with} \quad \frac{1}{\tau_{\mathbf{k}}} \approx 2\pi \sum_{\mathbf{k}'} |t_{\mathbf{k},\mathbf{k}'}|^2 \delta(\omega - \xi_{\mathbf{k}'}). \tag{11.61}$$

By iteration of Dyson's equation we find that $\mathcal{G}^{\text{SCBA}}$ is the sum of propagations with any number and any type of sequential wigwam-diagrams inside wigwam-diagrams but without crossings of any scattering lines:

$$\begin{aligned}
 \overline{\overline{\text{SCBA}}} = & \text{diagram 1} + \text{diagram 2} + \text{diagram 3} + \dots \\
 & + \text{diagram 4} + \text{diagram 5} + \dots \\
 & + \text{diagram 6} + \dots + \text{diagram 7} + \dots
 \end{aligned} \tag{11.62}$$

We have now resummed most of the diagrams in the diagrammatic expansion of $\langle \mathcal{G}_{\mathbf{k}} \rangle_{\text{imp}}$ with the exception of wigwam-diagrams with crossing lines. In Fig. 11.6 are shown two different types of irreducible diagrams of the same order in both n_{imp} and $u_{\mathbf{k}}$. Also sketched is the phase space Ω available for the internal momenta \mathbf{k}_1 and \mathbf{k}_2 in the two cases. At zero temperature the energy broadening around the Fermi energy ε_F is given by

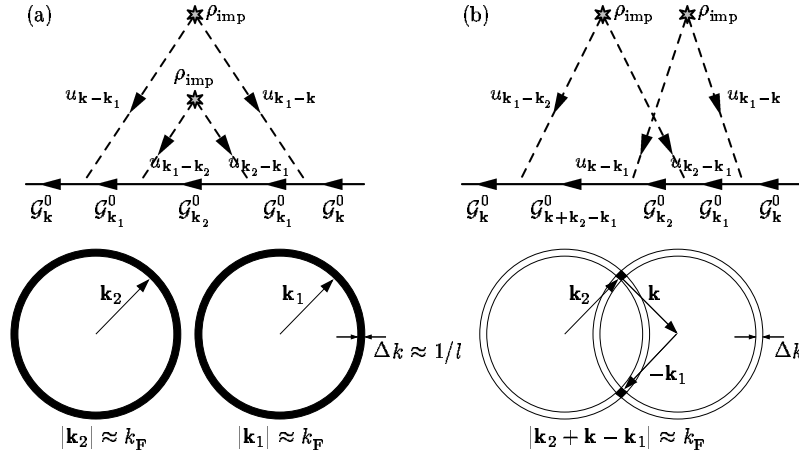


Figure 11.6: (a) The non-crossing wigwam diagrams, one inside the other, where \mathbf{k}_1 and \mathbf{k}_2 can take any value on the spherical shell of radius k_F and thickness $\Delta k \approx 1/l$. The phase space is $\Omega_a \propto (4\pi k_F^2 \Delta k)^2$. (b) The crossing wigwam diagram has the same restrictions for \mathbf{k}_1 and \mathbf{k}_2 as in (a) plus the constraint that $|\mathbf{k} + \mathbf{k}_2 - \mathbf{k}_1| \approx k_F$. For fixed \mathbf{k}_2 the variation of \mathbf{k}_1 within its Fermi shell is restricted to the intersection between this shell and the Fermi shell of $\mathbf{k} + \mathbf{k}_2 - \mathbf{k}_1$, i.e. to a ring with cross section $1/l^2$ and radius $\approx k_F$. The phase space is now $\Omega_b \propto (4\pi k_F^2 \Delta k)(2\pi k_F \Delta k^2)$. Thus the crossing diagram (b) is suppressed relative to the non-crossing diagram (a) with a factor $1/k_F l$.

$|\Sigma| \approx \hbar/\tau$ which relaxes $|\mathbf{k}_1|, |\mathbf{k}_2| = k_F$ a bit. In \mathbf{k} -space the broadening Δk is given by $\hbar^2(k_F + \Delta k)^2/2m \approx \varepsilon_F + \hbar/\tau$ which gives $\Delta k \approx 1/v_F \tau = 1/l$, i.e. the inverse scattering length. This means that \mathbf{k}_1 and \mathbf{k}_2 are both confined to a thin spherical shell of thickness $1/l$ and radius k_F .

In Fig. 11.6(a), where no crossing of scattering lines occurs, no further restrictions applies, so the volume of the available phase space is $\Omega_a = (4\pi k_F^2/l)^2$. In Fig. 11.6(b), where the scattering lines crosses, the Feynman rules dictate that one further constraint, namely $|\mathbf{k} + \mathbf{k}_1 - \mathbf{k}_2| \approx k_F$. Thus only one of the two internal momenta are free to be anywhere on the Fermi shell, the other is bound to the intersection between two Fermi shells, i.e. on a ring with radius $\sim k_F$ and a cross section $1/l^2$ as indicated in Fig. 11.6(b). So $\Omega_b = (4\pi k_F^2/l)(2\pi k_F/l^2)$. Thus by studying the phase space available for the non-crossed and the crossed processes we have found that the crossed ones are suppressed by a factor $\Omega_b/\Omega_a \approx 1/(k_F l)$. Such a suppression factor enters the calculation for each crossing of scattering lines in a diagram. Since for metals $1/k_F \sim 1 \text{ \AA}$ we find that

$$\frac{1}{k_F l} \ll 1, \quad \text{for } l \gg 1 \text{ \AA}. \quad (11.63)$$

In conclusion: all cases where the scattering length l is greater than 1 \AA we have by the various Born approximations indeed resummed the perturbation series for $\langle \mathcal{G}_{\mathbf{k}}(ik_n) \rangle_{\text{imp}}$ taking all relevant diagrams into account and obtained $\Sigma_{\mathbf{k}}(ik_n) = -i \frac{\text{sgn}(k_n)}{2\tau_{\mathbf{k}}}$. It is interesting to note that in e.g. doped semiconductors it is possible to obtain a degenerate electron

gas with a very low density. In these systems $1/k_F$ or the Fermi wavelength is much larger than in metals, and the condition in Eq. (11.63) is violated. In this case one may therefore observe deviations from the simple theory presented here. One example is the observation of weak localization, which is an increase in the resistivity due to quantum interference between scattering events involving several impurities at the same time. The weak localization effect is studied in Sec. 15.4.

11.6 Summary and outlook

In this chapter we have introduced the Feynman diagrams for elastic impurity scattering. We have applied the diagrammatic technique to an analysis of the single-particle Matsubara Green's function for electron propagation in disordered metals. The main result was the determination of the self-energy $\Sigma_{\mathbf{k}}(ik_n)$ in terms of the scattering time $\tau_{\mathbf{k}}$,

$$\Sigma_{\mathbf{k}}^{\text{FBA}}(ik_n) = -i \operatorname{sgn}(k_n) \frac{1}{2\tau_{\mathbf{k}}}, \quad \text{with} \quad \frac{1}{\tau_{\mathbf{k}}} \equiv 2\pi \sum_{\mathbf{k}'} |t_{\mathbf{k},\mathbf{k}'}|^2 \delta(\xi_{\mathbf{k}} - \xi_{\mathbf{k}'}),$$

and the scattering-time broadened spectral function

$$A_{\mathbf{k}}^{\text{1BA}}(\omega) = \frac{1/\tau_{\mathbf{k}}}{(\omega - \xi_{\mathbf{k}})^2 + 1/4\tau_{\mathbf{k}}^2}.$$

The structure in the complex plane of the Green's function was found to be:

$$\mathcal{G}_{\mathbf{k}}^{\text{1BA}}(ik_n) = \frac{1}{ik_n - \xi_{\mathbf{k}} + i\frac{\operatorname{sgn}(k_n)}{2\tau_{\mathbf{k}}}} \xrightarrow{ik_n \rightarrow z} \mathcal{G}_{\mathbf{k}}^{\text{1BA}}(z) = \begin{cases} \frac{1}{z - \xi_{\mathbf{k}} + \frac{i}{2\tau_{\mathbf{k}}}}, & \operatorname{Im} z > 0 \\ \frac{1}{z - \xi_{\mathbf{k}} - \frac{i}{2\tau_{\mathbf{k}}}}, & \operatorname{Im} z < 0. \end{cases}$$

These results will be employed in Chap. 15 in the study of the residual resistivity of metals.

The theory presented here provides in combination with the Kubo formalism the foundation for a microscopic quantum theory of resistivity. The technique can be extended to the study of quantum effects like weak localization (see Sec. 15.4) and universal conductance fluctuations (see Fig. 11.2). These more subtle quantum effects are fundamental parts of the modern research field known as mesoscopic physics. They can be explained within the theoretical framework presented here, by taking higher order correlations into account. For example is weak localization explained by treating crossed diagrams like the one in Fig. 11.6(b), which was neglected in calculation presented in this chapter.

Chapter 12

Feynman diagrams and pair interactions

It is in the case of interacting particles and fields that the power of quantum field theory and Feynman diagrams really comes into play. Below we develop the Feynman diagram technique for a system of fermions with pair interactions. The time-independent Hamiltonian H_0 of the unperturbed or non-interacting system is

$$H_0 = \sum_{\sigma} \int d\mathbf{r} \Psi^{\dagger}(\mathbf{r}) H_0 \Psi(\mathbf{r}), \quad (12.1)$$

while the interaction Hamiltonian W is given by

$$W = \frac{1}{2} \sum_{\sigma_1, \sigma_2} \int d\mathbf{r}_1 d\mathbf{r}_2 \Psi^{\dagger}(\sigma_1, \mathbf{r}_1) \Psi^{\dagger}(\sigma_2, \mathbf{r}_2) W(\sigma_2, \mathbf{r}_2; \sigma_1, \mathbf{r}_1) \Psi(\sigma_2, \mathbf{r}_2) \Psi(\sigma_1, \mathbf{r}_1). \quad (12.2)$$

We have specialized to the case where no spin flip processes occur at the vertices, this being the case for our coming main examples: electron-electron interactions mediated by Coulomb or by phonon interactions. The total Hamiltonian H governing the dynamics of the system is as usual given by $H = H_0 + W$. The main goal of this chapter is to derive the Feynman rules for the diagrammatic expansion in orders of W of the full single-particle Matsubara Green's function Eq. (10.33a)

$$\mathcal{G}(\sigma_b, \mathbf{r}_b, \tau_b; \sigma_a, \mathbf{r}_a, \tau_a) \equiv -\left\langle T_{\tau} \Psi(\sigma_b, \mathbf{r}_b, \tau_b) \Psi^{\dagger}(\sigma_a, \mathbf{r}_a, \tau_a) \right\rangle. \quad (12.3)$$

12.1 The perturbation series for \mathcal{G}

12.2 infinite perturbation series! Matsubara Green's function

The field operators in Eq. (12.3) defining \mathcal{G} are of course given in the Heisenberg picture, but using Eq. (10.16) we can immediately transform the expression for \mathcal{G} into the

interaction picture. With the short-hand notation $(\sigma_1, \mathbf{r}_1, \tau_1) = (1)$ we obtain

$$\mathcal{G}(b, a) = - \frac{\text{Tr} \left(e^{-\beta H} T_\tau \Psi(b) \Psi^\dagger(a) \right)}{\text{Tr} \left(e^{-\beta H} \right)} = - \frac{\left\langle T_\tau \left[\hat{U}(\beta, 0) \hat{\Psi}(b) \hat{\Psi}^\dagger(a) \right] \right\rangle_0}{\left\langle \hat{U}(\beta, 0) \right\rangle_0}. \quad (12.4)$$

The subscript 0 indicates that the averages in Eq. (12.4) are with respect to $e^{-\beta H_0}$ rather than $e^{-\beta H}$ as in Eq. (12.3). The expansion Eq. (10.12) for \hat{U} is now inserted into Eq. (12.4):

$$\mathcal{G}(b, a) = - \frac{\sum_{n=0}^{\infty} \frac{(-1)^n}{n!} \int_0^\beta d\tau_1 \dots \int_0^\beta d\tau_n \left\langle T_\tau \left[\hat{W}(\tau_1) \dots \hat{W}(\tau_n) \hat{\Psi}(b) \hat{\Psi}^\dagger(a) \right] \right\rangle_0}{\sum_{n=0}^{\infty} \frac{(-1)^n}{n!} \int_0^\beta d\tau_1 \dots \int_0^\beta d\tau_n \left\langle T_\tau \left[\hat{W}(\tau_1) \dots \hat{W}(\tau_n) \right] \right\rangle_0}. \quad (12.5)$$

Here we need to calculate τ -integrals of $\hat{W}(\tau)$. But one precaution must be taken regarding the ordering of the four operators in the basic two-particle interaction operator. According to Eq. (12.2) the two creation operators must always be to the left of the two annihilation operators. To make sure of that we add an infinitesimal time $\eta = 0^+$ to the time-arguments of $\Psi^\dagger(1)$ and $\Psi^\dagger(2)$, which gives the right ordering when the time-ordering operator T_τ of Eq. (12.4) acts. The τ -integrals of $\hat{W}(\tau)$ is therefore

$$\int_0^\beta d\tau_j \hat{W}(\tau_j) = \frac{1}{2} \int dj \int dj' \hat{\Psi}^\dagger(j_+) \hat{\Psi}^\dagger(j'_+) W_{j,j'} \hat{\Psi}(j') \hat{\Psi}(j), \quad (12.6)$$

where we have defined j_+ , $\int dj$, and $W_{j,j'}$ as

$$j_+ \equiv (\sigma_j, \mathbf{r}_j, \tau_j + \eta), \quad \int dj \equiv \sum_{\sigma_j} \int d\mathbf{r} \int_0^\beta d\tau_j, \quad W_{j,j'} \equiv W(\mathbf{r}_j, \mathbf{r}_{j'}) \delta(\tau_j - \tau_{j'}). \quad (12.7)$$

It is only in expressions where the initial and final times coincide that the infinitesimal shift in time of Ψ^\dagger plays a role. Next insert Eq. (12.6) for \hat{W} into Eq. (12.5) for \mathcal{G} :

$$\begin{aligned} \mathcal{G}(b, a) = & \quad (12.8) \\ & - \frac{\sum_{n=0}^{\infty} \frac{(-\frac{1}{2})^n}{n!} \int d1 d1' \dots dndn' W_{1,1'} \dots W_{n,n'} \left\langle T_\tau \left[\hat{\Psi}_1^\dagger \hat{\Psi}_1^\dagger \hat{\Psi}_1 \hat{\Psi}_1 \dots \hat{\Psi}_n^\dagger \hat{\Psi}_n^\dagger \hat{\Psi}_n \hat{\Psi}_n \hat{\Psi}_b \hat{\Psi}_a^\dagger \right] \right\rangle_0}{\sum_{n=0}^{\infty} \frac{(-\frac{1}{2})^n}{n!} \int d1 d1' \dots dndn' W_{1,1'} \dots W_{n,n'} \left\langle T_\tau \left[\hat{\Psi}_1^\dagger \hat{\Psi}_1^\dagger \hat{\Psi}_1 \hat{\Psi}_1 \dots \hat{\Psi}_n^\dagger \hat{\Psi}_n^\dagger \hat{\Psi}_n \hat{\Psi}_n \right] \right\rangle_0}. \end{aligned}$$

The great advantage of Eq. (12.8) is that the average of the field operators now involves bare propagation and thermal average both with respect to H_0 . In fact using Eq. (10.65), we recognize that the average of the products of field operators in the numerator is the bare $(2n+1)$ -particle Green's function $\mathcal{G}_0^{(2n+1)}(b, 1, 1', \dots, n'; a, 1, 1', \dots, n')$ times

$(-1)^{2n+1} = -1$, while in the denominator it is the bare $(2n)$ -particle Green's function $\mathcal{G}_0^{(2n)}(1, 1', \dots, n'; 1, 1', \dots, n')$ times $(-1)^{2n} = 1$. The resulting sign, -1 , thus cancels the sign in Eq. (12.8). Now is the time for our main use of Wick's theorem Eq. (10.79): the bare many-particle Green's functions in the expression for the full single-particle Green's function are written in terms of determinants containing the bare single-particle Green's functions $\mathcal{G}^0(l, j)$:

$$\mathcal{G}(b, a) = \frac{\sum_{n=0}^{\infty} \frac{(-\frac{1}{2})^n}{n!} \int d1 d1' \dots d n d n' W_{1,1'} \dots W_{n,n'}}{\sum_{n=0}^{\infty} \frac{(-\frac{1}{2})^n}{n!} \int d1 d1' \dots d n d n' W_{1,1'} \dots W_{n,n'}} \begin{vmatrix} \mathcal{G}^0(b, a) & \mathcal{G}^0(b, 1) & \mathcal{G}^0(b, 1') & \dots & \mathcal{G}^0(b, n') \\ \mathcal{G}^0(1, a) & \mathcal{G}^0(1, 1) & \mathcal{G}^0(1, 1') & \dots & \mathcal{G}^0(1, n') \\ \mathcal{G}^0(1', a) & \mathcal{G}^0(1', 1) & \mathcal{G}^0(1', 1') & \dots & \mathcal{G}^0(1', n') \\ \vdots & & & \ddots & \vdots \\ \mathcal{G}^0(n', a) & \mathcal{G}^0(n', 1) & \mathcal{G}^0(n', 1') & \dots & \mathcal{G}^0(n', n') \end{vmatrix} \quad (12.9)$$

This voluminous formula is the starting point for defining the Feynman rules for the diagrammatic expansion of \mathcal{G} in terms of the pair interaction W . We have suppressed, but not forgotten, the fact that the initial time τ_j in $\mathcal{G}^0(l, j)$ according to Eqs. (12.6) and (12.7) is to be shifted infinitesimally to $\tau_j + \eta$.

12.3 The Feynman rules for pair interactions






We formulate first a number of basic Feynman rules that are derived directly from Eq. (12.9). However, it turns out that using these basic rules leads to a proof that the denominator cancels out. This in turn leads to the formulation of the final Feynman rules to be used in all later calculations.

12.3.1 Feynman rules for the denominator of $\mathcal{G}(b, a)$

The basic Feynman rules for n 'th order term in the denominator of $\mathcal{G}(b, a)$ are

- (1) Fermion lines: $j_2 \bullet \leftarrow \bullet j_1 \equiv \mathcal{G}^0(j_2, j_1)$, $\tau_1 \rightarrow \tau_1 + \eta$.
- (2) Interaction lines: $j \bullet \text{---} \bullet j' \equiv W_{j,j'}$.
- (3) Vertices: $j \bullet \equiv \int dj \delta_{\sigma_j^{\text{in}}, \sigma_j^{\text{out}}}$, i.e. sum over internal variables, no spin flip.
- (4) Draw $(2n)!$ sets of n interaction lines $j \bullet \text{---} \bullet j'$.
- (5) For each set connect the $2n$ vertices with $2n$ fermion lines: one entering and one leaving each vertex. This can be done in $(2n)!$ ways.

(12.10a)

But this is not all, because what about the sign arising from the expansion of the determinant? Here the concept of fermion loops enters the game. A fermion loop is an uninterrupted sequence of fermion lines starting at some vertex j and ending there again after connecting to other vertices, e.g. j_1 , j_1 , or j_1  j_2 . The overall sign coming from the determinant is $(-1)^F$, where F is the number of fermion loops in the given diagram. An outline of the proof is as follows. The product of the diagonal terms in the determinant is per definition positive and in diagram form it consists of n factors $\textcircled{j \cdots j'}$, i.e. $F = 2n$ is even. All other diagrams can be constructed one by one simply by pair wise interchange of the endpoints of fermion lines. This changes the determinantal sign of the product since $\text{sgn}[\mathcal{G}^0(j_1, j'_1) \mathcal{G}^0(j_2, j'_2) \dots] = -\text{sgn}[\mathcal{G}^0(j_1, j'_2) \mathcal{G}^0(j_2, j'_1) \dots]$, and at the same time it changes the number of fermion loops by 1, e.g.  becomes . Thus we obtain the last Feynman rule

- (6) Multiply by $\frac{1}{n!}(-\frac{1}{2})^n(-1)^F$, F being the number of fermion loops, and add the resulting $(2n)!$ diagrams of order n .

(12.10b)

For all n there are $(2n)!$ terms or diagrams of order n in the expansion of the determinant in the denominator $\langle \hat{U}(\beta, 0) \rangle_0$ of $\mathcal{G}(b, a)$ in Eq. (12.9). Suppressing the labels, but indicating the number of diagrams of each order, this expansion takes the following form using Feynman diagrams:

$$\begin{aligned}
 \langle \hat{U}(\beta, 0) \rangle_0 = 1 &+ \left[\textcircled{\text{---}} + \textcircled{\text{---}} \right]_{2 \text{ terms}} \\
 &+ \left[\textcircled{\text{---}} + \textcircled{\text{---}} + \textcircled{\text{---}} + \dots + \textcircled{\text{---}} + \dots \right]_{24 \text{ terms}} \\
 &+ \left[\textcircled{\text{---}} + \dots + \textcircled{\text{---}} + \dots + \textcircled{\text{---}} + \dots \right]_{720 \text{ terms}} \\
 &+ \dots
 \end{aligned} \tag{12.11}$$

12.3.2 Feynman rules for the numerator of $\mathcal{G}(b, a)$

The numerator $\langle T_\tau[\hat{U}(\beta, 0)\hat{\Psi}(b)\hat{\Psi}^\dagger(a)] \rangle_0$ of $\mathcal{G}(b, a)$ differs from the denominator by the presence of the two external field operators $\hat{\Psi}(b)$ and $\hat{\Psi}^\dagger(a)$ that act at the external space-time points (b) and (a) . This raises the dimension of the n 'th order determinant from $2n$ to $2n+1$. Consequently, only Feynman rules (4) and (5) given for the denominator have to be changed to give the rules for the numerator:

- (4') Draw $(2n+1)!$ sets of n lines $j \bullet \text{---} \bullet j'$ and 2 external vertices $\bullet a$ and $\bullet b$.
 (5') For each set connect the $2n+2$ vertices with $2n+1$ fermion lines: one leaving a , one entering b , and one entering and leaving each internal vertex j .

(12.12)

Using these rules we obtain the diagrammatic expansion of the numerator:

$$\begin{aligned}
 \left\langle T_\tau[\hat{U}(\beta, 0) \hat{\Psi}(b) \hat{\Psi}^\dagger(a)] \right\rangle_0 = & \quad (12.13) \\
 & \begin{array}{c}
 \begin{array}{c} \bullet b \\ \uparrow \\ \bullet a \end{array} + \left[\begin{array}{c} \bullet b \\ \uparrow \\ \bullet a \end{array} \text{ with a loop} + \begin{array}{c} \bullet b \\ \uparrow \\ \bullet a \end{array} \text{ with a bubble} + \begin{array}{c} \bullet b \\ \uparrow \\ \bullet a \end{array} \text{ with a tadpole} + \begin{array}{c} \bullet b \\ \uparrow \\ \bullet a \end{array} \text{ with a vertex} + \begin{array}{c} \bullet b \\ \uparrow \\ \bullet a \end{array} \text{ with a cross} + \begin{array}{c} \bullet b \\ \uparrow \\ \bullet a \end{array} \text{ with a triangle} \right] \text{ 6 terms} \\
 + \left[\begin{array}{c} \bullet b \\ \uparrow \\ \bullet a \end{array} \text{ with two loops} + \begin{array}{c} \bullet b \\ \uparrow \\ \bullet a \end{array} \text{ with two bubbles} + \dots + \begin{array}{c} \bullet b \\ \uparrow \\ \bullet a \end{array} \text{ with two tadpoles} + \dots + \begin{array}{c} \bullet b \\ \uparrow \\ \bullet a \end{array} \text{ with two vertices} + \dots + \begin{array}{c} \bullet b \\ \uparrow \\ \bullet a \end{array} \text{ with two crosses} + \dots + \begin{array}{c} \bullet b \\ \uparrow \\ \bullet a \end{array} \text{ with two triangles} + \dots \right] \text{ 120 terms} \\
 + \dots
 \end{array}
 \end{aligned}$$

12.3.3 The cancellation of disconnected Feynman diagrams

It looks like we are drowning in diagrams, but in fact there is a major reduction at hand. We note that in Eq. (12.13) two classes of diagrams appear: those being connected into one piece with the external vertices a and b , the so-called connected diagrams (e.g. the last second-order diagram), and those consisting of two or more pieces, the so-called disconnected diagrams (e.g. the first second order diagram). We furthermore note that the parts of the diagrams in Eq. (12.13) disconnected from the external vertices are the same as the diagrams appearing in Eq. (12.11) order by order. We also note that a diagram containing two or more disconnected parts can be written as a product containing one factor for each disconnected part. A detailed combinatorial analysis (given at the end of this section) reveals that the denominator in \mathcal{G} cancels exactly the disconnected parts of

the diagrams in the numerator leaving only the connected ones:

$$\begin{aligned}
 \mathcal{G}(b, a) &= \frac{\left(\begin{array}{c} \bullet b \\ \uparrow \\ \bullet a \end{array} + \begin{array}{c} \bullet b \\ \nearrow \\ \bullet \\ \nwarrow \\ \bullet a \end{array} + \dots \right) \left(1 + \text{loop} + \dots \right)}{\left(1 + \text{loop} + \dots \right)} \\
 &= \left(\begin{array}{c} \bullet b \\ \uparrow \\ \bullet a \end{array} + \begin{array}{c} \bullet b \\ \nearrow \\ \bullet \\ \nwarrow \\ \bullet a \end{array} + \begin{array}{c} \bullet b \\ \nearrow \\ \bullet \\ \searrow \\ \bullet a \end{array} + \begin{array}{c} \bullet b \\ \uparrow \\ \bullet \\ \text{loop} \\ \bullet a \end{array} + \begin{array}{c} \bullet b \\ \uparrow \\ \bullet \\ \text{loop} \\ \bullet a \end{array} + \dots \right) \quad \text{connected} \quad (12.14)
 \end{aligned}$$

Being left with only the connected diagrams we find that since now all lines in the diagram are connected in a specific way to the external points a and b the combinatorics of the permutations of the internal vertex indices is particularly simple. There are $n!$ ways to choose the enumeration j of the n interaction lines $j \bullet \text{wavy} \bullet j'$, and for each line there are 2 ways to put a given pair of labels j and j' . We conclude that all $2^n n!$ diagrams with the same topology relative to the external points give the same value. Except for the sign this factor cancels the prefactor $\frac{1}{n!}(-\frac{1}{2})^n$, i.e. we are left with a factor of (-1) for each of the n interaction lines. In conclusion, for pair interactions the final version of the Feynman rules for expanding \mathcal{G} diagrammatically is:

- (1) Fermion lines: $j_2 \bullet \leftarrow \bullet j_1 \equiv \mathcal{G}^0(j_2, j_1)$, $\tau_1 \rightarrow \tau_1 + \eta$.
- (2) Interaction lines: $j \bullet \text{wavy} \bullet j' \equiv -W_{j,j'}$
- (3) Vertices: $j \bullet \equiv \int dj \delta_{\sigma_j^{\text{in}}, \sigma_j^{\text{out}}}$, i.e. sum over internal variables, no spin flip
- (4) At order n draw all topologically different, connected diagrams containing n interaction lines $j \bullet \text{wavy} \bullet j'$, 2 vertices $\bullet a$ and $\bullet b$, and $2n+1$ fermion lines, so that one leaves $\bullet a$, one enters $\bullet b$, and one enters and leaves each internal vertex $\bullet j$.
- (5) Multiply each diagram by $(-1)^F$, F being the number of fermion loops.
- (6) Sum over all the topologically different diagrams.

(12.15)

Pay attention to the fact that only the topology of the diagrams are mentioned. Thus they can at will be stretched, mirror inverted and otherwise deformed. No notion of a time-axis is implied in the imaginary time version of the Feynman diagrams.

For completeness we give the following proof of the cancellation of the disconnected diagrams, but the reader may skip it since the essential conclusion has already been given above. The proof goes through eight steps. We study the numerator of Eq. (12.9). (1) Since all internal vertices have one incoming and one outgoing fermion line, the external vertices a and b are always connected. (2) If vertex j somehow is connected to a , so is j' due to the interaction line $W_{j,j'}$. (3) In a diagram of order n , a is connected with r W -lines,

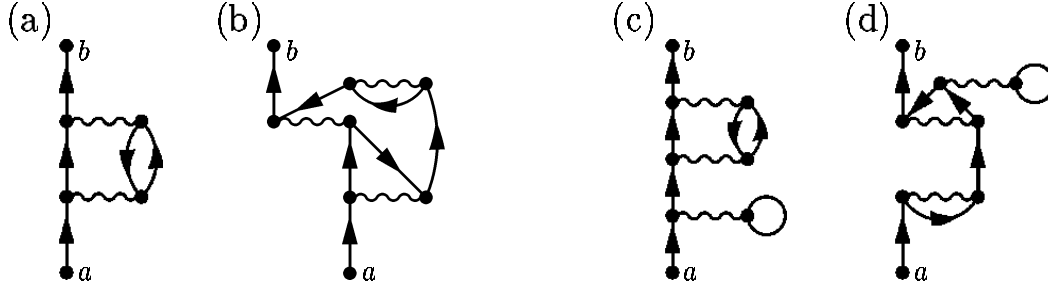


Figure 12.1: Examples of irreducible, (a) and (b), and reducible, (c) and (d), Feynman diagrams in the expansion of $\mathcal{G}(b, a)$ in the presence of pair-interactions.

where $0 \leq r \leq n$. The number of disconnected W -lines is denoted m , i.e. $m = n - r$. (4) In all terms of the expanded numerator the integral factorizes into a product of two integrals, one over the $2r$ variables connected to a and one over the $2m$ variables disconnected from a . (5) The r pairs of vertex variables j and j' connected to a can be chosen out of the available n pairs in $\frac{n!}{r!(n-r)!}$ ways, each choice yielding the same value of the total integral. (6) The structure of the sum is now:

$$\begin{aligned}
 & \sum_{n=0}^{\infty} \frac{1}{n!} \left(\frac{-1}{2} \right)^n I[1, 1', \dots, n, n'] \\
 &= \sum_{n=0}^{\infty} \frac{1}{n!} \left(\frac{-1}{2} \right)^n \sum_{r=0}^n \frac{n!}{r!(n-r)!} I[1, 1', \dots, r, r']_{\text{con}} I[r+1, (r+1)', \dots, n, n']_{\text{discon}} \\
 &= \sum_{r=0}^{\infty} \frac{1}{r!} \left(\frac{-1}{2} \right)^r I[1, 1', \dots, r, r']_{\text{con}} \sum_{m=0}^{\infty} \frac{1}{m!} \left(\frac{-1}{2} \right)^m I[r+1, (r+1)', \dots, (r+m), (r+m)']_{\text{discon}}.
 \end{aligned} \tag{12.16}$$

(7) In the connected part all $r!$ permutations of the vertex variable pairs (j, j') yield the same result, and so does all the 2^n ways of ordering each pair, if as usual $W_{j,j'} = W_{j',j}$.

(8) The disconnected part is seen to be $\langle \hat{U}(\beta, 0) \rangle_0$. We thus reach the conclusion

$$\left\langle T_{\tau} \hat{U}(\beta, 0) \hat{\Psi}(b) \hat{\Psi}^{\dagger}(a) \right\rangle_0 = \left\langle \hat{U}(\beta, 0) \right\rangle_0 \sum_{r=0}^{\infty} [-W(1, 1')] \dots [-W(r, r')] \text{Det} \left[\mathcal{G}^0 \right]_{\text{connected}}^{(2r+1) \times (2r+1)} \cdot \text{topological diff.} \tag{12.17}$$

12.4 Self-energy and Dyson's equation

In complete analogy with Fig. 11.3 for impurity scattering, we can now based on Eq. (12.14) define the concept of irreducible diagrams in $\mathcal{G}(b, a)$ in the case of pair interactions. As depicted in Fig. 12.1, such diagrams are the ones that cannot be cut into two pieces by cutting a single fermion line. Continuing the analogy with the impurity scattering case we can also define the self-energy $\Sigma(l, j)$ as

$$\begin{aligned}
\Sigma(l, j) &\equiv \left\{ \begin{array}{l} \text{The sum of all irreducible diagrams in } \mathcal{G}(b, a) \\ \text{without the two external fermion lines } \mathcal{G}^0(j, a) \text{ and } \mathcal{G}^0(b, l) \end{array} \right\} \\
&= \delta_{l,j} \text{ (loop) } + \text{ (self-energy) } + \text{ (bubble) } + \text{ (crossed bubble) } + \dots \\
&= \text{ (shaded blob) } \quad (12.18)
\end{aligned}$$

From Eqs. (12.14) and (12.18) we obtain Dyson's equation for $\mathcal{G}(b, a)$

$$\begin{aligned}
\mathcal{G}(b, a) &= \text{ (direct line) } \\
&= \text{ (direct line) } + \text{ (direct line) } \times \text{ (shaded blob) } \times \text{ (direct line) } + \dots \\
&= \text{ (direct line) } + \text{ (direct line) } \times \text{ (shaded blob) } \times \left(\text{ (direct line) } + \text{ (direct line) } \times \text{ (shaded blob) } \times \text{ (direct line) } + \dots \right) \\
&= \text{ (direct line) } + \text{ (direct line) } \times \text{ (shaded blob) } \times \text{ (direct line) } \\
&= \mathcal{G}^0(b, a) + \int dl \int dj \mathcal{G}^0(b, l) \Sigma(l, j) \mathcal{G}(j, a). \quad (12.19)
\end{aligned}$$

Note how Dyson's equation in this case is an integral equation. We shall shortly see that for a translation-invariant system it becomes an algebraic equation in \mathbf{k} -space.

12.5 The Feynman rules in Fourier space

For the special case where H_0 describes a translation-invariant system and where the interaction $W_{j,j'}$ only depends on the coordinate differences $\mathbf{r}_j - \mathbf{r}_{j'}$ and $\tau_j - \tau_{j'}$ it is a great advantage to Fourier transform the representation from (\mathbf{r}, τ) -space to (\mathbf{q}, iq_n) -space. Our main example of such a system is the jellium model for Coulomb interacting electrons studied in Sec. 2.2. In terms of the Fourier transform $W(\mathbf{q}) = 4\pi e_0^2/q^2$ the Coulomb interaction $W(\mathbf{r}\tau; \mathbf{r}', \tau')$ is written

$$W(\mathbf{r}\tau; \mathbf{r}'\tau') = \frac{1}{\beta\mathcal{V}} \sum_{\mathbf{q}, iq_n} W(q) e^{[i\mathbf{q} \cdot (\mathbf{r} - \mathbf{r}') - iq_n(\tau - \tau')]}. \quad (12.20)$$

It is important to realize that the Matsubara frequency iq_n is bosonic since the Coulomb interaction is bosonic in nature: *two* fermions are annihilated and *two* fermions are created by the interaction, i.e. *one* boson object is annihilated and *one* is created. Furthermore, we note that due to the factor $\delta(\tau - \tau')$ in Eq. (12.7) the Matsubara frequency iq_n appears only in the argument of the exponential function.

Likewise, using Eq. (10.39) we can express the electronic Green's function $\mathcal{G}_\sigma^0(\mathbf{r}\tau, \mathbf{r}'\tau')$ for spin σ in (\mathbf{k}, ik_n) -space as

$$\mathcal{G}_\sigma^0(\mathbf{r}\tau; \mathbf{r}'\tau') = \frac{1}{\beta\mathcal{V}} \sum_{\mathbf{k}, ik_n} \mathcal{G}_\sigma^0(\mathbf{k}, ik_n) e^{[i\mathbf{k}\cdot(\mathbf{r}-\mathbf{r}') - ik_n(\tau-\tau')]}, \quad (12.21)$$

where $\mathcal{G}_\sigma^0(\mathbf{k}, ik_n) = 1/(ik_n - \xi_{\mathbf{k}})$ depends on \mathbf{k} and ik_n , but not on σ . Here $\xi_{\mathbf{k}} \equiv \varepsilon - \mu$. In the case of the Coulomb interacting electron gas in the jellium model we thus see that both the Green's function \mathcal{G}_σ^0 and the interaction W depend only on the space and imaginary time differences $\mathbf{r} - \mathbf{r}'$ and $\tau - \tau'$. It follows from Eqs. (12.20) and (12.21) that it saves some writing to introduce the four-vector notation $\tilde{k} \equiv (\mathbf{k}, ik_n)$, $\tilde{r} \equiv (\mathbf{r}, \tau)$, and $i\tilde{k} \cdot \tilde{r} \equiv i\mathbf{k} \cdot \mathbf{r} - ik_n\tau$. Using this notation we analyze the Fourier transform of the basic Coulomb scattering vertex

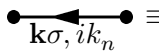
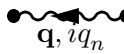


$$\int d\tilde{r} \mathcal{G}_\sigma^0(\tilde{r}_2, \tilde{r}) \mathcal{G}_\sigma^0(\tilde{r}, \tilde{r}_1) W(\tilde{r}_3; \tilde{r}) = \begin{array}{c} \tilde{r}_2 \\ \nearrow \tilde{p}\sigma \\ \tilde{r} \\ \nwarrow \tilde{k}\sigma \\ \tilde{r}_1 \end{array} \begin{array}{c} \tilde{q} \\ \text{---} \\ \tilde{r}_3 \end{array}, \quad (12.22)$$

where the (\mathbf{r}, τ) -space points \tilde{r}_1 , \tilde{r}_2 , \tilde{r}_3 , and \tilde{r} are indicated as well as the wave vectors \tilde{k} , \tilde{p} , and \tilde{q} to be used in the Fourier transform. On top of their usual meaning the arrows now also indicate the choice of sign for the four-momentum vectors: \tilde{k} flows from \tilde{r}_1 to \tilde{r} , \tilde{p} from \tilde{r} to \tilde{r}_2 , and \tilde{q} from \tilde{r} to \tilde{r}_3 . Inserting the Fourier transforms of Eqs. (12.20) and (12.21) into Eq. (12.22) yields with this sign convention

$$\begin{aligned} & \int d\tilde{r} \mathcal{G}_\sigma^0(\tilde{r}_2, \tilde{r}) \mathcal{G}_\sigma^0(\tilde{r}, \tilde{r}_1) W(\tilde{r}_3; \tilde{r}) \\ &= \int d\tilde{r} \frac{1}{(\beta\mathcal{V})^3} \sum_{\tilde{k}\tilde{p}\tilde{q}} \mathcal{G}_\sigma^0(\tilde{p}) \mathcal{G}_\sigma^0(\tilde{k}) W(\tilde{q}) e^{i[\tilde{p}\cdot(\tilde{r}_2-\tilde{r}) + \tilde{k}\cdot(\tilde{r}-\tilde{r}_1) + \tilde{q}\cdot(\tilde{r}_3-\tilde{r})]} \\ &= \frac{1}{(\beta\mathcal{V})^3} \sum_{\tilde{k}\tilde{p}\tilde{q}} \mathcal{G}_\sigma^0(\tilde{p}) \mathcal{G}_\sigma^0(\tilde{k}) W(\tilde{q}) e^{i[\tilde{p}\cdot\tilde{r}_2 - \tilde{k}\cdot\tilde{r}_1 + \tilde{q}\cdot\tilde{r}_3]} \int d\tilde{r} e^{-i(\tilde{p}-\tilde{k}+\tilde{q})\cdot\tilde{r}} \\ &= \frac{1}{(\beta\mathcal{V})^2} \sum_{\tilde{k}\tilde{q}} \mathcal{G}_\sigma^0(\tilde{k}-\tilde{q}) \mathcal{G}_\sigma^0(\tilde{k}) W(\tilde{q}) e^{i[\tilde{k}\cdot(\tilde{r}_2-\tilde{r}_1) + \tilde{q}\cdot(\tilde{r}_3-\tilde{r}_2)]}. \end{aligned} \quad (12.23)$$

From this follows that in Fourier space the four-momentum (\mathbf{k}, ik_n) is conserved at each Coulomb scattering vertex: $\tilde{k} = \tilde{p} + \tilde{q}$. Since each vertex consists of two fermion lines and one interaction line, the momentum conservation combined with the odd values of the fermion Matsubara frequencies leads, in agreement with our previous remarks, to even values for the Matsubara frequencies of the interaction lines. The momentum conservation rule for each of the $2n$ vertices also leads to $2n$ delta function constraints on the $2n$ internal fermion momenta and the n interaction line momenta, and whence the number of independent internal momenta equals n , i.e. the order of the diagram. For each independent momentum a factor $1/\beta\mathcal{V}$ remains from the corresponding Fourier transform. The topology of the diagram in (\mathbf{r}, τ) -space is not changed by the Fourier transform. We therefore end up with the following Feynman rules for the n -order diagrams in the expan-

sion of $\mathcal{G}_\sigma(\mathbf{k}, ik_n)$, where (\mathbf{k}, ik_n) is to be interpreted as the externally given four-vector momentum.

- (1) Fermion lines with four-momentum orientation:  $\equiv \mathcal{G}_\sigma^0(\mathbf{k}, ik_n)$.
- (2) Interaction lines with four-momentum orientation:  $\equiv -W(q)$.
- (3) Conserve the spin and four-momentum at each vertex, i.e. incoming momenta must equal the outgoing, and no spin flipping.
- (4) At order n draw all topologically different connected diagrams containing n oriented interaction lines $W(\tilde{q})$, two external fermion lines $\mathcal{G}_\sigma^0(\mathbf{k}, ik_n)$, and $2n$ internal fermion lines $\mathcal{G}_\sigma^0(\mathbf{p}_j, ip_j)$. All vertices must contain an incoming and an outgoing fermion line as well as an interaction line.
- (5) Multiply each diagram by $(-1)^F$, F being the number of fermion loops.
- (6) Multiply $\mathcal{G}_\sigma^0(\mathbf{k}, ik_n)$ in the 'same-time' diagrams  and  by $e^{ik_n\eta}$.
- (7) Multiply by $\frac{1}{\beta V}$ for each internal four-momentum \tilde{p} ; perform the sum $\sum_{\tilde{p}\sigma'}$.

(12.24)

Note how the two 'same-time' diagrams in rule (6) are the only ones where it is relevant to take explicitly into account the infinitesimal shift $\tau_j \rightarrow \tau_j + \eta$ mentioned in Eqs. (12.6) and (12.7). The factor $e^{ik_n\eta}$ follows directly from the Fourier transform when this shift is included.

In (\mathbf{k}, ik_n) -space the fourth Feynman rule concerning the conservation of four-momentum at the scattering vertices simplifies many calculations. Most noteworthy is the fact that Dyson's equation becomes an algebraic equation. Due to four-momentum conservation a four-momentum \tilde{k}_j entering a self-energy diagram, such as the ones shown in Eq. (12.18), must also exit it, i.e. $\tilde{k}_l = \tilde{k}_j$. The self-energy (with spin σ) is thus diagonal in \mathbf{k} -space,

$$\Sigma_\sigma(\tilde{k}, \tilde{k}') = \delta_{\tilde{k}, \tilde{k}'} \Sigma_\sigma(\tilde{k}), \quad \Sigma_\sigma(\tilde{k}) \equiv \Sigma_\sigma(\tilde{k}, \tilde{k}). \quad (12.25)$$

Dyson's equation Eq. (12.19) is therefore an algebraic equation,

$$\begin{aligned} \mathcal{G}_\sigma(\tilde{k}) &= \mathcal{G}_\sigma^0(\tilde{k}) + \mathcal{G}_\sigma^0(\tilde{k}) \Sigma_\sigma(\tilde{k}) \mathcal{G}_\sigma(\tilde{k}) \\ \text{---} \text{---} \text{---} &= \text{---} \text{---} \text{---} + \text{---} \text{---} \text{---} \end{aligned} \quad (12.26)$$

$$\text{with the solution } \mathcal{G}_\sigma(\mathbf{k}, ik_n) = \frac{\mathcal{G}_\sigma^0(\mathbf{k}, ik_n)}{1 - \mathcal{G}_\sigma^0(\mathbf{k}, ik_n) \Sigma_\sigma(\mathbf{k}, ik_n)} = \frac{1}{ik_n - \xi_{\mathbf{k}} - \Sigma_\sigma(\mathbf{k}, ik_n)}. \quad (12.27)$$

As in Eq. (11.41) the self-energy $\Sigma_\sigma(\mathbf{k}, ik_n)$, induced here by the Coulomb interaction W , appears as a direct additive renormalization of the bare energy $\xi_{\mathbf{k}} = \varepsilon_{\mathbf{k}} - \mu$.

12.6 Examples of how to evaluate Feynman diagrams

The Feynman diagrams is an extremely useful tool to gain an overview of the very complicated infinite-order perturbation calculation, and they allow one to identify the important

processes for a given physical problem. When this part of the analysis is done one is (hopefully) left with only a few important diagrams that then need to be evaluated. We end this chapter by studying the explicit evaluation of three simple Feynman diagrams in Fourier space using the Feynman rules Eq. (12.24).

12.6.1 The Hartree self-energy diagram

To evaluate a given diagram the first task is to label the fermion and interaction lines with four-momenta and spin obeying the conservation rules at each vertex, rule (3) in Eq. (12.24). We start with the so-called Hartree diagram \mathcal{G}_σ^H (which is zero in the presence of a charge compensating back-ground), where we in accordance with Eq. (12.18) strip off the two external fermion lines to obtain the self-energy Σ^H :

$$\mathcal{G}_\sigma^H(\mathbf{k}, ik_n) \equiv \text{diagram} = \frac{\mathcal{G}_\sigma^0(\mathbf{k}, ik_n)}{\mathcal{G}_\sigma^0(\mathbf{k}, ik_n)} \text{diagram} \quad (12.28)$$

The four-momentum transfer along the interaction line is zero, while the four-momentum (\mathbf{p}, ip_n) and the spin σ' in the fermion loop are free to take any value. The self-energy diagram is a first order diagram, i.e. $n = 1$. It contains one internal four-momentum, (\mathbf{p}, ip_n) , yielding a factor of $1/\beta\mathcal{V}$, one internal spin, σ' , and one fermion loop, i.e. $F = 1$. The Feynman rules therefore lead to the following expression for the Hartree self-energy diagram Eq. (12.28):

$$\begin{aligned} \Sigma_\sigma^H(\mathbf{k}, ik_n) \equiv \text{diagram} &= \frac{-1}{\beta\mathcal{V}} \sum_{\sigma'} \sum_{\mathbf{p}} \sum_{ip_n} [-W(0)] \mathcal{G}_{\sigma'}^0(\mathbf{p}, ip_n) e^{ip_n\eta} \\ &= \frac{2W(0)}{\beta} \int \frac{d\mathbf{p}}{(2\pi)^3} \sum_{ip_n} \frac{e^{ip_n\eta}}{ip_n - \xi_{\mathbf{p}}} \\ &= 2W(0) \int \frac{d\mathbf{p}}{(2\pi)^3} n_F(\xi_{\mathbf{p}}) = W(0) \frac{N}{\mathcal{V}}. \end{aligned} \quad (12.29)$$

Note the need for Feynman rule Eq. (12.24)(6) for evaluating this specific diagram. The spin sum turns into a simple factor 2. The Matsubara sum can easily be carried out using the method of Sec. 10.4.1. The evaluation of the \mathbf{p} -integral is elementary and yields $N/2$.

According to Eq. (12.27) the self-energy is the interaction-induced renormalization of the non-interacting single-particle energy. This renormalization we have calculated by completely different means in Sec. 4.2 using the Hartree-Fock mean field approximation. We see that the diagrammatic result Eq. (12.29) exactly equals the Hartree part of the mean field energy in Eq. (4.25b). In other words we have shown that the tadpole-shaped self-energy diagram is the diagrammatic equivalent of the Hartree mean field approximation.

12.6.2 The Fock self-energy diagram

We treat the Fock diagram \mathcal{G}_σ^F and Fock self-energy Σ_σ^F similarly:

$$\mathcal{G}_\sigma^F(\mathbf{k}, ik_n) = \text{diagram} = \mathcal{G}_\sigma^0(\mathbf{k}, ik_n) \text{diagram} \quad (12.30)$$

Once more the external fermion lines are written explicitly as two factors $\mathcal{G}_\sigma^0(\mathbf{k}, ik_n)$, leaving the Fock self-energy Σ_σ^F to be determined. The four-momentum transferred by the interaction line is $(\mathbf{k} - \mathbf{p}, ik_n - ip_n)$. This diagram is a first order diagram, i.e. $n = 1$. It contains one internal four-momentum, (\mathbf{p}, ip_n) , yielding a factor $1/\beta\mathcal{V}$. However, in contrast to Eq. (12.28) the internal spin σ' is now forced to be equal to the external spin σ . Finally, no fermion loops are present, i.e. $F = 0$. The Feynman rules therefore lead to the following expression for the Fock self-energy diagram Eq. (12.30):

$$\begin{aligned} \Sigma_\sigma^F(\mathbf{k}, ik_n) &\equiv \text{diagram} = \frac{1}{\beta\mathcal{V}} \sum_{\sigma'} \sum_{\mathbf{p}} \sum_{ip_n} [-W(\mathbf{k} - \mathbf{p})] \delta_{\sigma, \sigma'} \mathcal{G}_{\sigma'}^0(\mathbf{p}, ip_n) e^{ip_n \eta} \\ &= \frac{-1}{\beta} \int \frac{d\mathbf{p}}{(2\pi)^3} W(\mathbf{k} - \mathbf{p}) \sum_{ip_n} \frac{e^{ip_n \eta}}{ip_n - \xi_{\mathbf{p}}} \\ &= - \int \frac{d\mathbf{p}}{(2\pi)^3} W(\mathbf{k} - \mathbf{p}) n_F(\xi_{\mathbf{p}}). \end{aligned} \quad (12.31)$$

Note that also for this specific diagram we have used Feynman rule (6). The spin sum turned into a simple factor 1. The Matsubara sum can easily be carried out using the method of Sec. 10.4.1. The evaluation of the \mathbf{p} -integral is in principle elementary. We see that this self-energy diagram exactly equals the Fock part of the energy in Eq. (4.25b) calculated using the Hartree-Fock mean field approximation. We have thus shown that the half-oyster self-energy diagram¹ is the diagrammatic equivalent of the Fock mean field approximation.

12.6.3 The pair-bubble self-energy diagram

Our last example is the pair-bubble diagram \mathcal{G}_σ^P , which, as we shall see in Chap. 13, plays a central role in studies of the electron gas. We proceed as in the previous examples:

$$\mathcal{G}_\sigma^P(\mathbf{k}, ik_n) \equiv \text{diagram} = \mathcal{G}_\sigma^0(\mathbf{k}, ik_n) \text{diagram} \quad (12.32)$$

Removing the two external fermion lines $\mathcal{G}_\sigma^0(\mathbf{k}, ik_n)$ leaves us with the pair-bubble self-energy diagram Σ_σ^P . We immediately note that this diagram is of second order, i.e. $n = 2$, containing one fermion loop, i.e. $F = 1$. At the first vertex the incoming momentum

¹A full oyster diagram can be seen in e.g. Eq. (12.11)

(\mathbf{k}, ik_n) is split, sending (\mathbf{q}, iq_n) out through the interaction line, while the remainder $(\mathbf{k}-\mathbf{q}, ik_n-iq_n)$ continues in the fermion line. At the fermion loop, (\mathbf{q}, iq_n) is joined by the internal fermion momentum (\mathbf{p}, ip_n) and continues in a new fermion line as $(\mathbf{p}+\mathbf{q}, ip_n+iq_n)$. At the top of the loop the momentum (\mathbf{q}, iq_n) is sent out through the interaction line, where it ultimately recombines with the former fermion momentum $(\mathbf{k}-\mathbf{q}, ik_n-iq_n)$. We have thereby ensured that the exit momentum equals that of the entrance: (\mathbf{k}, ik_n) . The internal degrees of freedom are (\mathbf{q}, iq_n) , (\mathbf{p}, ip_n) , and σ' , the former two yielding a prefactor $1/(\beta\mathcal{V})^2$. The Feynman rules lead to the following expression for the pair-bubble self-energy Eq. (12.32):

$$\begin{aligned}
\Sigma_\sigma^P(\mathbf{k}, ik_n) &\equiv \text{Diagram: A fermion line with momentum } \mathbf{k} \text{ and frequency } ik_n \text{ enters from the left. It splits into two branches. The upper branch has momentum } \mathbf{k}-\mathbf{q} \text{ and frequency } ik_n-iq_n. \text{ The lower branch has momentum } \mathbf{p}+\mathbf{q} \text{ and frequency } ip_n+iq_n. \text{ These two branches meet at a vertex, forming a fermion loop. The loop has two vertices connected by interaction lines (dashed lines) with momentum } \mathbf{q} \text{ and frequency } iq_n. \text{ The loop is labeled } \tilde{q} \text{ and } \tilde{p}. \\
&= \frac{-1}{(\beta\mathcal{V})^2} \sum_{\sigma' \mathbf{p} \mathbf{q}} \sum_{ip_n iq_n} [-W(\mathbf{q})]^2 \mathcal{G}_{\sigma'}^0(\mathbf{p}, ip_n) \mathcal{G}_{\sigma'}^0(\mathbf{p}+\mathbf{q}, ip_n+iq_n) \mathcal{G}_\sigma^0(\mathbf{k}-\mathbf{q}, ik_n-iq_n) \\
&= \frac{1}{\beta} \sum_{iq_n} \int \frac{d\mathbf{q}}{(2\pi)^3} W(\mathbf{q})^2 \Pi^0(\mathbf{q}, iq_n) \mathcal{G}_\sigma^0(\mathbf{k}-\mathbf{q}, ik_n-iq_n), \tag{12.33}
\end{aligned}$$

where we have separated out the contribution $\Pi^0(\mathbf{q}, iq_n)$ from the fermion loop,

$$\Pi^0(\mathbf{q}, iq_n) \equiv \text{Diagram: A fermion loop with two vertices connected by interaction lines (dashed lines) with momentum } \mathbf{q} \text{ and frequency } iq_n. \\
= \frac{-2}{\beta} \sum_{ip_n} \int \frac{d\mathbf{p}}{(2\pi)^3} \frac{1}{(ip_n + iq_n - \xi_{\mathbf{p}+\mathbf{q}})} \frac{1}{(ip_n - \xi_{\mathbf{p}})}. \tag{12.34}$$

The loop contribution $\Pi^0(\mathbf{q}, iq_n)$ is traditionally denoted the pair-bubble, and we shall study it in more detail in the coming chapters. Here we just note that the spin sum becomes a factor 2, and that the Matsubara sum over ip_n can easily be carried out using the method of Sec. 10.4.1. The evaluation of the \mathbf{p} -integral is in principle elementary. Inserting the result for $\Pi^0(\mathbf{q}, iq_n)$ into the pair-bubble self-energy diagram Eq. (12.32) leads to a bit more involved Matsubara frequency summation over iq_n and momentum integration over \mathbf{q} . However, the calculation can be performed, and we shall return to it later.

12.7 Summary and outlook

In this chapter we have established the Feynman rules for writing down the Feynman diagrams constituting the infinite-order perturbation expansion of the full single-particle Green's functions $\mathcal{G}(b, a)$ or $\mathcal{G}_\sigma(\mathbf{k}, ik_n)$ in terms of the pair-interaction W . Our main example is the Coulomb interaction.

The Feynman diagram technique is a very powerful tool to use in the context of perturbation theory. It enables a systematic analysis of the infinitely many terms that need to be taken into account in a given calculation. Using the Feynman diagrammatic

analysis one can, as we shall see in the following chapters, identify which sub-classes of diagrams that give the most important contributions. We have already given explicit examples of how to evaluate some of the diagrams that are going to play an important role. Indeed, we show in Chap. 13 that the diagrams analyzed in Eqs. (12.31) and (12.34) are the ones that dominate the physics of the interacting electron gas in the high density limit. We shall learn how these diagrams determine the ground state energy of the system as well as its dielectric properties such as static and dynamic screening.

Chapter 13

The interacting electron gas

In Sec. 2.2 we studied the Coulomb interaction as a perturbation to the non-interacting electron gas in the jellium model. This was expected to be a valid procedure in the high density limit, where according to Eq. (2.35) the interaction energy is negligible. Nevertheless, the second order perturbation analysis of Sec. 2.2.2 revealed a divergence in the contribution $E_{\text{dir}}^{(2)}$ from the direct processes, see Eq. (2.49).

In this chapter we reanalyze the Coulomb-interacting electron gas in the jellium model using the Feynman diagram technique, and we show how a meaningful finite ground state energy can be found. To ensure well-behaved finite integrals during our analysis we work with the Yukawa-potential with an artificial range $1/\alpha$ instead of the pure long range Coulomb potential, see Eq. (1.103) and the associated footnote,

$$W(\mathbf{r} - \mathbf{r}') = \frac{e_0^2}{|\mathbf{r} - \mathbf{r}'|} e^{-\alpha|\mathbf{r} - \mathbf{r}'|}, \quad W(\mathbf{q}) = \frac{4\pi e_0^2}{q^2 + \alpha^2}. \quad (13.1)$$

The range $1/\alpha$ has no physical origin. At the end of the calculation we take the limit $\alpha \rightarrow 0$ to recover the Coulomb interaction. For example, with the Yukawa potential we can obtain a finite value for $E_{\text{dir}}^{(2)}$ in Eq. (2.49) if α is finite, but the divergence reappears as soon as we take the limit $\alpha \rightarrow 0$,

$$E_{\text{dir}}^{(2)} \propto \int_0^\infty dq \, q^2 \frac{1}{(q^2 + \alpha^2)^2} \frac{1}{q} \, q \, q \sim -\ln(\alpha) \xrightarrow{\alpha \rightarrow 0} \infty. \quad (13.2)$$

The main result of the following diagrammatic calculation is that the dynamics of the interacting system by itself creates a renormalization of the pure Coulomb interaction into a Yukawa-like potential independent of the value of α , which then without problems can be taken to zero. The starting point of the theory is the self-energy $\Sigma_\sigma(\mathbf{k}, ik_n)$.

13.1 The self-energy in the random phase approximation

To construct the diagrammatic expansion of the self-energy $\Sigma_\sigma(\mathbf{k}, ik_n)$ in (\mathbf{k}, ik_n) -space we use the Feynman rules Eq. (12.24). In analogy with Eq. (12.18) the self-energy is given by the sum of all the irreducible diagrams in $\mathcal{G}_\sigma(\mathbf{k}, ik_n)$ removing the two external fermion

lines $\mathcal{G}_\sigma^0(\mathbf{k}, ik_n)$. We recall that due to the charge compensating back ground in the jellium model the Hartree self-energy diagram vanishes, $\Sigma_\sigma^H(\mathbf{k}, ik_n) = \text{---}\bullet\text{---}\bigcirc = 0$. Thus:

$$\Sigma_\sigma(\mathbf{k}, ik_n) = \text{---}\bullet\text{---}\bigcirc + \text{---}\bullet\text{---}\bigcirc\text{---}\bullet\text{---}\bigcirc + \text{---}\bullet\text{---}\bigcirc\text{---}\bullet\text{---}\bigcirc + \text{---}\bullet\text{---}\bigcirc\text{---}\bullet\text{---}\bigcirc + \text{---}\bullet\text{---}\bigcirc\text{---}\bullet\text{---}\bigcirc + \dots \quad (13.3)$$

For each order of W we want to identify the most important terms, and then resum the infinite series taking only these terms into account. This is achieved by noting that each diagram in the expansion is characterized by its density dependence through the dimensionless electron distance parameter r_s of Eq. (2.37) and its degree of divergence in the cut-off parameter α .

13.1.1 The density dependence of self-energy diagrams

Consider an arbitrary self-energy diagram $\Sigma_\sigma^{(n)}(\mathbf{k}, ik_n)$ of order n :

$$\Sigma_\sigma^{(n)}(\mathbf{k}, ik_n) = \text{---}\bullet\text{---}\bigcirc\text{---}\bullet\text{---}\bigcirc\text{---}\bullet\text{---}\bigcirc \propto \underbrace{\int d\tilde{k}_1 \dots \int d\tilde{k}_n}_{n \text{ internal momenta}} \overbrace{W() \dots W()}^{n \text{ interaction terms}} \underbrace{\mathcal{G}^0() \dots \mathcal{G}^0()}_{2n-1 \text{ Green's fcts}}. \quad (13.4)$$

We then make the integral dimensionless by measuring momenta and frequencies in powers of the Fermi momentum k_F and pulling out the corresponding factors of k_F . We have $k \propto k_F$, $\varepsilon \propto k_F^2$, and $\frac{1}{\beta} \propto k_F^2$. Furthermore, $\int d\tilde{k}_1 \propto \frac{1}{\beta} \sum_{ik_n} \int \frac{d\mathbf{k}}{(2\pi)^3} \propto k_F^{2+3} = k_F^5$, while $W(\mathbf{q}) \propto \frac{1}{q^2 + \alpha^2} \propto k_F^{-2}$ and $\mathcal{G}_\sigma^0(\tilde{k}) = \frac{1}{ik_n - \varepsilon_{\mathbf{k}}} \propto k_F^{-2}$. The self-energy diagram therefore has the following k_F - and thus r_s -dependence:

$$\Sigma_\sigma^{(n)}(\mathbf{k}, ik_n) \propto \left(k_F^5\right)^n \left(k_F^{-2}\right)^n \left(k_F^{-2}\right)^{2n-1} = k_F^{-(n-2)} \propto r_s^{n-2}, \quad (13.5)$$

where in the last proportionality we have used $r_s = (9\pi/4)^{1/3}/(a_0 k_F)$ from Eq. (2.37). We can conclude that for two different orders n and n' in the high density limit, $r_s \rightarrow 0$, we have

$$n < n' \Rightarrow \left| \Sigma_\sigma^{(n)}(\mathbf{k}, ik_n) \right| \gg \left| \Sigma_\sigma^{(n')}(\mathbf{k}, ik_n) \right|, \text{ for } r_s \rightarrow 0. \quad (13.6)$$

Eqs. (13.5) and (13.6) are the precise statements for how to identify the most important self-energy diagrams in the high density limit.

13.1.2 The divergence number of self-energy diagrams

The singular nature of the Yukawa-modified Coulomb potential Eq. (13.1) in the limit of small q and α leads to a divergent behavior of the self-energy integrals. The more interaction lines carrying the same momentum there are in a given diagram, the more divergent is this diagram. For example (taking $\alpha = 0$) two lines with the momentum \mathbf{q} contributes with $W(\mathbf{q})^2$ which diverges as q^{-4} for $q \rightarrow 0$ independent of the behavior of any other internal momentum \mathbf{p} in the diagram. In contrast, two lines with different momenta \mathbf{q} and $\mathbf{q} - \mathbf{p}$ contributes with $W(\mathbf{q})W(\mathbf{q} - \mathbf{p})$, which diverges as q^{-4} only when both $q \rightarrow 0$ and $p \rightarrow 0$ at the same time, i.e. in a set of measure zero in the integral over \mathbf{q} and \mathbf{p} .

In view of this discussion it is natural to define a divergence number $\delta_\sigma^{(n)}$ of the self-energy diagram $\Sigma_\sigma^{(n)}(\mathbf{k}, ik_n)$ as

$$\delta_\sigma^{(n)} \equiv \left\{ \begin{array}{l} \text{the largest number of interaction lines in} \\ \Sigma_\sigma^{(n)}(\mathbf{k}, ik_n) \text{ having the same momentum } \mathbf{q}. \end{array} \right. \quad (13.7)$$











Consider two diagrams $\Sigma_\sigma^{(n,1)}$ and $\Sigma_\sigma^{(n,2)}$ of the same order n . With one notable exception, it is in general not possible to determine which diagram is the larger based alone on knowledge of the divergence number. The exception involves the diagram with the maximal divergence number, i.e. when all n momenta in the diagram are the same. In the limit $\alpha \rightarrow 0$ this diagram is the largest:

$$\delta_\sigma^{(n,1)} = n \quad \Rightarrow \quad \left| \Sigma_\sigma^{(n,1)}(\mathbf{k}, ik_n) \right| \gg \left| \Sigma_\sigma^{(n,2)}(\mathbf{k}, ik_n) \right|, \quad \left\{ \begin{array}{l} \text{for } \alpha \rightarrow 0 \text{ and any} \\ n\text{-order diagram } \Sigma^{(n,2)}. \end{array} \right. \quad (13.8)$$

13.1.3 RPA resummation of the self-energy

Using the order n and the divergence number δ , we now order the self-energy diagrams in a (n, δ) -table. According to Eqs. (13.6) and (13.8) the most important terms are those in the diagonal in this table where $\delta = n$. The first few diagrams (without arrows on the

interaction lines for graphical clarity) are

$\Sigma_\sigma(\tilde{k})$	$n = 1$	$n = 2$	$n = 3$	$n = 4$
$\delta = 1$				
$\delta = 2$	—			
$\delta = 3$	—	—		
$\delta = 4$	—	—	—	

(13.9)

It is clear that the most important diagrams in the high density limit are those having a low order. For each given order the diagrams with the highest divergence number are the most important. The self-energy in the random phase approximation (RPA) is an infinite sum containing diagrams of all orders n , but only the most divergent one for each n :

$$\Sigma_\sigma^{\text{RPA}}(\tilde{k}) \equiv \tilde{k} \begin{array}{c} \tilde{q} \\ \uparrow \\ \downarrow \\ \tilde{q} \end{array} + \tilde{k} \begin{array}{c} \tilde{q} \\ \uparrow \\ \tilde{p} + \tilde{q} \\ \downarrow \\ \tilde{q} \end{array} + \tilde{k} \begin{array}{c} \tilde{q} \\ \uparrow \\ \tilde{q} \\ \downarrow \\ \tilde{q} \end{array} + \tilde{k} \begin{array}{c} \tilde{q} \\ \uparrow \\ \tilde{q} \\ \downarrow \\ \tilde{q} \end{array} + \dots \quad (13.10)$$

Below we are going to analyze parts of the diagrams individually. This is straightforward to do, since the Feynman rules Eq. (12.24) are still valid for each part. An important part of the self-energy diagrams in Eq. (13.10) is clearly the pair-bubble $\Pi^0(\mathbf{q}, iq_n) \equiv \text{bubble}$ already introduced in Sec. 12.6.3. It plays a crucial role, because it ensures that all interaction lines $W(\mathbf{q})$ carry the same momentum \mathbf{q} . To make the fermion-loop sign from the pair-bubble appear explicitly we prefer to work with $\chi_0 \equiv -\Pi^0$, i.e.

$$\text{bubble} \equiv -\chi_0(\mathbf{q}, iq_n), \quad \chi_0(\mathbf{q}, iq_n) = \frac{2}{\beta} \sum_{ip_n} \int \frac{d\mathbf{p}}{(2\pi)^3} \frac{1}{(ip_n + iq_n - \xi_{\mathbf{p}+\mathbf{q}})} \frac{1}{(ip_n - \xi_{\mathbf{p}})}. \quad (13.11)$$

In fact, this χ_0 is the same correlation function as the one introduced for other reasons in Sec. 10.7.

By introducing a renormalized interaction line $-W^{\text{RPA}}(\tilde{q}) = \text{wavy line}$ we can, omitting interaction line arrows, rewrite the RPA self-energy as

$$\Sigma_{\sigma}^{\text{RPA}} = \text{vertical line} \times \left[\text{wavy line} + \text{bubble} + \text{chain of bubbles} + \dots \right] = \text{vertical line} \times \text{renormalized wavy line} \quad (13.12)$$

or, pulling out the convergent Fock self-energy bubble , as

$$\Sigma_{\sigma}^{\text{RPA}} = \text{bubble} + \text{vertical line} \times \left[\text{wavy line} + \text{bubble} + \text{chain of bubbles} + \dots \right] = \text{bubble} + \text{vertical line} \times \text{renormalized wavy line} \quad (13.13)$$

In the following we study the properties of the renormalized Coulomb interaction $W^{\text{RPA}}(\tilde{q})$.

13.2 The renormalized Coulomb interaction in RPA

The renormalized Coulomb interaction $W^{\text{RPA}}(\mathbf{q}, iq_n)$ introduced in Eqs. (13.12) and (13.13) can be found using a Dyson equation approach,

$$\begin{aligned} -W^{\text{RPA}}(\mathbf{q}, iq_n) \equiv \text{wavy line} &\equiv \text{wavy line} + \text{bubble} + \text{chain of bubbles} + \dots \\ &= \text{wavy line} + \text{bubble} \times \left[\text{wavy line} + \text{bubble} + \text{chain of bubbles} + \dots \right] \\ &= \text{wavy line} + \text{bubble} \times \text{wavy line} \end{aligned} \quad (13.14)$$

In (\mathbf{q}, iq_n) -space this is an algebraic equation with the solution

$$-W^{\text{RPA}}(\mathbf{q}, iq_n) = \text{wavy line} = \frac{\text{wavy line}}{1 - \text{bubble}} = \frac{-W(\mathbf{q})}{1 - W(\mathbf{q}) \chi_0(\mathbf{q}, iq_n)}. \quad (13.15)$$

Note the cancellation of the explicit signs from W and χ_0 in the denominator. We can now insert the specific form Eq. (13.1) for the Yukawa-modified Coulomb interaction, and let the artificial cut-off parameter α tend to zero. The final result is

$$W^{\text{RPA}}(\mathbf{q}, iq_n) \xrightarrow{\alpha \rightarrow 0} \frac{4\pi e_0^2}{q^2 - 4\pi e_0^2 \chi_0(\mathbf{q}, iq_n)}. \quad (13.16)$$

$W^{\text{RPA}}(\mathbf{q}, iq_n)$ thus has a form similar to $W(\mathbf{q})$, but with the important difference that the artificially introduced parameter α in the latter has been replaced with the pair-bubble function $-4\pi e_0^2 \chi_0(\mathbf{q}, iq_n)$ having its origin in the dynamics of the interacting electron gas. Note that the pair-bubble is a function of both momentum and frequency. From now on we no longer need a finite value of α , and it is put to zero in the following.

In the static, long-wave limit, $\mathbf{q} \rightarrow 0$ and $iq_n = 0 + i\eta$, we find that W^{RPA} appears in a form identical with the Yukawa-modified Coulomb interaction, i.e. a screened Coulomb interaction

$$W^{\text{RPA}}(\mathbf{q}, 0) \xrightarrow{\mathbf{q} \rightarrow 0} \frac{4\pi e_0^2}{q^2 + k_s^2}, \quad (13.17)$$

where the so-called Thomas-Fermi screening wavenumber, k_s has been introduced,

$$k_s^2 \equiv -4\pi e_0^2 \chi_0(0, 0). \quad (13.18)$$

In the extreme long wave limit we have

$$W^{\text{RPA}}(0, 0) = \frac{-1}{\chi_0(0, 0)}. \quad (13.19)$$

In the following section we calculate the pair-bubble $\chi_0(\mathbf{q}, iq_n)$, find the value of the Thomas-Fermi screening wavenumber k_s , and discuss a physical interpretation of the random phase approximation.

13.2.1 Calculation of the pair-bubble

In Eq. (12.34) the pair-bubble diagram is given in terms of a \mathbf{p} -integral and a Matsubara frequency sum. The sum was carried out in Eq. (10.85) using the recipe Eq. (10.54):

$$\chi_0(\mathbf{q}, iq_n) = 2 \int \frac{d\mathbf{p}}{(2\pi)^3} \frac{n_F(\xi_{\mathbf{p}+\mathbf{q}}) - n_F(\xi_{\mathbf{p}})}{\xi_{\mathbf{p}+\mathbf{q}} - \xi_{\mathbf{p}} - iq_n}. \quad (13.20)$$

The frequency dependence of the retarded pair-bubble χ_0^R can now be found by the usual analytical continuation $iq_n \rightarrow \omega + i\eta$. We still have to perform the rather involved \mathbf{p} -integral. However, it is a simple matter to obtain the static, long-wave limit $q \rightarrow 0$ and $iq_n = 0$, and thus determine $\chi_0^R(\mathbf{q}, 0)$. In this limiting case $\xi_{\mathbf{p}+\mathbf{q}} \rightarrow \xi_{\mathbf{p}}$, and we can perform a Taylor expansion in energy

$$\begin{aligned} \chi_0^R(\mathbf{q}, 0) \xrightarrow{q \rightarrow 0} 2 \int \frac{d\mathbf{p}}{(2\pi)^3} \frac{(\xi_{\mathbf{p}+\mathbf{q}} - \xi_{\mathbf{p}}) \frac{\partial n_F}{\partial \xi_{\mathbf{p}}}}{\xi_{\mathbf{p}+\mathbf{q}} - \xi_{\mathbf{p}}} &= - \int d\xi_{\mathbf{p}} d(\mu + \xi_{\mathbf{p}}) \left[-\frac{\partial n_F}{\partial \xi_{\mathbf{p}}} \right] \\ &\simeq -d(\varepsilon_F), \quad \text{for } k_B T \ll \varepsilon_F. \end{aligned} \quad (13.21)$$

In the static, long-wave limit at low temperatures $\chi_0^R(\mathbf{q}, 0)$ is simply minus the density of states at the Fermi level, and consequently, according to Eq. (13.19), $W^{\text{RPA}}(q \rightarrow 0, 0)$ becomes

$$W^{\text{RPA}}(q \rightarrow 0, 0) = \frac{1}{d(\varepsilon_F)}. \quad (13.22)$$

The Thomas-Fermi screening wavenumber k_s is found by combining Eq. (13.18) with Eqs. (2.31) and (2.36),

$$k_s^2 = -4\pi e_0^2 \chi_0^R(0,0) = 4\pi e_0^2 d(\varepsilon_F) = \frac{4}{\pi} \frac{k_F}{a_0}, \quad (13.23)$$

a_0 being the Bohr radius. This result is very important, because it relates the screening length $1/k_s$ to microscopic parameters of the electron gas. It is therefore useful for numerous applications. For metals $k_s \approx 0.1 \text{ nm}^{-1}$.

We now turn to the more general case, but limit the calculation of $\chi_0(\mathbf{q}, \omega + i\eta)$ to the low temperature regime $k_B T \ll \varepsilon_F$. Finite temperature effects can be obtained by using the Sommerfeld expansion or by numerical integration. In the low temperature limit an analytical expression is obtained by a straightforward but rather tedious calculation. In the \mathbf{p} -integral the only angular dependence of the integrand is through $\cos \theta$, and we have

$$\lambda \equiv \cos \theta, \quad \int \frac{d\mathbf{p}}{(2\pi)^3} = \int_0^\infty \frac{dp}{4\pi^2} p^2 \int_{-1}^1 d\lambda, \quad \xi_{\mathbf{p}-\mathbf{q}} - \xi_{\mathbf{p}} = \frac{1}{2m} (q^2 - 2pq\lambda). \quad (13.24)$$

In the low temperature limit the Fermi-Dirac distribution is a step-function, and the real part of χ_0 is most easily calculated by splitting Eq. (13.20) in two terms, substituting \mathbf{p} with $\mathbf{p} - \mathbf{q}$ in the first term, and collecting the terms again:

$$\text{Re } \chi_0(\mathbf{q}, \omega + i\eta) = -\mathcal{P} \int_0^{k_F} \frac{dp}{2\pi^2} p^2 \int_{-1}^1 d\lambda n_F(\xi_{\mathbf{p}}) \left[\frac{1}{\frac{1}{2m} (q^2 - 2pq\lambda) + \omega} + \frac{1}{\frac{1}{2m} (q^2 + 2pq\lambda) - \omega} \right]. \quad (13.25)$$

The integrand is now made dimensionless by measuring all momenta in units of k_F and all frequencies and energies in units of ε_F , such as

$$x \equiv \frac{q}{2k_F} \quad \text{and} \quad x_0 \equiv \frac{\omega}{4\varepsilon_F}, \quad (13.26)$$

and then the λ -integral followed by the p -integral is carried out using standard logarithmic integrals¹. The final result for the retarded function χ_0^R is

$$\text{Re } \chi_0^R(\mathbf{q}, \omega) = -2 d(\varepsilon_F) \left(\frac{1}{2} + \frac{f(x, x_0) + f(x, -x_0)}{8x} \right), \quad (13.27a)$$

where

$$f(x, x_0) \equiv \left[1 - \left(\frac{x_0}{x} - x \right)^2 \right] \ln \left| \frac{x + x^2 - x_0}{x - x^2 + x_0} \right|. \quad (13.27b)$$

The imaginary part of χ_0 in Eq. (13.20) is

$$\text{Im } \chi_0(\mathbf{q}, \omega + i\eta) = \int_0^{k_F} \frac{dp}{2\pi} p^2 \int_{-1}^1 d\lambda [n_F(\xi_{\mathbf{p}+\mathbf{q}}) - n_F(\xi_{\mathbf{p}})] \delta(\xi_{\mathbf{p}+\mathbf{q}} - \xi_{\mathbf{p}} - \omega). \quad (13.28)$$

¹Useful integrals are $\int dx \frac{1}{ax+b} = \frac{1}{a} \ln(ax+b)$ and $\int dx \ln(ax+b) = \frac{1}{a} [(ax+b) \ln(ax+b) - ax]$.

Using $\delta(f[x]) = \sum_{x_0} \delta(x - x_0)/|f'[x_0]|$, where x_0 are the zeros of $f[x]$, the λ -integral can be performed. A careful analysis of when the delta-function and the theta-functions are non-zero leads to

$$\text{Im } \chi_0^R(\mathbf{q}, \omega) = -d(\varepsilon_F) \begin{cases} \frac{\pi}{8x} \left[1 - \left(\frac{x_0}{x} - x \right)^2 \right], & \text{for } |x - x^2| < x_0 < x + x^2 \\ \frac{\pi}{2} \frac{x_0}{x}, & \text{for } 0 < x_0 < x - x^2 \\ 0, & \text{for other } x_0 \geq 0. \end{cases} \quad (13.29)$$

13.2.2 The electron-hole pair interpretation of RPA

We have learned above that the RPA results in a screened Coulomb interaction. To gain some physical insight into the nature of this renormalization, we study the pair-bubble diagram a little closer in the (\mathbf{q}, τ) -representation. Choosing $\tau > 0$ in Eq. (10.83) we arrive at

$$\chi_0(\mathbf{q}, \tau > 0) = - \sum_{\sigma} \int \frac{d\mathbf{p}}{(2\pi)^3} \langle c_{\mathbf{p}\sigma}(\tau) c_{\mathbf{p}\sigma}^{\dagger} \rangle_0 \langle c_{\mathbf{p}+\mathbf{q}\sigma}^{\dagger}(\tau) c_{\mathbf{p}+\mathbf{q}\sigma} \rangle_0. \quad (13.30)$$

Consequently we can interpret $\chi_0(\mathbf{q}, \tau > 0)$ as the sum of all processes of the following type: at $\tau = 0$ an electron is created in the state $|\mathbf{p}\sigma\rangle$ and a hole in the state $|\mathbf{p} + \mathbf{q}\sigma\rangle$, which correspond to an electron jumping from the latter state to the former. At the later time τ the process is reversed, and the electron falls back into the hole state. In the time interval from 0 to τ an electron-hole pair is thus present, but this corresponds to a polarization of the electron gas, and we now see the origin of the renormalization of the Coulomb interaction. The RPA scheme takes interaction processes into account thus changing the dielectric properties of the non-interacting electron gas. The imaginary part of $\chi_0^R(\mathbf{q}, \omega)$, describes the corresponding dissipative processes, where momentum \mathbf{q} and energy ω is absorbed by the electron gas (see also the discussion in Sec. 8.5).

In the remaining sections of the chapter we study how the effective RPA interaction influences the ground state energy and the dielectric properties (in linear response) of the electron gas.

13.3 The ground state energy of the electron gas

We first show how to express the ground state energy in terms of the single-particle Green's functions $\mathcal{G}(\mathbf{k}, ik_n)$. That this is at all possible is perhaps surprising due to the presence of the two-particle Coulomb interaction. But using the equation of motion technique combined with an “integration over the coupling constant” method we obtain the result.

Let λ be a real number $0 \leq \lambda \leq 1$, and define

$$H_{\lambda} \equiv H_0 - \mu N + \lambda W, \quad (13.31)$$

where H_0 is the kinetic energy and W the Coulomb interaction Eq. (2.34). For $\lambda = 0$ we have the non-interacting electron gas while for $\lambda = 1$ we retrieve the full Coulomb interacting electron gas. According to Eq. (1.119) the thermodynamic potential $\Omega \equiv U - TS - \mu N$ is given by

$$\Omega(\lambda) = -\frac{1}{\beta} \ln \text{Tr} \left[e^{-\beta(H_0 - \mu N + \lambda W)} \right]. \quad (13.32)$$

By differentiating with respect to λ we find

$$\frac{\partial \Omega}{\partial \lambda} = -\frac{1}{\beta} \frac{\text{Tr} \left[-\beta W e^{-\beta(H_0 - \mu N + \lambda W)} \right]}{\text{Tr} \left[e^{-\beta(H_0 - \mu N + \lambda W)} \right]} = \langle W \rangle_\lambda. \quad (13.33)$$

By integration over λ from 0 to 1 the change in Ω due to the interactions is found:

$$\Omega(1) - \Omega(0) = \int_0^1 \frac{d\lambda}{\lambda} \langle \lambda W \rangle_\lambda. \quad (13.34)$$

The subscript λ refers to averaging with respect to H_λ . At $T = 0$ we have $\Delta E = \Delta \Omega$, whence the ground state energy E of the system can be calculated as

$$E = E^0 + \lim_{T \rightarrow 0} \int_0^1 \frac{d\lambda}{\lambda} \langle \lambda W \rangle_\lambda. \quad (13.35)$$

The expectation value $\langle \lambda W \rangle_\lambda$ can be related to $\mathcal{G}_\sigma^\lambda(\mathbf{k}, ik_n)$ through the equation of motion for $\mathcal{G}_\sigma^\lambda(\mathbf{k}, \tau)$ using Eqs. (5.31) and (10.61b)

$$\begin{aligned} & -\partial_\tau \frac{1}{\mathcal{V}} \sum_{\mathbf{k}\sigma} \mathcal{G}_\sigma^\lambda(\mathbf{k}, \tau) \\ &= \delta(\tau) + \frac{1}{\mathcal{V}} \sum_{\mathbf{k}\sigma} \langle T_\tau [H_\lambda, c_{\mathbf{k}\sigma}] (\tau) c_{\mathbf{k}\sigma}^\dagger \rangle_\lambda \\ &= \delta(\tau) + \frac{1}{\mathcal{V}} \sum_{\mathbf{k}\sigma} \left(\varepsilon_{\mathbf{k}} \mathcal{G}_\sigma^\lambda(\mathbf{k}, \tau) - 2 \sum_{\mathbf{k}'\sigma'\mathbf{q}} \frac{\lambda}{2} W(\mathbf{q}) \langle T_\tau c_{\mathbf{k}'\sigma'}^\dagger(\tau) c_{\mathbf{k}'+\mathbf{q}\sigma'}(\tau) c_{\mathbf{k}-\mathbf{q}\sigma}(\tau) c_{\mathbf{k}\sigma}^\dagger \rangle_\lambda \right). \end{aligned} \quad (13.36)$$

We now let $\tau = 0^- = -\eta$ and note that the last term is nothing but the interaction part $\langle \lambda W \rangle_\lambda$ of the Hamiltonian. Furthermore, using Fourier transforms we can at $\tau = -\eta$ write $\mathcal{G}_\sigma^\lambda(\mathbf{k}, -\eta) = \frac{1}{\beta} \sum_{ik_n} \mathcal{G}_\sigma^\lambda(\mathbf{k}, ik_n) e^{ik_n \eta}$ and $\delta(-\eta) = \frac{1}{\beta} \sum_{ik_n} e^{ik_n \eta}$. We therefore arrive at the following compact expression,

$$\frac{1}{\beta \mathcal{V}} \sum_{ik_n \mathbf{k}\sigma} (ik_n - \varepsilon_{\mathbf{k}}) \mathcal{G}_\sigma^\lambda(\mathbf{k}, ik_n) e^{ik_n \eta} = \frac{1}{\beta \mathcal{V}} \sum_{ik_n \mathbf{k}\sigma} e^{ik_n \eta} + 2 \langle \lambda W \rangle_\lambda. \quad (13.37)$$

Collecting the sums on the left-hand side yields

$$\frac{1}{\beta \mathcal{V}} \sum_{ik_n \mathbf{k}\sigma} \left[(ik_n - \varepsilon_{\mathbf{k}}) \mathcal{G}_\sigma^\lambda(\mathbf{k}, ik_n) - 1 \right] e^{ik_n \eta} = 2 \langle \lambda W \rangle_\lambda. \quad (13.38)$$

We now utilize that $1 = [\mathcal{G}_\sigma^\lambda]^{-1} \mathcal{G}_\sigma^\lambda$ and furthermore that $[\mathcal{G}_\sigma^\lambda]^{-1} = ik_n - \varepsilon_{\mathbf{k}} - \Sigma_\sigma^\lambda$ to obtain

$$\langle \lambda W \rangle_\lambda = \frac{1}{2\beta \mathcal{V}} \sum_{ik_n} \sum_{\mathbf{k}\sigma} \Sigma_\sigma^\lambda(\mathbf{k}, ik_n) \mathcal{G}_\sigma^\lambda(\mathbf{k}, ik_n) e^{ik_n \eta}, \quad (13.39)$$

and when this is inserted in Eq. (13.35) we finally arrive at the expression for the ground state energy

$$E = E^0 + \lim_{T \rightarrow 0} \frac{1}{2\beta\mathcal{V}} \sum_{ik_n} \sum_{\mathbf{k}\sigma} \int_0^1 \frac{d\lambda}{\lambda} \Sigma_\sigma^\lambda(\mathbf{k}, ik_n) \mathcal{G}_\sigma^\lambda(\mathbf{k}, ik_n) e^{ik_n\eta}. \quad (13.40)$$

This expression allows for a diagrammatic calculation with the additional Feynman rule that $\lim_{T \rightarrow 0} \int_0^1 \frac{d\lambda}{\lambda}$ must be performed at the end of the calculation. Moreover, it is a remarkable result, because it relates the ground state energy of the interacting system to the single-particle Green's function and the related self-energy.

To improve the high-density, second-order perturbation theory of Sec. 2.2 we include in Eq. (13.40) all diagrams up to second order and, through RPA, the most divergent diagram of each of the higher orders. Since the self-energy Σ contains diagrams from first order and up, we do not have to expand the Green's function \mathcal{G} beyond first order:

$$\Sigma_\sigma^\lambda(\mathbf{k}, ik_n) \approx \text{diagram 1} + \text{diagram 2} + \text{diagram 3} + \text{diagram 4} \quad (13.41)$$

$$\mathcal{G}_\sigma^\lambda(\mathbf{k}, ik_n) \approx \text{diagram 5} + \text{diagram 6} \quad (13.42)$$

Note that only the second diagram in Eq. (13.41) needs to be renormalized. This is because only this diagram is divergent without renormalization. Combining Eq. (13.40) with Eqs. (13.42) and (13.41) we obtain to (renormalized) second order:

$$\begin{aligned} E - E^0 &\approx \lim_{T \rightarrow 0} \int_0^1 \frac{d\lambda}{\lambda} \left[\text{diagram 1} + \text{diagram 2} + \text{diagram 3} + 2 \text{diagram 4} \right] \\ &= \int_0^1 \frac{d\lambda}{\lambda} \left[\text{diagram 1} + \text{diagram 2} + \text{diagram 3} \right]. \end{aligned} \quad (13.43)$$

Note the similarity between the three diagrams in this expression for $E - E^0$ and the ones depicted in Fig. 2.6b, Fig. 2.8a, and Fig. 2.8b. We will not go through the calculation of these diagrams. The techniques are similar to those employed in the calculation of the pair-bubble diagram in Sec. 13.2.1. The RPA renormalization of the interaction line in the second diagram in Eq. (13.43) renders the diagram finite. Since the Thomas-Fermi wavenumber k_s replaced α as a cut-off, we know from Eq. (13.2) that this diagram must be proportional to $\log k_s$ and hence to $\log r_s$. We are now in a position to continue the expansion Eq. (2.43) of E/N in terms of the dimensionless distance parameter r_s ,

$$\frac{E}{N} \xrightarrow{r_s \rightarrow 0} \left(\frac{2.211}{r_s^2} - \frac{0.916}{r_s} + 0.0622 \log r_s - 0.094 \right) \text{ Ry}. \quad (13.44)$$

This expression ends the discussion of the ground state energy of the interacting electron gas in the jellium model. By employing the powerful quantum field theoretic method,

in casu resummation of the Feynman diagram series for the single-electron self-energy and Green's function, we could finally solve the problem posed by the failed second order perturbation theory.

Having achieved this solution, we will also be able to study other aspects of the interacting electron gas. In the following we focus on the dielectric properties of the system.

13.4 The dielectric function and screening

Already from Eq. (13.15) it is clear that the internal dynamics of the interacting electron gas lead to a screening of the pure Coulomb interaction. One suspects that also external potentials ϕ_{ext} will be screened similarly; and indeed, as we shall see below, this is in fact the case. As in Sec. 6.4 we study the linear response of the interacting system due to the perturbation H' caused by ϕ_{ext} ,

$$H' = \int d\mathbf{r} [-e \rho(\mathbf{r})] \phi_{\text{ext}}(\mathbf{r}, t), \quad (13.45)$$

where $\rho(\mathbf{r})$ is the particle density and not, as in Sec. 6.4, the charge density. Since the unperturbed system even with its Coulomb interacting electrons is translation-invariant, we write all expressions in Fourier (\mathbf{q}, ω) -space. The external potential $\phi_{\text{ext}}(\mathbf{q}, \omega)$ creates an induced charge density $-e\rho_{\text{ind}}(\mathbf{q}, \omega)$. Through the Coulomb interaction this in turn corresponds to an induced potential

$$\phi_{\text{ind}}(\mathbf{r}, t) = \int d\mathbf{r}' \frac{-e\rho_{\text{ind}}(\mathbf{r}', t)}{4\pi\epsilon_0|\mathbf{r} - \mathbf{r}'|} \quad \Rightarrow \quad \phi_{\text{ind}}(\mathbf{q}, \omega) = \frac{1}{e^2} W(\mathbf{q}) [-e \rho_{\text{ind}}(\mathbf{q}, \omega)]. \quad (13.46)$$

We divide with e^2 since $W(\mathbf{q})$ by definition contains this factor. Next step is to use the Kubo formula, which relates $[-e \rho_{\text{ind}}(\mathbf{q}, \omega)]$ with the external potential and with the retarded density-density correlator

$$[-e \rho_{\text{ind}}(\mathbf{q}, \omega)] = (-e)^2 C_{\rho\rho}^R(\mathbf{q}, -\mathbf{q}, \omega) \phi_{\text{ext}}(\mathbf{q}, \omega) \equiv e^2 \chi^R(\mathbf{q}, \omega) \phi_{\text{ext}}(\mathbf{q}, \omega). \quad (13.47)$$

Collecting our partial results we have

$$\phi_{\text{ind}}(\mathbf{q}, \omega) = W(\mathbf{q}) \chi^R(\mathbf{q}, \omega) \phi_{\text{ext}}(\mathbf{q}, \omega), \quad (13.48)$$

where $\chi^R(\mathbf{q}, \omega)$ is the Fourier transform of the retarded Kubo density-density correlation function $\chi^R(\mathbf{q}, t - t')$, see Eqs. (8.75) and (8.76),

$$\chi^R(\mathbf{q}, t - t') \equiv C_{\rho\rho}^R(\mathbf{q}t, -\mathbf{q}t') = -i\theta(t - t') \frac{1}{\mathcal{V}} \langle [\rho(\mathbf{q}t), \rho(-\mathbf{q}t')] \rangle_{\text{eq}}. \quad (13.49)$$

Here the subscript 'eq' refers to averaging in equilibrium, i.e. with respect to $H = H_0 + W$ omitting H' . Using Eq. (13.48) the total potential $\phi_{\text{tot}}(\mathbf{q}, \omega)$ can be written in terms of the polarization function χ^R ,

$$\phi_{\text{tot}}(\mathbf{q}, \omega) = \phi_{\text{ext}}(\mathbf{q}, \omega) + \phi_{\text{ind}}(\mathbf{q}, \omega) = [1 + W(\mathbf{q}) \chi^R(\mathbf{q}, \omega)] \phi_{\text{ext}}(\mathbf{q}, \omega). \quad (13.50)$$

When recalling that ϕ_{tot} corresponds to the electric field \mathbf{E} , and ϕ_{ext} to the displacement field $\mathbf{D} = \epsilon_0 \epsilon \mathbf{E}$, we see that the following expression for the dielectric function or electrical permittivity ϵ has been derived:

$$\frac{1}{\epsilon(\mathbf{q}, \omega)} = 1 + W(\mathbf{q}) \chi^R(\mathbf{q}, \omega). \quad (13.51)$$

So upon calculating $\chi^R(\mathbf{q}, \omega)$ we can determine $\epsilon(\mathbf{q}, \omega)$. But according to Eq. (10.30) and the specific calculation in Sec. 10.7 we can obtain $\chi^R(\mathbf{q}, \omega)$ by analytic continuation of the corresponding Matsubara Green's function

$$\chi^R(\mathbf{q}, \omega) = \chi(\mathbf{q}, iq_n \rightarrow \omega + i\eta), \quad (13.52)$$

where $\chi(\mathbf{q}, iq_n)$ is the Fourier transform in imaginary time of $\chi(\mathbf{q}, \tau)$ given by Eq. (10.81):

$$\chi(\mathbf{q}, \tau) = -\frac{1}{\mathcal{V}} \langle T_\tau \rho(\mathbf{q}, \tau) \rho(-\mathbf{q}, 0) \rangle_{\text{eq}}. \quad (13.53)$$

We will calculate the latter Green's function using the Feynman diagram technique.

From Eq. (1.96) we can read off the Fourier transform $\rho(\pm \mathbf{q})$:

$$\rho(\mathbf{q}) = \sum_{\mathbf{p}\sigma'} c_{\mathbf{p}\sigma'}^\dagger c_{\mathbf{p}+\mathbf{q}\sigma'}, \quad \rho(-\mathbf{q}) = \sum_{\mathbf{k}\sigma} c_{\mathbf{k}+\mathbf{q}\sigma}^\dagger c_{\mathbf{k}\sigma}. \quad (13.54)$$

Hence $\chi(\mathbf{q}, \tau)$ is seen to be a two-particle Green's function of the form

$$\begin{aligned} \chi(\mathbf{q}, \tau) &= -\frac{1}{\mathcal{V}} \langle T_\tau \sum_{\mathbf{p}\sigma' \mathbf{k}\sigma} c_{\mathbf{p}\sigma'}^\dagger(\tau) c_{\mathbf{p}+\mathbf{q}\sigma'}(\tau) c_{\mathbf{k}+\mathbf{q}\sigma}^\dagger c_{\mathbf{k}\sigma} \rangle_{\text{eq}} \\ &= \frac{1}{\mathcal{V}} \left[-\langle \rho_{\mathbf{q}=0} \rangle_{\text{eq}} \langle \rho_{\mathbf{q}=0} \rangle_{\text{eq}} + \sum_{\mathbf{p}\sigma' \mathbf{k}\sigma} \langle T_\tau c_{\mathbf{p}+\mathbf{q}\sigma'}(\tau) c_{\mathbf{k}\sigma} c_{\mathbf{p}\sigma'}^\dagger(\tau + \eta) c_{\mathbf{k}+\mathbf{q}\sigma}^\dagger(\eta) \rangle_{\text{eq}}^{\text{connected}} \right]. \end{aligned} \quad (13.55)$$

Here, as in Eq. (12.6), $\eta = 0^+$ has been inserted to ensure correct ordering, and we have divided the contributions to χ into two parts. One part where the two density operators are disconnected from one another, and the other part where they mix. The disconnected part is zero since the expectation of the charge density in the neutralized and homogeneous jellium model is zero. The second term has a structure similar to the simple pair-bubble diagram with an external momentum \mathbf{q} flowing through it.

It is now possible to apply the Feynman rules Eq. (12.24) directly and to write the diagrammatic expansion in (\mathbf{q}, iq_n) -space of $\chi(\mathbf{q}, iq_n) = \chi(\tilde{q})$. We only have to pay special attention to rule (4), where it for the single-particle Green's function is stated that the diagrams must contain two Green's functions with the external momentum \mathbf{k} . This rule was a direct consequence of the definition of $\mathcal{G}(\mathbf{k}, \tau)$,

$$\mathcal{G}(\mathbf{k}, \tau) = -\langle T_\tau c_{\mathbf{k}\sigma}(\tau) c_{\mathbf{k}\sigma}^\dagger \rangle \quad \Rightarrow \quad \bullet \xleftarrow{\tilde{k}} \dots \xleftarrow{\tilde{k}} \bullet \quad (13.56)$$

Likewise for $\chi(\mathbf{q}, \tau)$, except this is a two-particle Green's function with two operators at each of the external vertices instead of just one. One straightforwardly gets the following vertices corresponding to $\rho(\mathbf{q})$ and $\rho(-\mathbf{q})$:

$$\chi(\mathbf{q}, \tau) \sim \langle T_\tau c_{\mathbf{p}\sigma'}^\dagger(\tau) c_{\mathbf{p}+\mathbf{q}\sigma'}(\tau) c_{\mathbf{k}\sigma} c_{\mathbf{k}+\mathbf{q}\sigma}^\dagger \rangle \Rightarrow \begin{array}{c} \tilde{p} \quad \tilde{k} \\ \bullet \quad \quad \bullet \\ \tilde{p}+\tilde{q} \quad \tilde{k}+\tilde{q} \end{array} \quad \dots \quad (13.57)$$

The initial (right) vertex absorbs an external four-momentum \tilde{q} while the final (left) vertex reemits \tilde{q} . We must then have that $\chi(\tilde{q})$ is the sum of all possible diagrams that connect the two ρ -vertices and that involve any number of Coulomb interaction lines.

$$\begin{aligned} -\chi(\tilde{q}) &\equiv \begin{array}{c} \tilde{p} \quad \tilde{k} \\ \bullet \quad \quad \bullet \\ \tilde{p}+\tilde{q} \quad \tilde{k}+\tilde{q} \end{array} \quad \text{(diagram with cross-hatched box)} \\ &\equiv \begin{array}{c} \tilde{k} \\ \bullet \quad \quad \bullet \\ \tilde{k}+\tilde{q} \end{array} + \begin{array}{c} \tilde{p} \quad \tilde{k} \\ \bullet \quad \quad \bullet \\ \tilde{p}+\tilde{q} \quad \tilde{k}+\tilde{q} \end{array} \quad \text{(diagram with wavy line)} + \dots \\ &+ \begin{array}{c} \tilde{k} \\ \bullet \quad \quad \bullet \\ \tilde{k}+\tilde{q} \end{array} \quad \text{(diagram with two wavy lines)} + \dots \\ &+ \begin{array}{c} \tilde{k} \\ \bullet \quad \quad \bullet \\ \tilde{k}+\tilde{q} \end{array} \quad \text{(diagram with three wavy lines)} + \dots \end{aligned} \quad (13.58)$$

In analogy with the self-energy diagrams in Sec. 12.4, we define the irreducible diagrams in the χ -sum as the ones that cannot be cut into two pieces by cutting any single interaction line $\bullet \text{---} \text{wavy line} \text{---} \bullet$:

$$\begin{aligned} -\chi^{\text{irr}}(\tilde{q}) &\equiv \boxed{\text{the sum of all irreducible diagrams in } -\chi(\tilde{q})} \\ &= \begin{array}{c} \tilde{k} \\ \bullet \quad \quad \bullet \\ \tilde{k}+\tilde{q} \end{array} + \begin{array}{c} \tilde{p} \quad \tilde{k} \\ \bullet \quad \quad \bullet \\ \tilde{p}+\tilde{q} \quad \tilde{k}+\tilde{q} \end{array} \quad \text{(diagram with wavy line)} + \dots \\ &\equiv \begin{array}{c} \tilde{p} \quad \tilde{k} \\ \bullet \quad \quad \bullet \\ \tilde{p}+\tilde{q} \quad \tilde{k}+\tilde{q} \end{array} \quad \text{(diagram with diagonal-hatched box)} \end{aligned} \quad (13.59)$$

Hence we can resum $\chi(\tilde{q})$ in terms of $\chi^{\text{irr}}(\tilde{q})$ and obtain a Dyson equation for it,

$$\begin{aligned}
 -\chi(\tilde{q}) &= \text{diagram: bubble with cross-hatch} \\
 &= \text{diagram: bubble with diagonal hatch} + \text{diagram: bubble with diagonal hatch connected by wavy line to another bubble with diagonal hatch} + \dots \\
 &= \text{diagram: bubble with diagonal hatch} + \text{diagram: bubble with diagonal hatch connected by wavy line to a bracketed sum of diagrams} \\
 &= \text{diagram: bubble with diagonal hatch} + \text{diagram: bubble with diagonal hatch connected by wavy line to a cross-hatch bubble} = -\chi^{\text{irr}}(\tilde{q}) - \chi^{\text{irr}}(\tilde{q}) W(\tilde{q}) \chi(\tilde{q}), \quad (13.60)
 \end{aligned}$$

with the solution

$$-\chi(\tilde{q}) = \text{diagram: bubble with cross-hatch} = \frac{\text{diagram: bubble with diagonal hatch}}{1 - \text{diagram: bubble with diagonal hatch connected by wavy line to another bubble with diagonal hatch}} = \frac{-\chi^{\text{irr}}(\tilde{q})}{1 - W(\tilde{q}) \chi^{\text{irr}}(\tilde{q})} \quad (13.61)$$

With this result for $\chi(\mathbf{q}, iq_n)$ we can determine the dielectric function,

$$\frac{1}{\varepsilon(\mathbf{q}, iq_n)} = 1 + W(\mathbf{q}) \frac{\chi^{\text{irr}}(\mathbf{q}, iq_n)}{1 - W(\mathbf{q}) \chi^{\text{irr}}(\mathbf{q}, iq_n)} = \frac{1}{1 - W(\mathbf{q}) \chi^{\text{irr}}(\mathbf{q}, iq_n)}, \quad (13.62)$$

or more directly

$$\varepsilon(\mathbf{q}, iq_n) = 1 - W(\mathbf{q}) \chi^{\text{irr}}(\mathbf{q}, iq_n) = 1 - \frac{e^2}{\epsilon_0 q^2} \chi^{\text{irr}}(\mathbf{q}, iq_n). \quad (13.63)$$

Note it is e^2 and not e_0^2 that appears in the last expression. In RPA $\chi^{\text{irr}}(\mathbf{q}, iq_n)$ is approximated by the simple pair-bubble

$$-\chi^{\text{irr}}(\mathbf{q}, iq_n) = \text{diagram: bubble with diagonal hatch} \longrightarrow -\chi_{\text{RPA}}^{\text{irr}}(\mathbf{q}, iq_n) = \text{diagram: simple pair-bubble} = -\chi_0(\mathbf{q}, iq_n), \quad (13.64)$$

and the full correlation function $\chi(\mathbf{q}, iq_n)$ is approximated by $\chi^{\text{RPA}}(\mathbf{q}, iq_n)$,

$$-\chi^{\text{RPA}}(\mathbf{q}, iq_n) = \text{diagram: bubble with cross-hatch and 'RPA' label} = \frac{\text{diagram: simple pair-bubble}}{1 - \text{diagram: simple pair-bubble}} = \frac{-\chi_0(\mathbf{q}, iq_n)}{1 - W(\tilde{q}) \chi_0(\mathbf{q}, iq_n)}. \quad (13.65)$$

This results in the RPA dielectric function $\varepsilon^{\text{RPA}}(\mathbf{q}, iq_n)$

$$\varepsilon^{\text{RPA}}(\mathbf{q}, iq_n) = 1 - W(\mathbf{q}) \chi_0(\mathbf{q}, iq_n) = 1 - \frac{e^2}{\epsilon_0 q^2} \chi_0(\mathbf{q}, iq_n). \quad (13.66)$$

The entire analysis presented in this section leads to the conclusion that the external potentials treated in linear response theory are renormalized (or screened) in the exact same way as the internal Coulomb interactions of the previous section,

$$\phi_{\text{tot}}^{\text{RPA}}(\mathbf{q}, iq_n) = \frac{1}{\varepsilon^{\text{RPA}}(\mathbf{q}, iq_n)} \phi_{\text{ext}}(\mathbf{q}, iq_n) = \frac{\phi_{\text{ext}}(\mathbf{q}, iq_n)}{1 - \frac{e^2}{\epsilon_0 q^2} \chi_0(\mathbf{q}, iq_n)}. \quad (13.67)$$

This conclusion can be summarized in the following two diagrammatic expansions. One is the internal electron-electron interaction potential represented by the screened Coulomb interaction line W^{RPA} . The other is the external impurity potential Eqs. (11.25) and (11.30) represented by the screened electron-impurity line u^{RPA} .

$$-W^{\text{RPA}}(\mathbf{q}, iq_n) = \text{---} \text{---} \text{---} = \text{---} \text{---} \text{---} + \text{---} \text{---} \text{---} + \text{---} \text{---} \text{---} + \dots \quad (13.68)$$

$$u^{\text{RPA}}(\mathbf{q}) = \text{---} \text{---} \text{---} = \text{---} \text{---} \text{---} + \text{---} \text{---} \text{---} + \text{---} \text{---} \text{---} + \dots \quad (13.69)$$

13.5 Plasma oscillations and Landau damping

We now leave the static case and turn on an external potential with frequency ω . The goal of this section is to investigate the frequency dependence of the dielectric function $\varepsilon(\mathbf{q}, \omega)$. We could choose to study the full case described through $\chi_0^R(\mathbf{q}, \omega)$ by Eqs. (13.27a) and (13.29), but to draw some clear-cut physical conclusions, we confine the discussion to the case of high frequencies, long wave lengths and low temperatures, all defined by the conditions

$$v_F q \ll \omega \text{ (or } x \ll x_0), \quad q \ll k_F \text{ (or } x \ll 1), \quad k_B T \ll \varepsilon_F. \quad (13.70)$$

In this regime we see from Eq. (13.29) that $\text{Im} \chi_0^R = 0$. To proceed we adopt the following notation

$$\lambda \equiv \cos \theta, \quad \int \frac{d\mathbf{p}}{(2\pi)^3} = \int_0^\infty \frac{dp}{4\pi^2} p^2 \int_{-1}^1 d\lambda, \quad \xi_{\mathbf{p}+\mathbf{q}} - \xi_{\mathbf{p}} \approx v_{\mathbf{p}} q \lambda. \quad (13.71)$$

Utilizing this in Eq. (13.20) and Taylor expanding n_F as in Eq. (13.21) we obtain

$$\text{Re} \chi_0^R(\mathbf{q}, \omega) \approx \frac{1}{2\pi^2} \int dp p^2 \delta(\varepsilon_p - \varepsilon_F) \int_{-1}^1 d\lambda \frac{v_{\mathbf{p}} q \lambda}{\omega - v_{\mathbf{p}} q \lambda}. \quad (13.72)$$

We rewrite the delta-function in energy-space to one in k-space, and furthermore we introduce a small dimensionless variable z :

$$\delta(\varepsilon_{\mathbf{p}} - \varepsilon_F) = \frac{\delta(p - k_F)}{v_F}, \quad p \rightarrow k_F, \quad v_p \rightarrow v_F, \quad z \equiv \frac{q v_F}{\omega} \lambda \ll 1. \quad (13.73)$$

This is inserted in Eq. (13.72). The variable λ is substituted by z , and the smallness of this new variable permits the Taylor expansion $z/(1-z) \approx z + z^2 + z^3 + z^4$.

$$\begin{aligned} \text{Re } \chi_0^R(\mathbf{q}, \omega) &\approx \frac{1}{2\pi^2} k_F^2 \frac{1}{v_F} \frac{\omega}{qv_F} \int_{-qv_F/\omega}^{qv_F/\omega} dz \frac{z}{1-z} \\ &\approx \frac{1}{2\pi^2} \frac{k_F^2 \omega}{qv_F^2} \left[\frac{1}{2} z^2 + \frac{1}{3} z^3 + \frac{1}{4} z^4 + \frac{1}{5} z^5 \right]_{-qv_F/\omega}^{+qv_F/\omega} \\ &= \frac{n}{m} \frac{q^2}{\omega^2} \left[1 + \frac{3}{5} \left(\frac{qv_F}{\omega} \right)^2 \right], \end{aligned} \quad (13.74)$$

where in the last line we used $v_F = k_F/m$ and $3\pi^2 n = k_F^3$. Combining Eqs. (13.66) and (13.74) we find the RPA dielectric function in the high-frequency and long-wavelength limit to be

$$\varepsilon^{\text{RPA}}(\mathbf{q}, \omega) = 1 - \frac{\omega_p^2}{\omega^2} \left[1 + \frac{3}{5} \left(\frac{qv_F}{\omega} \right)^2 \right], \quad (13.75)$$

where the characteristic frequency ω_p , well known as the electronic plasma frequency, has been introduced,

$$\omega_p \equiv \sqrt{\frac{ne^2}{m\epsilon_0}}. \quad (13.76)$$

13.5.1 Plasma oscillations and plasmons

The plasma frequency is an important parameter of the interacting electron gas setting the energy scale for several processes, e.g. it marks the limit below which metals reflect incoming electromagnetic radiation, and above which they become transparent. Typical values are $\omega \approx 10^{16}$ Hz, putting it in the ultra-violet part of the electromagnetic spectrum. It is determined by the electron density n and the effective band-mass m of Eq. (2.16). The former parameter can be found by Hall effect measurements, while the latter can be determined from the de Haas-van Alphen effect². Using the observed parameters for aluminum, $n = 1.81 \times 10^{29} \text{ m}^{-3}$ and $m = 1.115 m_0$, we obtain $\omega_p^{\text{Al}} = 2.27 \times 10^{16} \text{ Hz} = 15.0 \text{ eV}$.

A very direct manifestation of the plasmon frequency is the existence of the collective charge density oscillations, the plasma oscillations. Theoretically, the existence of these oscillations is proved as follows. Consider the relation $\mathbf{D} = \varepsilon \epsilon_0 \mathbf{E}$ or the related one, $\phi_{\text{ext}}(\mathbf{q}, \omega) = \varepsilon(\mathbf{q}, \omega) \phi_{\text{tot}}(\mathbf{q}, \omega)$. Note that $\varepsilon(\mathbf{q}, \omega) = 0$ in fact allows for a situation where the total potential varies in space and time in the absence of any external potential driving these variations. We are thus about to identify an oscillatory eigenmode for the electron gas. Let us calculate its properties in RPA from Eq. (13.75).

$$\varepsilon^{\text{RPA}}(\mathbf{q}, \omega) = 0 \quad \Rightarrow \quad \omega^2 \approx \omega_p^2 + \frac{3}{5} (qv_F)^2 \quad \Rightarrow \quad \omega(q) \approx \omega_p + \frac{3}{10} \frac{v_F^2}{\omega_p} q^2. \quad (13.77)$$

²The de Haas-van Alphen effect is oscillations in the magnetization of a system as a function of an applied external magnetic field. The Fermi surface can be mapped out using this technique as described in Ashcroft and Mermin, *Solid State Physics*, chapter 14. For the determination of the electron band mass m in aluminum see N.W. Ashcroft, *Philos. Mag.* **8**, 2055 (1963) regarding aluminum.

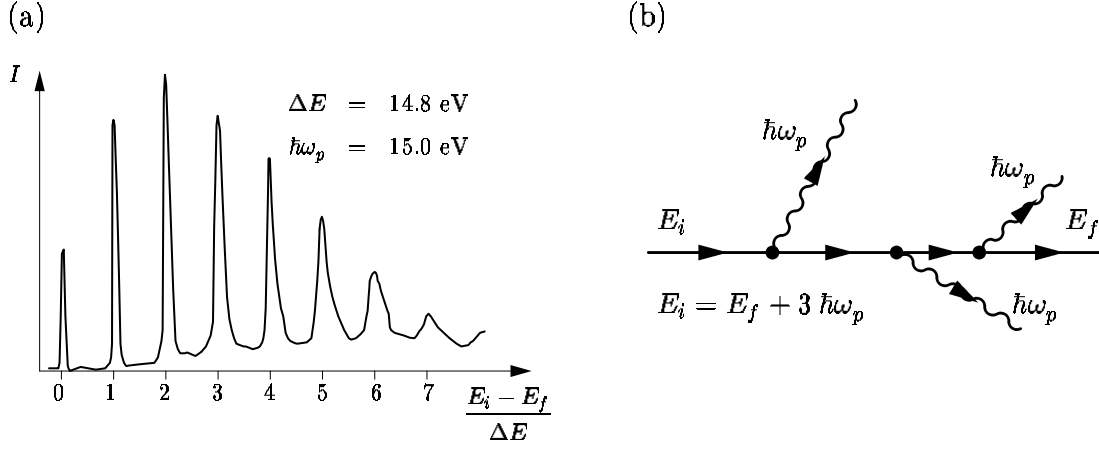


Figure 13.1: (a) Observation of plasmons in high-energy electron transmission spectroscopy on a 258 nm wide aluminum foil, by Marton et al. Phys. Rev. **126**, 182 (1962). The initial energy is $E_i = 20$ keV, and the final energy E_f is measured at zero scattering angle on the other side of the foil. The energy loss $E_i - E_f$ clearly reveals loss in quanta of ΔE . The energy quantum ΔE was found to be 14.8 eV in good agreement with the plasma frequency determined by other methods to be 15.0 eV. (b) A sketch of a typical microscopic process, here with the emission of three plasmon during the traversal.

Recall that in the high frequency regime $\text{Im } \chi_0^R$ and consequently $\text{Im } \epsilon$ is zero, so no damping occurs. Thus by Eq. (13.77) it is indeed possible to find oscillatory eigenmodes, the plasma oscillations. They have a simple quadratic dispersion relation $\omega(q)$ starting out from ω_p for $q = 0$ and then going up as q is increased.

But how could one be convinced of the existence of these oscillations? One beautiful and very direct verification is the experiment discussed in Fig. 13.1. If some eigenmodes exist with a frequency $\sim \omega_p$, then, as is the case with any harmonic oscillator, they must be quantized leading to oscillator quanta, denoted plasmons, with a characteristic energy of ω_p . In the experiment high energy electrons with an initial energy $E_i = 20$ keV are shot through a 258 nm wide aluminum foil. The final energy, E_f , is measured on the other side of the foil, and the energy loss $E_i - E_f$ can be plotted. The result of the measurement is shown in Fig. 13.1(a). The energy loss clearly happens in quanta of size ΔE . Some electrons traverse the foil without exciting any plasmons (the first peak), others excite one or more as sketched in Fig. 13.1(b). On the plot electrons exciting as many as seven plasmons are clearly seen. Note that the most probable process is not the plasmon-free traversal, but instead a traversal during which two plasmons are excited. The value of the energy loss quantum was measured to be $\Delta E = 14.8$ eV in very good agreement with the value of the plasma frequency of 15.0 eV for bulk aluminum.

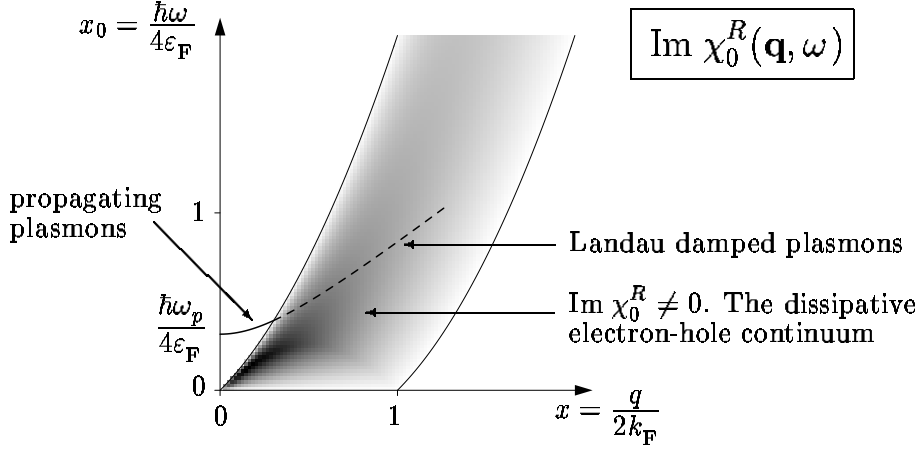


Figure 13.2: A gray scale plot of $\text{Im } \chi_0^R(\mathbf{q}, \omega)$. The darker a shade the higher the value. The variables are rescaled according to Eq. (13.26): $x = q/2k_F$ and $x_0 = \omega/4\varepsilon_F$. Note that $\text{Im } \chi_0^R(\mathbf{q}, \omega) \neq 0$ only in the gray scaled area, which is bounded by the constraint functions given in Eq. (13.29). Also shown is the plasmon branch with its propagating and damped parts. The parameters chosen for this branch are those of aluminum, $\varepsilon_F = 11.7$ eV and $\omega_p = 15.0$ eV.

13.5.2 Landau damping

Finally, we discuss the damping of excitations, which is described by the imaginary part $\text{Im } \chi_0^R(\mathbf{q}, \omega)$. The pure plasma oscillations discussed above are examples of undamped or long-lived excitations. This can be elucidated by going to the retarded functions in Eq. (13.67)

$$\phi_{\text{tot}}^{\text{RPA,R}}(\mathbf{q}, \omega) = \frac{\phi_{\text{ext}}(\mathbf{q}, \omega)}{1 - \frac{e^2}{\epsilon_0 q^2} \chi_0(\mathbf{q}, \omega + i\eta)}. \quad (13.78)$$

In the case of a vanishing imaginary part $\text{Im } \chi_0$ we find a pole on the real axis:

$$\phi_{\text{tot}}^{\text{RPA,R}}(\mathbf{q}, \omega) = \frac{\phi_{\text{ext}}(\mathbf{q}, \omega)}{1 - \frac{e^2}{\epsilon_0 q^2} \text{Re } \chi_0^R(\mathbf{q}, \omega) + i\eta}. \quad (13.79)$$

If, however, $\text{Im } \chi_0^R \neq 0$ we end up with a usual Lorentzian peak as a function of ω , signaling a temporal decay of the total potential with a decay time proportional to $\text{Im } \chi_0^R$,

$$\phi_{\text{tot}}^{\text{RPA,R}}(\mathbf{q}, \omega) = \frac{\phi_{\text{ext}}(\mathbf{q}, \omega)}{1 - \frac{e^2}{\epsilon_0 q^2} \text{Re } \chi_0^R(\mathbf{q}, \omega) + i \frac{e^2}{\epsilon_0 q^2} \text{Im } \chi_0^R(\mathbf{q}, \omega)}. \quad (13.80)$$

In Eq. (13.29) we have within RPA calculated the region the (q, ω) -plane of non-vanishing $\text{Im } \chi_0^R$, and this region is shown in Fig. 13.2. The physical origin of the non-zero imaginary part is the ability for the electron gas to absorb incoming energy by generating

electron-hole pairs. Outside the appropriate area in (q, ω) -space, energy and momentum constraints prohibit the excitation of electron-hole pairs, and the electron gas cannot absorb energy by that mechanism.

Another way to understand the effect of a non-vanishing $\text{Im } \chi_0^R$ is to link it to the conductivity σ of the electron gas. It is well-known that the real part of σ is associated with dissipation (Joule heating), when a current \mathbf{J} is flowing. But from Eq. (6.47) it follows that

$$e^2 \text{Im } \chi_0^R = -\frac{1}{\omega} \mathbf{q} \cdot (\text{Re } \sigma) \cdot \mathbf{q}, \quad (13.81)$$

whereby it is explicitly confirmed that a non-vanishing $\text{Im } \chi_0^R$ is associated with the ability of the system to dissipate energy.

Finally we remark that in Fig. 13.2 is shown the dispersion relation for the plasmon excitation. It starts out as a bona fide excitation in the region of the (q, ω) -space where the RPA dissipation is 0. Hence the plasmons have infinite life times for small q . However, at some point the dispersion curve crosses into the dissipative $\text{Im } \chi_0 \neq 0$ area, and there the plasmon acquires a finite life time. In other words for high q -values the plasmonic excitations are not exact eigenmodes of the system, and they are damped out as a function of time. In the literature this damping mechanism is denoted Landau damping.

13.6 Summary and outlook

In this chapter we have used the Feynman rules for pair-wise interacting particles to analyze the Coulomb-interacting electron gas in the jellium model. The main result was the RPA resummation of diagrams to all orders in perturbation theory valid in the high density limit. In particular we found the self-energy

$$\Sigma_{\sigma}^{\text{RPA}}(\mathbf{k}, ik_n) = \text{diagram} \times \left[\text{diagram} + \text{diagram} + \text{diagram} + \text{diagram} + \dots \right] = \text{diagram}$$

This result was used to calculate the ground state energy of the electron gas

$$\frac{E - E^0}{N} = \text{diagram} + \text{diagram} + \text{diagram} = \left(\frac{2.211}{r_s^2} - \frac{0.916}{r_s} + 0.0622 \log r_s - 0.094 \right) \text{ Ry}.$$

We also used the RPA analysis to study the dielectric properties of the electron gas. One main result was finding the screening of the Coulomb interaction both for the internal interaction and for external potentials, here expressed by their Dyson's equations

$$\begin{aligned} -W^{\text{RPA}}(\mathbf{q}, iq_n) &= \text{diagram} = \text{diagram} + \text{diagram} \\ u^{\text{RPA}}(\mathbf{q}) &= \text{diagram} = \text{diagram} + \text{diagram} \end{aligned}$$

Explicit expressions for the dielectric function $\varepsilon(\mathbf{q}, \omega)$ was found in two cases, (i) the static, long-wave limit and (ii) the high frequency, long-wave limit,

$$\begin{aligned}\varepsilon^{\text{RPA}}(\mathbf{q}, 0) &= 1 + \frac{k_s^2}{q^2}, \quad \text{where } k_s^2 = \frac{4}{\pi} \frac{k_F}{a_0} \\ \varepsilon^{\text{RPA}}(\mathbf{q}, \omega \gg qv_F) &= 1 - \frac{\omega_p^2}{\omega^2} \left[1 + \frac{3}{5} \left(\frac{qv_F}{\omega} \right)^2 \right].\end{aligned}$$

Finally, we studied the plasma oscillations of the electron gas found from the condition $\varepsilon^{\text{RPA}}(\mathbf{q}, \omega) = 0$, and found the dispersion relation involving the plasma frequency ω_p ,

$$\omega(q) = \omega_p + \frac{3}{10} \frac{v_F^2}{\omega_p} q^2, \quad \text{where } \omega_p \equiv \sqrt{\frac{ne^2}{m\epsilon_0}}.$$

The RPA analysis has already given us a good insight in some central physical properties of the electron gas. Moreover, it plays a crucial role in the studies of electron-impurity scattering, electron-phonon interaction, superconductivity, and of many other physical phenomena involving the electron gas.

Chapter 14

Fermi liquid theory

The concept of Fermi liquid theory was developed by Landau in 1957-59 and later refined by others¹. The basic conclusion is that a gas of interacting particles can be described by a system of almost non-interacting “quasiparticles”. These quasiparticles are approximate excitations of the system at sufficiently short time scales. What we mean by “sufficiently short” of course has to be quantified, and this condition will set the limits for the applicability of the theory.

The Fermi liquid theory is conceptually extremely important, because it explains why the apparently immensely complicated system of for example interacting electrons in a metal can be regarded as a gas of non-interacting particles. This is of course an enormous simplification, and it gives the theoretical explanation of why all the results that one gets from the widely used free electron model work so well.

The quasiparticle concept furthermore gives the theoretical foundation of the semi-classical description. The quasiparticle distribution function satisfies a kinetic equation, which may include scattering from one state to another for example due to impurity scattering. This equation is known as the Landau transport equation, and it is equivalent to the well-known Boltzmann equation from kinetic gas theory. In this description the potential is allowed to vary in space due to some external perturbation or due to interactions with the inhomogeneous density of quasiparticles. Using the Landau transport equation we shall see that the collective modes derived in the previous chapter also come out naturally from a semi-classical description and, furthermore, the conductivity, which is calculated from microscopic considerations in Chap. 15, also is easily understood in terms of scattering of quasiparticles.

14.1 Adiabatic continuity

The Fermi liquid theory is based on the assumption that starting from the non-interacting system of particles one can analyze the interacting case by applying perturbation theory. This is in fact a rather stringent criterion, because it means that one cannot cross a phase

¹See for example the collection of reprints in the book: D. Pines *The Many-body problem*, Addison-Wesley (1961,1997).

boundary line. This is because a phase transition, such as for example the ferromagnetic transition discussed in Chap. 4, cannot be reached by perturbation theory starting from the paramagnetic phase.²

If the excitations of the non-interacting system are connected to the excitations of the interacting system by a one-to-one correspondence (at least on short time scales as explained below) the two cases are said to be connected by “adiabatic continuity”. If you imagine that we start from the non-interacting system excited in some state and then turn on the interaction adiabatically, i.e. so slowly that the occupation numbers are not changed, then we would end up in a corresponding excited state of the interacting system. What we really are claiming is that the excited states of the interacting system can be labelled by the same quantum numbers as those we used to label the non-interacting system by.

As a simple example of adiabatic continuity we now consider a particle trapped in a one-dimensional potential. The one-dimensional potential will have a number of bound states with discrete eigenenergies and a continuum of eigenenergies corresponding to the delocalized states. We now imagine changing the potential slowly. As an example consider a potential of the form

$$V(x, t) = -V_0(t) \exp(-x^2/2x_0^2), \quad (14.1)$$

where the depth of the well is time dependent, and let us suppose that it is changing from an initial value V_{01} to a final value V_{02} . If this change is slow the solution of the Schrödinger equation

$$i\partial_t \psi(x, t) = H(t)\psi(x, t) = \left(\frac{p^2}{2m} + V(x, t) \right) \psi(x, t), \quad (14.2)$$

can be approximated by the adiabatic solution

$$\psi_{\text{adia}}(x, t) \approx \psi_{V_0(t)}(x) \exp(-iE_{V_0(t)}t), \quad (14.3)$$

where $\psi_{V_0(t)}(x)$ is the solution of the static (or instantaneous) Schrödinger equation, with energy $E_{V_0(t)}$

$$H(t)\psi_{V_0(t)}(x) = E_{V_0(t)}\psi_{V_0(t)}(x). \quad (14.4)$$

Note that both $\psi_{V_0(t)}(x)$ and $E_{V_0(t)}$ depend parametrically on the time through $V_0(t)$. The accuracy of the solution in Eq. (14.3) is estimated by inserting Eq. (14.3) into Eq. (14.2), which yields

$$i\partial_t \psi_{\text{adia}}(x, t) = E_{V_0(t)}\psi_{\text{adia}}(x, t) + \left(\frac{\partial \psi_{\text{adia}}(x, t)}{\partial V_0(t)} \right) \left(\frac{\partial V_0(t)}{\partial t} \right) = H\psi_{\text{adia}}(x, t). \quad (14.5)$$

Thus we have an approximate solution if the first term dominates over the second term.

Thus apparently our conclusion is that if the rate of change of $V_0(t)$ is small enough the solution for the new value of $V_0 = V_{02}$ can be found by starting from the solution

²This fact you can understand from the concept of broken symmetry explained in Sec. 4.3. The phase with broken symmetry can only occur if the ensemble of states in the statistical average is truncated.

with the old value of $V_0 = V_{01}$ and “adiabatically” changing it to its new value. For example if the first excited state is a bound state, it will change to a somewhat modified state with a somewhat modified energy, but most importantly it is still the first excited state and it is still a bound state. This may sound completely trivial, but it is not, and it is not always true. For example if the real solution during this change of V_0 from V_{01} to V_{02} changes from a bound state to an un-bound state (if V_{02} is small enough there is only one bound state), then it does not matter how slowly we change V_0 . The two states can simply not be connected through small changes of V_0 , because one is a decaying function and one is an oscillatory function. This is an example where perturbation theory to any order would never give the right answer. The important message is, however, that if we avoid these transitions between different kinds of states, adiabatic continuity does work. In the following this idea is applied to the case of interacting particles.

14.1.1 The quasiparticle concept and conserved quantities

The principle of adiabatic continuity is now utilized to study a system of interacting particles. It is used to bring the excitations of the interacting case back to the well-known excitations of the non-interacting case, thus making computation possible. In doing so we gain the fundamental understanding that the interacting and the non-interacting cases have a lot in common at least under some restricting circumstances. This turns out to be realized in many systems. The following arguments are meant to be the full theoretical explanation for the applicability of Fermi liquid theory, but rather to give a physical intuition for the reason why the quasiparticle picture is valid.

When calculating physical quantities, such as response functions or occupation numbers we are facing matrix elements between different states, for example between states with added particles or added particle-hole pairs. Since we are dealing with the low energy properties of the system, let us consider states with single particles or single electron-hole pairs added to the groundstate

$$|(\mathbf{k}\sigma)_p\rangle = c_{\mathbf{k}\sigma}^\dagger |G\rangle, \quad |(\mathbf{k}\sigma)_p; (\mathbf{k}'\sigma')_h\rangle = c_{\mathbf{k}\sigma}^\dagger c_{\mathbf{k}'\sigma'} |G\rangle, \quad \text{etc.} \quad (14.6)$$

where $|G\rangle$ is the groundstate of the interacting system. The first term inserts a particle while the second term creates both a particle and hole. If we now imagine letting time evolve according to a Hamiltonian where the interaction is gradually *switched off* at a rate ζ

$$H_\zeta = H_0 + H_{\text{int}} e^{-\zeta t}, \quad t > 0, \quad (14.7)$$

then according to Eq. (5.18) the time evolution with the time dependent Hamiltonian is

$$|\mathbf{k}\sigma\rangle(t) = e^{-iH_0 t} T_t \exp\left(-i \int_0^t dt' H_\zeta(t')\right) |\mathbf{k}\sigma\rangle \equiv U_\zeta(t, 0) |\mathbf{k}\sigma\rangle. \quad (14.8)$$

If, under the conditions of adiabaticity, we can bring the states ($|(\mathbf{k}\sigma)_p\rangle$, $|(\mathbf{k}\sigma)_p; (\mathbf{k}'\sigma')_h\rangle$, etc) all the way back to the non-interacting case, then the matrix elements are identical to those of the non-interacting case. For example

$$\langle(\mathbf{k}'\sigma')_p|(\mathbf{k}\sigma)_p\rangle = \langle(\mathbf{k}'\sigma')_p|U_\zeta^\dagger(t, 0)U_\zeta(t, 0)|(\mathbf{k}\sigma)_p\rangle \xrightarrow[t \rightarrow \infty]{} \langle(\mathbf{k}'\sigma')_p|(\mathbf{k}\sigma)_p\rangle_0. \quad (14.9)$$

There are two important assumptions built into this construction:

1. The adiabatic procedure is valid when the energy of the state is large compared to the rate of change, i.e. $\varepsilon_{k\sigma} \gg \zeta$, or, since typical excitation energies are of order of the temperature, this is equivalent to assuming $k_B T \gg \zeta$.
2. The interactions do not induce transitions of the states in question, or in other words the life-time τ_{life} of the state is long compared to ζ^{-1} , that is $\tau_{\text{life}} \gg \zeta^{-1}$.

This apparently leaves an energy window where the idea makes sense, namely when we can choose a switch-off rate ζ such that

$$\tau_{\text{life}}^{-1} \ll \zeta \ll k_B T. \quad (14.10)$$

The last condition can in principle always be met at high enough temperatures, whereas the first one is not necessarily possible. Below we shall see that it is indeed possible to make the approximations consistent, because the life-time turns out to be inversely proportional to the square of the temperature, $\tau_{\text{life}}^{-1} \propto T^2$. Thus there is always a temperature range at low temperature where Eq. (14.10) is fulfilled.

Next we discuss the properties of the state with an added particle, $|(\mathbf{k}\sigma)_p\rangle$. It is clear that the state where the interaction is switched off $U_\zeta(\infty, 0)|\mathbf{k}\sigma\rangle$ has a number of properties in common with the initial state $|(\mathbf{k}\sigma)_p\rangle$, namely those that are conserved by the Hamiltonian: (1) it has an excess charge e (compared to the groundstate), (2) it carries current $-e\hbar\mathbf{k}/m$, and (3) it has excess spin σ . Here $-e$ and m are charge and mass of the electrons, respectively. These properties are all conserved quantities because the corresponding operators (1) the total charge $Q = -eN$, (2) the total current $\mathbf{J}_e = -e \sum_{\mathbf{k}\sigma} \mathbf{v}_{\mathbf{k}} n_{\mathbf{k}\sigma}$, and (3) the total spin $\mathbf{S} = \sum_{\mathbf{k}\sigma} \sigma n_{\mathbf{k}\sigma}$ all commute with the Hamiltonian. Most importantly, the adiabatic continuity principle can also be used to calculate the distribution function, and therefore the distribution function $\langle c_{\mathbf{k}'\sigma'}^\dagger c_{\mathbf{k}\sigma} \rangle = \langle (\mathbf{k}'\sigma')_p | (\mathbf{k}\sigma)_p \rangle \mapsto \langle (\mathbf{k}'\sigma')_p | (\mathbf{k}\sigma)_p \rangle_0$ is a Fermi-Dirac distribution function. This leads us to the definition of quasiparticles:

Quasiparticles are the excitations of the interacting system corresponding to the creation or annihilation of particles (for example particle-hole pair state $|(\mathbf{k}\sigma)_p; (\mathbf{k}'\sigma')_h\rangle$). The quasiparticles can be labelled by the same quantum numbers as the non-interacting case, provided that the corresponding operators commute with the Hamiltonian. For a translation-invariant system of electrons interacting through the Coulomb interaction, the quasiparticles quantum numbers are thus \mathbf{k} and σ and they carry charge $-e$ and velocity $\mathbf{v}_{\mathbf{k}} = \hbar\mathbf{k}/m$. The quasiparticle concept only makes sense on time scales shorter than the quasiparticle life time. The quasiparticles are thus not to be thought of as the exact eigenstates. At low temperatures there are only a few quasiparticles, and they therefore constitute a dilute gas. Finally the quasiparticles are in equilibrium distributed according to the Fermi-Dirac distribution function.

In the following we make use of the quasiparticle concept to calculate the screening and the transport properties of an electron gas.

14.2 Semi-classical treatment of screening and plasmons

In Chap. 12 we saw how the collective modes of a charged Fermi gas came out of a rigorous diagrammatical analysis. Here we shall rederive some of this using a less rigorous but maybe physically more appealing approach. Consider a uniform electron gas which is subject to an external potential $\phi_{\text{ext}}(\mathbf{r}, t)$. We can include the external potential as a local change of the potential felt by the charged quasiparticles.³ Now, if the local potential of the quasiparticles is space and time dependent so is then the density of quasiparticles, because they will of course tend to move towards the low potential regions. This in turn changes the electrical potential because the quasiparticles are charged and therefore the total potential ϕ_{tot} is given by the sum of the external potential ϕ_{ext} and the induced potential ϕ_{ind} . The induced potential is caused by the excess or deficit of quasiparticles. Thus we write the resulting local potential $\phi_{\text{tot}}(\mathbf{r}, t)$ as

$$\phi_{\text{tot}}(\mathbf{r}, t) = \phi_{\text{ext}}(\mathbf{r}, t) + \phi_{\text{ind}}(\mathbf{r}, t). \quad (14.11)$$

The induced potential ϕ_{ind} created by the induced density ρ_{ind} , which in turn depends on the total potential, must be determined self-consistently.

³Note that we are here invoking a new concept namely local equilibrium, because otherwise we could not talk about a local potential. Clearly, this only makes sense on length scales larger than a typical thermalization length. The thermalization length is the length scale on which thermal equilibrium is established.

14.2.1 Static screening

First we consider linear static screening. To linear order in the local total potential and at low temperatures the induced charge density is given by

$$\begin{aligned}\rho_{\text{ind}}(\mathbf{r}) &= \frac{2}{V} \sum_{\mathbf{k}} \left[n_F(\xi_{\mathbf{k}} + (-e)\phi_{\text{tot}}(\mathbf{r})) - n_F(\xi_{\mathbf{k}}) \right] \\ &\approx -(-e)\phi_{\text{tot}}(\mathbf{r}) \frac{2}{V} \sum_{\mathbf{k}} \left(-\frac{\partial n_F(\xi_{\mathbf{k}})}{\partial \xi_{\mathbf{k}}} \right) \approx -(-e)\phi_{\text{tot}}(\mathbf{r}) d(\varepsilon_F),\end{aligned}\quad (14.12)$$

where $\xi_{\mathbf{k}}$ is quasiparticle energy measured relative to the equilibrium chemical potential and $d(\varepsilon_F)$ is the density of states at the Fermi level. From this we get the induced potential in real space and in \mathbf{q} -space as

$$\phi_{\text{ind}}(\mathbf{r}) = \frac{1}{-e} \int d\mathbf{r}' W(\mathbf{r}-\mathbf{r}') \rho_{\text{ind}}(\mathbf{r}') \Leftrightarrow \phi_{\text{ind}}(\mathbf{q}) = \frac{1}{-e} W(\mathbf{q}) \rho_{\text{ind}}(\mathbf{q}) = -W(\mathbf{q}) \phi_{\text{tot}}(\mathbf{q}) d(\varepsilon_F), \quad (14.13)$$

which when inserted into (14.11) yields

$$\phi_{\text{tot}}(\mathbf{r}) = \phi_{\text{ext}}(\mathbf{r}, t) - W(\mathbf{q}) d(\varepsilon_F) \phi_{\text{tot}}(\mathbf{q}) \Rightarrow \phi_{\text{tot}}(\mathbf{q}) = \frac{\phi_{\text{ext}}(\mathbf{q})}{1 + W(\mathbf{q}) d(\varepsilon_F)}, \quad (14.14)$$

and hence

$$\varepsilon(\mathbf{q}) = 1 + W(\mathbf{q}) d(\varepsilon_F), \quad (14.15)$$

in full agreement with the conclusions of the RPA results Eqs. (13.66) and (13.67) using $\chi_0^R = -d(\varepsilon_F)$ from Eq. (13.21).

14.2.2 Dynamical screening

In the dynamical case, we expect to find collective excitations similar to the plasmons found in Sec. 13.5. In order to treat this case we need to refine the analysis a bit to allow for the time it takes the charge to adjust to the varying external potential. Consequently, the induced charge density at point \mathbf{r} at time t now depends on the total potential at some other point \mathbf{r}' and at some other (previous) time t' . The way to describe this is to look at the deviation of the distribution function $n_{\mathbf{k}}$ of a quasiparticle with a given momentum $\mathbf{p} = \hbar\mathbf{k}$ (below we as usual use $\hbar = 1$). This depends on both \mathbf{r} and t , so that

$$n_{\mathbf{k}} = n_{\mathbf{k}(t)}(\mathbf{r}, t). \quad (14.16)$$

The dynamics are controlled by two things: the conservation of charge and the change of momentum with time. The first dependence arises from the flow of the distribution function. Because we are interested in times shorter than the life time of the quasiparticles, the number of quasiparticles in each state is conserved. The conservation of particles in state \mathbf{k} is expressed in the continuity equation

$$\dot{n}_{\mathbf{k}} + \nabla_{\mathbf{r}} \cdot \mathbf{j}_{\mathbf{k}} = 0, \quad (14.17)$$

where the current carried of quasiparticles in state \mathbf{k} is given by $\mathbf{j}_{\mathbf{k}} = \mathbf{v}_{\mathbf{k}} n_{\mathbf{k}} = (\hbar \mathbf{k}/m) n_{\mathbf{k}}$, and hence we get

$$\partial_t(n_{\mathbf{k}}) + \dot{\mathbf{k}} \cdot \nabla_{\mathbf{k}} n_{\mathbf{k}} + \mathbf{v}_{\mathbf{k}} \cdot \nabla_{\mathbf{r}} n_{\mathbf{k}} = 0, \quad (14.18)$$

which is known as the collision-free Boltzmann equation⁴.

The second dependence follows from how a negatively charged particle is accelerated in a field, i.e. simply from Newton's law

$$\dot{\mathbf{p}} = -(-e) \nabla_{\mathbf{r}} \phi_{\text{tot}}(\mathbf{r}, t). \quad (14.19)$$

Again it is convenient to use Fourier space and introducing the Fourier transform $n_{\mathbf{k}}(\mathbf{q}, \omega)$. Using Eq. (14.19) we find

$$(-i\omega + i\mathbf{q} \cdot \mathbf{v}_{\mathbf{k}}) n_{\mathbf{k}}(\mathbf{q}, \omega) = -ie (\mathbf{q} \cdot \nabla_{\mathbf{k}} n_{\mathbf{k}}) \phi_{\text{tot}}(\mathbf{q}, \omega) = ie (\mathbf{q} \cdot \nabla_{\mathbf{k}} \xi_{\mathbf{k}}) \left(-\frac{\partial n_{\mathbf{k}}}{\partial \xi_{\mathbf{k}}} \right) \phi_{\text{tot}}(\mathbf{q}, \omega). \quad (14.20)$$

To linear order in the potential ϕ_{tot} we can replace the $n_{\mathbf{k}}$ on the righthand side by the equilibrium distribution $n_{\mathbf{k}}^0 = n_F(\xi_{\mathbf{k}})$ and hence we find

$$n_{\mathbf{k}}(\mathbf{q}, \omega) = \frac{\mathbf{q} \cdot \nabla_{\mathbf{k}} \xi_{\mathbf{k}}}{\omega - \mathbf{q} \cdot \mathbf{v}_{\mathbf{k}}} \left(-\frac{\partial n_F(\xi_{\mathbf{k}})}{\partial \xi_{\mathbf{k}}} \right) (-e \phi_{\text{tot}}(\mathbf{q}, \omega)). \quad (14.21)$$

From this expression we easily get the induced density by summation over \mathbf{k}

$$\rho_{\text{ind}}(\mathbf{q}, \omega) = \frac{2}{\mathcal{V}} \sum_{\mathbf{k}} \frac{\mathbf{q} \cdot \nabla_{\mathbf{k}} \xi_{\mathbf{k}}}{\omega - \mathbf{q} \cdot \mathbf{v}_{\mathbf{k}}} \left(-\frac{\partial n_F(\xi_{\mathbf{k}})}{\partial \xi_{\mathbf{k}}} \right) (-e \phi_{\text{tot}}(\mathbf{q}, \omega)), \quad (14.22)$$

where the factor 2 comes from to spin degeneracy. This is inserted into Eqs. (14.13) and (14.11) and we obtain the dielectric function $\varepsilon = \phi_{\text{ext}}/\phi_{\text{tot}}$ in the dynamical case

$$\varepsilon(\mathbf{q}) = 1 - W(\mathbf{q}) \frac{2}{\mathcal{V}} \sum_{\mathbf{k}} \frac{\mathbf{q} \cdot \nabla_{\mathbf{k}} \xi_{\mathbf{k}}}{\omega - \mathbf{q} \cdot \mathbf{v}_{\mathbf{k}}} \left(-\frac{\partial n_F(\xi_{\mathbf{k}})}{\partial \xi_{\mathbf{k}}} \right). \quad (14.23)$$

At $\omega = 0$ we recover the static case in Eq. (14.15), because $\nabla_{\mathbf{k}} \xi_{\mathbf{k}} = v_{\mathbf{k}}$. At long wavelengths or large frequencies $qv \ll \omega$, we find by expanding in powers of q that

$$\varepsilon(\mathbf{q}) \approx 1 - \frac{W(\mathbf{q})}{\omega^2} \frac{2}{\mathcal{V}} \sum (\mathbf{q} \cdot \mathbf{v}_{\mathbf{k}})^2 \left(-\frac{\partial n_F(\xi_{\mathbf{k}})}{\partial \xi_{\mathbf{k}}} \right) = 1 - \left(\frac{\omega_p}{\omega} \right)^2, \quad (14.24)$$

which agrees with Eq. (13.75) in Sec. 13.5. Note that \mathbf{q} drops out because $W(\mathbf{q}) \propto q^{-2}$.

We have thus shown that in the long wavelength limit the semi-classical treatment, which relies on the Fermi liquid theory, gives the same result as the fully microscopic theory, based on renormalization by summation of the most important diagrams. We have also gained some physical understanding of this renormalization, because we saw explicitly how it was due to the screening of the external potential by the mobile quasiparticles.

⁴Here \mathbf{r} and t are independent space and time variables in contrast to the sometimes used fluid dynamical formulation where $\mathbf{r} = \mathbf{r}(t)$ follows the particle motion.

14.3 Semi-classical transport equation

Our last application of the semi-classical approach is the calculation of conductivity of a uniform electron gas with some embedded impurities. This will in fact lead us to the famous Drude formula. Historically, the Drude formula was first derived in an incorrect way, namely by assuming that the charge carriers form a classical gas. We know now that they follow a Fermi-Dirac distribution, but amazingly the result turns out to be the same. In Sec. 15 we will furthermore see how the very same result can be derived in a microscopic quantum theory starting from the Kubo formula and using a diagrammatic approach.

As explained in Chap. 10, the finite resistivity of metals at low temperatures is due to scattering against impurities or other imperfections in the crystal structure. These collisions take momentum out of the electron system, thus introducing a mechanism for momentum relaxation and hence resistivity. A simple minded approach to conductivity would be to say that the forces acting on a small volume of charge is the sum of the external force and a friction force that is taken to be proportional to the velocity of the fluid at the given point. In steady state these forces are in balance and hence

$$-(-e)\mathbf{E} + \frac{m\mathbf{v}}{\tau_{\text{p-relax}}} = 0 \quad \Rightarrow \quad \mathbf{J} = -en\mathbf{v} = \frac{e^2 n \tau_{\text{p-relax}}}{m} \mathbf{E} \quad \Rightarrow \quad \sigma = \frac{ne^2 \tau_{\text{p-relax}}}{m}, \quad (14.25)$$

where σ is the conductivity and $\tau_{\text{p-relax}}$ is the momentum relaxation time.

Microscopically the momentum relaxation corresponds to scattering of quasiparticles from one state $|\mathbf{k}\sigma\rangle$ with momentum $\hbar\mathbf{k}$ to another state $|\mathbf{k}'\sigma'\rangle$ with momentum $\hbar\mathbf{k}'$. For non-magnetic impurities, the ones considered here, the spin is conserved and thus $\sigma = \sigma'$. The new scattering process thus introduced means that the number of quasiparticles in a given \mathbf{k} -state is no longer conserved and we have to modify Eq. (14.17) to take into account the processes that change the occupation number $n_{\mathbf{k}}$. The rate of change is given by the rate, $\Gamma(\mathbf{k}'\sigma \leftarrow \mathbf{k}\sigma)$, at which scattering from the state $|\mathbf{k}\sigma\rangle$ to some other state $|\mathbf{k}'\sigma'\rangle$ occurs. It can be found from Fermi's golden rule

$$\Gamma(\mathbf{k}'\sigma \leftarrow \mathbf{k}\sigma) = 2\pi \left| \langle \mathbf{k}'\sigma | V_{\text{imp}} | \mathbf{k}\sigma \rangle \right|^2 \delta(\xi_{\mathbf{k}} - \xi_{\mathbf{k}'}), \quad (14.26)$$

where V_{imp} is the impurity potential. The fact that the scattering on an external potential is an elastic scattering is reflected in the energy-conserving delta function. The total impurity potential is a sum over single impurity potentials situated at positions \mathbf{R}_i (see also Chap. 11)

$$V_{\text{imp}}(\mathbf{r}) = \sum_i u(\mathbf{r} - \mathbf{R}_i) \quad (14.27)$$

We can then find the rate Γ by the adiabatic procedure where the matrix element $\langle \mathbf{k}'\sigma | V_{\text{imp}} | \mathbf{k}\sigma \rangle$ is identified with non-interacting counterpart $\langle \mathbf{k}'\sigma | V_{\text{imp}} | \mathbf{k}\sigma \rangle_0$, where $|\mathbf{k}\sigma\rangle_0 = e^{i\mathbf{k}\cdot\mathbf{r}}/\sqrt{\mathcal{V}}$, and we get

$$\Gamma(\mathbf{k}'\sigma \leftarrow \mathbf{k}\sigma) = \Gamma_{\mathbf{k}'\sigma, \mathbf{k}\sigma} = \frac{2\pi}{\mathcal{V}^2} \left| \sum_j \int d\mathbf{r} e^{-i\mathbf{k}'\cdot\mathbf{r}} u(\mathbf{r} - \mathbf{R}_j) e^{+i\mathbf{k}\cdot\mathbf{r}} \right|^2 \delta(\xi_{\mathbf{k}} - \xi_{\mathbf{k}'}). \quad (14.28)$$

Of course we do not know the location of the impurities exactly and therefore we perform a positional average. The average is done assuming only lowest order scattering, i.e. leaving out interference between scattering on different impurities. Therefore we can simply replace the sum over impurities by the number of scattering centers, $N_{\text{imp}} = n_{\text{imp}}\mathcal{V}$, and multiplied by the impurity potential for a single impurity $u(\mathbf{r})$. We obtain

$$\Gamma_{\mathbf{k}',\mathbf{k}} = 2\pi \frac{n_{\text{imp}}}{\mathcal{V}} \left| \int d\mathbf{r} e^{i(\mathbf{k}-\mathbf{k}')\cdot\mathbf{r}} u(\mathbf{r}) \right|^2 \delta(\xi_{\mathbf{k}} - \xi_{\mathbf{k}'}) \equiv \frac{n_{\text{imp}}}{\mathcal{V}} W_{\mathbf{k}',\mathbf{k}}. \quad (14.29)$$

Now the change of $n_{\mathbf{k}}$ due to collisions is included in the differential equation Eq. (14.17) as an additional term. The time derivative of $n_{\mathbf{k}}$ becomes

$$\dot{n}_{\mathbf{k}(t)}(\mathbf{r}, t) = \left(\frac{d}{dt} n_{\mathbf{k}} \right)_{\text{flow-force}} + \left(\frac{\partial}{\partial t} n_{\mathbf{k}} \right)_{\text{collisions}}, \quad (14.30)$$

where the change due to “flow and force” is given by the left hand side in Eq. (14.18). The new collision term is not a derivative but an integral functional of $n_{\mathbf{k}}$

$$\left(\frac{\partial}{\partial t} n_{\mathbf{k}} \right)_{\text{collisions}} = -\frac{n_{\text{imp}}}{\mathcal{V}} \sum_{\mathbf{k}'} [n_{\mathbf{k}}(1 - n_{\mathbf{k}'})W_{\mathbf{k}',\mathbf{k}} - n_{\mathbf{k}'}(1 - n_{\mathbf{k}})W_{\mathbf{k},\mathbf{k}'}]. \quad (14.31)$$

The first term in the sum represents the rate for being scattered out of the state \mathbf{k} and the second term represents the rate for being scattered into to state \mathbf{k} from the state \mathbf{k}' . The total rate is obtained from the Fermi golden rule expression (14.29) times the probability for the initial state to be filled and the final state to be empty. Because $W_{\mathbf{k},\mathbf{k}'} = W_{\mathbf{k}',\mathbf{k}}$, we have

$$\left(\frac{\partial}{\partial t} n_{\mathbf{k}} \right)_{\text{collisions}} = -\frac{n_{\text{imp}}}{\mathcal{V}} \sum_{\mathbf{k}'} W_{\mathbf{k}',\mathbf{k}} (n_{\mathbf{k}} - n_{\mathbf{k}'}), \quad (14.32)$$

and the full Boltzmann transport equation in the presence of impurity scattering now reads

$$\partial_t(n_{\mathbf{k}}) + \dot{\mathbf{k}} \cdot \nabla_{\mathbf{k}} n_{\mathbf{k}} + \mathbf{v}_{\mathbf{k}} \cdot \nabla_{\mathbf{r}} n_{\mathbf{k}} = -\frac{n_{\text{imp}}}{\mathcal{V}} \sum_{\mathbf{k}'} W_{\mathbf{k}',\mathbf{k}} (n_{\mathbf{k}} - n_{\mathbf{k}'}). \quad (14.33)$$

The Boltzmann equation for impurity scattering is rather easily solved in the linear response regime. First we note that $\dot{\mathbf{p}} = -e\mathbf{E}$, and therefore to linear order in \mathbf{E} the term $\nabla_{\mathbf{k}} n_{\mathbf{k}}$ multiplying $\dot{\mathbf{k}}$ can be replaced by the equilibrium occupation, which at zero temperature becomes $\nabla_{\mathbf{k}} n_{\mathbf{k}}^0 = \nabla_{\mathbf{k}} \theta(k_F - k) = -\hat{\mathbf{k}} \delta(k_F - k)$, where $\hat{\mathbf{k}}$ is a unit vector oriented along \mathbf{k} . Let us furthermore concentrate on the long wave-length limit such that $\nabla_{\mathbf{r}} n_{\mathbf{k}} \approx 0$. By going to the frequency domain, we obtain

$$-i\omega n_{\mathbf{k}} + e\mathbf{E} \cdot \hat{\mathbf{k}} \delta(k_F - k) = -\frac{n_{\text{imp}}}{\mathcal{V}} \sum_{\mathbf{k}'} W_{\mathbf{k}',\mathbf{k}} (n_{\mathbf{k}} - n_{\mathbf{k}'}). \quad (14.34)$$

Without the $n_{\mathbf{k}'}$ -term on the right hand side this equation is simple to solve, because the right hand side is then of the form $\tau^{-1} n_{\mathbf{k}}$ similar to $-i\omega n_{\mathbf{k}}$ on the left hand side. This

hints that we can obtain the full solution by some imaginary shift of ω , so let us try the ansatz

$$n_{\mathbf{k}}(\omega) = \frac{1}{i\omega - 1/\tau^{\text{tr}}} e\mathbf{E} \cdot \hat{\mathbf{k}} \delta(k_F - k), \quad (14.35)$$

where the relaxation time τ^{tr} needs to be determined. That this is in fact a solution is seen by substitution

$$\begin{aligned} & \frac{-i\omega}{i\omega - 1/\tau^{\text{tr}}} e\mathbf{E} \cdot \hat{\mathbf{k}} \delta(k_F - k) + e\mathbf{E} \cdot \hat{\mathbf{k}} \delta(k_F - k) \\ &= \frac{-e}{i\omega - 1/\tau^{\text{tr}}} \frac{n_{\text{imp}}}{\mathcal{V}} \sum_{|\mathbf{k}'|} W_{\mathbf{k}', \mathbf{k}} \left(\hat{\mathbf{k}} \delta(k_F - k) - \hat{\mathbf{k}}' \delta(k_F - k') \right) \cdot \mathbf{E}. \end{aligned} \quad (14.36)$$

Since $W_{\mathbf{k}', \mathbf{k}}$ includes an energy conserving delta function, we can set $k = k' = k_F$ and remove the common factor $\delta(k_F - k)$ to get

$$\frac{-i\omega}{i\omega - 1/\tau^{\text{tr}}} e\mathbf{E} \cdot \hat{\mathbf{k}} + e\mathbf{E} \cdot \hat{\mathbf{k}} = \frac{-e}{i\omega - 1/\tau^{\text{tr}}} \frac{n_{\text{imp}}}{\mathcal{V}} \sum_{|\mathbf{k}'|=k_F} W_{\mathbf{k}', \mathbf{k}} (\hat{\mathbf{k}} - \hat{\mathbf{k}}') \cdot \mathbf{E}. \quad (14.37)$$

which is solved by

$$\cos \theta_{\mathbf{k}} \frac{1}{\tau^{\text{tr}}} = \frac{n_{\text{imp}}}{\mathcal{V}} \sum_{k'=k_F} W_{\mathbf{k}', \mathbf{k}} (\cos \theta_{\mathbf{k}} - \cos \theta_{\mathbf{k}'}). \quad (14.38)$$

Here $\theta_{\mathbf{k}}$ is angle between the vector \mathbf{k} and the electric field \mathbf{E} . For a uniform system the result cannot depend on the direction of the electric field, and therefore we can put \mathbf{E} parallel to \mathbf{k} , and get

$$\frac{1}{\tau^{\text{tr}}} = \frac{n_{\text{imp}}}{\mathcal{V}} \sum_{k'=k_F} W_{\mathbf{k}', \mathbf{k}} (1 - \cos \theta_{\mathbf{k}, \mathbf{k}'}). \quad (14.39)$$

The time τ^{tr} is known as the transport time, because it is the time that enters the expression for the conductivity, as we see by calculating the current density

$$\begin{aligned} \mathbf{J} &= -\frac{2e}{\mathcal{V}} \sum_{\mathbf{k}} n_{\mathbf{k}} \mathbf{v}_{\mathbf{k}} \\ &= -\frac{2e}{\mathcal{V}} \sum_{\mathbf{k}} \left[\frac{e\delta(k_F - k)}{i\omega - 1/\tau^{\text{tr}}} \hat{\mathbf{k}} \cdot \mathbf{E} \right] \frac{\mathbf{k}}{m} \\ &= \frac{2e^2}{(2\pi)^2} \frac{\mathbf{E}}{-i\omega + 1/\tau^{\text{tr}}} \frac{1}{m} \int_0^\infty dk k^3 \delta(k_F - k) \int_{-1}^1 d(\cos \theta) \cos^2 \theta \\ &= \frac{2e^2 \mathbf{E}}{-i\omega + 1/\tau^{\text{tr}}} \frac{1}{(2\pi)^2 m} k_F^3 \frac{2}{3} = \frac{e^2 n}{(-i\omega + 1/\tau^{\text{tr}}) m} \mathbf{E}, \end{aligned} \quad (14.40)$$

where we have used the relation between density and k_F , $n = k_F^3/3\pi^2$. The result for the conductivity is

$$\sigma = \sigma_0 \frac{1}{1 - i\omega\tau^{\text{tr}}}; \quad \sigma_0 = \frac{ne^2\tau^{\text{tr}}}{m}, \quad (14.41)$$

which agrees with Eq. (14.25) found by the simplified analysis. The reason that the two approaches give the same result is that we can treat the quasiparticle as independent, and the analysis that was applied in the fluid dynamical picture in Eq. (14.25) is indeed applicable to each quasiparticle separately.

Often one uses an even simpler approximation for the collision term, namely the so-called relaxation time approximation. In this approximation the collision is replaced by

$$\left(\frac{\partial}{\partial t} n_{\mathbf{k}} \right)_{\text{collisions}} = - \frac{n_{\mathbf{k}} - n_{\mathbf{k}}^0}{\tau_0}, \quad (14.42)$$

where $n_{\mathbf{k}}^0$ is the equilibrium distribution function, and τ_0 is the relaxation time. This approximation in fact gives the correct answer if the relaxation time is identified with the transport time $\tau_0 = \tau^{\text{tr}}$. At first sight, it is tempting to think of the τ_0 as the time for scattering out of the state \mathbf{k} , i.e. the life time of the state \mathbf{k} . This would however only give the first term in the right hand side of Eq. (14.32) and it is therefore incorrect. The life time, which was also calculated in Eq. (11.49), is given by the first Born approximation

$$\frac{1}{\tau_{\text{life}}} = \frac{n_{\text{imp}}}{\mathcal{V}} \sum_{\mathbf{k}'} W_{\mathbf{k}', \mathbf{k}}. \quad (14.43)$$

This time expresses the rate for scattering out of a given state \mathbf{k} , but it does not tell us how much the momentum is degraded by the scattering process. This is precisely what the additional cosine-term in Eq. (14.39) accounts for. If the quasiparticle scatters forward, i.e. $\cos \theta \approx 1$, the state \mathbf{k} is destroyed but the momentum is almost conserved and such a process therefore does not effect the conductivity. On the contrary when the particle is scattered backward, i.e. $\cos \theta \approx -1$, there is a large change in momentum, corresponding to a large momentum relaxation. Therefore the transport time is precisely the momentum relaxation time defined in the simple fluid dynamical picture in Eq. (14.25).

14.3.1 Finite life time of the quasiparticles

Above we first assumed that the quasiparticles have an infinite life time. Then we included some finite life time induced by scattering against impurities. But we never included scattering of quasiparticle on other quasiparticles. Here we investigate the validity of this approach by studying the rate of quasiparticle-quasiparticle scattering. Clearly there is a mechanism for quasiparticle scattering against quasiparticles because they are charged and therefore interact through the Coulomb interaction. The interaction between the particles is screened by the other particles and we should use the RPA result for the interaction. The Coulomb interactions thus introduces a two-particle scattering where momentum and energy are exchanged, but of course both total momentum and total energy are conserved in the scattering event. If two particles in states $|\mathbf{k}\sigma; \mathbf{k}'\sigma'\rangle$ scatter, the final state will be a state $|\mathbf{k} + \mathbf{q}\sigma; \mathbf{k}' - \mathbf{q}\sigma'\rangle$, such that the initial and the final energies are the same $\varepsilon_{\mathbf{k}} + \varepsilon_{\mathbf{k}'} = \varepsilon_{\mathbf{k}+\mathbf{q}} + \varepsilon_{\mathbf{k}'-\mathbf{q}}$ or counting from the chemical potential $\xi_{\mathbf{k}} + \xi_{\mathbf{k}'} = \xi_{\mathbf{k}+\mathbf{q}} + \xi_{\mathbf{k}'-\mathbf{q}}$. The rate for quasiparticle-quasiparticle scattering can be calculated using Fermi's golden

rule

$$\Gamma_{\mathbf{k}+\mathbf{q}\sigma, \mathbf{k}'-\mathbf{q}\sigma'; \mathbf{k}'\sigma', \mathbf{k}\sigma} = 2\pi \left| \langle \mathbf{k}+\mathbf{q}\sigma, \mathbf{k}'-\mathbf{q}\sigma' | W^{\text{RPA}}(\mathbf{q}) | \mathbf{k}'\sigma', \mathbf{k}\sigma \rangle \right|^2 \delta(\xi_{\mathbf{k}} + \xi_{\mathbf{k}'} - \xi_{\mathbf{k}+\mathbf{q}} - \xi_{\mathbf{k}'-\mathbf{q}}), \quad (14.44)$$

where $W^{\text{RPA}}(\mathbf{q})$ is the RPA screened Coulomb interaction. From this rate we can obtain the total rate for changing the state of a given quasiparticle in state $|\mathbf{k}\sigma\rangle$ by the Coulomb interaction. To find that we must multiply Γ with the probability that the state $|\mathbf{k}'\sigma'\rangle$ is occupied and that final states are unoccupied and sum over all possible \mathbf{k}' and \mathbf{q} . The result for the “life-time” $\tau_{\mathbf{k}}$ of the state $|\mathbf{k}\sigma\rangle$ is then given by

$$\begin{aligned} \frac{1}{\tau_{\mathbf{k}}} = & \overbrace{2}^{\text{spin}} \frac{2\pi}{\mathcal{V}^2} \sum_{\mathbf{k}'\mathbf{q}} \overbrace{\left| \frac{W(\mathbf{q})}{\varepsilon^{\text{RPA}}(\mathbf{q}, 0)} \right|^2}^{\text{screened interaction}} \delta(\xi_{\mathbf{k}} + \xi_{\mathbf{k}'} - \xi_{\mathbf{k}+\mathbf{q}} - \xi_{\mathbf{k}'-\mathbf{q}}) \\ & \times \left\{ \underbrace{n_{\mathbf{k}} n_{\mathbf{k}'} [1 - n_{\mathbf{k}+\mathbf{q}}] [1 - n_{\mathbf{k}'-\mathbf{q}}]}_{\text{scattering out of state } \mathbf{k}} \right. \\ & \left. - \underbrace{[1 - n_{\mathbf{k}}] [1 - n_{\mathbf{k}'}] n_{\mathbf{k}+\mathbf{q}} n_{\mathbf{k}'-\mathbf{q}}}_{\text{scattering into state } \mathbf{k}} \right\}. \end{aligned} \quad (14.45)$$

The expression (14.45) can be evaluated explicitly for a particle in state \mathbf{k} added to a filled Fermi sea, i.e. $n_{\mathbf{k}} = 1$ and $n_{\mathbf{p}} = \theta(k_F - p)$ for \mathbf{p} equal to \mathbf{k}' , $\mathbf{k}' - \mathbf{q}$, or $\mathbf{k} + \mathbf{q}$. But for now we just want the energy dependence of the life-time. A simple phase space argument gives the answer, see also Fig. 14.1. We look at situation with a particle above the Fermi surface $\xi_{\mathbf{k}} > 0$. Suppose then we have integrated out the angle dependence, which takes care of the delta function. At $T = 0$ this gives the condition that $\xi_{\mathbf{k}} + \xi_{\mathbf{k}'} - \xi_{\mathbf{k}+\mathbf{q}} > 0$. Then we are left with two energy integrals over $\xi_{\mathbf{k}'} \equiv \xi' < 0$ and $\xi_{\mathbf{k}'-\mathbf{q}} \equiv \xi'' > 0$. We then have

$$\begin{aligned} \frac{1}{\tau_{\mathbf{k}}} & \sim |W|^2 [d(\varepsilon_F)]^3 \int_{-\infty}^0 d\xi' \int_0^{\infty} d\xi'' \Theta(\xi_{\mathbf{k}} + \xi' - \xi'') \\ & = |W|^2 [d(\varepsilon_F)]^3 \int_{-\infty}^0 d\xi' (\xi_{\mathbf{k}} + \xi') \Theta(\xi_{\mathbf{k}} + \xi') \\ & = |W|^2 [d(\varepsilon_F)]^3 \frac{\xi_{\mathbf{k}}^2}{2}, \quad \text{for } T < \xi_k, \end{aligned} \quad (14.46)$$

This is a very important result because it tells us that the life-time of the quasiparticles diverges as we approach the Fermi level and thus the notion of quasiparticles is a consistent picture. At finite temperature the typical excitation energy is $k_B T$ and $\xi_{\mathbf{k}}$ is replaced by $k_B T$

$$\frac{1}{\tau_{\mathbf{k}}} \propto T^2, \quad \text{for } T > \xi_k. \quad (14.47)$$

The conclusion from this analysis is: the life-time of the quasiparticles based on Fermi's golden rule diverges at low temperatures and therefore the condition for the adiabatic approach expressed in Eq. (14.10) holds as long the temperature is much smaller than the

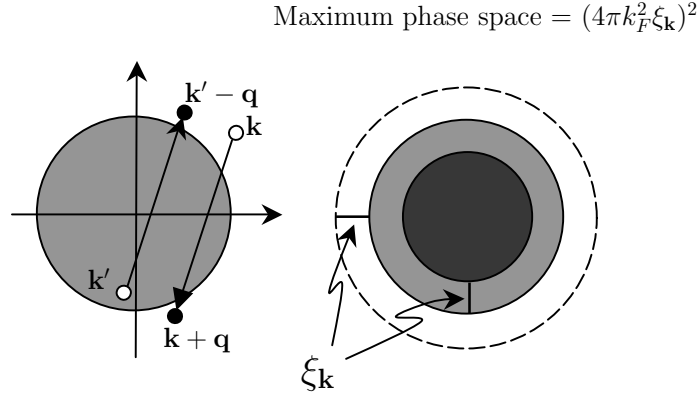


Figure 14.1: The two-particle scattering event that gives rise to a finite life time of the quasiparticles. Both momentum and energy have to be conserved. This together with the Pauli principle cause the phase space available for the scattering to be very limited, which is illustrated on the right hand figure. The dashed circle indicates the energy of the initial state. Since the particle can only loose energy, the other particle which is scattered out of state \mathbf{k}' can only gain energy. Furthermore, because of the Pauli principle the final states of both particles have to lie outside the Fermi surface and therefore the phase space volume for the final state $\mathbf{k} + \mathbf{q}$ (white area) and for the initial state \mathbf{k}' (gray area) both scale with ξ_k giving rise to a maximum total phase proportional to ξ_k^2 .

Fermi energy. Because the Fermi energy in for example metal is in general a fairly large energy scale, the condition in fact holds for even moderately elevated temperatures. As illustrated in Fig. 14.1 the physical reason for the smallness of the scattering rate is that although the Coulomb scattering matrix elements are big there is not much phase space available for scattering due to the Pauli principle.

14.4 Microscopic basis of the Fermi liquid theory

14.4.1 Renormalization of the single particle Green's function

The Fermi liquid theory relies on the assumption that the excitation created by adding a particle to the system, can be described by a free particle with a long life time. These were the quasiparticles. The function that measures precisely the density of states for adding particles is the retarded Green's function G^R . If the retarded Green's function of the interacting system turns out to be similar to that of free particles, the quasiparticle picture therefore has real physical meaning. This is what we are going to show in this section and thereby give a microscopic foundation of the Fermi liquid theory.

We consider the one-particle retarded Green's function, which in general can be written

as

$$G^R(\mathbf{k}\sigma, \omega) = \frac{1}{\omega - \xi_{\mathbf{k}} - \Sigma^R(\mathbf{k}\sigma, \omega)}, \quad (14.48)$$

where $\xi_k = k^2/2m - \mu$ is the free electron energy measured with the respect to the chemical potential μ , and where $\Sigma^R(\mathbf{k}, \omega)$ is the irreducible retarded self-energy. To calculate the self-energy we should in principle include all possible diagrams, which of course is not doable in the general case. Fortunately, important conclusions can be drawn from the first non-trivial approximation, namely the RPA which in Chap. 12 was shown to give the exact answer in the high density limit. Let us first write the general form of G^R by separating the self-energy in real and imaginary parts

$$G^R(\mathbf{k}\sigma, \omega) = \frac{1}{\omega - [\xi_{\mathbf{k}} + \text{Re } \Sigma^R(\mathbf{k}, \omega)] - i \text{Im } \Sigma^R(\mathbf{k}, \omega)}. \quad (14.49)$$

We then anticipate the quasiparticle picture by looking at \mathbf{k} -values close to the \tilde{k}_F , meaning close to the renormalized Fermi-energy. The renormalized Fermi wave number \tilde{k}_F is defined by the condition that the real part of the energy vanishes $\xi_{\tilde{k}_F} + \text{Re } \Sigma(\tilde{k}_F, 0) = 0$. At small energies and for k close to \tilde{k}_F , we can expand $(G^R)^{-1}$ in powers of $k - \tilde{k}_F$ and ω , which leads to

$$\begin{aligned} G^R(\mathbf{k}, \omega) &\approx \left[\omega - \omega \partial_\omega \text{Re } \Sigma^R - (k - \tilde{k}_F) \partial_{\mathbf{k}} (\xi + \text{Re } \Sigma^R) - i \text{Im } \Sigma^R \right]^{-1} \\ &\equiv Z \left[\omega - \tilde{\xi}_{\mathbf{k}} + \frac{i}{2\tilde{\tau}_{\mathbf{k}}(\omega)} \right]^{-1} \end{aligned} \quad (14.50)$$

where

$$Z^{-1} = 1 - \frac{\partial}{\partial \omega} \text{Re } \Sigma(\tilde{k}_F, \omega) \Big|_{\omega=0}, \quad (14.51)$$

$$\tilde{\xi}_{\mathbf{k}} = (k - \tilde{k}_F) Z \frac{\partial}{\partial \mathbf{k}} (\xi_{\mathbf{k}} + \text{Re } \Sigma(\mathbf{k}, 0))_{k=\tilde{k}_F}, \quad (14.52)$$

$$\frac{1}{\tilde{\tau}_{\mathbf{k}}(\omega)} = -2Z \text{Im } \Sigma^R(\mathbf{k}, \omega). \quad (14.53)$$

The imaginary part of $\Sigma^R(\mathbf{k}, \omega)$ is not expanded because we look at its form later. The effective energy $\tilde{\xi}_{\mathbf{k}}$ is usually expressed as

$$\tilde{\xi}_{\mathbf{k}} = (k - \tilde{k}_F) \tilde{k}_F / m^*, \quad (14.54)$$

where the effective mass by Eq. (14.52) is seen to be

$$\frac{m}{m^*} = Z \left(1 + \frac{m}{\tilde{k}_F} \frac{\partial}{\partial k} \text{Re } \Sigma(k, 0) \Big|_{k=\tilde{k}_F} \right). \quad (14.55)$$

In Sec. 14.3.1 we saw that the life-time goes to infinity at low temperatures. If this also holds here the spectral function therefore has a Lorentzian shape near $k = \tilde{k}_F$. For a very

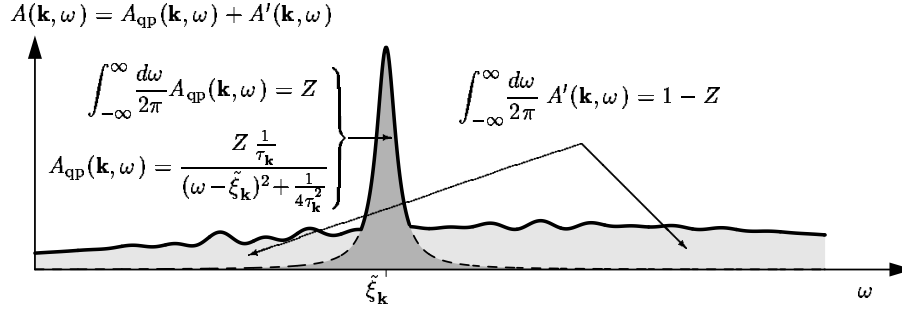


Figure 14.2: The spectral function $A(\mathbf{k}, \omega)$ as resulting from the analysis of the RPA approximation. It contains a distinct peak, which is identified with the quasiparticle. This part called A_{qp} however only carries part of the integrated spectral weight and the rest must therefore be contained in the background function A' stemming from other types of excitations.

small imaginary part we could namely approximate $\text{Im } \Sigma^R \approx -\eta$, and hence Eq. (14.50) gives

$$A(\mathbf{k}, \omega) = -2\text{Im } G^R(\mathbf{k}, \omega) \approx 2\pi Z \delta(\omega - \tilde{\xi}_{\mathbf{k}}). \quad (14.56)$$

This shows that with a small imaginary part, the Green's function and the spectral function has a sharp peak at $\omega = \tilde{\xi}_{\mathbf{k}}$. The peaked spectral function therefore resembles that of a free gas and the pole is identified as the quasiparticle that was defined in the Fermi liquid theory. However, because the general sum rule

$$\int_{-\infty}^{\infty} \frac{d\omega}{2\pi} A(\mathbf{k}, \omega) = 1, \quad (14.57)$$


is not fulfilled by Eq. (14.56), the integral only amounts to Z , the quasiparticle peak cannot be the whole story. There must be another part of the spectral function, which we denoted A' , that has an integrated weight given by $1 - Z$. See Fig. 14.2. Therefore we instead write

$$A(\mathbf{k}, \omega) = 2\pi Z \delta(\omega - \tilde{\xi}_{\mathbf{k}}) + A'(\mathbf{k}, \omega), \quad (14.58)$$

where the remaining contribution A' not associated with the pole, contains more complicated many body excitations not describable by a free electron like peak. The constant Z is called the renormalization constant and it is a measure of the quasiparticle weight. Typically Z is found from experiments to be between 0.7 and 1 for $r_s < 3$, where $r_s = (3/4\pi a_0^3 n)^{-1/3}$ is the parameter often used to parameterize the density of electron gases. The renormalization constant shows up for example in the distribution function $n(\mathbf{k})$, where the jump at the Fermi level is a direct measure of Z , see Exercise 13.2. For a discussion on the measurements of Z using Compton scattering see e.g. the book by Mahan.

We still need to show that the assumption of a large $\tau_{\mathbf{k}}$ is valid and we now turn to evaluating the imaginary part of the self-energy.

14.4.2 Imaginary part of the single particle Green's function

We base our analysis on the most important diagram, the RPA self-energy , in Eq. (13.12). In the Matsubara frequency domain it is given by

$$\Sigma_{\sigma}^{\text{RPA}}(\mathbf{k}\sigma, ik_n) = -\frac{1}{\beta} \sum_{i\omega_n} \frac{1}{\mathcal{V}} \sum_{\mathbf{q}} \frac{W(\mathbf{q})}{\varepsilon^{\text{RPA}}(\mathbf{q}, i\omega_n)} \mathcal{G}_0(\mathbf{k} + \mathbf{q}, \sigma; ik_n + i\omega_n). \quad (14.59)$$

where $W/\varepsilon^{\text{RPA}}$ is the screened interaction. As usual we perform the Matsubara summation by a contour integration

$$\Sigma_{\sigma}^{\text{RPA}}(\mathbf{k}\sigma, ik_n) = - \int_{\mathcal{C}} \frac{dz}{2\pi i} n_B(z) \frac{1}{\mathcal{V}} \sum_{\mathbf{q}} \frac{W(\mathbf{q})}{\varepsilon^{\text{RPA}}(\mathbf{q}, z)} \mathcal{G}_0(\mathbf{k} + \mathbf{q}, \sigma; ik_n + z), \quad (14.60)$$

where \mathcal{C} is a suitable contour that encloses all the bosonic Matsubara frequencies $z = i\omega_n$. The integrand is analytic everywhere but in $z = \xi_{\mathbf{k}+\mathbf{q}} - ik_n$ and for z purely real. If we therefore make a contour which is like the one in Fig. (10.3) $\mathcal{C} = \mathcal{C}_1 + \mathcal{C}_2$ then we include all the Matsubara frequencies except the one in origin (note that the points shown in Fig. (10.3) are the fermionic Matsubara frequencies). Therefore we include a loop around the origin so that the contour $\mathcal{C} = \mathcal{C}_1 + \mathcal{C}_2 + \mathcal{C}_3$ shown in Fig. 14.3 includes all boson Matsubara frequencies $z = i\omega_n$. The small loop \mathcal{C}_3 shown in Fig. 14.3 is now seen to cancel parts of the counters \mathcal{C}_1 and \mathcal{C}_2 so that they are modified to run between $]-\infty, -\delta]$ and $[\delta, \infty[$ only, and this is equivalent to stating that the integration are replaced by the principal part, when letting $\delta \rightarrow 0^+$. As seen in Fig. 14.3 we, however, also enclose the pole in $z = \xi_{\mathbf{k}+\mathbf{q}} - ik_n$, which we therefore have to subtract again. We now get

$$\begin{aligned} \Sigma^{\text{RPA}}(\mathbf{k}\sigma, ik_n) = & -\frac{1}{\mathcal{V}} \sum_{\mathbf{q}} \mathcal{P} \int_{-\infty}^{\infty} \frac{d\omega}{2\pi i} n_B(\omega) \\ & \times \left[\frac{W(\mathbf{q})}{\varepsilon^{\text{RPA}}(\mathbf{q}, \omega + i\eta)} \mathcal{G}_0(\mathbf{k} + \mathbf{q}, \sigma; ik_n + \omega) - (\eta \rightarrow -\eta) \right] \\ & + \frac{1}{\mathcal{V}} \sum_{\mathbf{q}} n_B(\xi_{\mathbf{k}+\mathbf{q}} - ik_n) \left[\frac{W(\mathbf{q})}{\varepsilon^{\text{RPA}}(\mathbf{q}, \xi_{\mathbf{k}+\mathbf{q}} - ik_n)} \right]. \end{aligned} \quad (14.61)$$

In the last term we should use that $n_B(\xi_{\mathbf{k}+\mathbf{q}} - ik_n) = -n_F(\xi_{\mathbf{k}+\mathbf{q}})$ because ik_n is a fermion frequency. Now that we have performed the Matsubara sum, we are allowed to get the

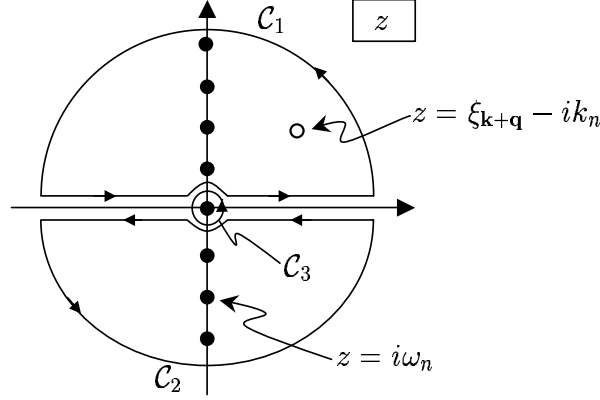


Figure 14.3: The contour $\mathcal{C} = \mathcal{C}_1 + \mathcal{C}_2 + \mathcal{C}_3$ used for integration for a the Matsubara sum that enters the RPA self-energy in Eq. (14.60). The poles from the boson frequencies are shown by black dots, while the that of \mathcal{G}_0 is the white dot. The contour \mathcal{C}_3 which picks up the contribution from the pole $z = 0$ cancels the parts of \mathcal{C}_1 and \mathcal{C}_2 given by the small loops.

retarded self-energy by the substitution $ik_n \rightarrow \varepsilon + i\eta$ which leads to

$$\begin{aligned} \Sigma^{\text{RPA},R}(\mathbf{k}\sigma, \varepsilon) = & -\frac{1}{\mathcal{V}} \sum_{\mathbf{q}} \mathcal{P} \int_{-\infty}^{\infty} \frac{d\omega}{2\pi i} n_B(\omega) \\ & \times (2i) \text{Im} \left[\frac{1}{\varepsilon^{\text{RPA}}(\mathbf{q}, \omega + i\eta)} \right] W(\mathbf{q}) G_0^R(\mathbf{k} + \mathbf{q}, \sigma; \varepsilon + \omega) \\ & - \frac{1}{\mathcal{V}} \sum_{\mathbf{q}} n_F(\xi_{\mathbf{k}+\mathbf{q}}) \left[\frac{W(\mathbf{q})}{\varepsilon^{\text{RPA}}(\mathbf{q}, \xi_{\mathbf{k}+\mathbf{q}} - \varepsilon - i\eta)} \right], \end{aligned} \quad (14.62)$$

because $[\varepsilon^{\text{RPA}}(\mathbf{q}, \omega + i\eta)] = [\varepsilon^{\text{RPA}}(\mathbf{q}, \omega - i\eta)]^*$. The imaginary part of the self-energy becomes

$$\text{Im} \Sigma^{\text{RPA}}(\mathbf{k}\sigma, \varepsilon) = \frac{1}{\mathcal{V}} \sum_{\mathbf{q}} [n_B(\xi_{\mathbf{k}+\mathbf{q}} - \varepsilon) + n_F(\xi_{\mathbf{k}+\mathbf{q}})] \text{Im} \left[\frac{W(\mathbf{q})}{\varepsilon^{\text{RPA}}(\mathbf{q}, \xi_{\mathbf{k}+\mathbf{q}} - \varepsilon + i\eta)} \right], \quad (14.63)$$

where we used that $-\text{Im} G_0^R(\mathbf{k} + \mathbf{q}, \sigma; \varepsilon + \omega) = \pi \delta(\varepsilon + \omega - \xi_{\mathbf{k}+\mathbf{q}})$ and then performed the ω -integration. Since we are interested in the case where a particle with $\xi_{\mathbf{k}}$ is scattered, we evaluate the imaginary part in $\varepsilon = \xi_{\mathbf{k}}$ and find

$$\begin{aligned} \frac{1}{\tau_{\mathbf{k}}} = & -2 \text{Im} \Sigma^{\text{RPA}}(\mathbf{k}\sigma, \xi_{\mathbf{k}}) = \frac{-2}{\mathcal{V}} \sum_{\mathbf{q}} [n_B(\xi_{\mathbf{k}+\mathbf{q}} - \xi_{\mathbf{k}}) + n_F(\xi_{\mathbf{k}+\mathbf{q}})] \left| \frac{W(\mathbf{q})}{\varepsilon^{\text{RPA},R}(\mathbf{q}, \xi_{\mathbf{k}+\mathbf{q}} - \xi_{\mathbf{k}})} \right|^2 \\ & \times \text{Im} \chi_0^R(\mathbf{q}, \xi_{\mathbf{k}+\mathbf{q}} - \xi_{\mathbf{k}}). \end{aligned} \quad (14.64)$$

The imaginary part of the polarization function follows from Eq. (13.20)

$$\text{Im} \chi_0^R(\mathbf{q}, \xi_{\mathbf{k}+\mathbf{q}} - \xi_{\mathbf{k}}) = \frac{2\pi}{\mathcal{V}} \sum_{\mathbf{k}'} [n_F(\xi_{\mathbf{k}'}) - n_F(\xi_{\mathbf{k}'-\mathbf{q}})] \delta(\xi_{\mathbf{k}'} - \xi_{\mathbf{k}'-\mathbf{q}} - \xi_{\mathbf{k}+\mathbf{q}} + \xi_{\mathbf{k}}) \quad (14.65)$$

(here we shifted $\mathbf{k}' \rightarrow \mathbf{k}' - \mathbf{q}$ as compared with Eq. (13.20)) and when this is inserted back into Eq. (14.64), we obtain

$$\begin{aligned} \frac{1}{\tau_{\mathbf{k}}} = -2 \text{Im} \Sigma^{\text{RPA}}(\mathbf{k}\sigma, \varepsilon) = & -\frac{4\pi}{\mathcal{V}} \sum_{\mathbf{q}\mathbf{k}'} [n_B(\xi_{\mathbf{k}+\mathbf{q}} - \xi_{\mathbf{k}}) + n_F(\xi_{\mathbf{k}+\mathbf{q}})] [n_F(\xi_{\mathbf{k}'}) - n_F(\xi_{\mathbf{k}'-\mathbf{q}})] \\ & \times \left| \frac{W(q)}{\varepsilon^{\text{RPA},R}(\mathbf{q}, \xi_{\mathbf{k}+\mathbf{q}} - \xi_{\mathbf{k}})} \right|^2 \delta(\xi_{\mathbf{k}'} - \xi_{\mathbf{k}'-\mathbf{q}} - \xi_{\mathbf{k}+\mathbf{q}} + \xi_{\mathbf{k}}). \end{aligned} \quad (14.66)$$

Let us study the occupation factors in this expression and compare with the Fermi's golden rule expression Eq. (14.45). For the first term in the first parenthesis we use the identity

$$n_B(\epsilon_1 - \epsilon_2)[n_F(\epsilon_2) - n_F(\epsilon_2)] = n_F(\epsilon_1)[1 - n_F(\epsilon_2)],$$

combined with $\xi_{\mathbf{k}} - \xi_{\mathbf{k}+\mathbf{q}} = -\xi_{\mathbf{k}'} + \xi_{\mathbf{k}'-\mathbf{q}}$. For the second term we use the obvious identity

$$n_F(\epsilon_1)[1 - n_F(\epsilon_2)] - n_F(\epsilon_2)[1 - n_F(\epsilon_2)] = n_F(\epsilon_1) - n_F(\epsilon_2)$$

and $n_F(-\epsilon) = 1 - n_F(\epsilon)$. All together this allows us to write the occupation factors in Eq. (14.66) as

$$-n_F(\xi_{\mathbf{k}'})[1 - n_F(\xi_{\mathbf{k}+\mathbf{q}})] [1 - n_F(\xi_{\mathbf{k}'-\mathbf{q}})] - [1 - n_F(\xi_{\mathbf{k}'})] n_F(\xi_{\mathbf{k}+\mathbf{q}}) n_F(\xi_{\mathbf{k}'-\mathbf{q}}) \quad (14.67)$$

At low temperature the first term is due to the energy conservation condition non-zero for $\xi_{\mathbf{k}} > 0$, while the last term is non-zero for $\xi_{\mathbf{k}} < 0$. The first term thus corresponds to the scattering out term in Eq. (14.45), while the second term corresponds to the scattering in term. If we furthermore approximate $\xi_{\mathbf{k}} - \xi_{\mathbf{k}+\mathbf{q}} \approx 0$ in ε^{RPA} we now see that the life time in Eq. (14.66) is equivalent to the Fermi's golden rule expression Eq. (14.45). We have thus verified that the imaginary part of the retarded Green's function indeed goes to zero. At least when employing the RPA approximation for the self-energy, but the RPA approximation in Chap. 12 was shown to be exact in the high density limit. An explicit calculation of Eq. (14.66) was done by Quinn and Ferrell⁵ who got

$$\frac{1}{\tau_{\mathbf{k}}} = \frac{\sqrt{3}\pi^2}{128} \omega_p \left(\frac{\xi_{\mathbf{k}}}{\varepsilon_F} \right)^2. \quad (14.68)$$

Going beyond RPA, it can in fact be shown that the imaginary part vanishes to all orders in the interaction. This was done by Luttinger⁶ who proved that the imaginary part of any diagram for the self-energy goes to zero as ξ^2 or faster. The derivation is rather lengthy and we do not give it here. It is however not hard to imagine that more complicated scattering events than the simple one depicted in Fig. 14.1 will have even more constraints on the energies. Hence after integration, they will result in higher powers of $\xi_{\mathbf{k}}$. This concludes our analysis of the single particle Green's function. The analysis indeed confirmed the physical picture put forward by Landau in his Fermi liquid theory.

⁵J. J. Quinn and R. A. Ferrell, Phys. Rev **112**, 812 (1958).

⁶J.M. Luttinger, Phys. Rev. **121**, 942 (1961).

14.4.3 Mass renormalization?

In the previous section we saw how the assumption of weakly interacting quasiparticles was justified by the long life time of the single particle Green's function. We also found that the effective mass of the quasiparticle was renormalized due to the interactions. This seems to contradict the postulate of the Fermi liquid theory that the current of the quasiparticles is independent of interactions, i.e. it is given by \mathbf{k}/m and not \mathbf{k}/m^* . The bare velocity of the quasiparticles was important for obtaining the Drude formula for the conductivity, $\sigma = ne^2\tau^{\text{tr}}/m$. How come the renormalized mass m^* appears in the Green's function whereas the physically observable conductivity contains the bare mass m ? The answer to this question is found by studying how the conductivity is calculated diagrammatically. The conductivity is as we remember from the Kubo formula related to the current-current correlation function. The calculation has to be done in a consistent way such that the diagrams included in the irreducible self-energy is also included in the diagrams for the two-particle correlation function. When the same type of diagrams are included both in the self-energy and in the lines that cross the two-particle "bubble" then the mass renormalization exactly cancels. In Chap. 15 we shall see an explicit example of this by calculating diagrammatically the finite resistance due to impurity scattering starting from the fully microscopic theory. See also Exercise 14.4

14.5 Outlook and summary

We have developed the semi-classical Fermi liquid theory of interacting particles. The theory is valid whenever perturbation theory is valid, i.e. when the interaction does not induce a phase transition. Miraculously, the interacting system of particles can be described by a gas of non-interacting particles. These particles we call quasiparticles and they can be labelled by the same quantum numbers of those of the non-interacting system, provided that the corresponding operators also commute with the full Hamiltonian. For a translation-invariant system the quantum numbers are \mathbf{k} and σ .

On long length and time scales we can use a semi-classical approach to study various properties. This approach is based on the Boltzmann equation

$$\partial_t(n_{\mathbf{k}}) + \dot{\mathbf{k}} \cdot \nabla_{\mathbf{k}} n_{\mathbf{k}} + \mathbf{v}_{\mathbf{k}} \cdot \nabla_{\mathbf{r}} n_{\mathbf{k}} = \left(\frac{\partial n_{\mathbf{k}}}{\partial t} \right)_{\text{collisions}}. \quad (14.69)$$

This equation is extremely useful since it in many situations gives a sufficiently accurate description of the physics. It has been widely used to explain numerous transport phenomena in gases and solids. One can include both electric and magnetic fields driving the system out of equilibrium. The driving fields enter through the Lorentz force as $\dot{\mathbf{p}} = \hbar \dot{\mathbf{k}} = (-e)(\mathbf{E} + \mathbf{v} \times \mathbf{B})$. On the right hand side of Eq. (14.69) we have included collisions due to impurities and particle-particle collisions. One can also include for example particle-phonon scattering in solids and thus explain the temperature dependence of the different transport coefficients.

Landau's phenomenological theory was shown to be justified by a rigorous microscopic calculation, using the random phase approximation result for the self-energy. The result

of this analysis was that even in the presence of interactions does the Fermi surface persist and near the Fermi surface the imaginary part of the single particle Green's function rapidly vanish as

$$\text{Im } \Sigma^R(k_F, \varepsilon) \propto \max(\varepsilon^2, T^2). \quad (14.70)$$

This explains why the Fermi liquid theory works: when the imaginary part goes to zero the single particle Green's function is identical to that of a free particle.

Chapter 15

Impurity scattering and conductivity

We now return to the problem of calculating the resistance of a metallic conductor due to scattering against impurities. The basic physics of impurity scattering was discussed in Chap. 10, where we saw how the single-particle Green's function acquired a finite life time after averaging over the positions of the impurities. In Chap. 13 the conductivity was calculated within the Boltzmann equation approach. We now rederive the Boltzmann equation result starting from a microscopic quantum approach. The advantage of this microscopic approach, besides giving a first principle justification of the Boltzmann equation, is that it can be extended to include correlation and coherence effects that cannot be described in the semiclassical Boltzmann approach. In order to get familiar with the techniques, we therefore start by deriving the semiclassical result. Then we go on to include the quantum mechanical effect known as weak localization, which is due to interference between time reversed paths. Weak localization involves coherent scattering on many impurities, and it can therefore not be explained semiclassically.

In 1979 the weak localization correction to resistivity was observed experimentally in large 2D samples at low temperatures. It was explained theoretically later the same year, and an extended research was initiated on the role of quantum coherence in transport properties. A few years later another low-temperature interference effect, the so-called universal conductance fluctuations, was discovered in small ($\sim \mu\text{m}$) phase-coherent structures. This discovery started the modern field of mesoscopic physics. To understand these smaller systems one must take into account the finite size of the conductors, which is the topic in Chap. 15. In this chapter we deal with extended systems and discuss the most important disorder-induced quantum corrections. The leading quantum correction is precisely the weak localization effect, at least in two dimensions. In one dimension, things are more complicated because there all states are localized and one cannot talk about a conductivity that scales in a simple fashion with the length of the system. In three dimensions, the situation is again different in that at some critical amount of impurity scattering there exists a metal-insulator transition known as the Anderson localization. This is however outside the scope of this book.

Based on the physical picture that emerged from the Fermi liquid description in Chap. 13, we assume in the first part of this chapter that we can describe the electrons as non-interacting. In the second part of the chapter we include electron-electron interactions together with impurity scattering and explicitly demonstrate that the non-interacting approximation is valid. This means that we shall see how the mass renormalization discussed in Sec. 14.4.3 is cancelled out. Furthermore, we shall see that in order to obtain meaningful results, it is absolutely imperative to include vertex corrections to the current-current correlation bubble diagrams. These corrections cannot be treated evaluating only single-particle Green's functions. They are thus genuine two-particle correlation effects, which can be described by diagrams where interaction lines “cross” the bubble diagrams.

15.1 Vertex corrections and dressed Green's functions

Let us start by the Kubo formula for the electrical conductivity tensor $\sigma_{\alpha\beta}$ given in Eq. (6.25) in terms of the retarded current-current correlation function Eq. (6.26). Here we shall only look at the dissipative part of the conductivity, and therefore we take the real part of Eq. (6.25)

$$\text{Re } \sigma_{\alpha\beta}(\mathbf{r}, \mathbf{r}'; \omega) = -\frac{e^2}{\omega} \text{Im } \Pi_{\alpha\beta}^R(\mathbf{r}, \mathbf{r}', \omega). \quad (15.1)$$

Note that the last, so-called “diamagnetic”, term of σ in Eq. (6.25) drops out of the real part. In the following we therefore only include the first, so-called “paramagnetic”, term in Eq. (6.25), denoted σ^∇ . For a translation-invariant system we consider as usual the Fourier transform

$$\sigma_{\alpha\beta}^\nabla(\mathbf{q}; \omega) = \frac{ie^2}{\omega} \Pi_{\alpha\beta}^R(\mathbf{q}, \omega). \quad (15.2)$$

The dc-conductivity is then found by letting¹ $q \rightarrow 0$ and then $\omega \rightarrow 0$. The dc-response at long wavelengths is thus obtained as

$$\text{Re } \sigma_{\alpha\beta} = -e^2 \lim_{\omega \rightarrow 0} \lim_{q \rightarrow 0} \frac{1}{\omega} \text{Im } \Pi_{\alpha\beta}^R(\mathbf{q}, \omega). \quad (15.3)$$

In this chapter we consider only homogeneous translation-invariant systems, i.e. the conductivity tensor is isotropic and therefore diagonal, $\sigma_{\alpha\beta} = \sigma \delta_{\alpha\beta}$. In particular we have no magnetic field and take $\mathbf{A} = 0$. In the computation we can choose α to be the x direction. Note that the system is translation-invariant even in the presence of impurities after performing the position average described in Chap. 10.

As usual we calculate the retarded function starting from the corresponding Matsubara function. The Matsubara current-current correlation function is

$$\Pi_{xx}(\mathbf{q}, \tau - \tau') = -\frac{1}{\mathcal{V}} \langle T_\tau J_x(\mathbf{q}, \tau) J_x(-\mathbf{q}, \tau') \rangle. \quad (15.4)$$

¹If in doubt always perform the limit $q \rightarrow 0$ first, because having a electric field $E(\mathbf{q}, \omega)$ where $\omega = 0$ and q finite is unphysical, since it would give rise to an infinite charge built up.

In the frequency domain it is

$$\Pi_{xx}(\mathbf{q}, iq_n) = -\frac{1}{\mathcal{V}} \int_0^\beta d(\tau - \tau') e^{iq_n(\tau - \tau')} \langle J_x(\mathbf{q}, \tau) J_x(-\mathbf{q}, \tau') \rangle, \quad (15.5)$$

where the time-ordering operator T_τ is omitted, because $\tau > \tau'$. We can now express $J_x(\mathbf{q}, \tau)$ in terms of $J_x(\mathbf{q}, iq_n)$ and obtain

$$\Pi_{xx}(\mathbf{q}, iq_n) = -\frac{1}{\mathcal{V}} \int_0^\beta d(\tau - \tau') e^{iq_n(\tau - \tau')} \frac{1}{\beta} \sum_{iq_l} \frac{1}{\beta} \sum_{iq_m} \langle J_x(\mathbf{q}, iq_l) J_x(-\mathbf{q}, iq_m) \rangle e^{-iq_l \tau} e^{-iq_m \tau'}. \quad (15.6)$$

The integration with respect to τ leads to $iq_n = iq_l$. Finally, since the result cannot depend on τ' , we must have $iq_n = -iq_m$, and whence

$$\Pi_{xx}(\mathbf{q}, iq_n) = -\frac{1}{\mathcal{V}\beta} \langle J_x(\mathbf{q}, iq_n) J_x(-\mathbf{q}, -iq_n) \rangle. \quad (15.7)$$

This we conveniently rewrite using the four-vector notation $\tilde{q} = (iq_n, \mathbf{q})$

$$\Pi_{xx}(\tilde{q}) = -\frac{1}{\mathcal{V}\beta} \langle J_x(\tilde{q}) J_x(-\tilde{q}) \rangle. \quad (15.8)$$

In order to begin the diagrammatical analysis we write the current density $J_x(\tilde{q})$ in four-vector notation

$$\begin{aligned} J_x(\tilde{q}) &= \int_0^\beta d\tau e^{iq_n \tau} \frac{1}{2m} \frac{1}{\mathcal{V}} \sum_{\mathbf{k}\sigma} (2\mathbf{k} + \mathbf{q})_x c_{\mathbf{k}\sigma}^\dagger(\tau) c_{\mathbf{k}+\mathbf{q}\sigma}(\tau) \\ &= \frac{1}{2m} \frac{1}{\beta} \sum_{ik_n} \frac{1}{\mathcal{V}} \sum_{\mathbf{k}\sigma} (2\mathbf{k} + \mathbf{q})_x c_{\mathbf{k}\sigma}^\dagger(ik_n) c_{\mathbf{k}+\mathbf{q}\sigma}(ik_n + iq_n), \\ &\equiv \frac{1}{2m} \frac{1}{\beta} \frac{1}{\mathcal{V}} \sum_{\tilde{k}} \sum_{\sigma} (2k_x + q_x) c_{\sigma}^\dagger(\tilde{k}) c_{\sigma}(\tilde{k} + \tilde{q}), \end{aligned} \quad (15.9)$$

which we draw diagrammatically as a vertex

$$J_x(\tilde{q}) = \text{diagram of a vertex with two outgoing lines labeled } \tilde{k} \text{ and } \tilde{k} + \tilde{q} \quad (15.10)$$

The vertex conserves four-momentum, and thus has the momentum $\tilde{q} = (iq_n, \mathbf{q})$ flowing out from it to the left.

We can now draw diagrams for the current-current correlation function using the Feynman rules. The procedure is analogous to that for the charge-charge correlation function in Chap. 12, however, here we include both the impurity lines $\bullet - - \star$ from Chap. 10 and

the Coulomb interaction lines $\bullet \cdots \bullet$ from Chap. 12. We obtain

$$\begin{aligned} \Pi_{xx}(\tilde{q}) = & \text{Diagram with a shaded rectangular region between two vertices} \\ \equiv & \text{Diagram 1} + \text{Diagram 2} + \text{Diagram 3} + \text{Diagram 4} \\ & + \text{Diagram 5} + \text{Diagram 6} + \text{Diagram 7} + \text{Diagram 8} \\ & + \text{Diagram 9} + \text{Diagram 10} + \text{Diagram 11} + \text{Diagram 12} \\ & + \text{Diagram 13} + \text{Diagram 14} \\ & + \text{Diagram 15} + \text{Diagram 16} + \dots \end{aligned} \quad (15.11)$$

We can perform a partial summation of diagrams to all orders by replacing each Green's function \mathcal{G}_0 by the full Green's function \mathcal{G} . In doing so we have in one step resummed Eq. (15.11) and are left with bubble diagrams where the only interaction and impurity lines to be drawn are those connecting the lower and upper electron Green's functions. Eq. (15.11) then becomes

$$\begin{aligned} \Pi_{xx}(\tilde{q}) = & \text{Diagram 1} + \text{Diagram 2} + \text{Diagram 3} + \text{Diagram 4} \\ & + \text{Diagram 5} + \text{Diagram 6} + \text{Diagram 7} + \text{Diagram 8} \\ & + \text{Diagram 9} + \text{Diagram 10} \\ & + \text{Diagram 11} + \text{Diagram 12} + \dots \end{aligned} \quad (15.12)$$

Here the double lines represent full Green's functions expressed by Dyson's equation as in

Eq. (12.19)

$$\begin{aligned}
 \mathcal{G}(\tilde{k}) &= \text{---} \text{---} \text{---} \\
 &= \text{---} \text{---} \text{---} + \text{---} \text{---} \text{---} \text{---} \text{---} \text{---} \\
 &= \mathcal{G}_0(\tilde{k}) + \mathcal{G}_0(\tilde{k}) \Sigma^{\text{irr}}(\tilde{k}) \mathcal{G}(\tilde{k}),
 \end{aligned} \tag{15.13}$$

where $\Sigma^{\text{irr}} = \text{---} \text{---} \text{---}$ is the irreducible self-energy. For example in the case where we include impurity scattering within the first Born approximation and electron-electron interaction in the RPA approximation, the irreducible self-energy is simply

$$\text{1BA + RPA: } \Sigma^{\text{irr}}(\tilde{k}) = \text{---} \text{---} \text{---} \approx \text{---} \text{---} \text{---} + \text{---} \text{---} \text{---} \tag{15.14}$$

where RPA means the following screening of all impurity and interaction lines

$$\text{---} \text{---} \text{---} = \text{---} \text{---} \text{---} + \text{---} \text{---} \text{---} \text{---} \text{---} \tag{15.15}$$

$$\text{---} \text{---} \text{---} \text{---} \text{---} = \text{---} \text{---} \text{---} \text{---} \text{---} + \text{---} \text{---} \text{---} \text{---} \text{---} \tag{15.16}$$

The next step is to organize the diagrams according to the lines crossing the bubbles from the upper to the lower fermion line in a systematic way. These diagrams are denoted vertex corrections. To obtain a Dyson equation for Π_{xx} we first introduce the irreducible line-crossing diagram Λ^{irr} consisting of the sum of all possible diagrams connecting the upper and lower fermion line, which cannot be cut into two pieces by cutting both the upper and the lower line just once²,

$$\Lambda^{\text{irr}} \equiv \text{---} \text{---} \text{---} \equiv \text{---} \text{---} \text{---} + \text{---} \text{---} \text{---} + \text{---} \text{---} \text{---} + \text{---} \text{---} \text{---} + \text{---} \text{---} \text{---} + \text{---} \text{---} \text{---} + \dots \tag{15.17}$$

²We do not include diagrams like the terms 9, 10, and 11 in Eq. (15.12). Diagrams of this type are proportional to q^{-2} and thus they vanish in the limit $q \rightarrow 0$.

Using Λ^{irr} we see that we can resum all diagrams in Π_{xx} in the following way

$$\begin{aligned}
\Pi_{xx}(\tilde{q}) &= \text{diagram 1} + \text{diagram 2} + \text{diagram 3} + \text{diagram 4} + \dots \\
&= \text{diagram 1} \times \left(\text{diagram 5} + \text{diagram 6} + \text{diagram 7} + \text{diagram 8} + \dots \right) \\
&\equiv \text{diagram 9} \\
&\equiv - \int d\tilde{k}' \Gamma_{0,x}(\tilde{k}', \tilde{k}' + \tilde{q}) \mathcal{G}(\tilde{k}') \mathcal{G}(\tilde{k}' + \tilde{q}) \Gamma_x(\tilde{k}' + \tilde{q}, \tilde{k}'), \tag{15.18}
\end{aligned}$$

where the unperturbed vertex is

$$\Gamma_{0,x}(\tilde{k}, \tilde{k} + \tilde{q}) = \frac{1}{2m} (2k_x + q_x), \tag{15.19}$$

and the “dressed” vertex function is given by an integral equation, which can be read off from Eq. (15.18)

$$\Gamma_x(\tilde{k} + \tilde{q}, \tilde{k}) \equiv \text{diagram 10} = \text{diagram 11} + \text{diagram 12} \tag{15.20a}$$

$$\equiv \Gamma_{0,x}(\tilde{k} + \tilde{q}, \tilde{k}) + \int d\tilde{q}' \Lambda^{\text{irr}}(\tilde{k}, \tilde{q}, \tilde{q}') \mathcal{G}(\tilde{k} + \tilde{q}') \mathcal{G}(\tilde{k} + \tilde{q}' + \tilde{q}) \Gamma_x(\tilde{k} + \tilde{q}' + \tilde{q}, \tilde{k} + \tilde{q}'), \tag{15.20b}$$

The notation for the arguments of the Γ functions is $\Gamma = \Gamma(\text{“out going”}, \text{“in going”})$.

The question is now which diagrams to include in Λ^{irr} . We have seen examples of how to choose the physically most important self-energies, both for the impurity scattering problem in Chap. 10 and for the case of interacting particles in Chap. 12. In the present case once the approximation for Σ^{irr} is chosen, the answer is simply that there is no freedom left in the choice for the vertex function Γ . If we include certain diagrams for the self-energy we must include the corresponding diagrams in the vertex function. This follows from a general relation between the self-energy and the vertex function. This relation, called the Ward identity,³ is derived using the continuity equation. Consequently,

³The Ward identity reads

$$iq_0 \Gamma_0(\tilde{k} + \tilde{q}, \tilde{k}) - i\mathbf{q} \cdot \Gamma(\tilde{k} + \tilde{q}, \tilde{k}) = -\mathcal{G}^{-1}(\tilde{k} + \tilde{q}) + \mathcal{G}^{-1}(\tilde{k}),$$

where the function Γ_0 is the charge vertex function, and Γ is the current vertex function. For more details see e.g. R.B. Schrieffer, *Theory of Superconductivity*, Addison-Wesley (1964).

not fulfilling this identity is equivalent to a lack of conservation of particles. Therefore a physically sensible approximation must obey Ward's identity, and one uses the term "conserving approximation" for the correct choice for the vertex function. For a derivation and discussion see for example the book by Schrieffer. Here we simply follow the rule as dictated by the Ward identity: if an irreducible diagram is included in Σ^{irr} the corresponding diagrams should also be included in Λ^{irr} .

If we consider the first Born approximation and RPA for Σ^{irr} as depicted in Eq. (15.14), we get for Λ^{irr}

$$\Lambda^{\text{irr}} = \text{[diagram: a square with diagonal lines]} \approx \text{[diagram: a vertical line with a star in the middle]} + \text{[diagram: a vertical wavy line]} \equiv \tilde{W}, \quad (15.21)$$

and in this case the integral function for Γ becomes

$$\Gamma_x(\tilde{k} + \tilde{q}, \tilde{k}) = \Gamma_{0,x}(\tilde{k} + \tilde{q}, \tilde{k}) + \int d\tilde{q}' \tilde{W}(\tilde{q}') \mathcal{G}(\tilde{k} + \tilde{q}') \mathcal{G}(\tilde{k} + \tilde{q}' + \tilde{q}) \Gamma_x(\tilde{k} + \tilde{q}' + \tilde{q}, \tilde{k} + \tilde{q}'), \quad (15.22)$$

where

$$\tilde{W}(\tilde{q}) = W^{\text{RPA}}(\tilde{q}) + n_{\text{imp}} \frac{u(\mathbf{q})}{\varepsilon^{\text{RPA}}(\tilde{q})} \frac{u(-\mathbf{q})}{\varepsilon^{\text{RPA}}(-\tilde{q})}. \quad (15.23)$$

This particular approximation is also known as the ladder sum, a name which perhaps becomes clear graphically if Eq. (15.21) for Λ^{irr} is inserted into the first line of Eq. (15.18) for Π_{xx} , and if for clarity we consider only the impurity scattering lines:

$$\Pi_{xx}(\tilde{q}) = \text{[diagram: a circle with two vertices]} + \text{[diagram: a circle with two vertices and one star]} + \text{[diagram: a circle with two vertices and two stars]} + \text{[diagram: a circle with two vertices and three stars]} + \dots \quad (15.24)$$

15.2 The conductivity in terms of a general vertex function

Having the expressions for both the single-particle Green's function \mathcal{G} and the vertex function Γ , we can obtain from Eq. (15.18) a general formula for the conductivity. This definition involves a summation over the internal Matsubara frequency. If we drop the four-vector notation in favor of the standard notation, and furthermore treat the case $\mathbf{q} = 0$, the current-current function is

$$\Pi_{xx}(0, iq_n) = -\frac{1}{\beta} \sum_{ik_n} \frac{1}{\mathcal{V}} \sum_{\mathbf{k}} \Gamma_{0,x}(\mathbf{k}, \mathbf{k}) \mathcal{G}(\mathbf{k}, ik_n) \mathcal{G}(\mathbf{k}, ik_n + iq_n) \Gamma_x(\mathbf{k}, \mathbf{k}; ik_n + iq_n, ik_n). \quad (15.25)$$

The Matsubara sum over ik_n is performed in the usual way by a contour integration over $z = ik_n$. The presence of two \mathcal{G} 's in the summand leads to two branch cuts; one along $z = \varepsilon$ and one along $z = -iq_n + \varepsilon$, with ε being real. Therefore we first study a summation

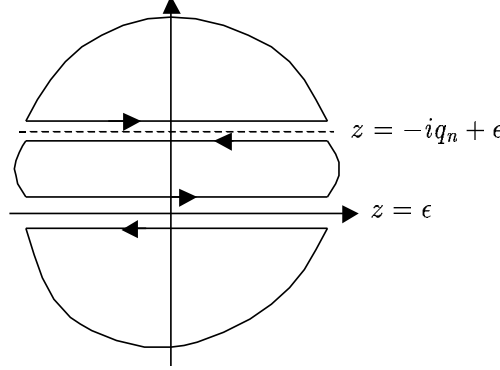


Figure 15.1: The contour used in the frequency summation in Eq. (15.26).

of the form

$$\begin{aligned}
 S_{2F}(iq_n) &= \frac{1}{\beta} \sum_{ik_n} f(ik_n, ik_n + iq_n) \\
 &= - \int_{\mathcal{C}} \frac{dz}{2\pi i} n_F(z) f(z, z + iq_n),
 \end{aligned} \tag{15.26}$$

where the integration contour \mathcal{C} is the one shown in Fig. (15.1) made of three contours leading to four integrals over ε

$$\begin{aligned}
 S_{2F}(iq_n) &= - \int_{-\infty}^{\infty} \frac{d\varepsilon}{2\pi i} n_F(\varepsilon) [f(\varepsilon + i\eta, \varepsilon + iq_n) - f(\varepsilon - i\eta, \varepsilon + iq_n)] \\
 &\quad - \int_{-\infty}^{\infty} \frac{d\varepsilon}{2\pi i} n_F(\varepsilon - iq_n) [f(\varepsilon - iq_n, \varepsilon + i\eta) - f(\varepsilon - iq_n, \varepsilon - i\eta)].
 \end{aligned} \tag{15.27}$$

At the end of the calculation we continue iq_n analytically to $\omega + i\eta$, and find

$$\begin{aligned}
 S_{2F}^R(\omega) &= - \int_{-\infty}^{\infty} \frac{d\varepsilon}{2\pi i} n_F(\varepsilon) [f^{RR}(\varepsilon, \varepsilon + \omega) - f^{AR}(\varepsilon, \varepsilon + \omega) \\
 &\quad + f^{AR}(\varepsilon - \omega, \varepsilon) - f^{AA}(\varepsilon - \omega, \varepsilon)],
 \end{aligned} \tag{15.28}$$

with the convention that $f^{AR}(\varepsilon, \varepsilon')$ means that the first argument is advanced, $\varepsilon - i\eta$, and the second argument is retarded, i.e. $\varepsilon + i\eta$, and so on. If we shift the integration variable $\varepsilon \rightarrow \varepsilon + \omega$ in the two last terms, we obtain

$$\begin{aligned}
 S_{2F}^R(\omega) &= \int_{-\infty}^{\infty} \frac{d\varepsilon}{2\pi i} [n_F(\varepsilon) - n_F(\varepsilon + \omega)] f^{AR}(\varepsilon, \varepsilon + \omega) \\
 &\quad - \int_{-\infty}^{\infty} \frac{d\varepsilon}{2\pi i} [n_F(\varepsilon) f^{RR}(\varepsilon, \varepsilon + \omega) - n_F(\varepsilon + \omega) f^{AA}(\varepsilon, \varepsilon + \omega)].
 \end{aligned} \tag{15.29}$$

Since we are interested in the low frequency limit, we expand to first order in ω . Furthermore, we also take the imaginary part as in Eq. (15.3). Since $(f^{AA})^* = f^{RR}$, we

find

$$\text{Im } S_{2F}^R(\omega) = -\omega \text{Im} \int_{-\infty}^{\infty} \frac{d\varepsilon}{2\pi i} \left(-\frac{\partial n_F(\varepsilon)}{\partial \varepsilon} \right) [f^{AR}(\varepsilon, \varepsilon) - f^{RR}(\varepsilon, \varepsilon)]. \quad (15.30)$$

At low temperatures, we can approximate the derivative of the Fermi-Dirac function by a delta function

$$\left(-\frac{\partial n_F(\varepsilon)}{\partial \varepsilon} \right) \approx \delta(\varepsilon) \quad (15.31)$$

and hence

$$\text{Im } S_{2F}^R(\omega) = \frac{\omega}{2\pi} \text{Re} [f^{AA}(0, 0) - f^{AR}(0, 0)]. \quad (15.32)$$

By applying this to Eq. (15.25) and then inserting into Eq. (15.3) one obtains

$$\begin{aligned} \text{Re } \sigma_{xx} = 2 \text{Re} \frac{e^2}{2\pi} \frac{1}{\mathcal{V}} \sum_{\mathbf{k}} \Gamma_{0,x}(\mathbf{k}, \mathbf{k}) & \left[G^A(\mathbf{k}, 0) G^R(\mathbf{k}, 0) \Gamma_x^{RA}(\mathbf{k}, \mathbf{k}; 0, 0) \right. \\ & \left. - G^A(\mathbf{k}, 0) G^A(\mathbf{k}, 0) \Gamma_x^{AA}(\mathbf{k}, \mathbf{k}; 0, 0) \right], \end{aligned} \quad (15.33)$$

where we have included a factor of 2 due to spin degeneracy. This is how far one can go on general principles. To proceed further, one must look at the specific physical cases and then solve for the vertex function satisfying Eq. (15.20b) and insert the result into (15.33). In the following we consider various cases. We will consider only cases where the disorder is weak and for this case it is shown in the next section that the product $G^R G^A$ exceeds $G^A G^A$ by a factor of order $1/\tau E_F$, where τ is the scattering time for impurity scattering. Hence in the weak disorder limit, we may replace the general formula in Eq. (15.33) by the first term only.

15.3 The conductivity in the first Born approximation

The conductivity was calculated in Sec. 14.3 using a semiclassical approximation for the scattering against the impurities. The semiclassical approximation is similar to the first Born approximation in that it only includes scattering against a single impurity and neglects interference effects. Therefore we expect to reproduce the semiclassical result if we only include the first Born approximation in our diagrammatical calculation. The starting point in this section is non-interacting electrons scattering on impurities. The RPA part of the self-energy in Eq. (15.14) is *not* included in this section. Later we discuss what happens if interactions are included.

The vertex function is now solved using the first Born approximation, i.e. the first diagram in Eq. (15.21). In this case, again taking $\mathbf{q} = 0$, the integral equation Eq. (15.22) becomes

$$\begin{aligned} \Gamma_x(\mathbf{k}, \mathbf{k}; ik_n + iq_n, ik_n) &= \Gamma_{0,x}(\mathbf{k}, \mathbf{k}) + \frac{1}{\mathcal{V}} \sum_{\mathbf{q}'} n_{\text{imp}} |u^{\text{RPA}}(\mathbf{q}')|^2 \mathcal{G}(\mathbf{k} + \mathbf{q}', ik_n) \\ &\quad \times \mathcal{G}(\mathbf{k} + \mathbf{q}', ik_n + iq_n) \Gamma_x(\mathbf{k} + \mathbf{q}', \mathbf{k} + \mathbf{q}'; ik_n + iq_n, ik_n), \end{aligned} \quad (15.34)$$

where the second term in Eq. (15.23) has been inserted and where $u^{\text{RPA}} = u/\varepsilon^{\text{RPA}}$. The Green's functions \mathcal{G} are, as we learned from the Ward identity, also those obtained in the first Born approximation. Note that there is no internal Matsubara sum because the impurity scattering conserves energy. Since we do not expect the dynamical screening to be important for the elastic scattering, we set the frequency in $\varepsilon^{\text{RPA}}(\mathbf{q}, 0)$ to zero. Remembering that Γ_x is a component of a vector function Γ and that the unperturbed vertex is $\Gamma_0(\mathbf{k}, \mathbf{k}) = \mathbf{k}/m$, we define for convenience a scalar function $\gamma(\mathbf{k}, \varepsilon)$ defined as $\Gamma(\mathbf{k}, \varepsilon) = \mathbf{k}\gamma(\mathbf{k}, \varepsilon)/m$. In doing so we in fact use that the system is isotropic which means that only the vector \mathbf{k} can give the direction. When inserting this into Eq. (15.34), multiplying by $(1/k^2)\mathbf{k}$, and shifting the variable \mathbf{q}' to $\mathbf{q}' = \mathbf{k}' - \mathbf{k}$, we get

$$\begin{aligned} \gamma(\mathbf{k}, \mathbf{k}; ik_n + iq_n, ik_n) &= 1 + \frac{1}{\mathcal{V}} \sum_{\mathbf{k}'} n_{\text{imp}} |u^{\text{RPA}}(\mathbf{k}' - \mathbf{k})|^2 \mathcal{G}(\mathbf{k}', ik_n) \\ &\quad \times \mathcal{G}(\mathbf{k}', ik_n + iq_n) \frac{\mathbf{k} \cdot \mathbf{k}'}{k^2} \gamma^{1\text{BA}}(\mathbf{k}', \mathbf{k}'; ik_n + iq_n, ik_n), \end{aligned} \quad (15.35)$$

In the formula Eq. (15.33) for the conductivity both Γ_x^{RA} and Γ_x^{RR} appear (or rather $\Gamma_x^{RR} = (\Gamma_x^{AA})^*$). They satisfy two different integral equations, which we obtain from Eq. (15.35) by letting $iq_n \rightarrow \omega + i\eta$ and $ik_n \rightarrow \varepsilon \pm i\eta$, and subsequently taking the dc-limit $\omega \rightarrow 0$. We arrive at

$$\gamma^{RX}(\mathbf{k}, \varepsilon) = 1 + \frac{1}{\mathcal{V}} \sum_{\mathbf{k}'} n_{\text{imp}} |u^{\text{RPA}}(\mathbf{k}' - \mathbf{k})|^2 G^X(\mathbf{k}', \varepsilon) G^R(\mathbf{k}', \varepsilon) \frac{\mathbf{k} \cdot \mathbf{k}'}{k^2} \gamma^{RX}(\mathbf{k}', \varepsilon), \quad (15.36)$$

where $X = A$ or R . One immediately sees that the small factor n_{imp} tends to kill the sum, and in the weak scattering limit one should expect the solution of this equation to be simply $\gamma^{RX}(\mathbf{k}, \varepsilon) \approx 1$. It is immediately seen that this is a consistent solution for the imaginary part of both γ^{RA} and γ^{RR} but it turns out that for the real part of γ^{RA} a factor $1/n_{\text{imp}}$ is contained in the Green's function. The lesson we learn here is that we have to be rather careful with products of Green's function carrying the same arguments, because in the limit of small n_{imp} , $\text{Im } G^X$ tends to a delta function, and the product of two delta functions has to be defined with care. Let us look more carefully into the products $G^A G^R$ and $G^R G^R$, which also appear in Eq. (15.33). This first combination is

$$\begin{aligned} G^A(\mathbf{k}, \varepsilon) G^R(\mathbf{k}, \varepsilon) &= |G^R(\mathbf{k}, \varepsilon)|^2 \equiv \left| \frac{1}{\varepsilon - \xi_{\mathbf{k}} - \Sigma^R(\mathbf{k}, \varepsilon)} \right|^2 \\ &= \frac{1}{\text{Im } \Sigma^R(\mathbf{k}, \varepsilon)} \text{Im } \frac{1}{\varepsilon - \xi_{\mathbf{k}} - \Sigma^R(\mathbf{k}, \varepsilon)} \\ &\equiv \frac{1}{-2 \text{Im } \Sigma^R(\mathbf{k}, \varepsilon)} A(\mathbf{k}, \varepsilon) \equiv \tau A(\mathbf{k}, \varepsilon), \end{aligned} \quad (15.37)$$

where $A = -2 \text{Im } G^R$ is the spectral function, and where as before the life-time τ is defined by $\tau^{-1} = -2 \text{Im } \Sigma^R(\mathbf{k}, \varepsilon)$. For the case of weak impurity scattering the scattering rate τ^{-1} is small, whence the spectral function is approximately a delta function. In the case of small n_{imp} we therefore get

$$G^A(\mathbf{k}, \varepsilon) G^R(\mathbf{k}, \varepsilon) \approx \tau 2\pi \delta(\varepsilon - \xi_{\mathbf{k}}). \quad (15.38)$$

Because $\tau \propto n_{\text{imp}}^{-1}$, the product $n_{\text{imp}} G^A G^R$ in Eq. (15.36) is finite in the limit $n_{\text{imp}} \rightarrow 0$. The combination $G^R G^R$ on the other hand is not divergent and in fact $n_{\text{imp}} G^R G^R \rightarrow 0$ as $n_{\text{imp}} \rightarrow 0$. That $G^R G^R$ is finite is seen as follows

$$\begin{aligned} G^R(\mathbf{k}, \varepsilon) G^R(\mathbf{k}, \varepsilon) &\approx \left(\frac{\varepsilon - \xi_{\mathbf{k}} - \frac{i}{2\tau}}{(\varepsilon - \xi_{\mathbf{k}})^2 + \left(\frac{1}{2\tau}\right)^2} \right)^2 \\ &= \frac{(\varepsilon - \xi_{\mathbf{k}})^2 - \left(\frac{1}{2\tau}\right)^2}{\left((\varepsilon - \xi_{\mathbf{k}})^2 + \left(\frac{1}{2\tau}\right)^2\right)^2} + i(\varepsilon - \xi_{\mathbf{k}}) A(\mathbf{k}, \varepsilon). \end{aligned} \quad (15.39)$$

The last term clearly goes to zero when τ is large and when A is approximated by a delta function. The first term is a peaked function at $\varepsilon - \xi_{\mathbf{k}} = 0$, but the integrated weight is in fact zero as can be checked by performing an integration over ε . From these arguments it follows that the terms with $G^R G^R$ can be omitted and only terms with $G^R G^A$ are kept. As explained above, we use the first Born approximation for the self-energy. In the following we therefore approximate τ with the first Born approximation life time τ_0

$$\tau^{-1} \approx \tau_0^{-1} \equiv 2\pi n_{\text{imp}} \sum_{\mathbf{k}'} |u(\mathbf{k} - \mathbf{k}')|^2 \delta(\xi_{\mathbf{k}} - \xi_{\mathbf{k}'}). \quad (15.40)$$

Because all energies are at the Fermi energy, this life time is independent of \mathbf{k} .

The conductivity Eq. (15.33) then becomes

$$\begin{aligned} \text{Re } \sigma_{xx} &= 2e^2 \text{Re} \frac{1}{\mathcal{V}} \sum_{\mathbf{k}} \Gamma_{0,x}(\mathbf{k}, \mathbf{k}) \tau_0 \delta(\xi_{\mathbf{k}}) \Gamma_x^{RA}(\mathbf{k}, \mathbf{k}; 0, 0) \\ &= 2e^2 \tau_0 \text{Re} \frac{1}{\mathcal{V}} \sum_{\mathbf{k}} \frac{k_x}{m} \delta(\xi_{\mathbf{k}}) \frac{k_x}{m} \gamma^{RA}(\mathbf{k}, \mathbf{k}; 0, 0) = \frac{e^2 n}{m} \tau_0 \gamma^{RA}(k_F, k_F; 0, 0) \end{aligned} \quad (15.41)$$

The remaining problem is to find $\gamma^{RA}(\mathbf{k}, \mathbf{k}; 0, 0)$ for $|\mathbf{k}| = k_F$. The solution follows from the integral equation Eq. (15.35)

$$\gamma^{RA}(\mathbf{k}) = 1 + \frac{2\pi}{\mathcal{V}} \sum_{\mathbf{k}'} n_{\text{imp}} |u^{\text{RPA}}(\mathbf{k}' - \mathbf{k})|^2 \tau_0 \delta(\xi_{\mathbf{k}'}) \frac{\mathbf{k} \cdot \mathbf{k}'}{k^2} \gamma^{RA}(\mathbf{k}'). \quad (15.42)$$

Since this equation has no dependence on the direction of \mathbf{k} , and since the lengths of both \mathbf{k} and \mathbf{k}' are given by k_F , γ^{RA} depends only on k_F . But k_F is constant, and we get

$$\gamma^{RA} = 1 + \left[\frac{2\pi}{\mathcal{V}} \sum_{\mathbf{k}'} n_{\text{imp}} |u^{\text{RPA}}(\mathbf{k}' - \mathbf{k})|^2 \delta(\xi_{\mathbf{k}'}) \frac{\mathbf{k} \cdot \mathbf{k}'}{k^2} \right] \tau_0 \gamma^{RA}. \quad (15.43)$$

The solution is thus simply

$$\gamma^{RA} = \frac{1}{1 - \lambda \tau_0}, \quad (15.44)$$

where

$$\lambda = \frac{2\pi}{\mathcal{V}} \sum_{\mathbf{k}'} n_{\text{imp}} |u^{\text{RPA}}(\mathbf{k}' - \mathbf{k})|^2 \delta(\xi_{\mathbf{k}'}) \frac{\mathbf{k} \cdot \mathbf{k}'}{k^2} = (\tau_0)^{-1} - (\tau^{\text{tr}})^{-1}. \quad (15.45)$$

Here the transport time τ^{tr} is defined as

$$(\tau^{\text{tr}})^{-1} \equiv \frac{2\pi}{\mathcal{V}} \sum_{|\mathbf{k}'|=k_F} n_{\text{imp}} |u^{\text{RPA}}(\mathbf{k}' - \mathbf{k})|^2 \left(1 - \frac{\mathbf{k} \cdot \mathbf{k}'}{k^2}\right). \quad (15.46)$$

This expression is precisely the transport time that we derived in the Boltzmann equation approach leading to Eq. (14.39). When inserted back into Eq. (15.44) γ^{RA} becomes

$$\gamma^{RA} = \frac{\tau^{\text{tr}}}{\tau_0}. \quad (15.47)$$

Finally, the conductivity formula (15.41) at zero temperature is

$$\sigma = \frac{e^2 \tau^{\text{tr}}}{m^2} \frac{1}{\mathcal{V}} \sum_{\mathbf{k}} \delta(\xi_{\mathbf{k}}) k_x^2 = \frac{e^2 n \tau^{\text{tr}}}{m}. \quad (15.48)$$

We thus find full agreement with the semiclassical result obtained in the previous chapter. This is what we expected, and thereby having gained confidence in the mathematical structure of the theory, we can go on to calculate various quantum corrections to the Drude formula; corrections not obtainable in the Boltzmann approach.

15.4 The weak localization correction to the conductivity

The Born approximation includes only scattering on one impurity at a time. We saw in Chap. 10 that there was in practice only little difference between the first Born and the full Born approximation. The reason is that even the full Born approximation depicted in Eq. (11.54), which does take into account multiple scattering does so only for multiple scatterings on the same impurity. Quantum effects such as interference between scattering on different impurities can therefore not be incorporated within the Born approximation scheme. In Sec. 11.5.4 it was hinted that such interference processes are represented by crossing diagrams as in Fig. 11.6. In this section we shall study in detail why that is.

As the temperature is lowered we expect quantum mechanical coherence to become more important because the phase coherence length ℓ_ϕ increases with decreasing temperature. When the coherence length ℓ_ϕ exceeds the mean free path ℓ_{imp} for impurity scattering, scattering on different impurities can interfere. Here the coherence length means the scale on which the electrons preserve their quantum mechanical phase, i.e. the scale on which the wave function evolves according to the one-particle Schrödinger equation. If an electron interacts with another electron or with a phonon through an inelastic scattering event its energy changes, and hence the evolution of its phase. Due to these processes the phase of the electron wave acquires some randomization or “dephasing”, and its coherence length becomes finite. At low temperatures the dominant dephasing mechanism is electron-electron scattering, and as we know from Chap. 13 the scattering rate for these processes is proportional to T^2 . Hence $\ell_\phi \propto T^{-2}$ can become very large at sufficiently low temperatures. At liquid helium temperature, 4.2 K, and below, typical coherence lengths are of the order 1-10 μm , spacing 10^4 - 10^5 atomic lattice spacings.

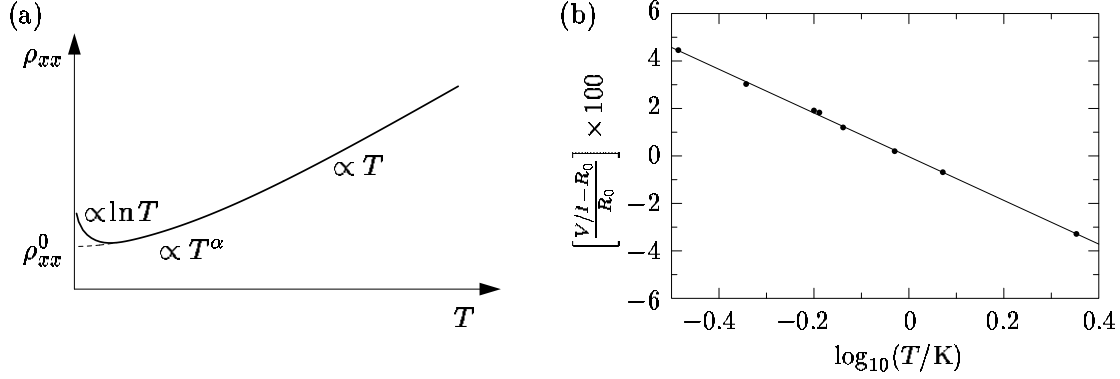


Figure 15.2: (a) A sketch of the electrical resistivity $\rho_{xx}(T)$ of a disordered metal as a function of temperature. As in Fig. 11.1 the linear behavior at high temperatures is due to electron-phonon scattering, but now at low temperatures we have added the small but significant increase due to the quantum interference known as weak localization. (b) Experimental data from measurements on a PdAu film by Dolan and Osherooff, Phys. Rev. Lett. **43**, 721 (1979), showing that the low-temperature weak localization correction to the resistivity increases logarithmically as the temperature decreases.

If the coherence length ℓ_ϕ is longer than the mean free path ℓ_0 , but still smaller than the sample size \mathcal{L} , most of the interference effects disappear. This is because the limit $\ell_\phi \ll \mathcal{L}$ effectively corresponds to averaging over many small independent segments, the so-called self-averaging illustrated in Fig. (11.2). However, around 1980 it was found through the observation of the so-called weak localization, shown in Fig. 15.2, that even in the case of large samples, $\ell_0 \ll \ell_\phi \ll \mathcal{L}$, one very important class of interference processes survive the self-averaging. Naturally, as discovered around 1985, much more dramatic quantum effects appear in small samples in the so-called mesoscopic regime (see also Chap. 7) given by $\mathcal{L} \simeq \ell_\phi$. In this regime all kinds of quantum interference processes become important, and most notably cause the appearance of the universal conductance fluctuations shown in Fig. (11.2).

In the following we study only the weak localization phenomenon appearing in large samples and not the universal conductance fluctuations appearing in small samples. To picture how averaging over impurity configurations influences the interference effects, we follow an electron after it has been scattered to a state with momentum \mathbf{k} by an impurity positioned at \mathbf{R}_1 . When the electron hits the next impurity at position \mathbf{R}_2 it has acquired a phase factor $e^{i\phi} = e^{i\mathbf{k} \cdot (\mathbf{R}_1 - \mathbf{R}_2)}$. Terms describing interference between the two scattering events will thus contain the factor $e^{i\mathbf{k} \cdot (\mathbf{R}_1 - \mathbf{R}_2)}$, and it is therefore intuitively clear that these terms vanish when one averages over \mathbf{R}_1 and \mathbf{R}_2 . *Only the interference processes which are independent of the impurity positions survive self-averaging.*

Interference generally means that the amplitude for two paths t_1 and t_2 are added as $t_1 + t_2$, so that when taking the absolute square $|t_1 + t_2|^2 = |t_1|^2 + |t_2|^2 + 2|t_1 t_2| \cos(\phi_1 - \phi_2)$, the cross-term expresses the interference. The relative phase $\phi_1 - \phi_2$ determines whether the contributions from the two paths interfere constructively or destructively. If we can

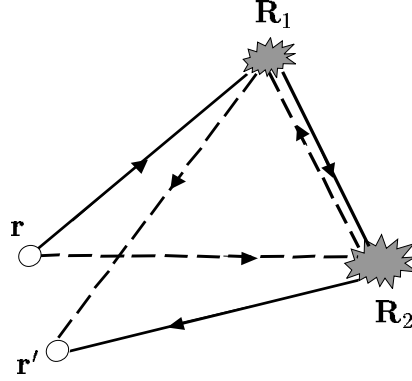


Figure 15.3: Illustration of the two interfering time-reversed paths discussed in the text.

find two paths where the relative phase is independent of the position of the impurities, the cross term would thus survive the impurity average. This is indeed possible, and two such paths are shown in Fig. 15.3. The key observation is that for each path that ends in the starting point after a specific sequence of scattering events, there is a corresponding reverse path which scatters on the same impurities but in the opposite order. Most remarkably, these two paths pick up exactly the same phase factor, and thus their relative phase $\phi_1 - \phi_2$ is always zero independent of the actual positions of the impurities. Thus for two such time-reversed paths there is always *constructive* interference. As a consequence there is an enhanced probability for returning to the same point, and the electrons therefore tend to be localized in space, hence the name “weak localization”⁴.

Having realized that the interference between time reversed paths survive impurity averaging, we now want to calculate the resulting correction to the conductivity. In order to do so we need to identify the corresponding diagrams. First we recall the Dyson equation for the single-particle Green’s functions in an external potential, which was derived in Chap. 10. Here the external potential is given by the impurity potential, U_{imp} . Writing it in the frequency domain and making analytic continuation, $ik_n \rightarrow \epsilon + i\eta$, we have for the retarded Green’s function

$$G^R(\mathbf{r}, \mathbf{r}', \epsilon) = G_0^R(\mathbf{r}, \mathbf{r}', \epsilon) + \int d\mathbf{r}'' G_0^R(\mathbf{r}, \mathbf{r}'', \epsilon) U_{\text{imp}}(\mathbf{r}'') G^R(\mathbf{r}'', \mathbf{r}', \epsilon). \quad (15.49)$$

If we for simplicity assume $U_{\text{imp}}(\mathbf{r}) \approx \sum_i U_0 \delta(\mathbf{r} - \mathbf{R}_i)$, i.e. short range impurities located at the positions $\{\mathbf{R}_i\}$, we have

$$G^R(\mathbf{r}, \mathbf{r}', \epsilon) = G_0^R(\mathbf{r}, \mathbf{r}', \epsilon) + \sum_i G_0^R(\mathbf{r}, \mathbf{R}_i, \epsilon) U_0 G^R(\mathbf{R}_i, \mathbf{r}', \epsilon). \quad (15.50)$$

Let us look at a specific process where an electron scatters at, say, two impurities located at \mathbf{R}_1 and \mathbf{R}_2 . To study interference effects between scattering at these two impurities we must expand to second order in the impurity potential. The interesting second order

⁴The term “strong localization” is used for the so-called Anderson localization where a metal-insulator transition is induced in three dimensions at a critical strength of the disorder potential.

terms (there are also less interesting ones where the electron scatters on the same impurities twice) are

$$G^{R(2)}(\mathbf{r}, \mathbf{r}', \epsilon) = G_0^R(\mathbf{r}, \mathbf{R}_1, \epsilon) U_0 G_0^R(\mathbf{R}_1, \mathbf{R}_2, \epsilon) U_0 G_0^R(\mathbf{R}_2, \mathbf{r}', \epsilon) \\ + G_0^R(\mathbf{r}, \mathbf{R}_2, \epsilon) U_0 G_0^R(\mathbf{R}_2, \mathbf{R}_1, \epsilon) U_0 G_0^R(\mathbf{R}_1, \mathbf{r}', \epsilon). \quad (15.51)$$

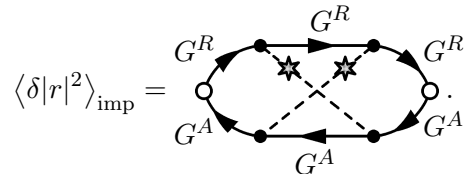
These two terms correspond to the transmission amplitudes t_1 and t_2 discussed above and illustrated in Fig. 15.3. The probability for the process is obtained from the absolute square of the Green's function, and because we want to find the correction $\delta|r|^2$ to the reflection coefficient, we set $\mathbf{r} = \mathbf{r}'$ at the end of the calculation. First the quantum correction due to interference to the transmission from \mathbf{r} to \mathbf{r}' is

$$\delta|t(\mathbf{r}, \mathbf{r}')|^2 \propto \text{Re} \left[G_0^R(\mathbf{r}, \mathbf{R}_1, \epsilon) U_0 G_0^R(\mathbf{R}_1, \mathbf{R}_2, \epsilon) U_0 G_0^R(\mathbf{R}_2, \mathbf{r}', \epsilon) \right. \\ \left. \times (G_0^R(\mathbf{r}, \mathbf{R}_2, \epsilon) U_0 G_0^R(\mathbf{R}_2, \mathbf{R}_1, \epsilon) U_0 G_0^R(\mathbf{R}_1, \mathbf{r}', \epsilon))^* \right]. \quad (15.52)$$

Now reflection is described by setting $\mathbf{r} = \mathbf{r}'$. Doing this and averaging over impurity positions \mathbf{R}_1 and \mathbf{R}_2 we find the quantum correction $\delta|r|^2$ to the reflection. In \mathbf{k} -space one gets

$$\langle \delta|r|^2 \rangle_{\text{imp}} \equiv \langle \delta|t(\mathbf{r} = \mathbf{r}')|^2 \rangle_{\text{imp}} \\ \propto \text{Re} \frac{1}{V^4} \sum_{\mathbf{p}_1 \mathbf{p}_2 \mathbf{p}_3 \mathbf{Q}} G_0^R(\mathbf{Q} - \mathbf{p}_1, \epsilon) U_0 G_0^R(\mathbf{Q} - \mathbf{p}_2, \omega) U_0 G_0^R(\mathbf{Q} - \mathbf{p}_3, \epsilon) \\ \times G_0^A(\mathbf{p}_1, \epsilon) U_0 G_0^A(\mathbf{p}_2, \epsilon) U_0 G_0^A(\mathbf{p}_3, \epsilon). \quad (15.53)$$

This formula can be represented by a diagram similar to the last one in Eq. (15.61) with the upper lines being retarded and the lower lines being advanced Green's functions. Notice however that contrary to the usual diagram for conductance the Green's function and the lower and upper branch run in same direction. If we however twist the lower branch such that the Green's function run in opposite directions while the impurity lines cross, the diagram looks like conductivity diagram if we furthermore join the retarded and advanced Green's function like this



$$\langle \delta|r|^2 \rangle_{\text{imp}} = \quad (15.54)$$

This hints that the interference term coming from time reversed paths can be summed by taking diagrams of this form into account. These crossed diagrams were not included in the Born approximation, which we used to derive the Boltzmann equation result, and in fact they were shown in Sec. 11.5.4 to be smaller than the Born approximation by a factor $1/k_F \ell$. Nevertheless, at low temperatures they do play a role as the leading

quantum correction. If we continue this line of reasoning we should include also diagrams where paths scattering on more than two impurities interfere with their time reversed counter parts. It is straightforward to see that the corresponding diagrams are of the same type as (15.54) but with more crossing lines. This class of diagrams are called *the maximally crossed diagrams*. We have now identified which diagrams we need to sum in order to get the leading quantum correction to the conductivity. Most importantly, this is a contribution which does not disappear upon self-averaging.

Let us return to the Kubo formula for conductance, and let us sum the maximally crossed diagrams. We write the current-current correlation function as $\Pi = \Pi^B + \Pi^{\text{WL}}$ where Π^B is the Boltzmann result derived in the previous section, and where

$$\Pi_{xx}^{\text{WL}}(\tilde{q}) = \text{Diagram 1} + \text{Diagram 2} \quad (15.55)$$

$$+ \text{Diagram 3} + \dots \quad (15.56)$$

The full electron Green's functions in these diagrams are as before the full Green's function with an appropriately chosen self-energy. Since we include crossed diagrams in the vertex function we should in principle also include these in the self-energy. However, they can safely be ignored, since they only give a small contribution, down by a factor $1/k_F v_F \tau_0$ (see the discussion in Fig. 11.6). The crossed diagrams we are about to evaluate are also small by the same factor, but as we shall see they nevertheless yield a divergent contribution. This divergence stems from summing the interference of many time-reversed paths. This sum is different from the ladder diagrams that we summed in the Born approximation. There is however a trick which allows for a summation just like a ladder diagram. Let us twist the diagram in Eq. (15.56) with for example three impurity lines so as to make the impurity lines parallel,

$$\Pi_{xx}^{\text{WL}(3)}(\tilde{q}) = \text{Diagram 4} \quad (15.57)$$

Then we see that the full series in Eq. (15.56) can be written as

$$\begin{aligned} \Pi_{xx}^{\text{WL}}(\tilde{q}) &= \text{Diagram 5} \quad (15.58) \\ &= -\frac{1}{(2m)^2} \frac{1}{v^2} \int d\tilde{k} \int d\tilde{k}' (2k_x + q_x) \mathcal{G}(\tilde{k}) \mathcal{G}(\tilde{k} + \tilde{q}) \mathcal{C}(\tilde{k}, \tilde{k}', \tilde{q}) \mathcal{G}(\tilde{k}') \mathcal{G}(\tilde{k}' + \tilde{q}) (2k'_x + q'_x), \end{aligned}$$

where the box \mathcal{C} is a sum of parallel impurity lines, i.e. analogous to the normal ladder sum of Eq. (15.24), but now with the fermion lines running in the same direction. This reversed

ladder sum, \mathcal{C} , which couples two electron lines or two hole lines rather one electron line and one hole line, is called a cooperon. The solution for the cooperon \mathcal{C} is found from the following Dyson-like equation

$$\mathcal{C} \equiv \text{[diagram 1]} + \text{[diagram 2]} + \text{[diagram 3]} + \dots \quad (15.59)$$

$$\mathcal{C} = \text{[diagram 1]} + \text{[diagram 2]} \quad (15.60)$$

In order to simplify our calculation, we only study the case $\mathbf{q} = 0$, and furthermore we restrict the analysis to the case of short range impurities so that we can approximate $W(\mathbf{q})$ by a constant, $W_0 = n_i |u_0|^2$. With these approximations, and denoting $\mathbf{k} + \mathbf{k}' \equiv \mathbf{Q}$ the cooperon becomes

$$\mathcal{C} = \text{[diagram 1]} + \text{[diagram 2]} + \text{[diagram 3]} + \dots \quad (15.61)$$

Because the impurity scattering conserves Matsubara frequencies the upper fermion lines all carry the frequency $ik_n + iq_n$, while the lower ones carry the frequency ik_n . It is now straightforward to solve the Dyson-equation for the cooperon ladder and obtain

$$\mathcal{C}(\mathbf{Q}; ik_n + iq_n, ik_n) = \frac{\frac{1}{V} \sum_{\mathbf{p}} W_0 \mathcal{G}(\mathbf{Q} - \mathbf{p}, ik_n + iq_n) \mathcal{G}(\mathbf{p}, ik_n) W_0}{1 - \frac{1}{V} \sum_{\mathbf{p}} W_0 \mathcal{G}(\mathbf{Q} - \mathbf{p}, ik_n + iq_n) \mathcal{G}(\mathbf{p}, ik_n)}. \quad (15.62)$$

This can then be inserted into the expression for the current-current correlation function Π_{xx}^{WL} in Eq. (15.58)

$$\begin{aligned} \Pi_{xx}^{\text{WL}}(0, iq_n) = & -\frac{1}{(2m)^2} \frac{1}{V^2} \frac{1}{\beta} \sum_{ik_n} \sum_{\mathbf{k}\mathbf{k}'} (2k_x) \mathcal{G}(\mathbf{k}, ik_n) \mathcal{G}(\mathbf{k}, ik_n + iq_n) \\ & \times \mathcal{C}(\mathbf{k} + \mathbf{k}'; ik_n + iq_n, ik_n) \mathcal{G}(\mathbf{k}', ik_n) \mathcal{G}(\mathbf{k}', ik_n + iq_n) (2k'_x). \end{aligned} \quad (15.63)$$

The Green's function \mathcal{G} is here the Born approximation Green's function which after analytic continuation is

$$G^R(\mathbf{k}, \varepsilon) = \mathcal{G}(\mathbf{k}, ik_n \rightarrow \varepsilon + i\eta) = \frac{1}{\varepsilon - \xi_{\mathbf{k}} + i/2\tau_0}, \quad (15.64)$$

where $[\tau_0]^{-1} = 2\pi W_0 d(\varepsilon_F)$. It is now simple to find the solution for the cooperon \mathcal{C} .

In the previous section we learned that only the $G^A G^R$ term in Eq. (15.33) contributed in the limit of weak scattering and therefore we should replace $ik_n + i\omega_n$ by a retarded frequency and ik_n by an advanced frequency. Likewise, we obtain from (15.63) the weak localization correction by the replacements $ik_n + iq_n \rightarrow \varepsilon + \omega + i\eta$ and $ik_n \rightarrow \varepsilon - i\eta$, followed by inserting the result into Eq. (15.33). Taking the dc-limit $\omega \rightarrow 0$ and the low temperature limit $T \rightarrow 0$, we have

$$\text{Re } \delta\sigma_{xx}^{\text{WL}} = 2 \times \frac{e^2}{2\pi} \left(\frac{1}{m} \right)^2 \frac{1}{\mathcal{V}^2} \sum_{\mathbf{k}\mathbf{k}'} (k_x k'_x) G^R(\mathbf{k}, 0) G^A(\mathbf{k}, 0) C^{AR}(\mathbf{k} + \mathbf{k}'; 0, 0) G^R(\mathbf{k}', 0) G^A(\mathbf{k}', 0). \quad (15.65)$$

As in the previous section we have factors of $G^A G^R$ appearing. However, here we cannot replace them by delta functions, because \mathbf{k} and \mathbf{k}' are connected through $C^{RA}(\mathbf{k} + \mathbf{k}')$. Instead we evaluate the cooperon as follows. After analytical continuation the cooperon in Eq. (15.62) becomes

$$C^{RA}(\mathbf{Q}) = \frac{W_0 \zeta(\mathbf{Q})}{1 - \zeta(\mathbf{Q})}, \quad (15.66)$$

$$\zeta(\mathbf{Q}) \equiv \frac{n_i}{\mathcal{V}} \sum_{\mathbf{p}} |u_0|^2 G^R(\mathbf{Q} - \mathbf{p}, 0) G^A(\mathbf{p}, 0), \quad (15.67)$$

where we have introduced the auxiliary function $\zeta(\mathbf{Q})$. Using Eq. (15.64) $\zeta(\mathbf{Q})$ becomes

$$\zeta(\mathbf{Q}) = n_i |u_0|^2 \frac{1}{\mathcal{V}} \sum_{\mathbf{p}} \frac{1}{-\xi_{\mathbf{Q}-\mathbf{p}} + i/2\tau_0} \frac{1}{-\xi_{\mathbf{p}} - i/2\tau_0}. \quad (15.68)$$

To proceed further we must now evaluate the \mathbf{p} -sum in $\zeta(\mathbf{Q})$. We begin by studying $\mathbf{Q} = 0$, in which case we have

$$\begin{aligned} \zeta(0) &= n_i |u_0|^2 d(\varepsilon_F) \int_{-\infty}^{\infty} d\xi \frac{1}{-\xi + i/2\tau_0} \frac{1}{-\xi - i/2\tau_0} \\ &= n_i |u_0|^2 d(\varepsilon_F) \int_{-\infty}^{\infty} d\xi \frac{1}{\xi^2 + (1/2\tau_0)^2} = n_i |u_0|^2 d(\varepsilon_F) 2\pi\tau_0 = 1, \end{aligned} \quad (15.69)$$

where we have used the definition of the life time τ_0 in the Born approximation. Combining Eqs. (15.66) and (15.69) it follows that C^{RA} diverges in the limit of small Q and small frequency. The dc conductivity is therefore dominated by the contribution from values of Q near zero. Consequently, we study this contribution by expanding Eq. (15.68) for small Q . Here small means small compared the width τ_0^{-1} of the spectral function, i.e. we study the limit $Q v_F \tau_0 \ll 1$ or $Q \ll \ell_0^{-1} = 1/v_F \tau_0$. Furthermore, by symmetry arguments the term linear in Q vanish, so we need to go to second order in Q

$$\begin{aligned} \zeta(\mathbf{Q}) &\approx 1 + n_i |u_0|^2 \frac{1}{\mathcal{V}} \sum_{\mathbf{p}} \left(\frac{1}{-\xi_{\mathbf{p}} + i/2\tau_0} \right)^2 \frac{1}{-\xi_{\mathbf{p}} - i/2\tau_0} \left(-\mathbf{v}_{\mathbf{p}} \cdot \mathbf{Q} + \frac{Q^2}{2m} \right) \\ &\quad + n_i |u_0|^2 \frac{1}{\mathcal{V}} \sum_{\mathbf{p}} \left(\frac{1}{-\xi_{\mathbf{p}} + i/2\tau_0} \right)^3 \frac{1}{-\xi_{\mathbf{p}} - i/2\tau_0} (\mathbf{v}_{\mathbf{p}} \cdot \mathbf{Q})^2, \end{aligned} \quad (15.70)$$

where it is indeed seen that the term linear in \mathbf{Q} is zero because $\mathbf{v}_{\mathbf{p}}$ is an odd function of \mathbf{p} . Now transforming the sum into integrations over ξ and performing the angular integrations, we find

$$\begin{aligned} \zeta(\mathbf{Q}) \approx & 1 + \frac{1}{2\pi\tau_0} \int_{-\infty}^{\infty} d\xi \left(\frac{1}{-\xi + i/2\tau_0} \right)^2 \frac{1}{-\xi - i/2\tau_0} \left(\frac{Q^2}{2m} \right) \\ & + \frac{1}{2\pi\tau_0} \int_{-\infty}^{\infty} d\xi \left(\frac{1}{-\xi + i/2\tau_0} \right)^3 \frac{1}{-\xi - i/2\tau_0} \frac{Q^2 v_F^2}{N_{\text{dim}}}, \end{aligned} \quad (15.71)$$

where N_{dim} is the number of dimensions. Closing the contour in the lower part of the complex ξ plan, we find that

$$\zeta(\mathbf{Q}) \approx 1 + \frac{2\pi i}{2\pi\tau_0} \left[\left(\frac{1}{i/\tau_0} \right)^2 \frac{Q^2}{2m} + \left(\frac{1}{i/\tau_0} \right)^3 \frac{Q^2 v_F^2}{N_{\text{dim}}} \right]. \quad (15.72)$$

To leading order in τ_0^{-1} , τ_0^3 dominates over τ_0^2 , and we end up with

$$\zeta(\mathbf{Q}) \approx 1 - \frac{1}{N_{\text{dim}}} Q^2 \ell_0^2 \equiv 1 - D\tau_0 Q^2, \quad (15.73)$$

where

$$\ell_0 = v_F \tau_0, \quad D = \frac{v_F^2 \tau_0}{N_{\text{dim}}}, \quad (15.74)$$

D being the diffusion constant. We emphasize that Eq. (15.73) is only valid for $Q \ll \ell_0^{-1}$. With this result for $\zeta(\mathbf{Q})$ inserted into (15.66) we obtain the final result for the cooperon

$$C^{RA}(\mathbf{Q}; 0, 0) = \frac{W_0(1 - D\tau_0 Q^2)}{D\tau_0 Q^2} \approx \frac{W_0}{\tau_0} \frac{1}{DQ^2}. \quad (15.75)$$

Because the important contribution comes from $Q \approx 0$, $\delta\sigma^{WL}$ in Eq. (15.65) becomes

$$\delta\sigma^{WL} = 2 \times \frac{e^2}{\pi} \left(\frac{1}{m} \right)^2 \frac{W_0}{\tau_0} \frac{1}{\mathcal{V}^2} \sum_{\mathbf{k}, Q < \ell_0^{-1}} (-k_x^2) G^R(\mathbf{k}, 0) G^A(\mathbf{k}, 0) \frac{1}{DQ^2} G^R(\mathbf{Q} - \mathbf{k}, 0) G^A(\mathbf{Q} - \mathbf{k}, 0). \quad (15.76)$$

First we perform the sum over \mathbf{k} . Since $Q < \ell_0^{-1}$, and hence smaller than the width of the spectral function, we can approximate $\mathbf{Q} - \mathbf{k}$ by just $-\mathbf{k}$ and obtain

$$\begin{aligned} \frac{1}{\mathcal{V}} \sum_{\mathbf{k}} k_x^2 G^R(\mathbf{k}, 0) G^A(\mathbf{k}, 0) G^R(-\mathbf{k}, 0) G^A(-\mathbf{k}, 0) &= d(\varepsilon_F) \frac{k_F^2}{N_{\text{dim}}} \int_{-\infty}^{\infty} d\xi \left(\frac{1}{\xi^2 + (1/2\tau_0)^2} \right)^2 \\ &= \frac{4\pi k_F^2}{N_{\text{dim}}} d(\varepsilon_F) \tau_0^3. \end{aligned} \quad (15.77)$$

From this follows

$$\delta\sigma^{WL} = -\frac{e^2}{\pi} \left(\frac{k_F}{m} \right)^2 \frac{2\tau_0}{N_{\text{dim}}} \frac{1}{\mathcal{V}} \sum_{Q < \ell^{-1}} \frac{1}{DQ^2} \quad (15.78)$$

We are then left with the \mathbf{Q} -integration, which amounts to

$$\frac{1}{\bar{v}} \sum_{Q < \ell_0^{-1}} \frac{1}{DQ^2} = \int_{Q < \ell_0^{-1}} \frac{d\mathbf{Q}}{(2\pi)^{N_{\text{dim}}}} \frac{1}{DQ^2} \propto \int_{Q < \ell_0^{-1}} dQ \frac{Q^{N_{\text{dim}}-1}}{DQ^2}. \quad (15.79)$$

It is evident that this integral is divergent in the small Q limit in both one and two dimensions. Physically this is because we have allowed interference between path of infinite length, which does not occur in reality. In a real system the electron cannot maintain coherence over arbitrarily long distances due to scattering processes that cause decoherence. We must therefore find a method to cut-off these unphysical paths. To properly describe the breaking of phase coherence between the time-reversed paths one should include coupling to other degrees of freedom such as coupling to phonons or electron-electron scatterings. Here we choose to do this in a phenomenological fashion instead. Let us suppose that each path in the sum over paths in Eq. (15.61) has a probability of being destroyed by a scattering event and that this probability is proportional to the length of the path, or equivalently to the number of impurity scattering events involved in the path. This can be modelled by including a factor $e^{-\gamma}$ in the impurity potential so that instead of W_0 we write $W_0 e^{-\gamma}$. Clearly a path with n scatterings will then carry a factor $e^{-n\gamma}$. The parameter γ is then interpreted as the amount of decoherence experienced within a mean free path, i.e. $\gamma = \ell_0/\ell_\phi$. With this modification, the function $\zeta(\mathbf{Q})$ is changed into

$$\zeta(\mathbf{Q}, \omega) \approx e^{-\gamma} (1 - D\tau_0 Q^2), \quad (15.80)$$

and hence the cooperon gets modified as

$$C^{RA}(\mathbf{Q}; 0, 0) = \frac{W_0}{1 - e^{-\gamma} + e^{-\gamma} DQ^2 \tau_0}. \quad (15.81)$$

In the limit of large ℓ_ϕ or small γ , we therefore have

$$C^{RA}(\mathbf{Q}; 0, 0) \simeq \frac{W_0}{\tau_0} \frac{1}{1/\tau_\phi + DQ^2}. \quad (15.82)$$

where $\tau_\phi = \ell_\phi/v_F$. This is a physical sensible result. It says that the paths corresponding to a diffusion time longer than the phase breaking time cannot contribute to the interference effect. If the phase coherence length becomes larger than the sample, the sample size \mathcal{L} must of course replace ℓ_ϕ as a cut-off length, because paths longer than the sample should not be included. We can now return to (15.79) and evaluate the integral in one, two and three dimensions, respectively

$$\begin{aligned} \int \frac{d\mathbf{Q}}{(2\pi)^{N_{\text{dim}}}} \frac{1}{1/\tau_\phi + DQ^2} &= \int_0^{1/\ell_0} dQ \frac{1}{1/\tau_\phi + DQ^2} \begin{pmatrix} \frac{1}{\pi} \\ \frac{1}{2\pi} Q \\ \frac{1}{2\pi^2} Q^2 \end{pmatrix} \\ &= \begin{cases} \frac{1}{\pi} \sqrt{\frac{\tau_\phi}{D}} \tan^{-1} \sqrt{\frac{D\tau_\phi}{\ell_0^2}}, & 1\text{D} \\ \frac{1}{4D\pi} \ln \left(1 + \frac{D\tau_\phi}{\ell_0^2} \right), & 2\text{D} \\ \frac{1}{2\pi^2 D \ell_0} - \frac{1}{2\pi^2 D \sqrt{D\tau_\phi}} \tan^{-1} \sqrt{\frac{D\tau_\phi}{\ell_0^2}}, & 3\text{D} \end{cases} \end{aligned} \quad (15.83)$$

which in the limit of large τ_ϕ gives us information about the importance of the quantum corrections:

$$\delta\sigma^{WL} \propto \begin{cases} -(\tau_\phi)^{1/2}, & 1\text{D} \\ -\ln\left(\frac{\tau_\phi}{\tau_0}\right), & 2\text{D} \\ (\tau_\phi)^{-1/2}, & 3\text{D}. \end{cases} \quad (15.84)$$

This is an important result, which states that due to the localization correction the conductivity decreases with increasing phase coherence time. Furthermore, in the one-dimensional case it tells us that in one dimension the localization correction is enormously important and may exceed the Drude result. In fact it can be shown that a quantum particle in a one dimensional disordered potential is always localized. In three dimensions the situation is more subtle, there a metal-insulator transition occurs at a critical value of the disorder strength. Two dimensions is in between these two cases, and it is in this case that the term “weak” localization makes sense, because here the correction is small. For the two dimensional case we have

$$\delta\sigma_{2\text{D}}^{\text{WL}} \approx -\frac{e^2}{2\pi^2} \ln\left(\frac{\tau_\phi}{\tau_0}\right). \quad (15.85)$$

This result is “universal” since, apart from the logarithmic factor, it does not depend on the details of the material or the impurity concentration. That it is a small correction to the Drude conductivity can be seen from the ratio

$$\frac{\delta\sigma_{2\text{D}}^{\text{WL}}}{\sigma_0} = -\frac{1}{\pi k_F \ell_0} \ln\left(\frac{\tau_\phi}{\tau_0}\right). \quad (15.86)$$

A way to measure this effect is to change the phase coherence time τ_ϕ and to look at the change of conductivity. The phase coherence can be changed in two ways. Foremost, one can apply a magnetic field which breaks the time-reversal symmetry giving rise to the fundamental interference between time-reversed paths. Secondly, decreasing the temperature increases the phase coherence time $\tau_\phi^{-1} \propto T^\alpha$, and a logarithmic increase of the conductivity is to be expected. Indeed $\delta\rho \propto -\delta\sigma \propto \ln \tau_\phi \propto -\ln T$ as is measured and shown in Fig. 15.2.

15.5 Combined RPA and Born approximation

This section will be added in the next edition of these notes. See also Exercise 14.4

Chapter 16

Green's functions and phonons

In this chapter we develop and apply the Green's function technique for free phonons and for the electron-phonon interaction. The point of departure is the second quantization formulation of the phonon problem presented in Chap. 3, in particular the bosonic phonon creation and annihilation operators $b_{-\mathbf{q},\lambda}^\dagger$ and $b_{\mathbf{q},\lambda}$ introduced in Eqs. (3.10) and (3.22) and appearing in the jellium phonon Hamiltonian Eq. (3.4) and in the lattice phonon Hamiltonian Eq. (3.23).

We first define and study the Green's functions for free phonons in both the jellium model and the lattice model. Then we apply the Green's function technique to the electron-phonon interaction problem. We derive the one-electron Green's function in the presence of both the electron-electron and the electron-phonon interaction. We also show how the high frequency Einstein phonons in the free-phonon jellium model become renormalized and become the usual low-frequency acoustic phonons once the electron-phonon interaction is taken into account. Finally, we prove the existence of the so-called Cooper instability of the electron gas, the phonon-induced instability which is the origin of superconductivity.

16.1 The Green's function for free phonons

It follows from all the Hamiltonians describing electron-phonon interactions, e.g. $H_{\text{el-ph}}^{\text{INA}}$ in Eq. (3.41) and $H_{\text{el-ph}}^{\text{jel}}$ in Eq. (3.43), that the relevant phonon operators to consider are not the individual phonon creation and annihilation operators, but rather the operators $A_{\mathbf{q}\lambda}$ and $A_{\mathbf{q}\lambda}^\dagger$ defined as

$$A_{\mathbf{q}\lambda} \equiv (b_{\mathbf{q}\lambda} + b_{-\mathbf{q}\lambda}^\dagger), \quad A_{\mathbf{q}\lambda}^\dagger \equiv (b_{\mathbf{q}\lambda}^\dagger + b_{-\mathbf{q}\lambda}) = A_{-\mathbf{q}\lambda}. \quad (16.1)$$

The phonon operator $A_{\mathbf{q}\lambda}$ can be interpreted as removing momentum \mathbf{q} from the phonon system either by annihilating a phonon with momentum \mathbf{q} or by creating one with momentum $-\mathbf{q}$. With these prerequisites the non-interacting phonons are described by H_{ph} and the electron-phonon interaction by $H_{\text{el-ph}}$ as follows:

$$H_{\text{ph}} = \sum_{\mathbf{q}\lambda} \Omega_{\mathbf{q}\lambda} \left(b_{\mathbf{q}\lambda}^\dagger b_{\mathbf{q}\lambda} + \frac{1}{2} \right), \quad H_{\text{el-ph}} = \frac{1}{V} \sum_{\mathbf{k}\sigma} \sum_{\mathbf{q}\lambda} g_{\mathbf{q}\lambda} c_{\mathbf{k}+\mathbf{q},\sigma}^\dagger c_{\mathbf{k}\sigma} A_{\mathbf{q}\lambda}. \quad (16.2)$$

Since H_{ph} does not depend on time, we can in accordance with Eq. (10.5) define the phonon operators $\hat{A}_{\mathbf{q}\lambda}(\tau)$ in the imaginary time interaction picture¹

$$\hat{A}_{\mathbf{q}\lambda}(\tau) \equiv e^{\tau H_{\text{ph}}} A_{\mathbf{q}\lambda} e^{-\tau H_{\text{ph}}}. \quad (16.3)$$

With this imaginary-time boson operator we can follow Eq. (10.17) and introduce the bosonic Matsubara Green's function $\mathcal{D}_{\lambda}^0(\mathbf{q}, \tau)$ for free phonons,

$$\mathcal{D}_{\lambda}^0(\mathbf{q}, \tau) \equiv -\langle T_{\tau} \hat{A}_{\mathbf{q}\lambda}(\tau) \hat{A}_{\mathbf{q}\lambda}^{\dagger}(0) \rangle_0 = -\langle T_{\tau} \hat{A}_{\mathbf{q}\lambda}(\tau) \hat{A}_{-\mathbf{q}\lambda}(0) \rangle_0, \quad (16.4)$$

where T_{τ} is the bosonic time ordering operator defined in Eq. (10.18) with a plus-sign. The frequency representation of the free phonon Green's function follows by applying Eq. (10.25),

$$\mathcal{D}_{\lambda}^0(\mathbf{q}, i q_n) \equiv \int_0^{\beta} d\tau e^{i q_n \tau} \mathcal{D}_{\lambda}^0(\mathbf{q}, \tau), \quad \omega_n = 2n\pi/\beta. \quad (16.5)$$

The specific forms for $\mathcal{D}_{\lambda}^0(\mathbf{q}, \tau)$ and $\mathcal{D}_{\lambda}^0(\mathbf{q}, i q_n)$ are found using the boson results of Sec. 10.3.1 with the substitutions $(\nu, \varepsilon_{\nu}, c_{\nu}) \rightarrow (\mathbf{q}\lambda, \Omega_{\mathbf{q}\lambda}, b_{\mathbf{q}\lambda})$. In the imaginary time domain we find

$$\mathcal{D}_{\lambda}^0(\mathbf{q}, \tau) = \begin{cases} -[n_{\text{B}}(\Omega_{\mathbf{q}\lambda}) + 1] e^{-\Omega_{\mathbf{q}\lambda}\tau} - n_{\text{B}}(\Omega_{\mathbf{q}\lambda}) e^{\Omega_{\mathbf{q}\lambda}\tau} & , \quad \text{for } \tau > 0, \\ -n_{\text{B}}(\Omega_{\mathbf{q}\lambda}) e^{-\Omega_{\mathbf{q}\lambda}\tau} - [n_{\text{B}}(\Omega_{\mathbf{q}\lambda}) + 1] e^{\Omega_{\mathbf{q}\lambda}\tau} & , \quad \text{for } \tau < 0, \end{cases} \quad (16.6)$$

while in the frequency domain we obtain

$$\mathcal{D}_{\lambda}^0(\mathbf{q}, i q_n) = \frac{1}{i q_n - \Omega_{\mathbf{q}\lambda}} - \frac{1}{i q_n + \Omega_{\mathbf{q}\lambda}} = \frac{2 \Omega_{\mathbf{q}\lambda}}{(i q_n)^2 - (\Omega_{\mathbf{q}\lambda})^2}, \quad (16.7)$$

where we have used that $n_{\text{B}}(\Omega_{\mathbf{q}\lambda}) = 1/[\exp(\beta\Omega_{\mathbf{q}\lambda}) - 1]$.

16.2 Electron-phonon interaction and Feynman diagrams

We next turn to the problem of treating the electron-phonon interaction perturbatively using the Feynman diagram technique. For clarity, in this section we do not take the Coulomb interaction between the electrons into account. The unperturbed Hamiltonian is the sum of the free electron and free phonon Hamiltonians, H_{el} and H_{ph} ,

$$H_0 = H_{\text{el}} + H_{\text{ph}} = \sum_{\mathbf{k}\sigma} \varepsilon_{\mathbf{k}} c_{\mathbf{k}\sigma}^{\dagger} c_{\mathbf{k}\sigma} + \sum_{\mathbf{q}\lambda} \Omega_{\mathbf{q}\lambda} \left(b_{\mathbf{q}\lambda}^{\dagger} b_{\mathbf{q}\lambda} + \frac{1}{2} \right). \quad (16.8)$$

When governed solely by H_0 the electronic and phononic degrees of freedom are completely decoupled, and as in Eq. (1.106) the basis states are given in terms of simple outer product states described by the electron occupation numbers $n_{\mathbf{k}\sigma}$ and the phonon occupation numbers $N_{\mathbf{q}\lambda}$,

$$|\Psi_{\text{basis}}\rangle = |n_{\mathbf{k}_1\sigma_1}, n_{\mathbf{k}_2\sigma_2}, \dots\rangle |N_{\mathbf{q}_1\lambda_1}, N_{\mathbf{q}_2\lambda_2}, \dots\rangle. \quad (16.9)$$

¹This expression is also valid in the grand canonical ensemble governed by $H_{\text{ph}} - \mu N$. This is because the number of phonons can vary, and thus minimizing the free energy gives $\partial F/\partial N \equiv \mu = 0$.

What happens then as the electron-phonon interaction $H_{\text{el-ph}}$ of Eq. (16.2) is turned on? We choose to answer this question by studying the single-electron Green's function $\mathcal{G}_\sigma(\mathbf{k}, \tau)$. In analogy with Eq. (12.5) we use the interaction picture representation, but now in momentum space, and substitutes the two-particle interaction Hamiltonian $\hat{W}(\tau)$ with the electron-phonon interaction $\hat{P}(\tau)$

$$\mathcal{G}_\sigma(\mathbf{k}, \tau) = - \frac{\sum_{m=0}^{\infty} \frac{(-1)^m}{m!} \int_0^\beta d\tau_1 \dots \int_0^\beta d\tau_m \left\langle T_\tau \hat{P}(\tau_1) \dots \hat{P}(\tau_m) \hat{c}_{\mathbf{k}\sigma}(\tau) \hat{c}_{\mathbf{k}\sigma}^\dagger(0) \right\rangle_0}{\sum_{m=0}^{\infty} \frac{(-1)^m}{m!} \int_0^\beta d\tau_1 \dots \int_0^\beta d\tau_m \left\langle T_\tau \hat{P}(\tau_1) \dots \hat{P}(\tau_m) \right\rangle_0}, \quad (16.10)$$

where the $\hat{W}(\tau)$ -integral of Eq. (12.6) is changed into a $\hat{P}(\tau)$ -integral,

$$\int_0^\beta d\tau_j \hat{P}(\tau_j) = \frac{1}{\mathcal{V}} \int d\tau_j \sum_{\mathbf{k}\sigma} \sum_{\mathbf{q}\lambda} g_{\mathbf{q}\lambda} \hat{c}_{\mathbf{k}+\mathbf{q},\sigma}^\dagger(\tau_j) \hat{c}_{\mathbf{k}\sigma}(\tau_j) \hat{A}_{\mathbf{q}\lambda}(\tau_j). \quad (16.11)$$

At first sight the two single-electron Green's functions in Eqs. (12.5) and (16.10) seems to be quite different since $\hat{W}(\tau)$ contains four electron operators and $\hat{P}(\tau)$ only two. However, we shall now show that the two expressions in fact are very similar. First we note that because the electronic and phononic degrees of freedom decouple the thermal average of the integrand in the m 'th term of say the denominator in Eq. (16.10) can be written as a product of a phononic and an electronic thermal average,

$$\begin{aligned} & \left\langle T_\tau \hat{A}_{\mathbf{q}_1\lambda_1}(\tau_1) \dots \hat{A}_{\mathbf{q}_m\lambda_m}(\tau_m) \hat{c}_{\mathbf{k}+\mathbf{q}_1\sigma}^\dagger(\tau_1) \hat{c}_{\mathbf{k}\sigma}(\tau_1) \dots \hat{c}_{\mathbf{k}+\mathbf{q}_m\sigma}^\dagger(\tau_m) \hat{c}_{\mathbf{k}\sigma}(\tau_m) \right\rangle_0 = \\ & \left\langle T_\tau \hat{A}_{\mathbf{q}_1\lambda_1}(\tau_1) \dots \hat{A}_{\mathbf{q}_m\lambda_m}(\tau_m) \right\rangle_0 \left\langle T_\tau \hat{c}_{\mathbf{k}+\mathbf{q}_1\sigma}^\dagger(\tau_1) \hat{c}_{\mathbf{k}\sigma}(\tau_1) \dots \hat{c}_{\mathbf{k}+\mathbf{q}_m\sigma}^\dagger(\tau_m) \hat{c}_{\mathbf{k}\sigma}(\tau_m) \right\rangle_0. \end{aligned} \quad (16.12)$$

It is clear from Eq. (16.1) that only an even number of phonon operators will lead to a non-zero contribution in the equilibrium thermal average, so we now write $m = 2n$. Next, we use Wick's theorem Eq. (10.79) for boson operators to break down the n -particle phonon Green's function to a product of n single-particle Green's functions of the form

$$\begin{aligned} g_{\mathbf{q}_i\lambda_i} g_{\mathbf{q}_j\lambda_j} \left\langle T_\tau \hat{A}_{\mathbf{q}_i\lambda_i}(\tau_i) \hat{A}_{\mathbf{q}_j\lambda_j}(\tau_j) \right\rangle_0 &= |g_{\mathbf{q}_i\lambda_i}|^2 \left\langle T_\tau \hat{A}_{\mathbf{q}_i\lambda_i}(\tau_i) \hat{A}_{-\mathbf{q}_i\lambda_i}(\tau_j) \right\rangle_0 \delta_{\mathbf{q}_j, -\mathbf{q}_i} \delta_{\lambda_i, \lambda_j} \\ &= -|g_{\mathbf{q}_i\lambda_i}|^2 \mathcal{D}_\lambda^0(\mathbf{q}_i, \tau_i - \tau_j) \delta_{\mathbf{q}_j, -\mathbf{q}_i} \delta_{\lambda_i, \lambda_j}. \end{aligned} \quad (16.13)$$

Note how the thermal average forces the paired momenta to add up to zero. In the final combinatorics the prefactor $(-1)^m/m! = 1/(2n)!$ of Eq. (16.10) is modified as follows. A sign $(-1)^n$ appears from one minus sign in each of the n factors of the form Eq. (16.13). Then a factor $(2n)!/(n!n!)$ appears from choosing the n momenta \mathbf{q}_j among the $2n$ to be the independent momenta. And finally, a factor $n!/2^n$ from all possible ways to combine the remaining n momenta to the chosen ones and symmetrizing the pairs, all choices leading to the same result. Hence we end up with the prefactor $(-1/2)^n/n!$. For each value of n

the $2n$ operators $\hat{P}(\tau_i)$ form n pairs, and we end with the following single-electron Green's function,

$$\mathcal{G}_\sigma(\mathbf{k}, \tau) = - \frac{\sum_{n=0}^{\infty} \frac{(-1)^n}{n!} \int_0^\beta d\tau_1 \dots \int_0^\beta d\tau_n \left\langle T_\tau \hat{P}(\tau_1) \dots \hat{P}(\tau_n) \hat{c}_{\mathbf{k}\sigma}(\tau) \hat{c}_{\mathbf{k}\sigma}^\dagger(0) \right\rangle_0}{\sum_{n=0}^{\infty} \frac{(-1)^n}{n!} \int_0^\beta d\tau_1 \dots \int_0^\beta d\tau_n \left\langle T_\tau \hat{P}(\tau_1) \dots \hat{P}(\tau_n) \right\rangle_0}, \quad (16.14)$$

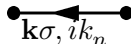

where the $\hat{P}(\tau)$ -integral substituting the original $\hat{P}(\tau)$ -integral of Eq. (16.10) is given by the effective two-particle interaction operator

$$\begin{aligned} \int_0^\beta d\tau_i \hat{P}(\tau_i) = & \int_0^\beta d\tau_i \int_0^\beta d\tau_j \sum_{\mathbf{k}_1\sigma_1} \sum_{\mathbf{k}_2\sigma_2} \sum_{\mathbf{q}\lambda} \frac{1}{2\mathcal{V}^2} |g_{\mathbf{q}\lambda}|^2 \mathcal{D}_\lambda^0(\mathbf{q}, \tau_i - \tau_j) \\ & \times \hat{c}_{\mathbf{k}_1+\mathbf{q},\sigma_1}^\dagger(\tau_j) \hat{c}_{\mathbf{k}_2-\mathbf{q},\sigma_2}^\dagger(\tau_i) \hat{c}_{\mathbf{k}_2\sigma_2}(\tau_i) \hat{c}_{\mathbf{k}_1\sigma_1}(\tau_j). \end{aligned} \quad (16.15)$$

From this interaction operator we can identify a new type of electron-electron interaction $V_{\text{el-el}}^{\text{ph}}$ mediated by the phonons

$$V_{\text{el-el}}^{\text{ph}} = \frac{1}{2\mathcal{V}} \sum_{\mathbf{k}_1\sigma_1} \sum_{\mathbf{k}_2\sigma_2} \sum_{\mathbf{q}\lambda} \frac{1}{\mathcal{V}} |g_{\mathbf{q}\lambda}|^2 \mathcal{D}_\lambda^0(\mathbf{q}, \tau_i - \tau_j) \hat{c}_{\mathbf{k}_1+\mathbf{q},\sigma_1}^\dagger(\tau_j) \hat{c}_{\mathbf{k}_2-\mathbf{q},\sigma_2}^\dagger(\tau_i) \hat{c}_{\mathbf{k}_2\sigma_2}(\tau_i) \hat{c}_{\mathbf{k}_1\sigma_1}(\tau_j). \quad (16.16)$$

This interaction operator resembles the basic two-particle Coulomb interaction operator Eq. (2.34), but while the Coulomb interaction is instantaneous or local in time, the phonon-mediated interaction is retarded, i.e. non-local in time, regarding both the operators and the coupling strength $(1/\mathcal{V}) |g_{\mathbf{q}\lambda}|^2 \mathcal{D}_\lambda^0(\mathbf{q}, \tau_i - \tau_j)$. The derivation of the Feynman rules in Fourier space, however, is the same as for the Coulomb interactions Eq. (12.24):

- (1) Fermion lines with four-momentum orientation:  $\equiv \mathcal{G}_\sigma^0(\mathbf{k}, ik_n)$
- (2) Phonon lines with four-momentum orientation:  $\equiv -\frac{1}{\mathcal{V}} |g_{\mathbf{q}\lambda}|^2 \mathcal{D}_\lambda^0(\mathbf{q}, iq_n)$
- (3) Conserve the spin and four-momentum at each vertex,
i.e. incoming momenta must equal the outgoing, and no spin flipping.
- (4) At order n draw all topologically different connected diagrams containing n oriented phonon lines $-\frac{1}{\mathcal{V}} |g_{\mathbf{q}\lambda}|^2 \mathcal{D}_\lambda^0(\mathbf{q}, iq_n)$, two external fermion lines $\mathcal{G}_\sigma^0(\mathbf{k}, ik_n)$, and $2n$ internal fermion lines $\mathcal{G}_\sigma^0(\mathbf{p}_j, ip_j)$. All vertices must contain an incoming and an outgoing fermion line as well as a phonon line.
- (5) Multiply each fermion loop by -1 .
- (6) Multiply by $\frac{1}{\beta\mathcal{V}}$ for each internal four-momentum \tilde{p} and perform the sum $\sum_{\tilde{p}\sigma\lambda}$.

(16.17)

16.3 Combining Coulomb and electron-phonon interactions

We now discuss the effect of the long range Coulomb interactions between electrons and ions and between electrons themselves. For simplicity we henceforth study only longitudinal phonons and hence drop all reference to the polarization index λ . In Fig. 3.1 we have already sketched the ion plasma oscillation that occurs, if we consider the interaction between the ions and the electron gas assuming the latter to be homogeneous and completely inert, i.e. disregarding all the dynamics of the electrons. A complete calculation is rather tedious, but in Sec. 3.1 we studied the ion plasma oscillations in the jellium model neglecting the electron dynamics. In the case of an ion density $\rho_{\text{ion}}^0 = N/\mathcal{V}$ we found the dispersion-less jellium phonon modes in the long wave length limit,

$$\Omega_{\mathbf{q}} = \Omega = \sqrt{\frac{Z^2 e^2 N}{\epsilon_0 M \mathcal{V}}}. \quad (16.18)$$

The coupling constant for the electron-electron interaction mediated by these jellium phonons is found by combining Eqs. (3.44) and (16.18),

$$\frac{1}{\mathcal{V}} |g_{\mathbf{q}}|^2 = \frac{1}{\mathcal{V}} \left(\frac{Z e^2}{q \epsilon_0} \right)^2 \frac{N \hbar}{2 M \Omega} = \frac{e^2}{\epsilon_0 q^2} \frac{\hbar \Omega}{2} = \frac{1}{2} W(q) \Omega, \quad (16.19)$$

which not surprisingly is proportional to the Coulomb interaction $W(q)$. Note that we have dropped \hbar in the last equality in accordance with the convention introduced in Sec. 5.1. The resulting, bare, phonon-mediated electron-electron interaction is

$$\frac{1}{\mathcal{V}} |g_{\mathbf{q}}|^2 \mathcal{D}^0(\mathbf{q}, i q_n) = W(q) \frac{\Omega^2}{(i q_n)^2 - \Omega^2}. \quad (16.20)$$

To discuss the role of the electron dynamics we now add the electron-electron Coulomb interaction $V_{\text{el-el}}$ of Eq. (2.34) and study the full Hamiltonian H for the electronic and phononic system,

$$H = H_{\text{el}} + V_{\text{el-el}} + H_{\text{ph}} + H_{\text{el-ph}}. \quad (16.21)$$

16.3.1 Migdal's theorem

When the electron-phonon coupling $H_{\text{el-ph}}$ is added, the question naturally arises of whether to study the influence of the electrons on the ions before that of the ions on the electrons, or vice versa. The answer is provided by Migdal's theorem. This theorem is the condensed matter physics analogue to the well-known Born-Oppenheimer approximation of molecular physics. The latter states that it is a good approximation to consider the coordinates \mathbf{R}_i of the slowly moving, heavy ions as parameters in the Schrödinger equation for the fast moving, light electrons, which is then solved. In the second stage the values of \mathbf{R}_i are then changed adiabatically. Likewise, it can be proven by phase space arguments that renormalization of the electron-phonon vertex is suppressed at least by a

factor $\sqrt{m/M} \sim 10^{-2}$, where m and M are the masses of the electron and ion, respectively. We will just outline the proof of Migdal's theorem here by studying the simplest phonon correction to the electron-phonon vertex,

$$\text{Diagram with loop} \approx \sqrt{\frac{m}{M}} \times \text{Bare Diagram} \quad (16.22)$$

The proof builds on a self-consistency assumption. We assume that the high frequency jellium phonons, Ω , get renormalized by electron screening processes to the experimentally observed low frequency acoustic phonons, $\omega_{\mathbf{q}} = v_s q$. If these phonons are used we can prove Eq. (16.22), and if, as shown in the following section, Eq. (16.22) is correct we can prove the assumed phonon renormalization.

The important frequencies for acoustic phonons are smaller than the Debye frequency ω_D , thus we concentrate on phonon frequencies $\omega_{\mathbf{q}} < \omega_D$. The diagram on the left hand side in Eq. (16.22) contains one phonon interaction line and two electron propagators more than the diagram on the right hand side. Now, according to Eq. (16.37) the typical (acoustic) phonon interaction line for low frequencies, $|iq_n| \ll \omega_D$, is $-W(q)/\epsilon^{\text{RPA}}$. Furthermore, due to four-momentum conservation, the two internal electron propagators are confined within ω_D to the Fermi surface. Consequently, a phase space factor of the order ω_D/ϵ_F must appear in front of the usual unrestricted contribution from two such lines, the pair-bubble of Eq. (13.21), $\chi_0 = -d(\epsilon_F)$. The ratio between the values of the two diagrams is therefore roughly given by

$$\frac{W(q)}{\epsilon^{\text{RPA}}} \times \frac{\hbar\omega_D}{\epsilon_F} \times d(\epsilon_F) = \frac{\hbar\omega_D}{\epsilon_F} = \frac{v_s k_D}{\frac{1}{2}v_F k_F} = 2\sqrt{\frac{Z}{3}} \sqrt{\frac{m}{M}} \frac{k_D}{k_F} \approx \sqrt{\frac{m}{M}}, \quad (16.23)$$

where we have used Eqs. (13.22) and (3.5) at the first and third equality sign, respectively. In the following we assume that we can neglect the phonon-induced renormalization of the electron-phonon vertex. We therefore study only the influence of the electronic degrees of freedom on the bare phonon degrees of freedom. The result of the analysis is that the assumption for Migdal's theorem indeed is fulfilled.

16.3.2 Jellium phonons and the effective electron-electron interaction

In more realistic calculations involving interacting electrons we need to consider the sum of the pure electronic Coulomb interaction and the phonon-mediated interaction. This combined interaction will be the basis for our analysis of the interacting electron gas henceforth. Combining the Feynman rules for these two interactions, Eqs. (12.24) and (16.17), yields the following bare, effective electron-electron interaction line,

$$-V_{\text{eff}}^0(\mathbf{q}, iq_n) \equiv -W(\mathbf{q}) - \frac{1}{\mathcal{V}} |g_{\mathbf{q}}|^2 \mathcal{D}^0(\mathbf{q}, iq_n) \quad (16.24)$$

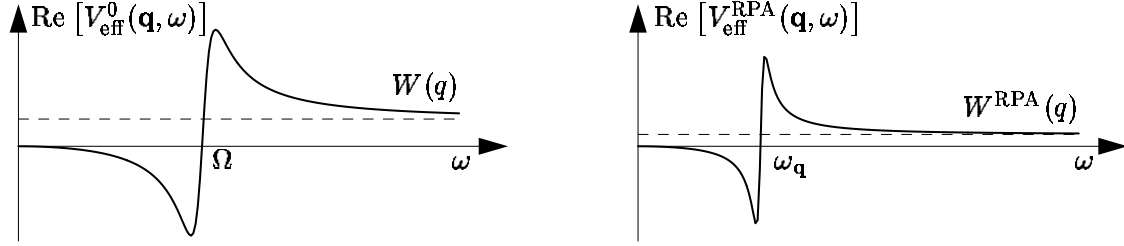


Figure 16.1: (a) The real part of the bare, effective electron-electron interaction $V_{\text{eff}}^0(\mathbf{q}, \omega)$ as a function of the real frequency ω for a given momentum \mathbf{q} . Note that the interaction is attractive for frequencies ω less than the jellium phonon frequency Ω , and that $V_{\text{eff}}^0(\mathbf{q}, \omega) \rightarrow W(q)$ for $\omega \rightarrow \infty$. (b) The same for the RPA renormalized effective electron-electron interaction $V_{\text{eff}}^{\text{RPA}}(\mathbf{q}, \omega)$, see Sec. 16.4. Now, the interaction is attractive for frequencies ω less than the acoustic phonon frequency $\omega_{\mathbf{q}}$, and $V_{\text{eff}}^{\text{RPA}}(\mathbf{q}, \omega) \rightarrow W^{\text{RPA}}(q)$ for $\omega \rightarrow \infty$.

The specific form of V_{eff}^0 is obtained by inserting Eq. (16.20) into Eq. (16.24),

$$V_{\text{eff}}^0(\mathbf{q}, iq_n) = W(q) + W(q) \frac{\Omega^2}{(iq_n)^2 - \Omega^2} = W(q) \frac{(iq_n)^2}{(iq_n)^2 - \Omega^2}, \quad (16.25)$$

or going to real frequencies, $iq_n \rightarrow \omega + i\eta$,

$$V_{\text{eff}}^0(\mathbf{q}, \omega) = W(q) \frac{\omega^2}{\omega^2 - \Omega^2 + i\tilde{\eta}}. \quad (16.26)$$

The real part of $V_{\text{eff}}^0(\mathbf{q}, \omega)$ is shown in Fig. 16.1(a). It is seen that the bare, effective electron-electron interaction becomes negative for $\omega < \Omega$, i.e. at low frequencies the electron-phonon interaction combined with the originally fully repulsive Coulomb interaction results in an attractive effective electron-electron interaction. At high frequencies the normal Coulomb interaction is recovered.

16.4 Phonon renormalization by electron screening in RPA

The electronic Coulomb interaction renormalizes the bare, effective electron-electron interaction. Migdal's theorem leads us to disregard renormalization due to phonon processes and only to consider the most important electron processes. Since $V_{\text{eff}}^0(\mathbf{q})$ is proportional to the bare Coulomb interaction, these processes, according to our main result in Chap. 13, in the limit high electron densities are given by RPA. Before we consider how the phonon propagator is renormalized by the electronic RPA, let us remind ourselves of the following expressions from Chap. 13, Eqs. (13.61)–(13.66) between the dielectric function ϵ^{RPA} , the

density-density correlator $-\chi^{\text{RPA}} = \text{diagram with a shaded box labeled RPA inside a bubble}$, and the simple pair-bubble $-\chi_0 = \text{diagram with a bubble}$,

$$\varepsilon^{\text{RPA}}(\mathbf{q}, iq_n) = 1 - W(q)\chi_0(\mathbf{q}, iq_n), \quad (16.27a)$$

$$\chi^{\text{RPA}}(\mathbf{q}, iq_n) = \frac{\chi_0(\mathbf{q}, iq_n)}{1 - W(q)\chi_0(\mathbf{q}, iq_n)} = \frac{\chi_0(\mathbf{q}, iq_n)}{\varepsilon^{\text{RPA}}(\mathbf{q}, iq_n)}, \quad (16.27b)$$

$$1 + W(q)\chi^{\text{RPA}}(\mathbf{q}, iq_n) = 1 + \frac{W\chi_0}{1 - W\chi_0} = \frac{1}{1 - W\chi_0} = \frac{1}{\varepsilon^{\text{RPA}}(\mathbf{q}, iq_n)}. \quad (16.27c)$$

Returning to the electron-phonon problem, we now extend the RPA-result Eq. (13.68) for W^{RPA} and obtain

$$-V_{\text{eff}}^{\text{RPA}}(\mathbf{q}, iq_n) = \text{diagram with a wavy line} = \text{diagram with a wavy line} + \text{diagram with a wavy line and a bubble}. \quad (16.28)$$

The solution for $V_{\text{eff}}^{\text{RPA}}(\mathbf{q}, iq_n)$ has the standard form

$$-V_{\text{eff}}^{\text{RPA}}(\mathbf{q}, iq_n) = \text{diagram with a wavy line} = \frac{\text{diagram with a wavy line}}{1 - \text{diagram with a bubble}} = \frac{-V_{\text{eff}}^0(\mathbf{q})}{1 - V_{\text{eff}}^0(\mathbf{q})\chi_0(\mathbf{q}, iq_n)}. \quad (16.29)$$

While this expression is correct, a physically more transparent form of $V_{\text{eff}}^{\text{RPA}}$ is obtained by expanding the infinite series Eq. (16.28), and then collecting all the diagrams containing only Coulomb interaction lines into one sum (this simply yields the RPA screened Coulomb interaction W^{RPA}), while collecting the remaining diagrams containing a mix of Coulomb and phonon interaction lines into another sum,

$$-V_{\text{eff}}^{\text{RPA}}(\mathbf{q}, iq_n) = -W^{\text{RPA}}(\mathbf{q}) + \text{diagram with a shaded box labeled RPA inside a bubble} + \text{diagram with a shaded box labeled RPA inside a bubble and a wavy line}. \quad (16.30)$$

Here the renormalized coupling $g_{\mathbf{q}}^{\text{RPA}} [(g_{\mathbf{q}}^{\text{RPA}})^*]$,

$$g_{\mathbf{q}}^{\text{RPA}} \equiv \text{diagram with a shaded box labeled RPA inside a bubble} = \text{diagram with a wavy line} + \text{diagram with a wavy line and a shaded box labeled RPA inside a bubble}, \quad (16.31)$$

is the sum of all diagrams between the outgoing left [incoming right] vertex and the first [last] phonon line, while the renormalized phonon line $\mathcal{D}^{\text{RPA}}(\mathbf{q}, iq_n)$,

$$-\mathcal{D}^{\text{RPA}}(\mathbf{q}, iq_n) = \text{diagram with a shaded box labeled RPA inside a bubble} = \text{diagram with a wavy line} + \text{diagram with a wavy line and a shaded box labeled RPA inside a bubble}, \quad (16.32)$$

is the sum of all diagrams between the first and the last phonon line, i.e. without contributions from the external coupling vertices. The solution for the RPA renormalized phonon line is

$$-\mathcal{D}^{\text{RPA}}(\mathbf{q}, iq_n) = \frac{\text{diagram with a wavy line}}{1 - \text{diagram with a shaded box labeled RPA inside a bubble}} = \frac{-\mathcal{D}^0(\mathbf{q}, iq_n)}{1 - \chi^{\text{RPA}}(\mathbf{q}, iq_n) \frac{1}{V} |g_{\mathbf{q}}|^2 \mathcal{D}^0(\mathbf{q}, iq_n)}. \quad (16.33)$$

Using first Eqs. (16.7) and (16.20) and then Eq. (16.27c) leads to

$$\mathcal{D}^{\text{RPA}}(\mathbf{q}, iq_n) = \frac{2\Omega}{[(iq_n)^2 - \Omega^2] - \Omega^2 W(q) \chi^{\text{RPA}}(\mathbf{q}, iq_n)} = \frac{2\Omega}{(iq_n)^2 - \omega_{\mathbf{q}}^2}, \quad (16.34)$$

where

$$\omega_{\mathbf{q}} \equiv \frac{\Omega}{\sqrt{\varepsilon^{\text{RPA}}(\mathbf{q}, iq_n)}} = \sqrt{\frac{Z^2 e^2 \rho_{\text{ion}}^0}{\varepsilon^{\text{RPA}} \epsilon_0 M}} = \sqrt{\frac{Z e^2 \rho_{\text{el}}^0}{\varepsilon^{\text{RPA}} \epsilon_0 M}}, \quad (16.35)$$

is the renormalized phonon frequency due to electronic RPA screening. In a moment we shall interpret this new frequency, but before doing so we study how also the coupling constant $g_{\mathbf{q}}$ gets renormalized in RPA and acquire the value $g_{\mathbf{q}}^{\text{RPA}}$,

$$g_{\mathbf{q}}^{\text{RPA}} \equiv \text{diagram} = \text{diagram} + \text{diagram} = (1 + W \chi^{\text{RPA}}) g_{\mathbf{q}} = \frac{g_{\mathbf{q}}}{\varepsilon^{\text{RPA}}(\mathbf{q}, iq_n)}. \quad (16.36)$$

The final form of the RPA screened phonon-mediated electron-electron interaction is now obtained by combining Eqs. (16.34) and (16.36),

$$\frac{1}{\mathcal{V}} |g_{\mathbf{q}}^{\text{RPA}}|^2 \mathcal{D}^{\text{RPA}}(\mathbf{q}, iq_n) = - \text{diagram} = \frac{|g_{\mathbf{q}}|^2 / \mathcal{V}}{(\varepsilon^{\text{RPA}})^2} \frac{2\Omega}{(iq_n)^2 - \omega_{\mathbf{q}}^2} = \frac{W(q)}{\varepsilon^{\text{RPA}}} \frac{\omega_{\mathbf{q}}^2}{(iq_n)^2 - \omega_{\mathbf{q}}^2}. \quad (16.37)$$

We now see that this renormalized propagator is identical to the free phonon propagator Eq. (16.20) where the unscreened phonon frequency Ω and the unscreened Coulomb interaction $W(q)$ have been replaced by their RPA screened counterparts $\omega_{\mathbf{q}}$ and $W(q)/\varepsilon^{\text{RPA}}$, respectively.

A further physical interpretation of this result is obtained by evaluating the expression Eq. (16.35) for $\omega_{\mathbf{q}}$ in the static, long wave length limit. We note from Eqs. (13.66) and (13.23) that in this limit $\varepsilon^{\text{RPA}}(\mathbf{q}, iq_n) \rightarrow k_s^2/q^2 = (4k_F/\pi a_0)/q^2$. Inserting this into Eq. (16.35) and using the relation $k_F^3 = 3\pi^2 \rho_{\text{el}}^0$ yields the following explicit form of $\omega_{\mathbf{q}}$:

$$\omega_{\mathbf{q}}(q \rightarrow 0, 0) = \sqrt{\frac{Z e^2 \rho_{\text{el}}^0}{k_s^2 \epsilon_0 M}} q = \sqrt{\frac{Z m}{3M}} v_F q. \quad (16.38)$$

This we recognize as the Bohm-Staver expression Eq. (3.5) for the dispersion of acoustic phonons in the jellium model. The significance of this result is that starting from the microscopic Hamiltonian Eq. (16.21) for the coupled electron and phonon problem, we have used the Feynman diagram technique to show how the phonon spectrum gets renormalized by interacting with the electron gas. The long range Coulomb forces of the non-interacting problem resulted in optical jellium phonons with the high frequency Ω . By introducing the electron-electron interaction the Coulomb forces get screened, and as a result the phonon dispersion gets renormalized to the usual low frequency acoustic dispersion $\omega_{\mathbf{q}} = v_s q$. In more elementary treatments this spectrum is derived by postulating short range forces following Hooke's law, but now we have proven it from first principles.

We end by stating the main result of this section, namely the explicit form of the effective electron-electron interaction due to the combination of the Coulomb and the

electron-phonon interaction, see also Fig. 16.1(b):

$$\begin{aligned}
 -V_{\text{eff}}^{\text{RPA}}(\mathbf{q}, iq_n) &= -W^{\text{RPA}}(\mathbf{q}) - \frac{1}{V} |g_{\mathbf{q}}^{\text{RPA}}|^2 \mathcal{D}^{\text{RPA}}(\mathbf{q}, iq_n) \\
 &= -W^{\text{RPA}}(q) \frac{(iq_n)^2}{(iq_n)^2 - \omega_{\mathbf{q}}^2}.
 \end{aligned} \quad (16.39)$$

16.5 The Cooper instability and Feynman diagrams

In 1956 Cooper discovered that the electron gas in an ordinary metal would become unstable below a certain critical temperature T_c due to the phonon-induced attractive nature of the effective electron-electron interaction $V_{\text{eff}}^{\text{RPA}}(\mathbf{q}, \omega)$ at low frequencies. This discovery soon lead Bardeen, Cooper and Schrieffer (BCS) to develop the microscopic theory explaining superconductivity.

In this section we will derive the Cooper instability using Feynman diagrams. The instability arises because a certain class of electron-electron scattering processes when added coherently yields a divergent scattering amplitude. We will first derive this divergence, and then we will discuss its physical interpretation. The divergence is due to repeated scattering between electron pairs occupying time-reversed states of the form $|\mathbf{k} \uparrow\rangle$ and $|\mathbf{-k} \downarrow\rangle$. Using the four-momentum notation $\tilde{k} = (\mathbf{k}, ik_n)$ we consider the following pair scattering vertex $\Lambda(\tilde{k}, \tilde{p}) = \text{[diagram]}$ given by the infinite ladder-diagram sum over scattering events between time-reversed electron pairs:

$$\begin{aligned}
 \Lambda(\tilde{k}, \tilde{p}) &= \text{[diagram]} + \text{[diagram]} + \text{[diagram]} + \dots \\
 &= \text{[diagram]} + \text{[diagram]} + \text{[diagram]} + \dots
 \end{aligned} \quad (16.40)$$

Suppressing all arguments and stripping away the external electron propagators we can recast Eq. (16.40) in the form of a Dyson equation for the pair-scattering vertex Λ ,

$$\text{[diagram]} = \text{[diagram]} + \text{[diagram]}, \quad (16.41)$$

which is equivalent to the following integral equation

$$\Lambda(\tilde{k}, \tilde{p}) = -V_{\text{eff}}^{\text{RPA}}(\tilde{k} - \tilde{p}) + \frac{1}{V\beta} \sum_{\tilde{q}} \left[-V_{\text{eff}}^{\text{RPA}}(\tilde{k} - \tilde{q}) \right] \mathcal{G}_{\uparrow}^0(\tilde{q}) \mathcal{G}_{\downarrow}^0(-\tilde{q}) \Lambda(\tilde{q}, \tilde{p}). \quad (16.42)$$

To proceed we make a simplifying assumption regarding the functional form of $V_{\text{eff}}^{\text{RPA}}(\mathbf{q}, iq_n)$. First we note that according to our analysis of the electron gas in Chap. 13 no instabilities arise due to the pure Coulomb interaction. Thus we are really only interested in the deviations of $V_{\text{eff}}^{\text{RPA}}(\mathbf{q}, iq_n)$ from $W^{\text{RPA}}(q)$. According to Eq. (16.39) and Fig. 16.1(b), $V_{\text{eff}}^{\text{RPA}}(\mathbf{q}, iq_n)$ rapidly approaches $W^{\text{RPA}}(q)$ for frequencies larger than the given acoustic phonon frequency $\omega_{\mathbf{q}}$, while it becomes attractive instead of repulsive for frequencies below $\omega_{\mathbf{q}}$. Further, according to the Debye model of acoustic phonons, Sec. 3.5, the density of phonon states, $D_{\text{ion}}(\varepsilon)$, is proportional to ε^2 or $\omega_{\mathbf{q}}^2$ for frequencies less than the Debye frequency $\omega_D = v_s k_D$ and zero otherwise, see Eq. (3.27). This means that most of

the phonons encountered have a frequency of the order ω_D . It is therefore a reasonable approximation to set $\omega_{\mathbf{q}} = \omega_D$. Finally, as a last simplification, we set the interaction strength to be constant. Hence we arrive at the model used by Cooper and by BCS:

$$V_{\text{eff}}^{\text{RPA}}(\mathbf{q}, iq_n) \approx \begin{cases} -V, & |iq_n| < \omega_D \\ 0, & |iq_n| > \omega_D. \end{cases} \quad (16.43)$$

The integral equation for $\Lambda(\tilde{k}, \tilde{p})$ thus only involves frequencies less than ω_D , and for those it takes the form

$$\Lambda(\mathbf{k}, \mathbf{p}) = V + \frac{1}{\beta} \sum_{iq_n}^{\omega_D} \frac{1}{V} \sum_{\mathbf{q}} V \mathcal{G}_{\uparrow}^0(\mathbf{q}, iq_n) \mathcal{G}_{\downarrow}^0(-\mathbf{q}, -iq_n) \Lambda(\mathbf{q}, \mathbf{p}). \quad (16.44)$$

The summand on the right hand side does not contain the external momentum \mathbf{k} , whence for the left hand side we conclude $\Lambda(\mathbf{k}, \mathbf{p}) = \Lambda(\mathbf{p})$, and thus for $\Lambda(\mathbf{q}, \mathbf{p})$ in the summand we can write $\Lambda(\mathbf{p})$. Now it is furthermore evident that the \mathbf{p} -dependence occurs only in the Λ -function, hence a consistent solution is obtained by taking $\Lambda(\mathbf{k}, \mathbf{p})$ to be a constant, which we naturally denote Λ . On the right hand side of Eq. (16.44) we can take Λ outside the sum, and solve for it:

$$\Lambda = \frac{V}{1 - \frac{V}{\beta} \sum_{|iq_n| < \omega_D} \frac{1}{V} \sum_{\mathbf{q}} \mathcal{G}_{\uparrow}^0(\mathbf{q}, iq_n) \mathcal{G}_{\downarrow}^0(-\mathbf{q}, -iq_n)}. \quad (16.45)$$

We see that at high temperatures, i.e. $\beta \ll 1/oD$, the resulting pair-interaction Λ equals the attractive pair-interaction strength V from Eq. (16.43). As T is lowered the denominator in Eq. (16.45) can approach zero from above resulting in an arbitrarily strong or divergent pair-interaction strength Λ . In quantum mechanics an infinite scattering amplitude signals a resonance, i.e. in the present case the formation of a bound state between the time-reversed pair of electrons. But in our model this would then happen simultaneously for all electron pairs within a shell of thickness ω_D of the Fermi surface, since the effective pair-interaction is attractive only for energy exchanges less than ω_D . The conclusion is clear: if the pair-interaction strength Λ diverge for a certain critical temperature T_c , the entire Fermi-surface becomes unstable at that temperature, and a new ground state is formed involving bound electron pairs in time-reversed states. This instability is called the Cooper instability, and the on-set of it marks the transition from a normal metallic state to a superconducting state.

The critical temperature $T = T_c$, or $\beta = \beta_c$, for the on-set of the Cooper instability is obtained by setting the denominator in Eq. (16.45) to zero using $\mathcal{G}_{\sigma}^0(\mathbf{q}, iq_n) = 1/(iq_n - \varepsilon_{\mathbf{q}})$

and $q_n = \frac{2\pi}{\beta_c}(n + \frac{1}{2})$:

$$\begin{aligned}
 1 &= \frac{V}{\beta_c} \sum_{|iq_n| < \omega_D} \frac{1}{\mathcal{V}} \sum_{\mathbf{q}} \frac{1}{iq_n - \varepsilon_{\mathbf{q}}} \frac{1}{-iq_n - \varepsilon_{\mathbf{q}}} = \frac{V}{\beta_c} \sum_{|iq_n| < \omega_D} \frac{d(\varepsilon_F)}{2} \int_{-\infty}^{\infty} d\varepsilon \frac{1}{q_n^2 + \varepsilon^2} \\
 &= \frac{V d(\varepsilon_F)}{2\beta_c} \sum_{|iq_n| < \omega_D} \frac{\pi}{|q_n|} = \frac{1}{2} V d(\varepsilon_F) \left[\sum_{n=0}^{\frac{1}{2\pi}\beta_c\omega_D} \frac{1}{n + \frac{1}{2}} - 2 \right] \\
 &\approx \frac{V d(\varepsilon_F)}{2} \ln \left(4 \frac{\beta_c\omega_D}{2\pi} \right), \quad \beta_c\omega_D \gg 1,
 \end{aligned} \tag{16.46}$$

where we use the density of states per spin, $d(\varepsilon_F)/2$. From this equation T_c is found to be

$$k_B T_c \approx \hbar\omega_D e^{-\frac{2}{V d(\varepsilon_F)}}. \tag{16.47}$$

Two important comments can be made at this stage. The first is that although the characteristic phonon energy $\hbar\omega_D$ is of the order 100 K, see e.g. Fig. 3.6b, the critical temperature T_c for the Cooper instability is lowered to about 1 K by the exponential factor. The second comment is that T_c is a non-analytic function of the pair-interaction strength V , since $T_c(V) \propto \exp(-\text{const}/V)$. Consequently, it is not possible to reach the new ground state resulting from the Cooper instability by perturbation theory in V of the normal metallic Fermi sea. These problems will be treated in some of the exercise of this chapter and in much greater detail in the next chapter concerning the BCS theory of superconductivity.

Chapter 17

Superconductivity

17.1 The Cooper instability

17.2 The BCS groundstate

17.3 BCS theory with Green's functions

17.4 Experimental consequences of the BCS states

17.4.1 Tunneling density of states

17.4.2 specific heat

17.5 The Josephson effect

Chapter 18

1D electron gases and Luttinger liquids

18.1 Introduction

18.2 First look at interacting electrons in one dimension

18.2.1 One-dimensional transmission line analog

18.3 The Luttinger-Tomonaga model - spinless case

18.3.1 Interacting one dimensional electron system

18.3.2 Bosonization of Tomonaga model-Hamiltonian

18.3.3 Diagonalization of bosonized Hamiltonian

18.3.4 Real space formulation

18.3.5 Electron operators in bosonized form

18.4 Luttinger liquid with spin**18.5 Green's functions****18.6 Tunneling into spinless Luttinger liquid****18.6.1 Tunneling into the end of Luttinger liquid****18.7 What is a Luttinger liquid?****18.8 Experimental realizations of Luttinger liquid physics****18.8.1 Edge states in the fractional quantum Hall effect****18.8.2 Carbon Nanotubes**

Appendix A

Fourier transformations

Fourier transformation is useful to employ in the case of homogeneous systems or to change linear differential equations into linear algebraic equations. The idea is to resolve the quantity $f(\mathbf{r}, t)$ under study on plane wave components,

$$f_{\mathbf{k}, \omega} e^{i(\mathbf{k} \cdot \mathbf{r} - \omega t)}, \quad (\text{A.1})$$

travelling at the speed $v = \omega/|\mathbf{k}|$.

A.1 Continuous functions in a finite region

Consider a rectangular box in 3D with side lengths L_x, L_y, L_z and a volume $\mathcal{V} = L_x L_y L_z$. The central theorem in Fourier analysis states that any well-behaved function fulfilling the periodic boundary conditions,

$$f(\mathbf{r} + L_x \mathbf{e}_x) = f(\mathbf{r} + L_y \mathbf{e}_y) = f(\mathbf{r} + L_z \mathbf{e}_z) = f(\mathbf{r}) \quad (\text{A.2})$$

can be written as a Fourier series

$$f(\mathbf{r}) = \frac{1}{\mathcal{V}} \sum_{\mathbf{k}} f_{\mathbf{k}} e^{i\mathbf{k} \cdot \mathbf{r}}, \quad \left\{ \begin{array}{l} k_x = \frac{2\pi n_x}{L_x}, \quad n_x = 0, \pm 1, \pm 2, \dots \\ \text{likewise for } y \text{ and } z, \end{array} \right. \quad (\text{A.3})$$

where

$$f_{\mathbf{k}} = \int_{\mathcal{V}} d\mathbf{r} f(\mathbf{r}) e^{-i\mathbf{k} \cdot \mathbf{r}}. \quad (\text{A.4})$$

Note the prefactor $1/\mathcal{V}$ in Eq. (A.3). It is our choice to put it there. Another choice would be to put it in Eq. (A.4), or to put $1/\sqrt{\mathcal{V}}$ in front of both equations. In all cases the product of the normalization constants should be $1/\mathcal{V}$.

An extremely important and very useful theorem states

$$\int d\mathbf{r} e^{-i\mathbf{k} \cdot \mathbf{r}} = \mathcal{V} \delta_{\mathbf{k}, 0}, \quad \frac{1}{\mathcal{V}} \sum_{\mathbf{k}} e^{i\mathbf{k} \cdot \mathbf{r}} = \delta(\mathbf{r}). \quad (\text{A.5})$$

Note the dimensions in these two expressions so that you do not forget where to put the factors of \mathcal{V} and $1/\mathcal{V}$. Note also that by using Eq. (A.5) you can prove that Fourier transforming from \mathbf{r} to \mathbf{k} and then back brings you back to the starting point: insert $f_{\mathbf{k}}$ from Eq. (A.4) into the expression for $f(\mathbf{r})$ in Eq. (A.3) and reduce by use of Eq. (A.5).

A.2 Continuous functions in an infinite region

If we let \mathcal{V} tend to infinity the \mathbf{k} -vectors become quasi-continuous variables, and the \mathbf{k} -sum in Eq. (A.3) is converted into an integral,

$$f(\mathbf{r}) = \frac{1}{\mathcal{V}} \sum_{\mathbf{k}} f_{\mathbf{k}} e^{i\mathbf{k}\cdot\mathbf{r}} \xrightarrow{\mathcal{V} \rightarrow \infty} \frac{1}{\mathcal{V}} \frac{\mathcal{V}}{(2\pi)^3} \int d\mathbf{k} f_{\mathbf{k}} e^{i\mathbf{k}\cdot\mathbf{r}} = \int \frac{d\mathbf{k}}{(2\pi)^3} f_{\mathbf{k}} e^{i\mathbf{k}\cdot\mathbf{r}}. \quad (\text{A.6})$$

Now you see why we choose to put $1/\mathcal{V}$ in front of $\sum_{\mathbf{k}}$. We have

$$f(\mathbf{r}) = \int \frac{d\mathbf{k}}{(2\pi)^3} f_{\mathbf{k}} e^{i\mathbf{k}\cdot\mathbf{r}}, \quad f_{\mathbf{k}} = \int d\mathbf{r} f(\mathbf{r}) e^{-i\mathbf{k}\cdot\mathbf{r}}, \quad (\text{A.7})$$

and also

$$\int \frac{d\mathbf{k}}{(2\pi)^3} e^{i\mathbf{k}\cdot\mathbf{r}} = \delta(\mathbf{r}), \quad \int d\mathbf{r} e^{-i\mathbf{k}\cdot\mathbf{r}} = (2\pi)^3 \delta(\mathbf{k}). \quad (\text{A.8})$$

Note that the dimensions are okay. Again it is easy to use these expressions to verify that Fourier transforming twice brings you back to the starting point.

A.3 Time and frequency Fourier transforms

The time t and frequency ω transforms can be thought of as an extension of functions periodic with the finite period \mathcal{T} , to the case where this period tends to infinity. Thus t plays the role of \mathbf{r} and ω that of \mathbf{k} , and in complete analogy with Eq. (A.7) – but with the opposite sign of i due to Eq. (A.1) – we have

$$f(t) = \int_{-\infty}^{\infty} \frac{d\omega}{2\pi} f_{\omega} e^{-i\omega t}, \quad f_{\omega} = \int_{-\infty}^{\infty} dt f(t) e^{i\omega t}, \quad (\text{A.9})$$

and also

$$\int_{-\infty}^{\infty} \frac{d\omega}{2\pi} e^{-i\omega t} = \delta(t), \quad \int_{-\infty}^{\infty} dt e^{i\omega t} = 2\pi \delta(\omega). \quad (\text{A.10})$$

Note again that the dimensions are okay.

A.4 Some useful rules

We can think of Eqs. (A.5), (A.8) and (A.10) as the Fourier transform of the constant function $f = 1$ to delta functions (and back):

$$1_{\mathbf{r}} \longleftrightarrow \mathcal{V} \delta_{\mathbf{k},0}, \quad 1_{\mathbf{k}} \longleftrightarrow \delta(\mathbf{r}), \quad \text{discrete } \mathbf{k}, \quad (\text{A.11a})$$

$$1_{\mathbf{r}} \longleftrightarrow (2\pi)^3 \delta(\mathbf{k}), \quad 1_{\mathbf{k}} \longleftrightarrow \delta(\mathbf{r}), \quad \text{continuous } \mathbf{k}, \quad (\text{A.11b})$$

$$1_t \longleftrightarrow 2\pi \delta(\omega), \quad 1_{\omega} \longleftrightarrow \delta(t), \quad \text{continuous } \omega. \quad (\text{A.11c})$$

Another useful rule is the rule for Fourier transforming convolution integrals. By direct application of the definitions and Eq. (A.8) we find

$$f(\mathbf{r}) = \int d\mathbf{s} h(\mathbf{r}-\mathbf{s}) g(\mathbf{s}) = \int d\mathbf{s} \frac{1}{\mathcal{V}^2} \sum_{\mathbf{k}, \mathbf{k}'} h_{\mathbf{k}} e^{i\mathbf{k} \cdot (\mathbf{r}-\mathbf{s})} g_{\mathbf{k}'} e^{i\mathbf{k}' \cdot \mathbf{s}} = \frac{1}{\mathcal{V}} \sum_{\mathbf{k}} h_{\mathbf{k}} g_{\mathbf{k}} e^{i\mathbf{k} \cdot \mathbf{r}}, \quad (\text{A.12})$$

or in words: a convolution integral in \mathbf{r} -space becomes a product in \mathbf{k} -space.

$$\int d\mathbf{s} h(\mathbf{r}-\mathbf{s}) g(\mathbf{s}) \longleftrightarrow h_{\mathbf{k}} g_{\mathbf{k}}. \quad (\text{A.13})$$

A related rule, the invariance of inner products going from \mathbf{r} to \mathbf{k} , is derived in a similar way (and here given in three different versions):

$$\int d\mathbf{r} h(\mathbf{r}) g^*(\mathbf{r}) = \int \frac{d\mathbf{k}}{(2\pi)^3} h_{\mathbf{k}} g_{\mathbf{k}}^*, \quad (\text{A.14})$$

$$\int d\mathbf{r} h(\mathbf{r}) g(\mathbf{r}) = \int \frac{d\mathbf{k}}{(2\pi)^3} h_{\mathbf{k}} g_{-\mathbf{k}}, \quad (\text{A.15})$$

$$\int d\mathbf{r} h(\mathbf{r}) g(-\mathbf{r}) = \int \frac{d\mathbf{k}}{(2\pi)^3} h_{\mathbf{k}} g_{\mathbf{k}}. \quad (\text{A.16})$$

Finally we mention the Fourier transformation of differential operators. For the gradient operator we have

$$\nabla_{\mathbf{r}} f(\mathbf{r}) = \nabla_{\mathbf{r}} \frac{1}{\mathcal{V}} \sum_{\mathbf{k}} f_{\mathbf{k}} e^{i\mathbf{k} \cdot \mathbf{r}} = \frac{1}{\mathcal{V}} \sum_{\mathbf{k}} f_{\mathbf{k}} \nabla_{\mathbf{r}} e^{i\mathbf{k} \cdot \mathbf{r}} = \frac{1}{\mathcal{V}} \sum_{\mathbf{k}} i\mathbf{k} f_{\mathbf{k}} e^{i\mathbf{k} \cdot \mathbf{r}}. \quad (\text{A.17})$$

Similarly for ∇^2 , $\nabla \times$, and ∂_t (remember the sign change of i in the latter):

$$\nabla_{\mathbf{r}} \longleftrightarrow i\mathbf{k}, \quad \partial_t \longleftrightarrow -i\omega, \quad (\text{A.18})$$

$$\nabla^2 \longleftrightarrow -\mathbf{k}^2, \quad \nabla \times \longleftrightarrow i\mathbf{k} \times. \quad (\text{A.19})$$

A.5 Translation invariant systems

We study a translation invariant system. Any physical observable $f(\mathbf{r}, \mathbf{r}')$ of two spatial variables \mathbf{r} and \mathbf{r}' can only depend on the difference between the coordinates and not on the absolute position of any of them,

$$f(\mathbf{r}, \mathbf{r}') = f(\mathbf{r}-\mathbf{r}'). \quad (\text{A.20})$$

The consequences in \mathbf{k} -space from this constraint are:

$$f(\mathbf{r}, \mathbf{r}') = \int \frac{d\mathbf{k}}{(2\pi)^3} \int \frac{d\mathbf{k}'}{(2\pi)^3} f_{\mathbf{k}, \mathbf{k}'} e^{i\mathbf{k} \cdot \mathbf{r}} e^{i\mathbf{k}' \cdot \mathbf{r}'} = \int \frac{d\mathbf{k}}{(2\pi)^3} \int \frac{d\mathbf{k}'}{(2\pi)^3} f_{\mathbf{k}, \mathbf{k}'} e^{i\mathbf{k} \cdot (\mathbf{r}-\mathbf{r}')} e^{i(\mathbf{k}'+\mathbf{k}) \cdot \mathbf{r}'}. \quad (\text{A.21})$$

Since this has to be a function of $\mathbf{r} - \mathbf{r}'$, it is obvious from the factor $e^{i(\mathbf{k}'+\mathbf{k}) \cdot \mathbf{r}'}$ that any reference to the absolute value of \mathbf{r}' only can vanish if $\mathbf{k}' = -\mathbf{k}$, and thus $f_{\mathbf{k}, \mathbf{k}'} \propto \delta(\mathbf{k} + \mathbf{k}')$.

To find the proportionality constant, we can also find the Fourier transform of f by explicitly using that f only depends on the difference $\mathbf{r} - \mathbf{r}'$

$$f(\mathbf{r}, \mathbf{r}') = \tilde{f}(\mathbf{r} - \mathbf{r}') = \int \frac{d\mathbf{k}}{(2\pi)^3} \tilde{f}_{\mathbf{k}} e^{i\mathbf{k} \cdot (\mathbf{r} - \mathbf{r}')}, \quad (\text{A.22})$$

and by comparing the two expressions Eqs. (A.21) and (A.22) we read off that

$$f_{\mathbf{k}, \mathbf{k}'} = (2\pi)^3 \delta(\mathbf{k} + \mathbf{k}') \tilde{f}_{\mathbf{k}}, \quad (\text{A.23})$$

or in short

$$f(\mathbf{r}, \mathbf{r}') \longleftrightarrow f_{\mathbf{k}, -\mathbf{k}'}, \quad \text{translation-invariant systems.} \quad (\text{A.24})$$

For the discrete case, we can go through the same arguments or use the formulae from above to get

$$f_{\mathbf{k}, \mathbf{k}'} = \mathcal{V} \delta_{\mathbf{k}, -\mathbf{k}'} \tilde{f}_{\mathbf{k}}. \quad (\text{A.25})$$

This result is used several times in the main text when we consider correlation functions of the form

$$g(\mathbf{r}, \mathbf{r}') = \langle \mathcal{A}(\mathbf{r}) \mathcal{B}(\mathbf{r}') \rangle, \quad (\text{A.26})$$

where \mathcal{A} and \mathcal{B} are some operators. For a translation-invariant system we now that $g(\mathbf{r}, \mathbf{r}') = g(\mathbf{r} - \mathbf{r}')$, and by using the result in Eq. (A.25) for $\mathbf{k} = -\mathbf{k}'$ we get that

$$g(\mathbf{k}) = \frac{1}{\mathcal{V}} \langle \mathcal{A}(\mathbf{k}) \mathcal{B}(-\mathbf{k}) \rangle. \quad (\text{A.27})$$

Appendix B

Exercises

Exercises for Chapter 1

Exercise 1.1

Prove Eq. (1.63) for fermions: $T_{\text{tot}} = \sum_{\nu_i, \nu_j} T_{\nu_i \nu_j} c_{\nu_i}^\dagger c_{\nu_j}$. Hints: write Eq. (1.60) with fermion operators c_ν^\dagger . Argue why in this case one has $c_{\nu_b}^\dagger = c_{\nu_b}^\dagger c_{\nu_{n_j}} c_{\nu_{n_j}}^\dagger$. Obtain the fermion analogue of Eq. (1.62) by moving the pair $c_{\nu_b}^\dagger c_{\nu_{n_j}}$ to the left. What about the fermion anti-commutator sign?

Exercise 1.2

Find the current density operator \mathbf{J} in terms of the arbitrary single particle basis states ψ_ν and the corresponding creation and annihilation operators a_ν^\dagger and a_ν . Hint: use the basis transformations Eq. (1.67) in the real space representation Eq. (1.99a).

Exercise 1.3

In some crystals the valence electrons are rather tightly bound to their host ions. A good starting point for analyzing such systems is to describe the kinetic energy by hopping processes, where with the probability amplitude t one valence electron can hop from an ion j to one of the nearest neighbor ions $j + \delta$ (as usual $\{c_j^\dagger, c_{j'}\} = \delta_{j,j'}$):

$$H = -t \sum_{j\delta} c_{j+\delta}^\dagger c_j,$$

This Hamiltonian is known as the tight-binding Hamiltonian.

(a) Consider a 1D lattice with N sites, periodic boundary conditions, and a lattice constant a . Here $j = 1, 2, \dots, N$ and $\delta = \pm 1$. Use the discrete Fourier transformation $c_j = (1/\sqrt{N}) \sum_k e^{ikja} c_k$ to diagonalize H in k -space and plot the eigenvalues ε_k as a function of k .

(b) In the high-temperature superconductors the conduction electrons are confined to parallel CuO-planes, where the ions form a 2D square lattice. In this case the 2D tight-binding model is applicable. Generalize the 1D model to a 2D square lattice also with the lattice constant a and plot contours of constant energy $\varepsilon_{k_x k_y}$ in the $k_x k_y$ plane.

Exercise 1.4

Consider a bosonic particle moving in 1D with the Hamiltonian

$$H = \hbar\omega \left(a^\dagger a + \frac{1}{2} \right) + \hbar\omega_0 \left(a^\dagger + a \right),$$

where $[a, a^\dagger] = 1$, while ω and ω_0 are positive constants. Diagonalize H by introducing the operator $\alpha \equiv a + \omega_0/\omega$ and its Hermitian conjugate α^\dagger , and determine the eigenenergies. What might be the physical origin of the second term in H (see Sec. 1.4.1)? Compare the result to a classical and a first quantized treatment of the problem.

Exercise 1.5

The Yukawa potential is defined as $V^{k_s}(\mathbf{r}) = \frac{e_0^2}{r} e^{-k_s r}$, with k_s being some real positive constant with the dimensions of a wavevector. Prove that the Fourier transform is $V_{\mathbf{q}}^{k_s} = \frac{4\pi e_0^2}{q^2 + k_s^2}$. Relate the result to the Coulomb potential. Hints: work in polar coordinates $\mathbf{r} = (r, \theta, \phi)$, and perform the $\int_0^{2\pi} d\phi$ and $\int_{-1}^{+1} d(\cos \theta)$ integrals first. The remaining $\int_0^\infty r^2 dr$ integral is a simple integral of the sum of two exponential functions.

Exercises for Chapter 2

Exercise 2.1

Iron (Fe) in its metallic state has valence II, and X-ray measurements have revealed that it forms a body-centered-cubic (BCC) crystal with side length $a = 0.287$ nm. Calculate the density n of the resulting gas of valence electrons, and use this value to determine the microscopic parameters k_F , ε_F , v_F , and λ_F .

Exercise 2.2

Use the variational principle to argue that although the expression Eq. (2.43) is not exact near the energy minimum density $r_s = r_s^* = 4.83$, the result $E^*/N = -1.29$ eV nevertheless ensures the stability of the electron gas.

Exercise 2.3

Starting from Eqs. (2.34) and (2.45) derive the expression Eq. (2.47) for the contributions from the direct Coulomb interaction processes to the interaction energy in second order perturbation theory.

Exercise 2.4

In Sec. 2.3.2 we saw an example of the existence of 2D electron gases in GaAs/Ga_{1-x}Al_xAs heterostructures. Derive, in analogy with the 3D case, the relation between the 2D Fermi wave vector k_F and the 2D electron density: $k_F^2 = 2\pi n$. Use the result to derive the 2D density of states per area, $d(\varepsilon)$.

Exercise 2.5

In Sec. 2.3.3 we saw an example of the existence of 1D electron gases in carbon nanotubes. Derive, in analogy with the 3D case, the relation between the 1D Fermi wave vector k_F and the 1D density of states per length, $d(\varepsilon)$. Use the result to derive the 1D electron density: $k_F = 2n/\pi$.

Exercises for Chapter 3**Exercise 3.1**

We want to study the influence of electron-phonon scattering on a given electron state $|\mathbf{k}\sigma\rangle$ using the simple Hamiltonian $H_{\text{el-ph}}^{\text{INA}}$ of Eq. (3.41). For simplicity we restrict our study to processes that scatter electrons out of $|\mathbf{k}\sigma\rangle$.

(a) Argue that in this case we need only consider the simple phonon absorption and emission processes given by

$$H_{\text{el-ph}} = H_{\text{el-ph}}^{\text{abs}} + H_{\text{el-ph}}^{\text{emi}} = \sum_{\mathbf{q}} g_{\mathbf{q}} c_{\mathbf{k}+\mathbf{q},\sigma}^{\dagger} c_{\mathbf{k}\sigma} b_{\mathbf{q}} + \sum_{\mathbf{q}} g_{\mathbf{q}} c_{\mathbf{k}+\mathbf{q},\sigma}^{\dagger} c_{\mathbf{k}\sigma} b_{-\mathbf{q}}^{\dagger}.$$

(b) The scattering rate corresponding to the emission processes is denoted $\tau_{\mathbf{k}}^{\text{emi}}$. It can be estimated using Fermi's Golden Rule (suppressing the unimportant spin index):

$$\frac{1}{\tau_{\mathbf{k}}^{\text{emi}}} = \frac{2\pi}{\hbar} \sum_f \left| \langle f | H_{\text{el-ph}}^{\text{emi}} | i \rangle \right|^2 \delta(E_f - E_i),$$

involving a sum over all possible final states with energy $E_f = E_i$, and an initial state $|i\rangle$ having the energy E_i and being specified by the occupation numbers $n_{\mathbf{k}\sigma}$ and $N_{\mathbf{q}}$ for electron states $|\mathbf{k}\sigma\rangle$ and phonon states $|\mathbf{q}\rangle$ (see Eq. (1.108)). Assume that $|i\rangle$ is a simple but unspecified product state, i.e. $|i\rangle = \left(\prod_{\{\mathbf{k}\sigma\}_i} c_{\mathbf{k}\sigma}^{\dagger} \right) \left(\prod_{\{\mathbf{q}\}_i} \frac{1}{\sqrt{N_{\mathbf{q}}!}} \left[b_{\mathbf{q}}^{\dagger} \right]^{N_{\mathbf{q}}} \right) |0\rangle$, and show that for a given $\mathbf{q} \neq 0$ in $H_{\text{el-ph}}^{\text{emi}}$ the only possible normalized final states is $\frac{1}{\sqrt{N_{\mathbf{q}}+1}} c_{\mathbf{k}+\mathbf{q}}^{\dagger} c_{\mathbf{k}} b_{\mathbf{q}}^{\dagger} |i\rangle$.

(c) Show for the state $|i\rangle$ that

$$\frac{1}{\tau_{\mathbf{k}}^{\text{emi}}} = \frac{2\pi}{\hbar} \sum_{\mathbf{q}} |g_{\mathbf{q}}|^2 (N_{\mathbf{q}}^i + 1) (1 - n_{\mathbf{k}+\mathbf{q}}^i) n_{\mathbf{k}}^i \delta(\varepsilon_{\mathbf{k}+\mathbf{q}} - \varepsilon_{\mathbf{k}} + \hbar\omega_{\mathbf{q}}).$$

Derive the analogous expression for the scattering rate $1/\tau_{\mathbf{k}}^{\text{abs}}$ due to absorption.

(d) Keeping $n_{\mathbf{k}} = 1$ fixed for our chosen state, argue why thermal averaging leads to

$$\frac{1}{\tau_{\mathbf{k}}^{\text{emi}}} = \frac{2\pi}{\hbar} \sum_{\mathbf{q}} |g_{\mathbf{q}}|^2 [n_{\text{B}}(\omega_{\mathbf{q}}) + 1] [1 - n_{\text{F}}(\varepsilon_{\mathbf{k}+\mathbf{q}})] \delta(\varepsilon_{\mathbf{k}+\mathbf{q}} - \varepsilon_{\mathbf{k}} + \hbar\omega_{\mathbf{q}}).$$

Exercise 3.2

We now determine the temperature dependence of the scattering rate $\tau_{\mathbf{k}}^{\text{emi}}$ in the high and low temperature limits. This immediately gives us the behavior of the total scattering rate $1/\tau_{\mathbf{k}} = 1/\tau_{\mathbf{k}}^{\text{emi}} + 1/\tau_{\mathbf{k}}^{\text{abs}}$, since at low T , due to the lack of phonons, $1/\tau_{\mathbf{k}}^{\text{abs}} \approx 0$, while at high T we have $1/\tau_{\mathbf{k}}^{\text{emi}} \approx 1/\tau_{\mathbf{k}}^{\text{abs}}$.

(a) To obtain realistic results we need to use the screened Coulomb or Yukawa potential for the ionic potential $V_{\mathbf{q}}$ (see Eq. (3.42) and Exercise 1.5). The electrons redistribute in an attempt to neutralize the ionic potential. As we shall see in Chap. 13 they succeed to do so for distances further away than $1/k_s$ from the ion. Show by dimensional analysis involving the Fourier component $e^2/(\epsilon_0 k_s^2)$, the Fermi energy ε_{F} , and the electron density n that $k_s^2 \approx k_{\text{F}}/a_0$.

(b) Show how Eq. (3.42) together with $\mathbf{k}' = \mathbf{k} + \mathbf{q}$ change $\frac{1}{\tau_{\mathbf{k}}^{\text{emi}}}$ from Exercise 3.1d to

$$\frac{1}{\tau_{\mathbf{k}}^{\text{emi}}} \propto \frac{2\pi}{\hbar} \sum_{\mathbf{q}} \omega_{\mathbf{q}} [n_{\text{B}}(\omega_{\mathbf{q}}) + 1] [1 - n_{\text{F}}(\varepsilon_{\mathbf{k}'})] \delta(\varepsilon_{\mathbf{k}'} - \varepsilon_{\mathbf{k}} + \hbar\omega_{\mathbf{q}}),$$

where we here and in the following do not care about the numerical prefactors.

(c) As usual, we are mainly interested in electrons moving relatively close to the Fermi surface (why?), i.e. $k', k \approx k_{\text{F}}$. Furthermore, we employ the Debye model of the phonon spectrum (see Sec. 3.5): $\omega_{\mathbf{q}} = v_{\text{D}} q$. We note that since \mathbf{k}' and \mathbf{k} are tied to the Fermi surface the largest q is $2k_{\text{F}}$, and the corresponding largest phonon energy is denoted $\hbar\omega_{\text{max}} \equiv 2v_{\text{D}} k_{\text{F}}$. Now use polar coordinates to obtain $\sum_{\mathbf{k}'} \propto \int d\varepsilon_{\mathbf{k}'} \int_{-1}^1 d(\cos \theta)$, and show using $q^2 = |\mathbf{k}' - \mathbf{k}|^2$ that $d(\cos \theta) \propto q dq$. With this prove that

$$\int_{-1}^1 d(\cos \theta) \delta(\varepsilon_{\mathbf{k}'} - \varepsilon_{\mathbf{k}} + \hbar\omega_{\mathbf{q}}) \propto \int_0^{2k_{\text{F}}} q dq \delta(\varepsilon_{\mathbf{k}'} - \varepsilon_{\mathbf{k}} + \hbar\omega_{\mathbf{q}}) \propto \begin{cases} \omega_{\mathbf{q}}, & \varepsilon_{\mathbf{k}} - \varepsilon_{\mathbf{k}'} < \hbar\omega_{\text{max}} \\ 0, & \varepsilon_{\mathbf{k}} - \varepsilon_{\mathbf{k}'} > \hbar\omega_{\text{max}} \end{cases}$$

Since $d\varepsilon_{\mathbf{k}'} = \hbar d\omega_{\mathbf{q}}$ show in the limit $\hbar\omega_{\text{max}} \ll \varepsilon_{\mathbf{k}} - \varepsilon_{\text{F}} \ll \varepsilon_{\text{F}}$ how to obtain

$$\frac{1}{\tau_{\mathbf{k}}^{\text{emi}}} \propto \int_0^{\omega_{\text{max}}} d\omega_{\mathbf{q}} \omega_{\mathbf{q}}^2 [n_{\text{B}}(\omega_{\mathbf{q}}) + 1] [1 - n_{\text{F}}(\varepsilon_{\mathbf{k}'})] \approx \int_0^{\omega_{\text{max}}} d\omega_{\mathbf{q}} \omega_{\mathbf{q}}^2 [n_{\text{B}}(\omega_{\mathbf{q}}) + 1].$$

(d) Show that the result in (c) leads to the following temperature dependencies:

$$\frac{1}{\tau_{\mathbf{k}}^{\text{emi}}} \propto \begin{cases} T, & \text{for } T \gg \hbar\omega_{\text{max}}/k_{\text{B}} \\ T^3 + \text{const.}, & \text{for } T \ll \hbar\omega_{\text{max}}/k_{\text{B}}. \end{cases}$$

Exercise 3.3

In analogy with the homogeneous 1D chain of Sec. 3.3 we now want to find the eigenmodes of the linear 1D chain with lattice constant a mentioned in Fig. 3.3(c). The ionic lattice has a unit cell with two different ions \bullet and \circ , respectively. All spring constants are the same, namely K . The masses, the momenta, and the displacements of the \bullet ions are denoted m , p_j and u_j , while for the \circ ions they are denoted M , P_j and U_j . The sites are numbered by j as $\dots, u_{j-1}, U_{j-1}, u_j, U_j, u_{j+1}, U_{j+1}, \dots$

(a) Verify that the Hamiltonian of the two-atoms-per-unit-cell chain is

$$H = \sum_j \left[\frac{1}{2m} p_j^2 + \frac{1}{2M} P_j^2 + \frac{1}{2} K (u_j - U_{j-1})^2 + \frac{1}{2} K (U_j - u_j)^2 \right]$$

(b) Use Hamilton's equations $\dot{u}_j = \frac{\partial H}{\partial p_j}$ and $\dot{p}_j = -\frac{\partial H}{\partial u_j}$ (similar for \dot{U}_j and \dot{P}_j), to obtain the equations for \ddot{u}_j and \ddot{U}_j .

(c) Assume the harmonic solutions $u_j \equiv u_k e^{i(kja - \omega t)}$ and $U_j \equiv U_k e^{i(kja - \omega t)}$ to derive a 2×2 matrix eigenvalue equation for (u_k, U_k) . Verify the dispersion curve $\omega_{\mathbf{k}}$ displayed in Fig. 3.3(c) and the eigenmode displayed in Fig. 3.4.

(d) Check that in the limit $M = m$ the dispersion ω_k in Eq. (3.9) of the one-atom-per-unit-cell is recovered.

Exercise 3.4

The task is to prove the Bohm-Staver expression Eq. (3.5). We study the situation described in Sec. 3.2, where the light and mobile electrons always follow the motion of the slow and heavy ions to maintain local charge neutrality. The ions are treated as the jellium of Sec. 3.1.

(a) Multiply the continuity equation by the ion mass M to obtain

$$M \partial_t \rho_{\text{ion}} + \nabla \cdot \boldsymbol{\pi} = 0,$$

where $\boldsymbol{\pi}$ is the momentum density.

(b) Take the time derivative and note that $\dot{\boldsymbol{\pi}}$ is the force density \mathbf{f} , which on the other hand is equal to the pressure gradient $-\nabla P$ due to the compression of the electron gas following the ionic motion:

$$\dot{\boldsymbol{\pi}} = \mathbf{f} = -\nabla P = \nabla \left(\frac{\partial E^{(0)}}{\partial \mathcal{V}} \right)_N,$$

where the electron gas ground state energy $E^{(0)}$ is given in Eq. (2.28).

(c) Combine the equations and derive the wave equation for ρ_{ion} , from which the (square of the) sound velocity v_s is read off:

$$M \partial_t^2 \rho_{\text{ion}} - \frac{2Z}{3} \varepsilon_F \nabla^2 \rho_{\text{ion}} = 0.$$

Exercise 3.5

Electrons and phonons in the jellium model In this exercise we quantize the jellium model of the ion system in a solid and derive the electron phonon interaction in a way which is somewhat different from the method used in the main text.

We take the case of a monovalent metal, i.e. each ion has charge $+e$. Because the system is charge neutral as a whole, we need only take into account interactions between deviations from equilibrium. We define

$$\begin{aligned}\rho_{\text{ion}}(\mathbf{r}) &= \rho_{\text{ion}}^0 + \delta\rho_{\text{ion}}(\mathbf{r}) \equiv \rho_{\text{ion}}^0 + \rho_{\text{ion}}^0 \nabla \cdot \mathbf{u}(\mathbf{r}), \\ \rho(\mathbf{r}) &= \rho_{\text{ion}}^0 + \delta\rho(\mathbf{r}),\end{aligned}$$

where \mathbf{u} is a displacement field describing the deviation of the ion density from equilibrium, and $\rho(\mathbf{r})$ is the electron density. The potential energy contributions which involves the ionic system are the ion-ion interaction and the electron-ion interaction

$$\begin{aligned}E_{\text{pot}}^{\text{ion-ion}} &= \frac{1}{2} \int d\mathbf{r} d\mathbf{r}' \delta\rho_{\text{ion}}(\mathbf{r}) V(\mathbf{r} - \mathbf{r}') \delta\rho_{\text{ion}}(\mathbf{r}'), \\ E_{\text{pot}}^{\text{ion-el}} &= - \int d\mathbf{r} d\mathbf{r}' \delta\rho(\mathbf{r}) V(\mathbf{r} - \mathbf{r}') \delta\rho_{\text{ion}}(\mathbf{r}'),\end{aligned}$$

with the usual definition

$$E_{\text{pot}}^{\text{el-el}} = \frac{1}{2} \int d\mathbf{r} d\mathbf{r}' \delta\rho(\mathbf{r}) V(\mathbf{r} - \mathbf{r}') \delta\rho(\mathbf{r}').$$

We have not explicitly included the electron-electron interaction here. When included it gives rise to the term in Eq. (2.34).

First we quantize the ion system and we start by looking at the isolated ion system. The classical Lagrangian for this system is

$$\begin{aligned}L_{\text{ion}}^0 &= T_{\text{ion}} - V_{\text{ion}} \\ T_{\text{ion}}^0 &= \frac{1}{2} \int d\mathbf{r} M \rho_{\text{ion}}(\mathbf{r}) v^2(\mathbf{r}) \\ V_{\text{ion}} &= E_{\text{pot}}^{\text{ion-ion}},\end{aligned}$$

where \mathbf{v} is the velocity field of the ions. Because we are interested in the low energy excitations we linearize the kinetic such that

$$T = \frac{1}{2} \int d\mathbf{r} M \rho_{\text{ion}}^0 v^2(\mathbf{r}).$$

Using particle conservation show that

$$\mathbf{v}(\mathbf{r}) = -\dot{\mathbf{u}}(\mathbf{r})$$

and using this, derive the Lagrangian as a functional of \mathbf{u}

$$L_{\text{ion}}^0[\mathbf{u}] = \frac{1}{2} \int d\mathbf{r} M \rho_{\text{ion}}^0 |\dot{\mathbf{u}}(\mathbf{r})|^2 - \frac{(\rho_{\text{ion}}^0)^2}{2} \int d\mathbf{r} d\mathbf{r}' [\nabla \cdot \mathbf{u}(\mathbf{r})] V(\mathbf{r} - \mathbf{r}') [\nabla \cdot \mathbf{u}(\mathbf{r}')].$$

Because the Lagrangian is quadratic in \mathbf{u} it is equivalent to a set of harmonic oscillators that describe sound waves of the ion system. What dispersion relation do you expect?

Next you should quantize the ion system and find the Hamiltonian. First show that the canonical momentum corresponding to the field \mathbf{u} is

$$\mathbf{p}(\mathbf{r}) = M\rho_{\text{ion}}^0 \dot{\mathbf{u}}(\mathbf{r}),$$

and show, using the well known relation $H = \int \mathbf{p} \cdot \dot{\mathbf{u}} - L$, that

$$\begin{aligned} H_{\text{ion}}^0 &= \frac{1}{2} \int d\mathbf{r} \frac{p^2(\mathbf{r})}{M\rho_{\text{ion}}^0} + \frac{(\rho_{\text{ion}}^0)^2}{2} \int d\mathbf{r} d\mathbf{r}' [\nabla \cdot \mathbf{u}(\mathbf{r})] V(\mathbf{r} - \mathbf{r}') [\nabla \cdot \mathbf{u}(\mathbf{r}')] \\ &= \frac{1}{2\mathcal{V}} \sum_{\mathbf{q}} \frac{\mathbf{p}(\mathbf{q}) \cdot \mathbf{p}(-\mathbf{q})}{M\rho_{\text{ion}}^0} + \frac{(\rho_{\text{ion}}^0)^2}{2\mathcal{V}} \sum_{\mathbf{q}} V(\mathbf{q}) [\mathbf{q} \cdot \mathbf{u}(\mathbf{q})] [\mathbf{q} \cdot \mathbf{u}(-\mathbf{q})]. \end{aligned}$$

The system is quantized by the condition (canonical quantization)

$$[u_i(\mathbf{r}), p_j(\mathbf{r}')] = i\delta_{ij}\delta(\mathbf{r} - \mathbf{r}').$$

Show that in \mathbf{k} -space this becomes

$$[u_i(\mathbf{q}), p_j(-\mathbf{q}')] = i\delta_{ij}\mathcal{V}\delta_{\mathbf{q}\mathbf{q}'}.$$

Now follow the standard scheme for diagonalization of the phonons modes. Define

$$\mathbf{u}_{\mathbf{q}} = \epsilon_{\mathbf{q}} \sqrt{\frac{\mathcal{V}}{2M\rho_{\text{ion}}^0\Omega}} (b_{\mathbf{q}} + b_{-\mathbf{q}}^\dagger), \quad \mathbf{p}_{-\mathbf{q}} = i\epsilon_{\mathbf{q}} \sqrt{\frac{\mathcal{V}M\rho_{\text{ion}}^0\Omega}{2}} (b_{\mathbf{q}}^\dagger - b_{-\mathbf{q}}),$$

where the polarization vector has the property that $\epsilon_{\mathbf{q}} = \epsilon_{-\mathbf{q}}$, i.e. one must choose a positive polarization direction. The polarization is here parallel to \mathbf{q} i.e. only longitudinal modes exist in the jellium model¹. Furthermore, Ω is chosen such that H is diagonal. Verify that

$$H = \sum_{\mathbf{q}} \Omega_0 \left(b_{\mathbf{q}}^\dagger b_{\mathbf{q}} + \frac{1}{2} \right); \quad \Omega_0 = \sqrt{\frac{4\pi e_0^2 \rho_{\text{ion}}^0}{M}}.$$

Explain the physics of this result.

Exercise 3.6

Bare electron-phonon interaction in the jellium model. Using the quantization from the previous exercise verify that the Hamiltonian describing the electron-phonon

¹In the general non-jellium case the polarization vectors are eigenvectors of the dynamical matrix $\mathbf{D}(\mathbf{q})$ in Eq. (3.14). In the jellium case, one thus has $D_{\alpha\beta}(\mathbf{q}) = q_\alpha q_\beta V(\mathbf{q})$ which only has one eigenvector with non-zero eigenvalue, namely $\epsilon_{\mathbf{q}}$, which you can easily check.

interaction is given by

$$\begin{aligned}
 H_{\text{ion-el}} &= \int d\mathbf{r} d\mathbf{r}' \delta\rho(\mathbf{r}) V(\mathbf{r} - \mathbf{r}') \delta\rho_{\text{ion}}(\mathbf{r}') \\
 &= \frac{\rho_{\text{ion}}^0}{\mathcal{V}} \sum_{\mathbf{q}} \rho(-\mathbf{q}) V(\mathbf{q}) (i\mathbf{q} \cdot \mathbf{u}(\mathbf{q})) \\
 &= \frac{1}{\sqrt{\mathcal{V}}} \sum_{\mathbf{q}} g(\mathbf{q}) \rho(-\mathbf{q}) A_{\mathbf{q}},
 \end{aligned} \tag{B.1}$$

where

$$g(\mathbf{q}) = iqV(\mathbf{q}) \sqrt{\frac{\rho_{\text{ion}}^0}{2M\Omega_0}}, \tag{B.2}$$

and

$$A_{\mathbf{q}} = b_{\mathbf{q}} + b_{-\mathbf{q}}^\dagger. \tag{B.3}$$

Exercises for Chapter 4

Exercise 4.1

(a) Consider the Hartree-Fock solution of the homogeneous electron gas in a positive background. After the mean-field approximation the Hamiltonian can be written as

$$H^{\text{HF}} = \sum_{\mathbf{k}} \varepsilon_{\mathbf{k}}^{\text{HF}} c_{\mathbf{k}\sigma}^\dagger c_{\mathbf{k}\sigma} + \text{constant}. \tag{1}$$

Argue why it is that in this case the Hartree-Fock energy follows from Eq. (4.25b) and is given by

$$\varepsilon_{\mathbf{k}}^{\text{HF}} = \varepsilon_{\mathbf{k}} + V_{\text{HF}}(k), \quad V_{\text{HF}}(\mathbf{k}) = - \sum_{\mathbf{k}'} V(\mathbf{k} - \mathbf{k}') n_{\mathbf{k}'\sigma}, \quad V(q) = \frac{4\pi e_0^2}{q^2} \tag{2}$$

The occupation numbers should of course be solved self-consistently. What is the self-consistency condition?

(b) Consider the zero temperature limit, and assume that $n_{\mathbf{k}'\sigma} = \theta(k_F - k')$, which then gives

$$V_{\text{HF}}(k) = -\frac{e_0^2 k_F}{\pi} \left(1 + \frac{k_F^2 - k^2}{2k_F k} \ln \left| \frac{k + k_F}{k - k_F} \right| \right). \tag{3}$$

$V_{\text{HF}}(k)$ is increasing monotonously with k (which you might check, e.g. graphically). Use this to argue that the guess $n_{\mathbf{k}'\sigma} = \theta(k_F - k')$ is in fact the correct solution.

(c) Now find the energy of the electron gas in the Hartree-Fock approximation. Is it given by

$$E_{\text{HF}} \stackrel{?}{=} \sum_{\mathbf{k}} \varepsilon_{\mathbf{k}}^{\text{HF}} n_F(\varepsilon_{\mathbf{k}}^{\text{HF}}), \tag{4}$$

and why not? Hint: show that the correct energy reduces to $E^{(1)}$ given in Eq. (2.39).

(d) The conclusion is so far that Hartree-Fock and first order perturbation theory are in this case identical. Is that true as well for the mean field solution of the Stoner model?

Exercise 4.2

The Hartree–Fock energies derived in the previous exercise have however some unphysical features. Show that the density of states as derived from Eq. (2) diverge at the Fermi level.

This conclusion contradicts both experiments and the Fermi liquid theory discussed in Chap. 14. It also warns us that the single-particle energies derived from a mean-field Hamiltonian are not necessary a good approximation of the excitation energies of the system, even if the mean-field approach gives a good estimate of the groundstate energy.

Exercise 4.3

In this exercise we calculate the density of states in the superconducting state. First go through the arguments that give the so-called coherence factors, $u_{\mathbf{k}}$ and $v_{\mathbf{k}}$, and the excitation energies, E , Eqs. (4.63) and (4.64). You can assume that Δ is real. Secondly, find the density of states for the excitations in energy space, $d(E)$. Show that it diverges at the “gap-edge”, near $d(\Delta)$. Hint: start with the density of states in k space and translate to a density in energy space. The square root singularity that you find, has been confirmed in great detail by experiments and is one of the many successes of the BCS theory. See also Table 4.6.

Exercise 4.4

In 1937 Landau developed a general phenomenological theory of symmetry breaking phase transitions. The basic idea is to expand the free energy in powers of the order parameter. Consider a transition to a state with a finite order parameter, η . For second order phase transitions only even terms are present in the free energy expansion

$$F(T, \eta) = F_0(T) + A(T)\eta^2 + C(T)\eta^4.$$

At the transition point η vanishes. Use this to argue that A also vanishes at the transition point, $T = T_C$, and that $A < 0$ for $T < T_C$, and $A > 0$ for $T > T_C$. Then write A and C as

$$A(T) = (T - T_C)\alpha, \quad C(T) = C,$$

and use the principle of minimal free energy to show that

$$\eta = \sqrt{\frac{-A}{2C}} = \sqrt{\frac{(T_C - T)}{T_C}}\eta(0), \quad \eta(0) = \sqrt{\frac{T_C\alpha}{2C}}.$$

Finally, make a sketch of the specific heat of the system and show that it is discontinuous at the transition point. Hint: recall that

$$C_V = -T \frac{\partial^2 F}{\partial T^2}.$$

Exercises for Chapter 5

Exercise 5.1

We return to the bosonic particle described by the Hamiltonian of Exercise 1.4. Write down the Heisenberg equations of motion for a^\dagger and a . Solve these equations by introducing the operator $\alpha^\dagger \equiv a^\dagger + \omega_0/\omega$. Express H in terms of $\alpha^\dagger(t)$ and $\alpha(t)$. Interpret the change of the zero point energy.

Exercise 5.2

Show that the third-order term $\hat{U}_3(t, t_0)$ of $\hat{U}(t, t_0)$ in Eq. (5.18) indeed has the form

$$\hat{U}_3(t, t_0) = \frac{1}{3!} \left(\frac{1}{i} \right)^3 \int_{t_0}^t dt_1 \int_{t_0}^{t_1} dt_2 \int_{t_0}^{t_2} dt_3 T_t \left(\hat{V}(t_1) \hat{V}(t_2) \hat{V}(t_3) \right).$$

Hint: study Eqs. (5.16) and (5.17) and the associated footnote.

Exercise 5.3

Use the Heisenberg picture to show that for the diagonal Hamiltonian H of Eq. (5.22) we have

$$H = \sum_{\nu'} \varepsilon_{\nu'} a_{\nu'}^\dagger a_{\nu'} \quad \Rightarrow \quad H(t) = \sum_{\nu'} \varepsilon_{\nu'} a_{\nu'}^\dagger(t) a_{\nu'}(t).$$

Exercise 5.4

Due to the equation of motion for operators Eq. (5.6) we will often need to calculate commutators of the form $[AB, C]$, for some operators A , B , and C . Show the very important relations

$$\begin{aligned} [AB, C] &= A[B, C] + [A, C]B, & \text{useful for boson operators,} \\ [AB, C] &= A\{B, C\} - \{A, C\}B, & \text{useful for fermion operators.} \end{aligned}$$

Exercise 5.5

In the jellium model of metals the kinetic energy of the electrons is described by the Hamiltonian H_{jel} of Eq. (2.19), while the interaction energy is given by $V'_{\text{el-el}}$ of Eq. (2.34). In the Heisenberg picture the time evolution of the electron creation and annihilation operators $c_{\mathbf{k}\sigma}^\dagger$ and $c_{\mathbf{k}\sigma}$ is governed by the total Hamiltonian $H = H_{\text{jel}} + V'_{\text{el-el}}$. In analogy with Eq. (5.31) derive the equation of motion for $c_{\mathbf{k}\sigma}(t)$. Apply the Hartree–Fock approximation to the result.

Exercises for Chapter 6

Exercise 6.1

As in Exercise 5.1 we consider a harmonic oscillator influenced by an external force $f(t)$, but now we treat this force as a time-dependent perturbation

$$H' = f(t) x.$$

Express x in terms of a and a^\dagger and calculate the linear response result for the expectation value $\langle x(t) \rangle$. Argue that this result is in fact exact, for example by considering the equation of motion for $\langle x(t) \rangle$.

Exercise 6.2

The spin susceptibility measures the response to a magnetic field. Suppose that a piece of some material is perturbed by external magnetic moments. These moments could for example be in the form of a neutron beam in a neutron scattering experiment. The perturbation is in this case given by

$$H' = -g\mu_B \int d\mathbf{r} \mathbf{B}_{\text{ext}}(\mathbf{r}, t) \cdot \mathbf{S}(\mathbf{r}),$$

where \mathbf{S} is the spin density operator $\mathbf{S}(\mathbf{r}) = \Psi^\dagger(\mathbf{r}) \mathbf{s} \Psi(\mathbf{r})$, see Sec. 1.4.3. Find the response to linear order in \mathbf{B} for the induced spin density in the material, $\langle \mathbf{S}(\mathbf{r}, t) \rangle$. Express your result in both real space and momentum space.

Neutron scattering experiments are the main source for obtaining experimental information about the distribution of spins in condensed matter systems.

Exercise 6.3

We study integrals of the form $\int_{-\infty}^{\infty} dx \frac{1}{x+i\eta} f(x)$, where $f(x)$ is any function with a well behaved Taylor expansion around $x = 0$, and $\eta = 0^+$ is a positive infinitesimal. Show that in this context $\frac{1}{x+i\eta}$ can be decomposed as the following real and imaginary parts

$$\frac{1}{x+i\eta} = \mathcal{P} \frac{1}{x} - i\pi \delta(x).$$

Here \mathcal{P} means Cauchy principle part:

$$\mathcal{P} \int_{-\infty}^{\infty} dx \frac{1}{x} f(x) \equiv \int_{-\infty}^{-\eta} dx \frac{1}{x} f(x) + \int_{\eta}^{\infty} dx \frac{1}{x} f(x).$$

Exercise 6.4

In this exercise we consider the conductivity of a translation- and rotational-invariant system. This means that the conductivity $\sigma(\mathbf{r}, \mathbf{r}')$ is a function of $\mathbf{r} - \mathbf{r}'$ only and that

the conductivity tensor is diagonal with identical diagonal components. Show that in the Fourier domain

$$\mathbf{J}_e(\mathbf{q}, \omega) = \sigma(\mathbf{q}, \omega) \mathbf{E}(\mathbf{q}, \omega).$$

Find the relation between the conductivity, i.e. $\sigma(\mathbf{q}, \omega)$ and the correlation function

$$\langle [J^\alpha(\mathbf{q}, t), J^\alpha(-\mathbf{q}, 0)] \rangle,$$

where $\mathbf{J}(\mathbf{q})$ is the particle current operator in momentum space.

Exercise 6.5

Consider again the conductivity of a translation-invariant and rotational-invariant system.

First consider the conductivity of a non-interacting electron gas at long wave lengths, $\mathbf{q} \rightarrow 0$. Derive the expression for the particle current operator in this limit,

$$\mathbf{J}(0, t) = \frac{1}{m} \sum_{\mathbf{k}\sigma} \mathbf{k} c_{\mathbf{k}\sigma}^\dagger(t) c_{\mathbf{k}\sigma}(t),$$

and show that it is time-independent in the Heisenberg picture. From this you can derive obtain the long wavelength conductivity

$$\sigma^{\alpha\beta}(0, \omega) = i\delta_{\alpha\beta} \frac{ne^2}{\omega m}.$$

How does this fit with the Drude result (13.42) in the clean limit, where the impurity induced scattering time τ tends to infinity (i.e. $\omega\tau \rightarrow \infty$)? How does the conclusions change for an *interacting* translation-invariant system?

Exercises for Chapter 7

Exercise 7.1

Verify that the self-consistent equations in Eqs. (8.16) and (8.17) both are solution to the Schrödinger equation in Eq. (8.13).

Exercise 7.2

In this exercise we prove that the propagator in Eq. (8.22) in fact is identical to the Green's function by showing that it obey the same differential equation, namely Eq. (8.14b). Hint: differentiate (8.22) with respect to time using that the derivative of the theta function is a delta function, and that

$$\langle \mathbf{r} | H | \phi \rangle = H(\mathbf{r}) \langle \mathbf{r} | \phi \rangle$$

Which you can see for example by inserting a complete set of eigenstates of H .

Exercise 7.3

Find the greater propagator, $G^>(\mathbf{r}, \mathbf{r}'; \omega)$ similar to Eq. (8.42), but now in one- and two dimensions. Can you suggest an experiment (at least in principle) that measures this propagator.

Exercise 7.4

Eqs. (8.50) are valid for fermions. Show that the corresponding results for bosons are

$$\begin{aligned} iG^>(\nu, \omega) &= A(\nu, \omega) [1 + n_B(\omega)], \\ iG^<(\nu, \omega) &= A(\nu, \omega) n_B(\omega). \end{aligned}$$

Exercise 7.5

The tunneling density of states for a superconductor has a characteristic shape which you find in this exercise. First find the retarded Green's function

$$G^R(\mathbf{k} \uparrow, t) = -i\theta(t) \langle \{c_{\mathbf{k}\uparrow}(t), c_{\mathbf{k}\uparrow}^\dagger\} \rangle$$

by expressing the c and c^\dagger operators in terms of the diagonal γ -operators called bogoliubons given in Eq. (4.65). Once you have done that the problem is reduced to finding the Green's function of a free particle, which you see from the Hamiltonian Eq. (4.66). Now calculate the tunneling current-voltage characteristics, assuming the tunneling matrix element to be approximately constant. Plot the results of I and dI/dV versus V .

Exercise 7.6

In this exercise we shall calculate the dc conductance of a perfect one-dimensional wire. From Sec. 6.3 we have that the conductance is given by

$$G = \frac{ie^2}{\omega} \Pi^R(\omega), \quad \Pi^R(x - x'; t - t') = -i\theta(t - t') \langle [I_p(xt), I_p(x't')] \rangle$$

where I_p is the operator for the particle current through the wire. Hints: use the one-dimensional version of the particle current operator

$$I_p(x) = \frac{\hbar}{mL} \sum_{kq\sigma} \left(k + \frac{q}{2}\right) c_{k\sigma}^\dagger c_{k+q\sigma} e^{iqx}.$$

The result for the dc conductance does not depend on where the current is evaluated (why?). Now you can use the method in Sec. 8.5 to find that

$$\begin{aligned} \Pi^R(x - x'; t - t') &= -i\theta(t - t') \left(\frac{\hbar}{mL}\right)^2 \sum_{kq\sigma} \left(n_F(\varepsilon_k) - n_F(\varepsilon_{k+q})\right) \\ &\quad \times \left(k + \frac{q}{2}\right)^2 e^{i(\varepsilon_k - \varepsilon_{k+q})(t-t')} e^{iq(x-x')}. \end{aligned}$$

Setting $x = x'$ find $\Pi^R(0, \omega)$ and study it in the low frequency limit. Show that

$$\lim_{\omega \rightarrow 0} \text{Im } \Pi^R(\omega) = \hbar \omega \pi \left(\frac{\hbar}{mL} \right)^2 \sum_{kq\sigma} \left[-\frac{\partial n_F(\partial \varepsilon_k)}{\varepsilon_k} \right] \delta(\varepsilon_k - \varepsilon_{k+q}) \left(k + \frac{q}{2} \right)^2.$$

Do the q -integral first and find

$$\begin{aligned} \lim_{\omega \rightarrow 0} \text{Im } \Pi^R(\omega) &= \hbar \omega \pi \left(\frac{\hbar}{m} \right)^2 \left(\frac{m}{\hbar^2} \right) \frac{1}{2\pi L} \sum_{k\sigma} \left(-\frac{\partial}{\partial \varepsilon_k} n_F(\varepsilon_k) \right) \frac{k^2}{|k|} \\ &= \frac{\omega}{\hbar \pi} \frac{1}{e^{-\beta \mu} + 1}. \end{aligned}$$

In the limit $\mu \gg kT$, you find the famous result for the conductance G of a perfect 1D channel

$$G = \frac{2e^2}{h}.$$

Exercise 7.7

Consider a 2D electron gas in the xy plane confined to the strip $0 < x < L$. What is the electron density as a function of the distance x from the left edge? Take for simplicity $T = 0$. What will change at larger temperatures? The oscillations that you will find are called Friedel oscillations.

Hints: Use standing waves in the x -direction fulfilling the proper boundary conditions, and assume quasi-continuous states with periodic boundary conditions in the y direction. Find the x -dependent density as $n(x) = \int dy \sum_{\nu} \langle c_{\nu}^{\dagger} c_{\nu} \rangle |\langle xy | \nu \rangle|^2$, where the ν -sum runs over the appropriately normalized states $|\nu\rangle$. You may need to know the integral $\int ds \sqrt{1-s^2} \sin^2(xs) = \frac{\pi}{8x} [x - J_1(2x)]$.

Exercises for Chapter 8

Exercise 8.1

Consider a physical system consisting of fermions allowed to occupy two orbitals. The Hamiltonian is given by

$$H = E_1 c_1^{\dagger} c_1 + E_2 c_2^{\dagger} c_2 + t c_1^{\dagger} c_2 + t^* c_2^{\dagger} c_1.$$

Find the Green's function $G^R(ij, \omega)$, where i and j can be both be either 1 or 2 and where $G^R(ij, t - t') = -i\theta(t - t') \langle \{c_i(t), c_j^{\dagger}(t')\} \rangle$. Use the equation of motion method. Don't forget to interpret the result.

Exercise 8.2

Derive Eqs. (9.22) and (9.23) by differentiating the Green's functions in (9.20) and (9.21).

Exercise 8.3

Consider an atom on a metal surface. The electronic states of the atom will hybridize with the conduction electrons in the metal. If we assume that only a single orbital couples to the metal states, then the atom and the metal can be described by the Anderson model Hamiltonian Eq. (9.18).

When a scanning tunneling microscope (STM) is placed near the atom current will flow from the STM tip through the atom to the metal. Since the atom is strongly coupled to the metal surface the bottleneck for the current is the tunneling from STM to atom, which we can describe by a tunneling Hamiltonian as in Eq. (8.60), and not the tunneling between atom and metal, described by Eq. (9.17). It is therefore a good approximation to assume that the atom is in equilibrium with the metal, and to use tunneling theory for the current between tip and atom.

Sketch the resulting dI/dV using the expression derived in Chap. 8 for the tunnel current and the mean field expression for the d electron Green's function, derived in Sec. 9.2.

Exercise 8.4

In this exercise we improve the solution of the Anderson model presented in Secs. 9.2.2 and 9.2.3. Start by combining Eqs. (9.22), (9.23), and (9.30b) to obtain the following equation of motion for $G^R(d \uparrow, \omega)$:

$$[\omega + i\eta - \varepsilon_d + \mu - \Sigma^R(\omega)] G^R(d \uparrow, \omega) = 1 + IUD^R(d \uparrow, \omega).$$

The two-particle Green's function $D^R(d \uparrow, t)$ is defined in Eq. (9.26). In Eq. (9.28) it was approximated by a product of two single-particle Green's functions, and the model was then solved at the level of single-particle Green's functions.

Here we go one step further and derive an equation of motion for $D^R(d \uparrow, t)$ and truncate it at the two-particle Green's function level. Thus we get a better approximation which takes pair correlations into account. First find the differential equation for D^R by differentiation with respect to t . When you do that the difficult commutator is

$$\begin{aligned} [H_{\text{hyb}}, n_{d\downarrow} d_{\uparrow}] &= n_{d\downarrow} [H_{\text{hyb}}, d_{\uparrow}] + [H_{\text{hyb}}, n_{d\downarrow}] d_{\uparrow} \\ &= n_{d\downarrow} [H_{\text{hyb}}, d_{\uparrow}] + \sum_{\mathbf{k}\sigma} \left(t_{\mathbf{k}}^* c_{\mathbf{k}\downarrow}^\dagger d_{\downarrow} - t_{\mathbf{k}} d_{\downarrow}^\dagger c_{\mathbf{k}\downarrow} \right) d_{\uparrow}, \end{aligned}$$

The last term contains a new type of processes giving rise to higher order correlations (corresponding to spin flips), and it is therefore omitted. This constitutes our new and improved approximation. The first term generates a two-particle Green's function denoted F^R given by

$$F^R(\mathbf{k}d \uparrow, t - t') = -i\theta(t - t') \langle \{ (n_{d\downarrow} c_{\mathbf{k}\uparrow})(t), d_{\uparrow}^\dagger(t') \} \rangle.$$

Note the similarity between F^R and the single-particle function $G_{kd}^R(\mathbf{k}d\sigma)$ of Eq. (9.21). Derive the equation of motion for F^R , and show that if you again neglect the term $[H_{\text{hyb}}, n_{d\downarrow}]$ no new Green's functions are generated. Instead F^R is coupled back to D^R .

Inset this result into the equation of motion you derived for D^R above, and show that the resulting equation for D^R is

$$[\omega + i\eta - \varepsilon_d + \mu - U - \Sigma(\omega)] D^R(d \uparrow) = \langle n_{d\downarrow} \rangle.$$

Finally, solve for G^R and show that the result is

$$G^R(d \uparrow) = \frac{1 - \langle n_{d\downarrow} \rangle}{\omega + i\eta - \varepsilon_d + \mu - \Sigma^R(\omega)} + \frac{\langle n_{d\downarrow} \rangle}{\omega + i\eta - \varepsilon_d - U + \mu - \Sigma^R(\omega)}.$$

Interpret this result physically, for example by considering how the result of Exercise 8.3 is changed.

Exercises for Chapter 9

Exercise 9.1

Find the Fermi-Dirac distribution by starting from the Matsubara Green's function and setting $\tau = 0^-$. Then show that

$$\langle c_\nu^\dagger c_\nu \rangle = \mathcal{G}_\sigma^0(\nu, \tau = 0^-) = \frac{1}{\beta} \sum_{ik_n} e^{-ik_n 0^-} \mathcal{G}_\sigma^0(\nu, ik_n) = n_F(\varepsilon_\nu)$$

How would you calculate $\langle c_\nu c_\nu^\dagger \rangle$?

Exercise 9.2

Repeat Exercise 7.6 but this time using the imaginary time formalism. Use the procedure going from Eq. (10.80) to Eq. (10.85).

Exercise 9.3

According to Eq. (10.63) the equation of motion for the Matsubara Green's function of a free particle is

$$\left(-\partial_\tau - \frac{\mathbf{p}^2}{2m} + \mu \right) \mathcal{G}_\sigma^0(\mathbf{r} - \mathbf{r}', \tau - \tau') = \delta(\mathbf{r} - \mathbf{r}') \delta(\tau - \tau').$$

Show (10.39) by Fourier transforming this equation. Note that both τ and τ' are greater than zero.

Exercises for Chapter 10

Exercise 10.1

Single impurity scattering. The Dyson equation for otherwise free electrons scattering against an external potential is written in Eqs. (11.5) and (11.9). Suppose now that the

electrons are confined to move in one dimension and that the external potential can be represented by a delta-function impurity potential, $U(x) = U_0\delta(x)$. Show that in this case the solution of the Dyson equation becomes

$$\mathcal{G}_\sigma(xx', ik_n) = \mathcal{G}_\sigma^0(xx', ik_n) + \mathcal{G}_\sigma^0(x0, ik_n) \frac{U_0}{1 - \mathcal{G}_\sigma^0(00, ik_n) U_0} \mathcal{G}_\sigma^0(0x', ik_n).$$

Hint: solve for $\mathcal{G}(0x', ik_n)$ first and insert that in the Dyson equation for $\mathcal{G}(xx', ik_n)$. To find the retarded Green's we thus need the unperturbed Green's function, which is

$$G_\sigma^{0R}(xx', \omega) = \mathcal{G}_\sigma^0(xx', \omega + i\eta) = \frac{1}{L} \sum_k \frac{e^{ik(x-x')}}{\omega - \varepsilon_k + \mu + i\eta} = \frac{1}{iv_\omega} e^{ik_\omega|x-x'|},$$

(do you agree?) where $k_\omega = \sqrt{2m(\omega + \mu)}$ and $v = \omega \partial\varepsilon_k/\partial k|_{k=k_\omega}$. Since the retarded Green's function tells us about the amplitude for propagation from point x' to point x , we can in fact extract the transmission and reflection amplitudes t and r . For $x' < 0$ we have

$$G_\sigma^R(xx', \omega) = t G_\sigma^{0R}(xx', \omega) \theta(x) + [1 + r e^{i\phi(x, x')}] G_\sigma^{0R}(xx', \omega) \theta(-x),$$

where $e^{i\phi(x, x')}$ is a phase factor, which is determined by the calculation. Find r and t and discuss the phase shifts that the electrons acquire when they are scattered.

Exercise 10.2

Resonant tunneling. In for example semiconductor heterostructures one can make quantum-well systems which to a good approximation can be described by a one-dimensional model of free electrons with two tunneling barriers. Here we simplify it somewhat further by representing the tunneling barriers by delta-function potentials situated at a_1 and a_2 . The Hamiltonian is then given by

$$H = H_0 + \int_{-\infty}^{\infty} dx \rho(x) U_0 [\delta(x - a_1) + \delta(x - a_2)],$$

where H_0 is the Hamiltonian for free electrons in one dimension. Write H in x -space and find a formal expression for the Matsubara Green's function using Dyson's equation. From the Dyson equation find the retarded Green's function for $x' < a_1 < a_2 < x$:

$$G_\sigma^R(xx', \omega) = \frac{e^{ik(x-x')}}{iv_\omega} \left[1 + \alpha \begin{pmatrix} e^{-ika_1} & e^{-ika_2} \end{pmatrix} \cdot \begin{pmatrix} 1 - \alpha & -\alpha e^{i\theta} \\ -\alpha e^{i\theta} & 1 - \alpha \end{pmatrix}^{-1} \cdot \begin{pmatrix} e^{ika_1} \\ e^{ika_2} \end{pmatrix} \right],$$

where $k = k_\omega$ (see previous exercise) and where $\alpha = U_0/iv$ and $\theta = k(a_2 - a_1)$. Use this to show that the transmission is unity for the particular values of θ satisfying

$$\alpha = i \cot \theta.$$

Derive the same result using the following simple argument involving two paths for an electron to go from x' to x : (1) $x' \rightarrow a_1 \rightarrow a_2 \rightarrow x$, and (2) $x' \rightarrow a_1 \rightarrow a_2 \rightarrow a_1 \rightarrow a_2 \rightarrow x$. The transmission is unity when these two paths interfere constructively – as does paths with any number of trips back and forth in the “cavity”.

Exercises for Chapter 11

Exercise 11.1

Matsubara frequency summation. Use the rule Eq. (10.54) for summing over functions with simple poles to perform the Matsubara frequency summation appearing in the following diagrams of Eqs. (12.30) and (12.34):

$$\Sigma_{\sigma}^F(\mathbf{k}, ik_n) \equiv \text{diagram of a fermion line with a self-energy loop} \quad \Pi^0(\mathbf{q}, iq_n) \equiv \text{diagram of a boson loop}$$

Exercise 11.2

The cancellation of disconnected diagrams in $\mathcal{G}(b, a)$. We study the one-particle Green's function, which in the interaction picture in the presence of the particle-particle interaction $W(\mathbf{r} - \mathbf{r}')$ becomes:

$$\mathcal{G}(b, a) = - \frac{\left\langle T_{\tau} \left[\hat{U}(\beta, 0) \hat{\Psi}(b) \hat{\Psi}^{\dagger}(a) \right] \right\rangle_0}{\left\langle \hat{U}(\beta, 0) \right\rangle_0}, \quad \text{with} \quad \hat{U}(\beta, 0) = T_{\tau} \exp \left(- \int_0^{\beta} d\tau \hat{W}(\tau) \right).$$

As in Eq. (12.14) use the Feynman rules to expand the denominator and the numerator, but now to second order in W , and show explicitly the cancellation of the disconnected diagrams. Hints. (1) Start with the simpler denominator (how many terms?). (2) Draw topologically identical diagrams only once and multiply with the number of them. (3) Get most of the diagrams in the numerator by cutting open and stretching out a Fermion line in the diagrams from the denominator (how many terms?).

Exercise 11.3

Feynman diagrams and Dyson's equation for the Anderson model. We return to Anderson's model for localized magnetic moments in metals, see Sec. 9.2. We wish to derive the Dyson equation Eq. (9.29) using Feynman diagrams. The unperturbed Hamiltonian is given by $H_0 = \sum_{\sigma} (\varepsilon_d - \mu) d_{\sigma}^{\dagger} d_{\sigma} + \sum_{\mathbf{k}\sigma} (\varepsilon_{\mathbf{k}} - \mu) c_{\mathbf{k}\sigma}^{\dagger} c_{\mathbf{k}\sigma}$, while the interaction part is given by $H_{\text{int}} = H_{\text{hyb}} + H_U^{\text{MF}}$, the sum of the hybridization Eq. (9.17) and on-site repulsion Eq. (9.27). We employ the mean-field approximation given by Eq. (9.27) where the σ spins only interact with the average density $\langle n_{d\bar{\sigma}} \rangle$ of the opposite $\bar{\sigma}$ spins.

We introduce the following rather obvious diagrammatic notation for the Matsubara Green's functions and interactions:

$$\begin{array}{lll} \text{---}\blacktriangleleft & \equiv & \mathcal{G}^0(d\sigma) \\ \text{==}\blacktriangleleft & \equiv & \mathcal{G}(d\sigma) \\ \text{---}\blacktriangleleft\text{---} & \equiv & \mathcal{G}^0(\mathbf{k}\sigma) \end{array} \quad \begin{array}{lll} \bullet & \equiv & \sum_{\mathbf{k}} t_{\mathbf{k}} \\ \text{---}\text{wavy}\text{---} & \equiv & U \end{array}$$

The electron mass for this material is $m^* = 0.067 m$, the relative permittivity is $\varepsilon_r = 13$, while the electron density ranges from $n^{2D} = 1 \times 10^{15} \text{ m}^{-2}$ to $5 \times 10^{15} \text{ m}^{-2}$.

The electron wave function for the two dimensional electron gas is restricted to be

$$\psi_{\mathbf{k}}(\mathbf{r}, z) = \frac{1}{\sqrt{L_x L_y}} e^{i\mathbf{k}\cdot\mathbf{r}} \zeta_0(z),$$

where $\mathbf{k} = (k_x, k_y)$ and $\mathbf{r} = (x, y)$, while $\zeta_0(z)$ is the lowest eigenstate in the z direction, i.e. $n = 0$ in Eq. (2.50). Write down the interaction part of the Hamiltonian and show that it is of the form

$$H^{2D} = \frac{1}{2\mathcal{A}} \sum_{\mathbf{k}\mathbf{k}'\mathbf{q}} \sum_{\sigma\sigma'} W^{2D}(\mathbf{q}) c_{\mathbf{k}+\mathbf{q},\sigma}^\dagger c_{\mathbf{k}'-\mathbf{q},\sigma'}^\dagger c_{\mathbf{k}',\sigma'} c_{\mathbf{k},\sigma}$$

where $\mathbf{q} = (q_x, q_y)$. For a strictly 2D system, i.e. $|\zeta_0(z)|^2 = \delta(z)$, show that

$$W^{2D}(\mathbf{q}) = \frac{e^2}{2\varepsilon_r \epsilon_0 q}.$$

Hint: use $\int_0^\pi d\theta \cos(\alpha \cos \theta) = \pi J_0(\alpha)$, where J_0 is the Bessel function of the first kind of order zero.

Exercise 12.3

Plasmons in two dimensions. Consider a translation-invariant electron gas in two dimensions fabricated in a GaAs heterostructure. The electron mass for this material is $m^* = 0.067 m$, the relative permittivity is $\varepsilon_r = 13$, while the electron density ranges from $n^{2D} = 1 \times 10^{15} \text{ m}^{-2}$ to $5 \times 10^{15} \text{ m}^{-2}$.

For such a system the RPA dielectric function is given by

$$\varepsilon_{\text{RPA}}^{2D}(\mathbf{q}, iq_n) = 1 - W^{2D}(\mathbf{q}) \chi_0^{2D}(\mathbf{q}, iq_n),$$

with $\mathbf{q} = (q_x, q_y)$ and where $\chi_0^{2D}(\mathbf{q}, iq_n)$ is the 2D version of the 3D pair bubble χ^0 given in Eq. (13.20). Show that at low temperatures, $k_B T \ll \varepsilon_F$, and long wave lengths, $q \ll \omega/v_F$, the plasmon dispersion relation is $\omega = v_F \sqrt{k_s^{2D} q/2}$, where k_s^{2D} is the Thomas-Fermi screening wavenumber in 2D. Find the relation between k_F and the electron density, n^{2D} . Express k_s^{2D} in terms of the parameters of the electron gas. Is it larger or smaller than k_F for $n^{2D} = 2 \times 10^{15} \text{ m}^{-2}$?

Exercise 12.4

Static screening in two dimensions. Show that in 2D the static RPA screened interaction at small wavevectors, $q \ll k_F$, and low temperatures, $k_B T \ll \varepsilon_F$, is given by

$$W_{\text{RPA}}^{2D}(\mathbf{q}, 0) \equiv \frac{W^{2D}(\mathbf{q})}{\varepsilon_{\text{RPA}}^{2D}(\mathbf{q}, 0)} = \frac{e^2}{2\varepsilon_r \epsilon_0 (q + k_s^{2D})}.$$

Exercise 12.5

Damping of two dimensional plasmons. The electron-hole pair continuum is the region in $q - \omega$ space where $\text{Im } \chi_0^{2D} \neq 0$. Find the condition for the plasmons not to be damped by single-particle excitations for $q < k_F$. In the estimate you can use the small- q expressions for the plasmon frequency and the polarization, that you found above. Are the plasmons damped in the region $q < k_F$ in GaAs with the parameters given above?

Exercise 12.6

Deriving the Feynman diagrams for $\chi(\tilde{q})$. The task is to understand the arguments leading to the diagrammatic expansion for $\chi(\tilde{q})$ given in Eq. (13.58). We are not asking for detailed calculations.

In the real space formulation $\chi(b, a) \equiv -\langle T_\tau \rho(b) \rho(a) \rangle_{\text{eq}} = -\langle T_\tau \Psi^\dagger(b) \Psi(b) \Psi^\dagger(a) \Psi(a) \rangle_{\text{eq}}$. Write down the expression for $\chi(b, a)$ analogous to Eq. (12.8) for $\mathcal{G}(b, a)$. Then apply Wick's theorem to obtain the analogue of Eq. (12.9). Following arguments similar to those of Eq. (12.16) it can be shown that the numerator also cancels in the case of $\chi(b, a)$ (you do not have to show that). Finally, argue with the help of Appendix A that for a translation-invariant system $\chi(\mathbf{q}, \tau) = -\frac{1}{V} \langle T_\tau \rho(\mathbf{q}, \tau) \rho(-\mathbf{q}, 0) \rangle_{\text{eq}}$ as stated in Eq. (13.53), see also the form of $\sigma(\mathbf{q}, \omega)$ in Exercise 6.4. Please note that $\langle \rho \rangle_{\text{eq}} = 0$ due to charge neutrality.

Alternatively, you may start with $\chi(\mathbf{q}, \tau)$ for a translation-invariant system, and write this in a form analogous to Eq. (12.8). Then apply Wick's theorem in this situation to obtain the starting point for the diagrammatic expansion directly in \mathbf{q} -space.

Exercises for Chapter 13**Exercise 13.1**

Semi-classical motion. We study Eqs. (14.17), (14.18), and (14.19). If the quasiparticles behaves like non-interacting particles why is then the number of quasiparticles conserved on the semi-classical level?

To answer this question we introduce the concept of a wave packet, i.e. a wave function fairly localized in both space and momentum space:

$$\psi(\mathbf{r}, t) = \int d\mathbf{k} f(\mathbf{k} - \mathbf{k}_0) e^{i[\mathbf{k} \cdot \mathbf{r} - \omega(\mathbf{k})t]}, \quad \text{e.g. with } f(\mathbf{k} - \mathbf{k}_0) = \exp\left(-\frac{(\mathbf{k} - \mathbf{k}_0)^2}{2(\Delta\mathbf{k})^2}\right).$$

Taylor expand $\omega(\mathbf{k})$ to first order and show that the wave packet can be written as

$$\psi(\mathbf{r}, t) \approx e^{i[\mathbf{k}_0 \cdot \mathbf{r} - \omega(\mathbf{k}_0)t]} F(\mathbf{r} - \partial_{\mathbf{k}} \omega(\mathbf{k}_0) t),$$

where F is some envelope function. What is the physical interpretation of $\partial_{\mathbf{k}} \omega(\mathbf{k}_0)$? In conclusion, the wave packet has the energy $\varepsilon_{\mathbf{k}}$ and the velocity $\mathbf{v}_{\mathbf{k}}$ given by

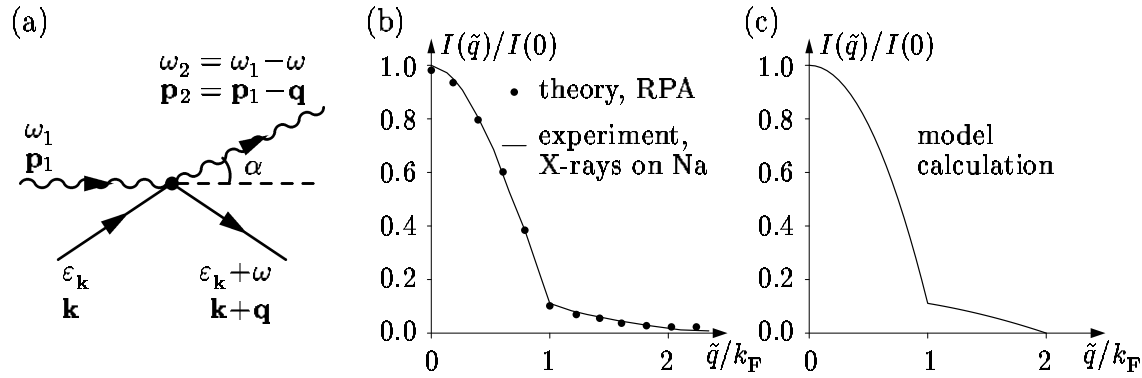
$$\varepsilon_{\mathbf{k}} = \hbar \omega_{\mathbf{k}}, \quad \mathbf{v}_{\mathbf{k}} = \partial_{\mathbf{k}} \omega_{\mathbf{k}} = \frac{1}{\hbar} \partial_{\mathbf{k}} \varepsilon_{\mathbf{k}}.$$

For external forces $\mathbf{F}(\mathbf{r}, t) = -\nabla V(\mathbf{r}, t)$ varying slowly in space and time, we can through the power $P_{\mathbf{k}}$ absorbed by the wave packet centered around \mathbf{k} deduce the time evolution of \mathbf{k} as follows. Combine the two classical expressions for the power, $P_{\mathbf{k}} = \mathbf{F} \cdot \mathbf{v}_{\mathbf{k}}$ and $P_{\mathbf{k}} = \dot{\varepsilon}_{\mathbf{k}}$, to show

$$\dot{\mathbf{k}} = \frac{1}{\hbar} \mathbf{F}.$$

Exercise 13.2

Measuring the discontinuity of the distribution function. For an interacting electron gas discuss the spectral function $A(\mathbf{k}, \omega)$ in Eq. (14.58) and use it to calculate the distribution function $\langle n_{\mathbf{k}} \rangle$. Demonstrate the existence of a Fermi surface characterized by the renormalization parameter Z . The value of Z can be inferred from X-ray Compton scattering on the electron gas, see Fig. (a).



In the so-called impulse approximation for Compton scattering, the intensity $I(\omega_1, \omega, \mathbf{q})$ of incoming photons of energy ω_1 being scattered with the energy and momentum loss ω and \mathbf{q} , respectively, is proportional to the number of scattering events on all electrons fulfilling the simple kinematic constraint: conservation of energy and momentum,

$$I(\omega_1, \omega, \mathbf{q}) = \mathcal{N}(\omega_1, \omega) \int d\mathbf{k} \langle n_{\mathbf{k}} \rangle \delta(\omega + \varepsilon_{\mathbf{k}} - \varepsilon_{\mathbf{k}+\mathbf{q}}) \propto \int d\mathbf{k} \langle n_{\mathbf{k}} \rangle \delta\left(\omega - \frac{1}{2m}q^2 - \frac{1}{m}\mathbf{q} \cdot \mathbf{k}\right).$$

We omit the explicit reference to the fixed ω_1 and work with $I(q, \tilde{q}) \equiv I(\omega_1, \omega, \mathbf{q})$. Show that

$$I(q, \tilde{q}) \propto \frac{1}{q} \int_{\frac{\tilde{q}^2}{2m}}^{\infty} d\varepsilon_{\mathbf{k}} \langle n_{\mathbf{k}} \rangle = \frac{1}{q} \int_{\frac{\tilde{q}^2}{2m}}^{\infty} d\varepsilon_{\mathbf{k}} \int_{-\infty}^{\infty} \frac{d\omega}{2\pi} A(\mathbf{k}, \omega) n_F(\omega).$$

where $A(\mathbf{k}, \omega)$ is the spectral function and $\tilde{q} \equiv m\omega/q - q/2$. Fig. (b) contains an experimental determination of $I(q, \tilde{q})$ from X-ray scattering on sodium. The experimental result is compared to theory based on RPA calculations of $A(\mathbf{k}, \omega)$.

Instead of using RPA, discuss the following simple model for $A(\mathbf{k}, \omega)$ containing the essential features. At low energies, $\varepsilon_{\mathbf{k}} < 4\varepsilon_F$, a renormalized quasiparticle pole of weight Z coexists with a broad background of weight $1 - Z$, while at higher energies, $\varepsilon_{\mathbf{k}} > 4\varepsilon_F$,

no renormalization occurs, and the quasiparticle is in fact the bare electron:

$$A(\mathbf{k}, \omega) = Z_{\mathbf{k}} 2\pi\delta(\omega - \xi_{\mathbf{k}}) + (1 - Z_{\mathbf{k}}) \frac{\pi}{W} \theta(W - |\omega|), \quad Z_{\mathbf{k}} = \begin{cases} Z, & \text{for } k < 2k_F \\ 1, & \text{for } k > 2k_F. \end{cases}$$

Here W is the large but unspecified band width of the conduction band. Explain Fig. (c).

Exercise 13.3

Detailed balance. The scattering life time in Eq. (14.45) expresses the time between scatterings assuming some unknown distribution function $n(\mathbf{k})$. The Boltzmann equation with inclusion of e-e scattering therefore reads

$$\partial_t(n_{\mathbf{k}}) + \dot{\mathbf{k}} \cdot \nabla_{\mathbf{k}} n_{\mathbf{k}} + \mathbf{v}_{\mathbf{k}} \cdot \nabla_{\mathbf{r}} n_{\mathbf{k}} = - \left(\frac{1}{\tau_{\mathbf{k}}} \right)_{\text{collisions}}.$$

In the homogenous and static case, i.e. absence of external forces, the left hand side is expected to be zero. Show that the usual Fermi-Dirac equation solves the Boltzmann equation in this case, i.e. that the right hand side is also zero if we use $n = n_F$. Hint: show and use that $n_F(\varepsilon) [1 - n_F(\varepsilon')] \exp(\beta(\varepsilon - \varepsilon')) = [1 - n_F(\varepsilon)] n_F(\varepsilon')$.

Exercise 13.4

Why are metals shiny? According to Eq. (13.75) we have in the semiclassical high frequency, long wave limit that $\varepsilon(0, \omega) = 1 - \omega_p^2/\omega^2$. Consider a monochromatic electromagnetic wave with $\mathbf{E} = E(x)e^{-i\omega t}\hat{\mathbf{e}}_z$ incident on a metal occupying the half-space $x > 0$. Use the high-frequency limit of Maxwell's equations in matter. Set $\mathbf{D} = \epsilon_0\epsilon(0, \omega)\mathbf{E}$ and prove that $\nabla^2 E(x) = \frac{\omega_p^2 - \omega^2}{c^2} E(x)$. Hint: you may need $\nabla \times \nabla \times \mathbf{E} = -\nabla^2 \mathbf{E}$. For which frequencies does the wave propagate through the metal, and for which is it reflected?

From X-ray diffraction we know that the unit-cell of Na is body-centered cubic (i.e. one atom in each corner and one in the center of the cube) with a side-length of 4.23 Å. It is observed that Na is transparent for UV-light with a wavelength shorter than 206 nm. Explain this, and explain why (polished) metals appear shiny. Hint: Each Na atom donates one electron to the conduction band.

Exercises for Chapter 14

Exercise 14.1

The integral equation for the vertex function in the Born approximation. This exercise deals with the Kubo formula method applied to impurity scattering in metals. The conductivity is in the weak scattering limit given by

$$\sigma_{xx} = \frac{e^2}{\pi} \frac{1}{\mathcal{V}} \sum_{\mathbf{k}} \left(\frac{k_x}{m} \right) G^R(\mathbf{k}, 0) G^A(\mathbf{k}, 0) \Gamma_x^{RA}(\mathbf{k}, \mathbf{k}; 0, 0).$$

In the Born approximation the Dyson equation for the vertex function is

$$\Gamma_x^{RA}(\mathbf{k}, \mathbf{k}; 0, 0) = \frac{k_x}{m} + \frac{1}{\mathcal{V}} \sum_{\mathbf{k}'} n_{\text{imp}} |u(\mathbf{k} - \mathbf{k}')|^2 G^R(\mathbf{k}', 0) G^A(\mathbf{k}', 0) \Gamma_x^{RA}(\mathbf{k}', \mathbf{k}'; 0, 0).$$

1. If the impurity potential is short ranged argue that we can approximate it by a constant $|u(\mathbf{k} - \mathbf{k}')|^2 \approx |u_0|^2$. Prove that in this case

$$\Gamma_x^{RA} = \frac{k_x}{m},$$

and use this to find that

$$\sigma = \frac{e^2 n \tau_0}{m},$$

where τ_0 is the Born approximation life time

$$\tau_0^{-1} = 2\pi d(\varepsilon_F) n_{\text{imp}} |u_0|^2.$$

2. Now relax the assumption of short range scatterers but assume instead that $u(\mathbf{k} - \mathbf{k}')$ is slowly varying on the scale given by the width of the spectral function, i.e. τ_0^{-1} . In this more realistic case, you will find for $|\mathbf{k}| = k_F$ that

$$\vec{\Gamma}^{RA}(\mathbf{k}) = \frac{\mathbf{k}}{m} + \frac{d(\varepsilon_F)}{2} \int d\Omega' |u(\mathbf{k} - \mathbf{k}')|^2 \vec{\Gamma}^{RA}(\mathbf{k}'),$$

with $|\mathbf{k}'| = k_F$ and $\int d\Omega' = \int d\phi' d\theta' \sin \theta'$ is an integration over the angle of \mathbf{k}' . Now show that

$$\sigma = \frac{e^2 n \tau^{\text{tr}}}{m},$$

where

$$(\tau^{\text{tr}})^{-1} = 2\pi d(\varepsilon_F) n_{\text{imp}} \int \frac{d\Omega'}{4\pi} |u(\mathbf{k} - \mathbf{k}')|^2 \left(1 - \frac{\mathbf{k} \cdot \mathbf{k}'}{k_F^2} \right).$$

Hint: use the ansatz $\vec{\Gamma}^{RA}(\mathbf{k}) = (\mathbf{k}/m)\gamma$.

Explain the physical meaning of the last term and why it does not appear in the result for point-like impurities.

Exercise 14.2

Life time of the Green's function in the Born approximation. Show that the retarded impurity averaged Green's function in the Born approximation decays exponentially in time and given a physical interpretation of this result.

Exercise 14.3

Weak localization at finite frequency. Here we consider the weak localization correction at finite frequency. The only change in the formula for the weak localization is through the Cooperon which becomes instead

$$C^{RA}(\mathbf{Q}, \omega) = \frac{W_0 \zeta(\mathbf{Q}, \omega)}{1 - \zeta(\mathbf{Q}, \omega)},$$

$$\zeta(\mathbf{Q}, \omega) = \frac{1}{V} \sum_{\mathbf{p}} |u_0|^2 G^R(\mathbf{p} - \mathbf{Q}, \omega) G^A(\mathbf{p}, 0).$$

Show that in this case, the low frequency $\omega\tau_0 \ll 1$ and long wavelength $Qv_F\tau_0 \ll 1$ limit of $\zeta(\mathbf{Q}, \omega)$ is

$$\zeta(\mathbf{Q}, \omega) \approx 1 + i\omega\tau_0 - D\tau_0 Q^2.$$

Show that the frequency provide a small Q cut-off in the conductivity correction and try to explain why.

Exercise 14.4

Mass renormalization in Drude formula? The mass that appears in the Drude formula is the bare electron mass (possibly including bandstructure effects). The impurities only enter in the scattering time. The Drude formula can be derived from e.g. the Boltzmann equation, where the mass enters through the velocity, $v_k = \hbar k/m$ and the impurity potential in the collision term.

If we think about impurity scattering from a microscopic point of view the self energy has both a real and an imaginary part. Let us for instance consider the lowest order self-consistent Born approximation. In this case the self-energy reads

$$\sum^{\text{ISBBA}}(\mathbf{k}, ik_n) = n_{\text{imp}} \sum_{\mathbf{k}'} |u_{\mathbf{k}-\mathbf{k}'}|^2 \mathcal{G}(\mathbf{k}', ik_n). \quad (\text{B.4})$$

Note that it is \mathcal{G} and not \mathcal{G}_0 that enters in the self-consistent approximation. The real part leads to a renormalization of the mass and to a renormalization of the spectral weight at the Fermi surface, i.e. when expanding the Green's function near the Fermi surface we can write

$$G^R(\mathbf{k}, \varepsilon) \approx \frac{Z}{\omega - \xi_{\mathbf{k}}^* + i \frac{2}{\tau^*}}. \quad (\text{B.5})$$

If we include the real part in this way (contrary to Sec. 14.3 and Exercise 5, where it is neglected) does it lead to a renormalization of the Drude formula?

Exercises for Chapter 15

Exercise 15.1

Conductance of a delta function barrier As a model system of a mesoscopic 1D channel take the following Hamiltonian

$$H = -\frac{\hbar^2}{2m} \frac{\partial^2}{\partial x^2} + V_0 \delta(x).$$

Consider a scattering state

$$\psi_k^+(x) = \begin{cases} \frac{1}{\sqrt{L}} (e^{ikx} + r e^{-ikx}), & x < 0, \\ \frac{1}{\sqrt{L}} t e^{ikx}, & x > 0, \end{cases}$$

and likewise for ψ^- . Show that

$$\psi'(0^+) - \psi'(0^-) = \frac{2m}{\hbar^2} V_0 \psi(0)$$

and use it to find r and t . Suppose now that the two ends of the wire have different chemical potential, so that the distribution function for electrons in the states ψ_k^+ is given by $n_F(\varepsilon_k - \mu_L)$, while the distribution function for electrons in states ψ_k^- is $n_F(\varepsilon_k - \mu_R)$. Show that the current at low temperature becomes

$$I = 2e \sum_{k>0} (v_k^+ n_F(\varepsilon_k - \mu_L) - v_k^- n_F(\varepsilon_k - \mu_R)) = \frac{2e^2}{h} \frac{1}{1 + (V_0/\hbar v_F)^2} V,$$

where $V = \frac{\mu_R - \mu_L}{e} \ll \varepsilon_F$.

Hints: $v_k^+ = \frac{\hbar}{2mi} ((\psi_k^+)^* \partial_x \psi_k^+ - \text{c.c.}) = |t|^2 = 1 - |r|^2$ with $t = (1 + iz)^{-1}$, $z = mV_0/\hbar k$.

Exercise 15.2

Landauer-Büttiker formula at finite temperatures. For a general mesoscopic system show that the linear conductance at finite temperature is generalized to

$$G = \frac{2e^2}{h} \sum_n \int_0^\infty dE \left(-\frac{\partial n_F(E - \mu)}{\partial E} \right) T_n(E),$$

where $T_n(E)$ is the transmission probability of a given mode $T_n(E) = \sum_{n'} t_{nn'}^* t_{n'n}$.

Using a model electron waveguide, where the potential in the transverse direction is a parabolic confinement, the transmission coefficient is supposed to be

$$T_n(E) = \Theta(E - E_n) = \Theta(E - (n + \frac{1}{2})\hbar\omega_T),$$

where ω_T is the frequency of transverse oscillation. Find an expression for the conductance G and plot the G as a function of μ . Plot for example $G(h/2e^2)$ versus $\mu/\hbar\omega_T$ for two different temperatures: $kT = (0.05, 0.15)\hbar\omega_T$. How would the result look if the transverse confinement was given by a square well?

Exercises for Chapter 16

Exercise 16.1

Phonon Green's function Prove Eq. (16.7).

Exercise 16.2

Cooper's instability In this exercise we shall see that an attractive electron-electron interaction leads to an instability of the Fermi surface.

BCS model Hamiltonian. In Chap. 16 it is shown that the electron-phonon interaction leads to an effective electron-electron interaction. It is attractive for small frequencies, i.e. for energies smaller than qv_s , where q is the exchanged momentum and v_s is the sound velocity. The scale of this energy is given by the Debye energy. This observation lead Cooper to study the following model Hamiltonian, which is also the starting point used by BCS,

$$H = H_0 + H' \quad (1a)$$

$$H_0 = \sum_{k\sigma} (\varepsilon_k - \mu) c_{k\sigma}^\dagger c_{k\sigma}, \quad (1b)$$

$$H' = -\frac{V_0}{2} \sum' c_{k+q\sigma}^\dagger c_{k'-q\sigma'}^\dagger c_{k'\sigma'} c_{k\sigma}. \quad (1c)$$

Here the sum is restricted such that all initial and final states lie in an interval given by $[\mu - \omega_D, \mu + \omega_D]$, i.e. in a shell around the Fermi surface. Anticipating the physical idea that the electrons due to the attractive interaction will form pairs with zero total momentum and spin, we look specifically at the interaction between such pairs. The pairs are thus supposed to consist of electrons with opposite momentum, which means that we choose $\mathbf{k}' = -\mathbf{k}$ and $\sigma = -\sigma'$. After relabelling we have

$$H' = -V_0 \sum' c_{\mathbf{k}'\uparrow}^\dagger c_{-\mathbf{k}'\downarrow}^\dagger c_{-\mathbf{k}\downarrow} c_{\mathbf{k}\uparrow}. \quad (2)$$

Variational calculation of FS with an added pair of electrons. We wish to find the energy of a pair of electrons added to a filled Fermi sea state, and with interactions according to (2). In order to separate the effect of the interaction on the Fermi sea and on the extra pair of electrons, the \sum' sum is further restricted to involve only states outside the Fermi sea. Thus Eq. (2) becomes

$$H' = -V_0 \sum_{k,k' > k_F} ' c_{\mathbf{k}'\uparrow}^\dagger c_{-\mathbf{k}'\downarrow}^\dagger c_{-\mathbf{k}\downarrow} c_{\mathbf{k}\uparrow}. \quad (3)$$

We look at the difference between the two situations: 1) The electron pair is added to the Fermi surface, i.e. with $|\mathbf{k}|, |\mathbf{k}'| = k_F$ and energy equal to zero. 2) The electron pair forms a coherent superposition of pairs not necessary at the Fermi surface. According to the variational principle the lowest energy of the two is closest to the groundstate energy.

For situation 2 we start by an Ansatz wavefunction, which is a superposition of so-called Cooper pairs

$$|\psi\rangle = \sum_{\mathbf{k}} \alpha_{\mathbf{k}} c_{\mathbf{k}\uparrow}^{\dagger} c_{-\mathbf{k}\downarrow}^{\dagger} |FS\rangle. \quad (4)$$

Show that $\alpha_{\mathbf{k}}$ satisfies the following equation.

$$\alpha_{\mathbf{k}}(2\varepsilon_{\mathbf{k}} - E_F) - V_0 \sum_{k' > k_F} ' \alpha_{\mathbf{k}'} = E \alpha_{\mathbf{k}}, \quad (5)$$

and that this leads to a condition for E given by

$$1 = V_0 \sum_{k' > k_F} ' \frac{1}{(2\varepsilon_{\mathbf{k}} - E_F) - E}. \quad (6)$$

In order to find the energy E you should make use of the following hierarchy of energy scales

$$E \ll \omega_D \ll E_F, \quad (7)$$

where the validity of the first one of course must be checked at the of the calculation. Find that (reinserting \hbar)

$$E = -2\hbar\omega_D \exp(-1/V_0 d(E_F)). \quad (8)$$

Discuss the following two important issues:

- Why does this result indicate an instability of the Fermi surface
- Could this result have been reached by perturbation theory in V_0 ?

Exercises for Chapter 17

Exercise 17.1

The Josephson effect. This exercise deals with the supercurrent across a tunnel junction, the so-called Josephson effect. We apply the relations to study the current-voltage characteristic of a tunnel junction in the so-called resistively shunted Josephson junction model.

Supercurrent in the equilibrium state. Consider a tunnel junction between two superconductors, i.e. two superconductors separated by an insulator. The tunnel Hamiltonian is

$$H_T = \sum_{kp} \left(t_{\mathbf{k}\mathbf{p}} c_{\mathbf{k}\sigma}^{\dagger} f_{\mathbf{p}\sigma} + t_{\mathbf{k}\mathbf{p}}^* f_{\mathbf{p}\sigma}^{\dagger} c_{\mathbf{k}\sigma} \right), \quad (1)$$

where the electron operators for the two sides are called c and f , respectively. In the following we assume for simplicity that in the energy range of interest the tunnel matrix element depends weakly on the states \mathbf{k} and \mathbf{p} , therefore

$$t_{\mathbf{k}\mathbf{p}} \approx t \quad (2)$$

The Hamiltonian for the two sides are the usual BCS Hamiltonians

$$H_c = \sum_{\mathbf{k}\sigma} \xi_k c_{\mathbf{k}\sigma}^\dagger c_{\mathbf{k}\sigma} - \Delta e^{i\phi_c} \sum_{\mathbf{k}} c_{\mathbf{k}\uparrow}^\dagger c_{-\mathbf{k}\downarrow}^\dagger - \Delta e^{-i\phi_c} \sum_{\mathbf{k}} c_{-\mathbf{k}\downarrow} c_{\mathbf{k}\uparrow}, \quad (3a)$$

$$H_f = \sum_{\mathbf{k}\sigma} \xi_k f_{\mathbf{k}\sigma}^\dagger f_{\mathbf{k}\sigma} - \Delta e^{i\phi_f} \sum_{\mathbf{k}} f_{\mathbf{k}\uparrow}^\dagger f_{-\mathbf{k}\downarrow}^\dagger - \Delta e^{-i\phi_f} \sum_{\mathbf{k}} f_{-\mathbf{k}\downarrow} f_{\mathbf{k}\uparrow}, \quad (3b)$$

where the two superconductors are assumed to be equal. The order parameter of each side of the junction have different phases, ϕ_c and ϕ_f , and Δ is here taking to be real. The phase difference between the two side can be absorbed as a phase shift of the tunnel matrix

$$t \rightarrow e^{-i(\phi_c - \phi_f)/2} t, \quad (4)$$

by the transformation

$$c \rightarrow e^{i\phi_c/2} c, \quad f \rightarrow e^{i\phi_f/2} f. \quad (5)$$

Show that the equilibrium current running between the two superconductors is

$$I_J = \langle I \rangle = (-2e) \langle \frac{\partial}{\partial \phi} H_T \rangle = (-2e) \frac{\partial F}{\partial \phi}, \quad (6)$$

where I is the operator for the electrical current $I = (-e) \dot{N}_c$, F is the free energy and $\phi = \phi_c - \phi_f$ is the phase difference.

This is a current which runs in thermodynamical equilibrium and hence is *dissipationless* in the sense that it runs without an applied bias (the chemical potential of the two sides is per definition identical in equilibrium). In the following we calculate this so-called supercurrent to second order in the tunneling amplitude.

Show that to second order in H_T

$$\langle \frac{\partial}{\partial \phi} H_T \rangle \approx - \int_0^\beta d\tau \langle T_\tau H_T(\tau) \frac{\partial}{\partial \phi} H_T \rangle_0 = - \frac{1}{2} \frac{\partial}{\partial \phi} \int_0^\beta d\tau \langle T_\tau H_T(\tau) H_T \rangle_0, \quad (7)$$

where the expectation value $\langle \rangle_0$ means taken with respect to Eqs. (2). Then show that

$$\begin{aligned} \frac{1}{2} \frac{\partial}{\partial \phi} \int_0^\beta d\tau \langle T_\tau H_T(\tau) H_T \rangle_0 &= \frac{\partial}{\partial \phi} \left(\int_0^\beta d\tau \sum_{\mathbf{k}\mathbf{p}} t^2 e^{i\phi} \mathcal{G}_{21}(\mathbf{k}, \tau) \mathcal{G}_{12}(\mathbf{p}, -\tau) + c.c. \right) \\ &= \frac{\partial}{\partial \phi} \left(\frac{1}{\beta} \sum_{ik_n} \sum_{\mathbf{k}\mathbf{p}} t^2 e^{i\phi} \mathcal{G}_{21}(\mathbf{k}, ik_n) \mathcal{G}_{12}(\mathbf{p}, ik_n) + c.c. \right) \end{aligned} \quad (8)$$

where \mathcal{G}_{12} and \mathcal{G}_{21} are the off-diagonal Nambu Green's functions defined in Exercise 3.

Verify the following steps

$$\begin{aligned} \sum_{\mathbf{k}} \mathcal{G}_{21}(\mathbf{k}, ik_n) &= \sum_{\mathbf{p}} \mathcal{G}_{12}(\mathbf{p}, ik_n) \\ &= \frac{\Delta d(\varepsilon_F)}{2} \int_{-\infty}^{\infty} d\xi \left(\frac{1}{(ik_n)^2 - E^2} \right) \\ &= - \frac{\Delta d(\varepsilon_F)}{2} \frac{\pi}{\sqrt{k_n^2 + \Delta^2}}, \end{aligned} \quad (9)$$

and use it to find that

$$\begin{aligned}
 I_J &= - \left(\frac{\pi \Delta d(\varepsilon_F) t}{2} \right)^2 \frac{1}{\beta} \sum_{ik_n} \frac{1}{k_n^2 + \Delta^2} \\
 &= \sin \phi \frac{e (\pi d(\varepsilon_F) t)^2}{2} \Delta \tanh \left(\frac{\Delta \beta}{2} \right) \\
 &= \sin \phi \frac{\Delta \pi}{2eR_N} \tanh \left(\frac{\Delta \beta}{2} \right), \tag{10}
 \end{aligned}$$

where the normal state tunnel resistance is given by $R_N^{-1} = \pi e^2 d^2 t^2 / \hbar$.

Exercise 17.2

RSJ model of a Josephson junction. With a finite bias voltage across the junction, one can still have a supercurrent running, i.e. a current carried by Cooper pairs and the relation

$$I_J = I_C \sin \phi, \tag{1}$$

is still valid. *This is known as the first Josephson relation.* The finite voltage changes the energy of electrons of the two sides and hence their phase. We can simply include this phase change in the time dependence of by the following substitution

$$c(t) \rightarrow c(t)e^{iVt/2}, \quad f(t) \rightarrow f(t)e^{-iVt/2}, \tag{2}$$

which corresponds to

$$\phi \rightarrow \phi + 2eVt, \tag{3}$$

or

$$\dot{\phi} = \frac{2e}{\hbar} V, \tag{4}$$

which is called the second Josephson relations.

The second Josephson relation adds interesting dynamics to the Josephson junction because of the intrinsic frequency $2eV/\hbar$. One can measure this frequency by applying external RF radiation to the junction. The Josephson junction thus acts as a voltage to frequency converter, which has many applications.

Now we look at the current-voltage characteristic of a Josephson junction in the RSJ model. The current is carried by two kinds of electrons: those that are paired and those that are not. The pair current is described by the Josephson relations while the normal current is supposed to be given by Ohm's law.

Consider a current biased setup, i.e. a junction with a fixed current, I . This current is made up by the sum of the supercurrent and the normal current. Thus

$$I = I_N + I_J = \frac{1}{R} V + I_C \sin \phi = \frac{\hbar}{2eR} \dot{\phi} + I_C \sin \phi. \tag{5}$$

Write this equation in the dimensionless form

$$\eta = \frac{I}{I_C} = \frac{d\phi}{d\tau} + \sin \phi, \quad \tau = \frac{2eI_C R}{\hbar} t. \tag{6}$$

The voltage is time dependent, but in a dc measurement one measures the average voltage. Integrate Eq. (6) and show that the average voltage becomes

$$\langle V \rangle = \begin{cases} 0, & I < I_C \\ RI_c \sqrt{(I/I_C)^2 - 1}, & I > I_C \end{cases} \quad (7)$$

Hint: first find solutions for $\dot{\phi} = 0$ and then a “running” solution where $\dot{\phi} \neq 0$. For the last situation the average voltage is $\langle V \rangle = \frac{1}{T} \int_0^T dt \frac{d\phi}{dt} = \frac{2\pi}{T}$. Here T is the period of the voltage or the time it takes to increase ϕ by 2π .

Index

- acoustic phonons
 - Debye phonons, 52
 - graphical representation, 51, 56
 - in second quantization, 55
- adiabatic continuity, 233
- advanced function, 163
- Aharonov-Bohm effect, 120
- analytic continuation, 162
- analytic function, 161
- Anderson's model for magnetic impurities, 147
- annihilation operators
 - 1D phonons, 55
 - bosons, 10
 - fermions, 13
 - time dependence, 91
 - time-derivative, 145
- anti-commutator, 13
- anti-symmetrization operator, 7
- antiferromagnetism, 73
- art, the art of mean field theory, 68
- atom
 - artificial, 153
 - Bohr radius a_0 , 40
 - electron orbitals, 3
 - ground state energy E_0 , 40
 - in metal, 31
- attractive pair-interaction, 281
- bandstructure diagram
 - extended zone scheme, 35
 - metal, semiconductor, insulator, 45
- Bardeen-Cooper-Schrieffer (see BCS), 78
- basis states
 - change in second quantization, 16
 - complete basis set, 3
 - Green's function, 130
 - many-particle boson systems, 12
 - many-particle fermion systems, 14
 - orthonormal basis set, 2
 - systems with different particles, 24
- BCS theory
 - effective Hamiltonian, 81
 - interaction potential model, 285
 - mean field Hamiltonian, 82
 - self-consistent gap equation, 83
 - tunneling spectroscopy, 140
- Bloch
 - Bloch theory of lattice electrons, 33
 - bandstructure, 35
 - Bloch's equation, density matrix, 158
 - Bloch's theorem, 34
- Bogoliubov transformation, 82
- Bohm-Staver sound velocity
 - from RPA-screened phonons, 283
 - semi-classical, 53
- Bohr radius a_0 , 40
- Boltzmann distribution, 26
- Boltzmann equation
 - collision free, 239
 - introduction, 233
 - with impurity scattering, 241
- Born approximation
 - first Born approximation, 190, 259
 - full Born approximation, 193
 - in conductivity, 261
 - self-consistent Born approximation, 194
 - spectral function, 1st order, 192
- Born-Oppenheimer approximation, 279
- Bose-Einstein distribution, 29, 51
- boson
 - creation/annihilation operators, 10
 - defining commutators, 11
 - definition, 5
 - frequency, 161, 165
 - many-particle basis, 12
- bra state, 2
- Brillouin zone
 - bandstructure diagram, 35
 - definition, 34
 - for 1D phonons, 54

- broadening of the spectral function, 136
- broken symmetry, 71
- canonical
 - ensemble, 27
 - momentum, 21
 - partition function, 26
- carbon nanotubes, 48
- charge-charge correlation function, 103
- chemical potential
 - definition, 27
 - temperature dependence, 39
- collapse of wavefunction, 2
- commutator
 - $[AB, C] = A[B, C] + [A, C]B$, 92
 - $[AB, C] = A\{B, C\} - \{A, C\}B$, 92
 - defining bosons, 11
 - defining fermions, 13
 - general definition, 11
- complete
 - basis states, 3
 - set of quantum numbers ν , 3
- conductance
 - conductance fluctuations, 186
 - Kubo formalism, 100
 - mesoscopic system, 113
 - universal fluctuations, 121
- conductance quantization, 116
- conductivity
 - cooperons, 269
 - introduction, 253
 - Kubo formalism, 98
 - relation to dielectric function, 104
 - semi-classical approach, 240
- connected Feynman diagrams, 203
- conservation of four-momentum, 208
- conserving approximation, 259
- continuity equation
 - for ions in the jellium model, 52
 - for quasiparticles, 238
- contour integral, 166
- convergence of Matsubara functions, 160
- Cooper
 - Cooper pairs, 81
 - instability of the Fermi surface, 81
 - instability, Feynman diagrams, 284
- cooperons in conductivity, 269
- core electron, 31
- correlation function
 - charge-charge correlation, 103
 - current-current correlation, 100, 254
 - general Kubo formalism, 97
- correlation hole around electrons, 65
- Coulomb blockade, 153
- Coulomb interaction
 - combined with phonons, 279
 - direct process, 43
 - divergence, 44, 213
 - exchange process, 44
 - in conductivity, 256
 - RPA renormalization, 217, 227
 - screened impurity scattering, 181
 - second quantization, 23
 - Yukawa potential, RPA-screening, 218
- coupling constant
 - electron interaction strength e_0^2 , 23
 - electron-phonon, general, 62
 - electron-phonon, jellium model, 64
 - electron-phonon, lattice model, 63
 - electron-phonon, RPA-renormalized, 283
 - integration over, 220
- creation operators
 - 1D phonons, 55
 - bosons, 10
 - fermions, 13
 - time dependence, 91
- critical temperature
 - Cooper instability, 285
 - ferromagnetism, 74
 - superconductivity, 84
- crossed diagram
 - definition, 267
 - maximally crossed, 268
- crossing diagrams
 - definition, 264
 - suppressed in the Born approx., 196
- current density operator
 - dia- and paramagnetic terms, 99
 - second quantization, 22
- current-current correlation function, Π
 - definition, 100
 - diagrammatics, 254
- d-shell, 148
- Debye
 - acoustical Debye phonons, 52
 - Debye energy or frequency ω_D , 59
 - Debye model, 52, 59, 284

- Debye temperature T_D , 59
- Debye wave number k_D , 59
- density of states, Debye model, 59
- frequency cut-off, BCS, 285
- delta function $\delta(\mathbf{r})$, 4
- density in second quantization, 22
- density matrix operator, 27
- density of states
 - measured by tunneling, 140
 - non-interacting electrons, 38
 - phonons, Debye model, 59
 - spectral function, 136
- density waves, 72
- density-density correlation function
 - the pair-bubble $\chi_0 \equiv -\Pi^0$, 216
 - the RPA-bubble χ^{RPA} , 226
 - the RPA-bubble and phonons, 282
- dephasing, 108, 264, 272
- determinant
 - first quantization, 7
 - in Wick's theorem, 172
 - Slater, 7
- diagonal Hamiltonian, 133
- diamagnetic term in current density, 99
- dielectric function ε
 - equation of motion derivation, 155
 - irreducible polarization function χ^{irr} , 226
 - Kubo formalism, 102
 - relation to polarization function χ , 223
 - relation to conductivity, 104
- differential conductance, 140
- differential equation
 - classical Green's function, 127
 - many-body Green's function, 131
 - single-particle Green's function, 146
- Dirac
 - bra(c)ket notation for quantum states, 2
 - delta function $\delta(\mathbf{r})$, 4
- disconnected Feynman diagrams, 203
- disorder, mesoscopic systems, 121
- dissipation
 - due to electron-hole pairs, 144, 231
 - of electron gas, 143
- distribution function
 - Boltzmann, 26
 - non-interacting bosons, 29
 - non-interacting fermions, 28
 - Boltzmann, Gibbs, 26
 - Bose-Einstein, 29
 - electron reservoir, 113
 - Fermi-Dirac, 28
 - Maxwell-Boltzmann, 45
- donor atoms, 46
- Drude formula, 240, 251, 264
- Dulong-Petit value for specific heat, 60
- dynamical matrix $\mathbf{D}(\mathbf{k})$, 57
- Dyson equation
 - Feynman diag., external potential, 179
 - first Born approximation, 190
 - for Π_{xx} , 257
 - for cooperon, 269
 - full Born approximation, 193
 - impurity and interaction, 256
 - impurity averaged electrons, 189
 - pair interactions in Fourier space, 208
 - pair interactions in real space, 205
 - pair-scattering vertex Λ , 284
 - polarization function χ , 226
 - self-consistent Born approximation, 194
 - single-particle in external potential, 178
- effective electron-electron interaction
 - Coulomb and phonons, jellium, 280
 - Coulomb and phonons, RPA, 283
 - phonon mediated, RPA, 283
- effective mass approximation, 35
- effective mass, renormalization, 246, 251
- eigenmodes
 - electromagnetic field, 19
 - lattice vibrations, 58
- eigenstate
 - definition, 1
 - superposition, 1
- eigenvalue, definition of, 1
- Einstein model of specific heat, 60
- Einstein phonons
 - in the jellium model, 52
 - optical phonons, 52
- elastic scattering
 - Matsubara Green's function, 179
- electric potential
 - classical theory, 127
 - external and induced, 237
- electron
 - core electrons, 31
 - density of states, 38
 - phase coherence, 184
 - valence electrons, 31

- electron gas, in general
 - 0D: quantum dots, 49
 - 1D: carbon nanotubes, 48
 - 2D: GaAs heterostructures, 46
 - 3D: metals and semiconductors, 45
 - introduction, 31
- electron gas, interacting
 - attractive interaction, 281
 - dielectric properties and screening, 223
 - first order perturbation, 41, 43
 - full self-energy diagram, 214
 - full theory, 213
 - general considerations, 39
 - ground state energy, 220, 222
 - Hartree–Fock mean field Hamiltonian, 70
 - infinite perturbation series, 214, 222
 - Landau damping, 230
 - plasma oscillations, 228
 - second order perturbation, 43
 - thermodynamic potential Ω , 220
- electron gas, non-interacting
 - Bloch theory, 33
 - density of states, 38
 - Feynman diagrams, 177
 - finite temperature, 38
 - ground state energy, 38
 - jellium model, 35
 - motion in external potentials, 177
 - static ion lattice, 33
- electron interaction strength e_0^2 , 23
- electron wave guides, 116
- electron-electron scattering
 - attractive interaction, 281
 - Cooper instability, 284
 - dephasing, 264, 272
 - life-time, 243
- electron-hole pairs
 - excitations, 144, 155
 - interpretation of RPA, 220
 - Landau damping, 231
- electron-phonon interaction
 - adiabatic electron motion, 53
 - basis states, 276
 - combined with Coulomb interaction, 279
 - Feynman diagrams, 276
 - general introduction, 51
 - graphical representation, 63
 - the jellium model, 63, 275
 - the lattice model, 61, 275
 - the sound velocity, 53
 - umklapp process, 63
- electronic plasma oscillations
 - graphical representation, 51
- equation of motion
 - Anderson’s model, 149
 - derivation of RPA, 153
 - for ions, 57
 - frequency domain, 147
 - Heisenberg operators, 88
 - in proof of Wick’s theorem, 171
 - introduction, 145
 - Matsubara Green’s function, 169
 - non-interacting particles, 147
 - single-particle Green’s function, 145
- ergodic, 121
- ergodicity assumption, 25
- extended zone scheme, 35
- Fermi
 - Fermi energy ε_F , 36
 - Fermi sea diagrams, 37
 - Fermi sea with interactions, 42
 - Fermi sea, Cooper instability, 286
 - Fermi sea, definition, 36
 - Fermi sea, excitations, 144
 - Fermi velocity v_F , 36
 - Fermi wave length λ_F , 36
 - Fermi wavenumber k_F , 36
 - Fermi’s golden rule, 240, 244, 250
 - Thomas-Fermi screening, 218, 219
- Fermi liquid theory
 - introduction, 233
 - microscopic basis, 245
- Fermi-Dirac distribution, 28, 237
- fermion
 - definition, 5
 - creation/annihilation operators, 13
 - defining commutators, 13
 - frequency, 161, 165
 - many-particle basis, 14
- fermion loop, 202
- ferromagnetism
 - critical temperature, 74
 - introduction, 73
 - order parameter, 72
 - Stoner model, 75
- Feynman diagrams
 - cancellation of disconnected diagrams, 203

- Cooper instability, 284
- electron-impurity scattering, 182
- electron-phonon interaction, 276
- external potential scattering, 179
- first Born approximation, 190
- full Born approximation, 193
- impurity averaged single-particle, 188
- interaction line in Fourier space, 208
- interaction line in real space, 204
- irreducible diagrams, imp. scattering, 189
- irreducible diagrams, pair interaction, 205
- pair interactions, 199
- polarization function χ , 225
- self-consistent Born approximation, 194
- single-particle, external potential, 177
- topologically different diagrams, 204
- Feynman rules
 - electron-impurity scattering, 184
 - external potential scattering, 179
 - impurity averaged Green's function, 188
 - pair interactions in Fourier space, 208
 - pair interactions in real space, 204
 - pair interactions, \mathcal{G} denominator, 201
 - pair interactions, \mathcal{G} numerator, 202
 - phonon mediated pair interaction, 278
- first quantization
 - many-particle systems, 4
 - name, 1
 - single-particle systems, 2
- Fock
 - approximation for interactions, 70
 - Fock self-energy for pair interactions, 209
 - Fock space, 10, 27
 - Hartree–Fock approximation, 69
- four-vector/four-momentum notation, 207, 255
- Fourier transformation
 - 1D ion vibrations, 54
 - basic theory, 291
 - Coulomb interaction, Matsubara, 206
 - equation of motion, 147
 - Matsubara functions, 161
- free energy
 - definition, 27
 - in mean field theory, 67
- GaAs/Ga_{1-x}Al_xAs heterostructures, 46
- gauge
 - breaking of gauge symmetry, 78
 - Landau gauge, 3
- radiation field, 19
- transversality condition, 19
- Gauss box, 47
- Gibbs distribution, 26
- grand canonical
 - density matrix, 27
 - ensemble, 27
 - partition function, 27
- gravitation, 1
- Greek letters, 158
- Green's function
 - n -particle, 170
 - classical, 127
 - dressed, 254
 - free electrons, 132
 - free phonons, 275
 - greater and lesser, 131
 - imaginary time, 160
 - introduction, 127
 - Lehmann representation, 134
 - Poisson's equation, 127
 - renormalization, 245
 - retarded, equation of motion, 145
 - retarded, many-body system, 131
 - retarded, one-body system, 130
 - RPA-screened phonons, 282
 - Schrödinger equation, 128
 - single-particle, many-body system, 131
 - translation-invariant system, 132
 - two particle, 141
- Hamiltonian
 - diagonal, 133
 - non-interacting particles, 135
 - quadratic, 135, 146, 150, 170
- harmonic oscillator
 - length, 18
 - second quantization, 18
- Hartree
 - approximation for interactions, 70
 - Hartree self-energy, pair interactions, 209
 - Hartree–Fock approximation, 69
- Hartree–Fock approximation
 - introduction, 69
 - mean field Hamiltonian, 70
 - the interacting electron gas, 70
- heat capacity
 - for electrons, 39
 - for ions, 52

- Heaviside's step function $\theta(x)$, 4
- Heisenberg
 - Heisenberg picture, 88
 - model of ferromagnetism, 73
- helium, Hamiltonian, 9
- heterostructures, GaAs/Ga_{1-x}Al_xAs, 46
- Hilbert space, 1
- hopping, 149
- Hubbard model, 75
- hybridization, 148
- hydrogen atom
 - Bohr radius a_0 , 40
 - electron orbitals, 3
 - ground state energy E_0 , 40
- imaginary time
 - discussion, 158
 - Greek letters, 158
 - Green's function, 160
- impurities, magnetic, 148
- impurity scattering, conductivity, 253
- impurity self-average, 184
- impurity-scattering line
 - Feynman rules, 188
 - in conductivity, 255
 - renormalization by RPA-screening, 227
- inelastic light scattering, 144
- infinite perturbation series
 - breakdown at phase transitions, 85
 - electron gas ground state energy, 222
 - self-energy for interacting electrons, 214
 - single-particle Green's function, 178
 - time-evolution operator $\hat{U}(t, t_0)$, 90
- infinitesimal shift η , 162
- integration over the coupling constant, 220
- interaction line
 - general pair interaction in real space, 204
 - pair interaction in Fourier space, 208
 - RPA screened Coulomb line, 217, 227
 - RPA screened impurity line, 227
- interaction picture
 - imaginary time, 159
 - introduction, 88
 - real space Matsubara Green's fct., 200
- interference, 264, 265
- ions
 - ionic plasma oscillations, 51
 - forming a static lattice, 33
 - Heisenberg model, ionic ferromagnets, 73
 - in a metal, 31
- irreducible Feynman diagrams
 - impurity scattering, 189
 - pair interaction, 205
 - polarization function χ^{irr} , 225
- iterative solution, integral eqs., 90, 128
- jellium model
 - effective electron-electron interaction, 280
 - Einstein phonons, 52
 - electron-phonon interaction, 63
 - full electronic self-energy, 214
 - oscillating background, 52
 - static case, 35
- ket state, 2
- kinetic energy operator
 - including a vector potential, 21
 - second quantization, 21
- kinetic momentum, 21
- Kronecker's delta function $\delta_{k,n}$, 4
- Kubo formalism
 - conductance, 100
 - conductivity, 98, 254
 - correlation function, 97
 - dielectric function, 102
 - general introduction, 95
 - Landauer-Büttiker formula, 115
 - RPA-screening in the electron gas, 223
 - time evolution, 97
 - tunnel current, 139
- ladder diagram, 259
- Landau
 - and Fermi liquid theory, 233
 - damping and plasma oscillations, 230
 - eigenstates, 3
 - gauge, 3
- Landauer-Büttiker formula
 - heuristic derivation, 113
 - linear response derivation, 115
- lattice model
 - basis in real space, 33
 - basis in reciprocal space, 33
 - Hamiltonian, 33
- lattice vibrations
 - 1D phonon Hamiltonian, 53
 - electron-phonon interaction, 61
- Lehmann representation
 - definition, 134

- for $G^>$, $G^<$, and G^R , 134
 - Matsubara function, 162
- life-time, 150, 236, 243, 262
- Lindhard function, 143, 155
- linear response theory
 - introduction, 95
 - Landauer-Büttiker formula, 115
 - mesoscopic system, 113
 - time evolution, 91
 - tunnel current, 139
- magnetic impurities, 148
- magnetic length, 3
- magnetic moment, 74, 147, 149
- magnetization, 72, 149
- many-body system
 - single-particle Green's function, 131
 - first quantization, 2
 - second quantization, 9
- mass renormalization, 254
- Matsubara
 - function, equation of motion, 169
 - convergence of, 160
 - Fourier transformation, 161
 - frequency, 161
 - Green's function, 160
 - relation to retarded function, 161
 - sums, evaluation of, 165
 - sums, simple poles, 167
 - sums, with branch cuts, 168
- Matsubara Green's function
 - elastic scattering, 179
 - electron-impurity scattering, 182
 - first Born approximation, 190
 - free phonons, 275
 - full Born approximation, 193
 - impurity averaged single-particle, 188
 - interacting elec. in Fourier space, 208
 - interacting electrons in Fourier space, 206
 - interacting electrons in real space, 199
 - RPA-screened phonons, 282
 - self-consistent Born approximation, 194
 - two-particle polarization function χ , 224
- maximally crossed diagrams, 268
- MBE, molecular beam epitaxy, 46
- mean field theory
 - Anderson's model, 150
 - BCS mean field Hamiltonian, 82
 - broken symmetry, phase transitions, 71
 - general Hamiltonian H_{MF} , 66
 - Hartree-Fock mean field Hamiltonian, 70
 - introduction, 65
 - mean field approximation, 67
 - partition function Z_{MF} , 67
 - the art of mean field theory, 68
- mean free path, 107
- measuring the spectral function, 137
- Meissner effect, 78
- mesoscopic
 - disordered systems, 121
 - physics, 253
 - regime, 265
 - systems, introduction, 107
- metal
 - disordering and random impurities, 181
 - electrical resistivity, 181
 - general description, 31
 - Hamiltonian, 32
 - observation of plasmons, 229
 - Thomas-Fermi screening in metals, 219
- Migdal's theorem, 279
- molecular beam epitaxy, MBE, 46
- momentum
 - canonical, 21
 - kinetic, 21
 - relaxation, 240, 243
- MOSFET, 46
- Newton's second law
 - for ions in the jellium model, 52
- non-interacting particles
 - distribution functions, 28
 - equation of motion, 147
 - Green's functions, 132
 - Hamiltonian, 135
 - in conductivity, 261
 - Matsubara Green's function, 164
 - quasiparticles, 233
 - retarded Green's function $G^R(\mathbf{k}\sigma, \omega)$, 135
 - spectral function $A_0(\mathbf{k}\sigma, \omega)$, 135
- normalization of quantum states, 3
- normalization, scattering state, 108
- nucleus, 31
- occupation number operator
 - bosons, 12
 - fermions, 14
 - introduction, 10

- occupation number representation, 10
- operator
 - adjoint, 2
 - boson creation/annihilation, 10
 - electromagnetic field, 19
 - expansion of e^{-iHt} , 87
 - fermion creation/annihilation, 13
 - first quantization, 7
 - Heisenberg equation of motion, 88
 - Hermitian, 1
 - real time ordering T_t , 90
 - second quantization, 14
 - time evolution operator $\hat{U}(t, t_0)$, 89
 - trace Tr , 27
- optical phonons
 - Einstein phonons, 52
 - graphical representation, 56
- optical spectroscopy, 141
- optical theorem, scattering theory, 194
- order parameter
 - definition, 72
 - list of order parameters, 72
- overlap of wavefunctions
 - localized/extended states, 148
 - particle propagation, 133
 - tunneling, 138
- pair condensate, 72
- pair interactions
 - Dyson equation in Fourier space, 208
 - Dyson equation in real space, 205
 - Feynman diagrams, 199
 - Feynman rules in Fourier space, 208
 - Feynman rules in real space, 204
 - self-energy in Fourier space, 208
 - self-energy in real space, 205
- pair-bubble
 - calculation of the pair-bubble, 218
 - Feynman diagram $\Pi^0(\mathbf{q}, iq_n)$, 211
 - in the RPA self-energy, 216
 - self-energy diagram, 210
 - the correlation function $\chi_0 \equiv -\Pi^0$, 216
- paramagnetic term in current density, 99
- particle-particle scattering
 - in the collision term, 251
 - life-time, 243
- partition function
 - canonical ensemble, 26
 - grand canonical ensemble, 27
 - in mean field theory, 67
- Pauli
 - exclusion principle, 5, 40
 - spin matrices, 21
- periodic boundary conditions
 - 1D phonons, 53
 - electrons, 36
 - photons, 19
- permanent
 - for bosons, 7
 - in first quantization, 7
 - in Wick's theorem, 172
- permutation, 171
- permutation group S_N , 7, 90
- perturbation theory
 - first order, electron gas, 41
 - infinite order, Green's function, 178
 - infinite order, ground state energy, 222
 - infinite order, interacting electrons, 214
 - linear response, Kubo formula, 95
 - second order, electron gas, 43
 - single particle wavefunction, 128
 - time-evolution operator $\hat{U}(t, t_0)$, 90
- phase coherence, 264
- phase coherence for electrons, 184
- phase coherence length l_φ , 186
- phase space, 244, 245
- phase transition
 - breakdown of perturbation theory, 85
 - broken symmetry, 71
 - order parameters, 72
- phonons
 - 1D annihilation/creation operators, 55
 - 1D lattice vibrations, 53
 - density of states, Debye model, 59
 - dephasing, 264, 272
 - eigenmodes in 3D, 58
 - Einstein model of specific heat, 60
 - free Green's function, 275
 - general introduction, 51
 - Hamiltonian for jellium phonons, 52
 - phonon branches, 55
 - relevant operator $A_{\mathbf{q}\lambda}$, 275
 - RPA renormalization, 281
 - RPA-renormalized Green's function, 282
 - second quantization, 55, 58
- plasma frequency
 - for electron gases in a metals, 228
 - ionic plasma frequency, 52

- plasma oscillations
 - electronic plasma oscillations, 51
 - interacting electron gas in RPA, 228
 - ionic plasma oscillations, 51
 - Landau damping, 230
 - plasmons, 228
- plasmons
 - dynamical screening, 238
 - experimental observation in metals, 229
 - plasma oscillations, 228
 - semi-classical treatment, 237
- Poisson's equation
 - GaAs heterostructures, 47
 - Green's function, 127
- polarization function χ
 - Dyson equation, 226
 - Feynman diagrams, 225
 - free electrons, 143, 173
 - irreducible Feynman diagrams, 225
 - Kubo formalism, 103
 - momentum space, 142
 - relation to dielectric function ϵ , 223
 - two-particle Matsubara Green's fct., 224
- polarization vectors
 - phonons, 57
 - photons, 19
- probability current conservation, 111
- probability distribution, 136
- propagator
 - Green's function, 130
 - single-particle in external potential, 178
- quadratic Hamiltonian, 135, 146, 150, 170
- quantum coherence
 - macroscopic in superconductivity, 79
 - single electrons, 184
- quantum correction, 253, 264, 273
- quantum dots
 - introduction, 49
 - tunneling spectroscopy, 140
- quantum effects, 107
- quantum field operator
 - definition, 17
 - Fourier transform, 17
- quantum fluctuations
 - in conductance, 186
- quantum number ν
 - Feynman rules, Dyson equation, 181
 - general introduction, 3
 - sum over, 4
- quantum point contact, 116
- quantum state
 - bra and ket state, 2
 - free particle, 2
 - hydrogen, 3
 - Landau states, 3
 - orthogonal, 2
 - time evolution, 2
- quasiparticle
 - definition, 236
 - discussion, 235
 - introduction, 233
 - life-time, 243
- quasiparticle-quasiparticle scattering, 243
- radiation field, 19
- Raman scattering, 144
- random impurities, 181
- random matrix theory, 121
- random phase approximation (see RPA), 213
- rational function, 163
- reciprocal lattice basis, 33
- reciprocal space, 33
- reduced zone scheme, 35
- reflection amplitude, 110
- reflectionless contact, 108, 113
- relaxation time approximation, 243
- renormalization
 - constant Z , 247
 - effective mass, 246, 251
 - Green's function, 245
 - of phonons by RPA-screening, 281
- reservoir, 25, 108
- resistivity (see conductivity), 240
- resummation of diagrams
 - current-current correlation, 256
 - impurity scattering, 188
 - the RPA self-energy, 215
- retarded function
 - convergence factor, 147
 - Green's function, 131, 132
 - relation to Matsubara function, 161
- Roman letters, 158
- RPA for the electron gas
 - Coulomb and impurity lines, 257
 - deriving the equation of motion, 153
 - electron-hole pair interpretation, 220
 - Fermi liquid theory, 238, 246

- plasmons and Landau damping, 227
- renormalized Coulomb interaction, 217
- resummation of the self-energy, 215
- the dielectric function ϵ^{RPA} , 226
- the polarization function χ^{RPA} , 226
- vertex corrections, 259
- Rydberg, unit of energy (Ry), 40
- scattering length, 193
- scattering matrix, S , 108
- scattering state, 108
- scattering theory
 - optical theorem, 194
 - Schrödinger equation, 128
 - transition matrix, 193
- Schrödinger equation
 - Green's function, 128
 - quantum point contact, 117
 - scattering theory, 128
 - time reversal symmetry, 112
 - time-dependent, 2
- Schrödinger picture, 87
- screening
 - dielectric properties of the elec. gas, 223
 - RPA-screened Coulomb interaction, 218
 - semiclassical, dynamical, 238
 - semiclassical, static, 238
 - Thomas-Fermi screening, 218
- second quantization
 - basic concepts, 9
 - basis for different particles, 24
 - change of basis, 16
 - Coulomb interaction, 23
 - electromagnetic field, 19
 - electron-phonon interaction, 61
 - free phonons in 1D, 55
 - free phonons in 3D, 58
 - harmonic oscillator, 18
 - kinetic energy, 21
 - name, 1
 - operators, 14
 - particle current density, 22
 - particle density, 22
 - spin, 21
 - statistical mechanics, 25
 - thermal average, 27
- self-average for impurity scattering
 - basic concepts, 184
 - weak localization, 265
- self-consistent equation
 - Anderson's model, 151
 - general mean-field theory, 67
- self-energy
 - due to hybridization, 150
 - first Born approximation, 190
 - Fock diagram for pair interactions, 209
 - full Born approximation, 193
 - Hartree diagram for pair interactions, 209
 - impurity averaged electrons, 189
 - interacting electrons, jellium model, 214
 - irreducible, 257
 - pair interactions in Fourier space, 208
 - pair interactions in real space, 205
 - pair-bubble diag., pair interactions, 210
 - RPA self-energy, interacting electrons, 216
 - self-consistent Born approximation, 194
- semi-classical
 - approximation, 261
 - screening, 237
 - transport equation, 240
- single-particle states
 - as N -particle basis, 6
 - free particle state, 2
 - hydrogen orbital, 3
 - Landau state, 3
- Slater determinant, fermions, 7
- Sommerfeld expansion, 39
- sound velocity
 - Bohm-Staver formula, RPA, 283
 - Bohm-Staver formula, semi-classical, 53
 - Debye model, 52
- sound waves, 51
- space-time, points and integrals, 177
- spectral function
 - Anderson's model, 151
 - broadening, 136
 - definition, 135
 - first Born approximation, 192
 - in sums with branch cuts, 169
 - measurement, 137
 - non-interacting particles, 135
 - physical interpretation, 135
- spectroscopy
 - optical, 141
 - tunneling, 137
- spin
 - Pauli matrices, 21
 - second quantization, 21

- spontaneous symmetry breaking
 - breaking of gauge symmetry, 78
 - introduction, 72
- statistical mechanics
 - second quantization, 25
- step function $\theta(x)$, 4
- STM, 138
- Stoner model of metallic ferromagnetism, 75
- superconductivity
 - critical temperature, 84
 - introduction, 78
 - Meissner effect, 78
 - microscopic BCS theory, 81
 - order parameter, 72
- symmetrization operator, 7
- thermal average, 27
- thermodynamic potential Ω
 - definition, 28
 - for the interacting electron gas, 220
- Thomas-Fermi screening, 218, 219, 222
- time dependent Hamiltonian, 95
- time evolution
 - creation/annihilation operators, 91
 - Heisenberg picture, 88
 - in linear response, 91
 - interaction picture, 88
 - linear response, Kubo, 97
 - operator, imaginary time, 159
 - Schrödinger picture, 87
 - unitary operator $\hat{U}(t, t_0)$, 89
- time-ordering operator
 - imaginary time T_τ , 160
 - real time T_t , 90
- time-reversal symmetry, 112
- time-reversed paths, 266, 268, 272
- topologically different diagrams, 204
- trace of operators, 27
- transition matrix, scattering theory, 193
- translation-invariant system
 - conductivity, 254
 - Green's function, 132
- transmission amplitude, 110, 130, 267
- transmission coefficients, 113
- transport equation, 233
- transport time, 242
- transversality condition, 19
- triangular potential well, 47
- truncation
 - Anderson's model, 150, 153
 - derivation of RPA, 154
 - discussion, 145
- tunneling
 - scanning microscope, 138
 - BCS superconductor, 140
 - current, 138
 - spectroscopy, 137
- umklapp process, 63
- unit cell, 55
- unitarity, S -matrix, 111
- universal conductance fluctuations, 121, 124
- valence
 - electrons, 31
- vector potential
 - electromagnetic field, 19
 - kinetic energy, 21
 - Kubo formalism, 99
- vertex
 - current vertex, 255
 - dressed vertex function, 258
 - electron-phonon vertex, 280
 - pair-scattering vertex Λ , 284
 - vertex correction, 254, 257
 - vertex function, 268
- Ward identity, 258, 262
- wavefunction collapse, 2
- weak localization
 - and conductivity, 264
 - introduction, 253
 - mesoscopic systems, 121, 123
- Wick's theorem
 - derivation, 170
 - interacting electrons, 201
 - phonon Green's function, 277
- WKB approximation, 119
- Yukawa potential
 - definition, 24, 213
 - RPA-screened Coulomb interaction, 218